

N72-32867-902

NASA TECHNICAL  
MEMORANDUM



NASA TM X-2637

NASA TM X-2637

CASE FILE  
COPY

## NASTRAN: USERS' EXPERIENCES

Second Colloquium held at  
Langley Research Center  
Hampton, Virginia  
September 11-12, 1972

NATIONAL AERONAUTICS AND SPACE ADMINISTRATION • WASHINGTON, D. C. • SEPTEMBER 1972

ERRATA

NASA Technical Memorandum X-2637

NASTRAN: USERS' EXPERIENCES

September 1972

In Paper No. 7 entitled "Some Applications of NASTRAN to the Buckling of Thin Cylindrical Shells With Cutouts" by Jerry G. Williams and James H. Starnes, Jr., the following pages should be corrected:

Page 82, line 27: Change "eight circumferential . . ." to "sixteen circumferential . . .".

Page 89, table II: In third column, change "same as case 5" to "same as case 4" for cases 6 and 7.

Page 93, figure 4: Model A should not contain a cutout.

Page 95, figure 6: For Model D (clamped case II, with two holes,  $0.91 \text{ m} \times 0.69 \text{ m}$ ), the magnitude  $P/P_{\text{ref}}$  should be 0.905.

Page 97, figure 8: Sublegends should read

(a) Model C.

and

(b) Model D.

1. Report No. NASA TM X-2637	2. Government Accession No.	3. Recipient's Catalog No.	
4. Title and Subtitle NASTRAN: USERS' EXPERIENCES		5. Report Date September 1972	
		6. Performing Organization Code	
7. Author(s)		8. Performing Organization Report No. L-8553	
		10. Work Unit No. 501-22-01-01	
9. Performing Organization Name and Address NASA Langley Research Center Hampton, Virginia 23365		11. Contract or Grant No. N/A	
		13. Type of Report and Period Covered Technical Memorandum	
12. Sponsoring Agency Name and Address National Aeronautics and Space Administration Washington, D.C. 20546		14. Sponsoring Agency Code	
		15. Supplementary Notes Compendium of papers prepared for Second NASTRAN Users' Colloquium, September 11-12, 1972, NASA Langley Research Center	
16. Abstract  This Technical Memorandum is comprised of selected papers prepared for the Second NASTRAN Users' Colloquium held at the NASA Langley Research Center, September 11-12, 1972. The authors discuss the application of NASTRAN to a wide variety of static and dynamic structural problems. Specifically, the papers focus on the following topics:  I. Statics and Buckling II. Vibrations and Dynamics III. Comparisons and Evaluations IV. New Capability V. General Applications			
17. Key Words (Suggested by Author(s)) NASTRAN, structures, finite element, NASTRAN Colloquium		18. Distribution Statement Unclassified - Unlimited	
19. Security Classif. (of this report) Unclassified	20. Security Classif. (of this page) Unclassified	21. No. of Pages 522	22. Price* \$6.00

NASTRAN: USERS' EXPERIENCES

Compendium of papers prepared for the Second NASTRAN Users' Colloquium

September 11-12, 1972

NASA Langley Research Center

FOREWORD

NASTRAN (NASA STRUCTURAL ANALYSIS) has been available to the public since late in 1970. As a large, comprehensive, nonproprietary, general purpose, finite element computer system for structural analysis, NASTRAN is finding widespread acceptance within NASA, other government agencies, and industry.

NASTRAN is available to the public at a cost of \$1,790, which covers reproducing and supplying the necessary system tapes. Furthermore, NASA has provided for the continuing maintenance and improvement of NASTRAN through the establishment of a NASTRAN Systems Management Office located at the Langley Research Center. At present, NASTRAN is in use at over 100 locations, including NASA centers, other government agencies, industry, and commercial computer data centers.

Because of the widespread interest in NASTRAN and because of a desire to better serve the community of NASTRAN users, the NASTRAN System Management Office organized the Second NASTRAN Users' Colloquium at the Langley Research Center, September 11-12, 1972. (The compendium of papers prepared for the First NASTRAN Users' Colloquium held September 13-15, 1971 was published as NASA TM X-2378.) The colloquium was planned to provide to everyone concerned an opportunity to participate in a comprehensive review of the current status of NASTRAN use, including the rate of user acceptance, unique applications, operational problems, most desired modifications including new capability, and comparisons with other applications programs.

Individuals actively engaged in the use of NASTRAN were invited to prepare papers for presentation at the colloquium. These papers are included in this volume. Only a limited editorial review was provided to achieve reasonably consistent format and content. The opinions and data presented are the responsibility of the authors and their respective organizations.

J. P. Raney, Head  
NASTRAN Systems Management Office  
Langley Research Center  
Hampton, Va. 23365  
September 1972



## CONTENTS

FOREWORD . . . . .	iii
1. NASTRAN: A PROGRESS REPORT . . . . . J. Philip Ranev and Deene J. Weidman (NASA Langley Research Center)	1
2. NASTRAN: DISSEMINATION EXPERIENCES AND USER BENEFITS . . . . . Joseph M. Carlson (NASA Headquarters)	13
3. TECHNICAL AND SOCIAL IMPACT OF NASTRAN . . . . . Thomas G. Butler (NASA Goddard Space Flight Center)	15
I. STATICS AND BUCKLING	
4. BUCKLING ANALYSIS OF A MISSILE INTERSTAGE . . . . . David P. Dudley (Aerojet Solid Propulsion Company)	29
5. NASTRAN BUCKLING ANALYSIS OF A THIN-WALLED CYLINDER . . . . . Ralph B. Wight (NASA Goddard Space Flight Center)	39
6. STRESS AND BUCKLING ANALYSIS OF A DOUBLE-BUBBLE TANK STRUCTURE . . . . . James C. Robinson (NASA Langley Research Center) and John H. Dutton (McDonnell Douglas Corporation)	53
7. SOME APPLICATIONS OF NASTRAN TO THE BUCKLING OF THIN CYLINDRICAL SHELLS WITH CUTOUTS . . . . . Jerry G. Williams and James H. Starnes, Jr. (NASA Langley Research Center)	73
8. ANALYSIS AND DESIGN OF ON-GRADE REINFORCED CONCRETE TRACK SUPPORT STRUCTURES . . . . . Francis G. McLean, Ronald D. Williams, and Lance R. Greening (Westenhoff and Novick, Inc.)	99
9. EXPERIENCES IN INTERFACING NASTRAN WITH ANOTHER FINITE ELEMENT PROGRAM . . . . . Dennis D. Schwerzler and Robert K. Leverenz (General Motors Corporation)	111
10. DELTA LAUNCH VEHICLE ISOGRID STRUCTURE NASTRAN ANALYSIS . . . . . Daniel J. Knighton (NASA Goddard Space Flight Center)	121

## II. VIBRATIONS AND DYNAMICS

11. A NASTRAN CORRELATION STUDY FOR VIBRATIONS OF A CROSS-STIFFENED SHIP'S DECK . . . . . 145  
Earl A. Thornton (Old Dominion University)
12. TRANSIENT ANALYSIS OF AN IVHM GRAPPLE IMPACT TEST . . . . . 161  
R. G. Hill (Hanford Engineering Development Laboratory)
13. MODELING TECHNIQUES OF THIN-WALLED BEAMS WITH OPEN CROSS SECTIONS . . . 179  
Knut S. Skattum (General Motors Corporation)
14. COMPLEX EIGENVALUE ANALYSIS OF ROTATING STRUCTURES . . . . . 197  
Jayant S. Patel (Teledyne Brown Engineering Company) and  
S. M. Seltzer (NASA George C. Marshall Space Flight Center)

## III. COMPARISONS AND EVALUATIONS

15. LEVEL 12 NASTRAN EXPERIENCES AT GENERAL DYNAMICS, CONVAIR AEROSPACE DIVISION, FORT WORTH OPERATION . . . . . 235  
Merle Allen (General Dynamics/Fort Worth)
16. NONAPPLICABILITY OF LINEAR FINITE ELEMENT PROGRAMS TO THE STRESS ANALYSIS OF TIRES . . . . . 263  
Michel Durand and Etienne Jankovich (Kleber-Colombes)
17. A COMPARISON OF THE CAPABILITIES OF THREE FINITE ELEMENT PROGRAMS . . . 277  
David D. Loendorf (Langley Directorate, U.S. Army Air Mobility Research and Development Laboratory)
18. ADAPTATION OF NASTRAN TO AN INTEGRATED SYSTEM OF STRUCTURAL DESIGN ANALYSIS . . . . . 289  
Gernot W. Hagenmacher (Lockheed-California Company)
19. COMPARISON OF NASTRAN AND STARDYNE STATIC ANALYSIS OF A GRAPHITE FIBER REINFORCED PLASTIC TRUSS STRUCTURE . . . . . 303  
George H. Honeycutt, Frank J. On, and Stuart L. Hanlein (NASA Goddard Space Flight Center)

## IV. NEW CAPABILITY

20. AN ISOPARAMETRIC QUADRILATERAL MEMBRANE ELEMENT FOR NASTRAN . . . . . 315  
Howard M. Adelman, Joseph E. Walz, and James L. Rogers, Jr.  
(NASA Langley Research Center)

21. SOME ASPECTS OF THE NASTRAN PROGRAM OUTPUT . . . . .	337
David J. Gregory (Grumman Aerospace Corporation)	
22. A DESIGN STUDY FOR THE ADDITION OF HIGHER-ORDER PARAMETRIC DISCRETE ELEMENTS TO NASTRAN . . . . .	361
E. L. Stanton (McDonnell Douglas Astronautics Company)	
23. MODIFICATIONS AND ADDITIONS TO NASTRAN AT MARSHALL SPACE FLIGHT CENTER - 1969-1972 . . . . .	375
Archie J. Jordan, Jr., and William G. Ward (Computer Sciences Corporation)	
24. THE NASTRAN CONTOUR PLOTTER . . . . .	385
Barbara M. Kelly (Naval Ship Research and Development Center)	
25. NASTRAN DATA GENERATION AND MANAGEMENT USING INTERACTIVE GRAPHICS . . .	399
M. Smoot Katow and Barry M. Cooper (Jet Propulsion Laboratory)	
26. THE BANDIT COMPUTER PROGRAM FOR THE REDUCTION OF MATRIX BANDWIDTH FOR NASTRAN . . . . .	407
Gordon C. Everstine (Naval Ship Research and Development Center)	

V. GENERAL APPLICATIONS

27. USE OF NASTRAN AS A TEACHING AID . . . . .	415
Michael T. Wilkinson (Louisiana Tech University)	
28. STRUCTURAL ANALYSIS FOR A 40-STORY BUILDING . . . . .	421
Lo-Ching Hua (Control Data Corporation)	
29. APPLICATIONS OF NASTRAN TO NUCLEAR PROBLEMS . . . . .	429
Embertus Spreeuw (NASA Langley Research Center)	
30. NASTRAN THERMAL ANALYZER - A GENERAL PURPOSE FINITE-ELEMENT HEAT TRANSFER COMPUTER PROGRAM . . . . .	443
Hwa-Ping Lee and James B. Mason (NASA Goddard Space Flight Center)	
31. VIEW - A MODIFICATION OF THE RAVFAC VIEW FACTOR PROGRAM FOR USE WITH THE NASTRAN THERMAL ANALYZER . . . . .	455
Edward F. Puccinelli and Clifton E. Jackson, Jr. (NASA Goddard Space Flight Center)	
32. STRUCTURAL DYNAMIC AND THERMAL STRESS ANALYSIS OF NUCLEAR REACTOR VESSEL SUPPORT SYSTEM . . . . .	465
James Chi-Dian Go (Computer Sciences Corporation)	

33. HIGH PRESSURE TURBINE BLADE STRESS ANALYSIS . . . . .	477
Robert R. Van Nimwegen and Samuel Tepper (AiResearch Manufacturing Company)	
34. APPLICATIONS OF NASTRAN SUBSTRUCTURING . . . . .	485
R. Narayanaswami (NASA Langley Research Center)	
35. DESIGN OF NASTRAN DEMONSTRATION PROBLEMS . . . . .	497
Alvin Levy (Grumman Aerospace Corporation)	

## NASTRAN: A PROGRESS REPORT

By J. Philip Raney and Deene J. Weidman  
NASA Langley Research Center

### INTRODUCTION

During the interval since the first NASTRAN Users' Colloquium September 13-15, 1971 (ref. 1), the number of NASTRAN users has increased by about 50 percent. At the present time NASTRAN is installed on over 100 computers. Government users include, in addition to NASA centers, DOD, DOT, and the AEC. Users in the private sector include most aerospace firms, the automotive industry, architectural engineers, and those who use NASTRAN at computer data centers. A partial sampling of some interesting domestic NASTRAN applications is included in a NASTRAN benefits study which was conducted for the Office of Technology Utilization, NASA Headquarters (ref. 2). On the international scene NASTRAN has been made available by American firms at computer data centers world wide. NSMO has received expressions of interest in NASTRAN from firms in nearly every West European country, Japan, and Israel.

The purpose of this report is to inform NASTRAN users of significant NASTRAN-related events of the past year, to describe the present operation of the NASTRAN Systems Management Office (NSMO), to discuss the new capabilities and improvements incorporated in Level 15 of NASTRAN, and to discuss priorities for future levels of NASTRAN.

### SIGNIFICANT MILESTONES

October 1971-September 1972

Four activities seem worthy of discussion as significant milestones: the NASTRAN Newsletter, the SPR Log, the generation of Level 15, and the 2nd NASTRAN Users' Colloquium including a NASA-Industry Working Session.

#### Newsletter

The first NASTRAN Newsletter was published August 20, 1971. Subsequent Newsletters were published December 7, 1971, March 13 and July 20, 1972. A variety of topics is normally included under NSMO Communications. Other items of user interest discussed in these Newsletters have included Level 15 Announcements, NASTRAN Publications, Level 12 Errors, DMAP Programs, and

Rigid Format Alter Packets. The Newsletter circulation is presently over 1,000 copies.

## SPR Log

A computerized data base of information from all Software Problem Reports (SPR's) was created in February. The first released SPR Log was designated Log 16 and was distributed by NSMO to 21 organizations for evaluation and comment. Log 17 was generated in March and was sent to 16 additional organizations and to COSMIC for further distribution. Log 19 was generated in July and is presently available from COSMIC. SPR Logs 16 and 17 consist of two parts. The first part is an alphabetical sort of the NASTRAN module in which the error was discovered. This is a brief listing and should be used as an index to the second part which is a listing by assigned SPR number and includes a complete description of the error and its present status. In SPR Log 19 a third listing is included which lists by SPR number the Level 12 errors that have been corrected in Level 15.

The SPR Log is a valuable reference for any NASTRAN user group. It provides a rapid assessment of all previously reported errors in any NASTRAN module.

## Level 15

The generation of Level 15 posed several formidable problems. Certain new capability and improvements which had been developed by the MacNeal-Schwendler Corporation (MSC) in their Level 11-based NASTRAN were scheduled to be incorporated in Level 15. These included a new GINO, efficiency improvements, heat transfer capability and several others. A contractual requirement stated that Level 15 would be built from NASA's Level 14 which was generated by the interim maintenance contractor, Computer Sciences Corporation (CSC), from Levels 12 and 13. In order to build Level 15 in a systematic, reproducible fashion and to retain all error corrections made by CSC in Level 14, the corresponding decks of both the MSC system and Level 14 were compared and the differences analyzed. Of a total of 939 decks 717 FORTRAN decks common to both systems were first compared line for line using a special purpose computer program. Either the Level 14 or the MSC deck was modified until a comparison showed perfect coincidence of the two decks. This computerized comparison effort resulted in changes to 307 decks from Level 14 and 370 decks from the MSC system. The remaining 222 decks were totally new design FORTRAN decks or were machine dependent and were not directly compared line for line. Of these, 125 decks were new additions from the MSC system, and 97 decks had been altered in both systems. For these decks the arduous task of hand comparison was performed. After thorough analysis and discussion, decisions were made which preserved nearly all previous error corrections and assured that the new decks would be free from previously reported errors. The Level 15 archive system was generated in May and incorporated all error corrections

which had been made by March 31. The completed code for each machine version was shipped to COSMIC early in July.

Level 15 documentation was a pacing item throughout the year. The camera-ready mats were finished for the Theoretical Manual SP-221(01) in mid-April, for the User's Manual SP-222(01) in mid-June, for the Demonstration Manual SP-224(01) in mid-June, and for the Programmer's Manual SP-223(01) in early September. COSMIC agreed to provide complimentary copies of the Level 12 manuals to persons ordering Level 15 until the Level 15 manuals became available.

Pre-release copies of Level 15 were made available in June to selected NASA centers and industry on the basis that evaluation reports would be returned to NSMO in a timely manner and thus preclude the possibility of serious undiscovered errors existing in Level 15 when released through COSMIC. Some errors that were discovered through pre-release testing have already been reported in the Newsletter and included in the SPR Log.

#### 1972 USERS' COLLOQUIUM

The 2nd NASTRAN Users' Colloquium was held at the Langley Research Center September 11-12. Papers were selected on the basis of abstracts received by NSMO by April 15. This volume contains a collection of the papers presented at the Colloquium.

An industry working session with representatives from several aerospace firms was held on the morning of the 13th. The purpose of this session was to provide the participants with an opportunity to formally apprise NSMO of their list of most needed NASTRAN improvements and new capabilities.

#### NSMO ACTIVITIES

The NSMO staff presently includes the following persons:

J. P. Raney, Head  
D. J. Weidman  
J. E. Walz  
H. M. Adelman  
J. L. Rogers, Jr.  
Sylvia Harris, Secretary

The major areas of activity of NSMO staff members include user communications, maintenance functions, development and installation of new capabilities.

## User Communication

One of the most important functions of NSMO requiring a greater than one man level of effort, is to provide open lines of communication with the users of NASTRAN. At present NSMO communications with NASTRAN users are handled in six ways:

Steering Committees: NSMO is represented on the Navy's NASTRAN Steering Committee and also serves on NASA's NASTRAN Advisory Group (NAG). Efforts to achieve a working interface with industry are also being made.

Newsletter: The NASTRAN Newsletter has been published by NSMO at a rate of about once every four months. The Newsletter provides a means of timely contact with NASTRAN users informing them of all maintenance activities and should be issued every two months.

NASTRAN Users' Colloquia: An annual colloquium provides a unique opportunity for users to share their experiences and evaluation of the NASTRAN system.

Talks and Papers: Last year the NSMO staff presented three papers and gave numerous presentations to groups at Langley and elsewhere.

SPR Log: The SPR Log, a spinoff of the maintenance activity, is essential as a guide to known errors in NASTRAN and can be used to identify and avoid potential pitfalls in previously untried applications or solution paths.

Telephone: The telephone is an expedient means of communication and, therefore, is in constant use. Telephone consultations alone account for most of the time devoted to user communications.

## Maintenance

The maintenance activity currently requires a nearly two man level of effort on the part of NSMO. Monitoring the maintenance contractor, establishment schedules and work priorities, and arranging for government furnished computers are important aspects of NSMO maintenance activity.

Initial screening of all SPR's is done by NSMO. NSMO receives an average of about 10 to 12 error reports each month. After an evaluation, and perhaps a computer verification of the reported error, a number and priority are assigned by NSMO and the SPR is then delivered to the maintenance contractor for in-depth evaluation and correction.

Maintenance of the NASTRAN manuals is performed jointly by NSMO and the maintenance contractor. Two editors have been assigned to each manual - an

NSMO editor and a contractor editor. Changes of the manuals for Level 15 proved to be quite extensive because of many modifications and the addition of new capability incorporated in this new level of NASTRAN. It was therefore decided to print new manuals rather than attempting to issue updates to the existing Level 12 documentation. Documentation was the pacing item of work in the preparation of Level 15. NSMO hopes to devote a continuous high level of effort to NASTRAN documentation requirements and thereby eliminate a major peaking of this activity during the generation of later levels of NASTRAN.

### New Capability

The selection and development of new capability also accounts for an expenditure of about a two man level-of-effort. In addition to monitoring contracts for the addition of solid isoparametric elements and of a family of linear strain elements, NSMO is installing inhouse a new isoparametric quadrilateral membrane element. A paper which describes this element is included in this volume. Significant time is required to evaluate and define new capability (including efficiency improvements) and to interface with the proposers of new capability for NASTRAN.

### LEVEL 15 A Comparison With Level 12

The improvements and modifications to Level 12 that led to the generation of Level 15 generally may be described as providing functional capabilities, or efficiency improvements, or user conveniences. The more significant of these are summarized below. A significant effort was also made to correct as many serious program errors as possible.

### Functional Capabilities

1. *Dummy structural elements* - Provision has been made for dummy structural elements to allow the user to investigate new structural elements with a minimum of difficulty. It is only necessary for the user to generate the code for the element matrices, and the procedures are such that a knowledge of Fortran is sufficient to accomplish the task of inserting a new element on a trial basis. These elements are still restricted to the six degrees of freedom currently in NASTRAN.
2. *Substructuring* - Substructuring procedures have been developed for both static and dynamic analysis. The basic matrix operations provided in Level 12 were used in the development of the substructuring procedures. Two new modules (INPUT11 and OUTPUT1) were developed to provide the capability for writing matrices on tape and reading

matrices from tape in NASTRAN format. Also, the PARTN and MERGE modules were rewritten for improved efficiency and capability. At present, an auxiliary program PARTVEC is used to generate partitioning vectors.

3. Solid polyhedra elements - The basic solid polyhedron element is the tetrahedron analyzed for constant strain and uniform isotropic materials. The wedge and hexahedron are assembled from basic tetrahedron elements, and are also elementary constant strain elements.
4. Heat transfer - Linear steady-state heat transfer analysis has been added. The NASTRAN heat flow capability may be used either as a separate analysis to determine temperatures or to determine temperature inputs to be used in a later run for structural problems.
5. Acoustic analysis - This application includes the calculation of the vibration modes of a compressible fluid in cavities with slots.
6. Compressible fluids in axisymmetric tanks - Compressibility of the fluid and the effects of gravity on a free surface are both included in the formulation, as well as consideration of the elasticity of the tank wall.
7. Improved differential stiffness for plate elements - An improved formulation of the differential stiffness for plate elements has reduced the error for buckling analysis to less than 10 percent with two elements per halfwave.
8. Thermal bending - Provision has been made to include thermal bending moments created by the presence of thermal gradients in bars and plate elements.

#### Efficiency Improvements

A number of important improvements in efficiency have been made in Level 15.

1. General input/output routines (GINO) - Many improvements were made in the efficiency of this machine-dependent routine. The IBM FORTRAN version of GINO was completely replaced with an assembly language routine, which also assumes the task of managing the secondary storage space on the disc storage files.
2. Matrix packing - The logic of the matrix packing routine was substantially revised, and the CDC and IBM versions were replaced with assembly language routines for efficiency.
3. Multiply/add (MPYAD) - The inner loops of all multiply/add routines were rewritten in assembly language for all three machines for

improved efficiency. In addition, the sparse matrix routine (Method 2) was completely rewritten.

4. Single precision - Most of the matrix operation routines on the CDC machine were revised to use only single-precision arithmetic. Some key operations still remain in double precision, and may be converted later.
5. Eigenvalue extraction - Improved shift decision logic and symmetric decomposition is now used in the inverse power method of eigenvalue extraction.
6. Frequency response - The use of symmetric decompositions and symmetric equation solution routines is available on an optional basis in the solution of frequency response problems.
7. Equation solution - The inner loops of the equation solution routines have been rewritten for improved efficiency.

A tabulation of the execution (CPU) times for the NASTRAN demonstration problems for both Levels 12 and 15 which indicates the areas of greatest improvement in efficiency is given in the Appendix.

#### User Conveniences

1. Diagnostic output - A number of new types of diagnostic output have been provided as indicated in the following partial list.
  - DIAG 8 - Print the size, form, type, and density of matrices as they are formed.
  - DIAG 13 - Print the amount of working storage available for each module.
  - DIAG 14 - Print the rigid format for all nonrestart runs.
  - DIAG 16 - Print details of the iteration steps for the real inverse power method of eigenvalue extraction.
2. User tapes - Two new modules (OUTPUT2 and INPUTT2) have been provided to allow the user to read information from tapes that have been written with external FORTRAN programs and to write information on tapes inside of NASTRAN that can be read by external FORTRAN programs. This provides an important interface between NASTRAN and other programs.
3. Partitioning matrices - Two new modules (VEC and UPARTN) have been provided to make it more convenient for the user to partition matrices in terms of the set notation that is used internally in NASTRAN.

4. Table printer - A new formatted table printer has been provided for the printing of selected NASTRAN tables in readable formats.
5. Matrix punching - A new module (OUTPUT3) has been provided to permit the user to punch matrices on DMI or bulk data cards.
6. Transliterator - Provision has been made to accept either 026 or 029 character sets, either as intermixed cards of these types or even as intermixed characters on a card.

PRIORITIES FOR FUTURE  
LEVELS OF NASTRAN

A new level of NASTRAN is generated when the bookkeeping associated with error corrections, system improvements, and new capability becomes excessive. At the present time well-defined plans for future release of NASTRAN include an intermediate version of Level 15 (Level 15 1/2) with major new capability, and Level 16.

Level 15 1/2 - January 1973

1. Complete Heat Transfer allows for analysis of steady state and transient heat transfer. Inputs include convection, conduction, and radiation.
2. Fully Stressed Design Module automatically sizes the ROD, BAR, TRMEM, QDMEM, TRPLT, QDPLT, TRIA1, QUAD1, TRIA2, and QUAD2 elements to provide maximum stress in each element.
3. Space Shuttle Improvements which include grid point force balance information and output of the element forces for the element listed under the Full Stressed Design Module.
4. Error Corrections

Level 16 - June 1973

1. Solid Isoparametric Elements developed by Universal Analytics, Inc.
2. Linear Strain Elements developed by Bell Aerospace Company.
3. New Structural Matrix Assembler
4. Complete Single/Double Precision Option
5. Extensive Efficiency Improvements
6. Error Corrections

Planning for FY 1974 has only recently commenced; however, it appears reasonably certain that at least a major update of Level 16 will occur before July 1, 1973.

## SUMMARY

The NASTRAN Systems Management Office has operated over the last year with a staff of five professionals who divide their time between user communications, maintenance, and new capability. Accomplishments of interest to NASTRAN users have included publishing four Newsletters, distribution of the new SPR Log, generation of Level 15, and organizing the 2nd NASTRAN Users' Colloquium. During FY '73 a major update of Level 15 is planned to incorporate a complete heat transfer capability. Level 16 is targeted to be released in June and will include major efficiency enhancements and new linear strain and solid isoparametric elements.

## REFERENCES

1. "NASTRAN: Users' Experiences," TM X-2378, September 1971.
2. "NASTRAN Benefits Analysis," CR-125882, February 15, 1972.

APPENDIX

Execution Times (CPU Seconds): Level 15 vs. Level 12

Demonstration Problems	IBM 360 Series						CDC 6000 Series			UNIVAC 1100 Series		
	Model 95		Model 67		Model 75		6600			1108		
	Level 12	Level 15	Level 12	Level 15	Level 15	Level 15	Level 15	Level 12	Level 15	Level 12	Level 15	
1-1	60	-	108	56	-	-	46	31	36	72	30	
1-1A	30	7	102	-	-	26	24	24	-	24	17	
1-1B	108	15	294	-	-	-	-	90	37	72	41	
1-2	84	-	264	114	-	-	-	72	22	60	55	
1-2A	48	10	144	-	-	41	36	36	-	30	25	
1-3	114	-	336	152	-	-	120	120	94	96	86	
1-3	NA	22	NA	-	-	-	NA	NA	85	NA	-	
1-4	1020	139	1464	-	-	-	666	666	323	1020	510	
1-4	NA	67	NA	-	-	-	NA	NA	316	NA	-	
1-4A	60	8	174	-	-	-	30	30	23	30	29	
1-4	380	179	-	-	-	-	-	-	429	NA	-	
1-4	NA	84	NA	-	-	-	NA	NA	421	NA	-	
1-4A	-	48	-	-	-	-	-	-	25	-	-	
1-5	660	111	1800	-	-	-	-	-	422	1080	477	
1-6	48	10	132	-	-	-	-	30	30	24	22	
1-7	60	21	270	-	-	-	-	120	127	90	115	
1-8	NA	16	NA	-	-	-	-	NA	90	NA	47	
1-9	NA	-	NA	128	-	-	148	NA	-	NA	76	
1-10	-	-	-	254	-	-	34	-	-	-	18	
1-11	-	30	-	-	-	-	-	-	-	-	83	
1-12	NA	-	NA	44	-	-	-	NA	81	NA	18	
2-1	72	-	168	66	-	-	42	30	26	24	24	
3-1	720	105	3900	-	-	-	-	828	366	660*4	422	
3-1	NA	92	NA	-	-	-	-	NA	352	NA	-	
3-1	610	228	-	-	-	-	354	-	-	-	-	
3-1	NA	510	NA	-	-	-	-	-	1062	NA	-	
3-2	NA	-	NA	-	-	-	-	NA	276	NA	405	
3-3	NA	79	NA	-	-	157	-	NA	274	NA	354	
3-4	NA	-	NA	-	-	182	-	NA	109	NA	107	
4-1	168	31	486	-	-	-	164	144	-	90*2	102	
5-1	408	-	1134	498	-	-	725	486	-	318*3	287	

Demonstration Problems		IBM 360 Series				CDC 6000 Series			UNIVAC 1100 Series		
		Model 95		Model 67	Model 65	Model 75	6400		6600		1108
No.	Form & Version	Level 12	Level 15	Level 12	Level 15	Level 15	Level 15	Level 12	Level 15	Level 12	Level 15
6-1	U	1714	353	5214*1	-	-	-	1956	323	270*3	1361
7-1	U	228	-	606	-	265	-	216	196	204	188
7-1	I	NA	-	NA	-	245	-	NA	176	NA	-
7-2	U-1	-	-	-	-	919	-	-	1225	-	765
7-2	U-2	-	-	-	-	388	-	-	1481	-	386
8-1	U-1	134	-	467	-	138	376	126	-	138	115
8-1	I-1	NA	-	NA	-	134	-	NA	127	NA	-
8-1	U-2	732	-	-	-	628	-	-	1354	-	-
8-1	I-2	NA	-	NA	-	940	-	NA	510	NA	-
9-1	U	90	-	372	-	66	57	30	40	36	24
9-2	U	396	81	1026	-	-	-	378	316	105	318
9-2	I	NA	78	NA	-	-	-	NA	307	NA	-
9-3	U	NA	286	NA	-	-	-	NA	464	NA	422
10-1	U	204	-	570	-	117	114	120	140	66	54
11-1	U	162	-	420	117	-	-	96	61	84	70
11-1A	R	36	8	114	-	-	24	18	-	18	16
11-2	U	942	271	2484	-	-	-	882	487	510*5	495
11-2	I	NA	124	NA	-	-	-	NA	504	NA	-
12-1	U	348	75	1032	-	-	-	336	147	294	167

I = INPUT generated deck  
 U = UMF generated deck  
 R = Restart deck  
 C = Card deck  
 NA = Not Applicable

FORMS  
 1-4 Version 1 = 5 x 50 elements  
 3-1 Version 1 = 5 x 60 element  
 7-2 Version 1 = 10 x 20 elements  
 8-1 Version 1 = 20 x 40 elements  
 2 = 3 harmonics  
 2 = 5 harmonics  
 2 = 10 x 10 elements  
 2 = 20 x 20 elements

VERSIONS  
 1 = 5 x 50 elements  
 2 = 5 x 60 element  
 1 = 10 x 20 elements  
 2 = 20 x 40 elements  
 1 = 3 harmonics  
 2 = 5 harmonics  
 1 = 10 x 10 elements  
 2 = 20 x 20 elements

\*1 25 loading increments  
 \*2 3 loading increments  
 \*3 4 loading increments  
 \*4 3 modes  
 \*5 20 modes



NASTRAN: DISSEMINATION EXPERIENCES  
AND USER BENEFITS

By Joseph M. Carlson  
Technology Utilization Office  
NASA Headquarters

It has long been contended in the NASA technology transfer program that the act of making computer programs openly available to all U.S. users would be one of the most visible kinds of transfer activities that we could undertake. This is because our other efforts tend to deal with technology and technical information less easily visualized, less well packaged, and which often requires the aggregation of inputs from many different research facilities and groups. Likewise the adaptation which is often necessary to convert aerospace technology to other purposes frequently constitutes a difficult investment decision: the share of the obtainable market compared to the cost of the adaptive engineering is a difficult analysis for the user to perform. Computer programs, however, come in more clearly defined packages; the elements of the package are usually all physically present in the same location; and the marginal costs of adaptation, while still difficult to judge, seem to be relatively easier to estimate than in other kinds of technology. Thus, it has appeared that whatever we could do to make programs available would be a good investment of our limited resources.

NASTRAN, of course, is too large, significant, and unique to justify a complete extrapolation from it to our entire program for software transfer. However, it is clear that if we can nearly replicate the value that has accrued to NASTRAN users in some other situations, the software dissemination program will be proven to be of great benefit to the American economy.

In the past year, a preliminary survey was conducted of the NASTRAN user community. Briefly, the study found that after NASTRAN had been publicly available for less than two years:

- . quantified annual user cost savings totaled at least \$14.5 million
- . new product development revenues to users totaled at least \$5.65 million

The significance of NASTRAN is indicated by the following, as of the time of the study:

- . users had spent at least \$1.732 million of their own funds to develop new applications and modifications
- . at least 186 discrete applications had been developed
- . at least 667 persons, primarily engineers, were found to have used NASTRAN

Applications have included the design and analysis of:

- . aircraft fuselages, wings and tail assemblies
- . automobile frames and other motor vehicle components
- . high speed railroad tracks
- . turbine blades
- . space vehicles and related launch facilities
- . skyscrapers
- . helicopter blades
- . a sports stadium roof, and many others

The past year has been instructive in that we have encountered some new experiences with NASTRAN. These have included the demonstration of significant foreign interest in the program, certainly not unique to NASTRAN but amplified by its exceptional value. This has contributed to several reviews of our policy on foreign dissemination. The many problems in servicing the program, borne primarily by the Langley NASTRAN Systems Management Office, and the distribution problems encountered by COSMIC have been unusual because of the sheer size of NASTRAN. The observation of how the industrial community has reacted, including the activities of service bureaus, large companies, universities, and entrepreneurial groups, has been very interesting. We anticipate that if we are able to do another user study, about 18 months to two years after the release of Level 15, this complex user interaction and response will prove even more interesting.

In summary, it is now clear that the economic and technical significance of the public availability of this new tool is very large and pervasive, and goes a long way to make the case for Federal computer software transfer programs.

# TECHNICAL AND SOCIAL IMPACT OF NASTRAN

Thomas G. Butler  
NASA Goddard Space Flight Center

## SUMMARY

Some estimates are made as to the direction in which a new generation of general purpose applications programs can be expected to migrate. NASA has released its new general purpose structures program, NASTRAN (NASA STRuctural ANalysis). Predictions are made as to the impacts that this newly available space technology is liable to have within the field of structural engineering and on the society in which it interacts.

## INTRODUCTION

NASTRAN is the first of a new generation of general purpose application programs for individual disciplines. It was established for the discipline of structural analysis. There is a strong possibility that other disciplines can adapt the NASTRAN format for a general purpose approach to their problems, and it is therefore timely to discuss this topic in an open forum such as the *NASTRAN Colloquium*.

The primary feature of NASTRAN as a general purpose management framework that should make it attractive for other disciplines is its freedom from semantic implications. It can manage a host of problem types without having the individual natures of these disciplines influence the logic of the management of the associated problems during the solution process on the computer. The basis for this statement will become apparent in the following discussion on characteristics.

## CHARACTERISTICS

### Computer Independence

All interfacing between the problem solution (Functional) Modules and the computer operating system is confined to a small section of the program called the "Executive." This allows the program to operate with and under the computer operating system. The Executive is organized about a central driver that stays resident in core. The central driver calls Executive Modules into core, consults a tape stored scheduler (called by the acronym OSCAR, which stands for Operating Sequence Control ARray) for the initiation of each module, and consults a file status table for peripheral service needs. The central driver also consults core resident tables that do the bookkeeping for file and core assignments and that contain the values or names of parameters, depending on whether they are constant or variable. These parameters either exert problem control or act as communication links between modules. The Executive Modules intercede for a Functional Module in invoking support from the operating system, such as reading and writing, or peripheral storage assignments. Naturally, some of these Executive Modules must be machine dependent, but these are a small fraction (about 1 percent) of the total program code so that there is a minimum of machine dependence.

The other design feature that has contributed to machine independence is the almost exclusive writing of Functional Modules in FORTRAN and using FORTRAN wherever possible (even in writing the machine-dependent Executive Modules). The FORTRAN language used was derived from the intersection of IBSYS FORTRAN IV, OS 360 FORTRAN IV, UNIVAC's FORTRAN V, and CDC's FORTRAN. Certain exceptions were allowed, e.g., in the area of nonstandard returns. Hence an interpreter is needed to generate the source decks for the CDC 6600 from the basic library.

The gross link/overlay design is essentially the same on each machine, but here again there are certain inherent uniquenesses that have to be accommodated. Thus for almost each computer model (not only for each computer manufacturer) there will be an individual strategy to build the architecture of the NASTRAN executable. The dimensions of NASTRAN level 15.0 are roughly 14 links wide with a depth of 7 levels of overlay in each link. To achieve seven levels of overlay on the 6000 class of CDC machines, a separate linkage editor/loader had to be written to replace that provided by the SCOPE operating system.

## Internal Storage Management

Initially, the operating system will make an assignment of core and an assignment of a combination of secondary storage devices with both serial and random access devices. A combined minimum of 30 serial and random access files is required for NASTRAN. From this point on, NASTRAN does its own internal dynamic management of files and core. File requirements are defined in terms of predetermined sets of data (called data blocks). Depending on the peculiarities of a given structural problem, a given physical file during one problem execution may have been occupied by a large succession of data blocks entirely under the control of a NASTRAN Executive Module. Each Functional Module is overlaid into core in a tightly packed fashion so that the maximum amount of remaining core is available as working space for the storage of matrices. This management of core and files, it must be reemphasized, is internal and is under the control of an Executive Module.

## Modularity, Open-Endedness, and Maintainability

The working basis of NASTRAN is through the companion pairs, modules, and data blocks. It takes the execution of many modules and several link control transfers to achieve a total cycle of a problem type relating to a given discipline. It takes a number of subroutines to compose the many functional steps of a module through several levels of overlay. A predetermined set of input data blocks, output data blocks, and scratch files belongs to each module. Information sources for data blocks can be tables or matrices. In nearly every instance, these various working parts have been made open ended. For instance, the number of links can be extended, the number of levels of overlay can be increased, the number of problem types can be expanded, the number of modules can be enlarged, the number of entries in tables can be augmented, the quantity of tables can be opened up, and the number of subroutines can grow. In rare instances, operational considerations have circumscribed the entries in a table, but these are sufficiently rare that it is fair to say that NASTRAN is generally open ended.

The modular design allows for program maintenance. Each module communicates only with the Executive and is not allowed to communicate directly with another module. Any communication that is needed between modules is accomplished by passing information to output data blocks that are used as input data blocks to succeeding modules or by

passing parameter values to parameter tables that can be accessed by a succeeding module. In this way, the interface with the Executive is fixed module by module so that an entire module can be replaced or revamped, so long as it maintains the same interface as previously. Hence no internal module change of this type has a cascading effect through the program. This modularity also allows for an internal input/output routine to process internal quantities in a machine-independent fashion. As the technology advances, new subroutines and modules can be added or inserted in place of old ones and the program can be kept modern without any organizational modification.

The matrix operations performed by the modules do not require that the amount of core working space be of a size to hold an entire matrix or set of matrices at once. Solution logic allows only portions of each matrix in an algebraic step to be present at any one time while the remaining portions are fed from secondary storage as operations on preceding portions are completed. This type of core usage vis-a-vis matrix operation is given the name "spill logic" and allows the program to operate on matrices of virtually unlimited size.

## Modules

Beside Executive Modules, the bulk of the program is composed of three kinds of modules: Utility, Mathematical, and Functional. Most of these are useful for any discipline. The Utility Modules are certainly discipline independent (having to do with printing matrices, performing coordinate transformations, etc.) and need no further discussion. The Mathematical Modules were written to perform operations on large matrices, because those routines provided by standard operating systems are not efficient enough to be functional for large matrices. "Large" is defined to be a combination of order and density\* so that the matrix will not fit in core even in packed form. A number of Mathematical Modules were written to take matrix characteristics into account, such as sparsity, bandedness, type (real or complex), or positive definiteness. Mathematical Modules are immediately adaptable to other disciplines.

Functional Modules currently favor structural mechanics, but conceivably they would be useful to other disciplines under different names. They have names such as Geometry

---

\*Density is a ratio of the nonzero elements to the maximum possible number of matrix elements.

Processors, Constraint Eliminators, Elastic Properties, Mass Properties, Damping Properties, Weight Generators, Load Generators, Simultaneous Algebraic Equation Solver, Eigenvalue Extraction, Stress Data Recovery, Piecewise Linear Analysis, and Differential Equation Integration. If there are other functions that other disciplines require, they can be generated and made part of a problem sequence, then their existence can be noted in the Module Property Table.

### Internal Compiler and Scheduler

The heart of its ability to adapt this Executive management to other applications programs resides in the way it organizes the functions to be performed. Various problem types peculiar to a given discipline (and in this case structural mechanics) are classified into categories such as statics, eigenvalue analysis, dynamic analysis, random analysis, and others. The steps needed to accomplish the solution of a problem of a given type are presented in an orderly sequence of module executions and Utility Executive operations. The statements of these solution steps are written in an internal language called "DMAP" (for Direct Matrix Abstraction Process). An internal reference library of statements for each problem type has been established with appropriate cataloguing. In the spirit of open endedness there is no requirement as to problem types to be kept in the library, so a given discipline (or combination of disciplines) can have as many problem types catalogued in the library as is convenient to the user. No matter to what discipline a set of statements belongs, the Executive merely calls out the set of statements by catalogue number according to an analyst's command.

In response to a user's call in the control section for a particular problem type, the Executive selects the corresponding sequence of DMAP statements and directs this sequence to the DMAP compiler. The output from the compiler in effect becomes the scheduler of module and utility executions. All loops are unwound and all jumps are translated into a purely serial string; all associated data block names and their file storage needs are tabulated in the scheduler. This scheduler, the OSCAR, is written onto tape and does not occupy core or disc space. The Executive central driver consults with OSCAR at the end of each module before calling a succeeding module. It is now evident how the Executive can operate on any discipline without semantic implications.

There are two operations that the Executive performs in conjunction with the problem type and the control section, to be discussed later. These operations have semantic implication and are only quasi-Executive operations. They are called, respectively, the Input File Processor (IFP) and the Output File Processor (OFP). The IFP checks on the legality of input bulk data and the logic of control section statements and organizes these input data into data blocks for eventual processing by the Functional Modules. The OFP does sorting on the solution vectors and organizes these results into formats that are suitable for a particular discipline. The IFP and OFP would have to be replaced entirely for the Executive to manage another discipline.

#### Control Versus Sets

The system to be analyzed is treated as the basic entity for purposes of defining a problem. In the case of structures the basic system is the geometric arrangement among elastic members. Most other quantities affecting the problem are less basic and are liable to frequent change, such as loads on the system, or constraints on the system, or partitions on the system from which response information is desired. The scheme for managing these varying conditions is based on sets.

As many sets of varying conditions that one desires may be assembled in a pool of information. These sets will remain dormant until they are individually activated. The analyst consequently is in a position to exercise quite precise control in the Case Control Section of the program by creating subcases wherein any of a particular load, a particular constraint, a particular spectrum, a particular sequence of time steps, or a particular series of output quantities and output locations can be activated from the data pool merely by specifying the appropriate set identifiers. As many subcases can be prepared for a single computer submittal as is convenient for the analyst.

The quantities that fall under the surveillance of the Case Control Section are kept in a table. In keeping with the open-ended spirit of the program, the table can be augmented so that unique quantities pertaining to other disciplines can be accommodated.

Another hierarchy of control is exercised to distinguish among major options within the program. This does not operate on the basis of sets but by fixed names. This portion is called the Executive Control Section.

### Plotter Independence

All interfacing between the solution results and the plotters that will be used to display them is confined to a section of the program called the Plot Module. The sorting by sets, the projection, the orientation, the color, labeling, and the general commands to produce these effects are accomplished without regard to the display hardware. A small translator subroutine will convert these plot commands from general internal expression to specific commands for execution on individual plotting machines. In this instance again, the general purpose character has been preserved with essential plotter independence.

### ADAPTATION TO OTHER DISCIPLINES

The ease with which the current NASTRAN general purpose organization can serve other disciplines will be examined by major program units. The reason for adaptation is to provide a general purpose applications program as opposed to a special purpose program.

#### Executive

The general purpose character of the Executive Section can make it immediately adaptable to other disciplines. The link/overlay management amply provides for the needs of most applications. The lean organization of having only a central driver permanently resident in core along with its vital tables, while all other Executive functions are provided by modules that are brought in temporarily to perform their jobs and then vacate core, is a concept that warrants preserving. The interrelationships between the Executive operations and computer operating systems have already been made and should certainly not be duplicated unnecessarily. When other computers have been added to the NASTRAN set, these too will become publicly available.

#### Modules

The particulars of a given discipline with respect to Functional Modules are considered here. It appears that if a discipline is based on potential theory, just as structural mechanics is based on the linear theory of elasticity, the existing Functional Modules could nicely serve merely by a change of name. If this is so, the existing forms could be preserved in their applications to another discipline simply by providing a new mask for input card mnemonics, headings of the output listings, and terms in the diagnostic messages. Because electrical engineering is based upon the potential theory of electromagnetics, we can draw

on analogies in NASTRAN. The existing Mass Properties Module could apply to an Inductance Property Generator; the existing Elastic Property Module could apply to a Capacitance Property Generator; and the existing Damping Property Module could apply to a Resistance Property Generator. Geometry Processor Modules could apply to the description of the Circuit/Nodal Pattern, while the Load Generator Module could apply to the External Voltage Array (or the Potential Gradient) at Nodes. Similar reasoning can be used in optics, electronics, and fluid flow. Presuming the universality of some of the Functional Modules, it is germane to return to the Executive Modules. IFP's can be preserved with respect to data input card reading and data block generation. Adaptation to electrical engineering would require a new mask for the terms in diagnostic messages concerning legality of input.

#### Compiler

One would not expect too much similarity between the way problem types are formed in different disciplines. It is reasonable to assume then that the catalogue of statements referring to the module executions for various problem types would be completely replaced. Because the sequence of statements is written in DMAP language, the creation of a new library of problem types is relatively trivial. The compiler and the generation of the OSCAR would remain intact. Quite possibly some new Functional Modules may want to be added to the existing structural set to round out the field for a given discipline, such as the counterpart to the Stress Data Recovery Module. Each discipline will probably have unique collateral characteristics recoverable from the solution vector.

In summary, a new discipline may provide a new name for the solution vector, such as acidity, voltage, humidity, light intensity, or population instead of elastic deformation, but most of the working portion of the program can probably be preserved with only a replacement mask for the names assigned to data.

The important factor in the ability to convert the program to other disciplines is the general purpose management approach in the Executive. Even though a few new modules and all new problem types will need to be added, the open-ended design will allow them to be easily integrated. Of course, it is a grubby job to comb through the code to prepare a new language mask, but the point to be made is that it is a relatively minor task compared to the generation of an entirely new general purpose applications program.

One of the huge benefits of adapting an existing general purpose applications program like NASTRAN to another discipline is the freedom from a major debugging exercise. The corollary advantage is the reliance on future maintenance that NASA is currently practicing.

## IMPACT ON THE STRUCTURES COMMUNITY

In narrowing the topic of discussion to general purpose programs in structural engineering only, it is interesting to indulge in some philosophical reflections.

Some sort of analysis has always been part of the design process in structural engineering, but until recently, analyses have been limited to the engineer's ability to solve only simpler approximations to the real structure and the usual attempt was to solve a pair of such approximations to bracket the real case. Analysis has advanced to the point where a very close representation of complicated three-dimensional structures is now possible. Because there was uneven advancement of structural analysis capability by problem type, for years there was a tendency to limit one's analytical skill to one or two specialties. A sufficiently broad range of structural problem types has advanced enough to warrant the investment in general purpose programs. Having access to general purpose programs, the structural analyst at long last is abandoning his fragmented approach to analysis and is applying a cohesive approach. As a result, analysis is now coming into its own as a vital part in the decision-making process of structural design.

The aerospace industry is a heavy user of analysis for structures. Here a large variety of tried-and-true special purpose programs does most of the analytical tasks. The full range of structural problems is generally being dealt with analytically in the aerospace industry. Engineers, however, are finding an increasing need to communicate analytical data. They would like to feed data that are being output from one special purpose program as the input to another special purpose program; but they find that they are frustrated by the lack of compatibility. A general purpose program on the other hand has the solution capability of the combined special purpose programs with no commensurability nor compatibility problems. In addition, the continual updating of some of the major general purpose programs is causing general purpose programs to enjoy increased popularity.

The civil engineering profession is rapidly moving toward analysis as an everyday tool. Static analyses for stress and deflection responses dominate the activity in civil

engineering problems; however, vibration analysis is on the increase. Only an occasional attempt is made at solving transients and most of these are from seismic excitation. Because their problems can become quite large, civil engineers are making use of general purpose programs.

Machinery manufacturers show the most diversity in their attitude toward analysis. The automotive and turbine industries head the list of those pledged to analysis; mining is the least active. As to the range of problem types, heavy industry is also the most varied. Boiler people are about the only ones doing random analyses. Rotating machinery designers are analyzing for vibrations. Statics is definitely the most popular. In several years, it is expected that heavy industry will become more involved with analysis.

Economics tends to prevent the use of analysis in consumer goods. Only on occasion when a sticky local problem is annoying him will a consumer goods manufacturer ask an engineering analyst to bail him out. Usually such problems are solved by consultants rather than by in-house engineers. It is not easy to say how big a part analysis will play in the design cycle of consumer goods in the years to come.

As part of the structures community, universities are showing an increased awareness of production analytical tools as opposed to those that concentrate on academic niceties. Probably general purpose programs will have the most far-reaching impact on engineering colleges and on the way that the engineering profession is practiced. The structural field has been fragmented into civil engineers, mechanical engineers, and aeronautical engineers. In industry the profession was further fragmented into dynamicists, thermal specialists, hydraulic engineers, propulsion specialists, weights engineers, and stochastics specialists. With the advent of general purpose programs, the tools are at the disposal of every engineer, enabling him to readily inquire into a host of problems. General purpose analytical capability will give rise to the education and training of engineers with broader backgrounds. Eventually they will become structural engineers spanning the whole range from statics through thermal to dynamics.

## SOCIAL IMPACT

Increased emphasis on analysis is bound to have an influence on deemphasizing some activities and promoting still others. The extensive development of general purpose

programs is symbolic of the maturity of analysis. As such, a revolution of sorts is being set into motion. The social impact of this revolution will be the realignment of the work force.

Until recently, the structural engineer has depended upon testing to serve two masters: as a proof of design and as a proof of manufacture. Constant improvement in instrumentation and test equipment has enhanced the dependency on testing. As an engineer becomes more proficient at analysis, he will find that the cost of using analysis for design certification will be far less than that of testing and that the time lapse between the completion of a design and the performance results will be far shorter. Lastly, he will discover that he will be able to inquire into the behavior of locations that were too remote to be accessible by instrumentation. The triple impact of less cost, less time, and more complete information will wean designers away from testing for design certification. We predict that analysis will eventually take its proper place so that the roles of analysis and testing can be encapsulated as—

Analysis is for proof of design.

Testing is for proof of manufacture.

This does not mean, of course, that no testing will be used for proof of design. For instance, photoelastic testing of machine parts with severe stress gradients will certainly remain as a practical check of design. For the most part, however, it is safe to say that analysis will invade the province of testing as the primary tool for checking on designs.

What will be the social impact of this shift of emphasis away from testing? It means that less mechanical test equipment will be manufactured, fewer testing laboratories will survive, and fewer testing personnel will be employed. The demand for the manufacture of test articles will slacken, with its attendant reduction in the need for model builders.

As the dependency on analysis increases, the need for digital programmers will be felt in the areas of debugging, advanced module writing for updating programs, the writing of pre-processors and post-processors to take the drudgery out of data handling, and the intensification of the writing of support routines for on-line interactive graphics. The net effect will be increased business for software houses and their increased employment of programmers.

Probably the design cycle will change to the extent that some design tasks will be done by the computer instead of being strictly the province of the designer. Conceivably for highly complicated structures, the task of producing the initial design would devolve on a highly creative designer. Subsequent tasks would be performed by structural analysts on the computer, first to analyze, then to synthesize in response to the characteristics shown by analysis, and last to optimize for achieving the most acceptable design with respect to a parameter such as cost or weight. Probably a minimum of demand for detailing the parts of the conceptual design will be made during the computer phase of the design evolution. At the termination of the computer phase, designers and detail draftsmen will be needed to make final manufacturing drawings. The social impact of reemphasis on the computer during the design stage will be the increased demand for highly creative designers and decreased demand for routine designers and detail draftsmen. There will also be an increase in demand for engineers who are structural analysts.

The shift in emphasis toward analysis should not have a depressing effect on the small design office or small consulting businesses. Even though the small offices cannot afford to install their own computers, they can nevertheless operate all of the latest analytical tools in support of these tasks. Fortunately, hardware technology has kept pace with software technology and the little man did not get caught in the squeeze. Computer terminals have come to the rescue of the small design offices. They can communicate via the terminals to the central computers operated by such companies as McDonnell Automation, CDC's Cybernet, CSC's Infonet, and IBM's Service Bureau. A rather complete library of structural analysis programs is available at these central computer installations to support the range of problems that the remote offices need to solve.

The social impact of this remote terminal support will be to preserve small business and to stimulate competition. Small design and consulting firms will be maintained and will possibly grow. Business from these numerous smaller firms should contribute to the incentives for competition among terminal manufacturers and among central computer operators. The demand for repairmen should offer new employment.

Finally, the increase in structural analysis has produced a further need for plotting equipment. The computer printout is an orderly form of record-keeping but is too

awkward for digesting the quantity of data that gush from these new analytical programs. Plotters and cathode ray display tubes are starting to fill this need. More and more clever ways of presenting plotted data are abetting programming employment. This mode of data reduction is also helping the plotter manufacturer and his staff of repairmen as well.

In presenting the social side of the trends in structural analysis, we plead that we have painted only a qualitative picture. We have not braved the more risky path of reducing these social effects into quantitative values in manpower or in a time frame. Nevertheless, we firmly believe that a minor revolution is currently in motion and that this revolution will not reach its full development for another 5 years. NASTRAN is an important influence in provoking this ferment. It is well checked out and available to the general public at a nominal cost. Its general purpose character and its degree of machine and plotter independence make it particularly attractive to those who are looking toward longevity of methods.



# BUCKLING ANALYSIS OF A MISSILE INTERSTAGE

By David P. Dudley

Aerojet Solid Propulsion Company

## SUMMARY

NASTRAN was used to find the buckling location and the degradation factor due to a specified temperature field for an interstage of a typical three stage missile. The model was made up of 6332 independent degrees of freedom. This large size required the use of an IBM 370/195 for evaluation of the eigenvalues. The effect of elevated temperature was to lower the critical buckling load by 3%.

## INTRODUCTION

A three dimensional buckling analysis, with and without temperature gradients, was performed on the aft skirt of a typical three stage missile using an IBM 370/195 computer and the NASTRAN computer program.

## OBJECTIVE

Static structural tests were performed on the aft skirt, at ambient temperature. The NASTRAN analysis was performed to provide a temperature degradation factor for use with the failure loads from the structural test program and to demonstrate adequacy of the second stage aft skirt when subjected to loading, including effects of temperature gradients. The analysis was to provide the following information for determination of the degradation factor.

The critical buckling failure load factor for the aft skirt at ambient temperature.

The critical buckling failure load factor for the aft skirt having radial, circumferential, and longitudinal thermal gradients computed for specific conditions.

The buckling mode.

The critical buckling location.

## MODELING

### Basic Grid

The model used for this analysis was designed to account for the load peaking caused by cutouts, and the effects of doublers and other stiffening members, as well as thermal effects. To minimize the size of the problems, the basic model was designed as a 180 degree section (from 210° through 360° to 30°) of an axisymmetric shell, using flat quadrilateral plate elements. The basic model, as shown in Figure 1, included the following structural components:

An aft segment of a second stage chamber (total segment length = 1.02 m (39.7 inches)) including a portion of the chamber and the aft skirt.

The aft closure was included from the aft Y-joint part way back.

To achieve results accurate to 5% or better<sup>1</sup> the basic grid was divided into elements approximately square; 5 degrees wide by approximately 0.063 m (2.5 in.) long. Each circumferential grid line was assigned a reference number (1, 2, 3, etc.), with odd numbers for the interstage, skirt flare, and chamber wall, and even numbers (2 through 10) for the aft closure. Each basic grid nodal point was then identified by a five-digit number, (e.g. 21015), beginning with three digits for the azimuth (e.g. 210°) and ending with a two-digit number for the circumferential line (e.g. 15) on which the point lies.

To better represent the stiffness of the Y-joint, the aft skirt and closure elements were joined at reference line 23, as shown in Figure 2, and a radially oriented element was connected between reference line 10 on the aft closure and an added line 12 on the skirt, at the Y-joint crotch. Representation of the aft chamber girth weld area is shown in Figure 3.

### Final Grid

Modifications were made to the basic model to obtain the final model which includes:

All skirt cutouts with doublers and debris deflectors.

Raceway on chamber skirt and barrel.

Disconnect bracket.

1-2 interstage attachment ring.

1-2 interstage raceway cutout.

1-2 interstage ordnance ports and doors.

1-2 interstage longitudinal ordnance (splice) joints.

To model in openings, doublers, brackets, etc., a local network of nodal points was established, forming a pattern of quadrilateral and triangular elements encompassing the shapes of all the layers of material to be included. Wherever two or more layers of material were involved, a separate set of elements was created for each layer and the appropriate material properties were assigned to each set of elements. This practice results in multiple elements occupying the same space, since overlying elements are formed by connecting the same grid points, which are all defined at the mean radius of the skirt or interstage skins. Some structural components were modeled as simple beam elements and nodal points were established at locations where these components were attached to the skirt/interstage structure. This model is shown in Figure 4.

### Temperatures

Buckling analysis runs were made for both "room temperature" (80°F) and for an elevated temperature. Since the temperatures were uniform circumferentially except near the raceway and the longitudinal splices, it was assumed that distribution could be extended circumferentially past 360° to the 30° azimuth.

For the motor aft chamber and skirt temperatures, a three-dimensional heat transfer analysis was performed using the TRW SINDA (Systems Improved Numerical Differencing Analyzer) computer program.

### PROCEDURE

#### Bandwidth Reduction

The time required to decompose a matrix in NASTRAN is proportional to the square of the bandwidth and the first power of the size of the matrix. To reduce running time to an acceptable level, the data deck for NASTRAN was processed by BANDIT. BANDIT is a computer program written by the Naval Ship Research and Development Center to minimize bandwidth for NASTRAN. The results of running BANDIT reduced the bandwidth by almost an order of magnitude. This required 10 minutes of computer time on a UNIVAC 1108.

#### Ambient Temperature Run

The first NASTRAN run, at a uniform temperature of 80°F, was evaluated by level L11.1.4 on an IBM 370/195. It required 800,000 bytes of core and ran for 104 minutes. Table 1 shows the timing information taken from the NASTRAN summary.

## Elevated Temperature Condition Run

The second NASTRAN run was similar to the first. The major difference was the use of temperature data.

### Subsection Elevated Temperature

Results of the elevated temperature condition run produced a mode of failure in the barrel instead of the skirt. To obtain the mode for the skirt a small section of the model was selected for further analysis.

The subsection was evaluated on the Univac 1108 and CDC 6600 computers using levels 12.1 and CDC NASTRAN. Deflections from Run 2 (elevated temperature run) were input as boundary conditions to the Univac 1108 computer version of NASTRAN. This version was used to calculate the equivalent load vector based on the input deflections. The CDC 6600 version of NASTRAN was then used to find the next mode of failure using the loads calculated from the Univac run. Table 1 also has the timing data for this analysis (Run 3).

## RESULTS

The results of the first run (room temperature) gave a minimum eigenvalue of 1.340, for buckling in the barrel at the forward end of the model as shown by Figure 5. Even though the lowest mode was found, it was not the mode of failure which was expected based on test data. Indeed, it was a mode which was due to the modeling technique and the way the load was applied. It is not uncommon in buckling problems of this size to find modes of failure other than those desired. This model has 6500 modes of failure! What is important is the fact that the lowest mode was found, and experience has shown that the modes will be packed together in a band. Therefore it is expected that the desired mode of failure has an eigenvalue very close to 1.340.

The second loading case (criteria condition temperatures) was run in a much shorter time by starting the eigenvalue search at a value of (1.3). The result was 1.302 and gave the same mode of failure as loading case one.

Since the expected mode of failure had not been found and the approximate location of this desired mode was known, it was decided to run a subsection of the model to find the next mode of failure. Table 2 lists the dimensional data to describe the submodel. Loading was accomplished by taking displacements from the results of the second run, evaluated by using both the UNIVAC 1108 and CDC 6600 computer. This submodel gave an eigenvalue of 1.304 and the correct mode shape. Figure 6 indicates this mode of failure. The buckling occurred at 250 degrees in an area near the dumpline port.

Based on this data the effect of temperature is to lower the buckling capacity of the structure by a factor of  $\frac{1.302}{1.340} = 0.972$ .

## CONCLUSIONS

The results of this computer study substantiate the ability of the aft skirt to withstand the elevated temperature condition loads with a positive margin of safety. Elevated temperatures were found to degrade the buckling capacity of the aft skirt by a factor of 0.972.

## REFERENCES

1. Broliar, Richard H., "A NASTRAN Buckling Analysis of a Large Stiffened Cylindrical Shell with a Cutout," NASA TM X-2378, September 13, 1971, pp 65-84.

TABLE 1

## NASTRAN TIMING DATA (MAJOR ROUTINES)

	Run 1 (IBM 370/195)		Run 3 (CDC 6600)	
	CPU Time, sec	Elapse Time, sec	CPU Time, sec	Elapse Time, sec
SMA1	276	343	223	263
SCE1	19	69	7	--
RBMG	317	441	64	293
FBS	115	326	14	33
DSMG	101	129	261	322
READ	1395	3932	187	1323
SDCØ	(277)	(373)	(55)	(78)
ITERATION	(459)	(1718)	--	--
TOTALS	2406	6254	851	2289
Bandwidth	309		125	
I.D.F.*	6332		867	
COST	\$2640 (Total)		\$369 + Printing Cost	

\*Independent Degrees of Freedom

TABLE 2  
SMALL PANEL DATA

I.	MODEL DATA	
	1. Elements	
	Bar	20
	Quadrilateral Plates	98
	Triangular Plates	233
	2. Grid Points	228
	3. Bandwidth	140
	4. Degrees of Freedom	1,110
II.	RUNNING TIME CDC 6600, 165000 <sub>8</sub> CORE	
	1236 Central Processor, sec	
	2964 Input/Output, sec	
	2587 Total System, sec	
III.	SOLUTION EIGENVALUE	
	$\lambda = 1.303$	

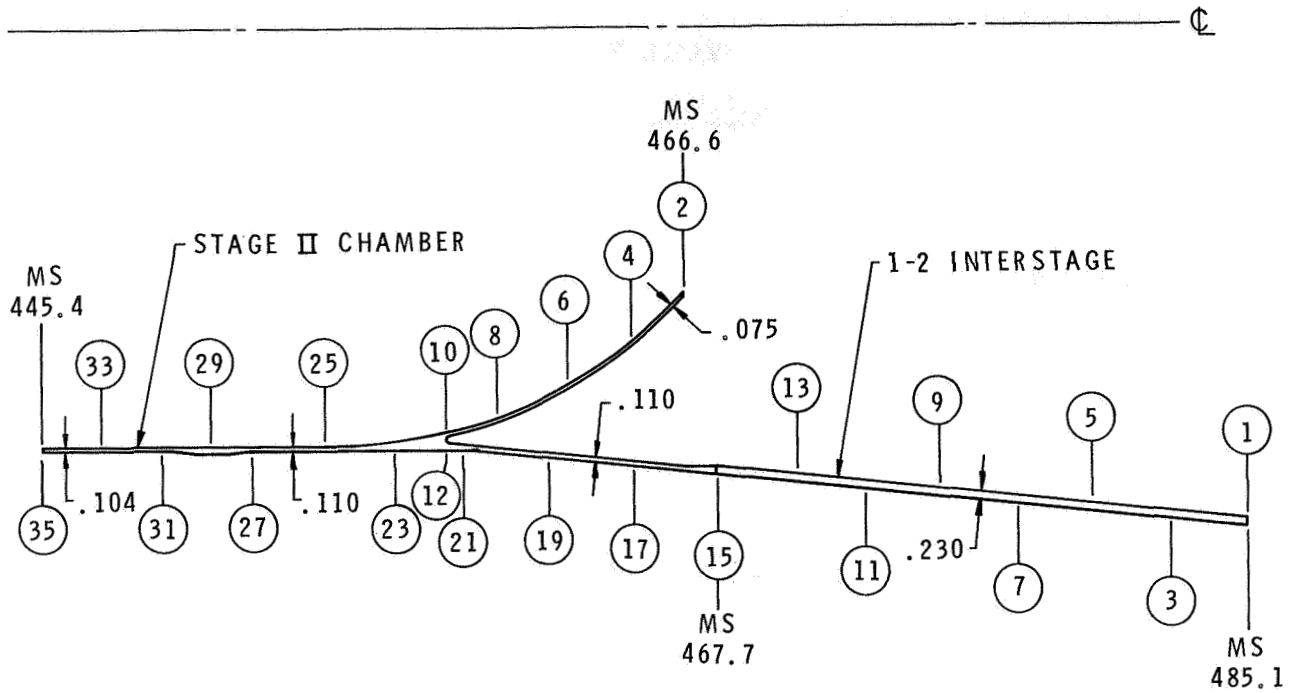


FIGURE 1

MAJOR COMPONENTS OF BASIC MODEL  
AND LONGITUDINAL REFERENCE POINTS

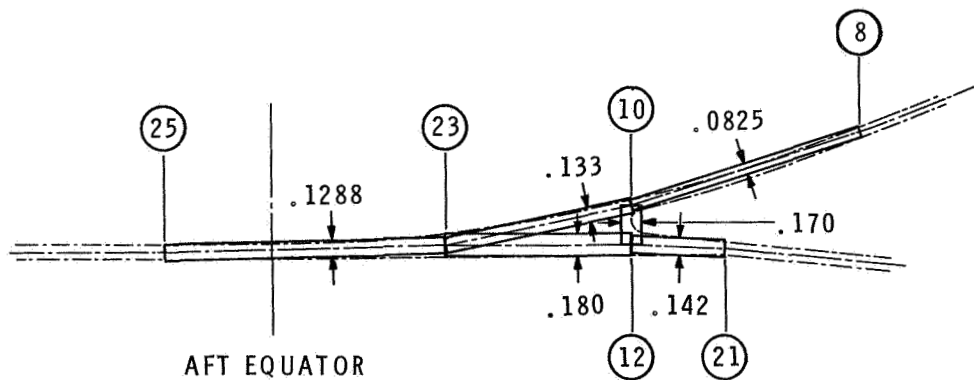


FIGURE 2

MODELING OF AFT Y-JOINT

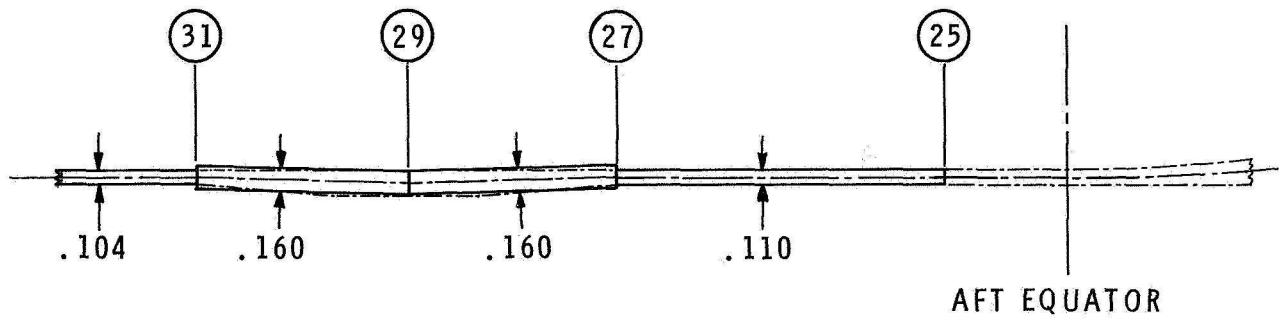


FIGURE 3  
MODELING OF AFT CHAMBER WELD AREA

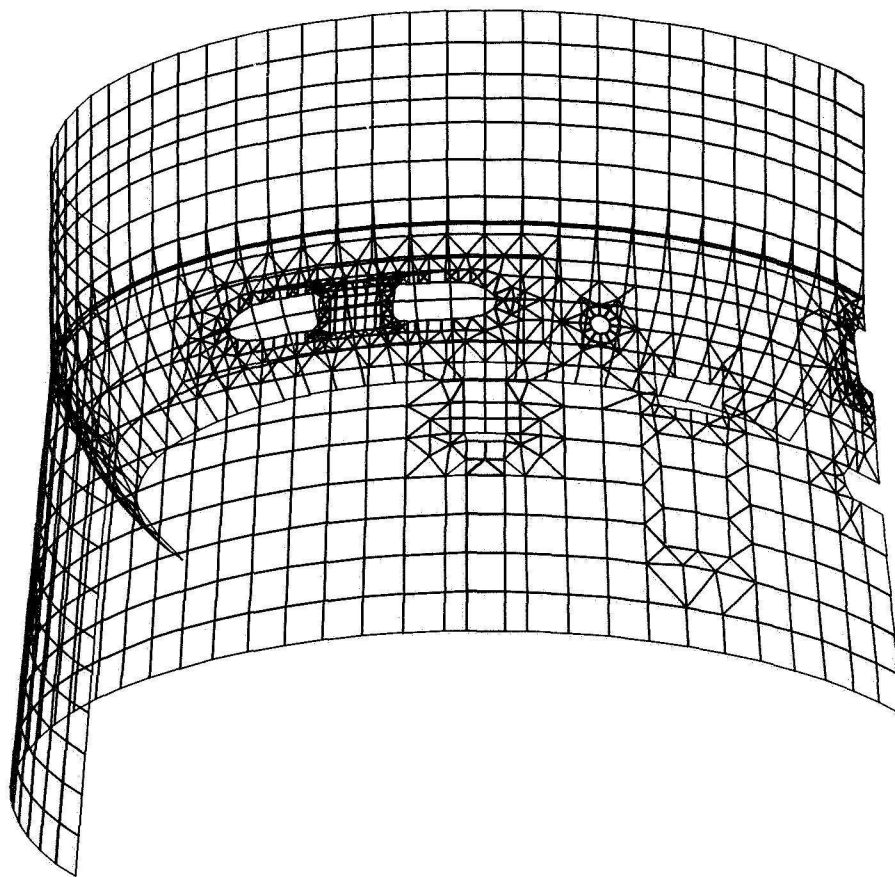


FIGURE 4  
NASTRAN MODEL IN UNDEFORMED SHAPE

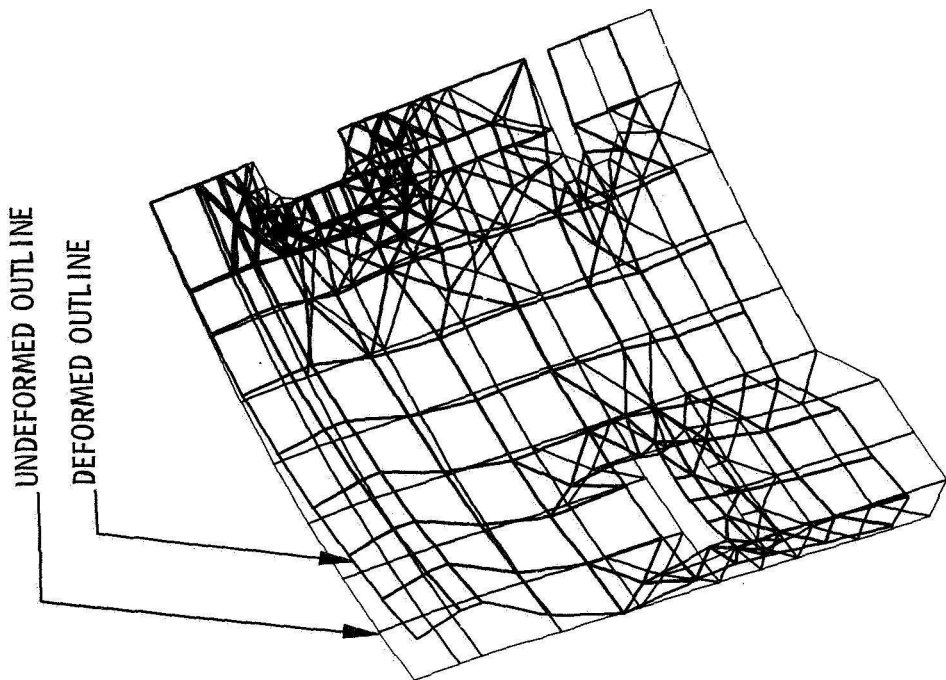


FIGURE 6  
DEFORMED SHAPE OF NASTRAN  
SUBSECTION MODEL

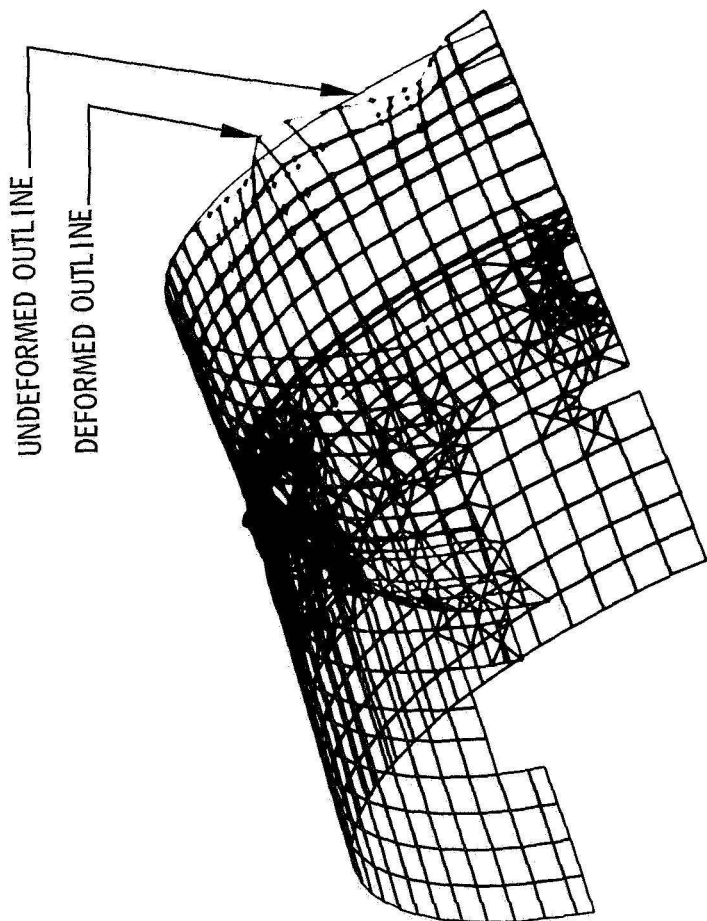


FIGURE 5  
FULL NASTRAN MODEL  
DEFORMED SHAPE

# NASTRAN BUCKLING ANALYSIS OF A THIN-WALLED CYLINDER

By Ralph B. Wight

NASA Goddard Space Flight Center

## SUMMARY

The computer run time required for a buckling analysis using NASTRAN is considerably greater than for a linear static analysis of the same structure. For this reason it is very important to obtain an optimal model size for the structure being analyzed, such that the model is neither so large as to increase running time unnecessarily, nor so small as to hinder accuracy. This paper studies the problem of critical load accuracy versus model complexity for a thin walled cylinder, using both Level 12 and Level 15 NASTRAN releases.

5

## INTRODUCTION

Buckling is generally the failure mode for thin-walled shells carrying axially compressive loads and NASTRAN has the capability of solving for the critical load of such problems. The problem which initially stimulated interest in this study was the buckling analysis of a thin-walled cone to be used on a NASA spacecraft. NASTRAN analysis yielded a wide range of answers by varying the finite element model used. No analytical solutions could be found for buckling of a cone which could be used to verify the NASTRAN results. Therefore the buckling analysis of a thin-walled cylinder of approximately the same dimensions as the cone was performed to determine the model complexity needed to obtain good agreement between NASTRAN and analytical solutions. The cylinder analyzed is 78.12 cm in diameter by 55.88 cm long with a wall thickness of 0.102 cm.

There have been complaints about the crudeness of the NASTRAN plate element for buckling analysis. (See, for example, ref. 1.) The majority of the runs made for this study used NASTRAN Level 12.1.2 on the IBM 360/95 computer at the Goddard Space Flight Center. These results are compared to Level 15.1.0 which includes a greatly improved plate element for buckling. This improvement was obtained by including an improved algorithm for the bending effects, whereas Level 12 analysis relied primarily on membrane contributions. A procedure was formulated to measure the effect of this improved plate element, as well as verify the advertised decrease in running time for Level 15.

## SYMBOLS

$K_{aa}$	stiffness matrix
$K_{3a}^d$	differential stiffness matrix
$\lambda$	eigenvalue
$u$	eigenvector
$\sigma_{cr}$	critical stress
$E$	Young's modulus of elasticity
$\mu$	Poisson's ratio
$t$	cylinder wall thickness
$m$	number of half sine waves
$L$	cylinder length
$R$	cylinder radius
$P_{cr}$	critical load
$F$	applied axial compressive load
$\theta$	angle subtended by one element

## NASTRAN MODEL AND THEORY

The bulk data required for a NASTRAN buckling analysis (Rigid Format 5) is identical to that required for a static analysis, with the addition of an EIGB card similar to the EIGR card used for normal mode analysis. The steps NASTRAN uses for solving the buckling problem as presented in ref. 2 are:

1. Solve the linear statics problem ignoring differential stiffness and calculate the internal element forces.
2. Use the element forces to obtain the differential stiffness matrix.

3. Find the eigenvalues and eigenvectors from the matrix equation:

$$\left[ K_{aa} + \lambda K_{aa}^d \right] \{u\} = 0 \quad (1)$$

where the eigenvalue ( $\lambda$ ) is the factor by which the arbitrary applied load is multiplied to obtain the critical load and the eigenvector ( $u$ ) represents the buckling mode shape.

Plate elements were used to model the cylinder. The AXIS data generating program was used to generate the NASTRAN data deck. (See ref. 4.) This program generates the GRID, CQUAD2 and PQUAD2 cards for a shell of revolution. The grid points are sequenced along circumferential rows to obtain the minimum band width and no active columns.

The critical load of the cylinder was obtained for various model sizes. All of these models were only portions of the complete cylinder, thus yielding only axisymmetric buckling modes. The effect of the rest of the cylinder is simulated by constraining to zero certain degrees of freedom along the edge of the model as described in ref. 3. These degrees of freedom are tangential translation, longitudinal rotation and radial rotation. (Degrees of freedom 2, 4, and 6 in Figure 1.)

#### ANALYTICAL SOLUTION

The analytical critical stress of a thin walled cylindrical shell under an axial compressive load is given in ref. 5 as

$$\sigma_{cr} = \frac{E}{12(1 - \mu^2)} \left[ \frac{\pi t m}{L} \right]^2 + E \left[ \frac{L}{\pi R m} \right]^2 \quad (2)$$

The number of half sine waves the cylinder buckles in is given by  $m$  in the above equation. Only the number of half sine waves which produces a minimum  $\sigma_{cr}$  is of interest, the others being fictitious numbers the cylinder will never see. This minimum occurs when

$$m = \frac{L}{\pi} \sqrt[4]{\frac{12(1 - \mu^2)}{R^2 t^2}} \quad (3)$$

Assuming the cylinder being analyzed is made of aluminum yields:

$$m \cong 16$$

$$\sigma_{cr} = 1.0859 \times 10^8 \text{ newton/meter}^2$$

$$P_{cr} = 2.7076 \times 10^5 \text{ newtons}$$

This critical load ( $P_{CR}$ ) was applied as a static load to the finite element model so that the eigenvalues would approach unity as the accuracy increased. The value of the force (F) applied to each grid point (See Figure 1) is calculated from

$$F = \frac{1}{2} \left( \frac{\theta}{360} \right) P_{cr} \quad (4)$$

## MODEL VARIABLES AND RESULTS

The model parameters which were varied are: the number of longitudinal elements, the number of circumferential elements, the length of the cylinder, the end fixity of the cylinder and the type of finite elements used. The eigenvalue ( $\lambda$ ) for each model was obtained by using NASTRAN.

### Longitudinal Elements

The accuracy of the solution is a function of the number of longitudinal elements, because the more elements per half sine wave the closer the actual buckling mode can be approximated. The purpose here is to perform a systematic variation of model complexity to obtain a curve of accuracy as a function of model complexity. Models containing 20, 40, 60, 80 and 120 longitudinal elements were analyzed. All these models were one element wide. Figure 2 plots the eigenvalue of each buckling mode for the various models as a function of the number of half sine waves. The analytical solution from equation (2) is also plotted. As was stated before, the only points on these curves which have real meaning are the minimum points. These minima are plotted to obtain the curve of primary interest (Figure 3). The number of elements per half sine wave required to obtain a given accuracy can be read directly from the graph. Also, the increased accuracy obtained from Level 15 can be seen.

### Circumferential Elements

A model more than one finite element wide, as has been used in ref. 1, does not necessarily increase the accuracy of the critical load obtained, because we are dealing with an axisymmetric phenomenon. To study this area various models of one, two and four circumferential elements were investigated. Table 1 clearly shows that the accuracy is not a function of the number of circumferential elements, but only a function of the number of longitudinal elements.

### Length

Equations (1) and (2) show that the critical stress, and therefore the critical load, is not a function of length. Table 2 shows how this parameter was varied in the NASTRAN model. The length of the 80-element, single-row model was cut in half and then in half

again, keeping the same element size. The theoretical solution was verified — the critical load is independent of length. This allows one to decrease the degrees of freedom of the axisymmetric model and still obtain the same accuracy as a full length model.

### End Fixity

Experimental solutions show that the critical load is independent of end fixity for long cylinders. (See ref. 6.) Ideally, failure of a pinned-pinned cylinder will occur simultaneously at each half sine wave along the length, but for a fixed-fixed cylinder the failure will occur near the center where the amplitude of the half sine wave is the same as that for a pinned-pinned condition as shown in Figure 4.

Table 3 shows the results of varying the end fixity of the NASTRAN model. The variation in critical load is less than one percent. This fact relieves the analyst of the burden of accurately approximating the actual end conditions of a thin-walled cylinder experiencing buckling.

### Type of Finite Elements

The use of triangular plates instead of quadrilateral plates will double the number of finite elements while keeping the degrees of freedom and the bandwidth, and therefore the decomposition time, constant. In the problem being studied this was done by dividing diagonally the quadrilateral plates, as shown in Figure 5. This substitution increased the accuracy of the solution as shown in Table 4. In the case being studied quadrilateral plates were more convenient, however, because the AXIS program generates quadrilateral plate elements.

### LEVELS OF NASTRAN

As was shown earlier in Figure 1, the improved plate element of Level 15 offers a great improvement in the accuracy of the critical loads obtained using Rigid Format 5. This allows the user to decrease the model size and still obtain the same accuracy as Level 12. Another great improvement in Level 15 is the decrease in running time for buckling problems. Running time for a finite-element model with a given bandwidth and number of degrees of freedom is reduced by a factor between 3 and 4, as shown in Table 5.

### CONCLUDING REMARKS

Many things can be done to reduce the computer time required to do a NASTRAN buckling analysis of a thin-walled cylinder. The optimal number of elements per half sine wave can be obtained from the graph of accuracy versus number of elements. For

axisymmetric buckling no increase in accuracy is obtained by increasing the number of rows of elements modeled. The critical load was found to be independent of length, allowing a reduction in model size. The use of triangular plate elements is recommended for improved accuracy, unless a data-generating program that produces quadrilateral plate elements is being used. Finally, Level 15 offers an increase in accuracy and a decrease in running time over the previous Level 12 NASTRAN.

Although this paper dealt with a thin-walled cylinder, which is easily solved by analytical methods, the conclusions reached are applicable to other problems which are more difficult to solve analytically. These problems include stiffened cylinders, thin-walled cones and cylinders with variable wall thickness.

#### REFERENCES

1. Broliar, Richard H.: A NASTRAN Buckling Analysis of a Large Stiffened Cylindrical Shell with a Cutout. NASTRAN: USERS EXPERIENCES. NASA TM X-2378, 1971.
2. The NASTRAN Theoretical Manual. R. H. MacNeal, ed., NASA SP-221, 1969.
3. Courtney, Roy L.: Structural Analysis and Design Optimization of Spacecraft Using NASTRAN. NASTRAN: USERS EXPERIENCES. NASA TM X-2378, 1971.
4. Cook, William L.: Automated Input Data Preparation for NASTRAN. NASA GSFC document X-321-69-237, 1969.
5. Timoshenko, S., and Gere J. M.: Theory of Elastic Stability. 2nd ed., New York: McGraw-Hill Book Company, Inc., 1961.
6. Barker, E. H., Cappelli, A. P., Kovalevsky, L., Rish, F. L., and Verette, R. M.: Shell Analysis Manual. NASA CR-912, 1968.

Table 1:  $\lambda$  vs Model Complexity

$$\lambda = \frac{\text{NASTRAN Critical Load}}{\text{Theoretical Critical Load}}$$

No. of Axial Elements	No. of Circumferential Elements		
	1	2	4
20	2.013	2.013	2.013
40	1.252	1.252	1.252
60	1.112	1.113	—
80	1.062	—	—

Table 2: Variation in Length

Length, (cm)	No. of Elements	$P_{cr}$ (kilonewton)
55.88	80	287.5
27.94	40	287.5
13.97	20	287.5

Table 3: Variation in End Fixity (60 Element Model)

Lower End Fixity	Upper End Fixity	$P_{cr}$ kilonewton
Free	Free	303.0
Pinned	Free	301.3
Pinned	Pinned	301.1
Fixed	Free	303.1
Fixed	Pinned	301.4
Fixed	Fixed	303.2

Table 4:  $\lambda$  vs Type of Elements

$$\lambda = \frac{\text{NASTRAN Critical Load}}{\text{Theoretical Critical Load}}$$

No. of Elements	Type of Elements	
	Quad.	Tria.
40	1.102	1.037
60	1.048	1.028
80	1.028	1.012

Table 5: CPU Time vs Level (IBM 360-95)

No. of Elements	CPU Time, sec		Ratio
	Level 12	Level 15	
20	132	35	3.8
40	250	70	3.6
60	430	124	3.5
80	556	178	3.1

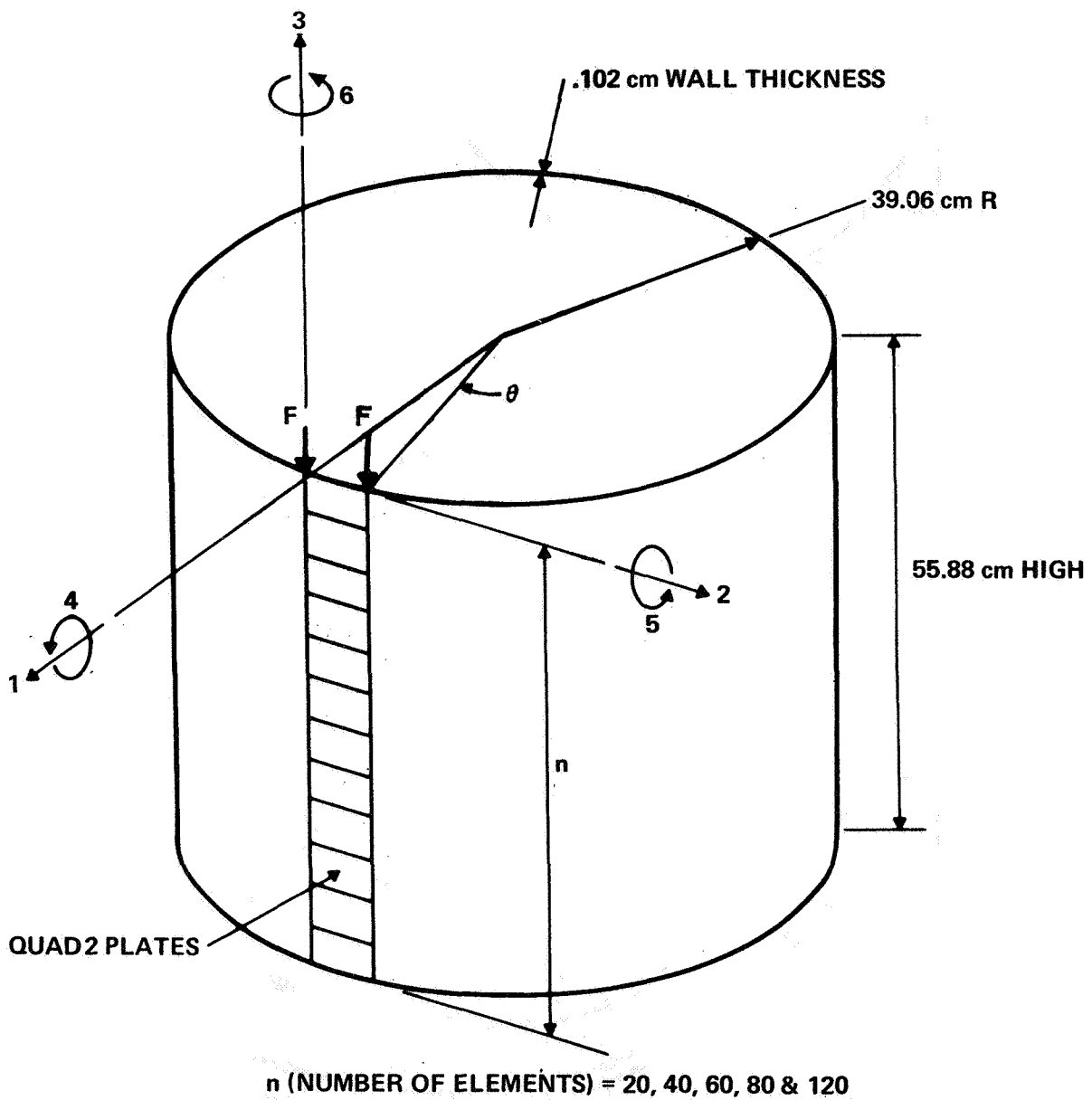


Figure 1.- Thin-walled cylinder.

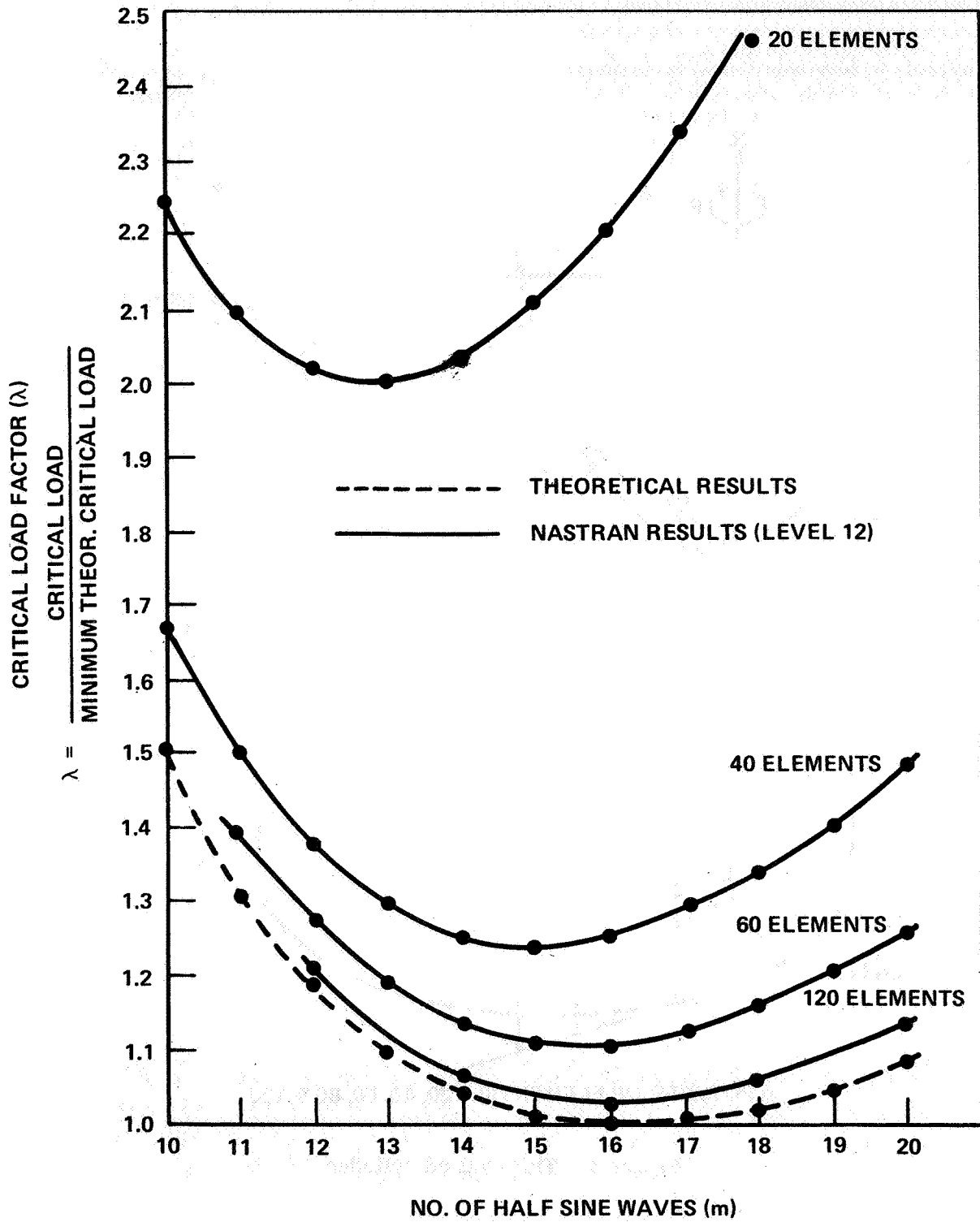


Figure 2.- Variation of  $\lambda$  with number of half-sine waves.

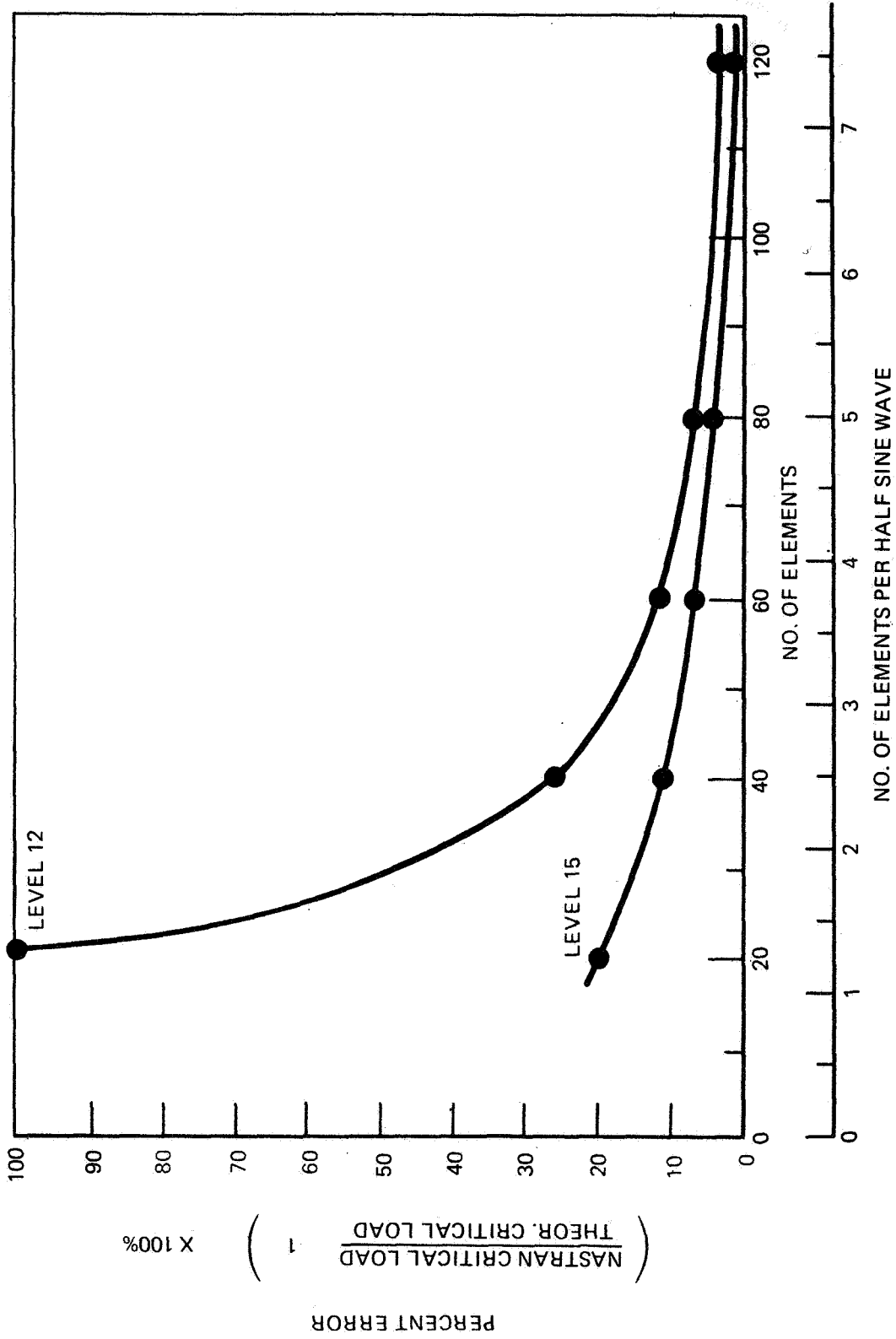
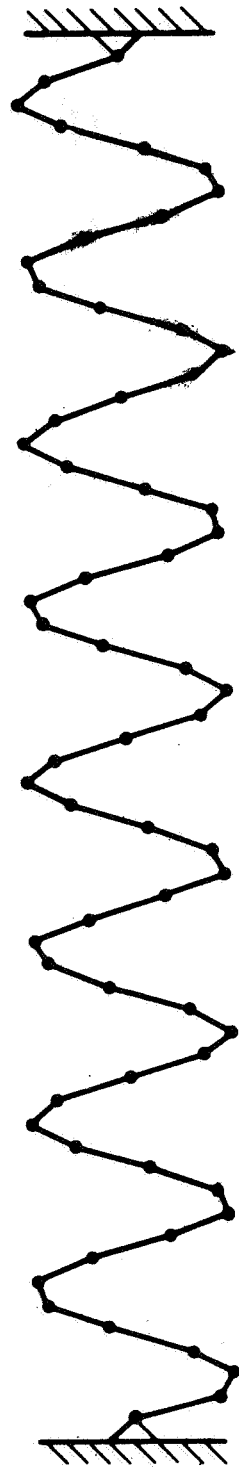
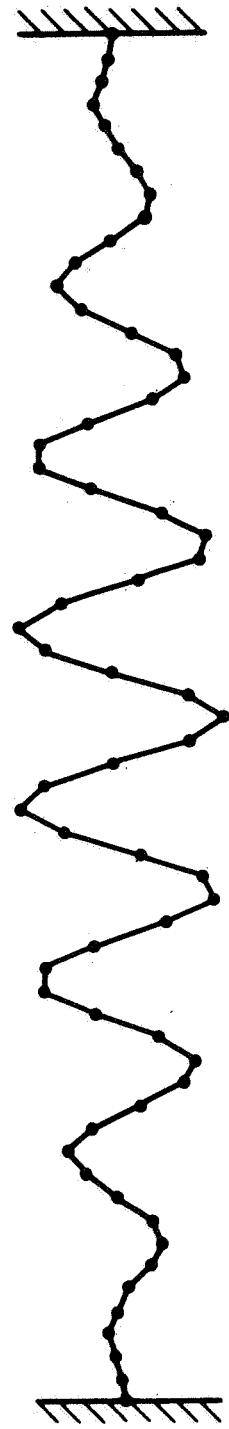


Figure 3.- Comparison of accuracy and model complexity.

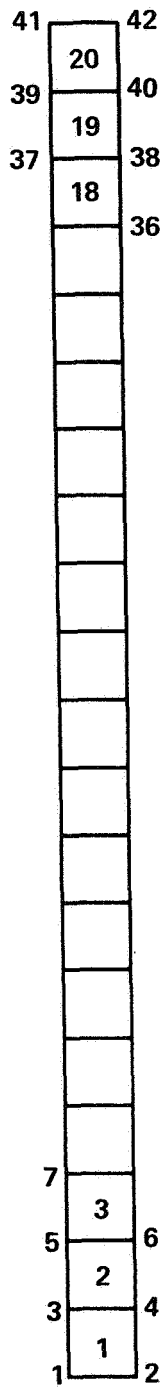


PINNED-PINNED

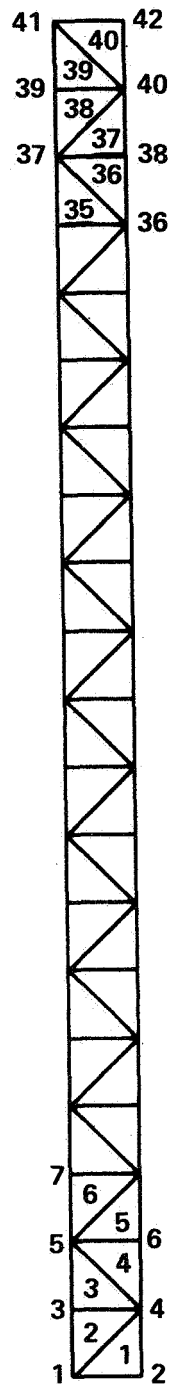


FIXED-FIXED

Figure 4.- Buckling mode shapes (60 element cylinder).



QUADRILATERAL  
ELEMENT MODEL



TRIANGULAR  
ELEMENT MODEL

Figure 5.- Finite-element model.



# STRESS AND BUCKLING ANALYSIS OF A DOUBLE-BUBBLE TANK STRUCTURE

By

James C. Robinson  
NASA Langley Research Center

and

John H. Dutton  
McDonnell Douglas Corporation

## SUMMARY

An analytical study of a two-lobed circular arc pressure vessel (double-bubble tank) with a local perturbation from the cylindrical shape has been made. From this study, it can be concluded that NASTRAN provides a good linear buckling analysis capability for structures that cannot be handled by other analysis techniques. However, at the present time, solutions are relatively expensive from a computational standpoint. Two worthwhile additions to the NASTRAN program would be the inclusion of a new beam element that adequately represents the shear transfer when modeling stiffeners on a shell and the capability, in a rigid format, to keep certain prescribed loads constant during the eigenvalue extraction process.

## INTRODUCTION

Some space shuttle orbiter configurations considered in the early stages of the Phase B studies had a two-lobed intersecting circular arc (double-bubble) pressure vessel for cryogenic propellant storage. In the orbiter configuration shown in figure 1, the tank was integrated into the orbiter as part of the primary fuselage structure and, therefore, was subjected to overall structural loads, such as axial compression, in addition to the loads induced by internal pressure. The fabrication method selected for the tank required that sections of the tank approximately 3.0 m (10 ft) in length be joined by full circumferential welds. Automatic welding was selected as the method to provide the weld quality required, but automatic welding equipment would not function satisfactorily in the cusp formed by the intersection of the two cylinders. Therefore, a local perturbation from the double-bubble shape was required to provide an acceptable radius on the

shell wall, as shown in figure 2.

The selection of an analysis method for the problem was limited by the complexity of the structure. The lack of axisymmetry precluded the use of shell-of-revolution programs for other than preliminary studies of modeling requirements and the existing form of a general shell program, STAGS, (ref. 1) was incapable of analyzing the shell with the perturbed shape. Thus, recourse to a finite element technique was required for detailed analysis.

The purpose of this paper is to present the results of a study using NASTRAN to determine the effect of the shape perturbation on the stress distribution and axial buckling load of the tank. A secondary purpose is to present some observations based on experience gained during the study in the use of NASTRAN for shell analyses.

## PRELIMINARY STUDIES

### Shell-of-Revolution Study

A preliminary study of a ring- and integral-stringer stiffened cylindrical shell having the same diameter and stiffener dimensions as one lobe of the tank was made using the shell-of-revolution analysis of reference 2 to gain some insight into modeling requirements for the tank analysis. Simply supported cylinders with a length equal to (1) a complete lobe between end domes, and (2) one bay of a lobe between tank rings were analyzed for a loading consisting of positive internal lateral pressure and net axial compressive loads. The results of this study (fig. 3) are that the longer cylinder (with rings and stringers considered distributed) buckles axisymmetrically and hence is independent of the ratio of the hoop stress resultant/axial stress resultant ( $N_y/N_x$ ). The buckling mode half-wave length of 23.0 cm (9.1 in.) approximates half the bay length between rings. The shorter cylinder buckles asymmetrically for small negative values of  $N_y/N_x$ , but approaches the analytical buckling load of the longer cylinder and buckles axisymmetrically with a half-wave length of 25.4 cm (10.0 in.) for values of  $N_y/N_x$  less than about -1.0.

These results and the details of the tank geometry, stiffness, and loads ( $N_y/N_x < -1$  for the stiffened area of the tank) suggest that a satisfactory approximation to the complete double-bubble tank could be obtained by limiting the model to one-half of one bay longitudinally and about twice that distance circumferentially to give a model covering an area of 25.4 by 55.4 cm (10 by 21.8 in.) (fig. 2a). The effect of the remainder of the structure was included by the use of assumed boundary conditions.

### Modeling Detail Studies

Several short studies were conducted to evaluate the effects of modeling details on the NASTRAN results. In one study, the effect of radius to thickness ratio ( $R/t$ ) on the axisymmetric buckling load of an unstiffened

cylinder was calculated using NASTRAN with a model composed completely of quadrilateral elements (CQUAD2). For dimensions similar to the NASTRAN demonstration problem ( $R/t$  of 32, ref. 3), the buckling load was 1.4 percent above the classical buckling load and the buckling mode shape was the classical shape of two longitudinal half-waves. As  $R/t$  was increased for a model containing the same number of elements (by decreasing the shell thickness), the discrepancy between buckling loads calculated with NASTRAN and those obtained from classical theory increased to 6.8 percent at  $R/t$  of 320. In addition, the NASTRAN analysis predicted a mode shape with six half-waves compared to seven for the classical solution. The increase in the number of half-waves with an increase in  $R/t$  requires more severe element deformation and is probably the cause for the increased discrepancy. These results suggest that for axisymmetric buckling problems, the number of elements per half-wave should be greater than the value of 3.3 obtained in the reduced thickness demonstration problem ( $R/t = 320$ ).

Another modeling detail study was designed to check the modeling of the longitudinally stiffened area of the tank. A stiffened circular cylinder of the same dimensions as one bay of the tank loaded by internal pressure and axial forces was analyzed using NASTRAN. BAR elements with bending stiffness were used in modeling the stiffeners to obtain the proper combination of axial and bending stiffness and adequate detail of stress output. However, modeling of a longitudinal stiffener as an offset BAR element produced unreasonable discrepancies in the stresses in adjacent elements when radial expansion of the end of the cylinder was prevented either by a ring or by radial displacement boundary conditions. A quadrilateral shear panel between the beam element and the shell was used to improve the model. Figure 4 shows the stresses due to a static loading in a longitudinal stiffener with and without the quadrilateral shear panels in the model. The smaller discontinuities in the calculated bending stresses using the model with the quadrilateral shear panels indicate that it is the better representation of the actual structure. The difference in stresses results from the mechanism of shear transfer in the composite section (stiffener and shell) and is similar to the problem discussed previously in reference 4. The inclusion in NASTRAN of the shear beam element discussed in reference 4, or an element with similar properties, should improve the NASTRAN modeling capability for this type of structure.

The axisymmetric buckling load for the cylinder discussed above, with the same boundary conditions as used in reference 2, was calculated using NASTRAN. This buckling load was about 2 percent higher than that given by the shell analysis of reference 2 and the buckling mode shape which had two half-waves was the same as that given by the shell analysis. It would appear, therefore, that the addition of longitudinal stiffeners to the relatively thin shell with an  $R/t$  of 1277 increases the local moment of inertia sufficiently to force a longer wave length for the buckling mode shape of the stiffened shell (10 elements per half-wave) and thus provides

satisfactory correlation between buckling predictions made with the use of classical theory and NASTRAN.

In the final modeling detail study, the validity of representing a complete cylinder by use of a single bay of that cylinder with assumed boundary conditions to simulate the remainder of the cylinder was evaluated by comparing the axisymmetric buckling load for a complete multi-bay cylinder with that for a single bay cylinder with assumed boundary conditions. NASTRAN was used to calculate the axisymmetric buckling load and mode shape of a complete five-bay cylinder. The cylinder selected (fig. 5) had relatively light rings and shorter end bays with rotationally restrained ends to insure buckling in the center portion. The loads were internal lateral pressure and enforced axial displacement. For the buckling calculation, the axial restraint was removed by the use of an ALTER package provided the NASTRAN Systems Management Office by Malcolm W. Ice of Boeing Computer Sciences, Inc. The buckling load for the five-bay cylinder was essentially the same as for the single bay cylinder and the buckling mode shape (fig. 5) is antisymmetric about the centerline, but the node locations do not occur at the frames. This may be due to the small frame extensional stiffness which is only about 12 percent of the shell extensional stiffness in the hoop direction. This agreement in the axisymmetric buckling loads for the two cylinders indicates that the use of assumed boundary conditions is satisfactory even with the use of light rings which do not force nodes to occur at the rings.

## DOUBLE-BUBBLE TANK STUDY

### Model and Loads

The tank was analyzed both with and without the shape perturbation to determine its effect on deflections, stresses, and buckling loads. The part of the double-bubble tank that was modeled is shown in figure 2, and the finite element model, a contour plot of the shape perturbation, and the shell thickness are shown in figure 6. The cylindrical portions of the shell were modeled with flat quadrilateral elements having membrane and bending properties (CQUAD2). The transition section of the perturbation was modeled with triangular elements having similar properties (CTRIA2). The integral longitudinal stiffeners were modeled as offset BAR elements with quadrilateral shear panels to provide a better approximation of the local shear transfer mechanism as determined in the preliminary studies (see fig. 4). The frame section was composed of rod elements and quadrilateral and triangular membrane elements. The frame was considered to elastically restrain the tank in the plane of the frame, but buckling of the frame was prevented by the imposition of deflection constraints normal to the plane of the frame.

To simulate the effect of the remainder of the structure on the portion of the tank that was modeled, appropriate restraint conditions were assumed for the boundaries of the model. Symmetric boundary conditions were assumed along the centerline of the double-bubble tank for both the prestress (static) and buckling computations. Symmetric boundary conditions were assumed along

the outer edge parallel to the tank centerline for both prestress and buckling computations. On the boundaries at the frame and along the bay centerline, zero rotation in the circumferential direction was assumed for the prestress calculations. For buckling, four combinations of symmetric and antisymmetric restraints were used to insure that the minimum value of the buckling load was obtained.

The loads imposed for prestress on the double-bubble tank resulted from a positive internal pressure of  $207 \text{ kN/m}^2$  (30.0 psi) and an enforced axial displacement of 0.051 cm (0.020 in.), which corresponds to a strain of 0.002. The enforced displacement was used to simulate overall compression of a structure of variable thickness at a distant location from the ends of the structure. This combination of loads produces a stress resultant ratio  $N_y/N_x$  of approximately -1.1. NASTRAN rigid format 5 requires that this ratio remain constant during buckling. Inasmuch as the tank internal pressure and the applied axial load are not physically coupled, it would have been desirable to have the option of letting only one stress resultant vary during buckling.

#### Numerical Results

The results of the NASTRAN calculations for the double-bubble tank both with and without the shape perturbation are shown in figures 7 through 10. All of these figures are nondimensionalized contour plots, where the contours are lines of constant percentage of the maximum value (shown in the subtitle) of the functions shown in the figure title. In all figures, plot (a) presents values for the tank without the shape perturbation, and plot (b) presents values for the tank with the perturbation. The plots were drawn by a computer program that is a modification of the contour plot program described in reference 5.

Comparison of the contour plots for the radial displacement of the tank without and with the perturbation (fig. 7) shows similar contour patterns, but the magnitudes are significantly different; the maximum deflection is increased approximately 38 percent by the presence of the perturbation.

The axial stress resultant ( $N_x$ ) patterns shown in figure 8 indicate that while the maximum values without the perturbation are fairly uniformly distributed adjacent to the double-bubble tank centerline (left side of figure), the maximum values with the perturbation are concentrated away from the tank centerline at the lower boundary and near the centerline at the upper boundary. In addition, the presence of the perturbation increases the maximum value by about 40 percent.

The hoop stress resultant ( $N_y$ ) contour patterns (fig. 9) show considerable differences near the double-bubble tank centerline. The presence of the perturbation with its reversal of curvature causes the large hoop stresses induced in the thickened weld area (upper boundary in the figure) to be diverted around the perturbation and even cause some hoop compression at the

centerline and also under the frame near the outer edge of the figure. While there are significant differences in the distribution of the hoop stress resultants, the maximum values are essentially the same.

The herring-bone pattern in the contours near the center of the left edge, which is particularly noticeable in figures 8b and 9b, is probably caused by the presence of high stress gradients in an area modeled with triangular elements.

The buckling mode shapes are shown in figure 10. In both cases, buckling occurred at an eigenvalue less than 1.0 indicating that the assumed prestress loading was higher than the buckling load. For comparison with the results for the cylinder, the local value of  $N_x$  in the integrally stiffened portion of the tank was used.

For the structure without the perturbation, the mode shape is fairly smooth and involves most of the area of the modeled structure. At the outer boundary (right edge), the mode shape becomes symmetric due to the assumed boundary conditions and the presence of the maximum radial displacement on this boundary indicates that an extension of the model in the circumferential direction would probably be desirable to reduce the effect of the boundary conditions on the mode shape. At buckling, the calculated value of  $N_x$  in the integrally stiffened area of the shell is  $242 \text{ kN/m}$  ( $1382 \text{ lb/in.}$ ). For the structure with the perturbation, the buckling mode shape shows local buckling of the tank shell between stiffeners in the integrally stiffened area. At buckling, the calculated value of  $N_x$  in the integrally stiffened area is  $236 \text{ kN/m}$  ( $1347 \text{ lb/in.}$ ). Local buckling probably occurs in this area because the hoop stress resultants in this area are compressive as shown in figure 9b. Therefore, the presence of the shape perturbation reduces the calculated buckling load very little (less than 3 percent), even though the maximum stress resultants are increased by amounts up to 40 percent, probably because the axial compressive loads do not change greatly in the area where buckling occurs.

In contrast to the relatively small reduction in buckling load due to the perturbation, is the reduction in the buckling load of the integrally stiffened portion of the shell when it comprises a portion of a double-bubble tank structure having variations in wall thickness and ring dimensions rather than comprising part of a uniform circular cylinder. This decrease in the value of the buckling load calculated by NASTRAN is about 22 percent.

#### COMPUTER TIME

Some typical NASTRAN run times on the CDC 6600 computer are shown in Table 1. The problems vary from about 300 to 900 degrees of freedom with central processor times varying from 300 seconds to 2228 seconds. A

comparison of the run times for the first three problems (NASTRAN demonstration problem and the demonstration problem with reduced thickness) shows that run times may vary considerably for what appears to be a similar problem. The large increase in run time for level 12.1.0 and  $R/t = 320$  may be due to the selection of the range on the EIGB card which was set very low to insure that the lowest mode would be obtained. For the reduced thickness demonstration problem, level 15.1.0 shows a speed advantage of about 4 compared to level 12.1.0. A comparison of the two double-bubble runs shown indicates the significant increase in run time required to obtain several eigenvalues. The reason for calculating more than one eigenvalue is to insure that the lowest eigenvalue has been determined. For succeeding runs, the eigenvalue extraction range can usually be selected such that only one eigenvalue is required which effects a substantial reduction in run time. It is of interest to make a comparison of the NASTRAN computation times with the time required by the SALORS shell-of-revolution analysis program for finite difference buckling calculations. For an assumed axisymmetric representation of the Apollo-Saturn short stack (ref. 6) with 436 finite difference points, 209 central processor seconds were required to calculate the buckling load. In comparison, the present analysis of shells using NASTRAN with quadrilateral and triangular elements is relatively time consuming. This time consideration is offset, however, by the fact that NASTRAN may be used to analyze structures that cannot be analyzed with existing shell programs.

## CONCLUSIONS

An analytical study of a two-lobed circular arc pressure vessel (double-bubble tank) with a local perturbation from the cylindrical shape has been made. From this study, it can be concluded that NASTRAN provides a good linear buckling analysis capability for structures that cannot be handled by other analysis techniques. However, at the present time, solutions are relatively expensive from a computational standpoint. Two worthwhile additions to the NASTRAN program would be the inclusion of a new beam element that adequately represents the shear transfer when modeling stiffeners on a shell, and the capability, in a rigid format, to keep certain prescribed loads constant during the eigenvalue extraction process.

## REFERENCES

1. Almroth, B. O.; and Brogan, F. A.: Bifurcation Buckling as an Approximation of the Collapse Load for General Shells. AIAA J., Vol. 10, No. 4, April 1972, pp. 463-467.
2. Block, David L.; Card, Michael F.; and Mikulas, Martin M., Jr.: Buckling of Eccentrically Stiffened Orthotropic Cylinders. NASA TN D-2960, 1965.
3. NASTRAN Demonstration Problem Manual. NASA SP-224, 1970.
4. Melosh, R. J.; and Merritt, R. G.: Evaluation of Spar Matrices for Stiffness Analysis, J. of Aero./Space Science, Vol. 25, No. 9, Sept. 1958, pp. 537-543.
5. Giles, Gary L.; and Blackburn, Charles L.: Procedure for Efficient Generating, Checking, and Displaying NASTRAN Input and Output Data for Analysis of Aerospace Vehicle Structures. NASTRAN:Users' Experiences. TM X-2378, 1971, pp. 679-696.
6. Anderson, M. S.; Fulton, R. E.; Heard, W. L., Jr.; and Walz, J. E.: Stress, Buckling, and Vibration Analysis of Shells of Revolution. Computers & Structures, Vol. 1, 1971, pp. 157-192.

TABLE I

CDC 6600 COMPUTER CENTRAL PROCESSOR TIMES FOR TANK BUCKLING LOADS CALCULATION<sup>1</sup>

<u>Problem</u>	<u>Level</u>	<u>Core (K OCTAL)</u>	<u>D.O.F.</u>	<u>Elements</u>	<u>Eigen- values</u>	<u>CPU Sec.</u>
Isotropic Cylinder ( $R/t = 32$ ) <sup>2</sup>	12.1.0	140	304	80	1	298
Isotropic Cylinder ( $R/t = 320$ ) <sup>3</sup>	12.1.0	140	304	80	0	1127 <sup>4</sup>
Isotropic Cylinder ( $R/t = 320$ ) <sup>3</sup>	15.1.0 <sup>5</sup>	140	304	80	1	301
5-Bay Continuous Stiffened Cylinder	12.1.0	160	880	332	1	974
Double-Bubble Tank	11.1.2	160	896	299	4	2228
Double-Bubble Tank	11.1.2	160	896	299	1	1194

1 Eigenvalue extraction method was inverse power.

2 NASTRAN demonstration axisymmetric cylinder buckling problem (ref. 3).

3 NASTRAN demonstration problem with increased  $R/t$ .

4 Run exceeded time limit without determining an eigenvalue.

5 Preliminary version of level 15.1.0.

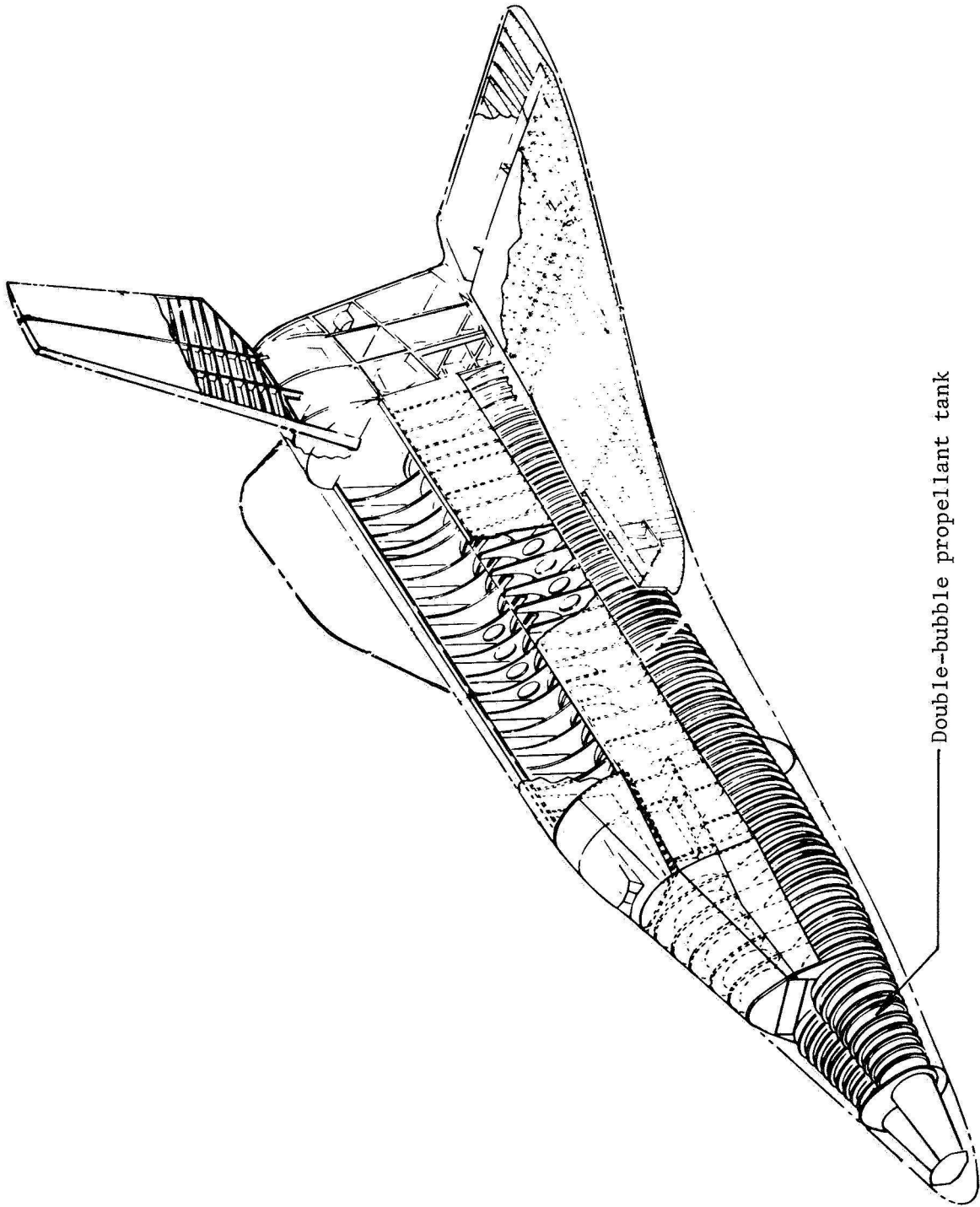
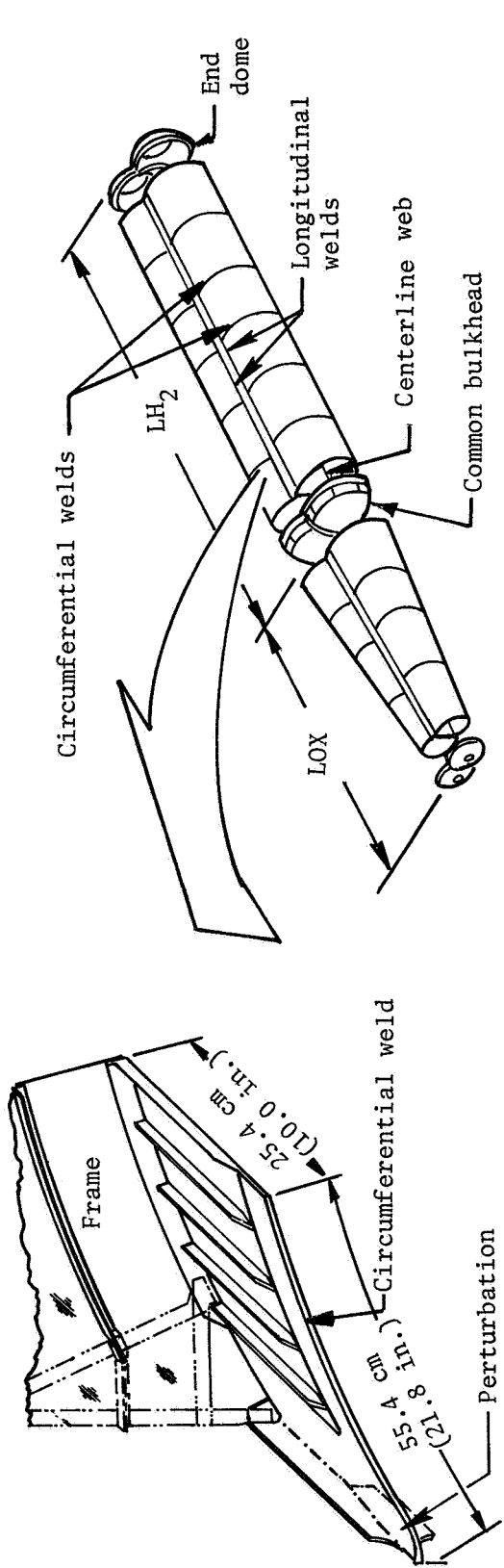
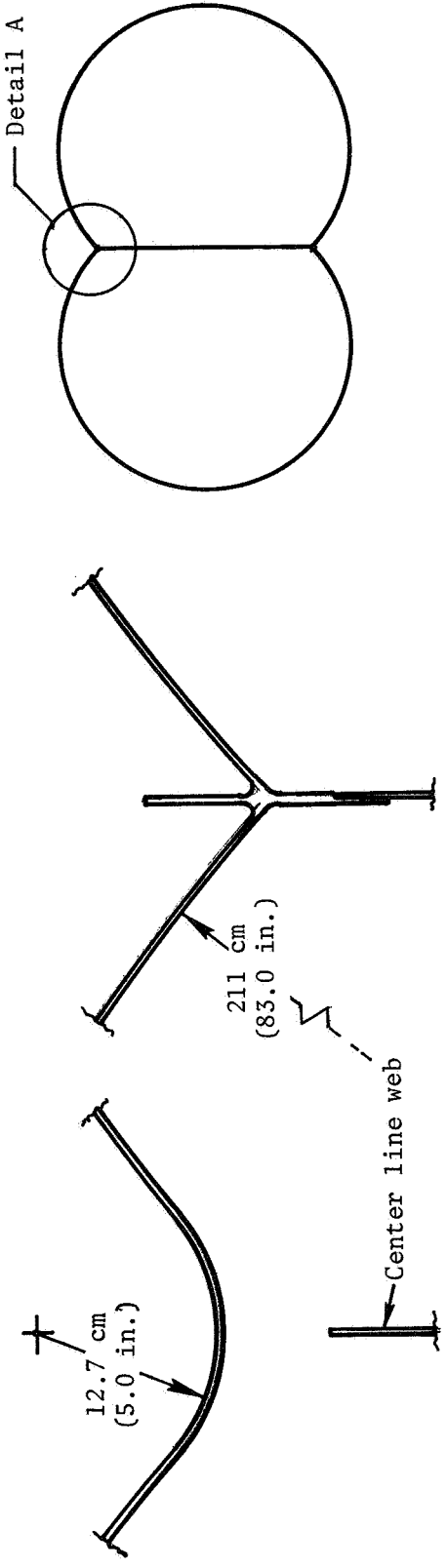


Figure 1.- Space shuttle orbiter concept with double-bubble cryogenic propellant tank.



(a) Structure modeled.

(b) Double-bubble tank.



Detail A at perturbation for weld.

Detail A away from weld.

Section thru double-bubble tank.

(c) Details of shape perturbation.

Figure 2.- Double-bubble tank and shape perturbation details.

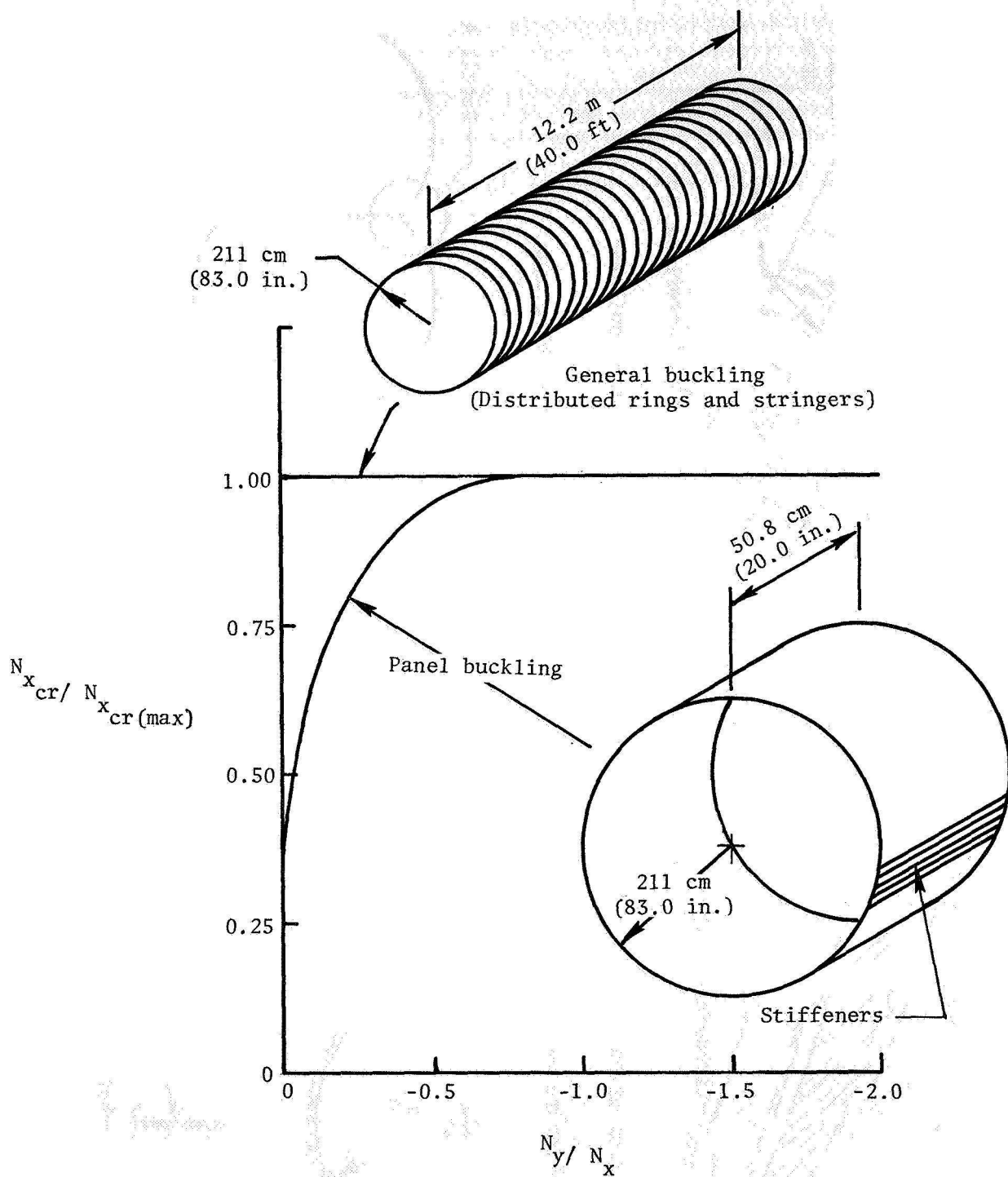


Figure 3.- Effects of stress ratio  $N_y / N_x$  on buckling of simply-supported ring- and stringer-stiffened cylindrical shells. Results obtained from analysis of reference 2.

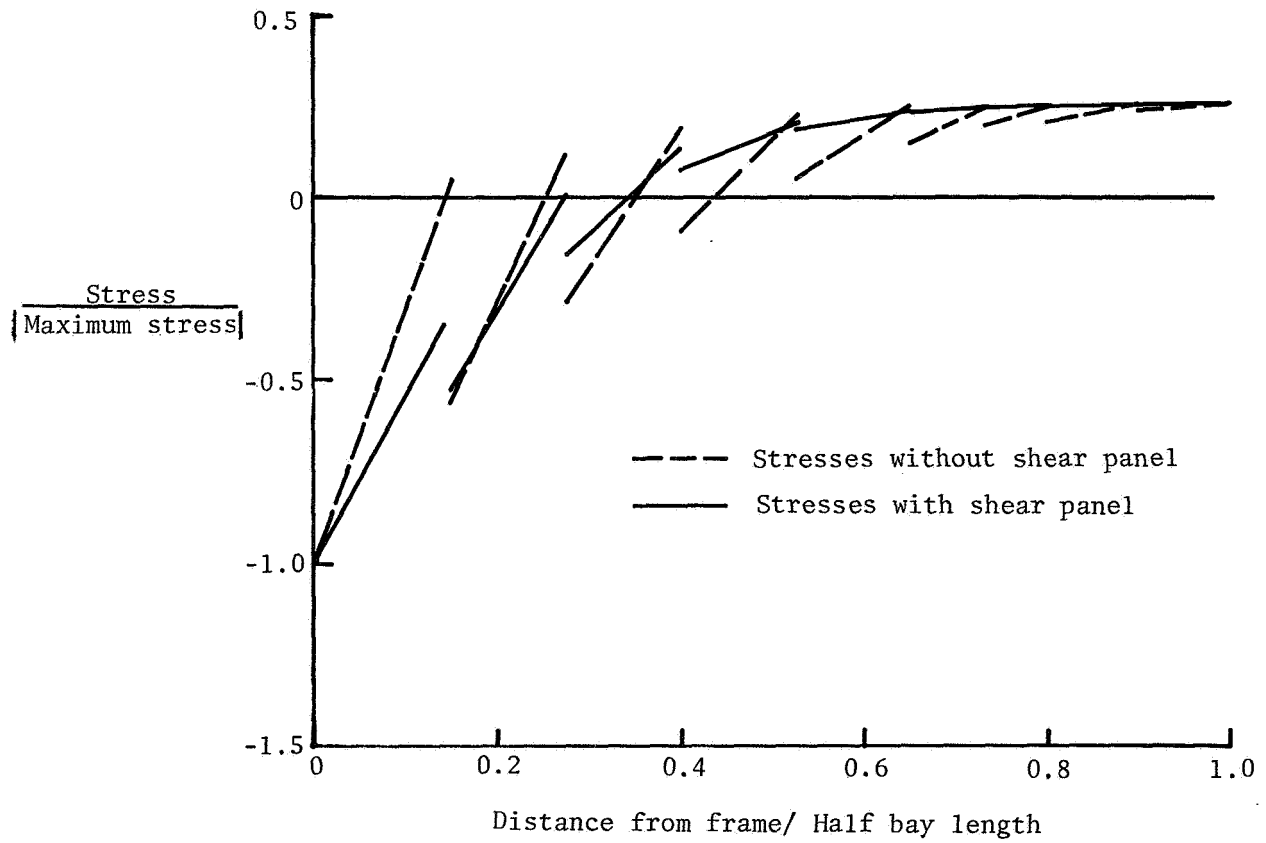
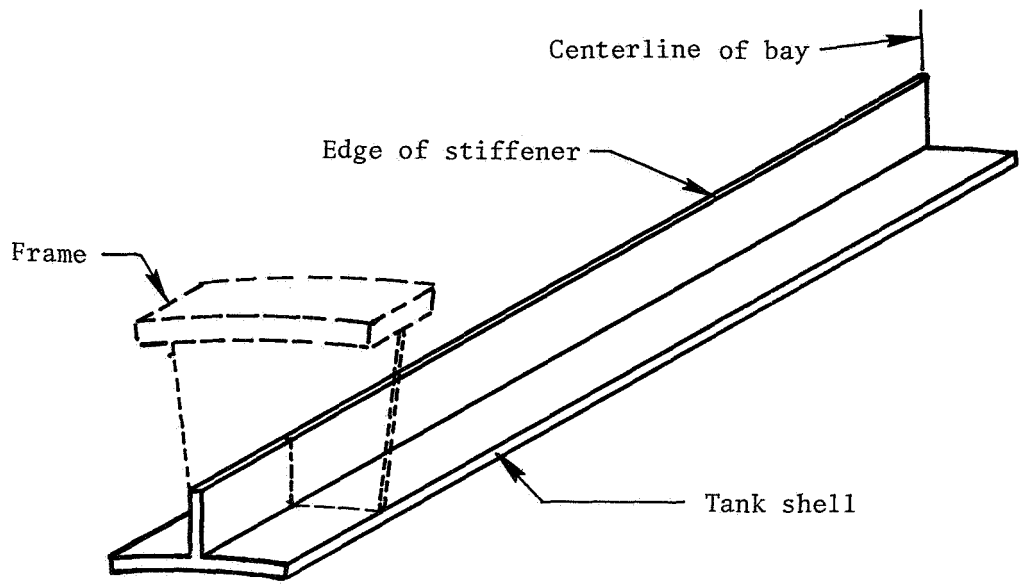
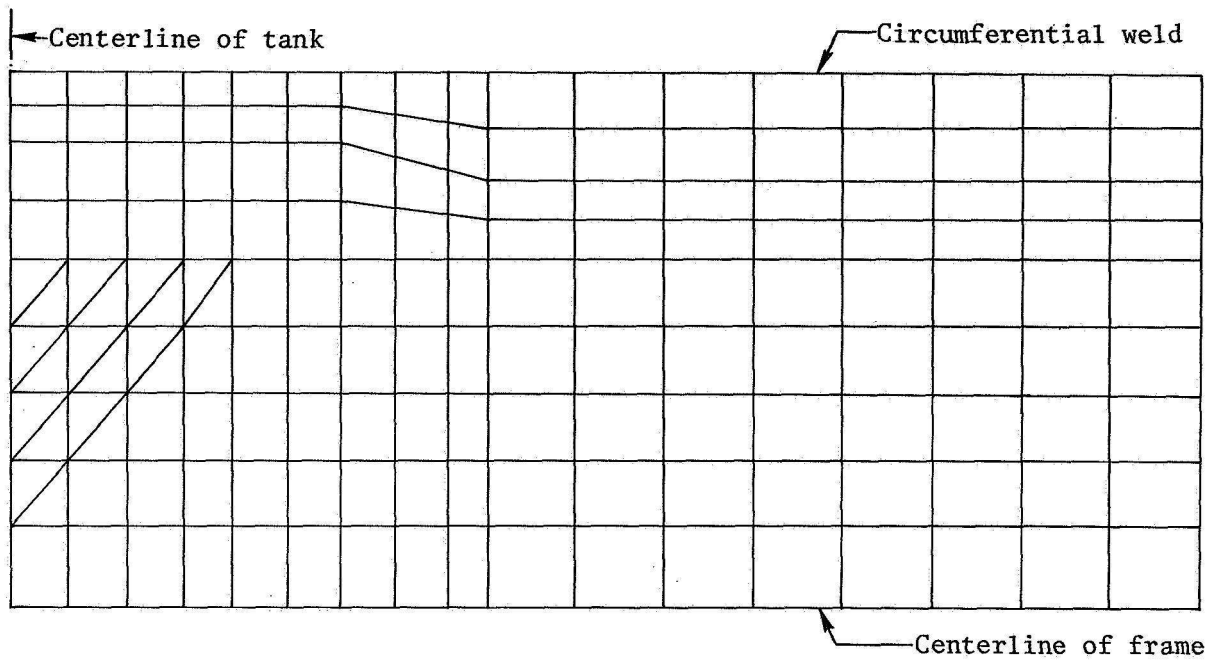
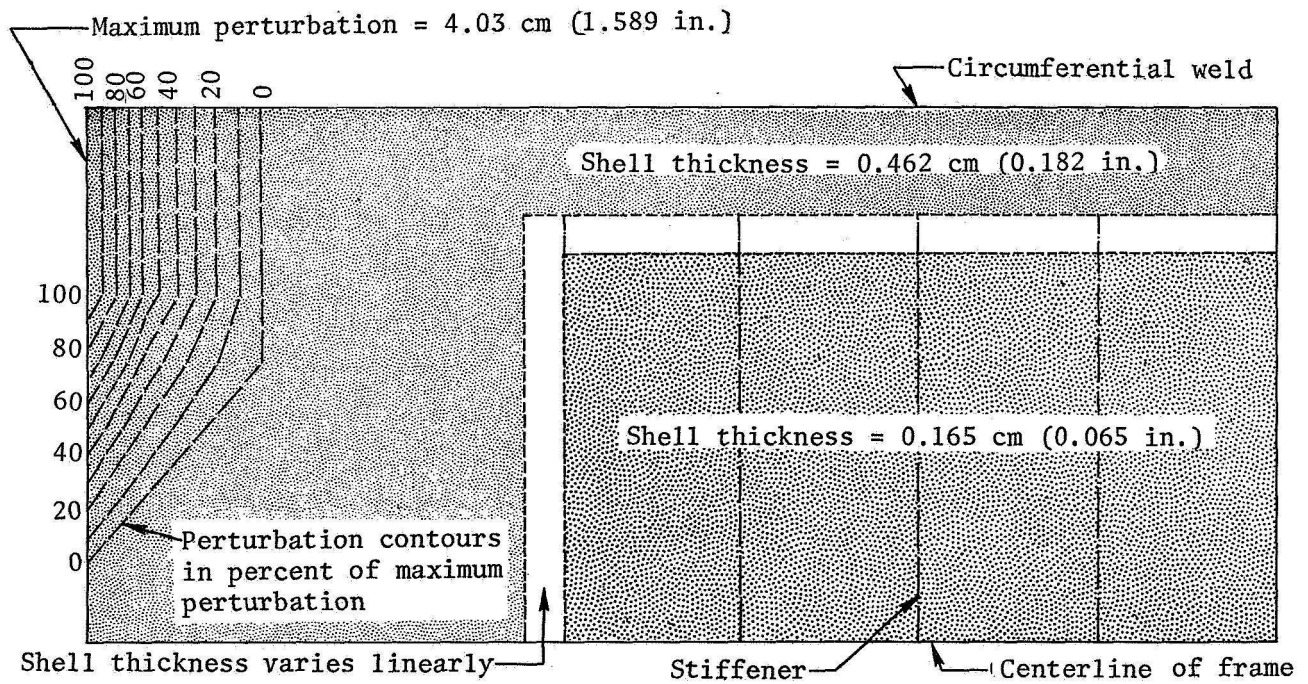


Figure 4.- Effect of stiffener modeling details on the NASTRAN calculated axial stress distribution in the edge of the stiffener.



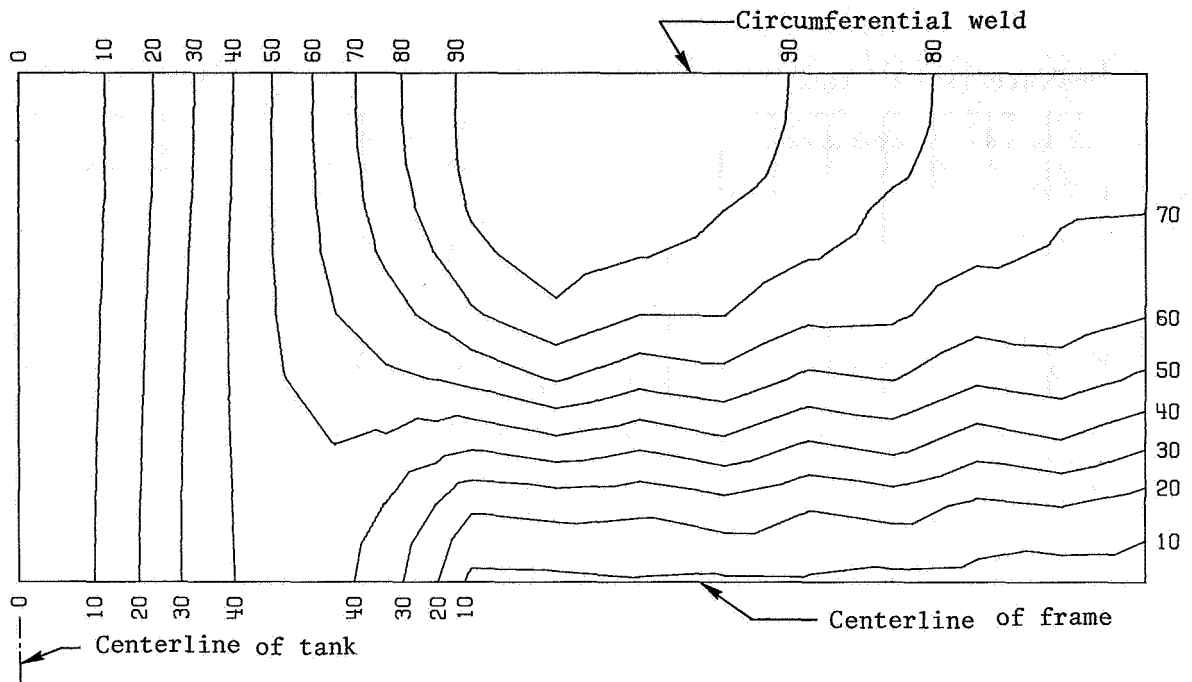


(a) Finite element model of double-bubble tank shell.

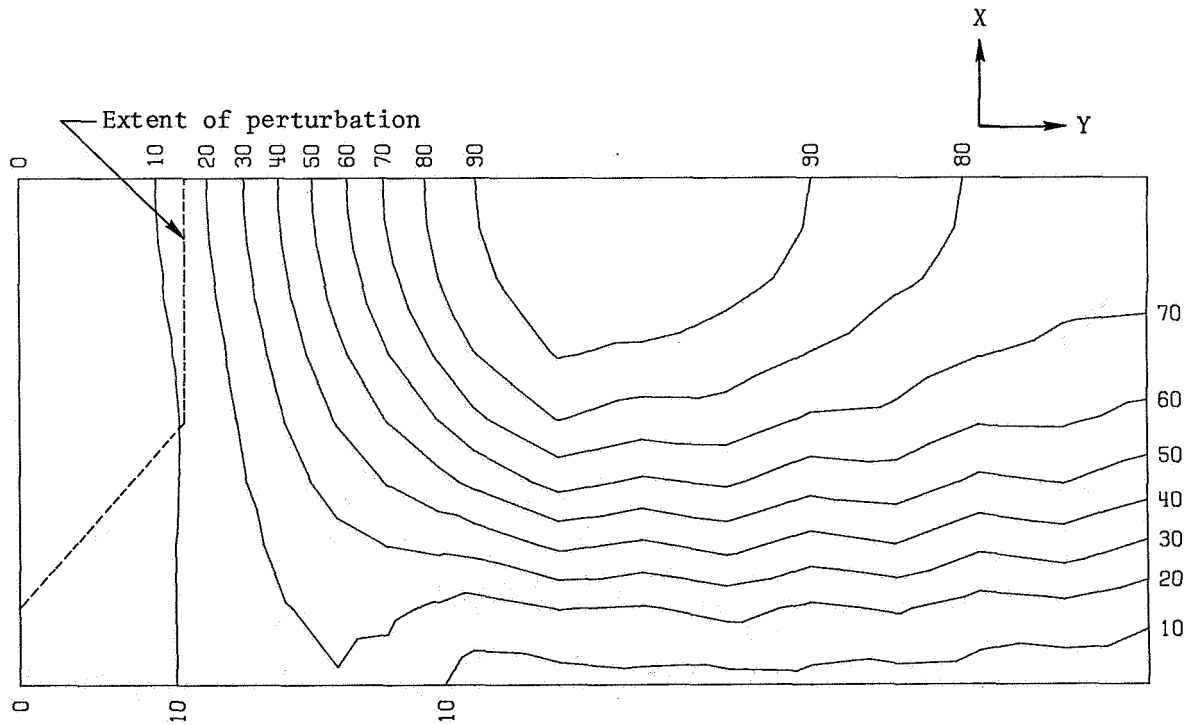


(b) Plot of shell thickness distribution and shape perturbation contours.

Figure 6.- Finite element model and shell details.

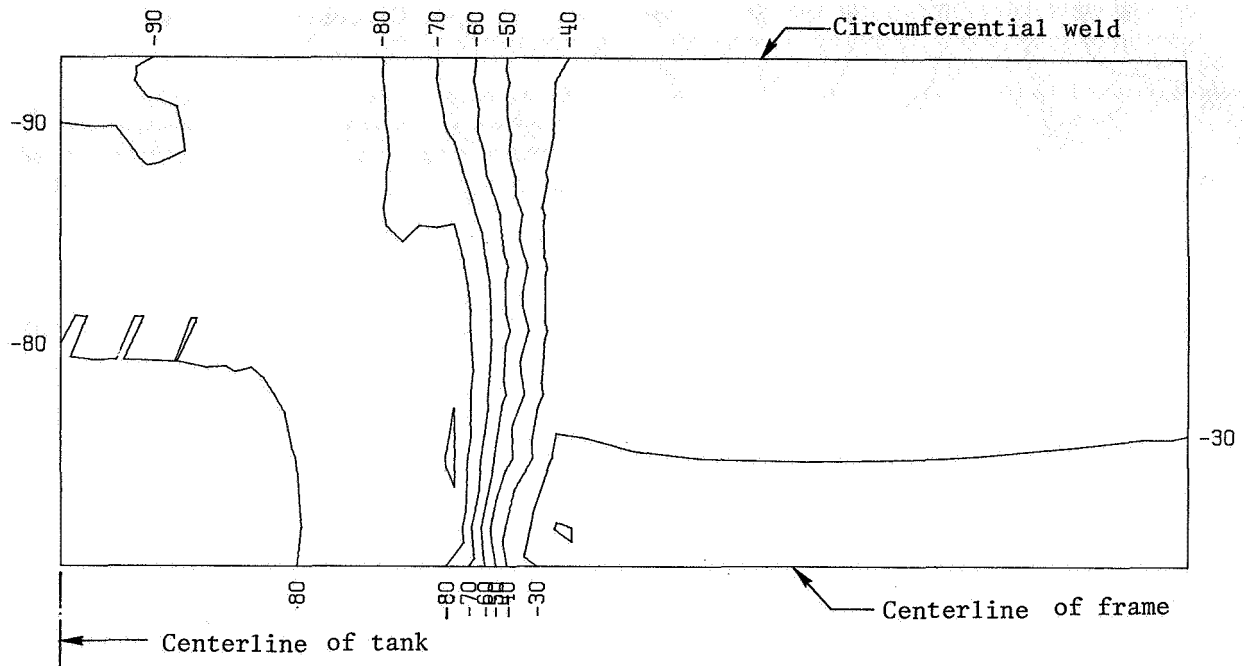


(a) Without shape perturbation. Maximum displacement = 0.620 cm (0.244 in.)

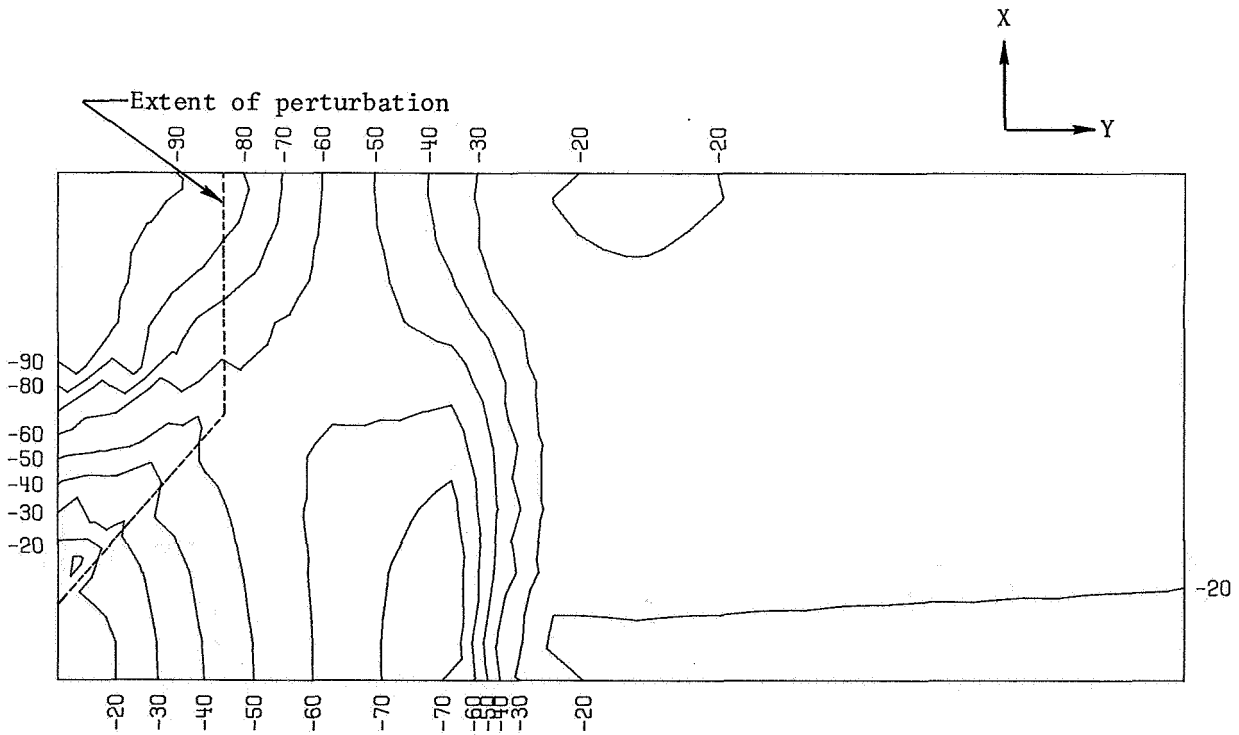


(b) With shape perturbation. Maximum displacement = 0.853 cm (0.336 in.)

Figure 7.- Contours of radial displacement under prestress loads for double-bubble tank model.

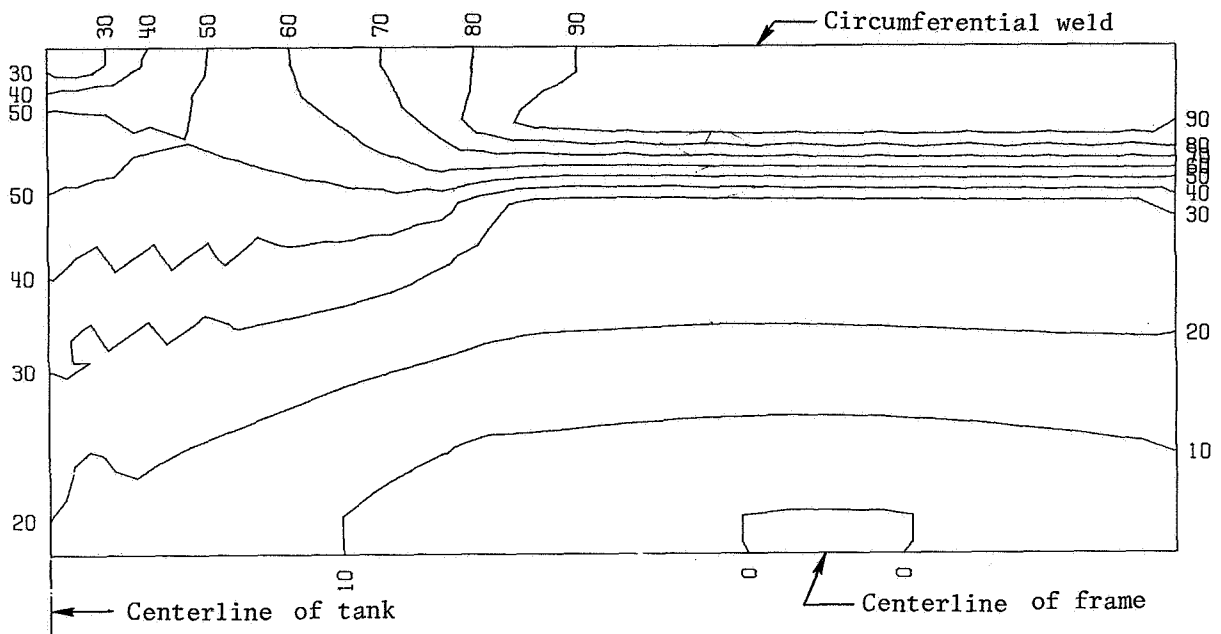


(a) Without shape perturbation. Maximum stress resultant =  $775.3 \text{ kN/m}$  ( $4427 \text{ lb/in.}$ )

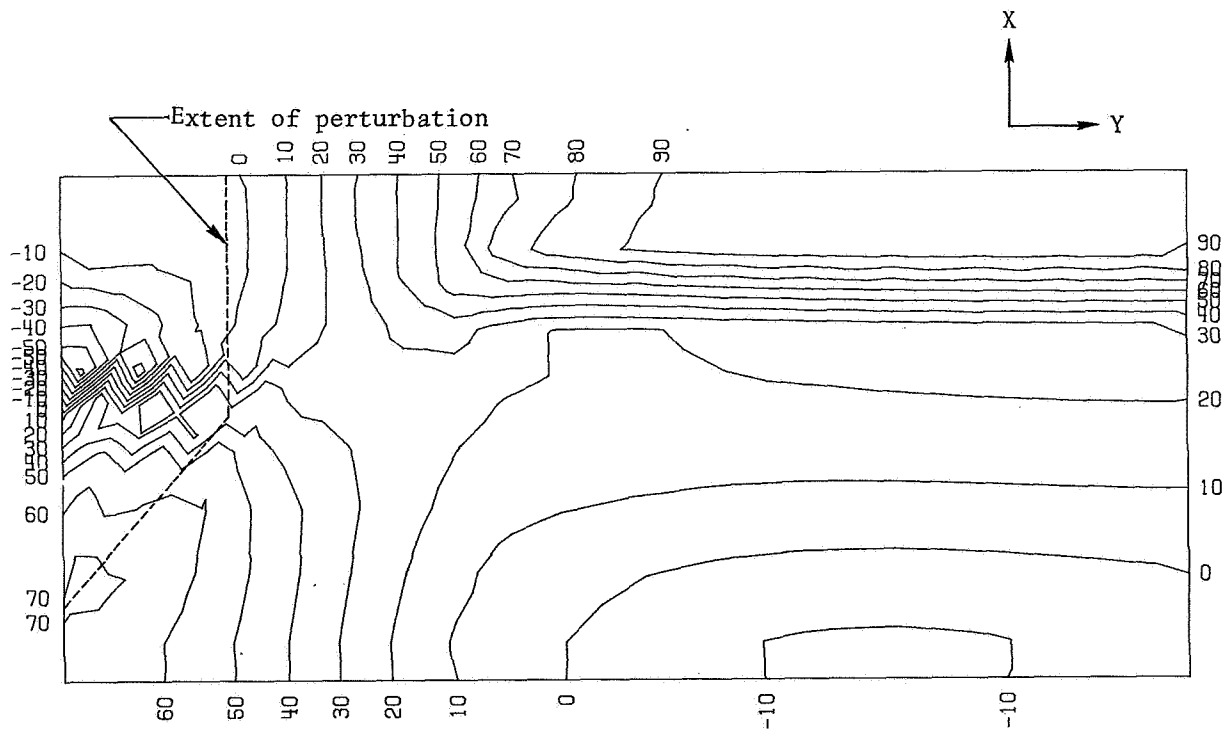


(b) With shape perturbation. Maximum stress resultant =  $1089.1 \text{ kN/m}$  ( $6219 \text{ lb/in.}$ )

Figure 8.- Contours of axial stress resultant  $N_x$  for double-bubble tank model.

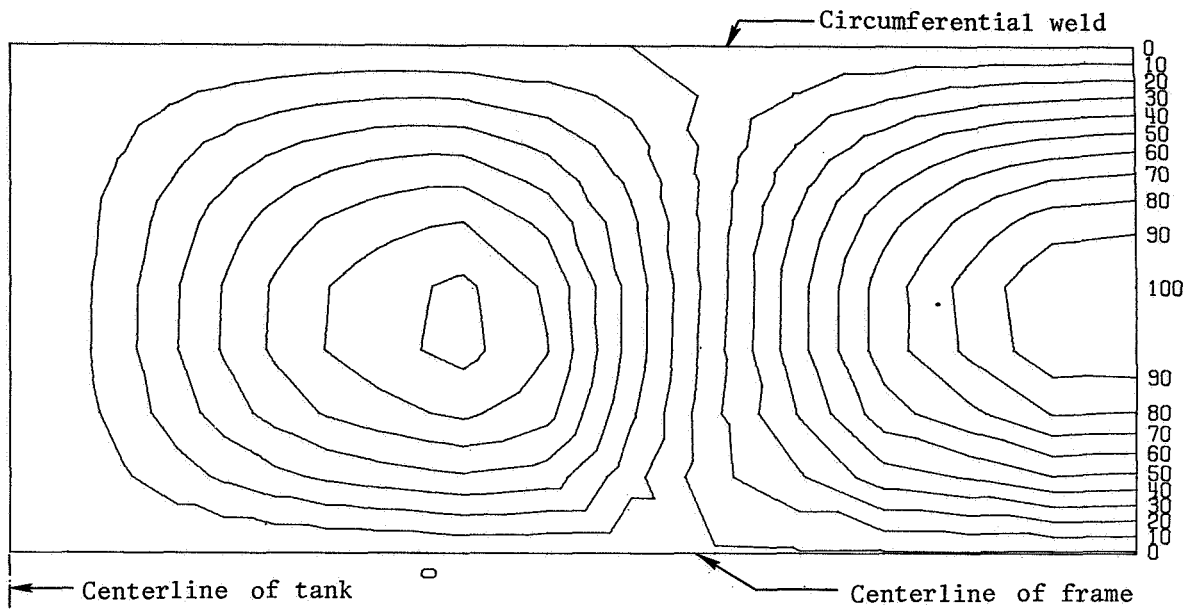


(a) Without shape perturbation. Maximum stress resultant =  $716.1 \text{ kN/m}$  (4089 lb/in.)

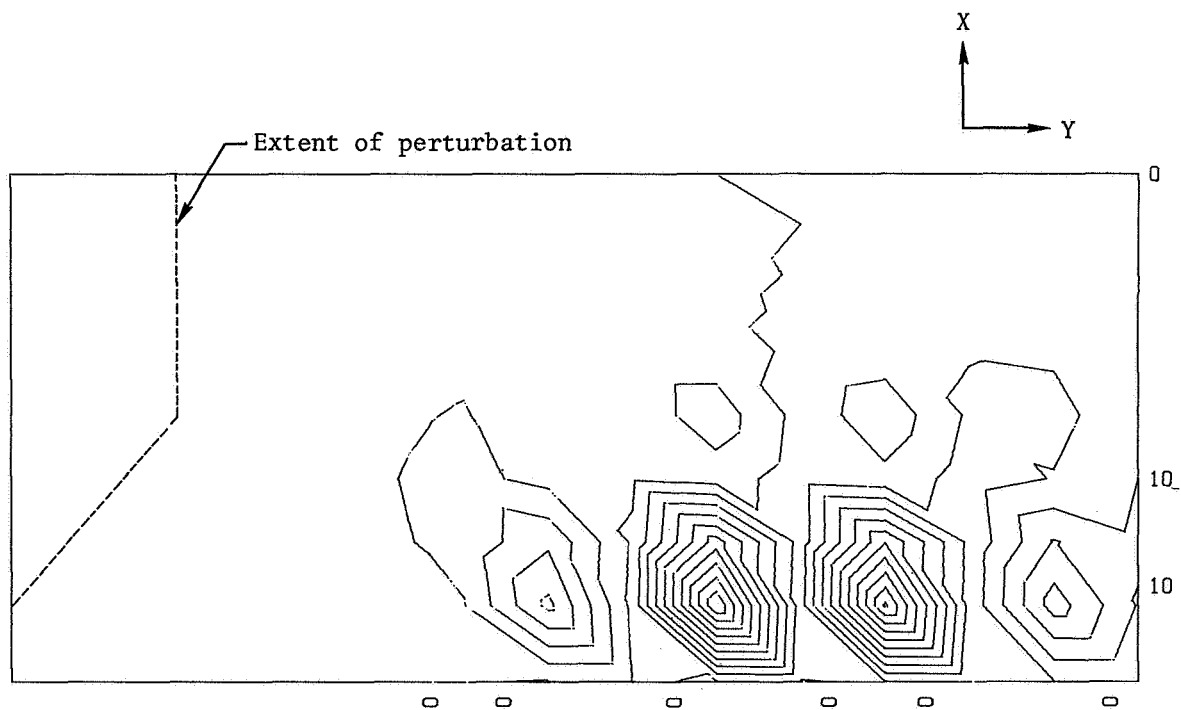


(b) With shape perturbation. Maximum stress resultant =  $724.7 \text{ kN/m}$  (4138 lb/in.)

Figure 9.- Contours of hoop stress resultant  $N_y$  for double-bubble tank model.



(a) Without shape perturbation.



(b) With shape perturbation.

Figure 10.- Contour plot of buckling mode shape for double-bubble tank model.



SOME APPLICATIONS OF NASTRAN TO THE BUCKLING OF THIN  
CYLINDRICAL SHELLS WITH CUTOUTS

By Jerry G. Williams and James H. Starnes, Jr.  
NASA Langley Research Center

SUMMARY

The buckling of isotropic and waffle stiffened circular cylinders with and without cutouts was studied using NASTRAN's Rigid Format 5 for the case of axial compressive loading. The results obtained for the cylinders without cutouts are compared with available reference solutions. The results for the isotropic cylinders containing a single circular cutout with selected radii are compared with available experimental data. For the waffle stiffened cylinder, the effect of two diametrically opposed rectangular cutouts was studied. A DMAP alter sequence was used to permit the necessary application of different prebuckling and buckling boundary conditions. Advantage was taken of available symmetry planes to formulate equivalent NASTRAN model segments which reduced the associated computational cost of performing the analyses. Limitations of the applicability of NASTRAN for the solution of problems with nonlinear characteristics are discussed.

## INTRODUCTION

Thin-walled circular cylindrical shells are commonly subjected to compressive type loading, and hence, buckling of these structures must be considered as a possible failure mode. The presence of cutouts in the sides of these structures can significantly reduce their load carrying capability as well as complicate the buckling analysis.

A limited number of experimental (refs. 1, 2, and 3) and finite-difference analytical (refs. 3 and 4) studies of the effects of cutouts on cylindrical shell buckling behavior have been reported. These investigations have been limited to isotropic cylinders with unreinforced circular cutouts and reinforced and unreinforced rectangular cutouts.

Current activities at the Langley Research Center include testing and analysis of small scale isotropic cylinders and very large waffle stiffened cylinders with cutouts. The NASTRAN finite-element program was used to perform the analytical studies of the buckling characteristics of these cylinders. Analytical studies were made of an isotropic cylinder with a single circular cutout at the midlength of the cylinder and a waffle stiffened cylinder with two diametrically opposed rectangular cutouts at midlength. The sizes of the cutouts were changed to determine the effect on the buckling load. The current paper describes the details of the NASTRAN analysis, presents some of the analytical results, and makes a comparison with experimental results for the buckling of a typical isotropic cylinder with a circular cutout.

## TEST CYLINDERS

### Isotropic Cylinder

The isotropic cylindrical shell test specimen studied in this investigation was 25.4 cm long, had a shell radius of 10.2 cm and a wall thickness of 0.025 cm. The test specimen was made from Mylar<sup>1</sup> polyester film. The modulus of elasticity of this material was experimentally determined to be equal to 5.0 GN/m<sup>2</sup> and Poisson's ratio was taken from reference 5 to be equal to 0.3. A series of single circular cutouts with selected radii

<sup>1</sup>DuPont registered trademark.

ranging up to approximately 3.11 cm were cut into the cylinder wall at mid-length. Thick aluminum end plates were attached to the ends of the cylinder to provide a clamped end boundary condition. A concentrated compressive force was applied at the center of the top end plate.

#### Waffle Stiffened Cylinder

A large waffle stiffened cylindrical shell soon to be tested is illustrated in figure 1. The cylinder has a radius of 1.53 m, a length of 2.39 m, and a skin thickness of 0.25 cm. The cylinder material is aluminum which has a modulus of elasticity of  $68.9 \text{ GN/m}^2$  and a Poisson's ratio of 0.333. The integral waffle stiffeners consist of circumferential rings and longitudinal stringers each with rectangular cross-section. A potential test configuration which was selected for the analytical study has two diametrically opposed rectangular cutouts of equal size located at the cylinder midlength. The rectangular cutouts have a circumferential arc length of 0.61 m and a longitudinal dimension of 0.69 m. The cylinder will be tested in axial compression in a test fixture which approximates clamped end boundary conditions.

#### NASTRAN MODELS

##### General Comments On Modeling and Boundary Conditions

A structural model should involve sufficient detail to represent accurately the physical problem yet be as simple as possible to reduce the computational cost. Since a curved plate element is not yet available in NASTRAN, a cylindrical shell must be modeled by the use of flat plate elements. This limitation requires that a relatively large number of circumferential grid points be used to obtain an accurate solution. In addition, it is the recommendation of reference 6 that NASTRAN quadrilateral plate elements be restricted to side dimension ratios between 1:1 and 1:1.5. Compliance with this recommendation requires that a correspondingly large number of gridpoints be used in the longitudinal direction.

The accuracy of the results for the buckling of cylinders without cutouts has been shown in reference 7 to depend on the number of grid points contained within a buckling mode half wave. These results indicate that approximately 3 grid points per half wave are required for an accuracy within 5 percent for stiffened cylinders, while approximately 5 grid points per half wave are required for an isotropic cylinder for the same accuracy. Reference 7 also suggests that the rotation about the radial axis be restrained at all grid points for cylinders modeled with flat plates. Low buckling loads are obtained if this restraint is not imposed because of the low inplane rotational stiffness of two nearly coplanar intersecting flat plates. This phenomenon is discussed further in reference 8.

The number of grid points necessary to model a structure accurately can be significantly reduced by taking advantage of existing loading and geometric symmetry. All of the models considered in this investigation had at least two planes of symmetry. For the model with one cutout at cylinder midlength, one plane of symmetry contained the cutout center and the cylinder axis of revolution, and the second plane passed through the cylinder at midlength normal to the axis of revolution. For cylinders containing two diametrically opposed holes at cylinder midlength, a third plane of symmetry exists which includes the axis of revolution and is normal to the cylinder diameter containing the two cutout centers. The applied loads were also symmetric since the concentrated load applied to the isotropic cylinder and the load resultant associated with the uniform end shortening of the waffle stiffened cylinder were collinear with the axis of revolution.

Taking advantage of these symmetry properties allows a cylinder with one cutout to be equivalently modeled by a one-quarter cylindrical segment and a cylinder with two cutouts to be represented by a one-eighth segment as illustrated in figure 2. These segments contain one true boundary (line 1 in figure 2) for which boundary conditions are prescribed to represent the actual edge conditions. In addition, there are three artificial boundary lines which have either symmetric or antisymmetric constraints imposed upon them. There are eight possible combinations of the symmetric and antisymmetric boundary constraints that can be imposed, and each combination should be considered to insure that the lowest eigenvalue has been found. In this

investigation results are presented only for symmetric boundary constraints.

The buckling capability provided by NASTRAN in Rigid Format 5 is a linear bifurcation buckling analysis for which the bifurcation occurs from a linear prebuckling state. This Rigid Format does not permit different prebuckling and buckling boundary conditions to be imposed. When the buckling of a thin cylindrical shell is approximated by a linear bifurcation buckling analysis, it is often necessary to impose different prebuckling and buckling boundary conditions. The buckling boundary conditions that are usually imposed for clamped or simple support conditions consist of one of the four sets of distinct boundary conditions at each end of the shell which accompany the formulation of the eighth order partial differential equation derived from classical shell theory. The capability of imposing different prebuckling and buckling boundary conditions was made possible in the present investigation through the use of a DMAP alter sequence which was provided by the NASTRAN Systems Management Office through the courtesy of Malcolm W. Ice of Boeing Computer Sciences, Inc. This DMAP sequence is presented in the appendix.

The prebuckling and buckling boundary conditions used in this investigation are presented in table I. The numbers 1, 2, and 3 in this table represent constrained displacements along the radial, circumferential and axial directions, respectively (see fig. 2) and the numbers 4, 5, and 6 represent constrained rotations about these three axes in a system of cylindrical coordinates. In this investigation one simple support and two clamped buckling boundary condition sets were examined. The prebuckling simple support boundary conditions allow uniform free expansion in the radial direction. The simple support buckling boundary condition set consisted of zero radial and circumferential displacements, zero edge bending moment, and a zero axial load perturbation. In the usual shell theory notation these conditions correspond to  $w = v = M_x = N_x = 0$ . The clamped prebuckling boundary conditions allowed axial displacements to occur freely and constrained all other edge displacements and slopes. One set of clamped buckling boundary conditions (case I) was identical to the prebuckling set. This is consistent in shell theory notation to setting  $N_x = v = w = w_{,x} = 0$  where  $w_{,x}$  represents the first derivative of the radial displacement with respect to the axial coordinate. The second clamped buckling boundary condition set

(case II) constrained all rotations and displacements. This is consistent in shell theory notation to setting  $u = v = w = w_{,x} = 0$  where  $u$  represents the axial displacement.

### Isotropic Cylindrical Models

Two NASTRAN modeling configurations were used to study the isotropic cylinder. The first configuration was a model of the complete cylinder without a cutout, and was used to determine the grid point network fineness necessary to provide an acceptable comparison with known analytical results. The uniformly spaced network of 720 grid points used for this model consisted of twelve axial stations and sixty circumferential stations. Following the suggestion of reference 7, the rotation about the radial axis was constrained for all grid points. The boundary conditions for this model were clamped case II as described above. The shell wall was modeled by CQUAD2 plate elements and the applied load resulted from imposing a uniform axial displacement.

The second model configuration was intended to simulate an experimental parametric study of the effect of a single unreinforced circular cutout on the buckling of a cylinder loaded by axial compression. Symmetry properties made it possible to represent this problem by an equivalent one-quarter cylindrical segment. A schematic representation of the cylinder geometry and end plate model is presented in figure 3(a). The aluminum end plate was modeled by a framework consisting of CBAR beam elements. The framework included one CBAR element between the grid point at the center of the end plate and each of the circumferential grid points on the shell boundary, and a CBAR element between each circumferential grid point around the cylinder boundary. The stiffness of these bar elements was extremely high ( $2.9 \text{ GN-m}^2$ ) to simulate the relative rigidity of the end plate. A concentrated axial force was applied at the grid point located at the center of the end plate.

The grid point network used for a typical circular cutout with radius  $a$  is presented in figure 3(b). An exploded view of the grid point refinement used in the vicinity of the cutout is presented in detail A. A very fine grid point network was used in the vicinity of the cutout to represent the high local prebuckling stress gradients shown to exist in this region by several authors (e.g., ref. 9 and 10). The extent of this highly refined

grid point network (detail A) was three hole radii and was guided by the prebuckling stress distribution presented in reference 9. Five cutout radii were considered ranging from approximately 0.406 cm to 1.27 cm and the corresponding models contained from 334 to 362 grid points. CQUAD2 and CTRIA2 plate elements were used to model the shell wall. Only symmetric boundary constraints were considered along the artificial boundary lines to limit the computational costs.

#### Waffle Stiffened Cylindrical Models

Four separate models were used in studying the buckling behavior of the waffle stiffened cylinder shown in figure 1. Details of the four models are presented in figure 4. The first configuration (model A) was a model of the complete cylinder without cutouts. The uniformly spaced network of 540 grid points used for this model consisted of nine axial stations and sixty circumferential stations. The second configuration (model B) was a one-eighth cylindrical segment with grid point spacing identical to model A and included 80 grid points. The third configuration (model C) was developed from model B by removing two grid points and the associated elements in order to represent two diametrically opposed cutouts at the cylinder midlength. The cutouts in the cylinder represented by model C were rectangular and have a circumferential arc length and axial length equal to 0.64 m and 0.60 m respectively. The actual cylinder shown in figure 1 was modeled using CQUAD2 flat plate elements to represent the skin and CBAR elements to represent the rings and stringers. Since the spacing of rings and stringers was closer for the actual cylinder than for model C, equivalent properties were assigned to the CBAR elements on the PBAR card. Each CQUAD2 element was bounded on all four sides by a CBAR element. The fourth configuration (model D) was also a one-eighth cylindrical segment representing a cylinder with two equal diametrically opposed rectangular cutouts. Two cutout sizes were considered for model D; one with dimensions 0.61 m by 0.69 m, and the other with dimensions 0.91 m by 0.69 m in the circumferential and axial directions, respectively. The grid point network in the vicinity of the hole was refined for model D such that a skin panel bounded by rings and stringers was represented by four CQUAD2 plate elements. CTRIA2 plate elements were used to make

the transition between regions of the shell with different grid point spacing. The grid point refinement in the vicinity of the hole was guided by the results for model C and by the high local prebuckling stress gradient expected to exist in this region. Model D contained 424 grid points. The hole edges for both models C and D were reinforced by rings and stringers with the properties identical to those used in the adjacent interior stiffener elements.

A uniform axial displacement was the applied loading condition for all four models. Boundary conditions used for these models included simple support, clamped case I, and clamped case II conditions as described in table I. The rotation about the radial axis was constrained for all grid points. Only symmetric boundary constraints were considered along the artificial boundary lines of models B, C, and D.

## RESULTS

### Isotropic Cylinders

The results of the NASTRAN study on the effects of a circular cutout on the buckling of a cylindrical shell loaded in axial compression are compared in figure 5 with some typical experimental results taken from reference 1. The buckling loads,  $P$ , of these studies have been nondimensionalized by the classical theoretical buckling load,  $P_{CL}$ , of a cylindrical shell without a cutout. These normalized buckling loads are plotted as a function of a non-dimensional geometric parameter

$$r = a/(Rt)^{1/2}$$

where  $a$  is the cutout radius,  $R$  is the shell radius, and  $t$  is the shell thickness. Analytical prebuckling solutions (e.g., ref. 9) and experimentally determined buckling loads have been shown to be related to this parameter.

The experimental results indicate that it is possible to identify ranges of the parameter  $r$  for which there were different buckling characteristics. For  $r$  less than approximately 0.5, it appears that there was no effect of the cutout on the experimental buckling load, and the familiar general collapse diamond pattern was always the buckling mode

(represented by square symbols on figure 5). For values of  $r$  between approximately 0.5 and 1.2 there was a sharp decline in the buckling load, and the shell still buckled in the general collapse pattern. It is suggested in reference 1 that the prebuckling stress concentration around the hole is apparently of sufficient magnitude to cause the hole region to snap into a local buckling configuration which could in turn provide enough of a disturbance at these applied stress levels to cause general collapse. For values of  $r$  greater than approximately 1.2 a stable local buckling mode occurred in the vicinity of the hole (represented by circular symbols on figure 5) which was followed by the general collapse of the shell when a small additional load was applied. The buckling loads continue to decline in this range as  $r$  is increased but at a much lower rate than for the previous range. For the larger values of  $r$ , visible local prebuckling deformations normal to the shell surface were observed in the region of the cutout implying a local nonlinear prebuckling behavior.

The buckling load from NASTRAN for the complete cylindrical model without a cutout was fourteen percent greater than the classical theoretical value. The mode shape consisted of fourteen circumferential half waves and one axial half wave. The model therefore had approximately four grid points per circumferential half wave. The solution took 4079 CPU seconds with a core storage of 300000<sub>8</sub> words on a Control Data Corporation 6600 computer. A greater refinement in the circumferential direction did not appear worth the cost. One suggestion for reducing the CPU time required to obtain a solution might be to reduce the number of axial grid points since for the present solution there were twelve grid points per axial half wave. However, this would increase the ratio of side lengths of the quadrilateral elements to values well above those recommended in reference 6 and the accuracy of the resulting solution may be questionable.

The NASTRAN results for the equivalent one-quarter cylindrical segment model for cylinders with cutouts are represented by the dashed curve on figure 5. The buckling mode shape predicted by NASTRAN for all cases considered was a local buckling mode in the region of the cutout. The existence of this local buckling mode shape gives credence to the suggestion that general collapse in the experiment was caused by a local buckling mode for

values of  $r$  between 0.5 and 1.2. For values of  $r$  less than approximately 1.5 the NASTRAN results provided an upper bound for the experimental results as should be expected from a solution technique based on the minimization of the total potential energy. For larger values of  $r$  the nonlinearities of the cutout problem become more pronounced and the linear bifurcation analysis provided by NASTRAN gives results below the experimental values. The limitations of using a linear bifurcation analysis to approximate a nonlinear buckling phenomenon are pointed out in reference 4 in which a comparison is made between linear and nonlinear buckling solutions for some typical thin shell structures (e.g., the collapse of a cylindrical panel due to an applied concentrated lateral load).

#### Waffle Stiffened Cylinders

A summary of the NASTRAN results for models of the waffle stiffened cylinder illustrated in figure 1 is presented in table II, and includes eight different cases. The critical buckling loads calculated using NASTRAN are normalized by the buckling load for a stiffened simply supported cylinder without cutouts obtained from the analysis presented in reference 11. A bar graph is presented in figure 6 to illustrate graphically the differences in results for the eight different solutions.

The NASTRAN results for the complete cylinder without holes (model A) with simple support end conditions was within two percent of the reference buckling load. The one-eighth cylindrical segment (model B) with simple support end constraints also agreed with this result, indicating that the symmetric constraints applied along the artificial boundary lines yielded the minimum solution. A NASTRAN generated plot of the buckling mode shape for models A and B is presented in figure 7. The mode shape included one longitudinal and eight circumferential half waves, which was the same as predicted by reference 11. The CPU time to generate these two results was 5.5 minutes for model B and 79 minutes for model A. Although all eight combinations of symmetry and antisymmetry were not executed for model B, it is projected that even if they had been, the cumulative time would have been less than that required for the solution for the entire cylinder (model A). In addition, a larger core storage is required for the execution of the entire cylinder model.

Buckling results obtained using models C and D for a simply supported cylinder containing two diametrically opposed holes are presented in table II as cases 3 and 4. The hole sizes for these two models were slightly different due to differences in modeling. The critical compressive buckling loads are in relatively close agreement (within eight percent). Contour plots of the buckling mode shapes for the two models is presented in figure 8.

Displacements have been normalized with respect to the maximum displacement amplitude which has been scaled to a value of 100. A discussion of the contour plotting technique is presented in reference 12. These two mode shapes are similar in character with the largest displacements occurring in the vicinity of the cutout. Although it is assumed for this solution that symmetric constraints exist along the three artificial boundaries (lines 2, 3, and 4 in figure 2), it may be assumed from a study of the displacement contour plots that it probably would not be necessary to exercise all eight combinations of symmetric and antisymmetric constraints to obtain the lowest eigenvalue. For example, an antisymmetric constraint along line 2 should yield essentially the same result as a symmetric constraint along this line since the magnitudes of the buckling displacements in the vicinity of line 2 are relatively small. The difference in the critical buckling load for models C and D with clamped case I boundary conditions (cases 5 and 6) was twelve percent. As for the simple support case, the buckling mode shapes were similar.

There was approximately a five percent decrease in the buckling load for cylinders with clamped case II boundary conditions (cases 7 and 8 in table II) when the circumferential hole dimension was increased by approximately fifty percent. Apparently, the rings and stringers in the vicinity of the hole are sufficiently stiff to allow a redistribution of the prebuckling stress to prevent significant decreases in the buckling load.

## CONCLUDING REMARKS AND RECOMMENDATIONS

NASTRAN has been used to study the complex problem of the buckling of cylindrical shells with and without cutouts. Reasonably acceptable agreement with known analytical results was achieved for isotropic and waffle stiffened cylinders without cutouts when the appropriate prebuckling and buckling boundary conditions were imposed. The capability of imposing different prebuckling and buckling boundary conditions (which is usually required for a linear bifurcation buckling analysis) was made possible through the use of a DMAP alter sequence. For isotropic cylinders with cutouts it was found that NASTRAN provided an upper bound for available experimental results for small cutouts, and provided solutions lower than the experimental results for large cutouts. For the large cutouts, the nonlinearities of the problem become pronounced, and therefore the linear bifurcation buckling analysis capability of NASTRAN cannot be expected to provide more than an approximation to the solution.

The computational cost of conducting a buckling analysis for a structure is several times the cost of performing a static stress analysis for the same model. Therefore, the user of Rigid Format 5 should seriously consider ways to reduce computational costs and the potentially high demands placed on the computational facility. In general, taking advantage of problem loading and geometric symmetries can reduce the cost of performing a buckling analysis. An argument can also be made that it is usually cost effective to select an eigenvalue search range on the EIGB card which is less than the expected eigenvalue to insure that the lowest root is obtained and therefore, that a restart is not required. It is recognized that some modules within the Rigid Format 5 DMAP sequence have greater storage requirements than others. Additional computational cost reductions and improvements in facility management could be made if it were possible to determine core storage requirements for certain DMAP modules before the module is executed. With this information it would be possible to adjust core storage requirements during the execution of a problem to a specified minimum and therefore release unnecessary core. This capability might be achieved automatically on certain computer systems or by the user through exercising the NASTRAN checkpoint and restart feature.

The systematic approach used in formulating a NASTRAN model simplifies the task of generating input data for general shells with complex geometries. Solutions for thin shell buckling problems by the use of NASTRAN, however, require an understanding of structural behavior to interpret properly the results. Therefore, NASTRAN must be used with discretion to obtain buckling loads for general shell structures because of the complexity of the problem, and the limited reported user experience for these problems.

APPENDIX

DMAP ALTER SEQUENCE FOR PRESCRIBING DIFFERENT  
PREBUCKLING AND BUCKLING BOUNDARY CONDITIONS

```
ALTER 2
FILE KDGG=APPEND,SAVE/KNN=SAVE/GM=SAVE $
ALTER 47
LABEL POINT1 $
ALTER 80
PARAM //C,N,SUB/V,N,TEST1/C,N,2/V,N,NSKIP $
COND POINT2,TEST1 $
*ALTER 104
PARAM //C,N,MPY/V,N,NSKIP/C,N,2/C,N,1 $
REPT POINT1,1 $
LABEL POINT2 $
ENDALTER
```

\* - Use ALTER 109 for level 15 or 104 for level 12.

The execution of the alter sequence requires three subcases in the Case Control Deck. Subcase 1 governs the prebuckling solution and subcases 2 and 3 govern the buckling solution.

```
SUBCASE 1
LOAD =
SPC =
MPC =
OUTPUT
```

```
SUBCASE 2
METHOD =
OUTPUT
```

```
SUBCASE 3
SPC =
MPC =
OUTPUT
```

## REFERENCES

1. Starnes, J. H.: The Effect of a Circular Hole on the Buckling of Cylindrical Shells. Ph. D. Thesis, California Institute of Technology, 1970.
2. Tennyson, R. C.: The Effects of Unreinforced Circular Cylindrical Shells Under Axial Compression. Journal of Engineering for Industry. November 1968, pp. 541-546.
3. Brogan, F.; and Almroth, B.: Buckling of Cylinders with Cutouts. AIAA Journal, Vol. 8, No. 2, February 1970, pp. 236-240.
4. Almroth, B. O.; and Brogan, F. A.: Bifurcation Buckling as an Approximation of the Collapse Load for General Shells. AIAA Journal, Volume 10, No. 4, April 1972, pp. 463-467.
5. Seide, P.; Weingarten, V. I.; and Morgan, E. J.: The Development of Design Criteria For Elastic Stability of Thin Shell Structures. AFBMD/TR-61-7, U. S. Air Force, December 31, 1960.
6. Haggemacher, Gernot W.: Some Aspects of NASTRAN Solution Accuracy. NASTRAN: Users' Experiences. NASA TM X-2378, 1971, pp. 47-63.
7. Broliar, Richard H.: A NASTRAN Buckling Analysis of a Large Stiffened Cylindrical Shell with a Cutout. NASTRAN: Users' Experiences. NASA TM X-2378, 1971, pp. 65-84.
8. Zienkiewicz, O. C.: The Finite Element Method in Engineering Science. McGraw-Hill Book Company Inc., 1971, pp. 212-238.
9. Lekkerkerker, J. G.: On the Stress Distribution in Cylindrical Shells Weakened By a Circular Hole. Ph. D. Thesis, Technological University, Delft, Netherlands, 1965.
10. Savin, G. N.: Stress Distribution Around Holes. NASA TT F-607, 1970.
11. Block, David L.; Card, Michael F.; and Mikulas, Martin M., Jr.: Buckling of Eccentrically Stiffened Orthotropic Cylinders. NASA TN D-2960, 1965.
12. Giles, Gary L.; and Blackburn, Charles L.: Procedure for Efficiently Generating, Checking, and Displaying NASTRAN Input and Output Data for Analysis of Aerospace Vehicle Structures. NASTRAN: Users' Experiences. NASA TM X-2378, 1971, pp. 679-696.

TABLE 1.- BOUNDARY CONDITIONS.

	<u>Constrained displacements and rotations<sup>a</sup></u>	
	<u>Prebuckling</u>	<u>Buckling</u>
Simple support - line 1 <sup>b</sup>	2,4,6	1,2,4,6
Clamped case I - line 1	1,2,4,5,6	1,2,4,5,6
Clamped Case II - line 1	1,2,4,5,6	1,2,3,4,5,6
Symmetry - line 2 or 4	2,4,6	2,4,6
Symmetry - line 3	3,4,5	3,4,5
Antisymmetry - line 2 or 4	2,4,6	1,2,4
Antisymmetry - line 3	3,4,5	1,3,4

a.- Numbers 1,2, and 3 represent radial, tangential, and axial displacements and 4,5, and 6 represent rotations about these axes, respectively in a cylindrical coordinate system.

b.- Lines 1,2,3, and 4 are defined in figure 1.

TABLE II.- NASTRAN BUCKLING RESULTS FOR A WAFFLE STIFFENED  
CYLINDRICAL SHELL.

CASE	MODEL	HOLE DESCRIPTION <sup>a</sup>	LOADING	END BOUNDARY CONDITION <sup>b</sup>	$\frac{P^c}{P_{ref}}$
1	A	no hole	uniform displacement, top and bottom	simple support	1.02
2	B	no hole	uniform displacement of top (line 1)	simple support	1.02
3	C	2 holes, 0.64 m x 0.60 m	uniform displacement of top (line 1)	simple support	0.712
4	D	2 holes, 0.61 m x 0.69 m	uniform displacement of top (line 1)	simple support	0.774
5	C	same as case 3	uniform displacement of top (line 1)	clamped case I	0.767
6	D	same as case 5	uniform displacement of top (line 1)	clamped case I	0.875
7	D	same as case 5	uniform displacement of top (line 1)	clamped case II	0.957
8	D	2 holes, 0.91 m x 0.69 m	uniform displacement of top (line 1)	clamped case II	0.905

<sup>a</sup> Hole size for complete cylinder located at midlength, two holes  $\pi$  radians apart, circumferential by axial dimensions.

<sup>b</sup> Where applicable, symmetric constraints were imposed along all three artificial boundary lines.

<sup>c</sup> The reference load is for a simply supported orthotropic cylinder without holes (reference 11).  
 $P_{ref} = 7.48 \text{ MN}$ .

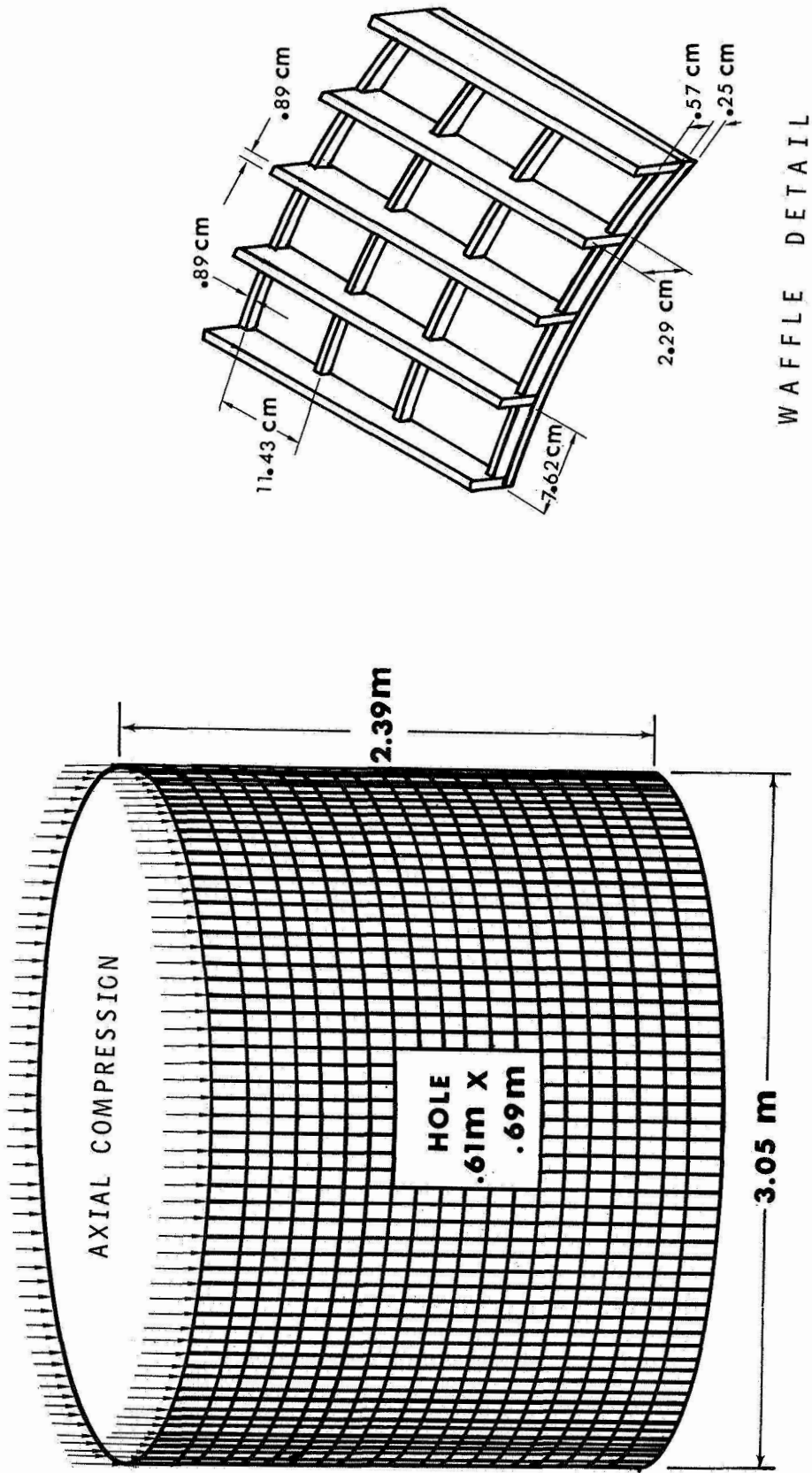
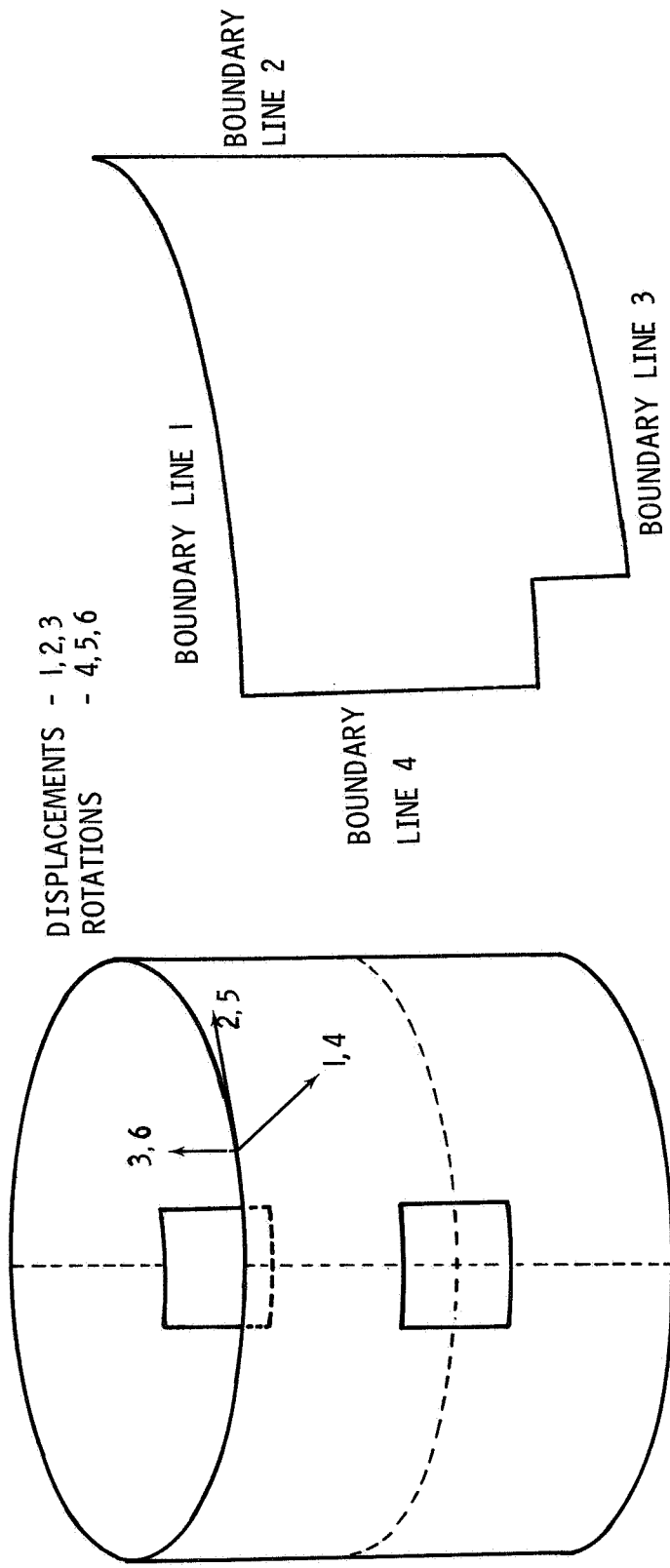


Figure 1.- Waffle stiffened cylinder containing two diametrically opposed holes located at midlength and  $\pi$  radians apart.

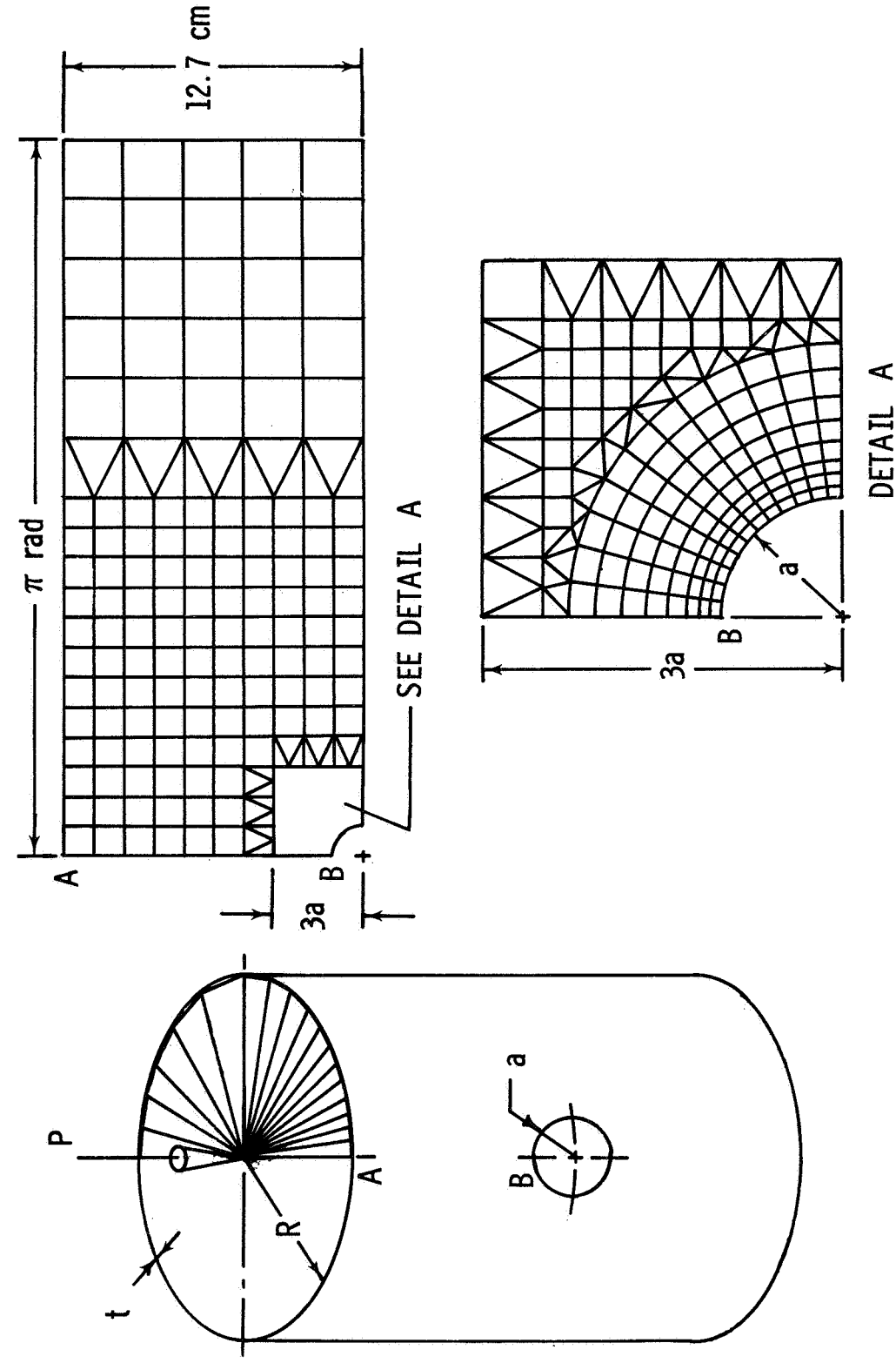


DISPLACEMENTS - 1,2,3  
 ROTATIONS - 4,5,6

CYLINDER WITH TWO DIAMETRICALLY OPPOSED HOLES LOCATED AT MIDLLENGTH

ONE-EIGHTH CYLINDRICAL SEGMENT MODEL

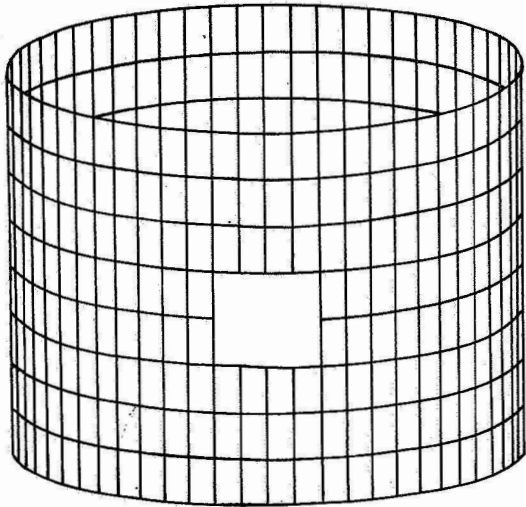
Figure 2.- Illustration of symmetry segmenting technique.



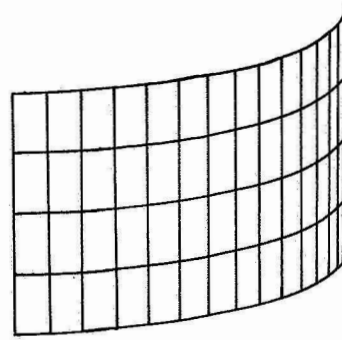
(a) Model Schematic

(b) Grid Point Network

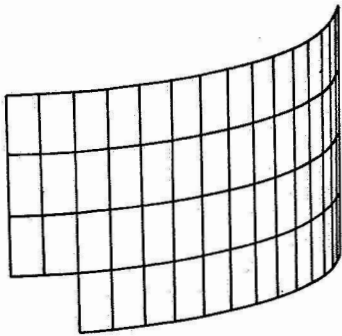
Figure 3.- Model of isotropic cylinder with a circular cutout.



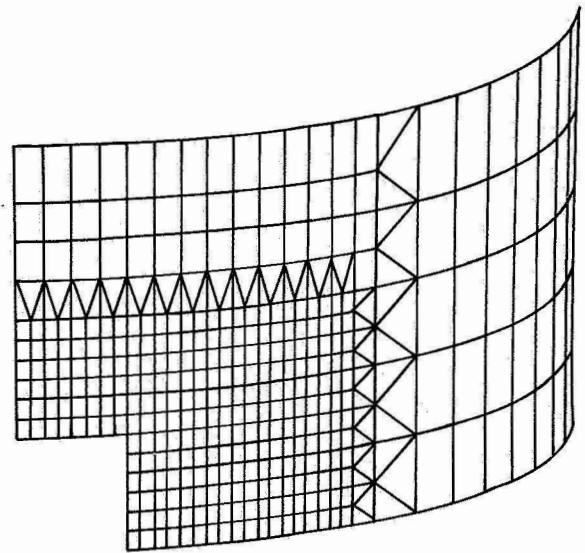
Model A



Model B



Model C



Model D

Figure 4.- Waffle stiffened cylindrical shell NASTRAN models.

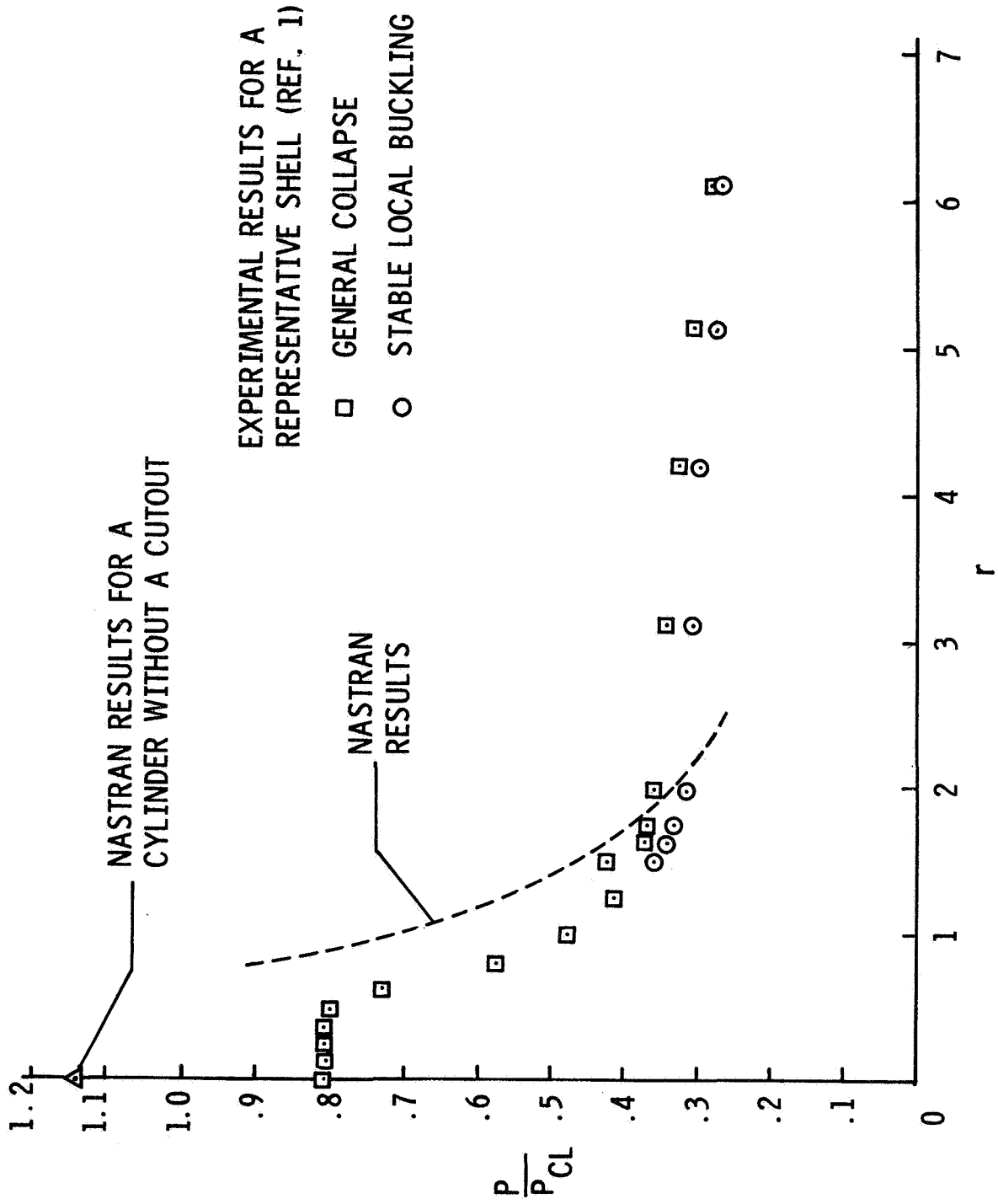


Figure 5.- Effect of circular cutout size on isotropic cylindrical shell buckling load where  $r$  is equal to  $a/(Rt)^{1/2}$ .

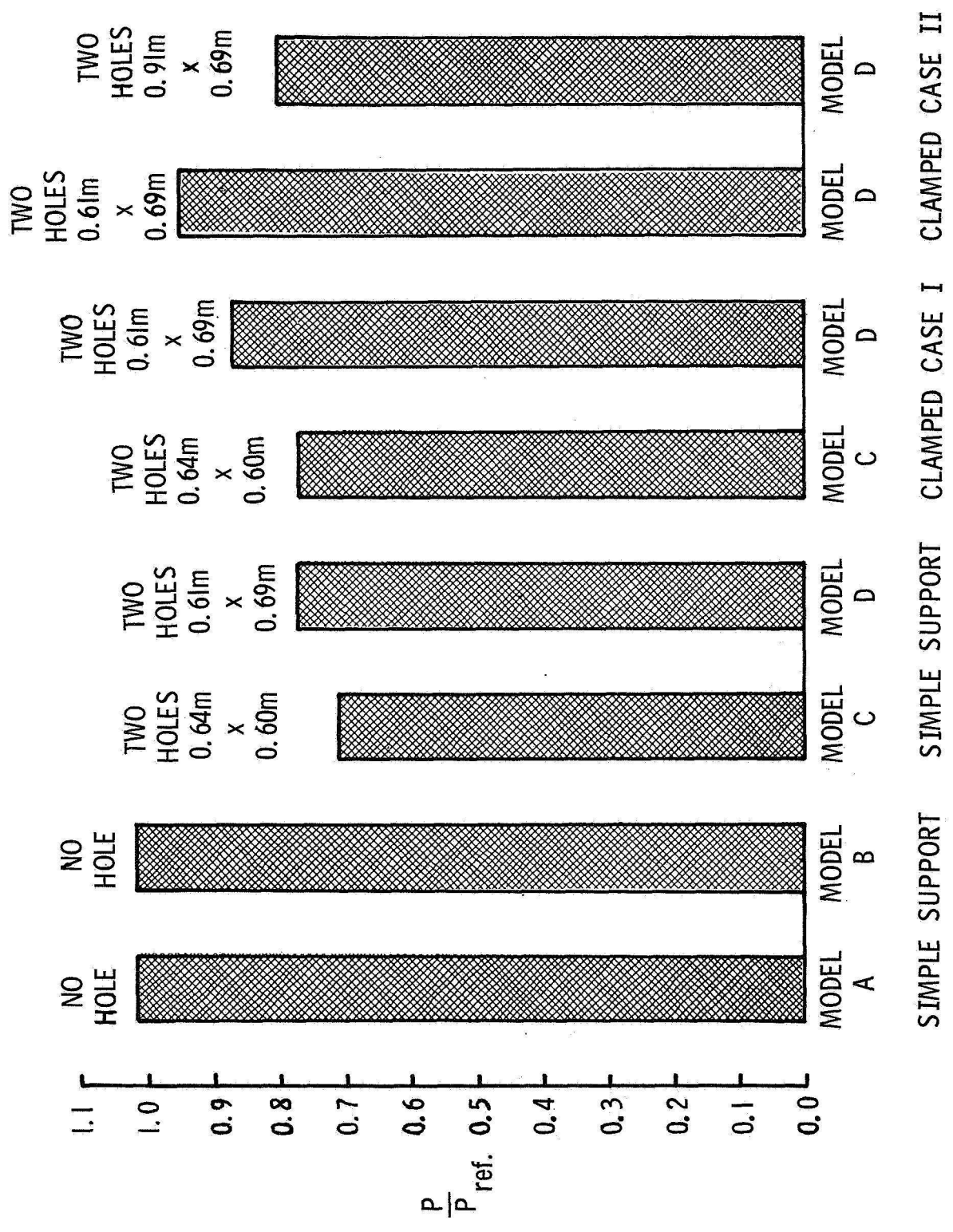
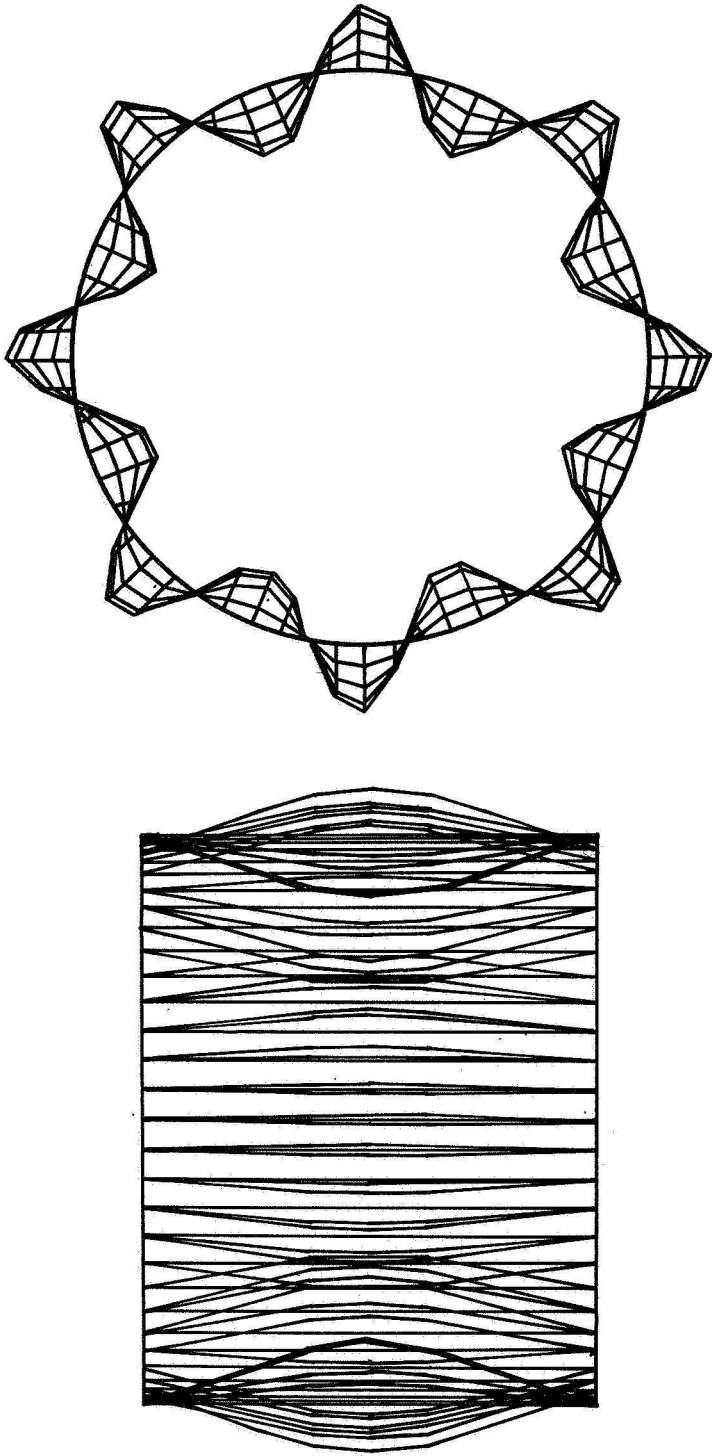
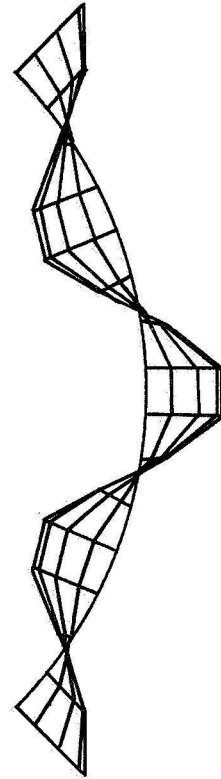


Figure 6.- Critical buckling load for waffle stiffened cylinders subjected to uniform axial displacement loading.

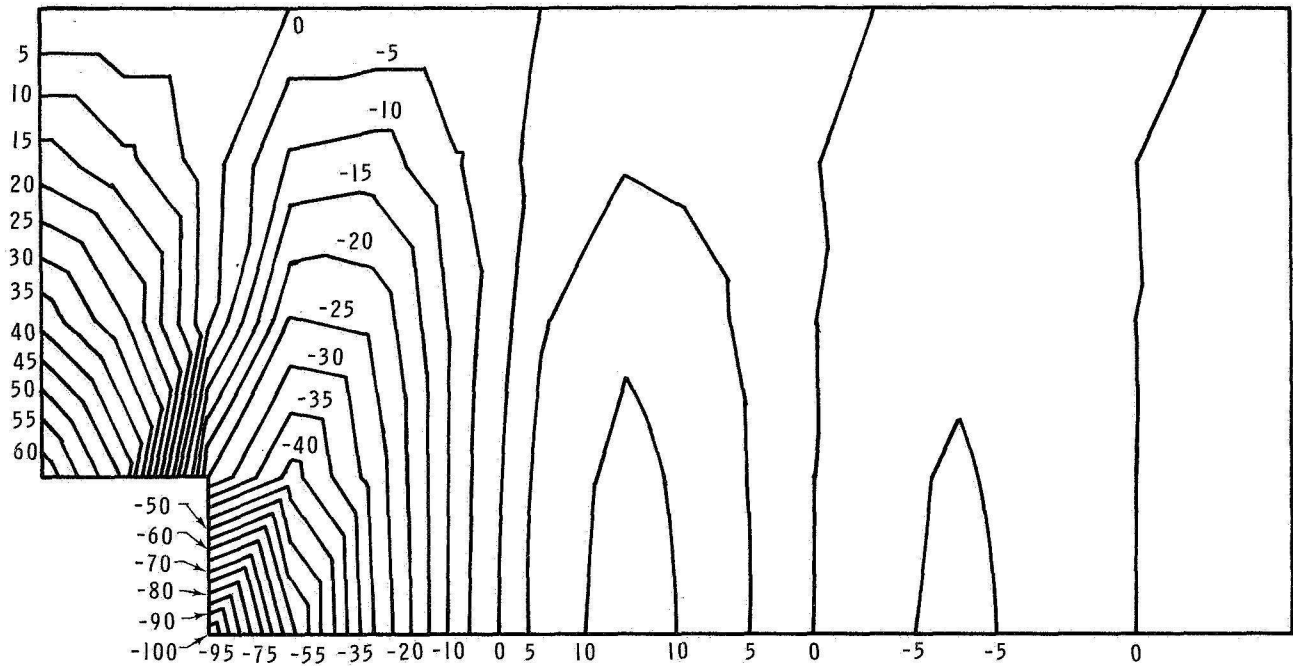


(a) Model A Results.

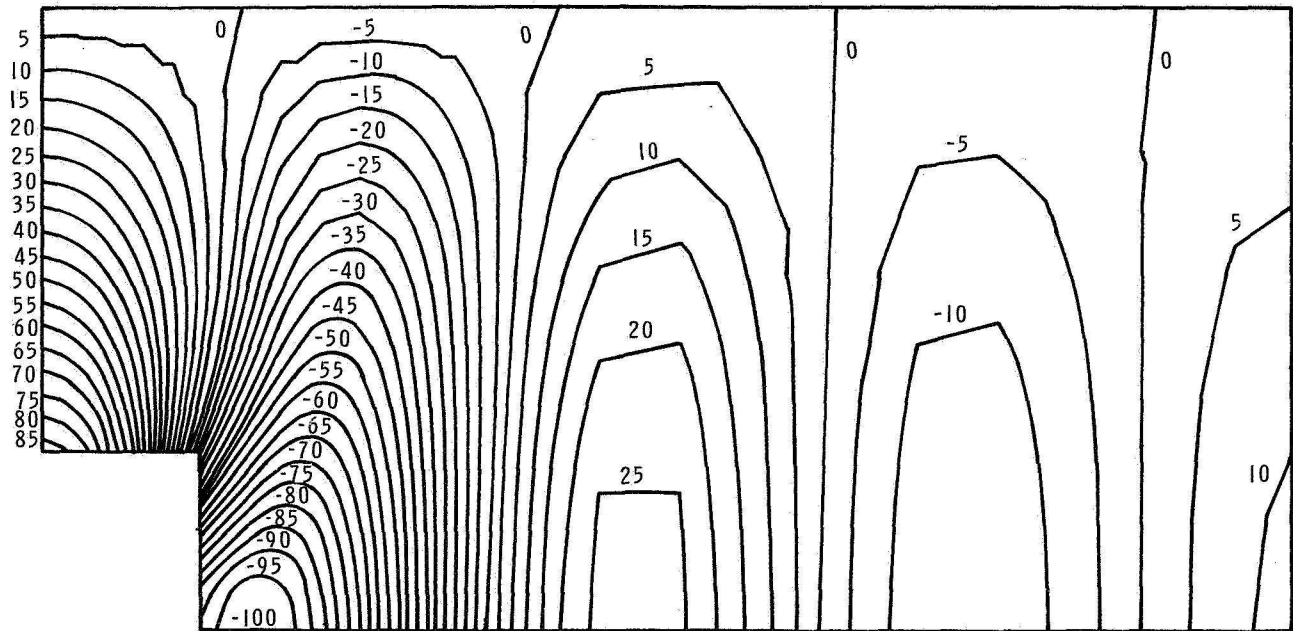


(b) Model B Results.

Figure 7.-- Buckling mode shapes for waffle stiffened cylindrical shell showing identical results for models A and B.



(a) Model B.



(b) Model C.

Figure 8.- Radial buckling displacement contour plot for a one-eighth segment of a simply supported waffle stiffened cylinder. All displacements scaled to a maximum displacement of 100.



ANALYSIS AND DESIGN OF  
ON-GRADE REINFORCED CONCRETE  
TRACK SUPPORT STRUCTURES

By Francis G. McLean, Ronald D. Williams,  
and Lance R. Greening

Westenhoff and Novick, Inc.  
Chicago, Illinois

SUMMARY

For the improvement of rail service, The Department of Transportation, Federal Rail Administration, is sponsoring a test track on the Atchison, Topeka, and Santa Fe Railway. The test track will contain nine separate rail support structures, including one conventional section for control and three reinforced concrete structures on grade, one slab and two beam sections. The analysis and design of these latter structures (ref.1) was accomplished by means of the finite element method, NASTRAN, and is presented herein.

INTRODUCTION

In order to provide fast, economical rail service, the development of improved, low maintenance track support systems is required. While seemingly a simple problem, the system of rail-fastener-structure-subgrade poses complex interaction problems. In addition, a random distribution of asymmetric lateral loads is applied by moving rail traffic.

In an effort to provide test data for use in developing such support systems, three non-conventional track structure systems are to be included as parts of the approximate two mile length of test track to be constructed by the U.S. Department of Transportation and the Santa Fe Railway Company. The three non-conventional track support structures, each 244 meters in length, are: twin cast-in-place continuously reinforced concrete beams joined by gaging (cross) members; a continuously reinforced concrete slab; and a system of twin precast beams made continuous at abutting ends and joined by gaging members.

As part of the research program related to developing practical, low maintenance, high quality track structures, studies

were carried out (refs. 2 and 3) to produce performance criteria and specifications for such structures. Analyses and tests showed that distinct subgrade pressure pulses are imparted by every passing axle load, and that subgrade deterioration is related to the number of impulses. As a result of those studies it was concluded that track support structures having a high structural rigidity would effectively reduce the load cycles to one per truck. A specific stiffness was determined and specified as design criteria, along with vertical and lateral wheel-rail load magnitudes. These criteria formed the basis for the static analyses performed to design and evaluate the sections shown in figure 1.

In the design and construction of the test sections the goal of removing all possible secondary variables and "weak links" was pursued in an effort to create structures whose performance and safety would be unimpaired. A test embankment was designed and constructed, under close control, to create uniform subgrade conditions throughout the entire test track. An unusual rail fastener was selected to insure that it would not be a controlling "weak link."

These instrumented systems will be integral parts of the Santa Fe's single track mainline, and will carry both eastward and westward trains approaching 50,000,000 gross tons annually, at speeds up to 120 kilometers/hour. Thus, the systems will be subjected to rigorous service, and it is anticipated that significant results for future use will be produced through the instrumentation and the observation of the performance of the components of the system.

In order to achieve the necessary safety in design, and handle the complex interaction and boundary conditions, the finite element method was chosen for analysis, and NASTRAN was used as the analytical tool. Design was accomplished using a combination of working stress and ultimate strength methods. All work was done in the British system of units.

## THE FINITE ELEMENT MODEL

The finite element models formulated for analysis are shown in figure 2. The models represent the rail, rail fastener, concrete structures and subgrade.

### Rail

Classically, little attention has been given to the torsional action of the rail in the track system. Hence, only bending

properties were available and the membrane analogy was applied to calculate the torsional coefficient for use in the analyses. CBAR elements were used to represent the rail in the NASTRAN model.

### Fastener

The direct fixation fastener selected for the project provides restraint to the rail in each of the six degrees of freedom. The selected fastener has not been in service, although a smaller scale version is on the market. Prestressed elastomers are utilized to provide restraint cushioning. The prototype fastener was tested to determine an order of magnitude for the load-deflection relations used for the CBAR element. The OFFSET provision was implemented to provide geometrical compatibility for the rail-fastener-slab connectivity.

### Slab and Beams

Since the distribution of subgrade pressures was desired as a result of the analyses, and the slab and beams were orthotropic in nature, the CQUAD 2 element was used with a MAT 2 formulation (ref. 4) to yield orthotropic properties. Longitudinal stiffnesses were as specified by the design criteria, while transverse stiffnesses were the result of transverse reinforcing for temperature and construction requirements. All design was based on cracked section properties.

### Subgrade

The subgrade was represented by three grounded CELAS 1 elements connected to each GRID point having CQUAD connectivity. One spring was in the vertical plane to represent a Winkler foundation. Properties used for these springs were obtained from field plate bearing tests (refs. 1 and 5) as shown in figure 3. Correlation for these properties were obtained using Vibroseismic methods (refs. 6, 7 and 8), and construction control tests obtained during construction of the test embankment (refs. 9 and 10). Two springs were used in the horizontal plane (longitudinally and transversely) to represent tractions on the concrete-subgrade interface. The elastic properties were derived from field tests (ref. 1) using large slabs with surcharge pressures; typical results are presented in figure 3.

## ANALYSIS PROCEDURES

A single preprocessor was written to generate the bulk data required for the structures, varying geometry, material properties, and connectivity as required. All analyses were performed on the Control Data Corporation Cybernet System using NASTRAN and, for simple parametric studies, EASE. Rigid Format 1, with RESTART, was used for all NASTRAN activity.

EASE models of a rail-fastener system on an infinitely stiff supporting structure were analyzed to determine the influence of rail torsional properties, and the effect of variation of fastener properties, on the distribution of load to the structures.

### Influence Length Study

A single axle and single truck load, figure 4, were applied to long models of both structures (2220 GRID, 520 CBAR, 5550 CELAS 1, and 1272 or 1440 CQUAD 2, having about 5.2 degrees of freedom average per GRID) to obtain influence lengths and approximation errors. Results of these studies indicated that one-half car length models would be satisfactory, but lateral load positioning required analysis of car length models until the occurrence of deflected structure symmetry was verified.

### Design Analyses

Car length models were used to analyze both the infinite and finite (end of test section) cases. Single Point Constraints were used to create a coupler to coupler model with plane of symmetry conditions in the deflected structure, while Multi-Point Constraints were used to give a mid-car to mid-car model with antisymmetric conditions in the deflected structure. Models with "softened" subgrade were also analyzed for the infinite case. Results of these analyses are shown in figures 5 and 6.

The finite structures were modeled by allowing inplane vertical displacements with no rotations of the GRIDs on one boundary, while allowing complete freedom on the other boundary for all but the rail GRIDs. Rail GRIDs were allowed to displace in the vertical plane with no rotation. A comparison of the spread of the beam structures, obtained for the infinite and finite cases, is shown on figure 6.

## DESIGN

ELFORCE output was used to verify the adequacy of the design criteria, to apportion reinforcing for the slab and beam structures, and to design tie-rods to restrain beam spread. The beam structures were reinforced for combined biaxial bending and torsion. Subgrade pressure distributions and structure-subgrade shears were evaluated, and validity of properties verified. Regions or items of probable "high maintenance" were located and inspection procedures formulated.

The project will be instrumented for strains in the rails, reinforcing, and embankment; for stresses in the subgrade; and for loads transmitted through the fasteners. In addition, a calibration series of static loads has been recommended to allow verification of the design procedures and analytical methods, and to allow a correlation base for dynamic readouts and subsequent analyses.

## CONCLUSION

The availability of NASTRAN was invaluable in carrying out this project since the sponsor had specified that no new codes were to be created. A more realistic design was achieved than would have been accomplished using conventional methods (ref. 11), or more simplistic models, which would not have defined the three-dimensional nature of the structure and would have resulted in an inadequate design.

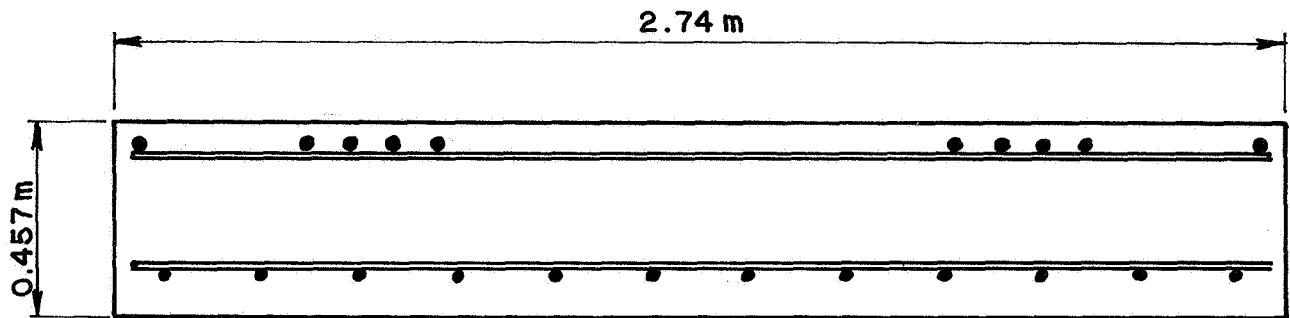
## ACKNOWLEDGMENTS

The work described herein was performed by Westenhoff and Novick, Inc. under contract to the Atchison, Topeka, and Santa Fe Railway. Funding sponsor for the research project is The Department of Transportation, Office of High Speed Ground Transportation, Federal Rail Administration.

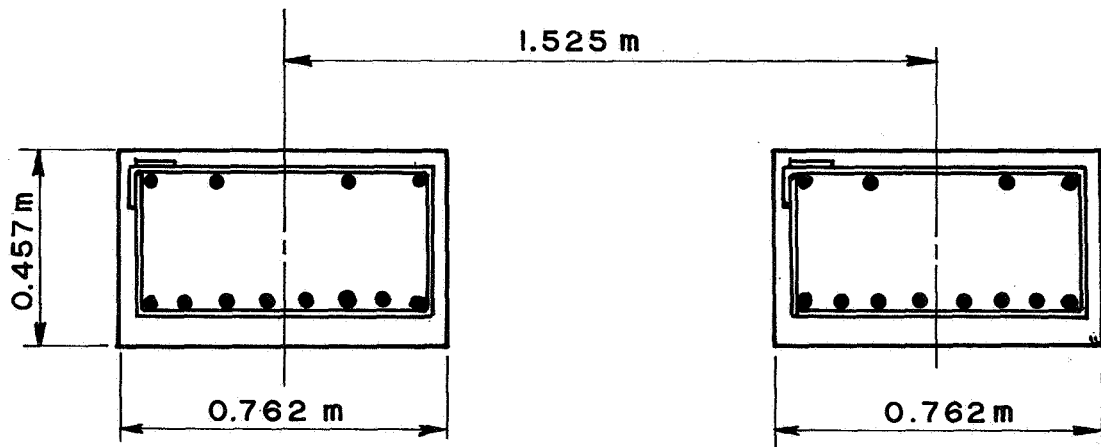
## REFERENCES

1. McLean, F.G., Turnbell, R.C., and Williams, R.D.: Design Report: Non-Conventional Track Structures, Kansas Test Track. Design Report from Westenhoff and Novick, Inc. to U.S. Department of Transportation, 1972.

2. Meacham, H.C., et. al.: Study of New Track Structure Designs, Phases I and II. Research Reports from Battelle Memorial Institute to U.S. Department of Transportation, 1968 and 1969.
3. Meacham, H.C., et. al.: Studies for Rail Vehicle Track Structures. Research Report from Battelle Memorial Institute to U.S. Department of Transportation, 1970.
4. Timoshenko, S.P., and Woinowsky-Krieger, S.: Theory of Plates and Shells. McGraw-Hill, 1959.
5. U.S. Corps of Engineers: Engineering and Design - Rigid Airfield Pavements. EM 1110-45-303.
6. Curro, J.R., Jr.: Vibroseismic Survey, Railroad Test Track Embankment. Report from U.S.C.E. Waterways Experiment Station to U.S. Department of Transportation, 1971.
7. U.S. Corps of Engineers: Engineering and Design - Foundation Subject to Vibratory Loads. EM 1110-45-310.
8. Barkan, D.D.: Dynamics of Bases and Foundations. McGraw-Hill, 1962.
9. Dietrich, R.J., and Salley, J.R.: Embankment Support for a Railroad Test Track, Design Studies. Report from Shannon and Wilson, Inc. to U.S. Department of Transportation, 1971.
10. Dietrich, R.J., and Salley, J.R.: Embankment Support for a Railroad Test Track, Embankment Construction and Instrumentation, Volume I. Report from Shannon and Wilson, Inc. to U.S. Department of Transportation, 1971.
11. Hetenyi, M.: Beams on Elastic Foundation. University of Michigan Press, 1946.

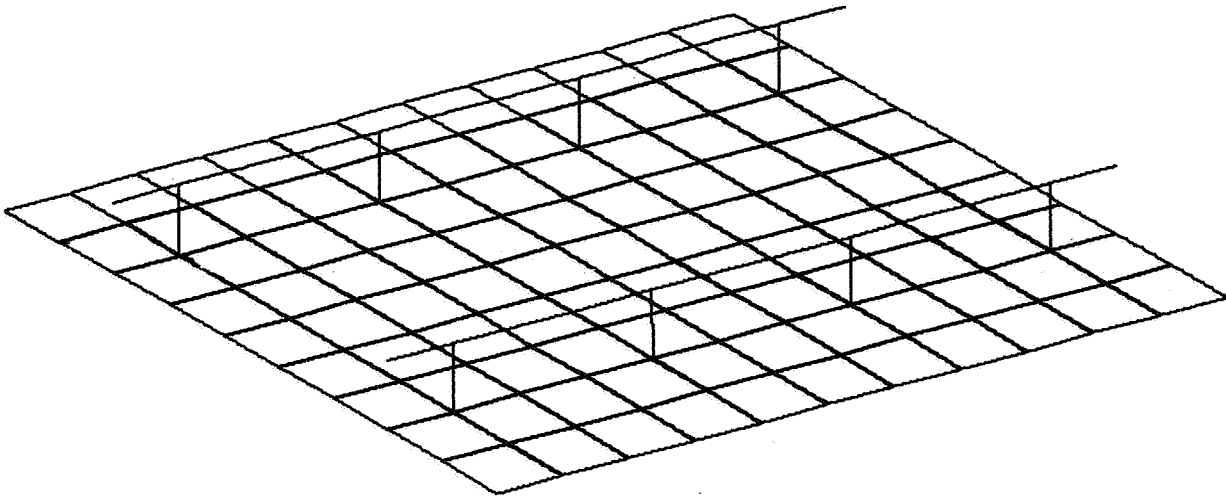


TYPICAL SLAB SECTION

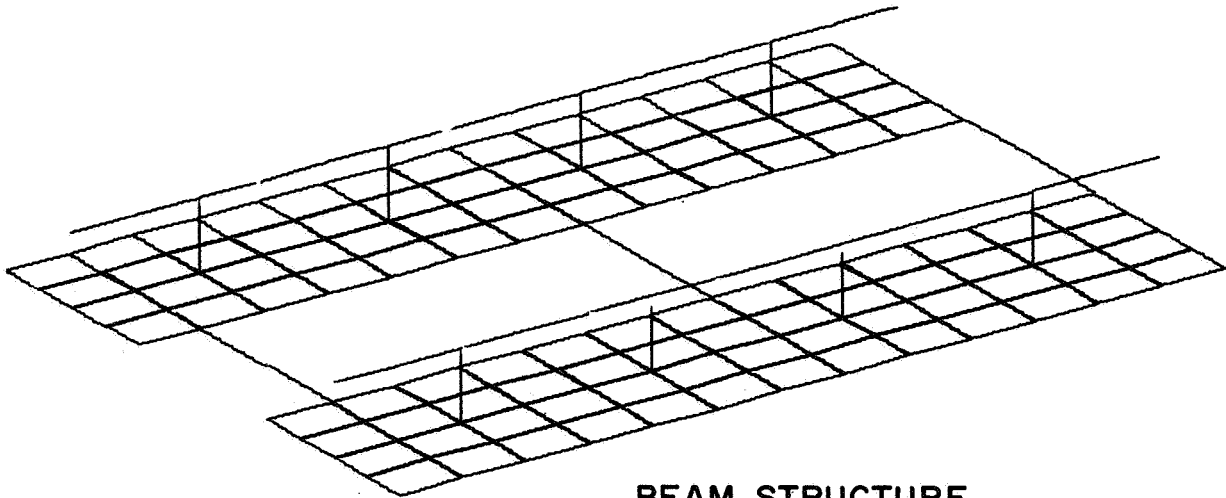


TYPICAL BEAM SECTION

FIGURE I: TYPICAL SECTIONS



**SLAB STRUCTURE**



**BEAM STRUCTURE**

**FIGURE 2: ELEMENT CONNECTIVITY**

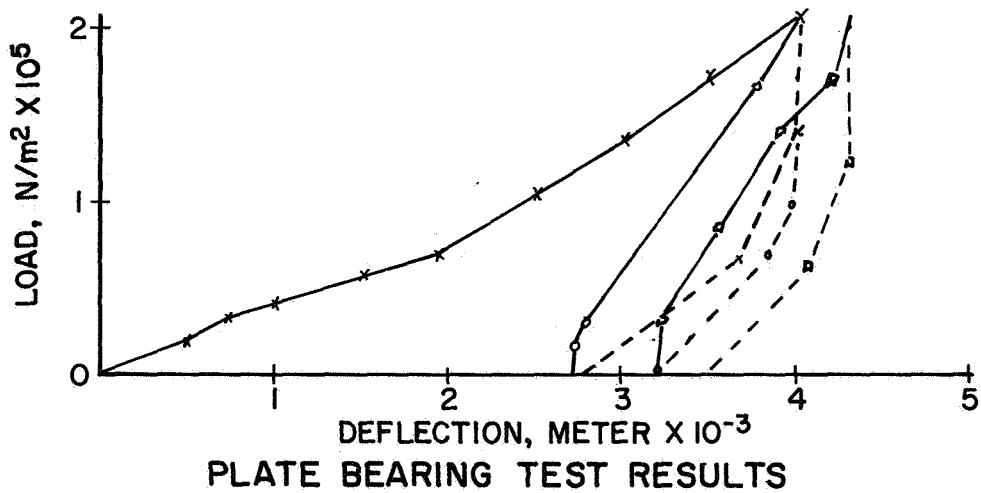
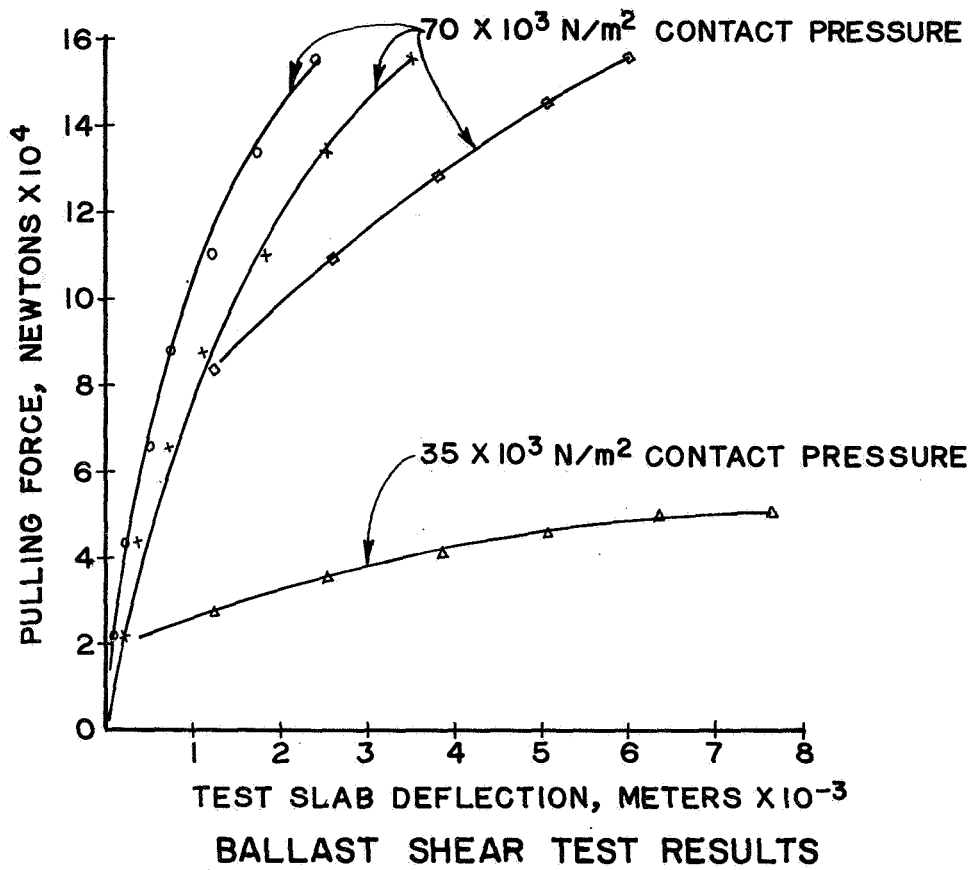
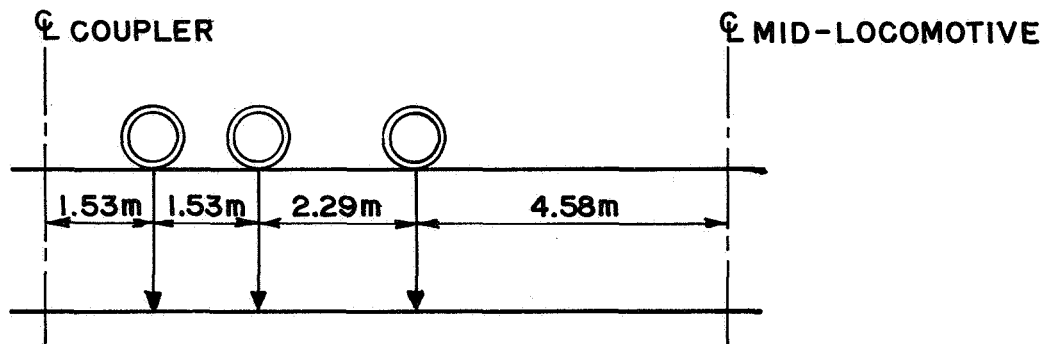
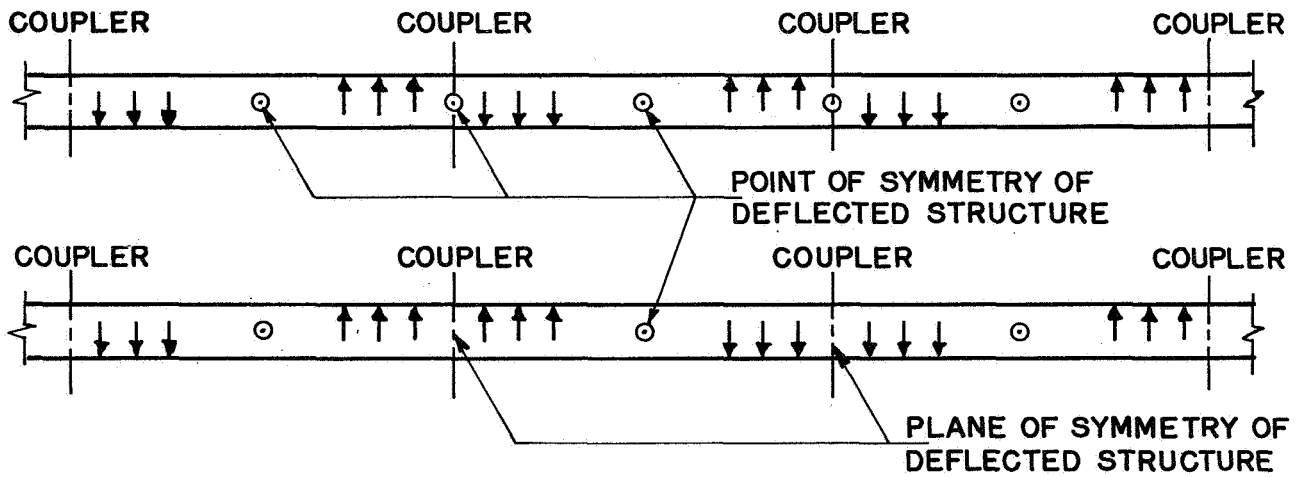


**FIGURE 3**



IDEALIZED LOCOMOTIVE TRUCK



IDEALIZED LATERAL LOAD PATTERN

FIGURE 4

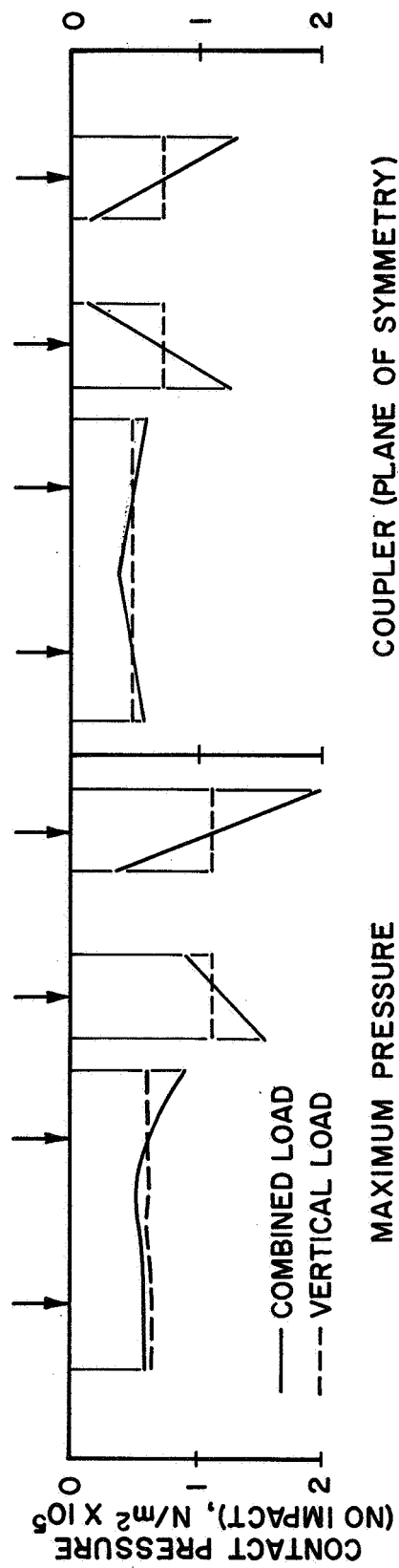
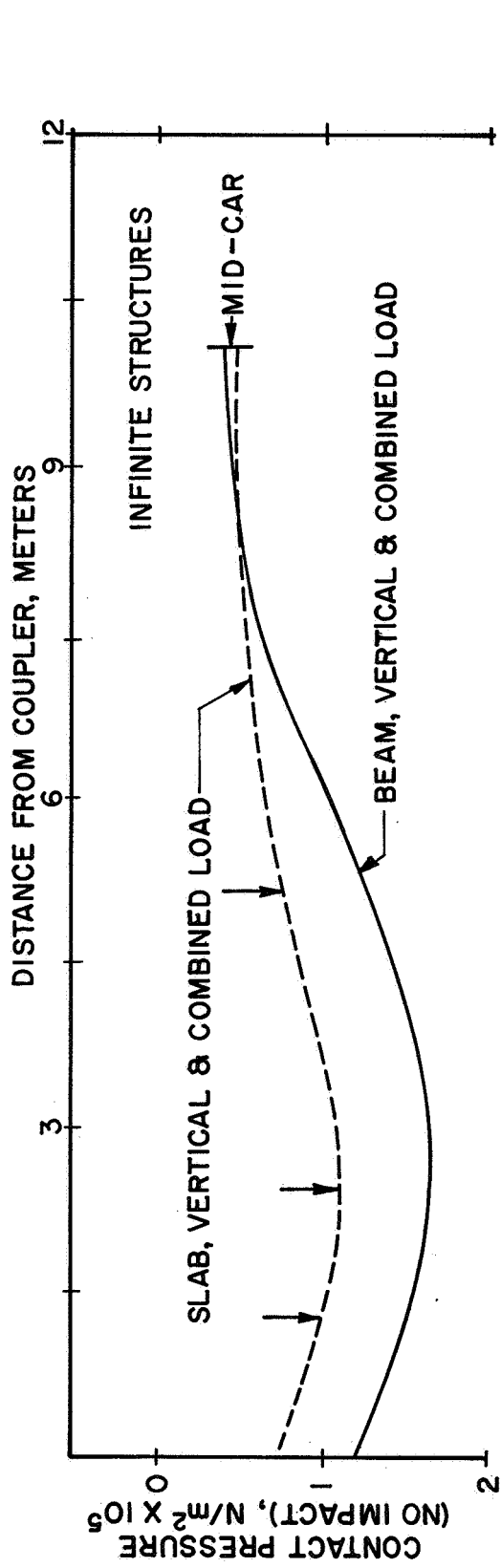


FIGURE 5: CONTACT PRESSURES

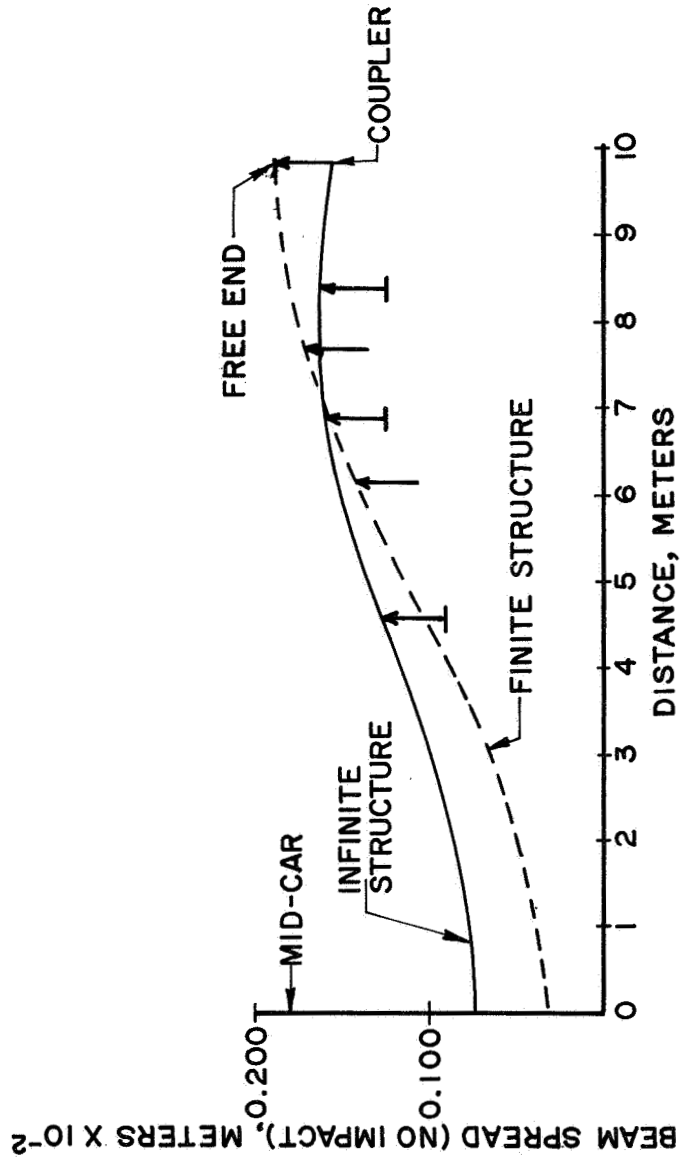
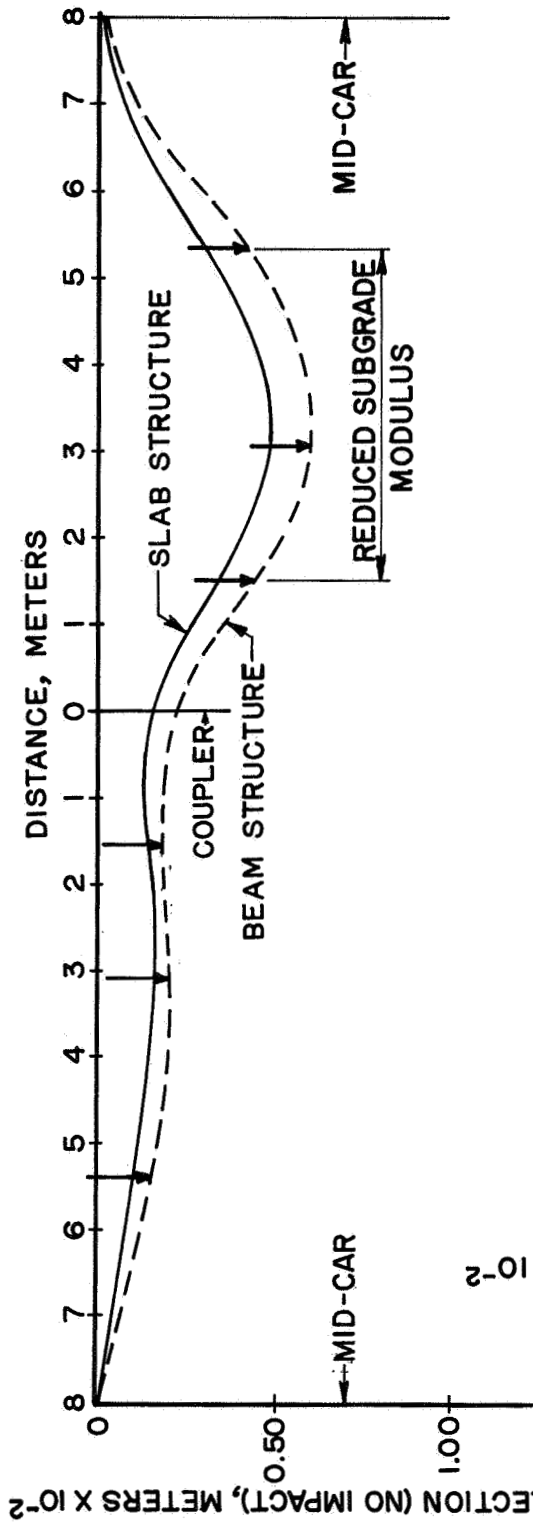


FIGURE 6: STRUCTURAL DEFLECTIONS

EXPERIENCES IN INTERFACING NASTRAN  
WITH ANOTHER FINITE ELEMENT PROGRAM

By Dennis D. Schwerzler and Robert K. Leverenz

Research Laboratories  
General Motors Corporation  
Warren, Michigan

SUMMARY

This paper deals with the coupling of NASTRAN to another finite element program which has been developed by the General Motors Research Laboratories for the static analysis of automotive structures. The two programs were coupled together to use the substructuring capability of the in-house program and the normal mode analysis capability of NASTRAN. Modifications had to be made to the NASTRAN program in order to make the coupling feasible. This information can be of use to other NASTRAN users since there are many in-house finite element programs that are specially designed for particular problems or have capabilities not found in NASTRAN. By coupling the two programs together, the capabilities of both programs can be utilized.

INTRODUCTION

An interface program was written to allow an in-house finite element program to be used for the static analysis and the NASTRAN program for the normal mode analysis of automotive structures. By using the in-house finite element program, the following benefits were gained: flexibility of substructuring, an extended element library, an easily modified program for particular problems, and reduced cost of execution. A majority of the geometric data had already been prepared and checked in a format compatible with the in-house program, thus, the coupling of the two programs saved redefining and debugging the data for the NASTRAN format. Since the in-house finite element program does not have dynamic capabilities and the NASTRAN dynamic software is reputed to be one of the best, it becomes a logical choice to couple these two programs rather than develop a dynamic analysis code or use another program.

This paper describes how the two programs are coupled together. The information contained in this paper is based on the use of NASTRAN version 12.1 on an IBM 370/165 computer.

## EXPLANATION OF INTERFACE PROGRAM DEVELOPED

When a substructure is modeled with the in-house code, the grid point data and the reduced stiffness matrix for the kept grid points are stored in a partitioned data set. When a normal mode analysis of one of these substructures is desired, this data, along with other user supplied data, is loaded into NASTRAN for the dynamic portion of the analysis by means of the interface program.

The input deck to the interface program is the NASTRAN executive control deck, the case control deck, and the bulk data deck, excluding grid point and element data. The interface program reads the input deck, converts any EBCDIC characters to BCD, and stores the card images in an output file for processing by NASTRAN. When processing the bulk data deck, the stiffness matrix for the substructure is inserted in its sorted position by placing the stiffness coefficients on DMIG cards. Likewise, GRID cards are also inserted in the bulk data deck in their correct sorted position.

An additional program processes the original data used to generate the substructure to determine the mass at each grid point by means of the lumped mass method. The mass at each grid point is then partitioned out to the kept grid points surrounding the grid point. This program then punches CØNM2 cards for the masses at each of the kept grid points. These cards are then read in as part of the bulk data input to the interface program.

Dummy rod elements are used to define the shape of the structure for plotting the mode shapes. To avoid changing the stiffness matrix, the rods are given an elastic modulus value of zero.

Grid point constraints imposed on the structure in the in-house finite element program are duplicated in the NASTRAN bulk data deck. This avoided calculating extraneous eigenvalues.

The stiffness values on the DMIG cards are read into the normal mode analysis format by means of the ALTER program shown below.

```
ALTER      26,27

MTRXIN,    ,MATPØØL,EQEXIN,SIL,/STIF,,/V,N,LUSET/V,N,NØM1/C,N,0/C,N,0 $

SMAL      CSTM,MPT,ECPT,GPCT,DIT/KGGY,,GPST/V,N,NØGENL/V,N,NØK4GG $

ADD       KGGY,STIF/KGGX/C,N,(1.0;0.0)/C,N,(1.0,0.0) $

CHKPNT    KGGX,GPST $

ENDALTER
```

This is similar to the alter program given in reference 1.

## MODIFICATIONS TO NASTRAN

Using the DMIG bulk data cards for inputting the stiffness matrix into NASTRAN creates several problems. Even though the stiffness matrix is symmetric, the entire matrix has to be read in since the direct matrix input method does not take advantage of symmetry. This requires reading in nearly twice as many cards as would normally be needed. When reading in large matrices, such as a 184 by 184, these extra values consume several minutes of computer time in order to pass through the input file processor.

Another disadvantage of the direct matrix input method is that only single precision values for the stiffness matrix can be read in. For the IBM 370, single precision is only six significant figures, therefore, round-off errors may significantly affect the accuracy of the solution. In order to read in six significant figures in an E field format, the large field format has to be used. A sorting problem developed when the large field format was used on the second DMIG type header card. The interface program outputs the DMIG cards in the correct sorted order such that GJ and CJ were in an increasing numerical order. However, NASTRAN sorted the deck with CJ in a decreasing numerical order. When the cards were input with CJ in a decreasing order, NASTRAN sorted them into the correct order of increasing CJ number. This problem could not be resolved, so it was reported to the NASTRAN system office for further study.

The sorting problem does not occur if the small field format is used for the second type header cards. However, if the small field format is used, a stiffness value must be placed on this header card, and the small field width does not allow inputting a stiffness value of six significant figures in an E field format. To overcome this restriction, a completely constrained fictitious grid point with a zero stiffness value is placed in this field.

After the sorting problem was corrected, problems still occurred in trying to pass a large number of cards (20,000) through the input file processor. Nine minutes of central processing time failed to pass these cards through the XSØRT subroutine. The problem was traced to a double DØ LØØP in the XSØRT subroutine in which a check was made for duplicate continuation cards. It appeared that in this subroutine each continuation card was compared to every other continuation card, resulting in  $(N)*(N-1)/2$  comparisons. Approximately 19,000 of the 20,000 cards were continuation cards resulting in approximately  $1.8 \times 10^8$  comparisons. At about 5 micro-seconds for each comparison on the IBM 370/165, it would have taken about 900 seconds to complete this cycle. By removing this double DØ LØØP without any other modifications to the subroutine, the 20,000 cards were processed by the XSØRT subroutine in 138 seconds.

Since most of the bulk data deck was created by the interface program which had been thoroughly checked out, and since the data was already sorted, it was felt that most of the checks performed by the XSØRT subroutine were not needed. A very brief, modified version of the XSØRT subroutine was created

especially for use with the interface program (Appendix). This modified subroutine reads in the data either from direct input, a UMF tape, or a check point tape, and outputs the data on the NPTP file tape. This subroutine can only be used for UMF tape or check pointed tape problems that require no corrections to the bulk data deck. The new subroutine further reduced the time to process the 20,000 cards from 138 to 79 seconds.

Initially, an attempt was made to read in the entire mass matrix by means of DMIG cards, using the ALTER program given in reference 1. However, the mass matrix MGG must be opened before the program reaches the ALTER DMAP instruction where the mass values, read in by the ALTER program, are added to MGG. If not, MGG will be an "ill defined matrix," and the addition would not be possible. The mass matrix must be opened by some means at DMAP operation 28, where MGG is formed. The easiest method is to put in a small mass at any grid point. For the problems that were considered only the diagonal mass terms were needed, and it was found to be easier to read in the mass matrix by means of the CONM2 cards. This method avoids the ill defined mass matrix problem.

#### OMITTING ROTATIONAL DEGREES OF FREEDOM

At first, all the degrees of freedom of each grid point were passed to NASTRAN for the dynamic analysis. The rotational degrees of freedom were then omitted in NASTRAN, since only the translational degrees of freedom were needed to adequately define the fundamental modes of the structures. The substructuring program was changed so that it performs a Guyan reduction of the stiffness matrix, omitting the rotational degrees of freedom, before passing the stiffness matrix to the interface program. This change has several advantages. Most of the structures considered are made up from several substructures, resulting in stiffness matrices which are densely populated. The Guyan reduction process, which tends to fill up the stiffness matrix, had little effect on the fullness of the stiffness matrix passed, but it did significantly reduce the size of the matrix. The structure which initially required 20,000 cards to define the stiffness matrix was reduced to 6,000 cards with very little change in the eigenvalues and eigenvectors. Since the number of cards was greatly reduced, the input file processor time was reduced from 79 seconds to 27 seconds.

This method has the advantage that the reduction process is performed with the original sixteen significant figures for each stiffness coefficient, instead of the rounded off six significant figures passed to NASTRAN when the rotational degrees of freedom are left in. Because these rotational degrees of freedom are omitted before being passed to NASTRAN, these degrees of freedom have to be constrained in the bulk data deck of the NASTRAN run. Back substitution to obtain deflections for the rotational degrees of freedom is not possible with this method.

## SPACE FRAME VERIFICATION PROBLEM

Figure 1 shows a diagram of the structure used to verify the interface program. The space frame structure shown consists of 22 grid points connected together by 32 rod elements. The space frame was modeled entirely in NASTRAN, and the resulting eigenvalues and eigenvectors were compared to those obtained by modeling the space frame in the substructuring program and passing the stiffness matrix over to NASTRAN by means of the interface program. A NASTRAN-generated mass matrix was used for both runs, being read in as CØNM2 data in the interface case. The values for the 66 eigenvalues and eigenvectors agreed to four significant figures. This example problem provided an assessment of the loss in accuracy due to the restriction of passing only six significant figures for the stiffness values. A comparison of the static analysis results between the two finite element programs produced exact agreement for the displacements.

The eigenvalues and eigenvectors for the analysis in which the rotational degrees of freedom were omitted before the data was passed to NASTRAN were closer to the values obtained by using NASTRAN directly than those values in which the stiffness values for the rotational degrees of freedom were passed to NASTRAN for omitting.

Omitting the rotational degrees of freedom with the substructuring program for the space frame increased the number of card images passed from 1,473 to 3,674. The reason for the increase was that the stiffness matrix for the space frame was very sparsely populated. The Guyan reduction process, although it reduced the size of the matrix, produced an almost fully populated matrix.

## CONCLUDING REMARKS

The interface program has been used on considerably more complicated structures than the space frame shown. The largest structure analyzed was a car body composed of 15 substructures which together contained over 3,000 degrees of freedom. The substructuring program was used to reduce the structure to 186 translational degrees of freedom for passage to NASTRAN for the normal mode analysis. The dynamic analysis of the structure was successfully completed in 425 seconds with the input file processor requiring 137 seconds. The modifications made to the XSØRT subroutine, and the use of the substructure program made this analysis technically feasible and computationally economical.

## REFERENCE

1. Jones, T. C. and Pinson, L. D., "Adaptation of NASTRAN to the Analysis of the Viking Space Vehicle," NASTRAN User's Experience, Sept. 12-15, 1971, p. 265, Vol. 1.

APPENDIX

```

SUBROUTINE XSORT
C* SORT READS BULK DATA CARDS FROM THE INPUT TAPE , ADJUSTS THE FIELDS,
C* PERFORMS AN ALPHA-NUMERIC SORT ON THE CARD IMAGES FROM LEFT TO RIGHT,
C* INSERTS CONTINUATION CARDS IN THEIR PROPER POSITION, AND
C* PLACES THE RESULTING SORTED IMAGES ON THE NEW PROBLEM TAPE.
  INTEGER BIMSK1,BIMSK2,BIMSK3,BIMSK4,BIMSK5,BIMSK6
  INTEGER BKMSK1,BKMSK2,          SHIFTS
  INTEGER STAR,PLUS,DOLLAR,STARL,SLASH,SFTM,BLANK
  INTEGER BK,BUF,CCNT,CORSZ,ECHOS,ECHOU,FCNT,OPTP,
1  OUTTAP,PTST,PSHIFT,SFTA,STARSW,ORF,ANDF,
2  TRJAL,TST,UMF,PID
  EXTERNAL LSHIFT,RSHIFT
  DIMENSION HEADU%32<,HEADS%32<,HEADN%32<,IBLKDA%2<,CDCNT%3<
  DIMENSION BK%4<,MK%4<,IBUF1%20<,IBUF2%20<,IBUF3%2<,KPARNT%2<
  DIMENSION IBUF1A%2<,IBUF2A%2<,NSORT%2<
  COMMON/SYSTEM/IBUFSZ,OUTTAP,NOGO,INTAPE,D1%14<,IECHO,D,IAPPRC,MACH
1  , DUM1 , IUEDIT
  COMMON/OUTPUT/DUM2%96<,HEAD1%32<,HEAD2%32<,HEAD3%32<
  COMMON/XMDMSK/DUM4%5<,ICPFLG
  COMMON/FSCRT/BUF%1<
  COMMON//ICOMON
  COMMON/XSORTD/BIMSK1%6<,BIMSK2%5<,BIMSK3%4<,BIMSK4%4<,BIMSK5%2<,
1  BIMSK6 ,BKMSK1%8<,BKMSK2 ,SHIFTS%4<,
2  ICCN1,ICCN2,STAR,PLUS,DOLLAR,STARL,SLASH,SFTM,MASK,BLANK,MKA,IS
  COMMON /STAPID/ KRAP%12<,KUMF
  EQUIVALENCE %BK%1<,BKMSK1%5<<,%MK%1<,BIMSK2%2<<,
1  %MKB ,BIMSK5%1<<,%INF ,BIMSK2%1<<,
2  %SFTA ,SHIFTS%2<<,%MKD ,BIMSK2%2<<,
3  %MKE ,BIMSK5%2<<,%MKC ,BIMSK4%1<<
  DATA HEADU/10*4H ,4H I N,4H P U,4H T ,4H B U,4H L K,4H D,
1  4H A T,4H A ,4H D E,4H C K,4H E,4H C H,4H O ,9*4H /
  DATA HEADS/11*4H ,4H S O,4H R T,4H E D,4H B,4H U L,4H K ,
1  4H D A,4H T A,4H E,4H C H,4H O ,10*4H /
  DATA HEACN/ 3*4H ,4H ,4H ,4H ,4H ,4H I ,4H ,4H ,
1  4H 2 ,4H ,4H 3 ,4H ,4H 4 ,4H ,4H 5 ,4H ,
2  4H 6 ,4H ,4H 7 ,4H ,4H 8 ,4H ,4H 9 ,4H ,
3  4H 10 ,4H ,5*4H /
  DATA CDCNT/4HCARC,4HCOUN,4HT /,NSORT/4HXSOR,4HT /
  DATA ECHOU,ECHOS/2*0/
  C DATA RK/4H000 ,4H00 ,4H0 ,4H /
  C DATA %MK%I<,I#1,4</0777777007777,0777700007777,0770000007777,00/
  C DATA MKA,MKB,INF,SFTA/0000000777777,037777777777,077777777777,6/
  C DATA MKC/000777777777777/,MKD/07777770077777/,MKE/0377777007777/
  DATA IEND1,IEND2/4HENDD,4HATA /,IEND/0/,ISEQ/0/,ICCBRK/0/
  C DATA STAR,PLUS,DOLLAR,STARL/4H000*,4H0000,4H$000,4H*000/
  DATA IBLKDA/4HBULK,4HDATA/,NCTSOR/0/,OPTP/4HOPTP/,NPTP/4HNPTP/
  DATA ITAPE1,ITAPE2,ITAPE3,ITAPE4,ITAPE5/301,302,303,304,305/
  DATA KIN/0/,UMF/4HUMF /
  C INITIALIZE XSORT
  C#####
  IPESTR # -IAPPRC
  IF%KUMF.LE.0< GO TO 90
  KIN#1
  CALL OPEN%$50,UMF,BUF%1<,2<
  C FIND PARTICULAR BULK DATA FILE ON UMF AS REQUESTED BY USER

```

```

10 CALL READ%$30,$60,UMF,PID,1,1,IFLG<
   IF%KUMF-PID< 30,80,20
20 CALL SKPFIL%UMF,1<
   GC TO 10
30 WRITE%OUTTAP,35< KUMF
35 FORMAT%52H0***USER FATAL MESSAGE 201,REQUESTED BULK DATA DECK 18,
   1 24H NOT ON USER MASTER FILE<
   NOGD#-1
   CALL CLOSE%UMF,1<
   RETURN
50 WRITE%OUTTAP,55<
55 FORMAT%1H0,23X,28H 202,UMF COULD NOT BE OPENED<
   GC TO 1800
60 WRITE%OUTTAP,65<
65 FORMAT%1H0,23X,23H 203,ILLEGAL EOR ON UMF<
   GC TO 1800
80 CALL CLCSE%UMF,2<
C#####
90 CALL INITCC
   IF%IECHO.LT.0< GC TO 110
   IF%IFCHO.EQ.1< ECHO# 1
   IF%IECHO.FQ.2< ECHOS# 1
   IF%IECHO.NF.3< GO TO 100
   ECHO# 1
   ECHOS# 1
100 IF%ICPFLG.NE.0< ECHOS# 1
110 CONTINUE
C START WORKING SORT BUFFER BELOW GING I/O BUFFERS
   II# 5* IBUFSZ& 1
   IBUG# II& 42
   IBUFLG# CORSZ%BUF%1<,ICOMON< - 21
   IF%IBUFLG-IBUG.LT.210< CALL MESSAGE%-8,0,NSORT<
   ITAPE# ITAPE1
   JTAPE# ITAPE2
   CALL OPEN %$1750,NPTP,BUF%4*IBUFSZ&1<,3<
   CALL WRITE %NPTP,IBLKDA,2,1<
   IF %IRESTR.GT.0 .OR. KIN.GT.0< GO TO 1400
180 READ %JNTAPE,190< IBUF1
   CALL XFADJ1 %IBUF1%1<,LSHIFT,0<
   IF %IBUF1%1<,FQ. IEND1 .AND. IBUF1%2<.EQ. IEND2< GO TO 560
190 FORMAT %20A4<
   CALL WRITE %NPTP,IBUF1,20,1<
   GO TO 180
560 CALL FCF %NPTP<
   CALL CLOSE %NPTP,1<
   RETURN
1400 IF %KIN.GT.0< GO TO 1430
   CALL OPEN %$1740,NPTP,9UF%1<,0<
1410 CALL READ %$1730,$1710,OPTP,IRUF3,2,1,IFLG<
   IF %IBUF3%1<.EQ. IBLKDA%1<.AND. IBUF3%2<.EQ. IBLKDA%2<< GO TO 1420
   CALL SKPFIL %OPTP,&1<
   GC TO 1410
1420 CALL READ %$1240,$1710,OPTP,IBUF1,20,1,IFLG<
   CALL WRITE %NPTP,IBUF1,20,1<
   GO TO 1420
1240 CALL CLOSE %OPTP,1<
   GO TO 560

```

```

1430 CALL OPEN %$50,UMF,BUF%1<,2<
      CALL READ%$1250,$1710,UMF,IBUF1,20,1,IFLG<
      CALL WRITE %NPTP,IBUF1,20,1<
      GO TO 1430
1250 CALL CLOSE %UMF,1<
      GO TO 560
1710 WRITE%OUTTAP,1711<
1711 FORMAT%1H0,23X,27H 211,ILLEGAL EOR ON SCRATCH<
      GO TO 1800
1730 WRITE%OUTTAP,1731<
1731 FORMAT%1H0,23X,24H 213,ILLEGAL EOF ON OPTP<
      GO TO 1800
1740 WRITE%OUTTAP,1741<
1741 FORMAT%1H0,23X,29H 214,OPTP COULD NOT BE OPENED<
      GO TO 1800
1750 WRITE%OUTTAP,1751<
1751 FORMAT%1H0,23X,29H 215,NPTP COULD NOT BE OPENED<
      GO TO 1800
1800 WRITE%OUTTAP,1801< PLUS
1801 FORMAT%A1,23H***SYSTEM FATAL MESSAGE<
      CALL MESSAGE%-37,0,NSORT<
      NCGO # -1
      RETURN
      END

```

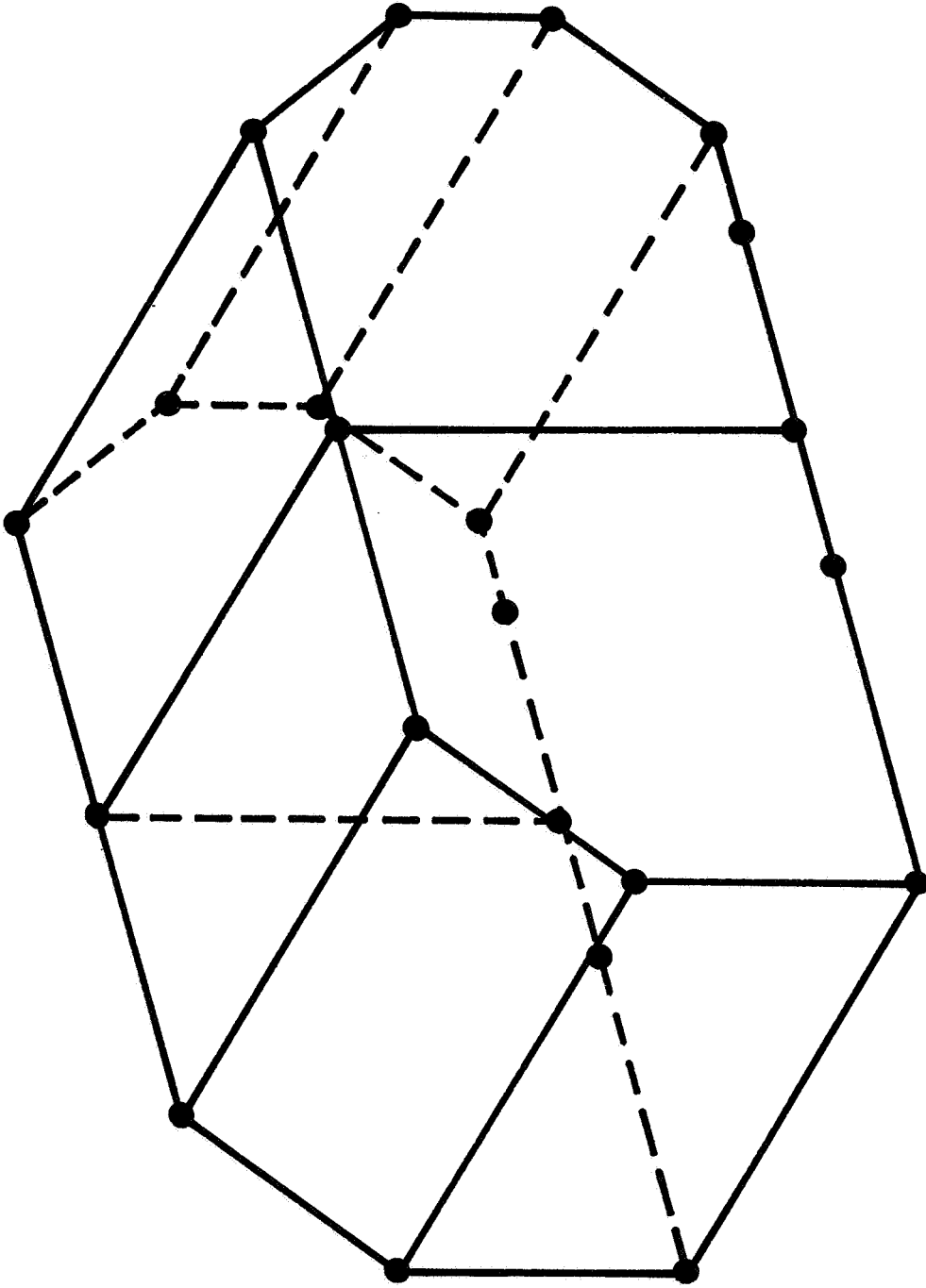


Figure 1. Space frame verification problem.



# DELTA LAUNCH VEHICLE ISOGRID STRUCTURE NASTRAN ANALYSIS

By Daniel J. Knighton

NASA Goddard Space Flight Center

## SUMMARY

The purpose of this paper is to present the varied structural analysis applications of NASTRAN on the new isogrid<sup>1</sup> structure of the Delta launch vehicle. Isogrid is a method employed to stiffen the booster cylindrical shell surface by integrally machining ribs and skin from one piece of metal. The ribs are arranged in a repetitive equilateral triangular pattern; this results in a structural surface whose stiffness is orthogonally isotropic. For that structure both static and general instability buckling analysis will be described and the theoretical results will be compared to test data. One of the parameters that has been included in this analysis is the effect of pressure loadings on the buckling allowable load. In addition, a description of a supplementary GSFC-originated computer program, without which this analysis could not have been performed, will be presented.

## INTRODUCTION

A brief description of the Delta launch vehicle and its performance advancements will be given with specific attention focused on the IBM 360/95 computer analysis of the recently innovated Delta external isogrid shell structure. The NASA Structural Analysis (NASTRAN) program has been successfully employed to (1) verify the isotropic property of isogrid, (2) show the variation in deflections and detail stress levels depending on loading versus the orientation of isogrid, (3) perform as an engineering liaison tool, and (4) determine the general instability buckling allowables for isogrid tank structures.

---

<sup>1</sup>Isogrid structure concept was developed for Delta by McDonnell Douglas in 1970.

## SYMBOLS

$a'$	side of isogrid triangle, cm (in.)
A	area, $\text{cm}^2$ (in.)
a, b	locations of CBAR
CBAR	NASTRAN bar element
CTRIA2	NASTRAN triangular plate element
d	rib height, cm (in.)
D	diameter of cylinder, cm (in.)
E	Young's modulus of elasticity, $\text{kN/m}^2$ (psi)
$\bar{E}$	isogrid modulus, $\text{kN/m}^2$ (psi)
f	force, N (lb)
$f_{rc}$	rib-allowable compression stress, $\text{kN/m}^2$ (psi)
$f_{sb}$	skin-allowable compression stress, $\text{kN/m}^2$ (psi)
F	force, N (lb)
G	modulus of rigidity, $\text{kN/m}^2$ (psi)
h	height of isogrid triangle, cm (in.)
I	moment of inertia, $\text{cm}^4$ (in. <sup>4</sup> )
J	polar moment of inertia, $\text{cm}^4$ (in. <sup>4</sup> )
K	form factor of cross section
$[K_{aa}]$	elastic stiffness
$[K_{aa}^d]$	differential stiffness
l	length, cm (in.)
m	moment, N-m (in.-lb)
M	bending moment, N-m (in.-lb)
$N_{GI}$	isogrid general instability allowable load, $\text{kN/m}$ (lb/in.)

$N_{rc}$	rib-allowable compression or crippling load, kN/m (lb/in.)
$N_{sb}$	skin-allowable compression or buckling load, kN/m (lb/in.)
$N_x$	equivalent compression load, kN/m (lb/in.)
$p$	pressure, kN/m <sup>2</sup> (psi)
$P$	applied axial load, N (lb)
$R$	radius, cm (in.)
$\bar{t}$	equivalent skin thickness, cm (in.)
$t_r$	rib thickness, cm (in.)
$t_s$	skin thickness, cm (in.)
$t_{wt. eq.}$	weight equivalent thickness (accounting for weld land and/or edge panel design)
$T$	torque, N-m (in.-lb)
$u$	linear displacement of CBAR grid point
$\{u\}$	eigenvector
$V$	shear, N (lb)
$dV$	infinitesimal element volume
$\epsilon_{xx}, \epsilon_{yy}$	extensional strain, cm/cm (in./in.)
$\epsilon_{xy}$	shear strain, cm/cm (in./in.)
$\theta$	rotation of CBAR grid point
$\lambda$	eigenvalue
$\nu$	Poisson's ratio
$\sigma_x, \sigma_y$	axial stress of isogrid in x, y directions, kN/m <sup>2</sup> (psi)
$\tau_{xy}$	shear stress, kN/m <sup>2</sup> (psi)
$\omega$	rotation of $dV$

## DELTA ISOGRID STRUCTURE

The Delta launch vehicle project began in 1959 shortly after the formation of NASA. It started with existing stages that were comprised of the Thor first stage and Vanguard second and third stages. Since that time it has been project policy to upgrade the Delta booster for increased performance and reliability at a minimum cost growth as shown on figure 1. The current launch vehicle and improved configurations are shown on figure 2.

One of the many upgraded design features of these new Delta vehicles is the incorporation of a cylindrically shaped isogrid structure. This design forms the external skin structure of the booster. The new tank skin is initially machined from flat 1.27-cm (1/2-in.) thick 14ST6 free-machining aluminum alloy plate, brake-formed into curved shapes, and finally welded into 2.44-m (8-ft) diameter tank shells. Typical integrally machined structures, waffle and isogrid, are shown in figure 3. Isogrid now replaces the less efficient rectangular waffle tank and skin, stringer, and frame interstage and fairing structures. The improved Delta isogrid tank construction is about 50 percent more efficient (weightwise), than the waffle and equivalent in efficiency to the built-up assemblies with regards to compressive local and general buckling capabilities. It is also interesting to note that isogrid is orthogonally isotropic in its overall strain characteristics.

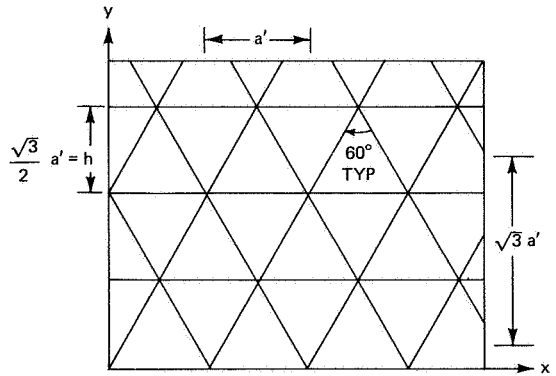
The first vehicles to employ the isogrid structure are now planned to carry the IMP H and TELESAT A spacecraft into orbit by the end of this year. Isogrid hardware is not only being fabricated for Delta vehicles but it is also being developed for the Shuttle (ref. 1) and Skylab programs under the cognizance of MSFC and is being proposed for more efficient Delta/Agena replacement second stages (fig. 4) in the Versatile Upper Stage (VUS) study (ref. 2) to GSFC requirements. Preliminary evaluations performed on Delta and the VUS indicate that isogrid structures are approximately 50 percent the cost of skin, stringer, and frame structures. This was the reason why the interstage and fairing were designed using isogrid for new model Deltas.

## ANALYSIS OF ISOGRID BY NASTRAN

The new structure, a relatively fine rib-node mesh, was modeled using NASTRAN program elements and procedures. Both static and buckling analysis were performed to give the Delta project a good understanding of the new structure being designed for Delta. Loadings applied to the isogrid model initially were only compression type but later were expanded to include pressure effects; i.e., hoop loadings. The compression loading included axial compression, equivalent axial compression due to bending, and offsetting axial tension forces  $pR/2$  due to internal pressure. The buckling analysis also included, for comparison only, the effects of an external pressure loading.

PROOF OF ISOTROPY OF ISOGRID

For an isogrid orientation having the  $a'$  and  $\sqrt{3}a'$  periodic grid distances shown to the right, it has been proven (ref. 3) that the material has isotropic elastic properties and that it obeys Hooke's law.



$$\sigma_x = \frac{\bar{E}}{1 - \nu^2} (\epsilon_{xx} + \nu \epsilon_{yy})$$

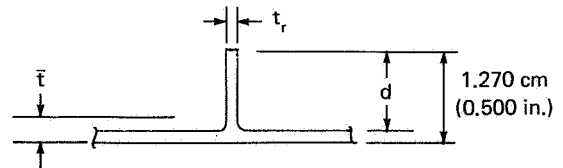
$$\sigma_y = \frac{\bar{E}}{1 - \nu^2} (\epsilon_{yy} + \nu \epsilon_{xx})$$

$$\tau_{xy} = \frac{\bar{E}}{1 + \nu} \epsilon_{xy}$$

where the isogrid elastic modulus  $\bar{E}$  is related to the actual material modulus  $E$  by  $\bar{E} = t_r E/h$ .

Subsequent to the previous analysis, the rib and plate elements were combined to produce an equivalent skin thickness  $\bar{t}$  such that the booster tank could be treated like an equivalent monocoque cylindrical structure. The equivalent monocoque skin thickness is

$$\bar{t} = t_s \left( 1 + \frac{t_r d}{t_s h} \right) = t_s + \frac{t_r d}{h}$$



The  $\bar{t}$  relation is important in solving for skin and rib compression allowables (ref. 4), which are

Skin buckling:

$$N_{sb} = 10.875 E \bar{t} \left( \frac{t_s}{h} \right)^2$$

$$f_{sb} = \frac{N_{sb}}{\bar{t}}$$

### Rib crippling:

$$N_{rc} = 0.422Et \left( \frac{t_r}{d} \right)^2$$
$$f_{rc} = \frac{N_{rc}}{t}$$

Isogrid, being isotropic, does possess an idiosyncrasy, i.e., its detail stresses must vary internally within the isogrid depending on the direction in which loadings are applied. The reason for this is that the isosceles triangular arrangement is oriented slightly differently in the x- and y-axis directions. To learn more about this novel structure, a small finite element model was fashioned using NASTRAN bar (CBAR) and triangular plate (CTRIA2) elements, figure 5. Specifically, this model was prepared to check the overall isotropic property of the integral rib and skin combination and to review the internal rib and skin stresses that result when the same magnitude of loading is placed in either the x or y directions.

The compression loading was selected from a typical Delta loading profile and is equated as follows:

$$N_x = \frac{P}{\pi D} + \frac{4M}{\pi D^2} = 308.2 \text{ kN/m (1760 lb/in.)}$$

$N_x$  was applied first in the negative x and then in the negative y directions. The results, including deflections and stress levels, are shown in figures 6 and 7. Note that the overall deflections, 1.346 mm (0.0530 in.), are the same for either x- or y-axis loadings, which indicates the overall isotropic characteristic of isogrid. Further, the rib and skin compressive stress levels in the center bay were lower for the x-axis loading direction (loads perpendicular to the main ribs) by 31 and 1 percent, respectively. Thus, to keep the compressive stresses at a minimum in the isogrid propellant tanks, the main ribs were located accordingly (on Delta stations, fig. 5).

The initial model, figure 5, was 46.94 cm (18.48 in.) square and required additional plate and bar elements. Two computer runs were made using heavy load support elements (50 times stiffer than isogrid CBAR members) and multiple point constraints at the load grid points and the same deflections and stress levels were obtained. The grid-point restraints are as noted on figure 6.

A third computer run was accomplished using a simpler model as shown in figure 8. Note that the model is 46.94 by 50.80 cm (18.48 by 20.00 in.) and contains fewer plate elements. The deflection and stresses are as shown in figures 9 and 10. The deflection and stresses are approximately the same as produced by the previous more complicated model. This simpler model was also utilized for the combined loading analysis, which is described in the next section.

## COMBINED LOADING OF ISOGRID

The previous NASTRAN models were loaded in compression only. Next, the preceding model, having a single fixed point (grid point 28), was loaded with axial compression (308.2 kN/m (1760 lb/in.)) and hoop tension (414 kN/m<sup>2</sup> (60 psi)) forces. For the levels of loading applied, the results are as shown in figures 11 and 12. The rib compressive stress level was 51 percent lower and the skin buckling level was 3 percent higher for the x-axis loading conditions where the compression loadings were perpendicular to the main ribs (fig. 11). A close look at the actual rib and skin stresses and a direct comparison with their respective allowable stresses is given in table 1. Note that the skin actual stress was closer to its allowable stress. For the combined loads case analyzed, the skin stress will be a minimum if the compression load is in line with the isogrid main rib. Because past tests (ref. 5) indicate that local skin buckling will reduce general instability allowables (by approximately 20 percent), it is important to keep the skin actual stresses as low as possible.

TABLE 1.--Rib and Skin Compression Stresses

Element	Actual stress, kN/m <sup>2</sup> (psi)	Allowable stress, kN/m <sup>2</sup> (psi)	$\left(\frac{\text{Allowable stress}}{\text{Actual stress}} - 1\right) 100,$ percent
Rib	-252 067 (-36 558)	-424 042 (14ST651 yield corrected for plasticity; -61,500)	+68
Skin	-173 637 (-25 183)	-202 024 (-29 300)	+16

## LIAISON COMPUTER ANALYSIS

During the early stages of fabrication, there have been occasions when isogrid skins have been machined improperly. In the cases where skin pockets and rib thicknesses were undersized at random locations, the small NASTRAN model previously described was used effectively. Having the actual stress levels throughout the model, it was quite easy to determine rib and skin margin of safety and whether reinforcements were required.

ISOGRID TANK STATIC AND BUCKLING ANALYSIS  
(MOVE AND NASTRAN PROGRAMS)

This analysis was performed to determine the general instability theoretical allowables for axial compression and various tank hydrostatic loadings; i.e., negative or external, zero, or positive or internal pressure loadings.

The fact that tank pressure loading can be handled quite easily by the NASTRAN program made this a more interesting and comprehensive study. The results of this analysis compared with test data and other methods of analysis (ref. 6) will be summarized later. Before discussing the model and the results, a brief description of the theory will be presented.

BUCKLING THEORY

NASTRAN buckling analysis (ref. 7) is based on the elastic and differential stiffnesses of the structure analyzed. The elastic properties of a structure are generally dependent on shear  $AG/K$ , torsion  $JG$ , bending  $EI$ , and axial  $AE$  stiffness characteristics. The differential stiffness is based on the static loading, displacement, and geometry of the structure. An example of a bar element differential stiffness matrix is shown in figure 13 (ref. 7). The approach presented in reference 7 is essentially based on using Lagrange's equations of motion on a structural system with a finite number of degrees of freedom.

The steps (ref. 7) for including differential stiffness in a structural problem are as follows:

- (1) Solve the linear static response problem for the structure in the absence of differential stiffness and compute the internal forces in each element.
- (2) Using the results of (1), calculate the differential stiffness matrix for the individual elements and apply the standard reduction procedure (constraints and partitioning) to form the differential stiffness matrix  $[K_{aa}^d]$  in final form.
- (3) For the buckling problem, find the characteristic eigenvalue and eigenvectors for

$$[K_{aa} + \lambda K_{aa}^d] \{u\} = 0$$

For the isogrid cylinder buckling problem, the inverse power method was used to determine the eigenvalues. Because the above-defined set of buckling equations are homogeneous, the assignment of one arbitrary eigenvector (within NASTRAN) must be made to start the analysis. The solution of the first trial eigenvalue permits the determination for convergence; the redetermination of the eigenvalue, if necessary; and the subsequent final solution of all eigenvector ratios  $\{u\}$  or of the mode shape.

It is the eigenvalue that is the factor by which the applied compression static loading is multiplied to produce the theoretical threshold of buckling. Once obtained, the theoretical buckling load is multiplied by a 65-percent reduction factor. That factor has evolved from testing full-scale isogrid cylinders and it accounts for manufacturing tolerances and distortions that are present in hardware.

#### BUCKLING MODEL DESCRIPTION

During June 1971, three isogrid tank segments (244-cm diameter by 244-cm length (8-ft diameter by 8-ft length)) were fabricated from free-machining 2014T6 aluminum; subsequently, compression tested with zero internal pressure. The mathematical model was determined, based on those compression test tank sizes, in order to correlate computer results with test values.

The NASTRAN model, being an exact replica of the tested tank segments, was a rather fine and detailed model. This model size is believed to be the largest structural model analyzed at NASA Goddard Space Flight Center. The model was composed of NASTRAN triangular plate (CTRIA2) and bar (CBAR) elements. A complementary computer program, MOVE (ref. 8), was utilized to simplify the task. A model such as ours, having 1850 grid points and 7986 elements, would have been extremely difficult, if not impossible within the time available, to construct had it not been for the help of the MOVE program.

The MOVE program was designed to generate repeat bulk data for structures having a number of identical segments. All one need do is to generate one basic NASTRAN bulk data segment and MOVE does the rest. The strip model selected for our problem was a longitudinal segment shown in figure 14. By moving that segment 66 times ( $5.45^\circ$  per move circumferentially), the complete cylinder was generated as shown in figure 15. It should be noted here that all of the undeformed and deformed figures in this report were made by the Stromberg-Carlson 4060 plotter, which is one of several systems that may be specified in NASTRAN programming.

When the MOVE program was first programmed, it was designed for a relatively small structural problem. Thus, the initial trial of that program on a large structural model was not successful. The reason was that the MOVE program could not handle CBAR continuation cards and a very large number of repeat cycles. Further, the MOVE program was written to place its bulk data output on punched cards. This feature could have been quite cumbersome to handle for our large buckling problem (approximately 8 data card file boxes, or 8000 cards). Including the output data on tape was a far superior way of handling an immense quantity of data. That program, written in PL-1 language, was subsequently revised to rectify the above problem areas and to store its output data on magnetic tape.

Having accomplished the MOVE programming successfully, the next step was to input the data using NASTRAN programming methods. Here too, initial attempts were not good because of an assortment of program problems involving the

application of the MOVE data tape and the determination of a practical size storage requirement for our isogrid structural model. The solutions were readily available by properly arranging the executive control section of NASTRAN and adjusting the storage requirement from 500 000 to 1 000 000 places. Incidentally, the isogrid tank buckling computer analysis required all but 5000 places for some of the NASTRAN routines--that was measuring storage quite close. Yet still another problem occurred: The computer program timed out at 120 min of requested central processing unit (CPU) time. Rather than increase the run time, the model was reduced, but reduced in such a way that the original size tank configuration could be maintained. This was achieved by reducing the NASTRAN model to one-quarter the original size, limiting the buckling problem by analyzing only the first four symmetric-symmetric modes as shown in figure 16, and establishing the constraints or degrees of freedom accordingly.

To accomplish the reduction in model size to one-quarter the original, the grid points were modified to include 1 through 13 (fig. 14) only and the MOVE rotations ( $5.45^\circ$ /rotation) were reduced from 66 to 33. The MOVE program was rerun and the reduced data (on tape) were submitted via NASTRAN for a plot of the one-quarter-scale model shown in figure 17.

The buckling analysis was again attempted and constraint problems were encountered. A more careful look at the symmetric-symmetric modes and the loaded end conditions led to grid-point degrees of freedom revisions that subsequently produced good buckling results as shown in table 2. Plots of the statically deformed and buckled structure are presented in figures 18 to 24.

But how dependable was the general instability buckling analysis using NASTRAN? To answer this question, the NASTRAN output was compared directly to another analysis (ref. 6) and to isogrid tank compression test data (refs. 4 and 9) as shown in figure 25. For that figure the theoretical buckling values were multiplied by a 65-percent test correlation factor (ref. 4) and compared to 99 percent probability buckling test values (2.340 lower than the average of nine test data points). The lower than theoretically predicted buckling allowables thus achieved account for imperfections that are inherent in large structures. Such imperfections are generally attributable to built-in residual forming stresses, slight amounts of tank out-of-roundness, and local rib and skin waviness.

Figure 25 graphically documents instability buckling levels for the Delta isogrid and waffle designs as compared to monocoque designs. It also shows the allowable skin buckling running load for the isogrid design. The graph has been produced by placing the weight equivalent thickness ( $t_{wt. eq.}$ ) along the abscissa and the allowable compressive load ( $N_{GI}$  or  $N_{sb}$ ) along the ordinate.

By scanning figure 25, it becomes apparent that the general instability allowables obtained through the use of NASTRAN correlate very well with the test data point and the cylindrical shell analysis by W. Flugge (ref. 6) and McDonnell Douglas H312 analysis. Because the symmetric-symmetric buckling results appeared to be quite good, further analyses in the asymmetric buckling modes were not performed.

TABLE 2.--Isogrid Tank Structure NASTRAN Buckling Analysis Data

Item no.	Loading condition	Run time, min		Rigid format	Date of run	Output		Maximum compression N, kN/m (lb/in.)	Theoretical buckling N, kN/m (lb/in.)	NGI = 0.65 AN, kN/m (lb/in.)
		CPU	I/O			Modes	Eigen-value, $\lambda$			
1	414-kN/m <sup>2</sup> (60-psi) uniform external pressure plus unsymmetrical compression loads 	84	79	12.1.1	1/8/72	12	1.042	302.8 (1730)	315.5 (1803)	204.8 (1170)
2	414-kN/m <sup>2</sup> (60-psi) uniform internal pressure plus unsymmetrical compression loads 	65	72	12.1.2	2/5/72	3	1.433	302.8 (1730)	433.8 (2479)	281.8 (1610)
3	Unsymmetrical compression loads 	41	46	12.1.2	3/11/72	1	1.338	302.8 (1730)	405.1 (2315)	263.4 (1505)

Note also that the instability plots are based on compression loadings and no internal pressure. To verify the pressure effect, analysis was performed using NASTRAN for the conditions of compression loading and  $414\text{-kN/m}^2$  (60-psi) internal and external pressure. These data points are also shown in figure 25. It is interesting to observe that internal pressure (through pressure stiffening of skin and rib) improves the zero-pressure buckling allowable by 7 percent, and the external pressure degrades the zero-pressure buckling level by -22 percent. The 7-percent improvement correlates fairly well with a 4-percent gain seen during testing of scaled-down lexan isogrid models (ref. 5).

Observe also that isogrid is local skin buckling critical from a thickness of 2.39 mm (0.093 in.) and lower. During the previously mentioned scaled-down lexan isogrid test program, local skin buckling levels with and without internal pressure were evaluated. The results are what would be expected--the general instability buckling load level was improved by 20 percent by adding an internal pressure loading. The reason for that improvement was that internal pressure stiffened the ribs and skin pocket areas such that 100 percent of the theoretical general instability level could be achieved. It is for this reason that a combined loads (compression, shear, and internal pressure) research and development task has been proposed. The combined loads would be applied to several full-scale aluminum isogrid tank segments (2.44-m diameter by 2.44-m length (8-ft diameter by 8-ft length)).

#### CONCLUSIONS

The NASTRAN program techniques have been advantageously employed on the Delta launch vehicle isogrid structure in the following areas:

- (1) The combined loads isogrid model served as an excellent analytical tool in accomplishing liaison stress analysis. That isogrid is orthogonally isotropic was proved by NASTRAN.
- (2) NASTRAN buckling analysis produces good general instability buckling allowable load levels. It also has the capability of combining axial compression, bending, shear, and pressure loadings. Shear effects were omitted in this analysis in order to correlate test and other analyses.
- (3) Buckling analysis of the isogrid cylinder determined that internal pressure loading, when combined with axial compression loading, provides a 7-percent improvement in the general instability allowable. Because both local skin pocket and instability buckling allowables are improved by internal pressure stiffening effects, a combined loads development task has been proposed.

## ACKNOWLEDGMENTS

The author wishes to acknowledge the assistance of Margorie Johns (NASA GSFC) and William Gorman and Karl Swenson (Computer Sciences Corp. at GSFC) for their work on the MOVE and NASTRAN program support phases. Recognition is also given to Robert Meyer (McDonnell Douglas) for the many years of research in isogrid development and for his enthusiastic assistance. In addition, special thanks go to Thomas Butler (NASA GSFC) for his help in the theory behind NASTRAN and in his encouragement during the course of this analytical study.

## REFERENCES

1. Meyer, R. R.: Booster Airframe. Pt. III of Space Shuttle Data, Rept. MDC EO375, McDonnell Douglas, June 30, 1971.
2. Nelson, L. M.; et al.: Phase A Advanced Versatile Upper Stage (VUS) Study. Vol. I, Tech. Book I, Astronautics Rept. GD/CA BNZ72-006, General Dynamics/Convair, May 1972.
3. Meyer, R. R.; and Bellifante, R. J.: Isotropic Analysis. Pt. I of Fabrication and Experimental Evaluation of Common Domes Having Waffle-Like Stiffening, Rept. SM-47742, Douglas Aircraft Corp., Nov. 1964, p. 78.
4. Chen, R.: Isogrid Strength Allowables--Delta Booster Tanks and Interstage. Rept. MDC G2833, McDonnell Douglas, Apr. 1972.
5. Jenkins, W. C.: Determination of Critical Buckling Loads for Isogrid Stiffened Cylinders. Rept. MDC G2792, McDonnell Douglas, Feb. 1972.
6. Flugge, W.: Stresses in Shells. Springer Verlag (Berlin), 1962.
7. MacNeal, Richard H.: NASTRAN Theoretical Manual. NASA SP-221, Sept. 1970.
8. Cook, W. L.: Automated Input Data Preparation for NASTRAN. NASA TM X-63607, Apr. 1969.
9. Sternitzke, J. F.: (DELTA) Isogrid Cylinder Buckling Capabilities.. Vol. I, Rept. MDC G2472, McDonnell Douglas, Aug. 1971.

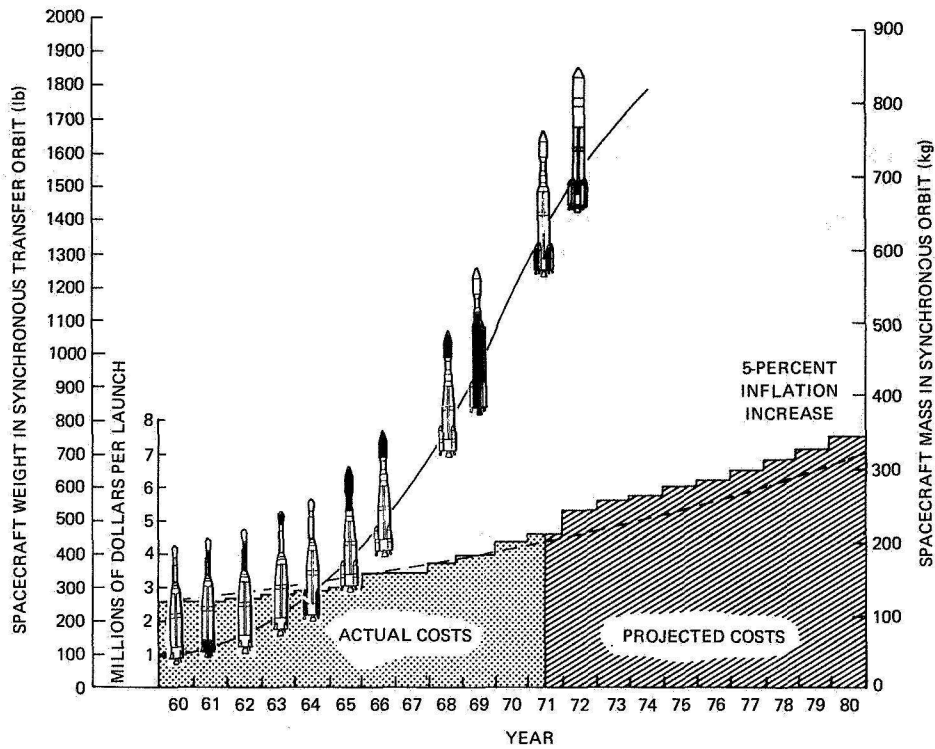


Figure 1.--Delta performance and cost history.

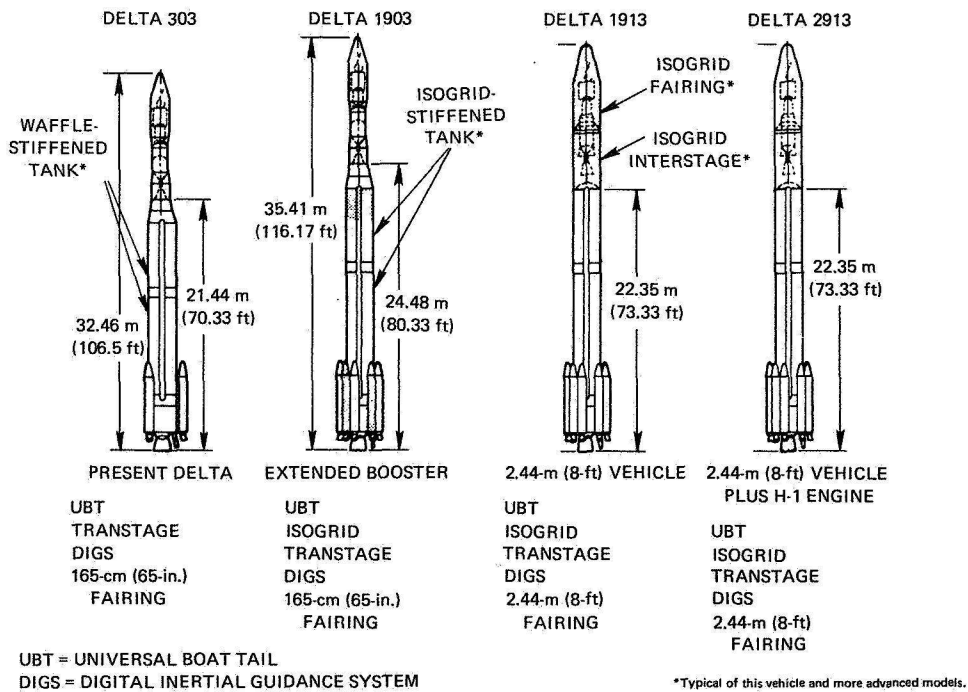


Figure 2.--Configuration development plan.

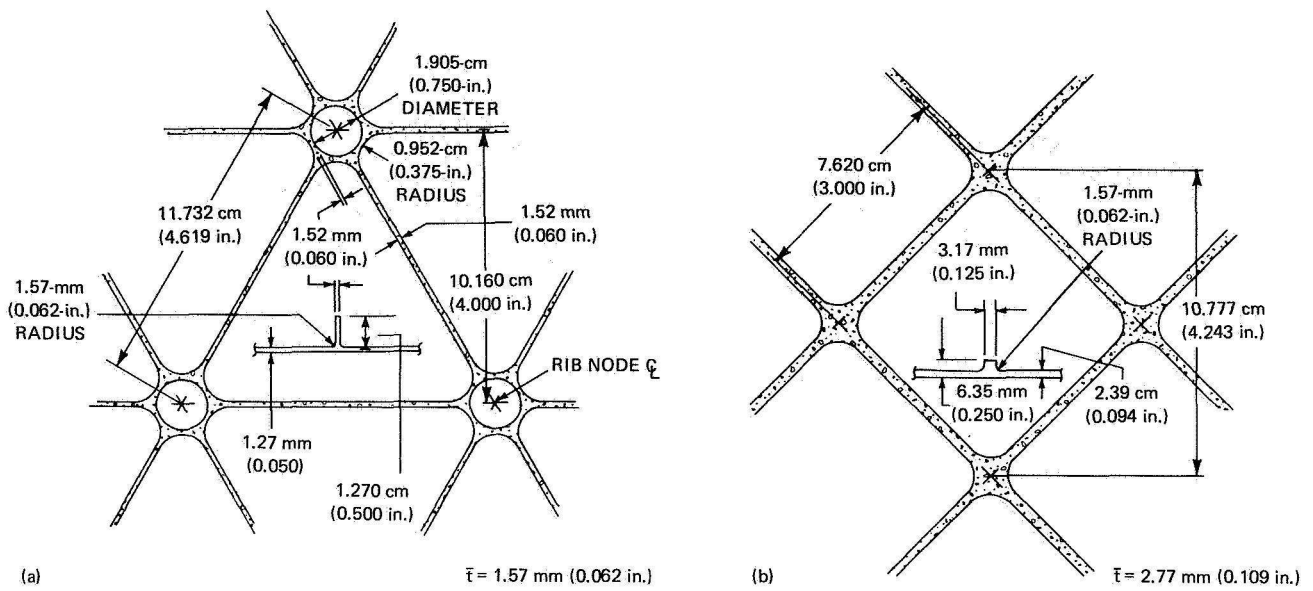


Figure 3.--Thor tank grid pattern. (a) Isogrid. (b) Waffle.

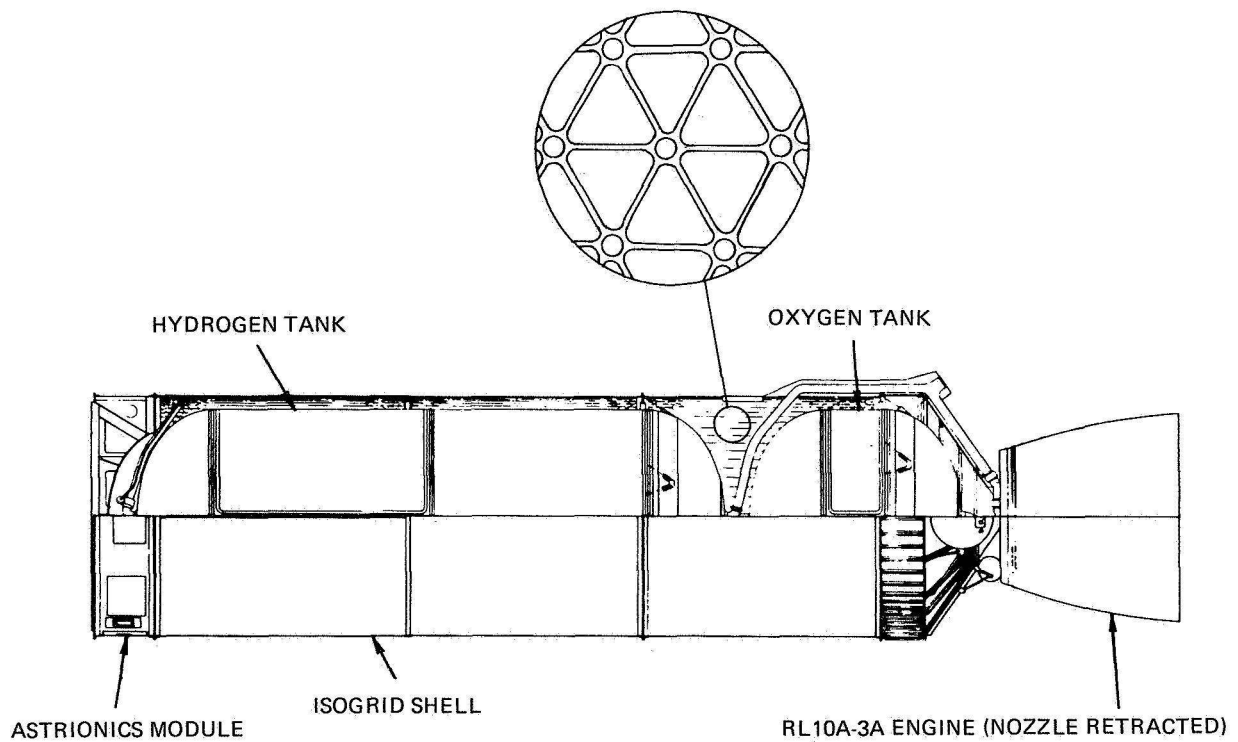


Figure 4.--Delta/Agena replacement stage.

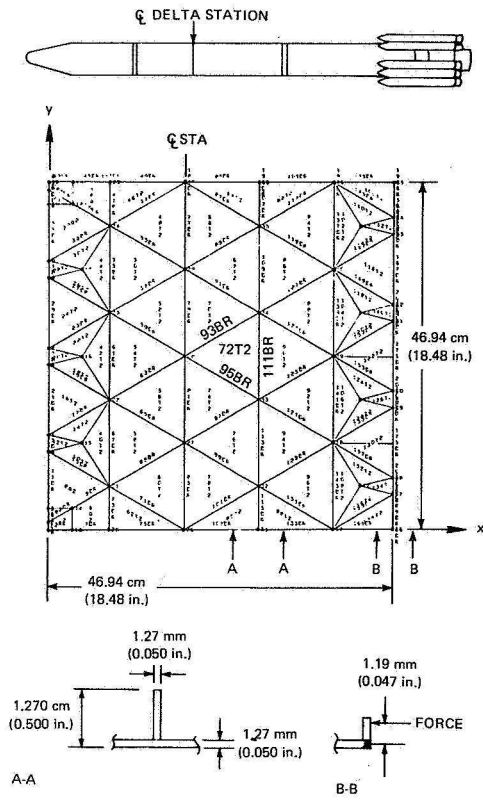


Figure 5.--Delta isogrid NASTRAN model .

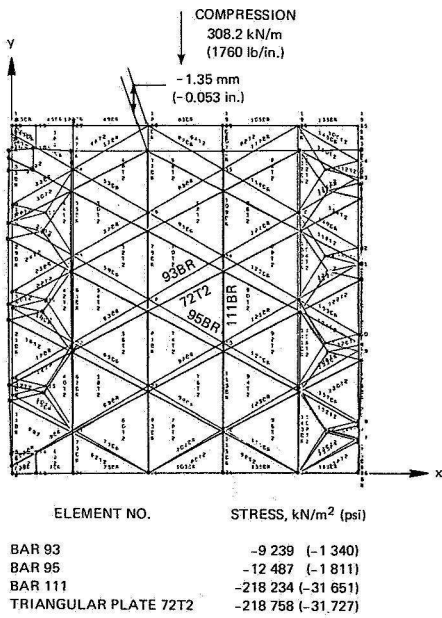


Figure 7.--Deflection and stresses, compression load in -y direction.

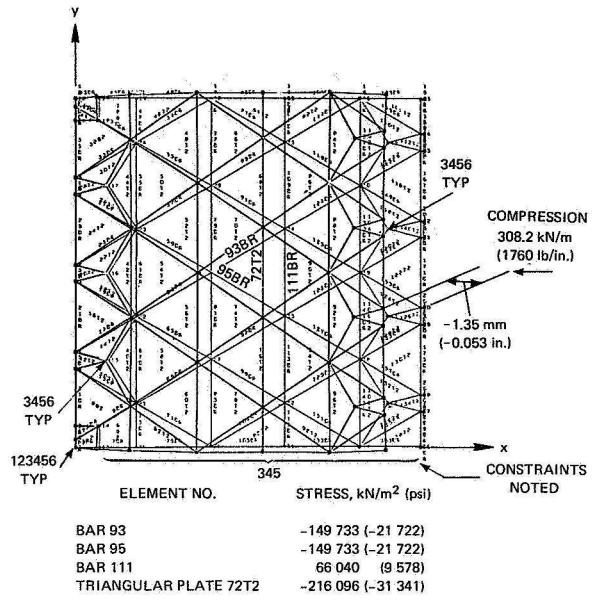


Figure 6.--Deflection and stresses, compression load in -x direction.

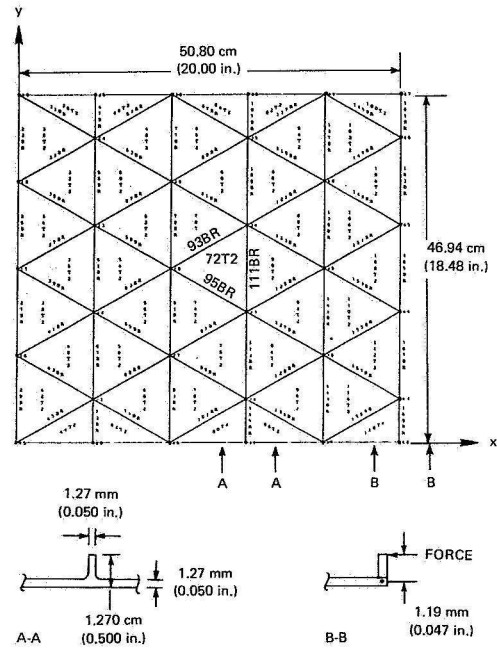
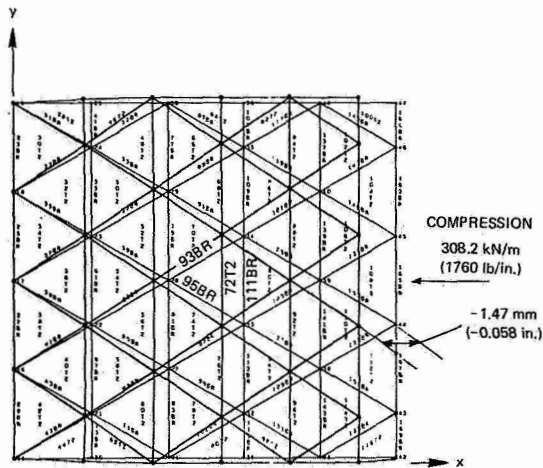
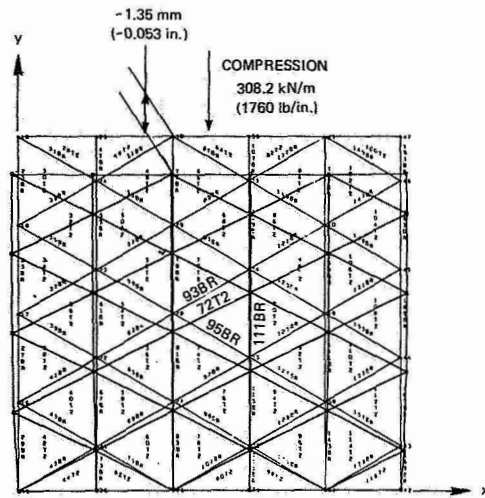


Figure 8.--Delta isogrid NASTRAN model (simplified).



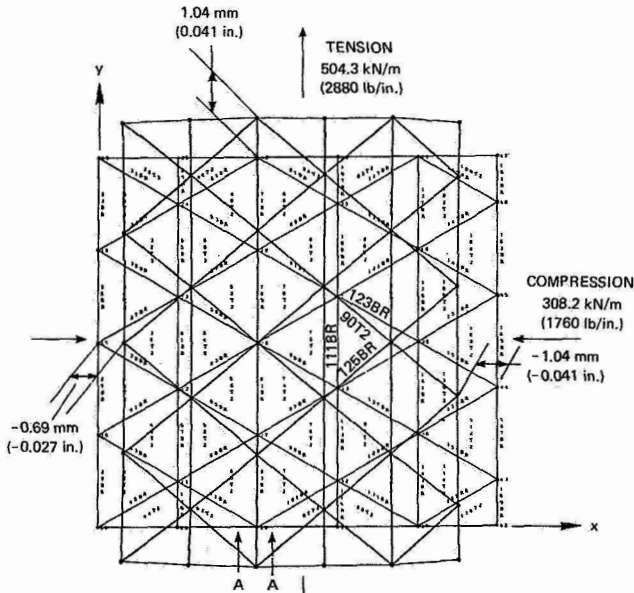
ELEMENT NO.	STRESS, kN/m <sup>2</sup> (psi)
BAR 93	-153 993 (-22 334)
BAR 95	-153 993 (-22 334)
BAR 111	64 737 (9 389)
TRIANGULAR PLATE 72T2	-222 198 (-32 226)

Figure 9.--Deflection and stresses, compression load in -x direction.



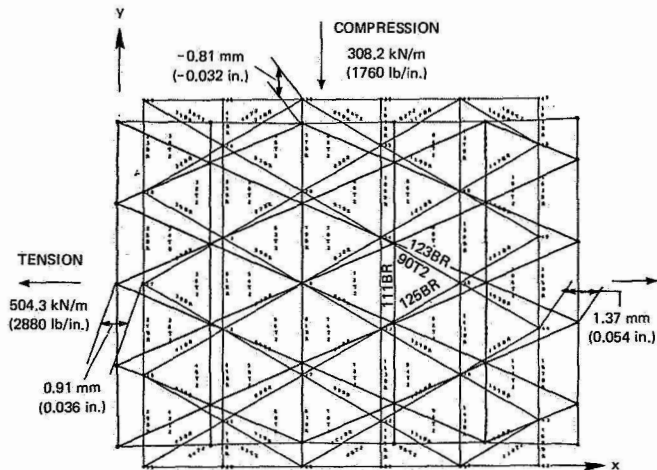
ELEMENT NO.	STRESS, kN/m <sup>2</sup> (psi)
BAR 93	-6 592 (-956)
BAR 95	-14 459 (-2 097)
BAR 111	-217 944 (-31 609)
TRIANGULAR PLATE 72T2	-219 309 (-31 807)

Figure 10.--Deflection and stresses, compression load in -y direction.



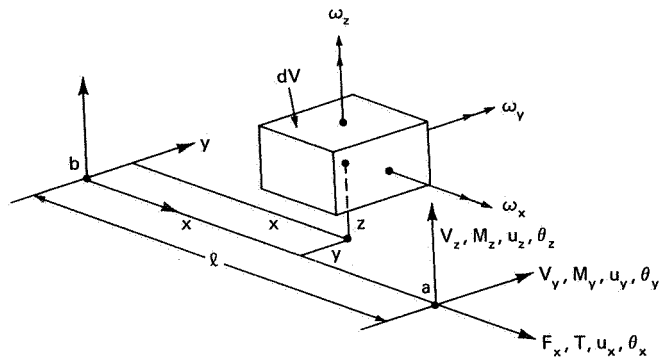
ELEMENT NO.	STRESS, kN/m <sup>2</sup> (psi)
BAR 123	-122 055 (-17 702)
BAR 125	-122 055 (-17 702)
BAR 111	327 954 (47 564)
TRIANGULAR PLATE 90T2	-173 637 (-25 183)

Figure 11.--Deflection and stresses, compression and tension loadings (tension parallel to main ribs).



ELEMENT NO.	STRESS, kN/m <sup>2</sup> (psi)
BAR 123	196 473 (28 495)
BAR 125	196 473 (28 495)
BAR 111	-252 067 (-36 558)
TRIANGULAR PLATE 90T2	-168 059 (-24 374)

Figure 12.--Deflection and stresses, compression and tension loadings (compression parallel to main ribs).



$$[K_{aa} + \lambda K_{aa}^d] \{u\} = 0$$

$f_{ya}$	$\frac{6F_x}{5l}$	0	$\frac{M_{yb}}{l}$	0	$-\frac{F_x}{10}$	$-\frac{6F_x}{5l}$	0	$\frac{M_{ya}}{l}$	0	$-\frac{F_x}{10}$	$u_{ya}$
$f_{za}$	0	$\frac{6F_x}{5l}$	$\frac{M_{zb}}{l}$	$\frac{F_x}{10}$	0	0	$-\frac{6F_x}{5l}$	$\frac{M_{za}}{l}$	$\frac{F_x}{10}$	0	$u_{za}$
$m_{xa}$	$\frac{M_{yb}}{l}$	$\frac{M_{zb}}{l}$	$\frac{IF_x}{l^2 A}$	$-\frac{lV_y}{6}$	$-\frac{lV_z}{6}$	$-\frac{M_{yb}}{l}$	$-\frac{M_{zb}}{l}$	$-\frac{IF_x}{l^2 A}$	$\frac{lV_y}{6}$	$\frac{lV_z}{6}$	$\theta_{xa}$
$m_{ya}$	0	$\frac{F_x}{10}$	$-\frac{lV_y}{6}$	$\frac{2l}{15} F_x$	0	0	$-\frac{F_x}{10}$	$\frac{lV_y}{6}$	$-\frac{lF_x}{30}$	0	$\theta_{ya}$
$m_{za}$	$-\frac{F_x}{10}$	0	$-\frac{lV_z}{6}$	0	$\frac{2l}{15} F_x$	$\frac{F_x}{10}$	0	$\frac{lV_z}{6}$	0	$-\frac{lF_x}{30}$	$\theta_{za}$
$f_{yb}$	$-\frac{6F_x}{5l}$	0	$-\frac{M_{yb}}{l}$	0	$\frac{F_x}{10}$	$\frac{6F_x}{5l}$	0	$-\frac{M_{ya}}{l}$	0	$\frac{F_x}{10}$	$u_{yb}$
$f_{zb}$	0	$-\frac{6F_x}{5l}$	$-\frac{M_{zb}}{l}$	$-\frac{F_x}{10}$	0	0	$\frac{6F_x}{5l}$	$\frac{M_{za}}{l}$	$-\frac{F_x}{10}$	0	$u_{zb}$
$m_{xb}$	$\frac{M_{ya}}{l}$	$\frac{M_{za}}{l}$	$-\frac{IF_x}{l^2 A}$	$\frac{lV_y}{6}$	$\frac{lV_z}{6}$	$-\frac{M_{ya}}{l}$	$-\frac{M_{za}}{l}$	$\frac{IF_x}{l^2 A}$	$-\frac{lV_y}{6}$	$-\frac{lV_z}{6}$	$\theta_{xb}$
$m_{yb}$	0	$\frac{F_x}{10}$	$\frac{lV_y}{6}$	$-\frac{lF_x}{30}$	0	0	$-\frac{F_x}{10}$	$-\frac{lV_y}{6}$	$\frac{2lF_x}{15}$	0	$\theta_{yb}$
$m_{zb}$	$-\frac{F_x}{10}$	0	$\frac{lV_z}{6}$	0	$-\frac{lF_x}{30}$	$\frac{F_x}{10}$	0	$-\frac{lV_z}{6}$	0	$\frac{2lF_x}{15}$	$\theta_{zb}$

Figure 13.--Prismatic beam and differential stiffness.

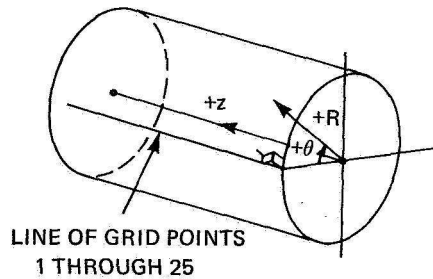
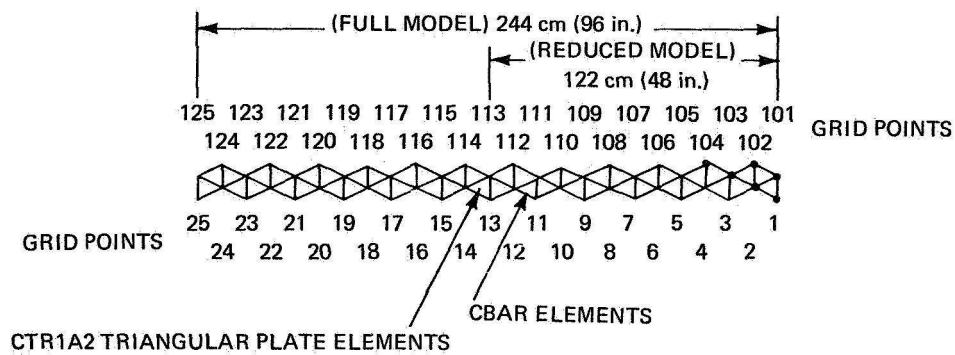


Figure 14.--NASTRAN segment for MOVE program.

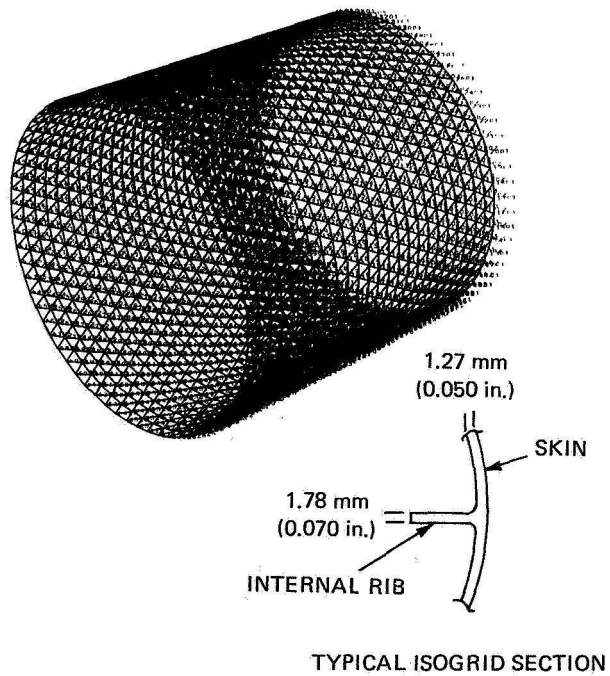


Figure 15.--Isogrid tank structural model (1850 grid points; 7986 elements).

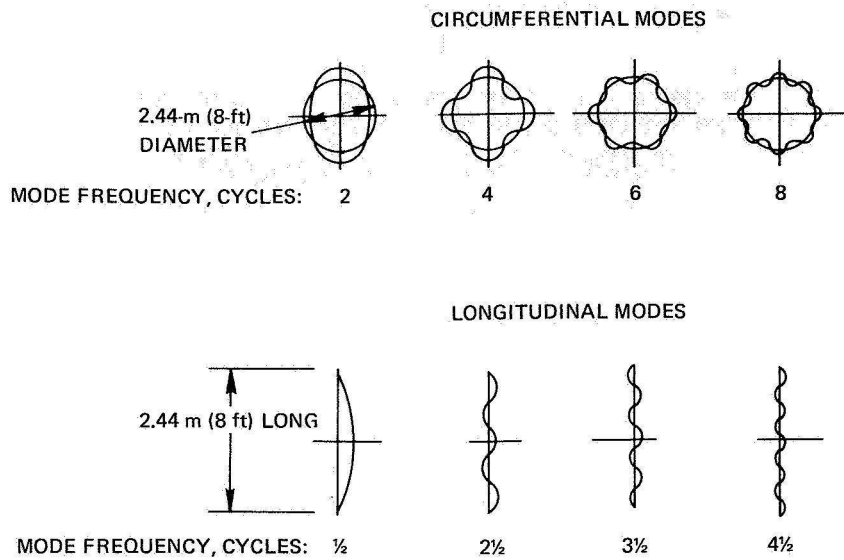


Figure 16.--Symmetric-symmetric modes for isogrid tank 2.44 m (8 ft) in diameter and 2.44 m (8 ft) in length.

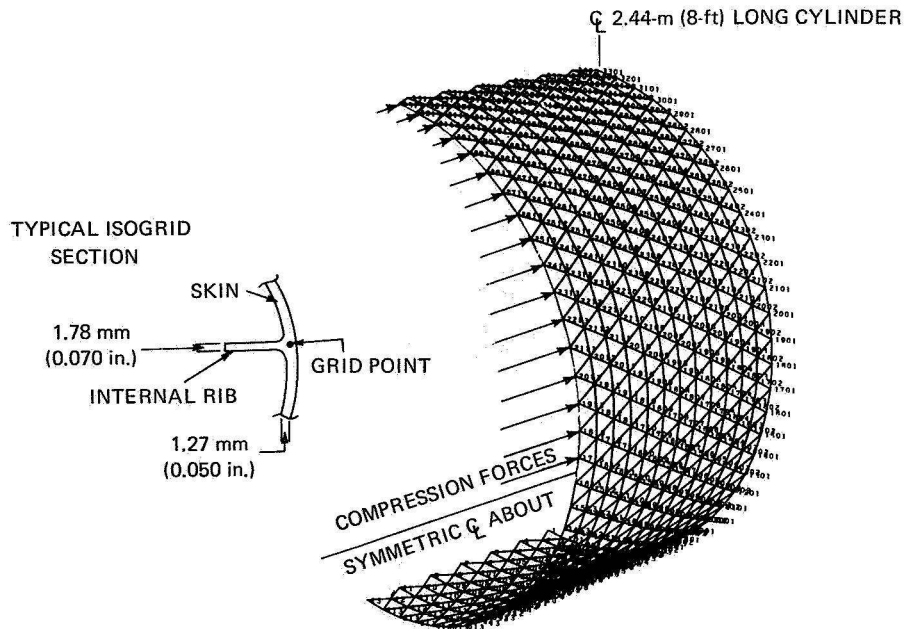


Figure 17.--One quarter tank model undeformed (1.2-m (4-ft) length, 1.2-m (4-ft) radius). Axial compression forces include bending moment equivalent force, axial force, and offsetting pressure equivalent force.

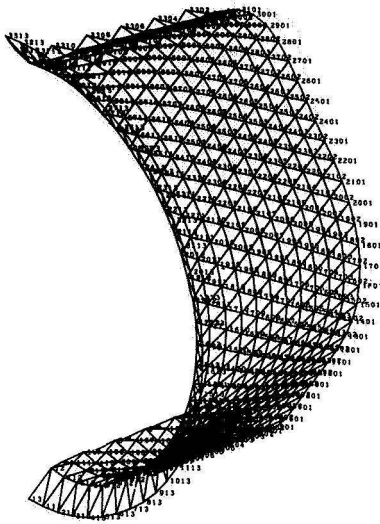


Figure 18.--Static deflections, compression load plus  $414\text{-kN/m}^2$  ( $60\text{-psi}$ ) external pressure.

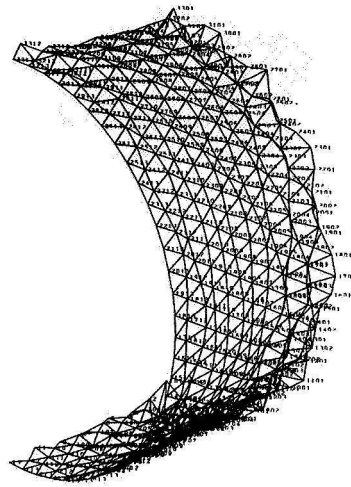


Figure 19.--First buckling mode, compression load plus  $414\text{-kN/m}^2$  ( $60\text{-psi}$ ) external pressure.

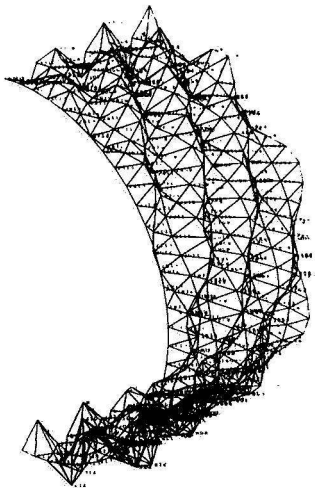


Figure 20.--Second buckling mode, compression load plus  $414\text{-kN/m}^2$  ( $60\text{-psi}$ ) external pressure.

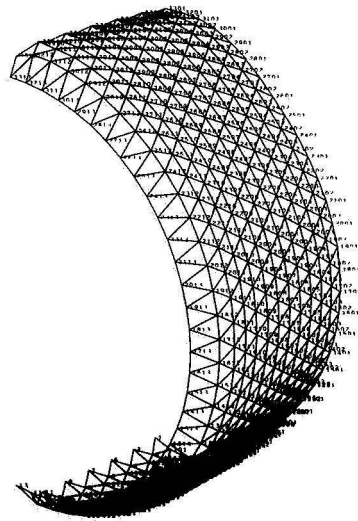


Figure 21.--Static deflections, compression load plus  $414\text{-kN/m}^2$  ( $60\text{-psi}$ ) internal pressure.

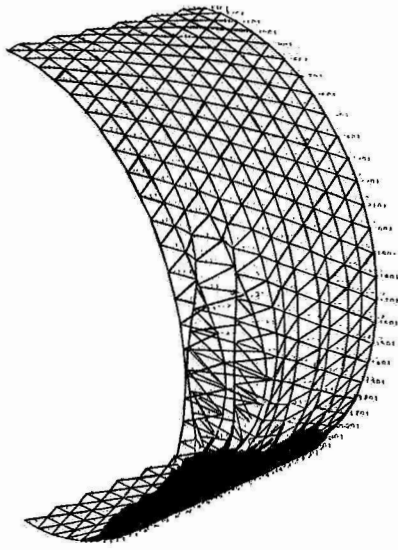


Figure 22.--First buckling mode, compression load plus 414-kN/m<sup>2</sup> (60-psi) internal pressure.

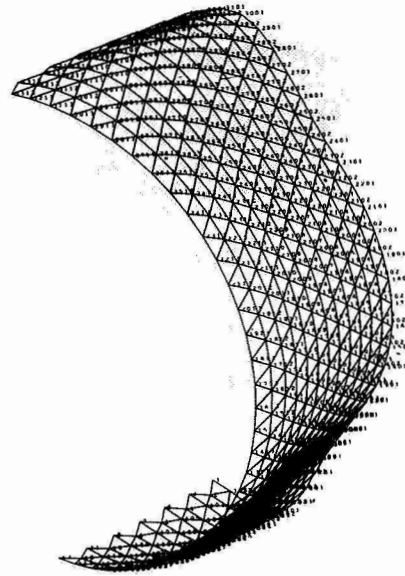


Figure 23.--Static deformation, compression load plus zero internal pressure.

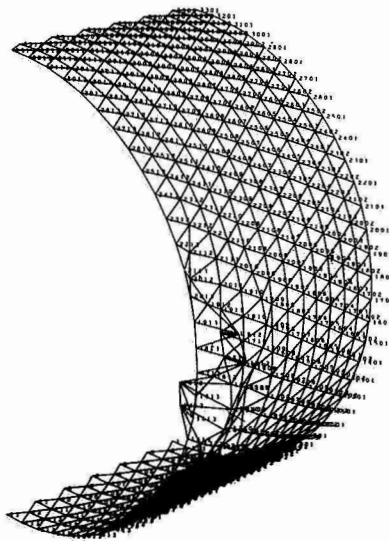


Figure 24.--First buckling mode, compression load plus zero internal pressure.

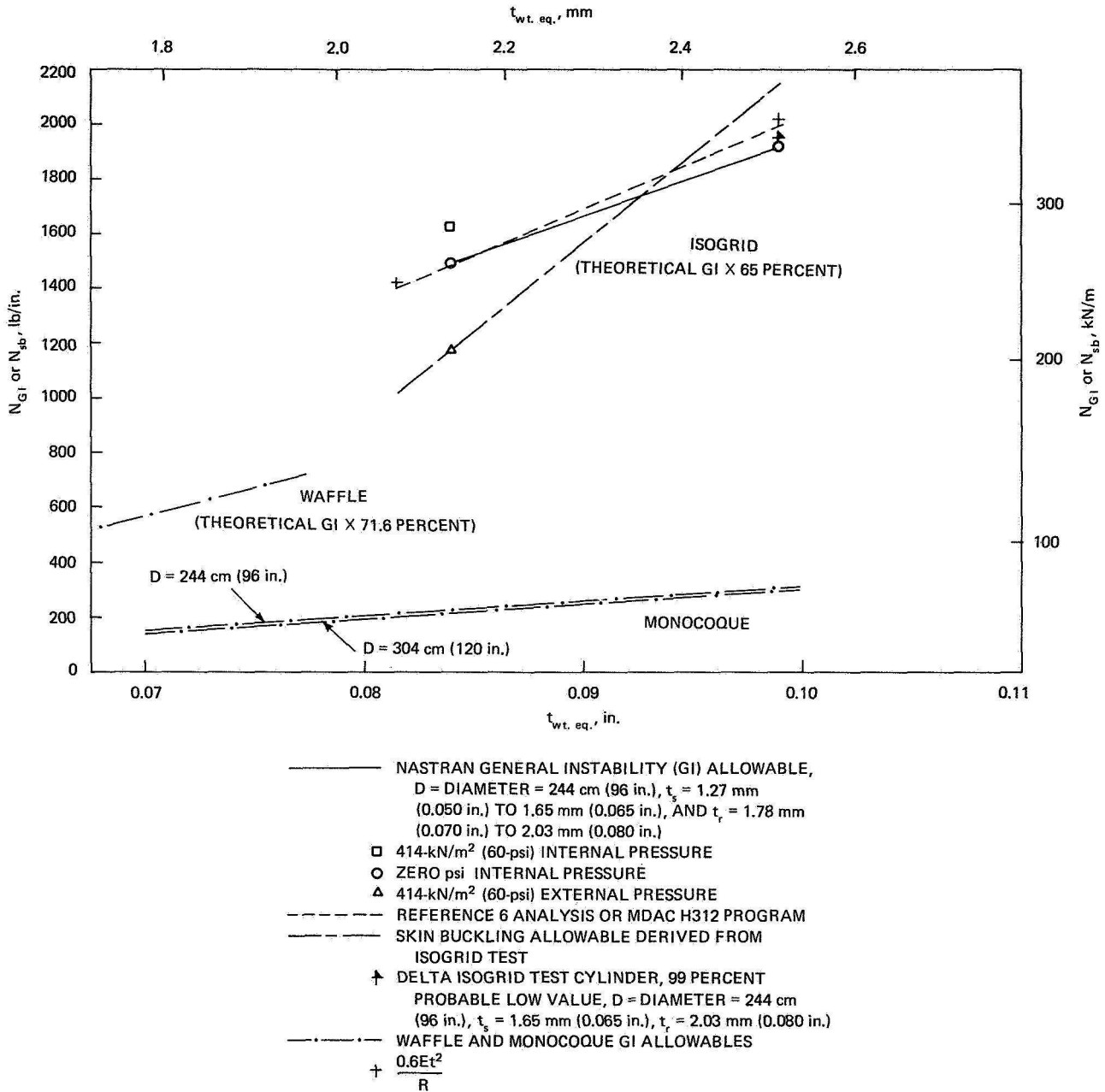


Figure 25.--Buckling allowables, 14ST6 aluminum cylinders.



A NASTRAN CORRELATION STUDY FOR VIBRATIONS  
OF A CROSS-STIFFENED SHIP'S DECK

By Earl A. Thornton

Old Dominion University

SUMMARY

To evaluate the effectiveness of NASTRAN for predicting the vibration modes of panels with bending-membrane coupling, a cross-stiffened ship's deck has been analyzed. In correlations with experimental data, one NASTRAN finite element representation gave results slightly more accurate than a previous analytical solution. Computational time was excessively long due to the Guyan method of reducing the eigenvalue problem. It is recommended that a more efficient method of matrix reduction be implemented for the lumped mass formulation.

INTRODUCTION

In studies concerning the shock environment of surface ships, the dynamic behavior of decks is of basic importance. Studies (References 1-4) performed at the Naval Ship Research and Development Center have established that the shock response of a deck can be predicted in terms of the input motions of the deck provided the modal characteristics of the deck are known.

The classical approach used to analyze the bending behavior of stiffened decks has been to use the concept of an equivalent orthotropic plate. After modification to include the effects of a few large, widely spaced stiffeners (References 1 and 2), the orthotropic plate approach has been used to successfully predict the vibration modes of a cross-stiffened ship's deck. In addition (References 3 and 4), the effect of local mass loadings on the vibration modes of the deck model has been studied by incorporating point masses in the modified orthotropic plate approach.

The application of this type of analytical representation is limited, of course, to highly idealized mathematical models of realistic ship structures. For this reason, it is of interest to evaluate the effectiveness of general purpose Finite Element programs such as NASTRAN by correlations with previous analytical and experimental studies.

A stiffened deck modeled with the finite element approach using a combination of plate and bar elements is characterized by a coupling between in-plane and transverse bending displacements. This behavior is characteristic of a number of other panel problems including corrugated panels which are among candidate thermal protection systems for the space shuttle. For this reason also, it is of interest to evaluate the effectiveness of NASTRAN for the prediction of vibration modes of stiffened decks.

The present paper describes a correlation study performed using NASTRAN to predict the vibration frequencies and modes of the 1/4-scale model of the cross-stiffened ship's deck studied in References 1-4. This structure was selected for investigation primarily because of availability of previous analytical and experimental results. The structure is also of further interest since its construction details are representative of a realistic ship structure. Thus, the study provides insight into the effectiveness of finite element modeling as used in NASTRAN when applied to a prototype ship structure.

The specific objectives of the study were to predict natural frequencies and nodal patterns of the model deck and correlate these with the available analytical and experimental results.

The study was performed from the viewpoint that the analyst would like to employ a detailed finite element representation of all details of the deck construction for accurate prediction of frequencies, as well as detailed predictions of mode shapes and modal stress distributions. Moreover, it would be desirable for the computational scheme to give a fast, accurate prediction of a large number of modes in one pass using an eigenvalue routine which protects the analyst from overlooking modes. The NASTRAN analysis was formulated and performed to satisfy these characteristics. The results of the NASTRAN analysis, after correlation with previous results, were evaluated in terms of these criteria.

## STIFFENED DECK MODEL

The model ship's deck studied is the top deck of a 1/4-scale model of a compartment of a surface ship constructed and used by the Naval Ship Research and Development Center for shock and vibration studies. The details of the deck are shown in Figure 1. The center panel of the deck between the two interior bulkheads was the subject of the previous investigations reported in References 1-4. The center panel is stiffened in the transverse direction by a large number of closely spaced stiffeners and in the longitudinal direction by two widely spaced, deep

stiffeners. Attempts were made in the design and construction of the model to provide clamped boundary conditions at the two edges of the panel supported by the interior bulkheads. The model was constructed in a Naval Shipyard using fabrication techniques representative of prototype ship construction.

#### PREVIOUS ANALYTICAL METHOD

The classical approach of representing the bending stiffness of ship's decks uses orthotropic plate theory. This approach was investigated in Reference 1. It was demonstrated that the presence of the two deep longitudinal stiffeners limited the accuracy of the orthotropic solution to only a few lower modes. As an improvement on the orthotropic theory, the flexure of the longitudinal stiffeners was considered separately which led to a modified version of the orthotropic plate equation. This approach, the Separated Stiffener Method, gave good agreement with the experimental frequencies for the EC-2 deck for up to nine half waves along the deep stiffeners.

The differential equation describing the eigenfunctions  $\phi$  of the stiffened deck by the Separated Stiffener Method has the form

$$L[\phi] = \lambda M[\phi] \quad (1)$$

where the eigenvalues  $\lambda$  are related to the unknown natural frequencies  $\omega$ , by  $\lambda = \omega^2$ . In this differential equation, the stiffness operator  $L$  is given by

$$L = D_x \frac{\partial^4}{\partial x^4} + 2H \frac{\partial^4}{\partial x^2 \partial y^2} + [D_y + \sum D_{y_i} \delta(x-a_i)] \frac{\partial^4}{\partial y^4} \quad (2)$$

and the mass operator

$$M = \rho + \sum \mu_i \delta(x-a_i) \quad (3)$$

In the above equations,  $D_x$ ,  $H$ ,  $D_y$  are the orthotropic plate stiffnesses,  $D_{y_i}$  is the bending stiffness of the  $i$ th longitudinal stiffener and associated plating,  $\rho$  is the orthotropic plate mass per unit area,  $\mu_i$  is the beam mass per unit length, and  $\delta$  is the Dirac delta function.

For the boundary conditions of the EC-2 deck, this equation was solved by separation of variables in the form,

$$\phi_{mn} = X_{mn}(x) Y_n(y) \quad (4)$$

where  $m$  and  $n$  are integers. Beam mode shapes were used for the  $Y_n$  functions in connection with an energy approach to obtain the  $X_{mn}$  functions. These results are tabulated in Reference 1. It may be noted from the form of equation (4) that the Separated Stiffener Method always predicts straight nodal lines. The results of the Separated Stiffener analysis will be presented later for correlation with experimental findings and the results of the NASTRAN analysis.

## NASTRAN ANALYSIS

### NASTRAN Finite Element Models

Two NASTRAN analyses were performed. In the first analysis, NASTRAN Model 1, the center panel of the deck was analyzed for direct comparison with the previous analytical predictions. In the second analysis, NASTRAN Model 2, the entire deck of the EC-2 deck was represented in hopes of obtaining improved agreement with the experimental results.

The finite element mesh for the two NASTRAN models is shown in Figure 2. In the NASTRAN Model 1 analysis, the interior deck panel was modeled using 1/2 symmetry. The deck plating was represented with 220 CQUAD2 plate elements. All stiffeners were represented with offset CBAR elements; 240 bar elements were used. The entire deck was represented as NASTRAN Model 2 using 1/4 symmetry. In the NASTRAN Model 2 analysis, 143 CQUAD2 elements and 132 CBAR elements were employed. Element properties for these two models are tabulated in Table I. Before constraints, NASTRAN Model 1 had 1265 degrees of freedom and NASTRAN Model 2 had 840 degrees of freedom.

### NASTRAN Computations

All NASTRAN computations were performed using the lumped mass formulation. Prior to eigenvalue extraction, rotational and in-plane degrees of freedom were omitted using the NASTRAN Guyan reduction method. Eigenvalue extraction was performed for both analyses using the Givens method. Degrees of freedom at each stage in the analyses are shown in Table II.

Plots of the nodal patterns for the NASTRAN analyses were obtained from a separate FORTRAN program. During each NASTRAN execution, printed and punched output for the eigenvectors was requested. After execution the eigenvectors were copied from the punchfile onto a tape. This tape was subsequently used as

input to the FORTRAN program which calculated nodal points by linear interpolation between grid point displacements. Nodal points were calculated by first making sweeps along lines parallel to the x-axis and then along lines parallel to the y-axis. The resulting nodal points were then plotted using a DDI plotter to yield the nodal patterns.

Significant computational times in various modules as well as total times are tabulated in Table III. All computations were performed on LRC, CDC 6600 computers. A salient characteristic of both analyses is that a very large amount of time was required to perform the Guyan reductions.

## DISCUSSION OF RESULTS

Comparisons of the experimental and predicted frequencies are given in Table IV. Measured frequencies are compared with the analytical solution previously described and the results of the two NASTRAN analyses. Measured nodal patterns are compared with NASTRAN predicted patterns in Figure 3.

The NASTRAN frequency predictions, on the average, are in slightly better agreement with the experimental results than the analytical solution. NASTRAN Model 1, which has the same boundary conditions as the analytical solution, has an average percentage difference of 8.5% whereas the analytical solution has an average percentage difference of 10.9%. The second NASTRAN model, which predicted the fundamental frequency almost exactly, generally predicted lower frequencies than the experimental results.

The fact that the second NASTRAN model predicted frequencies which were generally too low may be attributed to the simply supported boundary condition assumed on the interior bulkheads. The model was designed for the interior bulkheads to represent clamped edges. The experimental nodal patterns show, however, that some rotation is permitted. From the second NASTRAN analysis it may be concluded that the boundary conditions at the bulkheads are most nearly represented as fully clamped since assuming simple supports predicts frequencies consistently much too low.

The nodal patterns predicted by NASTRAN Model 1 show good agreement with the experimental results. Although the analytical prediction of nodal lines were unavailable these results consist of intersecting straight lines. NASTRAN predicted nodal lines which were generally nonintersecting and curved.

The disappointing feature of the NASTRAN analyses was the long computer times required to reduce the degrees of freedom prior

to eigenvalue extraction. In the NASTRAN Model 1 analysis, the Guyan reduction required approximately 3000 CPU seconds out of a total of 5300 CPU seconds. Of the 3000 seconds required in the Guyan reduction, over 70% of the time was required in reduction of the mass matrix.

One of the reasons that NASTRAN was relatively inefficient in the present analyses is that no attempt is made to take advantage of the lumped mass formulation. Considerable time-savings would have been accomplished if a distinction was made between the reduction used for the lumped mass and consistent mass formulations. For a considerable number of vibration problems (see Reference 5), the gain in computational efficiency offered by the lumped mass formulation more than offsets advantages of the increased accuracy and bounded nature of the consistent mass formulation.

#### CONCLUDING REMARKS

To evaluate the effectiveness of NASTRAN for predicting the vibration modes of panels with bending-membrane coupling, a cross-stiffened ship's deck has been analyzed. A fine mesh of beam and plate elements was used. To obtain a large number of modes and to insure that all modes were obtained, the matrix eigenvalue problem was reduced by a Guyan reduction and solved by the Given's method.

For one NASTRAN finite element model, the matrix reduction for the stiffness matrix required about 850 CPU seconds, and the mass matrix reduction required about 2200 CPU seconds. The long computational time was required because of large matrix multiplications in the Guyan reduction.

In correlations with experimental data one NASTRAN finite element model was slightly more accurate for frequency predictions and nodal patterns than a previous analytical method. Agreement with experimental results was good.

It can be concluded that NASTRAN was effective in meeting all of the evaluation criteria with the exception of computational time. Excessively large computer time was required because of the Guyan method of reducing the mass matrix. It is recommended that the NSMO consider investigating and implementing other more efficient methods of mass matrix reduction for the lumped mass formulation.

## ACKNOWLEDGEMENT

This study was performed at the NASA Langley Research Center during the summer of 1971 under the sponsorship of the NASA-ASEE Summer Faculty Fellowship program.

The author is pleased to acknowledge the assistance of a number of LRC personnel particularly Barbara J. Durling who wrote the FORTRAN program for plotting the nodal patterns.

## REFERENCES

1. Short, R. D., Jr., "Theoretical Determination of Natural Modes of Deck Vibrations," Marine Technology, Vol. 3, No. 1, January 1966.
2. Short, R. D., Jr., and Moore, D., "Analysis of the Response of a Ship's Deck to Underwater Explosions," Naval Ship Research and Development Center Report C-2193, July 1967.
3. Thornton, E. A., "Effect of Equipment Mass on the Shock Motions of Decks," 40th Shock and Vibration Symposium, Hampton, Virginia, October 1969.
4. Thornton, E. A., "A Method for the Prediction of Shock Motions at Deck Mounted Equipment, Naval Ship Research and Development Center Report C-2544, December 1969.
5. Clough, R., "Analysis of Structural Vibrations and Dynamic Response," Recent Advances in Matrix Methods of Structural Analysis and Design, edited by R. H. Gallagher, Y. Yamada, and J. T. Oden, The University of Alabama Press, 1971.

Table I  
Bar Element Properties

Stiffener	Components of Offset Vector			Area cm <sup>2</sup>	Moments of Inertia			Torsional Constant cm <sup>4</sup>
	Z1 cm	Z2 cm	Z3 cm		I1 cm <sup>4</sup>	I2 cm <sup>4</sup>	I12 cm <sup>4</sup>	
Transverse y = constant	0.0	0.4298	3.167	1.785	3.694	0.9121	-1.061	.0420
Longitudinal x = 129.5 cm	-1.183	0.0	8.659	9.149	157.9	36.06	-43.75	.6919
x = 281.9 cm	1.183	0.0	8.659	9.149	157.9	36.06	43.75	.6919

Table II  
Degrees of Freedom (DOF) During Computations

	NASTRAN Model 1 (one-half symmetry)	NASTRAN Model 2 (one-quarter symmetry)
DOF Before Constraints	1265	840
DOF After SPC	1028	648
DOF Omitted	798	516
DOF for Eigenvalue Problem	230	132

Table III  
Computational Times for NASTRAN Analyses

Operation (Module)	CPU Time (seconds)	
	NASTRAN Model 1	NASTRAN Model 2
Generate Stiffness Matrix (SMA1)	210	136
Generate Mass Matrix (SMA2)	9	4
Impose SPC (SCE1)	26	17
Reduction of Stiffness Matrix (SMPI)	852	911
Reduction of Mass Matrix (SMP2)	2198	
Eigenvalue Extraction (READ)	1453	348
Eigenvector Recovery for 25 Modes (SDR1)	249	118
Total CPU for Above Operations	4997 Seconds	1534 Seconds
Total CPU for all Operations	5344 Seconds	1674 Seconds
Total PPU for all Operations	3260 Seconds	927 Seconds

Table IV  
Measured and Computed Natural Frequencies of Deck

Analytical Half-Wave Numbers		Measured Frequency	Analytical Solution (Ref. 1)		NASTRAN Model 1		NASTRAN Model 2	
n*	m*	HZ	HZ	%Diff.	HZ	%Diff.	HZ	%Diff.
1	1	29	35.0	20.7	33.2	14.5	28.9	0.3
	2	47	44.4	5.5	43.1	8.3	36.5	22.3
	3	67	57.5	14.2	58.6	12.5	51.1	23.7
3	1	88	96.3	9.4	86.7	1.5	83.1	5.6
	2	84	79.8	5.0	79.9	4.9	69.0	17.9
	3	62	57.8	6.8	68.1	9.8	64.5	4.0
5	1		105.0		97.5		94.4	
	2		87.0		91.2		84.0	
	3	76	64.6	15.0	81.9	7.8	76.2	0.2

\*n denotes the number of half waves along the y-axis; m denotes the number of half waves along the x-axis.

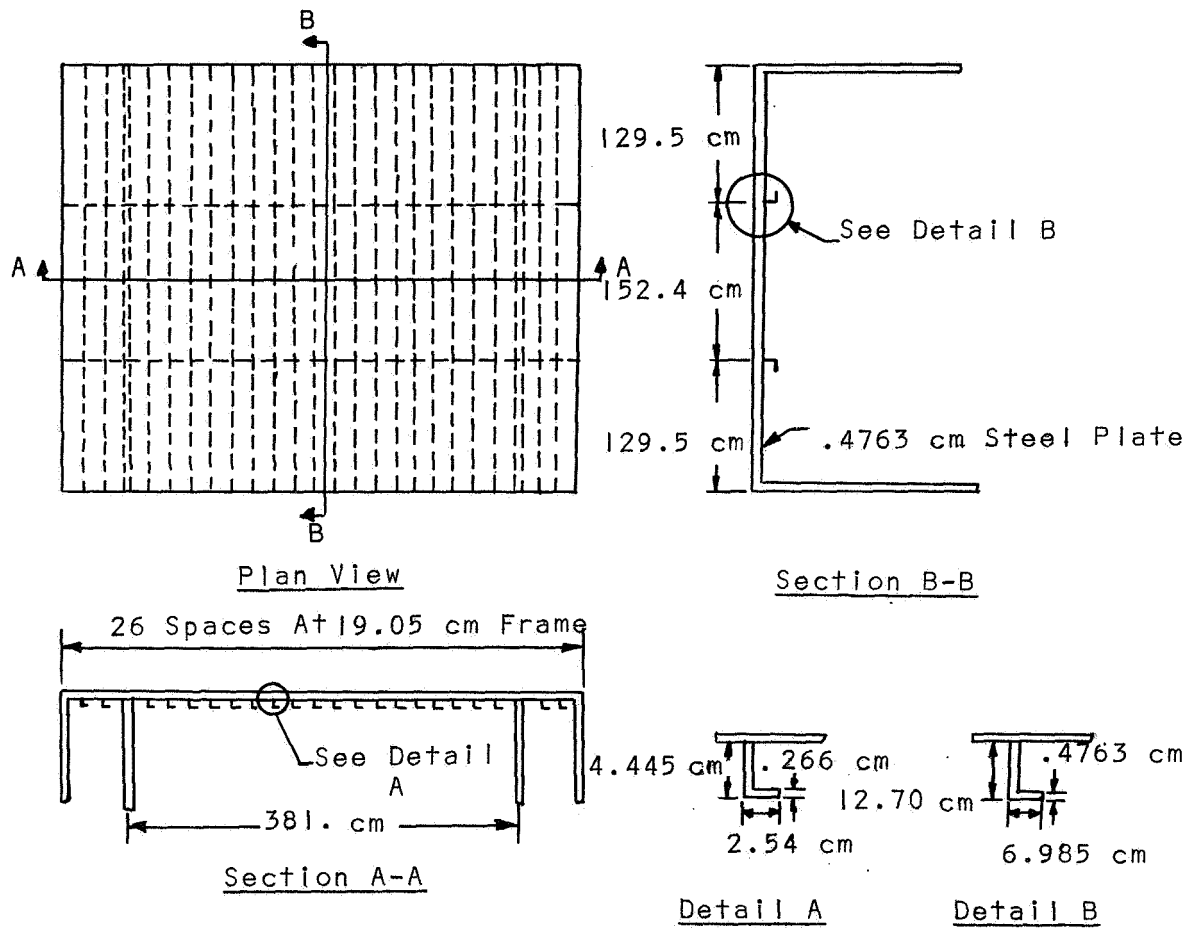


Figure 1.- Cross-stiffened model of ship's deck.

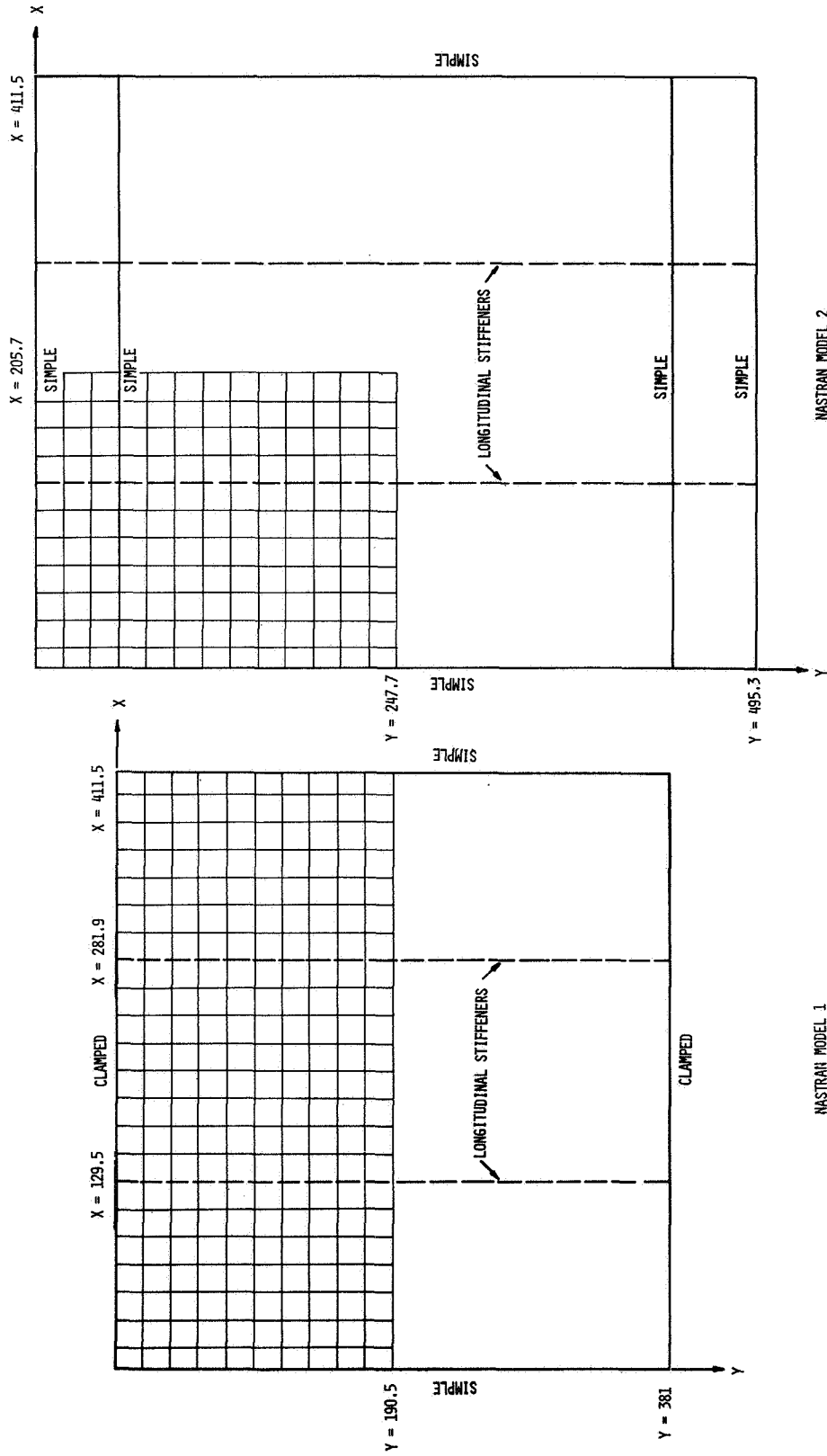
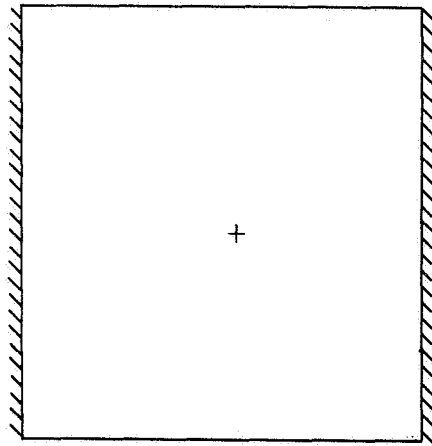
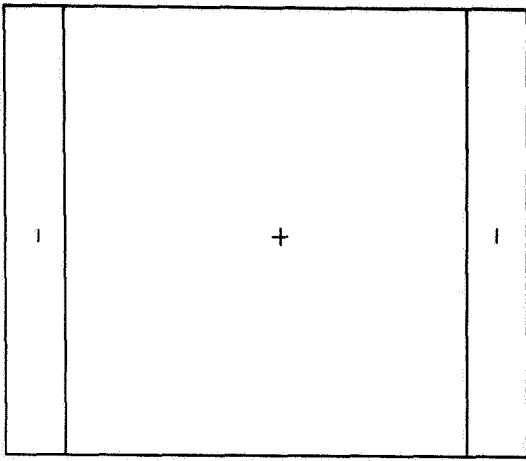
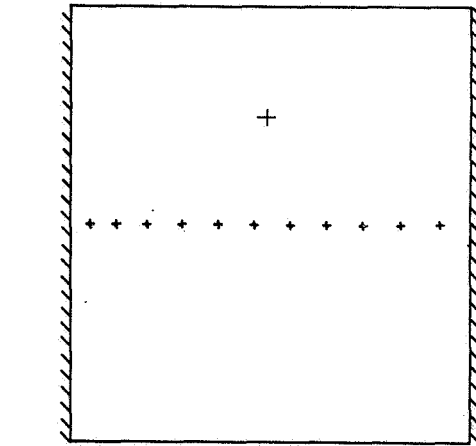
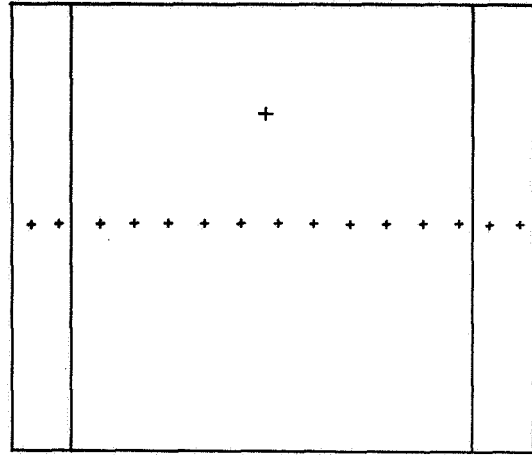


Figure 2.- NASTRAN finite element models.



NASTRAN MODEL 2 28.9 HZ

NASTRAN MODEL 1 33.2 HZ



NASTRAN MODEL 2 36.5 HZ

NASTRAN MODEL 1 43.1 HZ

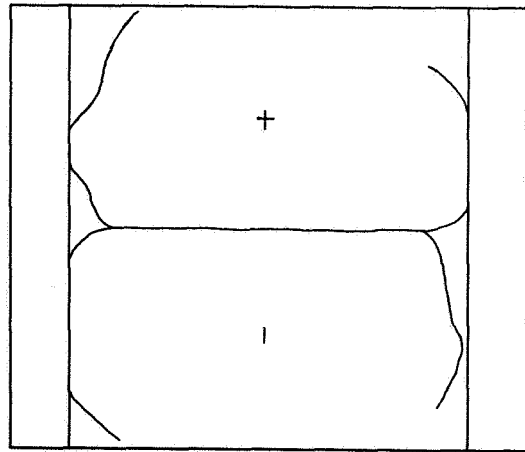
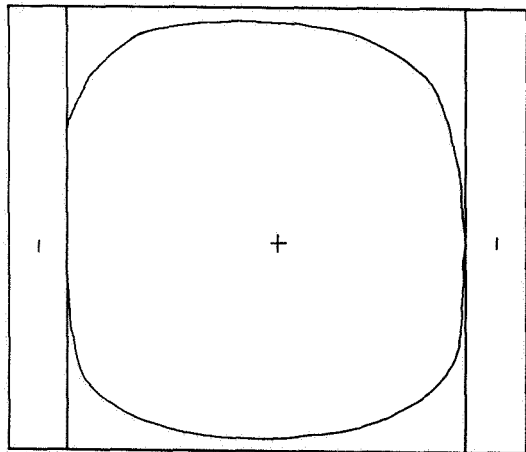
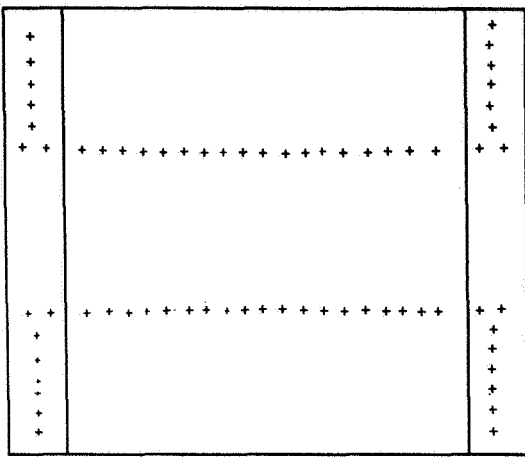
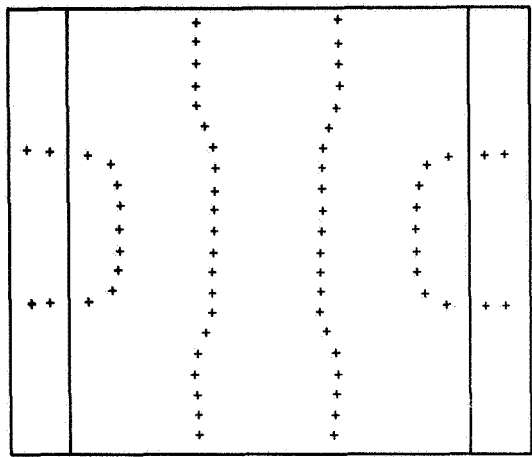


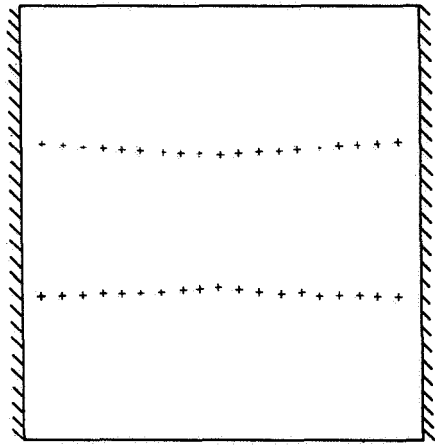
Figure 3.- Experimental and NASTRAN nodal patterns.



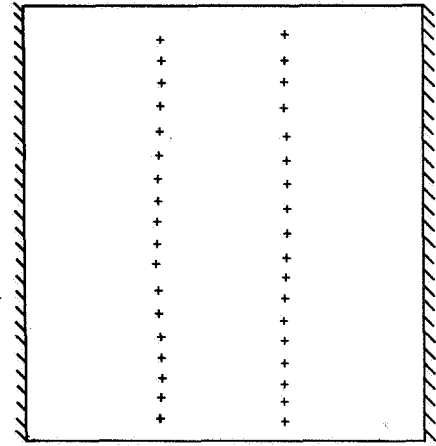
NASTRAN MODEL 2 51.1 HZ



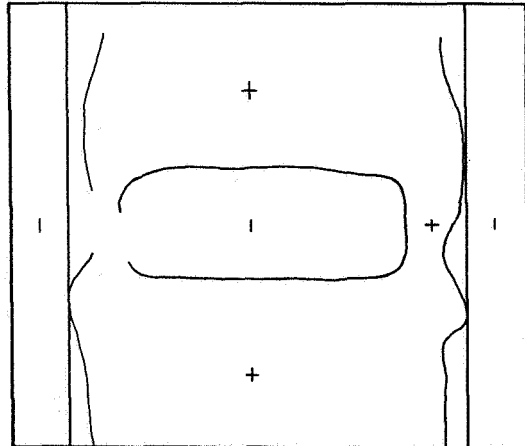
NASTRAN MODEL 2 83.1 HZ



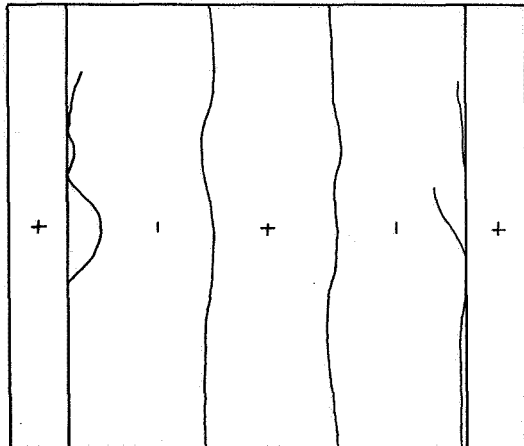
NASTRAN MODEL 1 58.6 HZ



NASTRAN MODEL 1 86.7 HZ



N = 1, M = 3 EXP. FREQUENCY 67 HZ



N = 3, M = 1 EXP. FREQUENCY 88 HZ

Figure 3.- Experimental and NASTRAN nodal patterns - Continued.

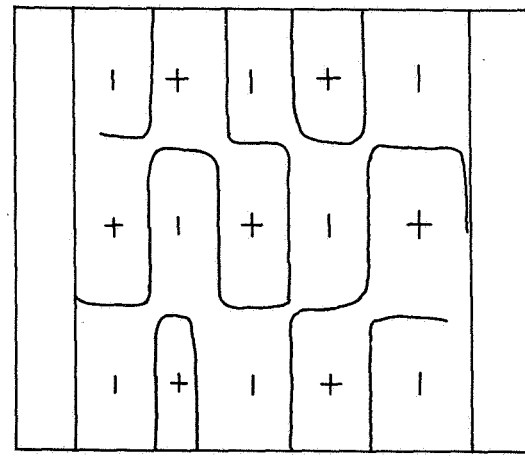
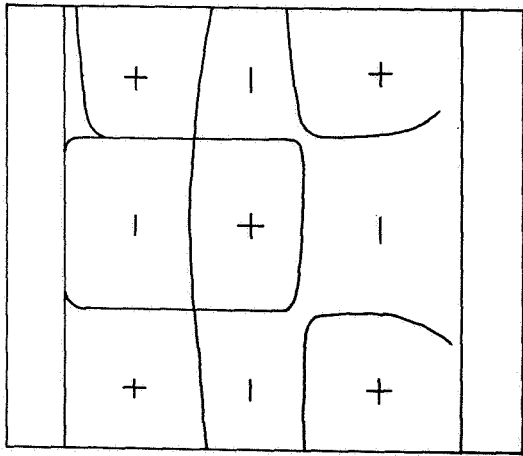
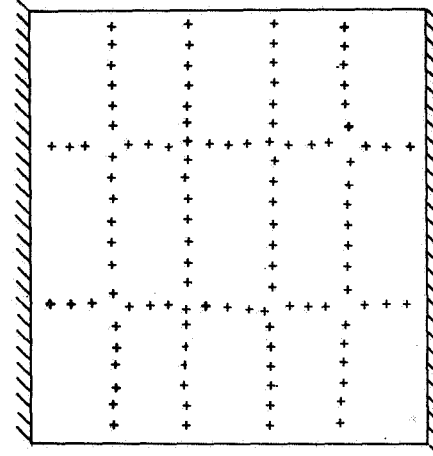
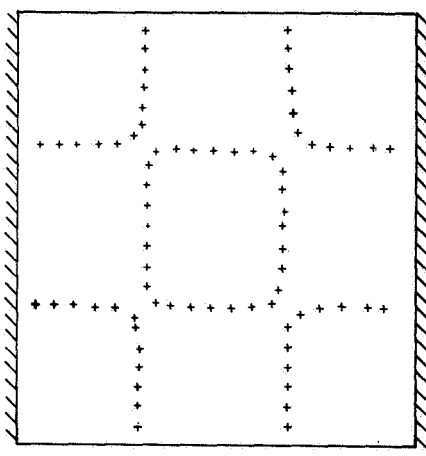
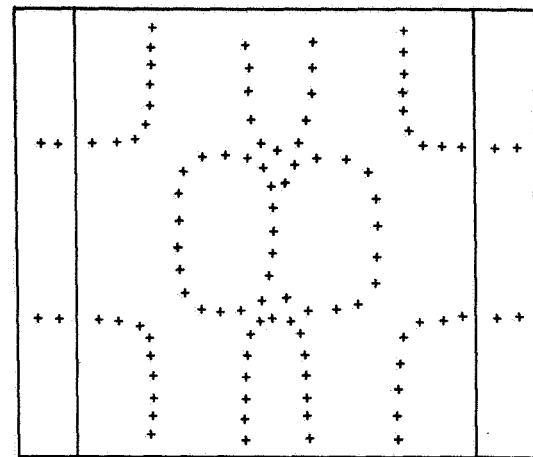
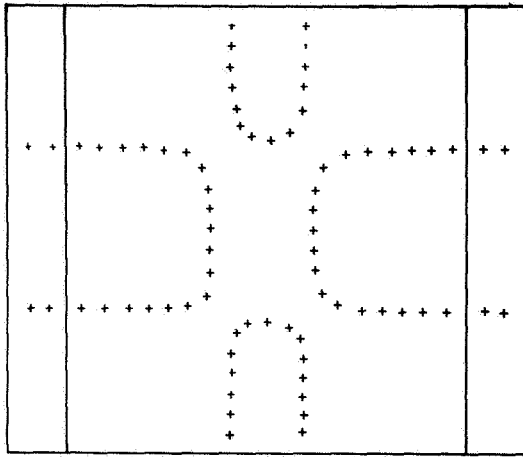


Figure 3.- Experimental and NASTRAN nodal patterns - Concluded.



# TRANSIENT ANALYSIS OF AN IVHM GRAPPLE IMPACT TEST

By R. G. Hill  
Hanford Engineering Development Laboratory

## SUMMARY

A lumped-mass model has been used to represent the impact condition between a fuel duct and an IVHM (In-Vessel Fuel Handling Machine). The non-linear effects of a Bellville spring and the free fall impact of the fuel duct on the IVHM were included. The purpose of the tests was to determine the loads on the fuel duct due to the impact. A comparison between experimental and theoretical results is presented.

## INTRODUCTION

In the operation of the FTR (Fast Test Reactor) an IVHM is used to handle core components under various component and core conditions. The component under consideration is a fuel duct which interfaces with the IVHM by means of a grapple mechanism. The grapple grips a nozzle-handling socket mounted on the end of the fuel duct. Under certain operating conditions the fuel duct drops a short distance to impact on the grapple fingers. A simulated mechanical mockup of the FTR core and the IVHM was set up, and IVHM fuel duct withdrawal and insertion tests were conducted. During these tests high accelerations were measured on the simulated fuel duct. The experimental data indicated that the acceleration loads were due to the impact of the fuel duct on the grapple. This paper describes how the results of the analysis and tests of the impact are interpreted in terms of the response of the simulated fuel duct and the IVHM structure.

## SYMBOLS

a	acceleration
B	scalar damper
d	drop distance
g	structural damping
t	time

## DESCRIPTION OF IVHM

The FFTF (Fast Flux Test Facility) simulated core test facility and an IVHM positioned for fuel duct insertion are shown in figure 1. The IVHM consists of a motor-driven mechanism mounted on a lead screw and a grapple assembly as shown in figures 1 to 3. Four fuel duct support fingers (fig. 3) support the weight of the fuel duct during insertion and provide for the withdrawal forces. The IVHM is used to transfer fuel duct components from the

active core to fixed storage positions located outside the core region. Fuel handling problems can occur due to distortion of the individual fuel ducts and the core. The distortion effects can be induced by stainless steel swelling and thermal creep (ref. 1). Twelve core restraint yokes located hexagonally at two levels maintain the lateral position and compactness of the core.

#### Free Fall Condition

There are two operating conditions of the IVHM that have been investigated in this report. The first is a free fall impact of the fuel duct on the grapple and, secondly, a free fall impact combined with an initial condition of pre-load on the IVHM and fuel duct. During the insertion of the fuel duct, the above core load pad contacts the core (fig. 1), and a gap exists between the fingers on the grapple and the fuel duct. The core restraint yokes are retracted, the respective fuel duct position opens and the fuel duct drops the gap distance to impact on the grapple support fingers.

#### Pre-Load Conditions

Certain core conditions (ref. 1) require that a compressive force be applied to the fuel duct for insertion. The lead screw on the IVHM is used to apply the compressive force through the grapple (turnbuckle effect) to the fuel duct. Again, as the grapple engages the top of the fuel duct for the compressive load a gap exists between the grapple fingers and the nozzle-handling socket on the fuel duct.

When insertion occurs the fuel duct experiences a free fall with an initial condition of pre-load. The compressive pre-load (turnbuckle effect) is relieved on both the fuel duct and the IVHM during the first milliseconds of fuel duct free fall. The fuel duct then impacts on the grapple support fingers. The load cell oscillogram indicated that the 1000 lb pre-load initial condition was a ramp function with a time duration of 0.026 second. The effect of the pre-load on the initial acceleration of the fuel duct is unknown. Due to the manner in which the accelerations were recorded, the change in free fall time due to the pre-load could not be determined.

### LUMPED-MASS MODEL

#### Basic Model

After a review of the test facility and test data, it was decided to use a relatively simple model to represent the IVHM and fuel duct so that the results of the analysis would be available quickly. The physical properties used in the model in most cases were calculated from the results of load deflection and other tests on the simulated IVHM. Figure 4 shows the scalar elements that were chosen to represent the stiffnesses, masses, and damping properties of the IVHM and the fuel duct. The IVHM and fuel duct were idealized with six degrees of freedom with instrumentation locations and areas of nonlinear response considered in the selection of grid points and lumped masses. The scalar damper values shown in the NASTRAN Input (fig. 5) were calculated from the frequency and measured structural damping values (see ref. 2 for equation). A structural

damping value ( $g = 15$  percent) was calculated for the assembled IVHM by considering the rate of decay and of successive rebounds of the fuel duct on grapple support fingers, as shown by the IVHM load cell oscillogram (fig. 6). A structural damping value of  $g = 2$  percent was calculated for fuel duct. The fuel duct was empty except for a lead weight mounted in bottom of the duct to simulate the components of the fuel duct.

#### Nonlinear Considerations

Two nonlinear conditions were considered in the model shown in figure 4, a Bellville spring with stiffness different in tension than in compression, Element 4, and the free fall gap, Element 5. For these conditions the nonlinear provision of NASTRAN was used. The nonlinear effects were treated through the use of an additional applied load vector and by means of a transfer function, the NONLIN 1 and TF input cards. (See figure 5 for NASTRAN input.) To use the nonlinear provision requires rigid format 9, Direct Transient Response. In this format (ref. 3) numerical integration of the coupled equations is achieved by employing a central difference equivalent step-by-step procedure. It was found that the solution became unstable as the time step was increased or as the value of the lumped masses was reduced. The stability problem was evident through large and/or plus or minus oscillating displacements. A discussion of the stability problems described here is found in appendix C of reference 4.

#### COMPARISON OF RESULTS

Results from the lumped-mass model for displacement, force, and acceleration parameters are shown in figure 7 to figure 12 for the  $1\frac{5}{16}$  in. and  $1\frac{3}{8}$  in. free fall conditions. On the two displacement curves (figs. 7 and 10) the theoretical free fall times ( $d = \frac{1}{2}at^2$ ) for the  $1\frac{5}{16}$  in. and  $1\frac{3}{8}$  in. gap distances are shown. The theoretical time for a single mass provides a close approximation of the free fall time of the two degree of freedom fuel duct model. The peak displacement and acceleration did not occur at first time of impact. This is shown by both the NASTRAN and experimental results and is due to the response of the multi-degree of freedom system (figs. 6, 7, and 10).

A comparison of the wave forms between the experimental and NASTRAN results for the IVHM load cell (figs. 6 and 8) indicates that structural damping is larger than the 15 percent value used in the lumped-mass model. The structural damping ( $g = 15$  percent) was determined from the rate of decay of successive rebounds. It was difficult to determine a consistent damping parameter after the impact event from the load cell oscillogram.

It was found from the NASTRAN results that structural damping had a very small effect on the amplitude of the first impact event. However, the value of structural damping made a significant change in the response of the IVHM subsequent to the first impact. Structural damping was varied from 0 to 15 percent.

The response of the IVHM due to the initial condition of the 1000 lb pre-load is shown in figure 11. The pre-load was input to the model at Grid Point 4 as a ramp function with a time duration of 0.026 second. No pre-load was applied to the fuel duct Grid Point 5 for the reasons previously noted in this report. Nominally, the free fall time could be expected to be less than the theoretical time because of the increase in acceleration of the fuel duct. (See fig. 10.) Nevertheless the response characteristics shown in figures 9, 10, and 12 yield an approximation of the effect of the pre-load condition on the IVHM.

Figures 9 and 12 show the acceleration response of the fuel duct and the IVHM. The bounce effect, due to the multi-degree of freedom response, and the successive rebounds are illustrated. In both instances, the  $1\frac{5}{16}$  in. and  $1\frac{3}{8}$  in. free falls, the accelerations on the IVHM are higher than on the fuel duct.

A comparison (fig. 13) is made of the experimental and NASTRAN results for the accelerometer on the top of the fuel duct and the IVHM load cell. The effect of the pre-load is to reduce the amplitude of acceleration on the fuel duct but to increase it on the IVHM. (See figs. 9 and 12.)

#### CONCLUDING REMARKS

The experience gained in the application of NASTRAN to a complex reactor component impact condition has been presented.

Comparison of the results obtained with NASTRAN with results from the experiments and theory shows NASTRAN to be very effective in calculating the transient response of the IVHM and fuel duct.

The fuel duct loads determined by these tests and analyses should be considered qualitative. The simulated fuel duct has different dynamic properties than the prototype FTR fuel duct. The two mass models of the fuel duct should be extended to include the principal dynamic characteristics of the components of the FTR fuel duct.

#### REFERENCES

1. Waymire, G. R.: The Significance of Applied Mechanics In Designing the Fast Test Reactor. Nuclear Engineering and Design, vol. 19, no. 1, Apr. 1972.
2. Tong, K. N.: Theory of Mechanical Vibration. John Wiley & Sons, Inc., 1960.
3. MacNeal, R. K.: The NASTRAN Theoretical Manual. NASA SP-221, Oct. 1969.
4. Peterson, L.: SADSAM User's Manual. MSR-10, Dec. 1970.

FIGURE 1. FFTF SIMULATED CORE AND IVHM

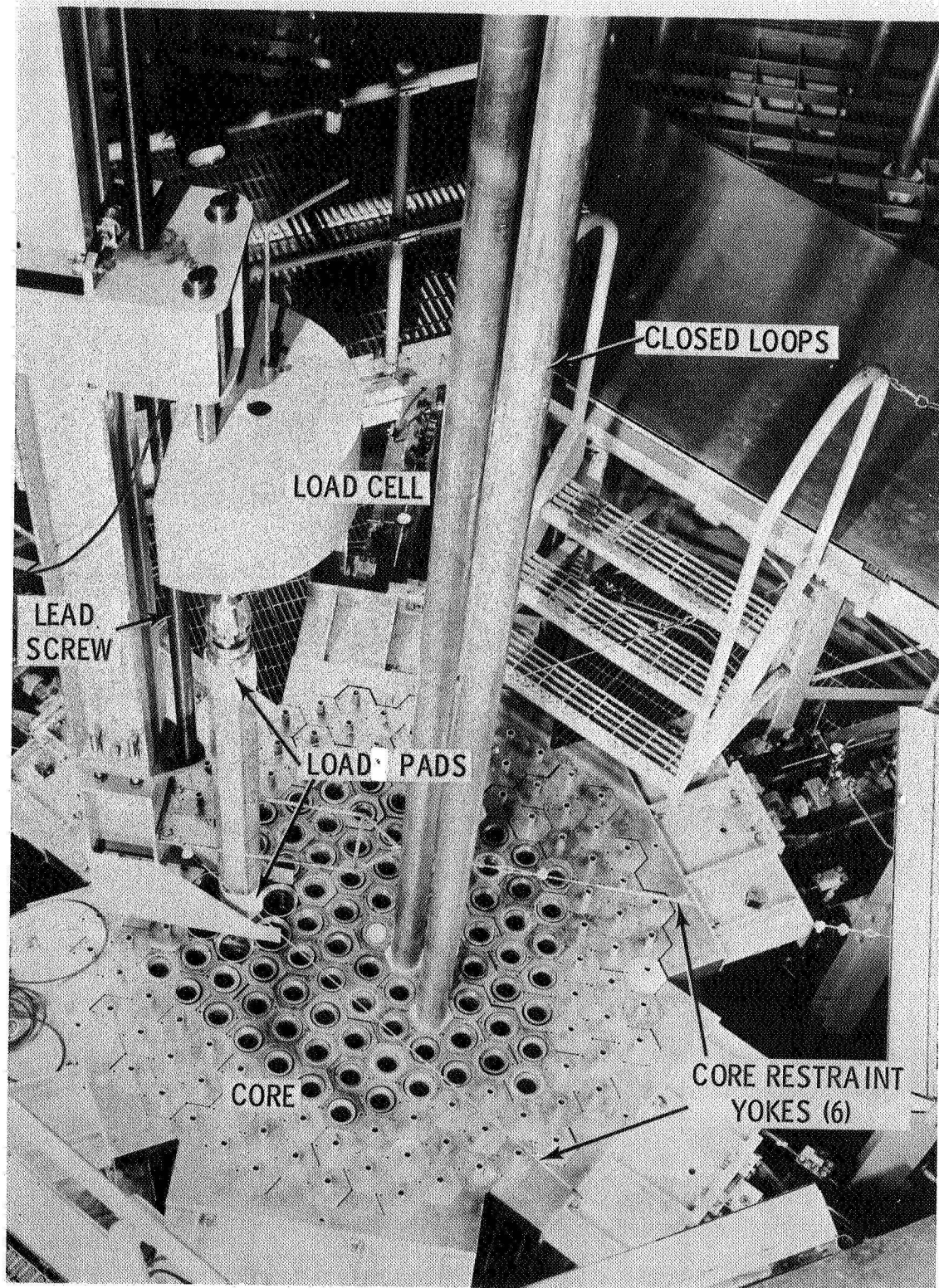


FIGURE 2. SIMULATED GRAPPLE AND FUEL DUCT ASSEMBLY

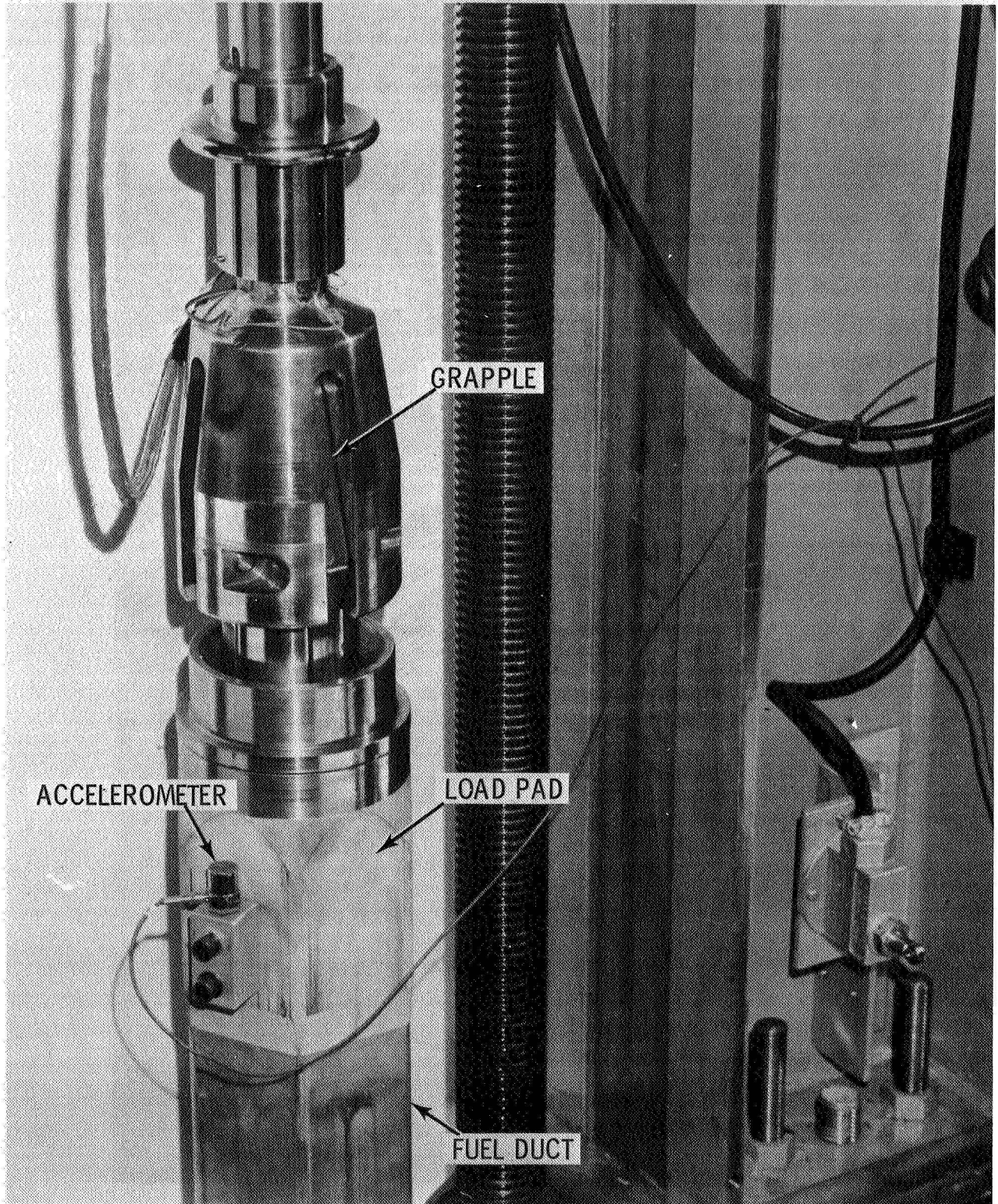


FIGURE 3. IVHM SIMULATED GRAPPLE

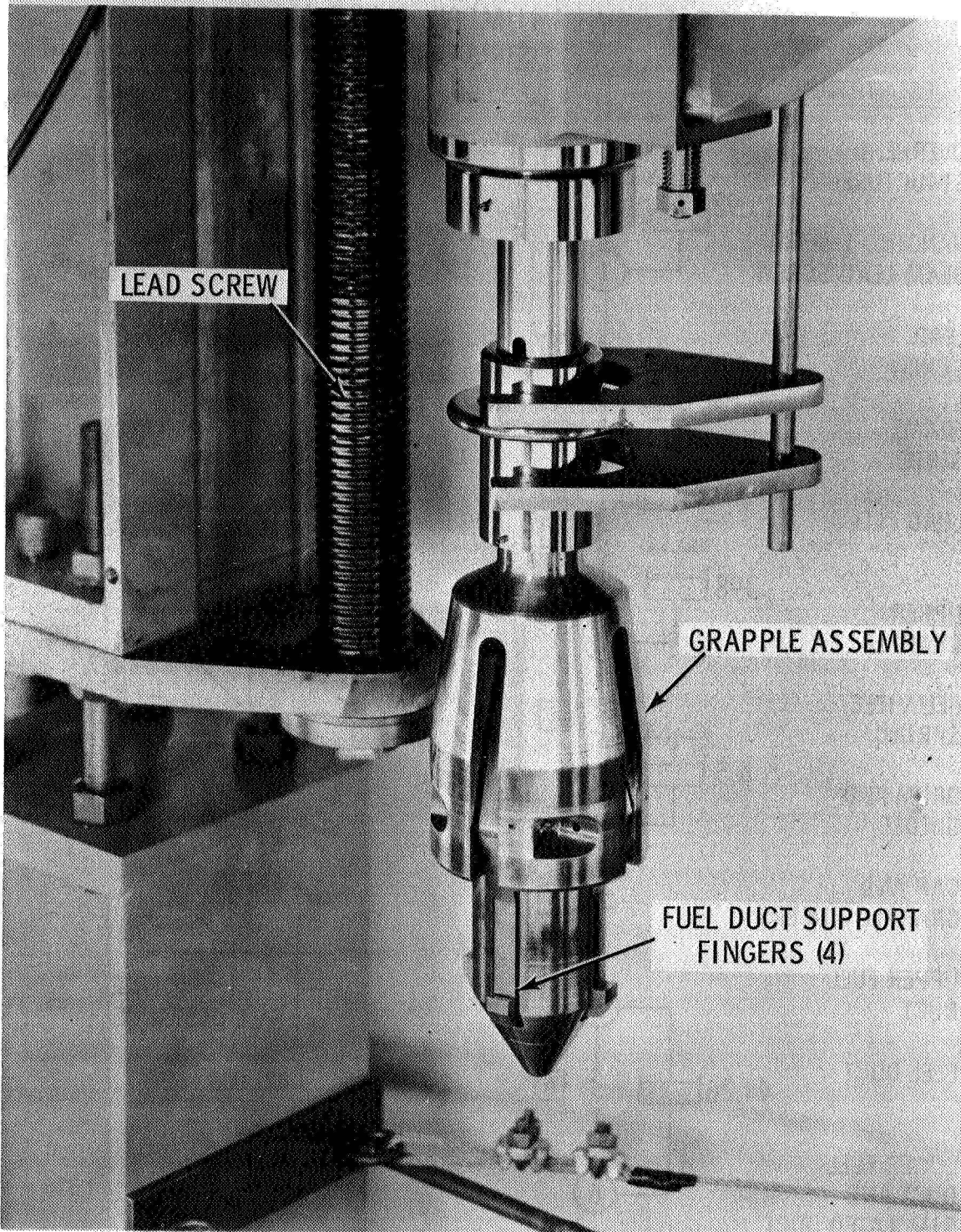
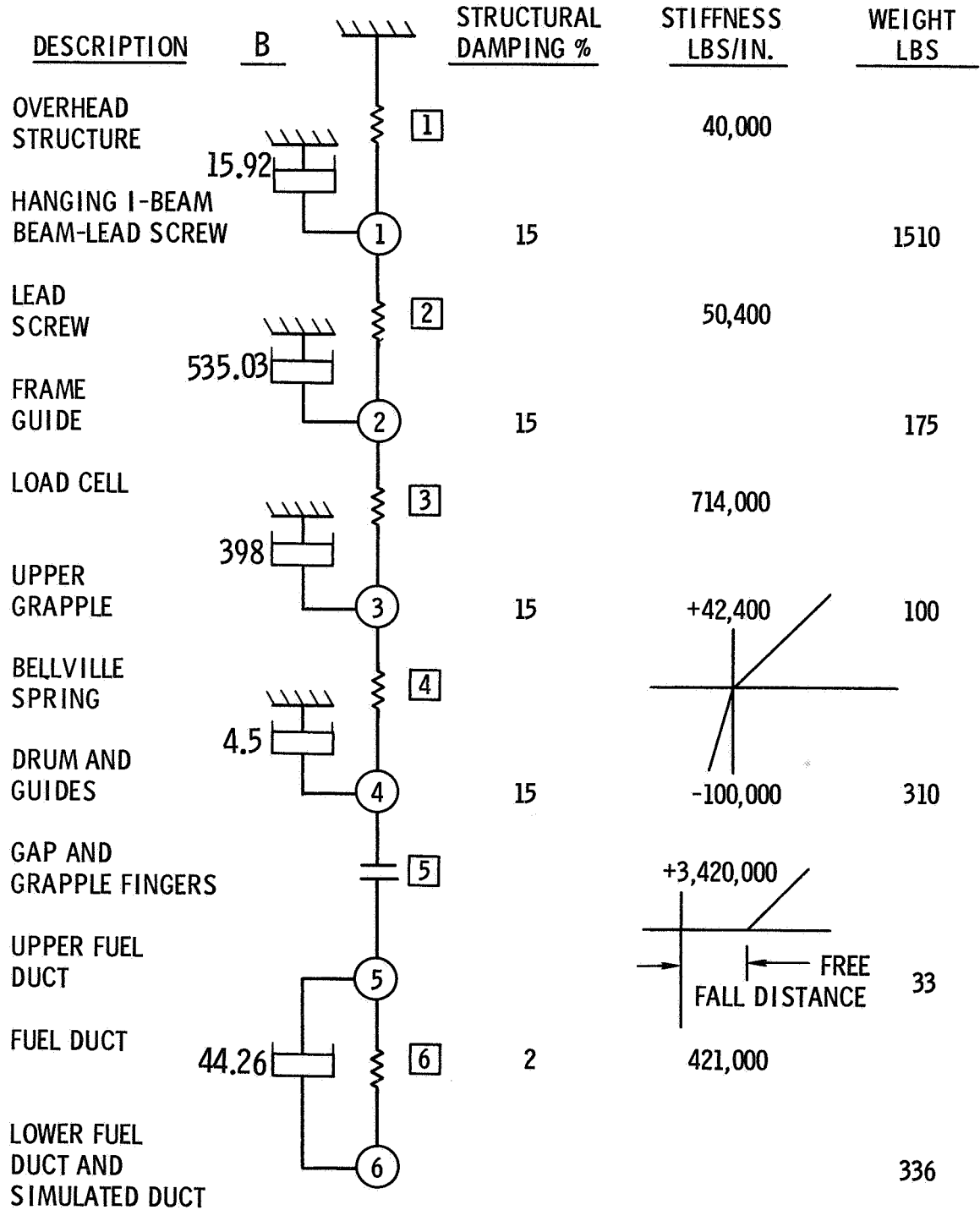


FIGURE 4. IVHM LUMPED-MASS MODEL



## FIGURE 5. NASTRAN COMPUTER INPUT DATA

NASTRAN EXECUTIVE CONTROL DECK

72

PAGE 1

```
ID   GRAPPLE, RUN 102
APP  DISPLACEMENT
SOL  9,0
TIME 15
DIAG 2,3,5,6,9,13
CEND
```

IVHM GRAPPLE IMPACT  
NONLINEAR BELLVILLE SPRING - 2 PERCENT STRUCTURAL DAMPING

```

CASE CONTROL DECK ECHO

CARD
COUNT
1  TITLE = IVHM GRAPPLE IMPACT TEST
2  SUBTITLE = NONLINEAR BELLVILLE SPRING - 2 PER CENT STRUCTURAL DAMPING
3  SET 1 = 3,4,5
4  SET 2 = 5,6
5  SUBCASE 1
6  DLOAD = 1
7  TSTEP = 10
8  NONLINEAR = 100
9  TFL = 1000
10 OUTPUT
11 LINE = 38
12 MAXLINES = 40000
13 NLLOAD = 1
14 ACCELERATION = ALL
15 DISPLACEMENT = ALL
16 ELFORCE = ALL
17 OLOAD = 2
18 OUTPUT (XYPLOT)
19 PLOTTER CALCOMP, MODEL 765,205 DENSITY 556 BPI
20 XAXIS = YES
21 YAXIS = YES
22 XGRID LINES = YES
23 YGRID LINES = YES
24 XTITLE = TIME SECONDS
25 YTITLE = DISPLACEMENT IN.
26 TCURVE = * * * * GRID PTS. 4 AND 5 * * * *
27 XYPLOT = DISP / 4(T1) , 6(T1)
28 TCURVE = * * * * GRID PTS. 4 AND 6 * * * *
29 XYPLOT = DISP / 4(T1) , 6(T1)
30 YTITLE = LOAD LBS.
31 TCURVE = NONLIN FORCE GRID PTS. 4 AND 5
32 XYPLOT = NONLINEAR / 4 (T1) , 5 (T1)
33 TCURVE = LOAD CELL FORCE ELEMENT 3
34 XYPLOT = ELFORCE / 3(2)
35 YTITLE = ACCELERATION IN. / SEC.2
36 TCURVE = ACCELERATION GRID PTS. 4 AND 6
37 XYPLOT = ACCE / 4 (T1) , 6(T1)
38 BEGIN BULK
```

## FIGURE 5. (cont.) NASTRAN COMPUTER INPUT DATA

IVHM GRAPPLE IMPACT TEST  
NONLINEAR BELLVILLE SPRING - 2 PERCENT STRUCTURAL DAMPING

72

PAGE 2

SORTED BULK DATA ECHO										
CARD COUNT	. 1 .	. 2 .	. 3 .	. 4 .	. 5 .	. 6 .	. 7 .	. 8 .	. 9 .	. 10
1*	CDAMP4	101	15.92	1						
2*	CDAMP4	102	535.03	2						
3*	CDAMP4	103	398.	3						
4*	CDAMP4	104	4.5	4						
5*	CDAMP4	106	44.26	5	6					
6*	CELAS4	1	.040 +6	0	1					
7*	CELAS4	2	2.559+6	1	2					
8*	CELAS4	3	.714 +6	2	3					
9*	CELAS4	6	.421+6	.5	6					
10*	CMASS4	11	3.909	1						
11*	CMASS4	22	.453	2						
12*	CMASS4	33	.8022	4						
13*	CMASS4	44	.0854	5						
14*	CMASS4	55	.8420	6						
15*	CMASS4	222	.264	3						
16*	DAREA	10	5		+1.0					
17*	DAREA	20	6		+1.0					
18*	DLOAD	1	1.0	1.0	2	1.0	3			
19*	GRID	100		1.0	.0	.0		23456		
20*	GRID	200		2.0	.0	.0		23456		
21*	NOLIN1	100	3		+1.0	200	1	200		
22*	NOLIN1	100	4		-1.0	200	1	200		
23*	NOLIN1	100	4		+1.0	100	1	100		
24*	NOLIN1	100	5		-1.0	100	1	100		
25*	TABLED1	10								TAB10
26*	+AB10	0.0	0.0	0.0005	33.0	10.0	33.0	ENDT		
27*	TABLED1	20								TAB20
28*	+AB20	0.0	0.0	0.0005	336.0	10.0	336.0	ENDT		
29*	TABLED1	100								TAB30
30*	+AB30	0.0	0.0	1.3125	0.0	11.3125	34.2+6	ENDT		
31*	TABLED1	200								TAB40
32*	+AB40	-0.001	-.100+3	.0	0.0	10.0	42.4 +4	ENDT		
33*	TF	1000	100	1	+1.0					TF101
34*	+F101	4		+1.0						TF102
35*	+F102	5		-1.0						
36*	TF	1000	200	1	+1.0					TF103
37*	+F103	3		+1.0						TF104
38*	+F104	4		-1.0						
39*	TLOAD1	2	10			10				
40*	TLOAD1	3	20			20				
41*	TSTEP	10	3000	.0001	5					
	ENDDATA									

FIGURE 6. EXPERIMENTAL RESULTS - 1 5/16 FREE FALL - TEST NO. 19.5.3

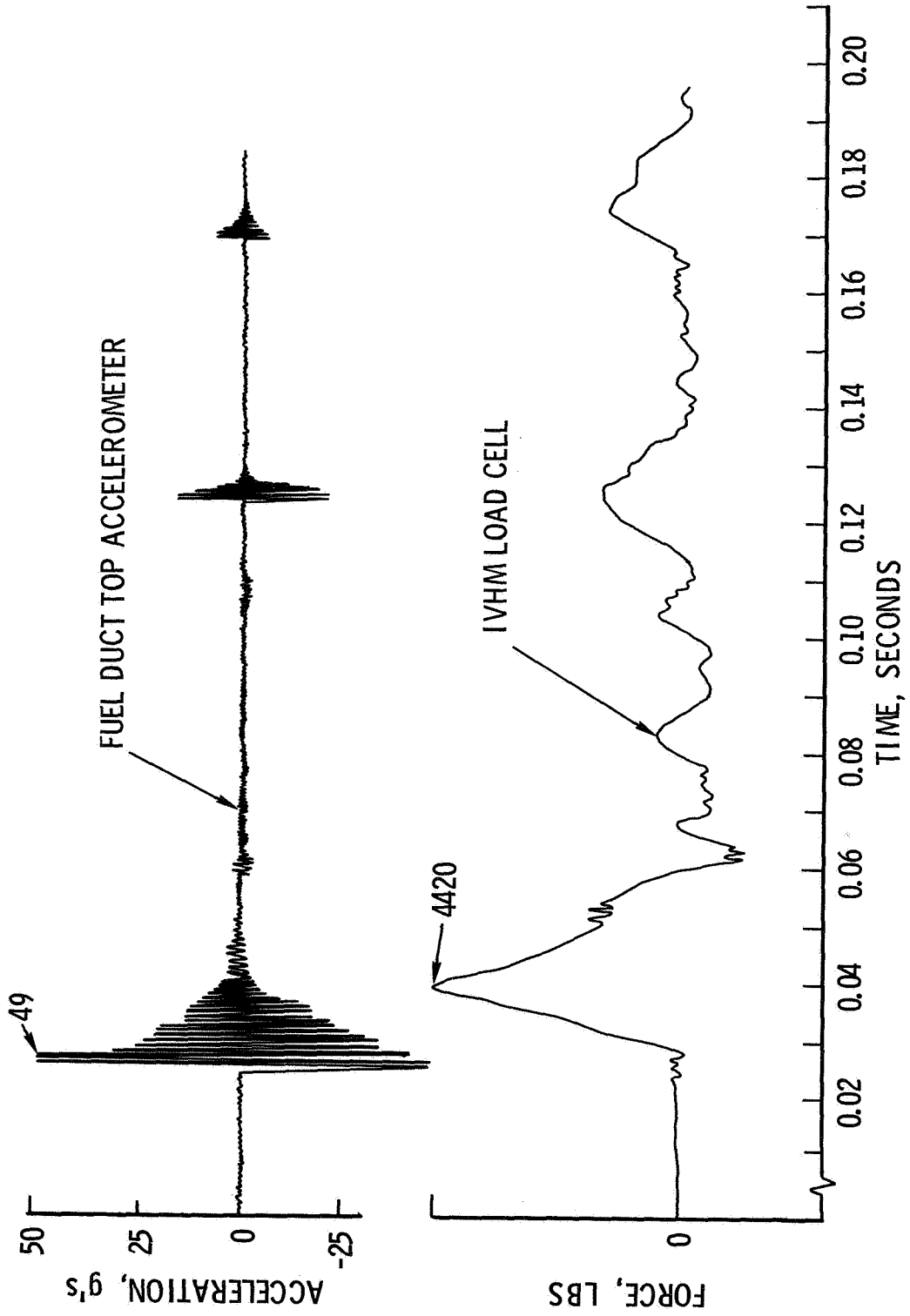


FIGURE 7. GRAPPLE AND FUEL DUCT DISPLACEMENTS - 1 5/16 IN. FREE FALL

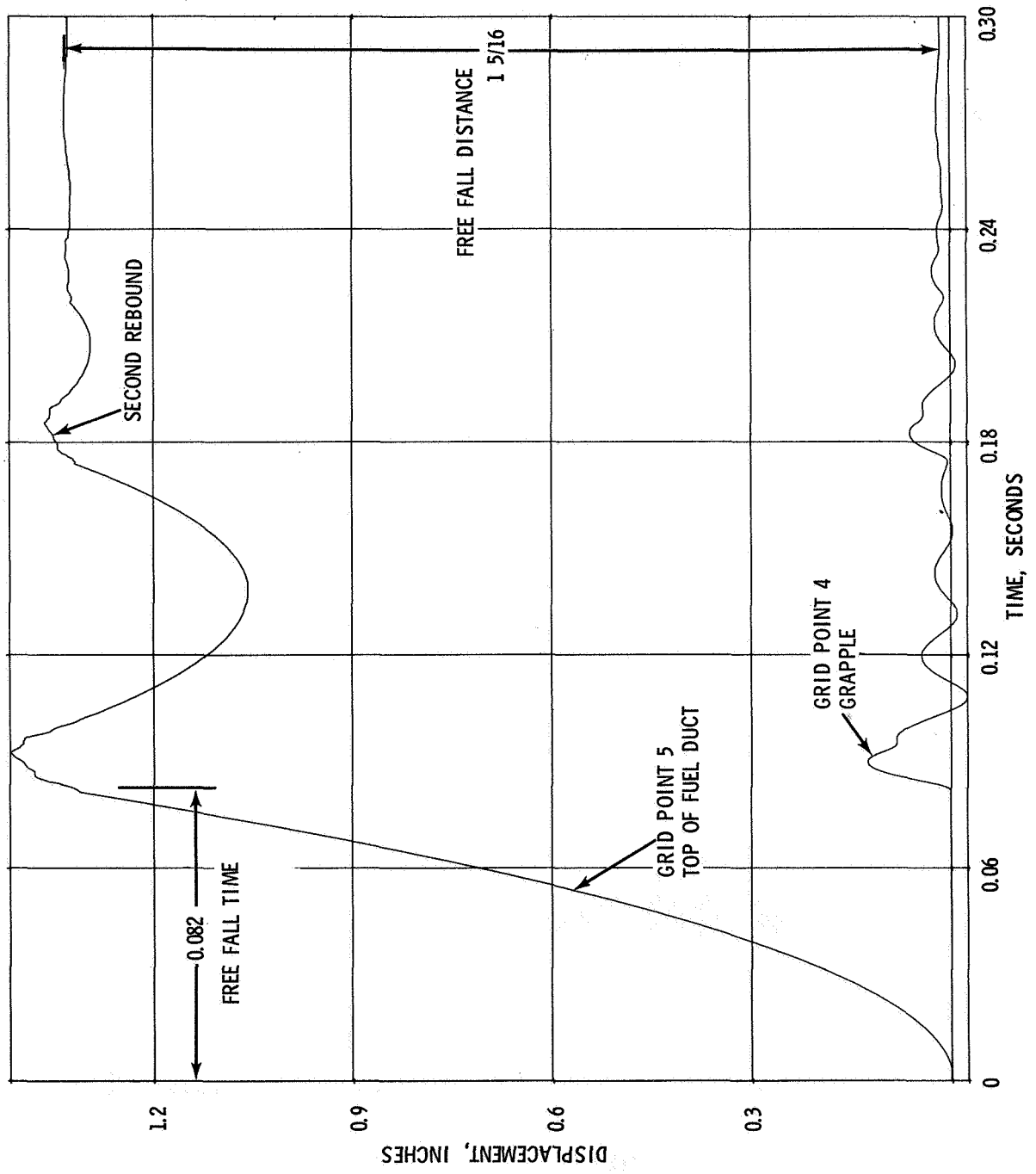


FIGURE 8. LOAD CELL FORCE - 1 5/16 IN. FREE FALL

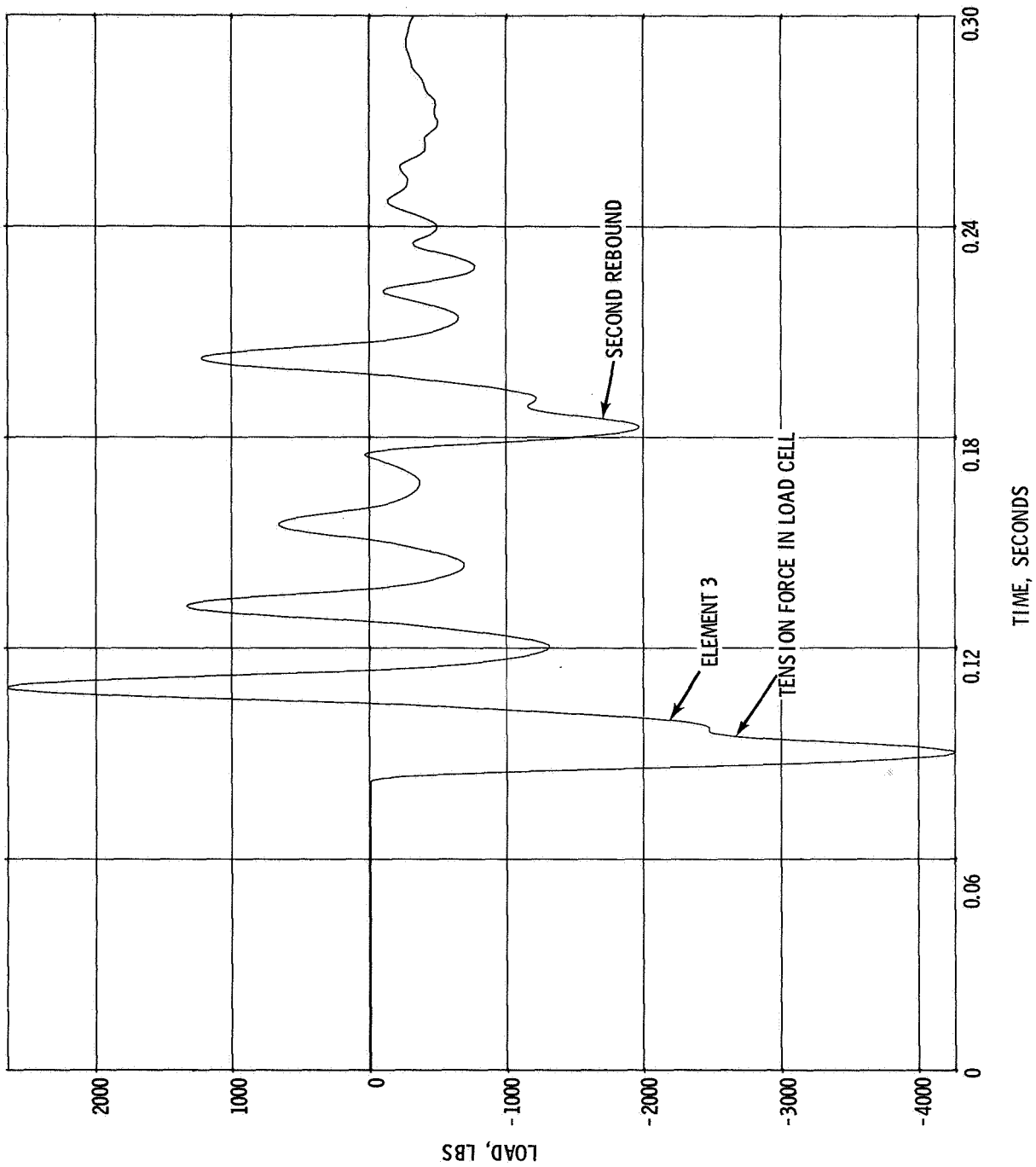


FIGURE 9. GRAPPLE AND FUEL DUCT ACCELERATIONS - 1 5/16 IN. FREE FALL

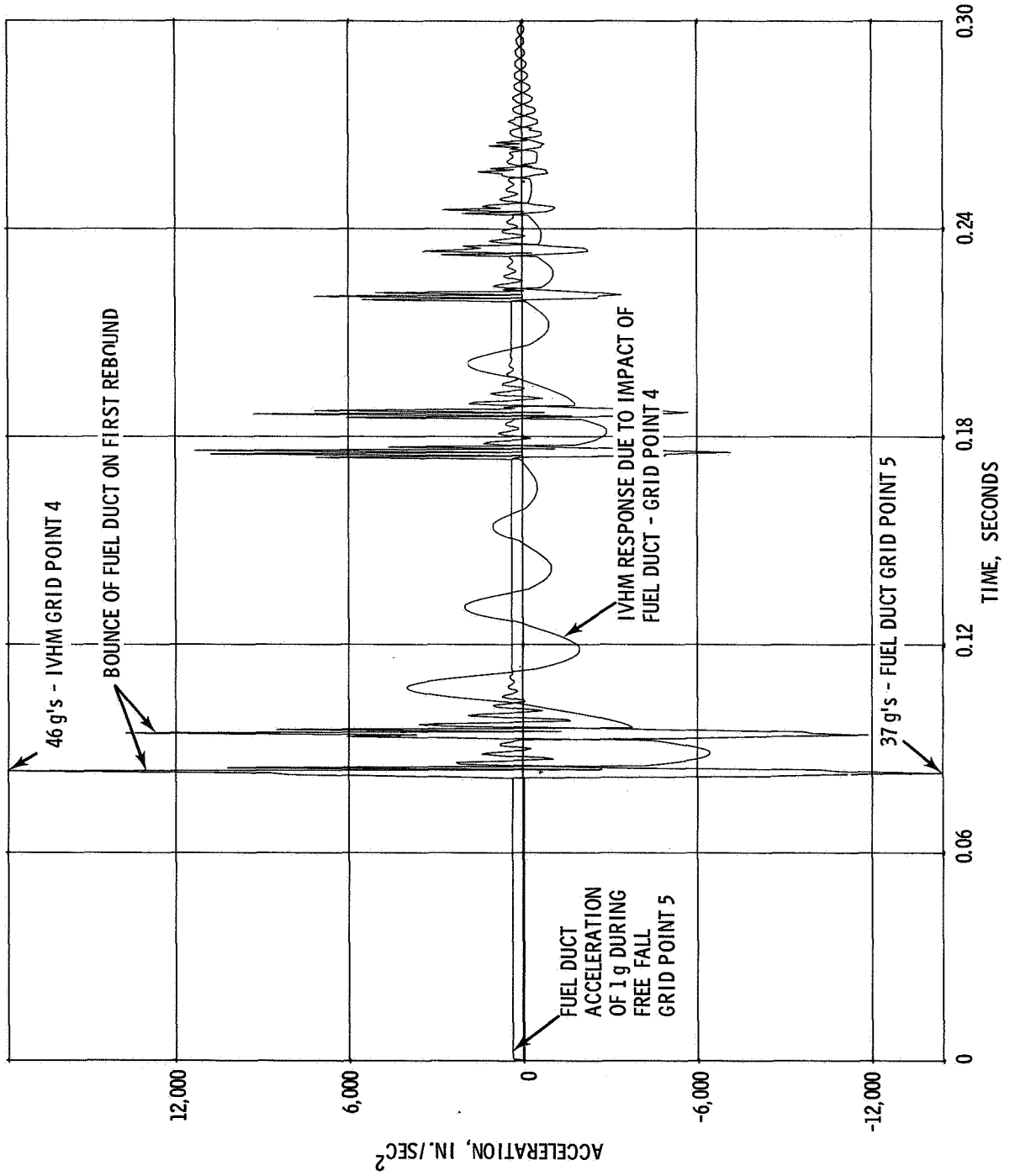


FIGURE 10. GRAPPLE AND FUEL DUCT DISPLACEMENTS - 1 3/8 IN. FREE FALL - 1,000 LB PRELOAD

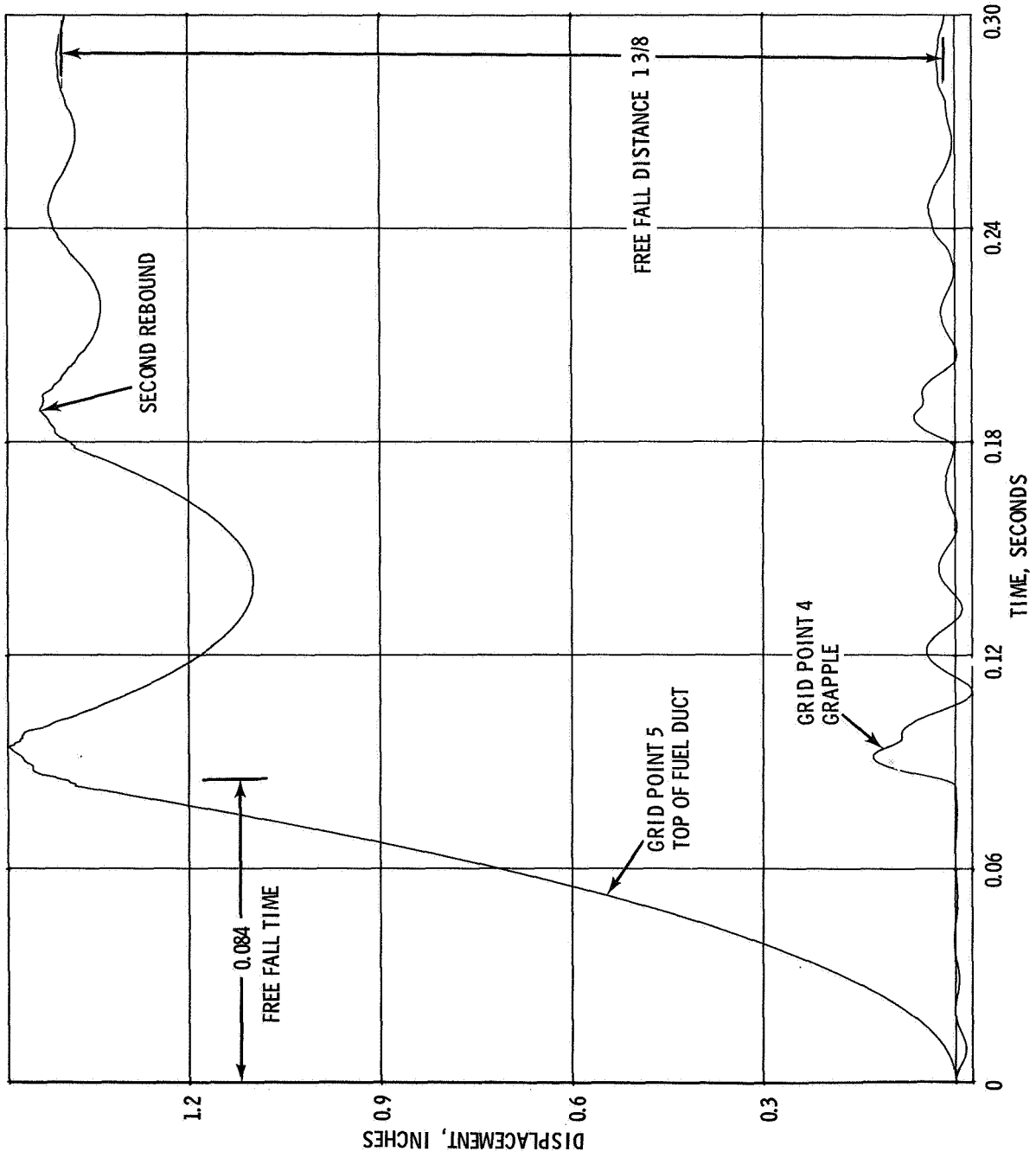


FIGURE 11. LOAD CELL FORCE - 1 3/8 IN. FREE FALL - 1,000 LB PRELOAD

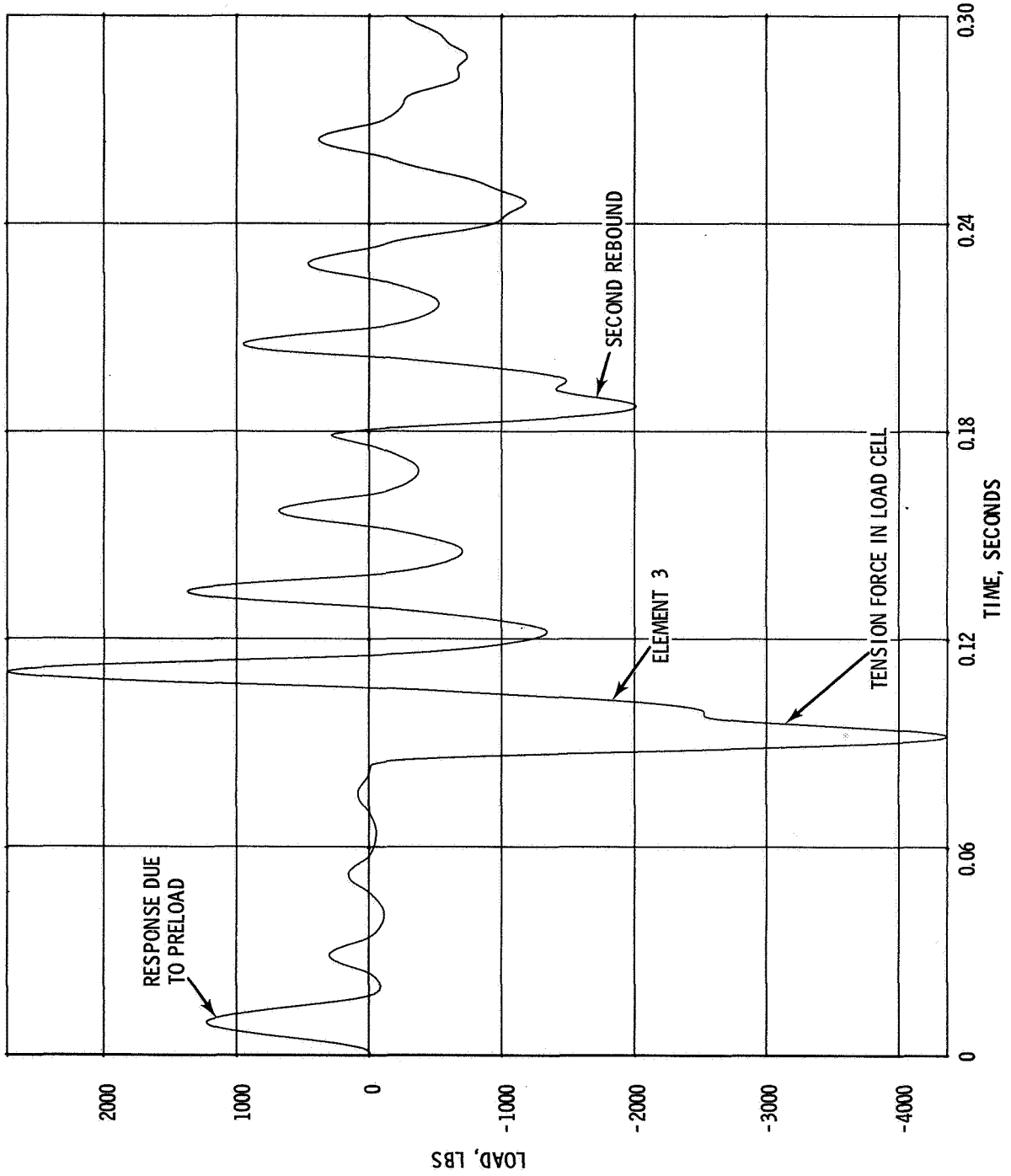


FIGURE 12. GRAPPLE AND FUEL DUCT ACCELERATIONS - 1 3/8 IN. FREE FALL - 1,000 LB PRELOAD

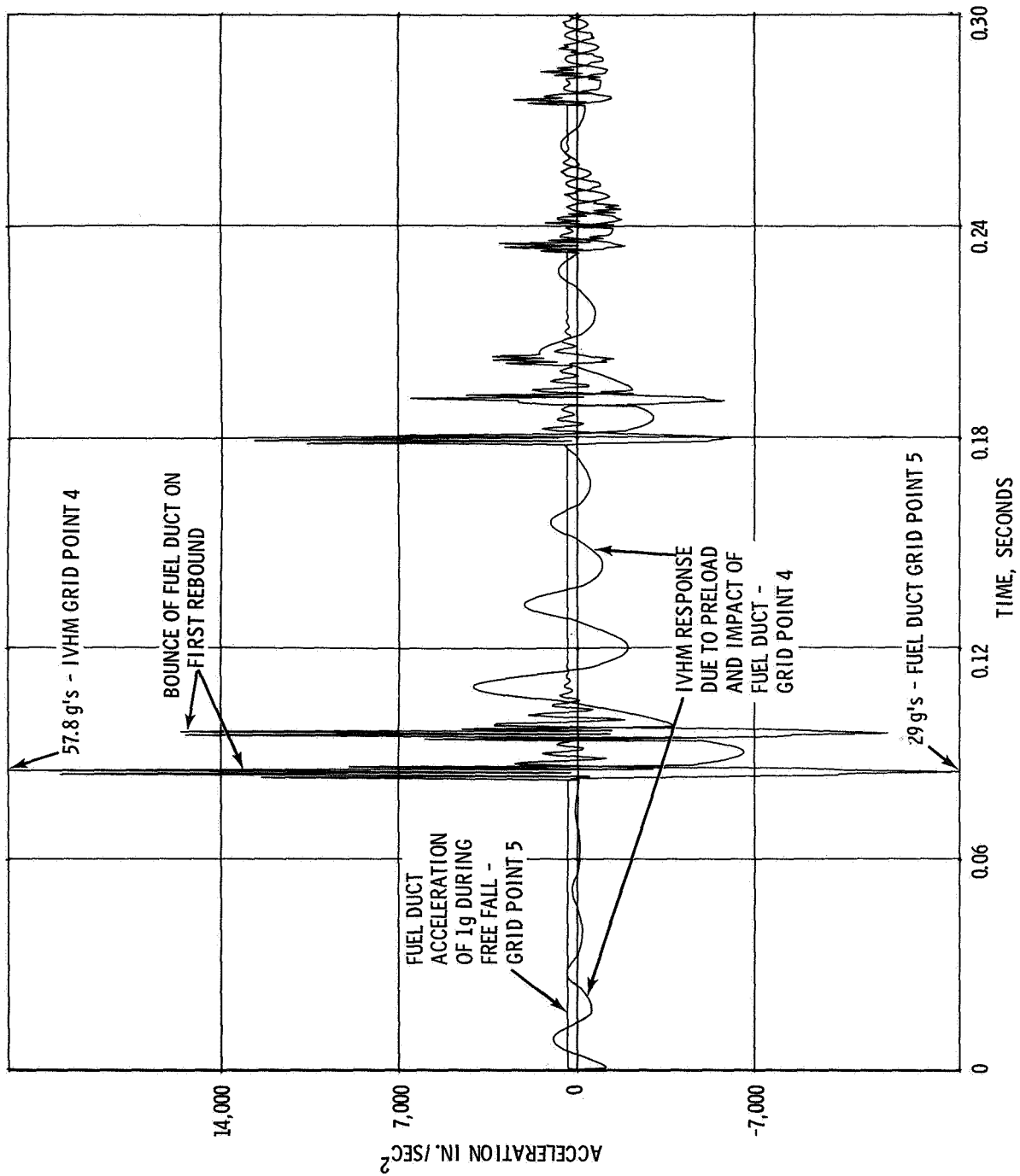


FIGURE 13. COMPARISON OF PEAK VALUES FROM EXPERIMENTAL  
AND ANALYTICAL RESULTS

CONDITION	LOAD	ELEMENT	ACCELEROMETER	GRID POINT
	CELL LBS	NO.3 LBS	TOP OF DUCT g's	NO.5 g's
1 5/16 IN. FREE FALL*	4,420	4,300	49	37
1 3/8 IN. FREE FALL**	4,580	4,400	32	29

\* TEST NO. 19.5.3

\*\* 1.375 IN. FREE FALL WITH AN INITIAL CONDITION OF 1,000 LBS  
(PRE-LOAD) - TEST NO. 19.8.2

MODELING TECHNIQUES OF THIN-WALLED BEAMS  
WITH OPEN CROSS SECTIONS

By Knut S. Skattum  
Research Laboratories  
General Motors Corporation  
Warren, Michigan

ABSTRACT

Warping constraints of thin-walled beams of open cross sections may significantly add to the torsional rigidity of the beams. This property is not included in the conventional beam element available in NASTRAN and makes it impossible to model such beams properly.

This paper presents a composite element which includes the effects of warping and offset shear centers. It is shown to be mathematically consistent with thin-walled open beam theory and can easily be incorporated into any structural analysis program by use of NASTRAN'S standard elements.

A numerical example analyzing the vibration of a channel beam is presented, and, by using the composite element, the numerical results agreed very well with theoretical data.

INTRODUCTION

Thin-walled beams of open cross sections are commonly used in automotive and aircraft structures where it is imperative to insure maximum flexural efficiency without violating practical fabrication and assembly requirements. It turns out that for many cases the static and dynamic response of these structures depends strongly upon the warping constraints of the members. Consequently, proper modeling techniques are essential to insure good numerical results.

The most general beam element available in the present version of NASTRAN (level 12) is based upon the well-known Timoshenko beam theory. This theory, however, neglects warping displacements and assumes that the elastic and centroidal axes coincide. Both these conditions are usually too restrictive when thin-walled open beams are modeled.

Several books and articles have been published treating the theory and applications of thin-walled beams of open cross sections. A thorough presentation is found in Vlasov's book (Ref. 1). Timoshenko and Gere have done a

buckling analysis (Ref. 2), and contributions to the vibrational analysis are due to Timoshenko (Ref. 3), Gere (Ref. 4), Gere and Lin (Ref. 5), and Christiano and Salmela (Ref. 6).

This paper presents a new element which includes the effects of warping and noncoincidental elastic and centroidal axes. It is a composite element derived from a variational principle consistent with the thin-walled open beam formulation. Also, in addition to being mathematically correct, this model can very easily be incorporated into any structural analysis program by using elements now available in NASTRAN.

As a numerical example on how the model is constructed, the vibration of a channel beam is analyzed, and good agreement between theoretical and numerical results are obtained.

#### THEORY OF THIN-WALLED OPEN BEAMS

A thin-walled beam is usually defined by restricting its dimensions so that

$$L > 10d \quad (1)$$

$$d > 10t \quad (2)$$

where  $L$  is the length of the bar,  $d$  the depth of the cross section, and  $t$  the largest thickness (Fig. 1). The first relation makes it possible to assume uniformity of the longitudinal stresses along the axis (St. Venant's Principle) while Eq. 2 is used in making assumptions on the shear stresses in the section. Particularly for beams of open cross sections which will be considered in this analysis, it will be assumed that the middle surface is free of shear. In addition, the material and sectional properties of the beam are assumed to be constant along the length, and the displacements are considered to be small such that the cross sections do not change shapes during deformation.

Figure 1 shows a general thin-walled open beam. Included is also a detail of the cross section giving the locations of the center of gravity (CG) and the shear center (SC). The shear center is the point on the cross section through which the resultant of the transverse shearing forces always passes. Locus of the shear centers along a beam is called the elastic axis, and similarly, the centroidal axis passes through the CG of the cross sections.

Before the differential equations can be presented, it is very important to clearly define the coordinate and displacement system used. Referring to Fig. 1, the  $x$ -coordinate coincides with the centroidal axis of the beam, and the  $y$ - and  $z$ -coordinates are the principal axes of the cross section. The displacements are defined by

$u$  = longitudinal displacement of centroid  
 $v$  = vertical displacement of shear center

w = horizontal displacement of shear center  
 $\theta$  = rotational displacement of shear center

and are also indicated in the figure.

Based on these definitions and the assumptions mentioned above, the full set of differential equations for a thin-walled open beam can be written as (Ref. 1)

$$EA \frac{d^2 u}{dx^2} = -q_x \quad (3)$$

$$EI_1 \frac{d^4 v}{dx^4} = q_y \quad (4)$$

$$EI_2 \frac{d^4 w}{dx^4} = q_z \quad (5)$$

$$EC_\omega \frac{d^4 \theta}{dx^4} - GJ \frac{d^2 \theta}{dx^2} = m_\theta \quad (6)$$

in which E = modulus of elasticity; G = shear modulus; A = cross sectional area;  $I_1$  = moment of inertia about z axis;  $I_2$  = moment of inertia about y-axis; J = torsion constant;  $C_\omega$  = warping constant;  $q_x$  = longitudinal surface load applied to the centroid;  $q_y$  and  $q_z$  = transverse loads applied at the shear center; and  $m_\theta$  = twisting moment about the elastic axis.

It should be observed that the above set of differential equations differs from the regular beam equation by the fact that v, w, and  $\theta$  (and correspondingly  $q_y$ ,  $q_z$ , and  $m_\theta$ ) are displacements (and forces) relating to the shear center rather than the centroid, and that the term

$$EC_\omega \frac{d^4 \theta}{dx^4}$$

relating to the warping of the cross section, has been added. Also, the four equations are completely uncoupled, a very desirable feature made possible by letting some of the displacements be associated with the shear center.

#### MODELING OF THIN-WALLED OPEN BEAMS

The conventional beam element available in the NASTRAN computer program is essentially based upon the same assumptions given above, but in addition, two other conditions are made:

1. Plane sections remain plane (i.e., no warping deformations)
2. Centroidal- and elastic-axes coincide.

These two additional restrictions were also pointed out in the last section by looking at the differential equations.

Warping is a phenomenon that occurs in all bars subjected to twist, with the exception of circular cross sections (Ref. 7). Only for open sections though can the strain associated with the warping be large enough to cause significant contribution to the rotational stiffness of the beam. By excluding warping, the rotational stiffness is too flexible; a factor of two or more is quite common depending upon the cross-sectional properties and how the beam rotates. There have been some attempts to incorporate warping in the conventional beam element by defining an effective torsional constant  $J_e$ . From Eq. 6 it is observed that this can be accomplished by the equation

$$GJ_e \frac{d\theta}{dx} = GJ \frac{d\theta}{dx} - EC_w \frac{d^3\theta}{dx^3} \quad (7)$$

but it is also noticed that  $J_e$  then necessarily must depend upon the solution  $\theta$ . For static analysis, this approach might be used effectively where the rotational displacement  $\theta$  can be estimated fairly accurately, but for dynamic analysis, where different modes are extracted in the same analysis, large errors will be introduced.

When centroidal and elastic axes do not coincide, the beam element should be modeled along the elastic axis. Otherwise, it can easily be observed that the bending moment created by the applied transverse forces will not be encountered. This modeling will unfortunately introduce new problems, namely, the bending moment caused by the longitudinal forces which, according to Eq. 3, should coincide with the centroidal axis. In many cases, though, the effect of axial forces can be neglected.

In order to treat thin-walled open beams in a finite element computer program and include the effects of warping and offset shear center, it will be necessary to either 1) develop a new element that includes these effects, 2) model the beams by a number of plate elements, or 3) arrange the available finite elements in a way consistent with the thin-walled open beam theory. While there exists an element (Ref. 8) with the above features, it is not readily available, and in particular, not for NASTRAN users. A beam modeled by plate elements usually increases the number of grid points tremendously. This also increases the degrees of freedom, and the procedure will often become impractical and uneconomical. One is thus often left to model a thin-walled open beam by the existing beam element which will introduce errors as discussed above or create a new composite element. The following section presents such an element where the effects of warping and offset shear centers are included.

## DERIVATION OF A COMPOSITE ELEMENT

Before describing a suitable finite element model, a fictitious continuous beam is presented (Fig. 2). The differential equations of vibration and the corresponding boundary conditions for this beam will be derived by the Hamilton's Variational Principle

$$\delta \int_{t_0}^{t_1} (T - U) dt = 0 \quad (8)$$

where T is the total kinetic and U the total potential energy of the system.

Referring to Fig. 2, the fictitious element consists of a rod coinciding with the centroidal axis, a beam coinciding with the elastic axis, and two flanges displaced  $h$  from the elastic axis in a direction parallel to the  $y$  coordinate. The rod accepts only axial deformations, and the corresponding strain energy over the whole length,  $L$ , of the rod can thus be written as

$$U_R = \frac{1}{2} \int_0^L EA \left( \frac{\partial u}{\partial x} \right)^2 dx \quad (9)$$

where  $u$  is the longitudinal displacement of the centroid as defined in the last section.

As indicated in the figure, the beam has all capabilities of a regular beam except that the area is neglected such that no axial strain exists. The strain energy is then given by

$$U_B = \frac{1}{2} \int_0^L \left[ EI_1 \left( \frac{\partial^2 v}{\partial x^2} \right)^2 + EI_2^* \left( \frac{\partial^2 w}{\partial x^2} \right)^2 + GJ \left( \frac{\partial \theta}{\partial x} \right)^2 \right] dx \quad (10)$$

in which  $I_2^*$  is the moment of inertia about the  $y$ -axis while the other properties, including the displacements, are as defined earlier.

The two flanges are displaced from the elastic axis an arbitrary distance  $h$  which will be determined later. Only bending deflections are admitted for the flanges, and by defining the displacements parallel to the  $z$ -axis as  $w_1$  and  $w_2$ , as indicated on Fig. 2, the strain energy becomes

$$U_F = \frac{1}{2} \int_0^L EI_F \left[ \left( \frac{\partial^2 w_1}{\partial x^2} \right)^2 + \left( \frac{\partial^2 w_2}{\partial x^2} \right)^2 \right] dx \quad (11)$$

The rod is assumed to carry all the mass of the elements such that the kinetic energy will be written in terms of the rod displacements  $u$ ,  $v^*$ ,  $w^*$ , and  $\theta^*$ . Neglecting rotational inertia, the kinetic energy is

$$T = \frac{1}{2} \int_0^L \rho A \left[ \left( \frac{\partial u}{\partial t} \right)^2 + \left( \frac{\partial v^*}{\partial t} \right)^2 + \left( \frac{\partial w^*}{\partial t} \right)^2 + \frac{I_p}{A} \left( \frac{\partial \theta^*}{\partial t} \right)^2 \right] dx \quad (12)$$

where  $I_p$  is the centroidal polar moment of inertia and  $\rho$  is the mass density of the material.

The nine displacement parameters used will next be reduced to four by the relations

$$\theta^* = \theta \quad (13)$$

$$v^* = v + c_z \theta \quad (14)$$

$$w^* = w - c_y \theta \quad (15)$$

$$w_1 = w + h\theta \quad (16)$$

$$w_2 = w - h\theta \quad (17)$$

$c_y$  and  $c_z$  are the distances between C.G. and S.C. in the  $y$  and  $z$  direction respectively. Substituting these equations into the above expressions for strain and kinetic energies, Hamilton's equation (8) can be formed. The variation is then accomplished by varying  $u$  by  $\delta u$ ,  $v$  by  $\delta v$ ,  $w$  by  $\delta w$  and  $\theta$  by  $\delta \theta$  where it is understood that the variation vanishes at  $t = t_0$  and  $t = t_1$ . This procedure produces the differential equations

$$EA \frac{\partial^2 u}{\partial x^2} = \rho A \frac{\partial^2 u}{\partial t^2} \quad (18)$$

$$EI_1 \frac{\partial^4 v}{\partial x^4} = -\rho A \frac{\partial^2 v}{\partial t^2} - \rho A c_z \frac{\partial^2 \theta}{\partial t^2} \quad (19)$$

$$E (I_2^* + 2I_F) \frac{\partial^4 w}{\partial x^4} = -\rho A \frac{\partial^2 w}{\partial t^2} + \rho A c_y \frac{\partial^2 \theta}{\partial t^2} \quad (20)$$

$$2EI_F h^2 \frac{\partial^4 \theta}{\partial x^2} - GJ \frac{\partial^2 \theta}{\partial x^2} = -\rho A \left( c_z^2 + c_y^2 + \frac{I_p}{A} \right) \frac{\partial^2 \theta}{\partial t^2} - \rho A c_z \frac{\partial^2 v}{\partial t^2} + \rho A c_y \frac{\partial^2 w}{\partial t^2} \quad (21)$$

and the boundary conditions (at  $x = 0$  and  $x = 1$ )

$$\frac{\partial^2 v}{\partial x^2} \cdot \frac{\partial v}{\partial w} = 0 \quad (22)$$

$$\frac{\partial^3 v}{\partial x^3} \cdot v = 0 \quad (23)$$

$$\frac{\partial^2 w}{\partial x^2} \cdot \frac{\partial w}{\partial x} = 0 \quad (24)$$

$$\frac{\partial^3 w}{\partial x^3} \cdot w = 0 \quad (25)$$

$$\frac{\partial u}{\partial x} \cdot u = 0 \quad (26)$$

$$\frac{\partial^2 \theta}{\partial x^2} \cdot \frac{\partial \theta}{\partial x} = 0 \quad (27)$$

$$\left( 2EI_F h^2 \frac{\partial^3 \theta}{\partial x^3} - GJ \frac{\partial \theta}{\partial x} \right) \cdot \theta = 0 \quad (28)$$

The differential equations presented for the thin-walled open beam, Eqs. 3 through 6, can easily be transformed into the form given for the fictitious beam by substituting inertia loads for  $q_x$ ,  $q_y$ ,  $q_z$ , and  $m_\theta$  (Ref. 1). Equations 18 through 21 will then become identical with the thin-walled open beam equations if the following two substitutions are made

$$I_2^* = I_2 - 2I_F \quad (29)$$

$$I_F = \frac{C \omega}{2h^2} \quad (30)$$

It should be observed that the boundary conditions also will be identical with these substitutions.

Because of the mathematical identity between the fictitious and thin-walled open beams, a finite element model for the first will also be a model for the latter. Figure 3 shows how the fictitious beam can be modeled and how the different elements are constrained at the grid points  $a_0$  and  $b_0$ . Four elements will be used; a rod, without torsional rigidity, coinciding with the centroid; a beam, without axial rigidity and mass, coinciding with the elastic axis; and two flanges (or beams), resisting only bending deformations, and displaced  $h$  parallel to the  $y$ -axis away from the elastic axis. The second

moment of inertia (NASTRAN notation) for the beam and the flanges is as defined in Eqs. 29 and 30, otherwise the notation given in Fig. 3 refers to the original properties of the thin-walled beam. The distance  $h$  is arbitrarily chosen, but should be large enough such that  $I_2^*$  is positive.

At each grid point, which is arbitrarily taken to be the centroid, the beam is offset by a rigid link to its shear center location. This will insure that the forces acting on the grid points will be transmitted correctly to the beam elements, and the grid point displacements will obey Eqs. 13, 14, and 15 used in the development of the fictitious beam.

Similarly, the displacements of the two flanges must be made dependent upon those at the shear center as restricted by Eqs. 16 and 17. If warping is constrained at the grid point, i.e.,

$$\frac{d\theta}{dx} = 0 \quad (31)$$

then the connections between the flanges and the centroid can be made rigid. Otherwise, as in the case of interior points of a thin-walled open beam, warping is admissible, and Eqs. 16 and 17 imply that

$$\frac{dw_1}{dx} \neq \frac{dw}{dx}, \quad \frac{dw_2}{dx} \neq \frac{dw}{dx} \quad (32)$$

This makes it necessary to create special grid points ( $a_1$ ,  $a_2$ ,  $b_1$  and  $b_2$  on Fig. 3) for the flanges where the transverse displacements are made dependent displacements, and the rotational displacements

$$\frac{dw_1}{dx} \quad \text{and} \quad \frac{dw_2}{dx}$$

are unrestricted. The four other displacements must, in this case, be constrained in order to avoid singular matrices.

The only difference between the composite model and the fictitious beam is that while Eqs. 16 and 17 are satisfied continuously for the mathematical beam, they are satisfied only at discrete intervals for the model. This implies that the flanges between the grid points will deform according to the law of minimum energy, contributing less to the torsional rigidity than theoretically assumed. Although usually small, this error can be made still smaller by using more grid points along the length of the beam.

#### NUMERICAL EXAMPLE

A numerical example is presented next to illustrate the use of the composite element and to compare the numerical results with data obtained from theory. The example chosen is the dynamic response of a channel beam whose properties are given by

$A = 0.884 \text{ in}^2$	$\rho = 0.733 \cdot 10^{-3} \text{ lbs sec}^2 \text{ in}^{-4}$
$I_1 = 7.66 \text{ in}^4$	$C = 3.52 \text{ in}^6$
$I_2 = 0.294 \text{ in}^4$	$c_\omega = 0.0 \text{ in}$
$J = 0.00168 \text{ in}^4$	$c_y = 0.94 \text{ in}$
$E = 29 \cdot 10^6 \text{ lbs in}^{-2}$	$L^z = 120 \text{ in}$
$G = 11 \cdot 10^6 \text{ lbs in}^{-2}$	

In the pure vibration of the channel beam, the differential equation in the axial displacement  $u$  (Eq. 18) uncouples from the other equations. Since  $c_y$  is zero in this example, Eq. 20 will uncouple also. The problem then reduces to a coupled vibrational problem in the  $v$ - and  $\theta$ - displacements, Eqs. 19 and 21. For simply supported ends,

$$v = \frac{\partial^2 v}{\partial x^2} = \theta = \frac{\partial^2 \theta}{\partial x^2} = 0 \quad (33)$$

and the theoretical solution, as given by the natural frequencies of vibration,  $p_i$ , can be written as (Ref. 3)

$$p_i^2 = \frac{\omega_{ti}^2 + \omega_{bi}^2 \pm \sqrt{(\omega_{ti}^2 - \omega_{bi}^2)^2 + 4\lambda c_z \omega_{bi}^2 \omega_{ti}^2}}{2(1 - \lambda c_z)} \quad (34)$$

where

$$\lambda = \frac{Ac_z}{I_o} \quad (35)$$

$$I_o = I_p + A(c_y^2 + c_z^2) \quad (36)$$

and  $\omega_{ti}$  and  $\omega_{bi}$  are the  $i^{\text{th}}$  uncoupled frequencies in twist and bending, respectively;

$$\omega_{ti}^2 = \frac{GJ\pi^2 L^2 i^2 + EC_\omega \pi^4 i^4}{\rho I_o L} \quad (37)$$

$$\omega_{bi}^2 = \frac{EI_1 \pi^4}{\rho A L^4} i^4 \quad (38)$$

When warping is not included in the analysis,  $\omega_{ti}$  reduces to

$$\omega_{ti}^2 = \frac{GJ\pi^2L^2i^2}{\rho I_o L^4} \quad (39)$$

The data obtained by using these equations are given in Table 1, cases 1 through 4. It can be observed that warping increases the twisting frequencies more than 100% while an increase of about 5% is seen for the bending frequencies by going from uncoupled to the coupled theory.

The channel is modeled by five equal elements 24 inches in length. Seven different modeling techniques have been tried, and the result is given in Table 1. Cases 5 through 8 show the channel modeled by the conventional Timoshenko beam element coinciding with the centroidal or elastic axis. In the first case only the uncoupled frequencies are obtained, while case 8 reflects the coupled frequencies without taking warping into effect. Also noticeable are the bending frequencies obtained in case 7, which because of the coupling between  $v$  and  $\theta$ , actually represents the twisting frequencies.

Warping is included in the last three cases in Table 1 by using a composite element similar to the one given in Fig. 3, but the rod element is excluded since no axial forces are present during the vibration considered. Because of the boundary conditions, Eq. 33, the flanges must be free to rotate at the ends. This is accomplished by modeling the ends similar to all the interior points with a semi-rigid link where  $w_1$  and  $w_2$  are restricted, but the rotations about the  $y$ -axis are free. The bulk data cards used for case 11 are given in the Appendix. Case 9, where the flanges are rigidly linked to the shear center, is included to show how important it is to free the rotational coordinates of the flanges, while cases 10 and 11 show the composite element properly used, including bending displacement and both bending ( $v$ ) and twisting ( $\theta$ ) displacements, in the numerical analysis. It is noticed that good correlation is obtained between theoretical (case 4) and numerical (case 11) data, the latter results being slightly below the first. This can be reasoned by the fact that few elements are used in the analysis, which implies 1) reduced torsional rigidity as explained above, and 2) concentrated inertia forces at the grid points instead of a continuous distribution.

Although the example did not use the rod element, this must be considered a very special case. For other structures and other loading conditions, the effect of excluding the rod can be significant. This will especially be the case where thin-walled open beams are used as members in between closed beams and where the axial load transfer is large. The example has shown, though, that

- (1) warping effects are properly taken into account by the composite element
- (2) inclusion of rotational displacements are necessary
- (3) good results are obtained with few elements.

## CONCLUSION

The composite element presented in this paper has been shown both mathematically and numerically to properly represent the thin-walled open beam. Since it is derived upon the differential equations for such beams, the model can be made as accurate as the theory is. In fact, in the limit as the length of the element gets smaller and smaller, the composite beam element is an exact model of the thin-walled open beam.

In conclusion, it is hoped that future editions of NASTRAN can present a true thin-walled beam element since the need for proper modeling will increase. Until that time, the present composite element is available, it is accurate, and easy to use.

## ACKNOWLEDGEMENT

The author expresses his gratitude to Dr. Curtis F. Vail for his many valuable suggestions in carrying out this work.

## REFERENCES

1. Vlasov, V. Z., "Thin-Walled Elastic Beams," OTS 61-11400, National Science Foundations, Washington, D.C. (1961).
2. Timoshenko, S. P. and Gere, J. M., Theory of Elastic Stability, Chapter 5, McGraw-Hill, New York, 1961.
3. Timoshenko, S. P., Vibration Problems in Engineering, 3rd Edition, D. Van Nostran Co., Inc., New York, 1955.
4. Gere, J. M., "Torsional Vibration of Beams of Thin-Walled Open Cross Section," Journal of Applied Mechanics, A.S.M.E., December 1954, pp. 381, 387.
5. Gere, J. M. and Lin, Y. K., "Coupled Vibrations of Thin-Walled Beams of Open Cross Section," Journal of Applied Mechanics, Transactions, A.S.M.E., Vol. 80, 1958, p. 373.
6. Christiano, P. and Salmela, L., "Frequencies of Beams with Elastic Warping Restraint," Tech. Note, Journal of the Structural Division, A.S.C.E., Vol. 97, No. ST6, June 1971.
7. Sokolnikoff, I. S., Mathematical Theory of Elasticity, 2nd Edition, McGraw-Hill, New York, 1956.
8. Schrem, E. and Roy, J. R., "An Automatic System for Kinematic Analysis," ASKA Part 1, ISD Report No. 98, Stuttgart, Germany, 1971.

APPENDIX

NASTRAN COMPUTER INPUT DECK

NASTRAN BUFFSIZE=511  
 ID SKATTUM,NASTRAN  
 APP DISPLACEMENT  
 SOL 3,0  
 TIME 5  
 CEND

TITLE= TEXT BOOK EXAMPLE OF CHANNEL  
 METHOD = 13  
 MPC = 100

OUTPUT  
 DISPLACEMENTS = ALL  
 BEGIN BULK

BAR0R							20.	1	
CBAR	1	27	1	2					+CB1
+CB1			0.0	-0.94	0.0	0.0	-0.94	0.0	
CBAR	2	27	2	3					+CB2
+CB2			0.0	-0.94	0.0	0.0	-0.94	0.0	
CBAR	3	27	3	4					+CB3
+CB3			0.0	-0.94	0.0	0.0	-0.94	0.0	
CBAR	4	27	4	5					+CB4
+CB4			0.0	-0.94	0.0	0.0	-0.94	0.0	
CBAR	5	27	5	6					+CB5
+CB5			0.0	-0.94	0.0	0.0	-0.94	0.0	
CBAR	6	2	7	11					
CBAR	7	2	8	15					
CBAR	8	2	14	9					
CBAR	9	2	18	10					
CBAR	12	2	11	12					
CBAR	13	2	12	13					
CBAR	14	2	13	14					
CBAR	22	2	15	16					
CBAR	23	2	16	17					
CBAR	24	2	17	18					
CJNM2	1	1		0.0078					+C21
+C21	0.0767								
CJNM2	2	2		0.0156					+C22
+C22	0.1534								
CJNM2	3	3		0.0156					+C23
+C23	0.1534								
CJNM2	4	4		0.0156					+C24
+C24	0.1534								
CJNM2	5	5		0.0156					+C25
+C25	0.1534								
CJNM2	6	6		0.0078					+C26
+C26	0.0767								
EIGR	13	GIV	0.0	2000.0		10			+13
+13	MAX								
GRID	1		0.0				1234		
GRID	2		24.0						
GRID	3		48.0						
GRID	4		72.0						
GRID	5		96.0						
GRID	6		120.0				1234		
GRID	7		0.0	-0.94	4.0		12345		

GRID	8		0.0	-0.94	-4.0				12345
GRID	9		120.0	-0.94	4.0				12345
GRID	10		120.0	-0.94	-4.0				12345
GRID	11		24.0	-0.94	4.0				1345
GRID	12		48.0	-0.94	4.0				1345
GRID	13		72.0	-0.94	4.0				1345
GRID	14		96.0	-0.94	4.0				1345
GRID	15		24.0	-0.94	-4.0				1345
GRID	16		48.0	-0.94	-4.0				1345
GRID	17		72.0	-0.94	-4.0				1345
GRID	18		96.0	-0.94	-4.0				1345
MAT1	2	29.+6	1.1+7						
MPC	1	11	2	1.	2	2		-1.0	+MP1
+MP1		2	4	4.0					
MPC	2	12	2	1.0	3	2		-1.0	+MP2
+MP2		3	4	4.0					
MPC	3	13	2	1.0	4	2		-1.0	+MP3
+MP3		4	4	4.0					
MPC	4	14	2	1.0	5	2		-1.0	+MP4
+MP4		5	4	4.0					
MPC	5	15	2	1.0	2	2		-1.0	+MP5
+MP5		2	4	-4.0					
MPC	6	16	2	1.0	3	2		-1.0	+MP6
+MP6		3	4	-4.0					
MPC	7	17	2	1.0	4	2		-1.0	+MP7
+MP7		4	4	-4.0					
MPC	8	18	2	1.0	5	2		-1.0	+MP8
+MP8		5	4	-4.0					
MPCADD	100	1	2	3	4	5	6	7	+MPA
+MPA		8							
OMIT1	5	1	6						
OMIT1	6	7	8	9	10	1	6	18	+OM1
+OM1	17	11	12	13	14	15	16		
OMIT1	1256	2	3	4	5				
PBAR	2	2	0.0	0.0	0.11	0.0			
PBAR	27	2	0.884	7.66	0.074	0.00168			
SEQGP	7	1.2	8	1.4	11	2.2	15	2.4	
SEQGP	12	3.2	16	3.4	13	4.2	17	4.4	
SEQGP	14	5.2	18	5.4					

TABLE 1. FREQUENCIES (CYCLES/SEC.) FOR CHANNEL VIBRATION

Case	Displacement Included	Warping Included	Natural Frequencies					
			Twist			Bending		
			<u>1</u>	<u>2</u>	<u>3</u>	<u>1</u>	<u>2</u>	<u>3</u>
1. Uncoupled theory (Eq. 38)	v	--	--	--	--	63.9	255.5	574.8
2. Uncoupled theory (Eq. 39)	$\theta$	No	7.1	14.2	21.2	--	--	--
3. Uncoupled theory (Eq. 37)	$\theta$	Yes	15.5	56.9	125.8	--	--	--
4. Coupled theory (Eq. 34)	v, $\theta$	Yes	15.4	56.8	125.5	67.1	268.3	603.7
5. Beam along centroidal axis	v	No	--	--	--	63.8	254.4	563.3
6. Beam along centroidal axis	v, $\theta$	No	7.0	13.3	18.2	63.8	254.4	563.3
7. Beam along elastic axis	v	No	--	--	--	7.0	12.9	17.7
8. Beam along elastic axis	v, $\theta$	No	6.7	12.7	17.5	66.6	265.7	588.1
9. Beam along elastic axis	v, $\theta$	Yes*	81.2	134.7	187.3	59.0	269.9	591.0
10. Beam along elastic axis	v	Yes	--	--	--	17.8	63.9	138.5
11. Beam along elastic axis	v, $\theta$	Yes	14.8	54.1	117.7	66.7	266.2	589.1

\* Flanges are rigidly linked to the shear center.

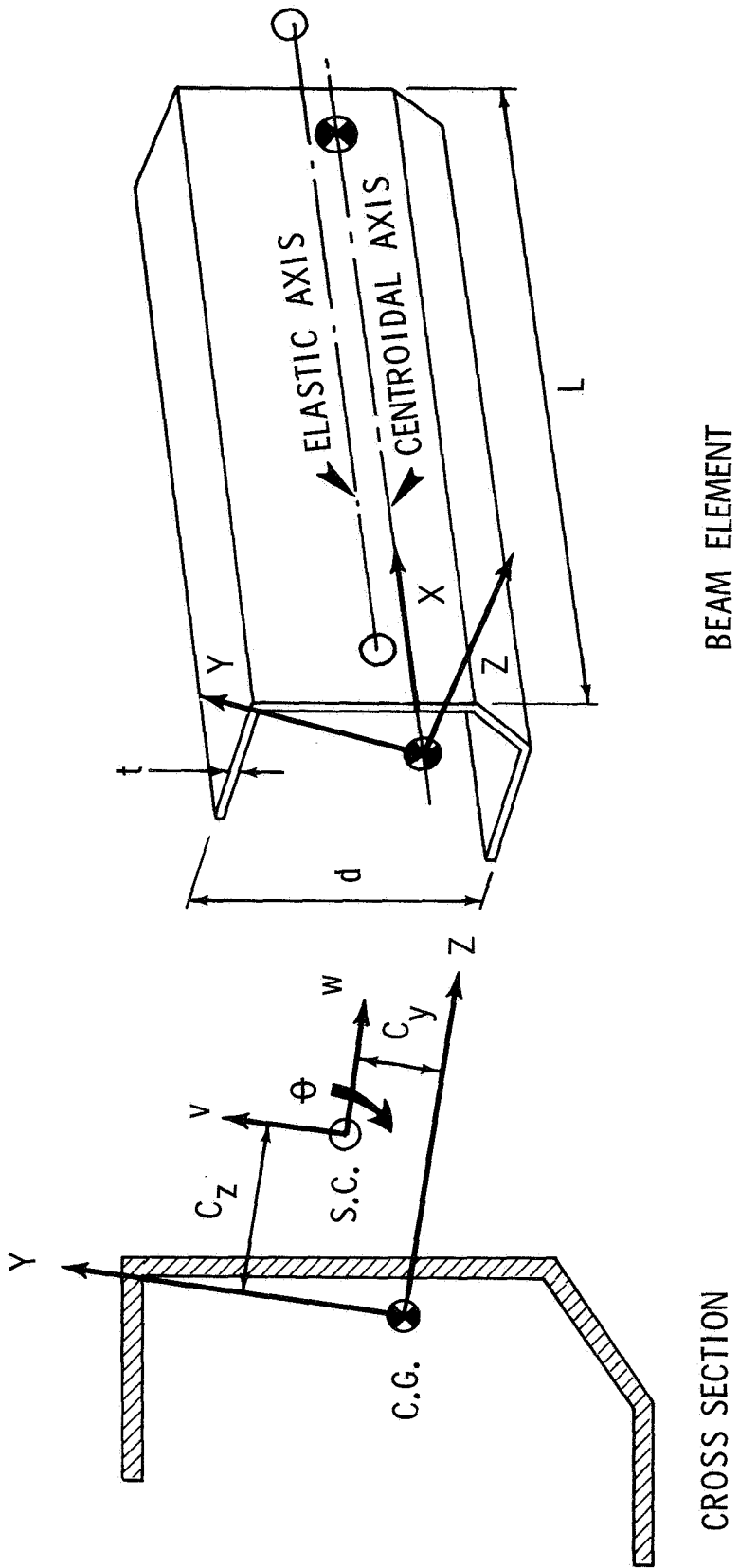


FIG. 1 THIN-WALLED OPEN BEAM

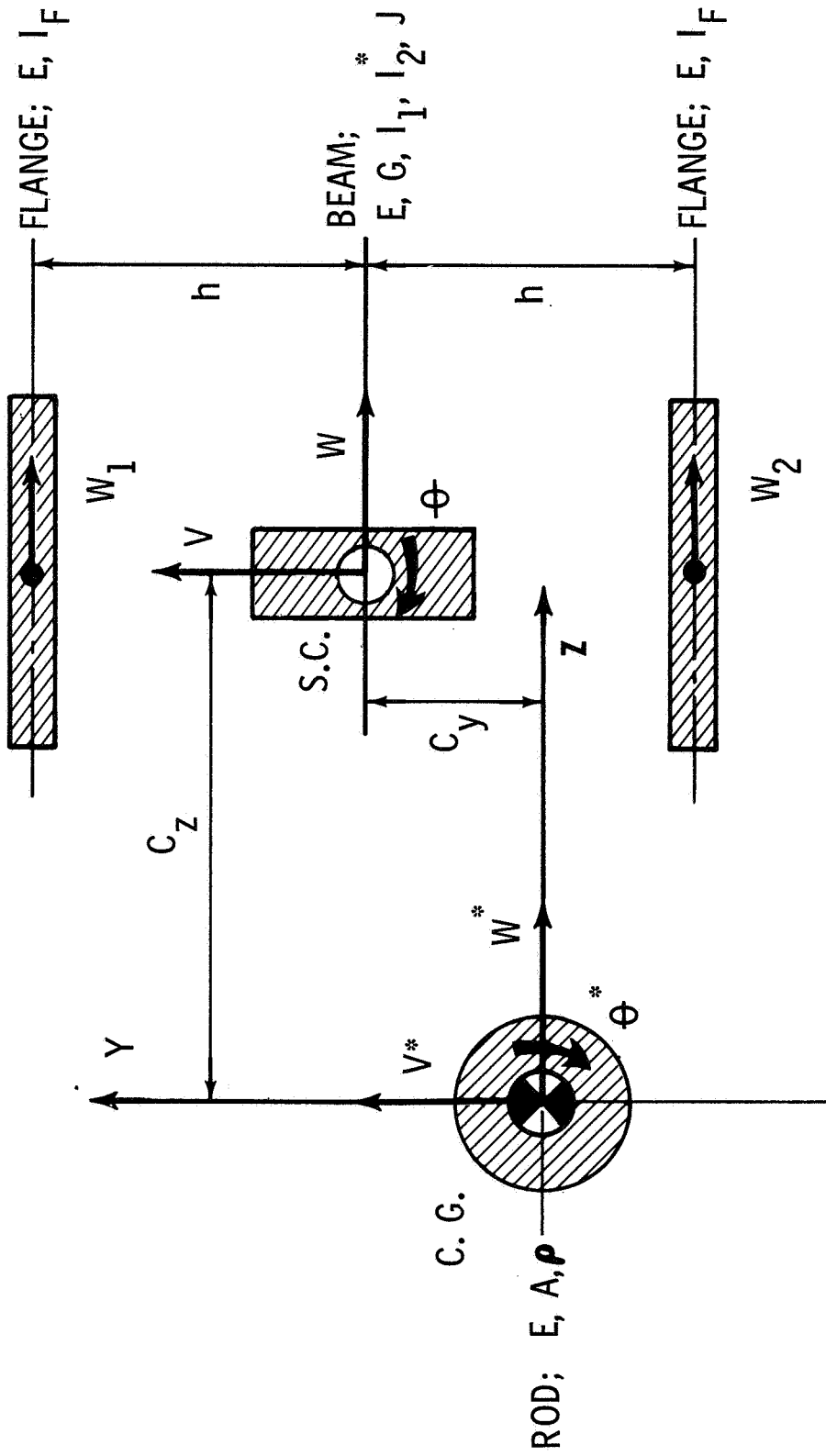


FIG. 2 FICTITIOUS COMPOSITE BEAM

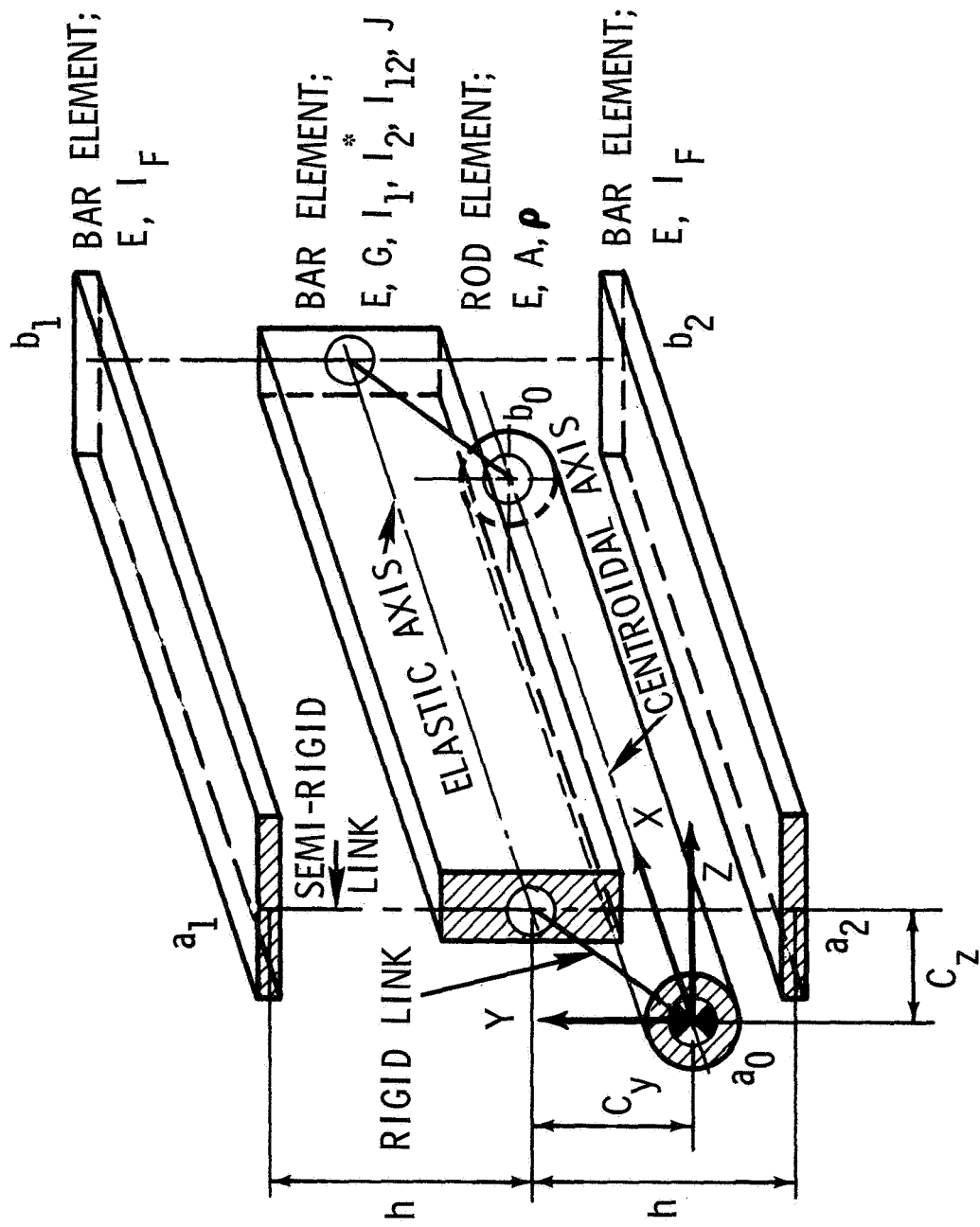


FIG. 3 MODELING OF THIN-WALLED BEAMS OF OPEN CROSS SECTIONS



# COMPLEX EIGENVALUE ANALYSIS OF ROTATING STRUCTURES

Jayant S. Patel  
Principal Engineer  
Teledyne Brown Engineering  
Company  
Huntsville, Alabama

S. M. Seltzer  
Sr. Research Engineer, Astrionics Lab.  
George C. Marshall Space Flight Center  
Marshall Space Flight Center, Alabama

## INTRODUCTION

Even though the NASA Structural Analysis (NASTRAN) program is designed to solve numerous structural dynamic problems through the use of available rigid formats, an important class of problems, where the structures are spinning at a constant angular velocity, has been omitted. Rotating shafts, blades of spinning turbines, rotating linkages, and spin stabilized satellites are examples of problems falling within this class. These problems differ from the nonspinning structures in several significant ways. The accelerations of the masses in a nonrotating stationary frame are represented by the second derivatives with respect to time of the spatial variables. In the case of a structure spinning at a constant angular velocity, expressions for the accelerations of the discrete masses contain terms arising from the second derivatives of the spatial variables; in addition, they contain terms caused by coriolis accelerations, which are proportional to the velocities of the masses in the rotating frame. Finally, these expressions reflect the variations in steady-state centripetal accelerations caused by the small displacements of the masses in the rotating frame. The steady-state centrifugal forces set up the steady stresses that give rise to the geometric stiffness matrix.

Since NASTRAN does not construct coriolis and centripetal acceleration matrices, and a centrifugal load vector due to spin about a selected point or about the mass center of the structure, a Fortran subroutine to construct these matrices is added in NASTRAN. The rigid translational degrees of freedom can be removed by using a transformation matrix  $T$  and its explicitly given inverse,  $T^{-1}$ . These matrices are generated in the above Fortran subroutine and their explicit expressions are given in Appendix A.

The complex eigenvalue subroutine of NASTRAN does not measure up to the excellence it has shown in assembling the matrices. If the user desires, an option is available to write out the matrices generated by NASTRAN on a magnetic tape which, in turn, can be used as the input to another eigenvalue program. The probable advantages in using another eigenvalue program are that the user may be able to solve a larger problem within the available core and he may use a more efficient eigenvalue routine if one is available to him. If it is required, the user can write out certain information generated by NASTRAN on a magnetic tape unit using the subroutines OUTPUT2 and WRTAPE used in this program.

### THEORETICAL DESCRIPTION<sup>1,2</sup>

The equations of motion of a spinning structure are briefly derived here to show how they differ from those of a nonspinning structure. The direct use of the Newton-Euler equations gives

$$\begin{aligned}\underline{F}^s &= m^s \underline{A}^s \\ \underline{T}^s &= \frac{i}{dt} \underline{H}^s\end{aligned}\quad (1)$$

for the  $s^{\text{th}}$  rigid body of a flexible appendage; where  $m^s$  is the mass,  $\underline{A}^s$  is the absolute translational acceleration vector.  $\underline{F}^s$  and  $\underline{T}^s$  are the sum of the external and connection force and torque vectors, respectively.  $\underline{H}^s$  is the angular momentum vector and  $i$  denoted differentiation in the inertial frame of reference.

For a rigid body of an appendage spinning nominally in the steady state with an angular velocity  $\underline{\omega}$  (fig. 1), the expression for acceleration is written as

$$\begin{aligned}\underline{A}^s &= \frac{b_d^2}{dt^2} (\underline{c} + \underline{u}^s) + 2\underline{\omega} \times \frac{b_d}{dt} (\underline{c} + \underline{u}^s) + \underline{\omega} \times (\underline{\omega} \times (\underline{c} + \underline{u}^s)) + \underline{\omega} \times (\underline{\omega} \times \underline{r}^s) \\ &+ \frac{i}{dt} \underline{\omega} \times (\underline{c} + \underline{u}^s + \underline{r}^s) + \frac{i^2}{dt^2} \underline{R}\end{aligned}\quad (2)$$

$$\begin{aligned}
\underline{T}^s &= \frac{i_d}{dt} (\underline{I}^s \cdot \underline{\omega}^s) = \frac{i_d}{dt} (\underline{I}^s \cdot (\underline{\omega} + \underline{\beta}^s)) \\
&= \underline{I}^s \cdot \left[ \frac{i_d}{dt} \underline{\omega} + \frac{b_d^2}{dt^2} \underline{\beta}^s + \underline{\omega} \times \frac{b_d}{dt} \underline{\beta}^s \right] \\
&\quad + \underline{\omega} \times \underline{I}^s \cdot \underline{\omega} + \underline{\omega} \times \underline{I}^s \cdot \frac{b_d}{dt} \underline{\beta}^s + \frac{b_d}{dt} \underline{\beta}^s \times \underline{I}^s \cdot \underline{\omega} \tag{3}
\end{aligned}$$

where  $\underline{c}$  is a vector representing the location of the mass center at time  $t$  with respect to its steady state position.  $\underline{u}^s$  and  $\underline{\beta}^s$  are vectors representing the displacement and small rotation, respectively, of the  $s^{\text{th}}$  rigid body from its steady state configuration.  $\underline{r}^s$  is a vector representing the location of the  $s^{\text{th}}$  rigid body of the appendage in its steady state configuration measured from the steady state mass center location.  $\underline{I}^s$  is the inertia dyadic of the  $s^{\text{th}}$  rigid body. Superscript  $b$  denotes differentiation in the reference frame  $\underline{b}$  imbedded in the rigid body with the origin at the steady state mass center location.

For zero spin ( $\underline{\omega} = 0$ ), eq. (2) and (3) reduce to the familiar form

$$\underline{A}^s = \frac{i_d^2}{dt^2} (\underline{R} + \underline{c} + \underline{r}^s + \underline{u}^s) \tag{2-a}$$

$$\underline{T}^s = \underline{I}^s \cdot \frac{i_d^2}{dt^2} \underline{\beta}^s \tag{3-a}$$

In matrix notation the second term on the right hand side of eq. (2), which is due to coriolis acceleration, gives rise to a skew-symmetric matrix; whereas, the third term, which is due to the centripetal acceleration, yields a symmetric matrix. The fourth term in eq. (2) and (3) represents a steady state centripetal acceleration which describes the steady state configuration. Stretching forces, moments and rotations obtained therefrom, give rise to the second order geometric stiffness matrix. In the absence of angular acceleration, the fifth term of eq. (2) vanishes. If rotational dynamics are the primary concern, the effect of translation of the orbit is disregarded and the last term of eq. (2) also vanishes. The last two terms in eq. (3) will cancel each other if the inertia matrix is diagonal with all the terms having the same magnitude. In the computer program no such restriction is imposed on the  $\underline{I}^s$  matrix.

Conservation of linear momentum provides the relation

$$\underline{c} = -\frac{1}{M} \sum_{s=1}^n m^s \underline{u}^s \quad (4)$$

where  $M$  is the cumulative mass of all appendages and the central rigid body, and  $n$  is the total number of masses representing all of the appendages.

Conservation of angular momentum is not imposed. As a result, the central rigid body is restricted against variations in rotations. Conservation of linear momentum permits the translation of the central rigid body, thus allowing the coupling of the vibrations of all the appendages attached to the central rigid body.

The set of equations representing the motion of all the rigid bodies in the appendage about the steady state configuration is obtained by substituting eq. (4) into eq. (2) and writing the resulting eq. (2) and (3), for all rigid bodies in matrix form:

$$[M'] \{\ddot{u}\} + [G'] \{\dot{u}\} + [K''' + K_e + K_g] \{u\} = [F] \quad (5)$$

The steady state equation in matrix form is:

$$[K_e + K'''] \{u\}^s = \{P\}^s \quad (6)$$

The use of eq. (4) eliminates the remaining translational rigid body degrees-of-freedom. As a result, the mass matrix  $M'$  is a symmetric non-diagonal matrix. Matrix  $G'$  is in general, a fully populated skew-symmetric matrix of coriolis acceleration terms. Matrix  $K'''$  is a fully populated non-symmetric matrix of centrifugal acceleration terms.  $K_e$  and  $K_g$  are elastic and geometric (differential) stiffness matrices, respectively, (and are obtained from the NASTRAN program) and  $\{u\}$  is the vector of generalized displacements about the steady state configuration. In the absence of spin, matrices  $G'$ ,  $K'''$ , and  $K_g$  will all be identically zero, and the eigenvalue problem reduces to the standard eigenvalue problem of a free-free structure or a cantilever.  $\{u\}^s$  is the vector of the steady state generalized displacements from the unstrained configuration  $\{r\}$  of the appendages. Since the steady state deformations  $\{u\}^s$  are very small compared to the unstrained configuration  $\{r\}$ , it is assumed that the steady state configuration is given by  $\{r\}$  instead of  $\{r\} + \{u\}^s$ . The steady state force vector  $\{P\}^s$  is used to obtain the geometric stiffness matrix,  $K_g$ .

Matrices  $M'$ ,  $G'$ , and  $K'''$  have the following properties:

$$\begin{aligned} [M'] &= [M] [T] \\ [G'] &= [G] [T] \\ [K'''] &= [K''] [T] \end{aligned} \quad (7)$$

Relations (7) afford a transformation

$$\{y\} = [T] \{u\} \quad (8)$$

Substitution of transformation (8) into eq. (5) gives

$$[M] \{\ddot{y}\} + [G] \{\dot{y}\} + [K'' + [K_e + K_g] T^{-1}] \{y\} = 0 \quad (9)$$

where

- $u$  = Vector of displacements from the steady state configuration of the nodal masses in spinning body frame.
- $T$  = Transformation matrix relates the displacements of nodal masses in the body frame with the origin at steady state mass center to the displacements in another body frame obtained by translating the above frame to the instantaneous mass center. In the absence of vibrations both above body frames coincide. If the axis of rotation and the origin of the body frame are both fixed in inertial space,  $T$  and  $T^{-1}$  become identity matrices, additionally.
- $M$  = NASTRAN generated mass matrix
- $G$  = Dummy module generated coriolis acceleration matrix
- $K''$  = Dummy module generated centripetal acceleration matrix
- $P_g$  = Dummy module generated steady state centrifugal force vector
- $K_g$  = NASTRAN generated differential stiffness matrix using the above load vector  $P_g$
- $K_e$  = NASTRAN generated elastic stiffness matrix.

Explicit forms of the above matrices are given in Appendix A.

## DMAP DESCRIPTION

The following information and options are made available through the input of vector WW with five elements using DMI\* cards. The first of the two cards never changes for this program. WW(1), WW(2), WW(3) are the components of the spin vector in the body frame. Terms WW(4), WW(5) can take the values either 0.0 or 1.0. If WW(4) = 1.0 the structure is spinning about the mass center of vehicle, and if WW(4) = 0.0 the structure is spinning about a fixed point in the space. The calculation of matrices T and  $T^{-1}$ , which removes the rigid body translational degrees of freedom, is performed if WW(5) = 1.0. If WW(5) = 0.0, matrices T and  $T^{-1}$  are identity matrices which means that the structure is supported and does not have the rigid body translational degrees of freedom.

The following options can be exercised through the use of WW(4) and WW(5).

Case I. WW(4) = WW(5) = 1.0, GRID 1 constrained in all six directions. The structure is spinning about the vehicle mass center, and the rigid body translational degrees of freedom are removed. GRID No. 1 is connected by a rigid link to the mass center of the vehicle in the steady state configuration and one or more appendages are cantilevered from GRID No. 1. GRID No. 1 should be constrained in all six directions by use of SPC cards or permanent SPC on GRID cards.

Case II. WW(4) = WW(5) = 0.0, GRID 1 constrained in all six directions. The structure is assumed to be spinning about a point (GRID 1) fixed in inertial space, e.g., a spinning shaft with GRID 1 at bearing.

Case III. WW(4) = 1.0 WW(5) = 0.0, GRID 1 constrained in all six directions. Node No. 1 is rigidly connected to the steady state mass center which is fixed in inertial space. The structure is spinning about mass center.

Case IV. WW(4) = 0.0 WW(5) = 1.0, GRID 1 constrained in all six directions. The structure is spinning about GRID 1 with rigid body translational degrees of freedom removed.

\* Refer to NASTRAN User's Manual for definitions of card names used herein.

The DMAP sequence given in Appendix B solves eq. (9) and eigenvectors  $y_i$  (PHI in DMAP) thus obtained are transformed to  $u_i$  (PHID in DMAP) which are the eigenvectors of eq. (8).

It is essential that two subcases are used in the case control deck as shown below for successful completion of the NASTRAN run.

```
CASE CONTROL DECK
TITLE
:
SUBCASE 1
DISPLACEMENT = ALL
:
SUBCASE 2
DSCOEFFICIENT = DEFAULT
BEGIN BULK
```

No provision for checkpoint is made since the time taken to assemble the matrices is just a fraction of the time taken to find a few eigenvalues.

## FUNCTIONAL MODULE PROGRAMING NOTES

In writing a functional module for NASTRAN, the concept of open core should be employed even if the corresponding logic for an open core array is not used. This gives the generality and possibility of later expansions without having to alter the program extensively. This does not mean that the fixed dimensioned arrays cannot be used in NASTRAN functional modules. The details of the open core concept are given in Section 1.5 of the Programmer's Manual. Once the dimensions are set either by open core or by fixed locations, the next steps are either to retrieve the data (input blocks) to be used for further computations or to store the computed data (output blocks) in a prescribed format within NASTRAN. The data as described in Section 2.2 of the Programmer's Manual may be in the form of a matrix, a table or bulk data cards.

A matrix data are stored in two separate parts. One part constitutes the name of the matrix in alpha-numeric form (Header Information). The columns of the matrix are stored on random access peripheral equipments.

The second part is called the Trailer Information and is stored in FIAT which is an executive system table of NASTRAN. The first part is stored as a set of logical records: the first record is the Header information, and the second and subsequent logical records until the end of file is reached are the columns of a matrix. The Trailer informations, which is the collection of the properties (size, real, complex, symmetric, etc.) of all the matrices used in NASTRAN are given in the Programmer's Manual but if new matrices are created, their Trailer information should be stored according to the instructions on page 2.2-2 of the Programmer's Manual. Either of the above two parts describing a matrix can be called, as shown later, without disturbing the other.

Each of the matrices, whether constructed by NASTRAN or computed in a functional module and designated as an input or output block in a particular DMAP statement should be referred to by a file number. The numbering system of a file is standardized by NASTRAN as consisting of three digits. The first digit takes value 1 if it is an input block and 2 if it is an output block; the second and third digits refer to matrix location in the string of input or output data blocks. For example, file number 102 in DMAP statement DUMMOD1 given in Appendix B refers to the second input block which is an unreduced mass matrix M<sub>gg</sub> whereas 203 refers to the third output block which is the coriolis acceleration matrix G.

In order to read the desired matrix, the following set of calls to subroutines listed below will unpack and read the matrix data. In each of the subroutines the file number for the appropriate matrix data block must be included in appropriate argument.

```
CALL RDTRL
CALL OPEN
CALL FWDREC
CALL UNPACK
:
CALL UNPACK
CALL CLOSE
```

The subroutine RDTRL calls on the file number appearing in its argument for the Trailer information. A call on RDTRL can also be made after calling OPEN, if desired. Subroutine OPEN opens the file to be read. FWDREC positions the requested file forward one logical record thereby skipping the first record in this particular example. If for

some reason two logical records need to be skipped, FWDREC is called twice. Each call to UNPACK allows the reading of one column (a logical record) of a matrix at a time. The call to UNPACK can be put within a DO-loop once the information on the number of columns of the matrix is obtained from Trailer information. After the reading of columns is completed the subroutine CLOSE is called to close the file as soon as practicable.

If the data are in tabular form, instead of calling UNPACK, call READ to read the data. Each call to READ reads one logical record of the data. The programmer's manual should be consulted for structure of the record read. The call to READ can be put either within a DO-loop once the information on the number of records is obtained from Trailer information or within an unending DO-loop in which case, when the end of file is reached, the transfer will be made to a statement number appearing in the argument of READ. The set of calls is shown as

```
CALL RDTRL
CALL OPEN
CALL FWDREC
CALL READ
  :
  :
CALL READ
CALL CLOSE
```

If the data on Bulk Data Cards are desired to be retrieved the following set of calls to subroutines should be employed.

```
CALL PRELOC
CALL LOCATE
CALL READ
  :
  :
CALL READ
CALL CLOSE
```

Subroutine PRELOC locates the file on which the bulk data card images are stored and LOCATE locates the desired number of cards in the file.

In DMAP statement DUMMOD1 file number 101 which is GEOM1, contains the geometric information from Bulk Data Cards. This file number is called in PRELOC subroutine. For each bulk data card to be read, subroutine READ should be called.

To pack the matrices calculated in a subroutine and appearing as output data block the following set of calls to subroutines is required.

```
CALL OPEN
CALL FNAME (finds Header information)
Prepare Trailer information (e.g. M(1), M(2), --M(7) )
    according to instructions appearing in Section 2.2-2
    of the Programmer's Manual.
CALL WRITE (writes Header information)
```

Perform computations.

```
CALL PACK (----, ----, WRITE, M)
:
CALL PACK
CALL WRTTRL (M(1))
CALL CLOSE
```

Subroutine OPEN opens the file to be written on and FNAME finds and stores the Header information as appearing in DMAP subroutine (e.g., if file number 204 is referred in OPEN, FNAME will go to the fourth output block of DUMMOD1 which is matrix AA and store AA as the Header information). Next prepare the Trailer information in the vector M according to the instructions in Programmer's Manual with the following exceptions. On page 2.2-2 of the Programmer's Manual M has the dimension 6 which is an error, it should be dimensioned M(7) and M(1) = File Number

M(2) = 0

M(3) = M(2) of the Programmer's Manual

:

M(7) = M(6) of the Programmer's Manual.

Note that M(2) is set equal to zero and not one as implied in the Programmer's Manual. If M(2) = 1, the information on the number of columns stored in Trailer information will show one more than the value desired. Hence when this Trailer information is used to read the columns, the READ will try to take it past the end of file resulting in fatal error.

Subroutine WRITE writes the Header information and then one column at a time is packed by subroutine PACK. Call WRTTRL to write Trailer information and then call subroutine CLOSE.

If it is desired when developing functional modules, the number of input, output blocks and parameters can be altered by altering the information in MPL (subroutine XMPLBD). In the development of this program, four functional modules are written. In addition several other functional modules for other NASA projects at MSFC have also been written. All these functional modules are given dummy names as given in User's Manual. Because the procedure given in NASTRAN's program manual are either incomplete or in error, attempts to add new functional modules with unique name and unique MPL (Module Properties List) have not been met any degree of success.

It is acknowledged that most of the information presented in this section may be found throughout the Programmer's Manual. However, it will take a considerable time to assemble and use. Here we have presented the information we collected through trial and error and months of diligent work by two expert programmers. We present it with the hopes that someone wishing to write their new functional modules will not have to encounter the same difficulties.

#### ACKNOWLEDGEMENT

The help of Mr. Archie Jordan and Mr. Tommy Franklin of Computer Science Corporation of Huntsville, Alabama in successfully completing the programming of this altered version of NASTRAN to solve the Complex Eigenvalue Analysis of Rotating Structures is appreciated. This effort was made possible by Bettye L. Harrison of Marshall Space Flight Center's Computation Laboratory.

#### REFERENCES

1. Likins, P. W.: Dynamics and Control of Flexible Space Vehicles. NASA TR-32-1329, Revision 1, January 1970.
2. Patel, J. S. and Seltzer, S. M.: Complex Eigenvalue Solution to a Spinning Skylab Problem. NASA TM-X-2378, Vol. II, September 1971.
3. "Eigenvalue Analysis of Rotating Structures." Job No. 310261, April 25, 1972. NASA Computation Lab. Bldg. 4663. Marshall Space Flight Center, Huntsville, Alabama 35805.

APPENDIX A

$$[K'] = \begin{bmatrix} [K']^1 & & & & & \\ & [K']^2 & & & & \\ & & [K']^3 & & & \\ & & & \cdot & & \\ & & & & \cdot & \\ & & & & & \cdot \\ & & & & & & [K']^n \end{bmatrix}_{6n \times 6n}$$

A-1

where

$$[K']^i = \begin{bmatrix} [K'_{11}]^i & \vdots & 0 \\ \hline 0 & \vdots & [K'_{22}]^i \end{bmatrix}$$

and

$$[K'_{11}]^i = \begin{bmatrix} -m^i(\omega_2^2 + \omega_3^2) & m^i\omega_1\omega_2 & m^i\omega_1\omega_3 \\ m^i\omega_1\omega_2 & -m^i(\omega_1^2 + \omega_3^2) & m^i\omega_2\omega_3 \\ m^i\omega_1\omega_3 & m^i\omega_2\omega_3 & -m^i(\omega_1^2 + \omega_2^2) \end{bmatrix}$$

$$[K'_{22}] = \begin{bmatrix} k_{11} & k_{12} & k_{13} \\ k_{21} & k_{22} & k_{23} \\ k_{31} & k_{32} & k_{33} \end{bmatrix}$$

$$k_{11} = (I_{22}^i - I_{33}^i)(\omega_2^2 - \omega_3^2) + 4I_{23}^i\omega_2\omega_3 + I_{12}^i\omega_1\omega_2 + I_{13}^i\omega_1\omega_3$$

$$k_{12} = (I_{33}^i - I_{11}^i)\omega_1\omega_2 - 2I_{31}^i\omega_2\omega_3 \\ + I_{21}^i(\omega_3^2 - \omega_2^2) - I_{32}^i\omega_1\omega_3$$

$$k_{13} = I_{31}^i(\omega_2^2 - \omega_3^2) - I_{32}^i\omega_1\omega_2 \\ - 2I_{21}^i\omega_2\omega_3 - (I_{11}^i - I_{22}^i)\omega_1\omega_3$$

$$k_{21} = I_{21}^i(\omega_3^2 - \omega_1^2) - I_{31}^i\omega_2\omega_3 \\ - (I_{22}^i - I_{33}^i)\omega_1\omega_2 - 2I_{32}^i\omega_1\omega_3$$

$$k_{22} = (I_{33}^i - I_{11}^i)(\omega_3^2 - \omega_1^2) + I_{32}^i\omega_2\omega_3 \\ + 4I_{31}^i\omega_1\omega_3 + I_{21}^i\omega_2\omega_1$$

$$k_{23} = (I_{11}^i - I_{22}^i)\omega_2\omega_3 - 2I_{21}^i\omega_1\omega_3 \\ - I_{32}^i(\omega_3^2 - \omega_1^2) - I_{31}^i\omega_1\omega_2$$

$$k_{31} = (I_{22}^i - I_{33}^i)\omega_1\omega_3 - 2I_{32}^i\omega_1\omega_2 \\ - I_{31}^i(\omega_1^2 - \omega_2^2) - I_{21}^i\omega_2\omega_3$$

$$k_{32} = I_{32}^i(\omega_1^2 - \omega_2^2) - I_{21}^i\omega_1\omega_3 \\ - (I_{33}^i - I_{11}^i)\omega_2\omega_3 - 2I_{31}^i\omega_1\omega_2$$

$$k_{33} = (I_{11}^i - I_{22}^i)(\omega_1^2 - \omega_2^2) \\ + 4I_{21}^i\omega_1\omega_2 + I_{31}^i\omega_1\omega_3 + I_{32}^i\omega_2\omega_3$$

$$[P^S] = \begin{bmatrix} [P^i]_1 \\ [P^i]_2 \\ [P^i]_3 \\ \vdots \\ [P^i]_n \end{bmatrix}_{6n} \quad \text{where } [P^i] = \begin{bmatrix} [P_1^i] \\ \vdots \\ [P_2^i] \end{bmatrix}$$

and

$$[P_1^i] = \begin{bmatrix} -m^i [-(\omega_2^2 + \omega_3^2)R_1^i + \omega_1\omega_2R_2^i + \omega_1\omega_3R_3^i] \\ -m^i [\omega_1\omega_2R_1^i - (\omega_1^2 + \omega_3^2)R_2^i + \omega_2\omega_3R_3^i] \\ -m^i [\omega_1\omega_3R_1^i + \omega_2\omega_3R_2^i - (\omega_1^2 + \omega_2^2)R_3^i] \end{bmatrix}$$

$$[P_2^i] = \begin{bmatrix} (I_{22}^i - I_{33}^i)\omega_2\omega_3 - I_{32}^i(\omega_2^2 - \omega_3^2) - I_{31}^i\omega_1\omega_2 + I_{21}^i\omega_1\omega_3 \\ (I_{33}^i - I_{11}^i)\omega_1\omega_3 - I_{31}^i(\omega_3^2 - \omega_1^2) - I_{21}^i\omega_2\omega_3 + I_{32}^i\omega_1\omega_2 \\ (I_{11}^i - I_{22}^i)\omega_1\omega_2 - I_{21}^i(\omega_1^2 - \omega_2^2) - I_{32}^i\omega_1\omega_3 + I_{31}^i\omega_2\omega_3 \end{bmatrix}$$

$$R_1^i = R_1^i - R_{1G}$$

$$R_2^i = R_2^i - R_{2G}$$

$$R_3^i = R_3^i - R_{3G}$$

$$\text{where } R_{jG} = \sum_{i=1}^n R_{ji}^i / M \quad j = 1, 2, 3$$

$$[G] = \begin{bmatrix} [G]^1 & & & & & \\ & [G]^2 & & & & \\ & & [G]^3 & & & \\ & & & 0 & & \\ & & & & 0 & \\ & & & & & [G]^n \end{bmatrix}$$

A-3

6n x 6n

where  $[G]^i = \begin{bmatrix} G_{11} & | & 0 \\ \hline 0 & | & G_{22} \end{bmatrix}$

and

$$G_{11} = \begin{bmatrix} 0 & -2m^i \omega_3 & 2m^i \omega_2 \\ 2m^i \omega_3 & 0 & -2m^i \omega_1 \\ -2m^i \omega_2 & 2m^i \omega_1 & 0 \end{bmatrix}$$

$$G_{22} = \begin{bmatrix} 0 & (I_{33}^i - I_{11}^i - I_{22}^i) \omega_3 & (I_{33}^i + I_{11}^i - I_{22}^i) \omega_2 \\ & + 2I_{32}^i \omega_2 + 2I_{31}^i \omega_1 & -2I_{32}^i \omega_3 - 2I_{21}^i \omega_1 \\ (I_{11}^i + I_{22}^i - I_{33}^i) \omega_3 & 0 & (I_{11}^i - I_{22}^i - I_{33}^i) \omega_1 \\ -2I_{32}^i \omega_2 - 2I_{31}^i \omega_1 & & + 2I_{21}^i \omega_2 + 2I_{31}^i \omega_3 \\ (I_{22}^i - I_{33}^i - I_{11}^i) \omega_2 & (I_{22}^i + I_{33}^i - I_{11}^i) \omega_1 & \\ + 2I_{32}^i \omega_3 + 2I_{21}^i \omega_1 & -2I_{21}^i \omega_2 - 2I_{31}^i \omega_3 & 0 \end{bmatrix}$$



The inverse of this matrix is expressed in the following form, rather than inverting [T] by some matrix inversion technique.

$$[T]^{-1} = \begin{pmatrix}
 \left( \begin{array}{cccc}
 1 + \frac{\mu_1^1}{s_{10}} & 0 & 0 & 0 \\
 0 & 1 + \frac{\mu_2^1}{s_{20}} & 0 & 0 \\
 0 & 0 & 1 + \frac{\mu_3^1}{s_{30}} & 0 \\
 0 & 0 & 0 & 1
 \end{array} \right) & \begin{pmatrix} \frac{\mu_1^2}{s_{10}} & 0 & 0 & 0 \\ 0 & \frac{\mu_2^2}{s_{20}} & 0 & 0 \\ 0 & 0 & \frac{\mu_3^2}{s_{30}} & 0 \\ 0 & 0 & 0 & 0 \end{pmatrix} & \begin{pmatrix} \frac{\mu_1^n}{s_{10}} & 0 & 0 & 0 \\ 0 & \frac{\mu_2^n}{s_{20}} & 0 & 0 \\ 0 & 0 & \frac{\mu_3^n}{s_{30}} & 0 \\ 0 & 0 & 0 & 0 \end{pmatrix} \\
 \begin{pmatrix} 0 & 0 & 0 & 1 \\ 0 & 0 & 0 & 0 \\ 0 & 0 & 0 & 0 \\ 0 & 0 & 0 & 0 \end{pmatrix} & \begin{pmatrix} 0 & 0 & 0 & 0 \\ 0 & 0 & 0 & 0 \\ 0 & 0 & 0 & 0 \\ 0 & 0 & 0 & 0 \end{pmatrix} & \begin{pmatrix} 0 & 0 & 0 & 0 \\ 0 & 0 & 0 & 0 \\ 0 & 0 & 0 & 0 \\ 0 & 0 & 0 & 0 \end{pmatrix} \\
 \begin{pmatrix} \frac{\mu_1^1}{s_{10}} & 0 & 0 & 0 \\ 0 & \frac{\mu_2^1}{s_{20}} & 0 & 0 \\ 0 & 0 & \frac{\mu_3^1}{s_{30}} & 0 \\ 0 & 0 & 0 & 0 \end{pmatrix} & \begin{pmatrix} \frac{\mu_1^n}{s_{10}} & 0 & 0 & 0 \\ 0 & \frac{\mu_2^n}{s_{20}} & 0 & 0 \\ 0 & 0 & \frac{\mu_3^n}{s_{30}} & 0 \\ 0 & 0 & 0 & 0 \end{pmatrix} & \begin{pmatrix} 0 & 0 & 0 & 0 \\ 0 & 0 & 0 & 0 \\ 0 & 0 & 0 & 0 \\ 0 & 0 & 0 & 0 \end{pmatrix} \\
 \begin{pmatrix} 0 & 0 & 0 & 0 \\ 0 & 0 & 0 & 0 \\ 0 & 0 & 0 & 0 \\ \vdots & \vdots & \vdots & \vdots \\ 0 & 0 & 0 & 0 \end{pmatrix} & \begin{pmatrix} 0 & 0 & 0 & 0 \\ 0 & 0 & 0 & 0 \\ 0 & 0 & 0 & 0 \\ \vdots & \vdots & \vdots & \vdots \\ 0 & 0 & 0 & 0 \end{pmatrix} & \begin{pmatrix} 0 & 0 & 0 & 0 \\ 0 & 0 & 0 & 0 \\ 0 & 0 & 0 & 0 \\ \vdots & \vdots & \vdots & \vdots \\ 0 & 0 & 0 & 0 \end{pmatrix} \\
 \begin{pmatrix} \frac{\mu_1^1}{s_{10}} & 0 & 0 & 0 \\ 0 & \frac{\mu_2^1}{s_{20}} & 0 & 0 \\ 0 & 0 & \frac{\mu_3^1}{s_{30}} & 0 \\ 0 & 0 & 0 & 0 \end{pmatrix} & \begin{pmatrix} \frac{\mu_1^n}{s_{10}} & 0 & 0 & 0 \\ 0 & 1 + \frac{\mu_2^n}{s_{20}} & 0 & 0 \\ 0 & 0 & 1 + \frac{\mu_3^n}{s_{30}} & 0 \\ 0 & 0 & 0 & 0 \end{pmatrix} & \begin{pmatrix} 0 & 0 & 0 & 0 \\ 0 & 0 & 0 & 0 \\ 0 & 0 & 0 & 0 \\ 0 & 0 & 0 & 0 \end{pmatrix} \\
 \begin{pmatrix} 0 & 0 & 0 & 0 \\ 0 & 0 & 0 & 0 \\ 0 & 0 & 0 & 0 \end{pmatrix} & \begin{pmatrix} 0 & 0 & 0 & 0 \\ 0 & 0 & 0 & 0 \\ 0 & 0 & 0 & 0 \end{pmatrix} & \begin{pmatrix} 0 & 0 & 0 & 1 \\ 0 & 0 & 0 & 0 \\ 0 & 0 & 0 & 0 \end{pmatrix}
 \end{pmatrix}$$

$6n \times 6n$

where

$$\mu_k^i = \begin{cases} \frac{m^i}{M_0 + \sum_{j=1}^n m^j} & \text{if the motion of mass at node } i \text{ in } k\text{th} \\ & \text{direction is not constrained to be} \\ & \text{zero} \\ 0 & \text{if the motion of mass at node } i \text{ in } k\text{th} \\ & \text{direction is constrained to be zero} \end{cases}$$

$$S_{k0} = 1 - \sum_{j=1}^n \mu_k^j$$

where  $m^i$  is the mass at the  $i$ th node point of the total of ' $n$ ' nodes and  $I_{jk}^i$  is the moment of inertia of the rigid body at the  $i$ th node,  $M_0$  is the mass of the central rigid body and  $\{\omega\}$  is the spin vector.

Matrices  $[G]$ ,  $[K'']$ ,  $[T]$ , and  $[T^{-1}]$  are the square matrices of the dimension  $6n \times 6n$ . Rows and columns corresponding to the degree-of-freedom which are either constrained to be zero or have no mass should be removed. This will reduce the above matrices to  $N \times N$  where  $N$  is the total degree-of-freedom of the problem.

## APPENDIX B

```

1 BEGIN      EIGENVALUE ANALYSIS OF ROTATING STRUCTURES. $
2 GP1       GEØM1,GEØM2,/GPL,EQEXIN,GPDT,CSTM,BGPDT,SIL/V,N,LUSET/C,N,123/
           V,N,NØGPDT $
3 SAVE      LUSET $
4 GP2       GEØM2,EQEXIN/ECT $
5 PLTSET    PCDB,EQEXIN,ECT/PLTSETX,PLTPAR,GPSETS,ELSETS/V,N,NSIL/V,N,
           JUMPPLØT $
6 SAVE      NSIL,JUMPPLØT $
7 PRTMSG    PLTSETX// $
8 SETVAL    //V,N,PLTFLG/C,N,1/V,N;PFILE/C,N,0 $
9 SAVE      PLTFLG,PFILE $
10 CØND     P1,JUMPPLØT $
11 PLØT     PLTPAR,GPSETS,ELSETS,CASECC,BGPDT,EQEXIN,SIL,,/PLØTX1/V,N,
           NSIL/V,N,LUSET/V,N,JUMPPLØT/V,N,PLTFLG/V,N,PFILE $
12 SAVE     JUMPPLØT,PLTFLG,PFILE $
13 PRTMSG    PLØTX1// $
14 LABEL    P1 $
15 GP3       GEØM3,EQEXIN,GEØM2/SLT,GPPT/C,N,123/V,N,NØGRAV/C,N,123 $
16 TA1,     ,ECT,EPT,BGPDT,SIL,GPPT,CSTM/EST,,GEI,ECPT,GPCT/V,N,LUSET/C,N,
           123/V,N,NØSIMP/C,N;O/V,N,NØGENL/V,N,GENEL $
17 SAVE     NØGENL,NØSIMP,GENEL $
18 CØND     ERRØR1,NØSIMP $
19 PURGE    ØGPST/GENEL $
20 SMA1     CSTM,MPT,ECPT,GPCT,DIT/KGGX,,GPST/V,N,NØGENL/V,N,NØK4GG $
21 SMA2     CSTM,MPT,ECPT,GPCT,DIT/MGG;/V,Y,WTMASS=1.0/V,N,NØMGG/V,N,NØBGG/
           V,Y,CØUPMASS=-1 $
22 SAVE     NØMGG $
23 CØND     LBL1,GRDPNT $
24 CØND     ERRØR4,NØMGG $
25 GPWG     BGPDT,CSTM,EQEXIN,MGG/ØGPWG/V,Y,GRDPNT=-1/V,Y,WTMASS $
26 ØFP      ØGPWG,,//V,N,CARDNØ $
27 SAVE     CARDNØ $
28 LABEL    LBL1 $
29 EQUIV    KGGX,KGG/NØGENL $
30 CØND     LBL11,NØGENL $
31 SMA3     GEI,KGGX/KGG/V,N,LUSET/V,N,NØGENL/V,N,NØSIMP $
32 LABEL    LBL11 $
33 PARAM    //C,N,MPY/V,N,NSKIP/C,N,O/C,N,0 $
34 GP4      CASECC,GEØM4,EQEXIN,SIL,GPDT/RG,YS,USET/V,N,LUSET/V,N,MPCF1/V,
           N,MPCF2/V,N,SINGLE/V,N,ØMIT/V,N,REACT/V,N,NSKIP/V,N,REPEAT/V,
           N,NØSET/V,N,NØL/V,N,NØA $
35 SAVE     MPCF1,MPCF2,SINGLE,ØMIT,REACT,NSKIP,REPEAT,NØSET,NØL,NØA $
36 CØND     ERRØRS,NØL $
37 PURGE    GM/MPCF1/GØ,KØØB,LØØ,UØØ,PØ,UØØV,RUØV/ØMIT/PS,KFS,KSS,QG/
           SINGLE/UBØØV/ØMIT/YBS,PBS,KBFS,KBSS,KDFS,KDSS/SINGLE $
38 EQUIV    KGG,KNN/MPCF1/MGG,MNN/MPCF1 $
39 CØND     LBL4Ø,REACT $
40 JUMP     ERRØR2 $
41 LABEL    LBL4Ø $
42 CØND     LBL4,GENEL $
43 GPSP     GPL,GPST,USET,SIL/ØGPST $
44 ØFP      ØGPST,,//V,N,CARDNØ $
45 SAVE     CARDNØ $
46 LABEL    LBL4 $
47 CØND     LBL2,MPCF2 $
48 MCE1     USET,RG/GM $
49 MCE2     USET,GM,KGG,MGG,,/KNN,MNN,, $
50 LABEL    LBL2 $
51 EQUIV    KNN,KFF/SINGLE/MNN,MFF/SINGLE $
52 CØND     LBL3,SINGLE $

```

```

53 SCE1      USET,KNN,MNN,,/KFF,KFS,KSS,MFF,, $
54 LABEL    LBL3 $
55 EQUIV    KFF,KAA/ØMIT/MFF,MAA/ØMIT $
56 CØND    LBL5,ØMIT $
57 SMP1     USET,KFF,MFF,,/GØ,KAA,KØØB,LØØ,UØØ,MAA,MØØB,MØAB,, $
58 LABEL    LBL5 $
59 DUMMØD1  GEØM1,MGG,BGPDT,WW;USET,,,/KP,PS,G;AA,T,TI,RPP,NDØF/ $
60 EQUIV    PG,PL/NØSET $
61 RBMG2    KAA/LLL,ULL $
62 CØND    LBL10,NØSET $
63 SSG2     USET,GM,YS,KFS,GØ,;PG;/PØ,PS,PL $
64 LABEL    LBL10 $
65 SSG3     LLL,ULL,KAA,PL,LØØ;UØØ;KØØB,PØ/ULV,UØØV,RULV,RUØV/V,N,ØMIT/
V,Y,IRES=-1 $
66 CØND    LBL9,IRES $
67 MATGPR   GPL;USET,SIL,RULV//C,N;L $
68 MATGPR   GPL,USET,SIL,RUØV//C,N;Ø $
69 LABEL    LBL9 $
70 SDR1     USET,PG,ULV,UØØV,YS,GØ;GM,PS,KFS,KSS,/UGV,PGG,QG/C,N,1/C,N,DSØ $
71 DUMMØD2  UGV,,,;/UGVX,,,;/V,Y;IUGV=0 $
72 SAVE     IUGV $
73 MATPRN   UGVX,,,// $
74 CØND    LBB,IUGV $
75 DSMG1    CASECC,GPTT,SIL,EDT,UGV,CSTM,MPT,ECPT,GPCT,DIT/KP3G/
V,N,DSCØSET $
76 SAVE     DSCØSET $
77 ADD      KP3G,KGGX/KDGG/C,Y;ALPHA=(1.0,0.0)/C,Y,BETA=(1.0,0.0) $
78 EQUIV    KDGG,KDNN/MPCF2 $
79 CØND    LBL2D,MPCF2 $
80 MCE2     USET,GM,KDGG,,,/KDNN,, $
81 LABEL    LBL2D $
82 EQUIV    KDNN,KDFF/SINGLE $
83 CØND    LBL3D,SINGLE $
84 SCE1     USET,KDNN,;/KDFF,KDFS,KDSS,,, $
85 LABEL    LBL3D $
86 EQUIV    KDFF,KDAA/ØMIT $
87 CØND    LBL5D,ØMIT $
88 SMP1     USET,KDFF,;/GØØ,KDAA,KØØB1,LØØ1,UØØ1,,,, $
89 LABEL    LBL5D $
90 LABEL    LBB $
91 EQUIV    KAA;KDAA/IUGV/GØ,GØØ/IUGV $
92 MATPRN   KAA,GØ,,,// $
93 MPYAD    KDAA,TI,/KSUM/C,N,0/C,N,1/C,N,0/C,N,1 $
94 MPYAD    KAA,TI,/KSUM2/C,N,0/C,N,1/C,N,0/C,N,1 $
95 ADD      KSUM,KP/KSUM1/C,Y,ALPHA=(1.0,0.0)/C,Y,BETA=(1.0,0.0) $
96 DPD     DYNAMICS,GPL,SIL,USET/GPLD,SILD,USED,TFPØØL,,,,,EED,EQDYN/
V,N,LUSET/V,N,LUSETD/V,N,NØTFL/V,N,NØDLT/V,N,NØPSDL/
V,N,NØFRL/V,N,NØNFLT/V,N,NØTRL/V,N,NØEED/C,N,123/V,N,NØUE $
97 ØUTPUT2  RPP,NDØF,TI,,,/C,Y;P1=-1/C,Y,P2=-1 $
98 ØUTPUT2  MAA,KSUM2,KSUM;KP,G//C;Y,P1=-1/C,Y,P2=-1 $
99 CEAD     KSUM1,G,MAA,EED,CASECC/PHI;CLAMA,ØCEIGS/V,N,EIGVS $
100 SAVE    EIGVS $
101 ØFP     ØCEIGS;CLAMA,,,//V,N,CARDNØ $
102 SAVE    CARDNØ $
103 CØND    LBL16,EIGVS $
104 MPYAD    TI;PHI;/PHID/C;N,0/C,N,1/C,N,0/C,N,1 $
105 MATPRN   PHID,PHI,,,// $
106 NØDG    AA;PHID//C;N,-1 $
107 VDR     CASECC;EQDYN,USED;PHID;CLAMA,;/ØPHID,/C,N,CEIGN/C,N,DIRECT/
C,N,0/V,N,NØD/V,N,NØP/C,N,0 $
108 SAVE    NØD;NØP $

```

```

109 CØND      LBL15,NØD $
110 ØFP       ØPHID, , , , //V,N,CARDNØ $
111 SAVE      CARDNØ $
112 LABEL     LBL15 $
113 CØND      LBL16,NØP $
114 EQUIV     PHID,CPHIP/NØA $
115 CØND      LBL17,NØA $
116 SDR1      USETD, ,PHID, , ,GØØ,GM, ,KFS, /CPHIP, ,QPC/C,N,1/C,N,DYNAMICS $
117 LABEL     LBL17 $
118 SDR2      CASECC, CSTM, MPT, DIT, EQDYN, SILD, , , , CLAMA, QPC, CPHIP, EST, /, ØQPC1,
ØCPHIP, ØESC1, ØEFC1 /C,N, CEIG $
119 ØFP       ØCPHIP, ØQPC1, ØEFC1, ØESC1, , //V,N,CARDNØ $
120 SAVE      CARDNØ $
121 LABEL     LBL16 $
122 JUMP      FINIS $
123 LABEL     ERRØR1 $
124 PRTPARM   //C,N,-1/C,N,MØDES$
125 LABEL     ERRØR2 $
126 PRTPARM   //C,N,-2/C,N,DIFFSTIF$
127 LABEL     ERRØR4 $
128 PRTPARM   //C,N,-4/C,N,DIFFSTIF$
129 LABEL     ERRØRS $
130 PRTPARM   //C,N,-5/C,N,DIFFSTIF$
131 LABEL     FINIS $
132 END       $

```

## Description of DMAP Operations for Eigenvalue Analysis of Rotating Structures

2. GP1 generates coordinate system transformation matrices, table of grid point locations, and tables for relating internal and external grid point numbers.
4. GP2 generates Element Connection Table with internal indices.
5. PLTSET transforms user input into a form used to drive structure plotter.
7. PRTMSG prints error messages associated with structure plotter.
10. Go to DMAP No. 14 if no undeformed structure plot request.
11. PLOT generates all requested undeformed structure plots.
13. PRTMSG prints plotter data and engineering data for each undeformed plot generated.
15. GP3 generates Grid Point Temperature Table.
16. TA1 generates element tables for use in matrix assembly and stress recovery.
18. Go to DMAP No. 123 and print error message if there are no structural elements.
20. SMA1 generates stiffness matrix  $[ K_{gg}^x ]$  and Grid Point Singularity Table.
21. SMA2 generates mass matrix  $[ M_{gg} ]$ .
23. Go to DMAP No. 28 if no weight and balance request.
24. Go to DMAP No. 127 and print error message if no mass matrix exists.
25. GPWG generates weight and balance information.
26. OFP formats weight and balance information and places it on the system output file for printing.

29. Equivalence  $[ K_{gg}^x ]$  to  $[ K_{gg} ]$  if no general elements.
30. Go to DMAP No. 32 if no general elements.
31. SMA3 adds general elements to  $[ K_{gg}^x ]$  to obtain stiffness matrix  $[ K_{gg} ]$ .
34. GP4 generates flags defining members of various displacement sets (USET), forms multipoint constraint equations  $[ R_g ] \{ u_g \} = 0$  and forms enforced displacement vector  $\{ Y_s \}$ .
36. Go to DMAP No. 129 and print error message if no independent degrees of freedom are defined.
38. Equivalence  $[ K_{gg} ]$  to  $[ K_{nn} ]$  and  $[ M_{gg} ]$  to  $[ M_{nn} ]$  if no multipoint constraints.
39. Go to DMAP No. 41 if no free-body supports supplied.
40. Go to DMAP No. 125 and print error message if free-body supports are present.
42. Go to DMAP No. 46 if general elements present.
43. GPSP determines if possible grid point singularities remain.
44. OFP formats table of possible grid point singularities and places it on the system output file for printing.
47. Go to DMAP No. 50 if MCE1 and MCE2 have already been executed for current set of multipoint constraints.
48. MCE1 partitions multipoint constraint equations  $[ R_g ] = [ R_m | R_n ]$  and solves for multipoint constraint transformation matrix  $[ G_m ] = -[ R_m ]^{-1} [ R_n ]$ .
49. MCE2 partitions stiffness and mass matrices

$$[ K_{gg} ] = \begin{bmatrix} \overline{K}_{nn} & | & \overline{K}_{nm} \\ \hline \overline{K}_{mn} & | & \overline{K}_{mm} \end{bmatrix} \quad \text{and} \quad [ M_{gg} ] = \begin{bmatrix} \overline{M}_{nn} & | & \overline{M}_{nm} \\ \hline \overline{M}_{mn} & | & \overline{M}_{mm} \end{bmatrix}$$

and performs matrix reductions

$$[K_{nn}] = [\bar{K}_{nn}] + [G_m^T] [K_{mn}] + [K_{mn}^T] [G_m] \\ + [G_m^T] [K_{mm}] [G_m] \text{ and}$$

$$[M_{nn}] = [\bar{M}_{nn}] + [G_m^T] [M_{mn}] + [M_{mn}^T] [G_m] \\ + [G_m^T] [M_{mm}] [G_m].$$

51. Equivalence  $[K_{nn}]$  to  $[K_{ff}]$  and  $[M_{nn}]$  to  $[M_{ff}]$  if no single-point constraints.
52. Go to DMAP No. 54 if no single-point constraints.
53. SCE1 partitions out single-point constraints.

$$[K_{nn}] = \left[ \begin{array}{c|c} K_{ff} & K_{fs} \\ \hline K_{sf} & K_{ss} \end{array} \right] \text{ and } [M_{nn}] = \left[ \begin{array}{c|c} M_{ff} & M_{fs} \\ \hline M_{sf} & M_{ss} \end{array} \right].$$

55. Equivalence  $[K_{ff}]$  to  $[K_{aa}]$  and  $[M_{ff}]$  to  $[M_{aa}]$  if no omitted coordinates.
56. Go to DMAP No. 58 if no omitted coordinates.
57. SMP1 partitions constrained stiffness and mass matrices

$$[K_{ff}] = \left[ \begin{array}{c|c} \bar{K}_{aa} & K_{ao} \\ \hline K_{oa} & K_{oo} \end{array} \right] \text{ and } [M_{ff}] = \left[ \begin{array}{c|c} \bar{M}_{aa} & M_{ao} \\ \hline M_{oa} & M_{oo} \end{array} \right]$$

solves for transformation matrix  $[G_o] = -[K_{oo}]^{-1} [K_{oa}]$ ,

and performs matrix reductions  $[K_{aa}] = [\bar{K}_{aa}] + [K_{oa}^T] [G_o]$

$$\text{and } [M_{aa}] = [\bar{M}_{aa}] + [M_{oa}^T] [G_o] + [G_o^T] [M_{oa}] \\ + [G_o^T] [M_{oo}] [G_o].$$

59. Dummy module DUMMOD1 constructs coriolis acceleration matrix  $[G]$ , centripetal acceleration matrix  $[K''']$ , transformation matrix  $[T]$  and its inverse  $[T]^{-1}$ , and centrifugal load vector  $\{P_g\}$ . Rows and columns corresponding to the degrees of freedom constrained to be zero or have no mass have been removed from  $[G]$ ,  $[K''']$ ,  $[T]$ , and  $[T]^{-1}$ . Centrifugal load vector  $\{P_g\}$  is in g-set and is reduced in the following D-MAP statements.

60. Equivalence  $\{P_g\}$  to  $\{P_1\}$  if no constraints applied.

61. RMBG2 decomposes constrained stiffness matrix  $[K_{11}] = [L_{11}][U_{11}]$ .

62. Go to DMAP No. 64 if no constraints applied.

63. SSG2 applies constraints to static load vectors

$$\{P_g\} = \begin{Bmatrix} \bar{P}_n \\ - \\ P_m \end{Bmatrix}, \quad \{P_n\} = \{\bar{P}_n\} + [G_m^T] \{P_m\},$$

$$\{P_n\} = \begin{Bmatrix} \bar{P}_f \\ - \\ P_s \end{Bmatrix}, \quad \{P_f\} = \{\bar{P}_f\} - [K_{fs}] \{Y_s\},$$

$$\{P_f\} = \begin{Bmatrix} P_a \\ - \\ P_o \end{Bmatrix} \quad \text{and} \quad \{P_1\} = \{P_a\} + [G_o^T] \{P_o\}.$$

65. SSG3 solves for displacements of independent coordinates

$$\{u_1\} = [K_{11}]^{-1} \{P_1\},$$

solves for displacements of omitted coordinates

$$\{u_o\} = [K_{oo}]^{-1} \{P_o\},$$

calculates residual vector (RULV) and residual vector error ratio for independent coordinates

$$\{\delta P_1\} = \{P_1\} - [K_{11}] \{u_1\}$$

$$\epsilon_1 = \frac{\begin{Bmatrix} u_1^T \\ \end{Bmatrix} \{\delta P_1\}}{\begin{Bmatrix} P_1^T \\ \end{Bmatrix} \{u_1\}}$$

and calculates residual vector (RUOV) and residual vector error ratio for omitted coordinates

$$\{\delta P_o\} = \{P_o\} - [K_{oo}] \{u_o^o\} ,$$

$$\epsilon_o = \frac{\{u_o^T\} \{\delta P_o\}}{\{P_o^T\} \{u_o^o\}} .$$

66. Go to DMAP No. 69 if residual vector is not to be printed.
67. Print residual vector for independent coordinates (RULV).
68. Print residual vector for omitted coordinates (RUOV).
70. SDR1 recovers dependent displacements

$$\{u_o\} = [G_o] \{u_1\} + \{u_o^o\} ,$$

$$\begin{Bmatrix} u_a \\ \bar{u}_o \end{Bmatrix} = \{u_f\} , \quad \begin{Bmatrix} u_f \\ \bar{Y}_s \end{Bmatrix} = \{u_n\} ,$$

$$\{u_m\} = [G_m] \{u_n\} , \quad \begin{Bmatrix} u_n \\ \bar{u}_m \end{Bmatrix} = \{u_g\} ,$$

and recovers single-point forces of constraint

$$\{q_s\} = - \{P_s\} + [K_{fs}^T] \{u_f\} + [K_{ss}] \{Y_s\} .$$

71. DUMMOD2 checks if vector  $\{u_g\}$  is a null vector. IUGV = -1 if  $\{u_g\}$  is null (geometric stiffness matrix KDGG is also a null matrix) otherwise IUGV = 0.
74. Go to DMAP No. 90 if IUGV = -1.
75. DSMG1 generates differential stiffness matrix  $[K_{gg}^p]$ .
77. ADD elastic and geometric stiffness matrices in g-set

$$[K_{gg}^x] + [K_{gg}^p] = [K_{gg}^d] .$$

78. Equivalence  $[K_{gg}^d]$  to  $[K_{nn}^d]$  if no multipoint constraints.

79. Go to DMAP No. 81 if no multipoint constraints.

80. MCE2 partitions differential stiffness matrix

$$[K_{gg}^d] = \left[ \begin{array}{c|c} \bar{K}_{nn}^d & K_{nm}^d \\ \hline K_{mn}^d & K_{mm}^d \end{array} \right]$$

and performs matrix reduction  $[K_{nn}^d] = [\bar{K}_{nn}^d] + [G_m^T] [K_{mn}^d]$

$$+ [K_{mn}^d] [G_m] + [G_m^T] [K_{mm}^d] [G_m].$$

82. Equivalence  $[K_{nn}^d]$  to  $[K_{ff}^d]$  if no single-point constraints.

83. Go to DMAP No. 85 if no single-point constraints.

84. SCE1 partitions out single-point constraints.

$$[K_{nn}^d] = \left[ \begin{array}{c|c} K_{ff}^d & K_{fs}^d \\ \hline K_{sf}^d & K_{ss}^d \end{array} \right]$$

86. Equivalence  $[K_{ff}^d]$  to  $[K_{aa}^d]$  if no omitted coordinates.

87. Go to DMAP No. 89 if no omitted coordinates.

88. SMP1 partitions constrained stiffness matrix

$$[K_{ff}^d] = \left[ \begin{array}{c|c} \bar{K}_{aa}^d & K_{ao}^d \\ \hline K_{oa}^d & K_{oo}^d \end{array} \right],$$

solves for transformation matrix  $[G_{oo}] = -[K_{oo}^d]^{-1} [K_{oa}^d]$ ,

and performs matrix reductions  $[K_{aa}^d] = [\bar{K}_{aa}^d] + [K_{oa}^{Td}] [G_{oo}]$ .

91. Equivalence  $[K_{aa}^d]$  to  $[K_{aa}]$  and  $[G_o]$  to  $[G_{oo}]$  if geometric stiffness matrix  $[K_{gg}^d]$  is a null matrix.
93. Multiplies the matrices  $[K_{aa}^d] [T]^{-1} = [KSUM]$  .
94. Multiplies the matrices  $[K_{aa}] [T]^{-1} = [KSUM2]$  .
95. Adds matrix KSUM and the centripetal acceleration matrix  $[K''']$  .
96. DPD generates flags defining members of various displacement sets used in dynamic analysis (USETD), tables relating internal and external grid point numbers, including extra points introduced for dynamic analysis, and prepared Transfer Function Pool and Eigenvalue Extraction Data.
97. Matrices  $[R_p^I]$ ,  $[NDOF]$  and  $[T]^{-1}$  are output on magnetic tape.  
 $[R_p^I]$  is  $(n \times 4)$  matrix where  $n =$  no. of grid points. First three columns represent the coordinates of grid points in basic coordinates and fourth column stores the mass data at grid points.  
 $[NDOF]$  is  $(3 \times n)$  matrix. Value of 1.5 is written if the translational D.O.F. at a grid point is not constrained by SPC, MPC, OMIT or permanent SPC on GRID cards. Otherwise it is written 0.0.
98. Matrices  $[M_{aa}]$ ,  $[K_{aa}]$ ,  $[K_{aa}^d]$ ,  $[K''']$ ,  $[G]$  are output on magnetic tape.  
 $[K_{aa}]$  is the reduced elastic stiffness matrix  
 $[K_{aa}^d]$  is the reduced (elastic + geometric) stiffness matrix  
 $[K''']$  is the reduced centripetal acceleration matrix  
 $[G]$  is the reduced coriolis acceleration matrix.
99. CEAD extracts complex eigenvalues from the equation

$$[M_{dd}p^2 + B_{dd}p + K_{dd}] \{u_d\} = 0$$

and normalizes eigenvectors according to one of the following user requests:

- (1) Unit magnitude of selected coordinate
- (2) Unit magnitude of largest component.

101. OFF formats the summary of complex eigenvalues and summary of eigenvalue extraction information and places them on the system output file for printing.

103. Go to DMAP No. 121 if no eigenvalues found.

104.  $\{\phi\}$ , the eigenvector of

$$[Mp^2 + Gp + [K''' + [K_e + K_g] T^{-1}]] \{\phi\} = 0$$

is given by complex eigenvalue analysis step #91.

$\{\phi_d\}$ , the eigenvector of

$$[MTp^2 + GTP + K''' T + K_e + K_g] \{\phi_d\} = 0$$

is obtained in this step  $\{\phi_d\} = [T]^{-1} \{\phi\}$ .

105. Eigenvectors  $\{\phi_d\}$  and  $\{\phi\}$  are printed.

106.  $[\delta^T \delta]$ , a (3 x 3) matrix for each of the eigenvector  $\{\phi_d\}$  is constructed and printed.

107. VDR prepares eigenvectors for output, using only the independent degrees of freedom.

109. Go to DMAP No. 112 if no output request for the independent degrees of freedom.

110. OFF formats the eigenvectors for independent degrees of freedom and places them on the system output file for printing.

113. Go to DMAP No. 121 if no output request involving dependent degrees of freedom or forces and stresses.

114. Equivalence  $\{\phi_d\}$  to  $\{\phi_p\}$  if no constraints applied.

115. Go to DMAP No. 117 if no constraints applied.

116. SDR1 recovers dependent components of eigenvectors

$$\{\phi_o\} = [G_{oo}^d] \{\phi_d\}, \quad \left\{ \begin{array}{c} \phi_d \\ \phi_o \end{array} \right\} = \{\phi_f + \phi_e\},$$

$$\left\{ \begin{array}{c} \phi_f + \phi_e \\ \phi_s \end{array} \right\} = \{\phi_n + \phi_e\}, \quad \{\phi_m\} = [G_m^d] \{\phi_n + \phi_e\},$$

$$\left\{ \begin{array}{c} \phi_n + \phi_e \\ \phi_m \end{array} \right\} = \{\phi_p\}$$

and recovers single-point forces of constraint

$$\{q_s\} = [K_{fs}^T] \{\phi_f\}.$$

118. SDR2 calculates element forces and stresses (OESC1, OEFC1) and prepares eigenvectors and single-point forces of constraint for output (OCPHIP, OQPC1).
119. OFP formats tables prepared by SDR2 and places them on the system output file for printing.
122. Go to DMAP No. 131 and make normal exit.
124. Normal mode analysis error message No. 1 - Mass matrix required for real eigenvalue analysis.
126. Static analysis with differential stiffness error message No. 2 - Free body support not allowed.
128. Static analysis with differential stiffness error message No. 4 - Mass matrix required for weight and balance calculations.
130. Static analysis with differential stiffness error message No. 5 - No independent degrees of freedom have been defined.

```

SUBROUTINE DUMM01
INTEGER TYPIN, TYP0UT, TDGF, SYSBUF, C0RSZ
REAL M, MU(300)
EXTERNAL WRITE
EXTERNAL READ
DIMENSION HEAD(5), HEAD2(5), HEAD3(5), HEAD4(5), IC0NM(2)
D      ,IC0NM(2), A(8), B(13), R(4), RG(4), W(5), M(300)
D      , TDGF(300), NDEGF(6,300), NFRE(300), XKP(1)
D      ,AA(3,300), RP(300,3), MM(7)
D      ,RHEAD(5)
DIMENSION XI11(300)
D      ,XI21(300), XI22(300), XI31(300), XI32(300), XI33(300)
D      ,XMG(300), D0F(6,300)
COMMON /DUM0PN/ XKP
COMMON /PACKX/ TYPIN, TYP0UT, I1, N1, INCR
COMMON /UNPAKX/ ITYPE, JJ, N, JINCR
COMMON /SYSTEM/ SYSBUF, 0UTAPE
COMMON XXX
EQUIVALENCE (A(1), ID)
1      ,(A(7), IA)
2      ,(B(2), IG)
C
C
C      OPEN CORE ARRAY
EQUIVALENCE (XKP(2000), NDEGF)
E      ,(XKP(3800), M )
E      ,(XKP(4100), NFRE )
E      ,(XKP(4400), TDGF )
E      ,(XKP(4700), A )
E      ,(XKP(4708), B )
E      ,(XKP(4721), R )
E      ,(XKP(4725), HEAD )
E      ,(XKP(4730), HEAD1)
E      ,(XKP(4735), HEAD2)
E      ,(XKP(4740), HEAD3)
E      ,(XKP(4745), HEAD4)
E      ,(XKP(4750), AA )
EQUIVALENCE (XKP(5650), RP )
E      ,(XKP(6550), MU )
E      ,(XKP(6850), XI11 )
E      ,(XKP(7150), XI21 )
E      ,(XKP(7450), XI22 )
E      ,(XKP(7750), XI31 )
E      ,(XKP(8050), XI32 )
E      ,(XKP(8350), XI33 )
E      ,(NDEGF, D0F)
DATA NAM1, NAM2, NAM3, NAM4 / 201, 202, 203, 204 /
C*****
C
C      IFL(101) REFERS TO GE0M1-THE FIRST INPUT DATA BLOCK OF DMAP
C      STATEMENT DUMM01.
C      IC0NM REFERS TO MGG-THE SECOND INPUT DATA BLOCK OF DUMM01.
C      IBG REFERS TO BGPOT-THE THIRD INPUT DATA BLOCK OF DUMM01.
C      IWW(104) REFERS TO WW-THE BLOCK CONTAINING W-S AND R-T FLAGS.
C      NAM5 REFERS TO USET-THE FIFTH INPUT DATA BLOCK OF DUMM01.
C
C      THE GENERAL PROCEDURE FOR READING A DATA BLOCK IS-FIRST,
C      OPEN THE FILE CONTAINING THE BLOCK SUCH AS IC0NM,IBG ETC.
C      THEN SKIP THE HEADER RECORD BY CALLING FWDREC. THE NEXT STEP
C      IS TO DETERMINE IF THE DATA IS A MATRIX EG. MGG. FOR MATRICES,

```

```

DM100100
DM100200
DM100300
DM100400
DM100500
DM100600
DM100700
DM100800
DM100900
DM101000
DM101100
DM101200
DM101300
DM101400
DM101500
DM101600
DM101700
DM101800
DM101900
DM102000
DM102100
DM102200
DM102300
DM102400
DM102500
DM102600
DM102700
DM102800
DM102900
DM103000
DM103100
DM103200
DM103300
DM103400
DM103500
DM103600
DM103700
DM103800
DM103900
DM104000
DM104100
DM104200
DM104300
DM104400
DM104500
DM104600
DM104700
DM104800
DM104900
DM105000
DM105100
DM105200
DM105300
DM105400
DM105500
DM105600
DM105700
DM105800
DM105900
DM106000

```

```

C THE NEXT STEP IS TO CALL UNPACK. EACH CALL TO UNPACK BRINGS INTO MEMORY ONE COLUMN OF THE MATRIX. FOR NON-MATRIX INPUT, THE RECORD STRUCTURE MUST BE LOOKED UP IN THE NASTRAN PROGRAMMER-S MANUAL. EACH RECORD CAN THEN BE BROUGHT INTO MEMORY BY CALLING READ. ONE CALL TO READ BRINGS IN ONE RECORD.
C THE EXCEPTION IN THIS CASE IS DATA READ EXACTLY AS IT APPEARS ON BULK DATA CARDS. FOR THIS, THE PROCEDURE IS CALL PRELOC, THEN LOCATE, THEN READ FOR EACH BULK DATA CARD. THIS IS USED FOR IFL.
C*****
DATA NAM5, NAM6 /205, 206/
DATA NAM7, NAM8 /207, 208/
DATA IGRID /4501, 45/ IFL /101/
DATA TW0, E0R /2, 1/
DATA IC0N /102/ IC0NM /1501, 15/ IBG /103/
C THIS IS THE MAIN ROUTINE FOR COMPUTING THE K-PRIME, P-PRIME, G AND MASS MATRICES USED IN SOLVING THE ROTATING FLEXIBLE STRUCTURE PROBLEM
C READ IN OMEGA VALUES AND RG + T-INVERSE FLAGS
C
IWW = 104
ITYPE = 1
JJ = 1
N = 5
JINCR = 1
CALL OPEN($1000, IWW, XKP(LC0L+1), 0)
CALL FWDREC($1000, IWW)
CALL FNAME(IWW, RHEAD(1))
CALL UNPACK($1000, IWW, W, READ)
CALL CLOSE(IWW, 1)
C WRITE COMMENTS ON OUTPUT LISTING
C
WRITE(6, 601)
601 FORMAT(1H, - RESTRICTIONS ***-//
F- 1. ID NO. 1 ON GRID CARDS SHOULD BE USED FOR THE CENTRAL RIGID-BODY OTHERWISE THE TRANSFORMATION MATRICES T AND T-INVERSE WILL BE INCORRECT-//
F- 2. THE USE OF THE T AND T-INVERSE PERMIT THE BASE MOTION WITH THE TRANSLATIONAL RIGID BODY MOTION SWEPT OUT FROM THE EQS.-//
F- OF MOTION -)
WRITE(6, 604)
604 FORMAT(1H,
F- 3. IT IS ASSUMED THAT THE AXIS OF ROTATION PASSES THROUGH THE CENTER OF MASS OF THE ENTIRE VEHICLE. IF THE AXIS OF ROTATION IS TO PASS THROUGH A POINT OTHER THAN THE MASS CENTER, THE CORRESPONDING GRID POINT SHOULD BE DEFINED AS GRID NO. 1-)
WRITE(6, 605)
605 FORMAT(
F- 4. LOCATION OF THE CENTER OF ROTATION (C.R.) GOVERNS THE CALCULATIONS OF DELTA TRANSPOSE DELTA MATRICES AND THE CENTRIFUGAL FORCES WHICH IN TURN AFFECTS THE GEOMETRIC STIFFNESS MATRIX. THE OPTION TO SELECT THE C.R. IS AVAILABLE THRU DMI CARDS. W(4)=0.0-CG IS NOT CALCULATED AND C.R. IS ASSUMED TO BE GRID NO. 1. W(4)=1.0-CG IS CALCULATED AND C.R.

```

```

F / DM112200
F- IS C.G.- DM112300
F- W(5)=1.0 PERMITS THE CALCULATIONS OF T AND T-INVERSE.-/ DM112400
F- W(5)=0.0 MAKES T AND T-INVERSE IDENTITY MATRICES.-/ DM112500
F- IN GENERAL THE FOLLOWING COMBINATIONS SHOULD BE USED.-/ DM112600
F- W(4)=W(5)=0.0 OR W(4)=W(5)=1.0. W(4)=W(5)=0.0 ASSUMES THE- DM112700
WRITE(6,899) DM112800
899 F0RMAT( DM112900
F- STRUCTURE ROTATES ABOUT GRID NO. 1 AND ONLY THE CANTILEVER-/ DM113000
F- MODES ARE AVAILABLE. W(4)=W(5)=1.0 ASSUMES THE STRUCTURE-/ DM113100
F- ROTATES ABOUT THE C.G. WITH TRANSLATIONAL RIGID BODY D0F-/ DM113200
F- SWEEPED OUT-/ DM113300
F- 5. IN THE CALCULATION OF THE CENTER OF MASS OF THE VEHICLE ALL-/ DM113400
F- THE GRID POINTS WITH MASSES ARE USED. IF THERE IS A DUMMY- / DM113500
F- GRID POINT FOR THE DEFINITION OF THE PLANE FOR CBAR CARDS,-/ DM113600
F- DO NOT PUT ANY MASS AT THAT DUMMY GRID POINT OTHERWISE WRONG- DM113700
F/ DM113800
F- C. M. WILL BE COMPUTED-) DM113900
WRITE(6,606) DM114000
606 F0RMAT( DM114100
F- 6. THE NUMBER OF GRID POINTS IN THE PROBLEM SHOULD BE LESS-/ DM114200
F- THAN 300; THIS ALLOWS UP TO 1800 D0F.-) DM114300
WRITE(6,602) DM114400
602 F0RMAT(1H0,- THE FOLLOWING DATA WAS TAKEN FROM GRID CARDS BY THE DDM114500
FUMMY MODULE***/) DM114600
WRITE(6,612) W(1),W(2),W(3) DM114700
612 F0RMAT(/ 1H / -SPIN RATE VECTOR*** OMEGA1 = -F10.4, 5X, DM114800
F -OMEGA2 = -F10.4, 5X, -OMEGA3 = -F10.4) DM114900
IF(W(4) .LT. 0.01) WRITE(6,695) DM115000
695 F0RMAT(1H , -THE FOLLOWING ANALYSIS ASSUMES ROTATION ABOUT GRID NO. DM115100
1 1.-) DM115200
IF(W(4) .GT. 0.0) WRITE(6,696) DM115300
696 F0RMAT(1H , -IN THIS ANALYSIS THE STRUCTURE SPINS ABOUT THE C.G. OF DM115400
1 THE SYSTEM DESCRIBED IN THE BULK DATA-) DM115500
IF(W(5) .LT. 0.01) WRITE(6,697) DM115600
697 F0RMAT(1H , -THE FOLLOWING ANALYSIS GIVES CANTILEVER MODES OF A SPIDM115700
FNNING STRUCTURE BY MAKING T AND-/1H , -T-INVERSE IDENTITY MATRICES- DM115800
F) DM115900
IF(W(5) .GT. 0.0) WRITE(6,698) DM116000
698 F0RMAT(1H , -THE FOLLOWING ANALYSIS CALCULATES THE MATRICES T AND T DM116100
F-INVERSE THUS SWEEPING OUT THE-/1H , -TRANSLATIONAL RIGID BODY D0F- DM116200
F) DM116300
WRITE(6,611) DM116400
C DM116500
C SET UP PACK COMMON AND LOCATE END OF CORE DM116600
C DM116700
611 F0RMAT(1H0,- N0DE D0F MASS I11 I21 I22 DM116800
F I31 I32 I33 R1 R2 R3-/) DM116900
TYPIN = 1 DM117000
TYP0UT = 1 DM117100
II = 1 DM117200
INCR = 1 DM117300
LZ = C0RSZ(XXX, XKP) DM117400
LC0L = LZ - SYSBUF DM117500
IL = LC0L DM117600
IXX = LZ - 2*SYSBUF -2 DM117700
IBGR = IXX - SYSBUF - 1 DM117800
D0 750 II=1,3 DM117900
750 RB(II) = 0.0 DM118000
XM = 0.0 DM118100

```

C		DM118200
C	LØCATE FILE THAT GRID PØINTS ARE STØRED ØN	DM118300
C		DM118400
	CALL PRELØC(\$1000, XKP(IL), IFL)	DM118500
	CALL LØCATE(\$1000, XKP(ILL), IGRID, IFLG)	DM118600
C		DM118700
C	LØCATE FILE THAT BASIC GRID PØINT CØ-ØRDINATES ARE STØRED ØN	DM118800
C		DM118900
	CALL ØPEN(\$1000, IBG, XKP(IGR), 0)	DM119000
	CALL FWDREC(\$700, IBG)	DM119100
	NØDE = 0	DM119200
C	BUILD MASS AND INERTIA TABLE	DM119300
C		DM119400
C	UNPACK MGG MATRIX TØ GET MASS AND INERTIAS	DM119500
C		DM119600
	N = 300	DM119700
	CALL ØPEN(\$1000, ICØN, XKP(IXX), 0)	DM119800
	CALL FWDREC(\$1000, ICØN)	DM119900
	CALL FNAME(ICØN, RHEAD(1))	DM120000
C		DM120100
C	WHEN AN END ØF FILE IS ENCØUNTERED BY FWDREC, READING ØF MGG STØPSØ	DM120200
C		DM120300
	950 CALL FWDREC(\$699, ICØN)	DM120400
	CALL FWDREC(\$699, ICØN)	DM120500
	NØDE = NØDE + 1	DM120600
	ND1 = (NØDE-1)*6	DM120700
	CALL UNPACK(\$951, ICØN, XMGG, READ)	DM120800
	M(NØDE) = XMGG(ND1+3)	DM120900
	XM = XM + M(NØDE)	DM121000
	951 CALL UNPACK(\$952, ICØN, XMGG, READ)	DM121100
	XI11(NØDE) = XMGG(ND1+4)	DM121200
	952 CALL UNPACK(\$953, ICØN, XMGG, READ)	DM121300
	XI21(NØDE) = XMGG(ND1+4)	DM121400
	XI22(NØDE) = XMGG(ND1+5)	DM121500
	953 CALL UNPACK(\$950, ICØN, XMGG, READ)	DM121600
	XI31(NØDE) = XMGG(ND1+4)	DM121700
	XI32(NØDE) = XMGG(ND1+5)	DM121800
	XI33(NØDE) = XMGG(ND1+6)	DM121900
	GØ TØ 950	DM122000
	699 NØDE = 0	DM122100
	700 CØNTINUE	DM122200
	CALL READ(\$710, \$710, IFL, A, 8, 0, IFLG)	DM122300
	NØDE = NØDE + 1	DM122400
C		DM122500
C	BASIC GRID PØINT INFØ.	DM122600
	CALL READ(\$710, \$710, IBG, R, 4, 0, IFLG)	DM122700
C	IF MØTION AT A GRID PØIT IS RESTRAINED IN ALL DIRECTIØNS THE LØGIC	DM122800
C	IN THE CØDE CAUSES THE GRID PØINT TØ BE DISREGARDED	DM122900
C		DM123000
	WRITE(6,610) ID, IA, M(NØDE), XI11(NØDE), XI21(NØDE), XI22(NØDE)	DM123100
	W, XI31(NØDE), XI32(NØDE), XI33(NØDE), R(2), R(3),	DM123200
	W, R(4)	DM123300
	610 FØRMAT(1I5,1I8,10F10,4)	DM123400
	IF(W(4) .GT. 0.0) GØ TØ 720	DM123500
	IF(ID .GT. 1) GØ TØ 725	DM123600
	DØ 733 II=1,3	DM123700
	733 RG(II) = R(II+1)	DM123800
	GØ TØ 725	DM123900
	720 CØNTINUE	DM124000
	DØ 701 II=1,3	DM124100
	701 RG(II) = RG(II) + M(NØDE)*R(II+1)	DM124200

```

725 CONTINUE DM124300
    GO TO 700 DM124400
710 CONTINUE DM124500
1000 CONTINUE DM124600
    IFW(4) .EQ. 0.0) GO TO 719 DM124700
    DO 734 II=1,3 DM124800
734 RG(II) = RG(II)/XM DM124900
719 CONTINUE DM125000
    WRITE(6,607) DM125100
607 FORMAT(1H , -RG GIVES THE COORDINATES OF THE CENTER OF ROTATION-) DM125200
    WRITE(6,615) XM, RG(1), RG(2), RG(3) DM125300
615 FORMAT(1H0 , - TOTAL MASS = -,1E15.8, - RG(1) = -,1E15.8, - RG(2) = DM125400
    F-, 1E15.8, - RG(3) = -, 1E15.8) DM125500
    WRITE(6,620) DM125600
620 FORMAT(1H0 , - MOTION CONSTRAINTS IN 1 THRU 6 DIRECTION AND TOTAL DM125700
    FOF AT EACH NODE-//= NODE CONSTRAINTS TOTAL DOF -) DM125800
    CALL CLOSE(IFL, 1) DM125900
    CALL CLOSE(ICON, 1) DM126000
C***** DM126100
C NAMI(201) REFERS TO PG-THE FIRST OUTPUT DATA BLOCK OF DUMM0D1. DM126200
C . . . DM126300
C NAM8(208) REFERS TO D0F-THE EIGHTH OUTPUT DATA BLOCK OF DUMM0D1. DM126400
C DM126500
C THE PROCEDURE FOR PACKING A MATRIX IS-OPEN THE FILE(EG. 201), DM126600
C CALL FNAME, CALL WRITE TO WRITE THE HEADER RECORD, THEN PACK. DM126700
C ALSO BUILD THE TRAILER ARRAY, THEN CALL WRITRL. SEE 2.2-1 OF THE DM126800
C NASTRAN PROGRAMMER-S MANUAL FOR TRAILER INFORMATION. DM126900
C DM127000
C ALWAYS CLOSE THE FILES OUT AS SOON AS POSSIBLE DM127100
C DM127200
C CALL CLOSE(IBG, 1) DM127300
C CALL DFRE(LC0L, N0DE) DM127400
C DO 672 II=1,N0DE DM127500
    NFRE(II) = NDEGF(1,II) + NDEGF(2,II) + NDEGF(3,II) DM127600
    NFREE = NDEGF(4,II) + NDEGF(5,II) + NDEGF(6,II) DM127700
672 TDGF(II) = NFRE(II) + NFREE DM127800
    WRITE(6,625) (II, (NDEGF(JJ,II),JJ=1,6), TDGF(II), II=1,N0DE) DM127900
625 FORMAT(1I5, 9X, 6I1, 1I11) DM128000
    CALL OPEN($300, NAMI, XKP(LC0L+1), 1) DM128100
    CALL FNAME(NAMI, HEAD(1) ) DM128200
    CALL WRITE(NAMI, HEAD(1), TW0, E0R) DM128300
C DM128400
C ZERO OUT ROWS AND COLS. OF EACH 6X6 SUBMATRIX WHERE THE DEGREE OF DM128500
C FREEDOM IS NOT USED ; EG FOR NDEGF(3) = 0 , THIRD ROW AND COL ARE ZERO DM128600
C THE NON-ZERO ELEMENTS ARE THEN MOVED TO THE TOP LEFT CORNER OF SUBMAT DM128700
C DM128800
C ZERO OPEN CORE DM128900
C DM129000
C NC0R = 6*N0DE DM129100
C DO 817 II=1,NC0R DM129200
    XKP(II) = 0.0 DM129300
817 CONTINUE DM129400
    DO 818 II=1,N0DE DM129500
        DO 818 JJ=1,6 DM129600
818 ITT = NDEGF(JJ,II) + ITT DM129700
    CALL KPRIM(N0DE, W) DM129800
300 CONTINUE DM129900
    CALL CLOSE(NAMI, 1) DM130000
    CALL OPEN($501, NAM2, XKP(LC0L+1), 1) DM130100
    CALL FNAME(NAM2, HEAD2(1) ) DM130200

```

CALL WRITE(NAM2, HEAD2(1); TWØ, EØR)	DM130300
CALL ØPEN(\$501, IBG, XKP(IBGR), 0)	DM130400
CALL FWDREC(\$501, IBG)	DM130500
CALL PPRIM(RG, NØDE, W)	DM130600
501 CØNTINUE	DM130700
CALL CLØSE(NAM2, 1)	DM130800
CALL CLØSE(ØBG, 1)	DM130900
C	DM131000
C ZERØ ØUT ØPEN CØRE	DM131100
C	DM131200
DØ 2001 II=1,NI	DM131300
2001 XKP(II) = 0.0	DM131400
CALL ØPEN(\$3000, NAM3, XKP(LCØL+1), 1)	DM131500
CALL FNAME(NAM3, HEAD3(1) )	DM131600
CALL WRITE(NAM3, HEAD3(1); TWØ, EØR)	DM131700
CALL GMAT(XM, NØDE, W)	DM131800
3000 CØNTINUE	DM131900
CALL CLØSE(NAM3, 1)	DM132000
C	DM132100
C ZERØ ØUT ØPEN CØRE	DM132200
C	DM132300
DØ 3001 II=1,NI	DM132400
XKP(II) = 0.0	DM132500
3001 CØNTINUE	DM132600
CALL ØPEN(\$4000, NAM4, XKP(LCØL+1), 1)	DM132700
CALL FNAME(NAM4, HEAD4(1) )	DM132800
CALL WRITE(NAM4, HEAD4(1); TWØ, EØR)	DM132900
C	DM133000
CALL AMAT(NØDE)	DM133100
CALL CLØSE(NAM4, 1)	DM133200
C	DM133300
CALL ØPEN(\$4000, NAM5, XKP(LCØL+1), 1)	DM133400
CALL FNAME(NAM5, HEAD4(1))	DM133500
CALL WRITE(NAM5, HEAD4(1); TWØ, EØR)	DM133600
CALL TMAT(XM, NØDE, W, ITT)	DM133700
CALL CLØSE(NAM5, 1)	DM133800
C	DM133900
CALL ØPEN(\$4000, NAM6, XKP(LCØL+1), 1)	DM134000
CALL FNAME(NAM6, HEAD4(1))	DM134100
CALL WRITE(NAM6, HEAD4(1); TWØ, EØR)	DM134200
CALL TIMAT(NØDE, W, ITT, XM)	DM134300
CALL CLØSE(NAM6, 1)	DM134400
C	DM134500
C	DM134600
C	DM134700
CALL ØPEN(\$4000, NAM7, XKP(LCØL+1), 1)	DM134800
CALL FNAME(NAM7, HEAD4(1))	DM134900
CALL WRITE(NAM7, HEAD4(1); TWØ, EØR)	DM135000
NI = NØDE	DM135100
MM(1) = 207	DM135200
MM(2) = 0	DM135300
MM(3) = NØDE	DM135400
MM(4) = 2	DM135500
MM(5) = 1	DM135600
MM(6) = NØDE	DM135700
DØ 3500 II=1,3	DM135800
CALL PACK(RP(1,II), NAM7, WRITE, MM)	DM135900
3500 CØNTINUE	DM136000
C	DM136100
C	DM136200
C	DM136300
C	DM136300

	CALL PACK(M, NAM7, WRITE, MM)	DM136400
	CALL WRTTRL(MM(1))	DM136500
	CALL CLØSE(NAM7, 1)	DM136600
C		DM136700
C	PACK DØF	DM136800
C		DM136900
	CALL ØPEN(\$4000, NAM8, XKP(LCØL+1), 1)	DM137000
	CALL FNAME(NAM8, HEAD4(1))	DM137100
	CALL WRITE(NAM8, HEAD4(1), TWØ, EØR)	DM137200
	DØ 3550 II=1,6	DM137300
	DØ 3550 JI=1,NØDE	DM137400
3550	IF(NDEGF(II,JI) .GT. 0) DØF(II,JI) = 1.5	DM137500
	NI = 3	DM137600
	MM(1) = 208	DM137700
	MM(2) = 0	DM137800
	MM(3) = 6	DM137900
	MM(4) = 2	DM138000
	MM(5) = 1	DM138100
	MM(6) = 6	DM138200
	DØ 3600 II=1,NØDE	DM138300
	CALL PACK( DØF(1;II),NAM8,WRITE, MM)	DM138400
3600	CØNTINUE	DM138500
	CALL WRTTRL(MM(1))	DM138600
	CALL CLØSE(NAM8,1)	DM138700
4000	CØNTINUE	DM138800
	RETURN	DM138900
	END	DM139000

For complete listing of this program on Univac 1108 Computer,  
write to Reference 3.

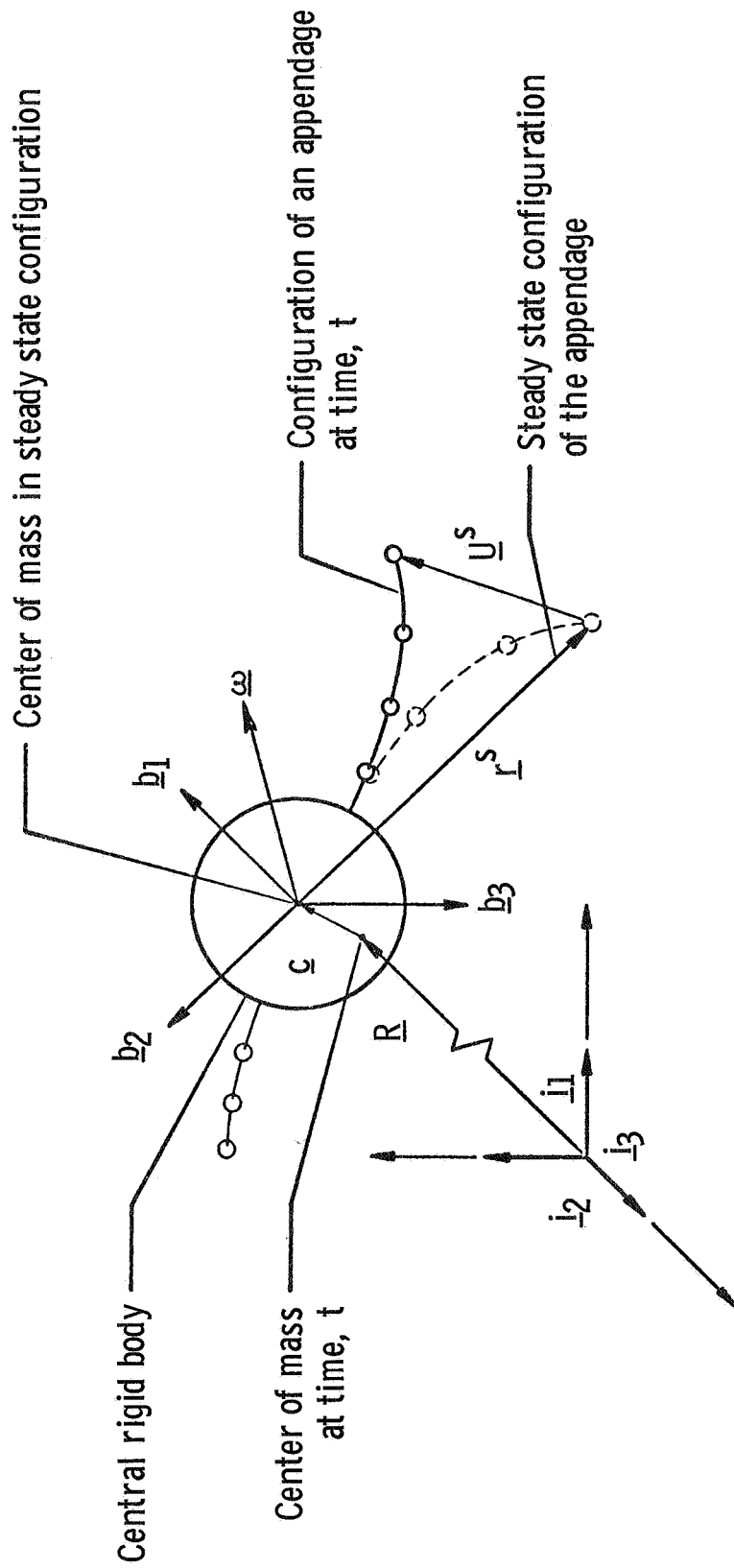


FIGURE 1. GEOMETRY OF SPINNING FLEXIBLE APPENDAGE AND CENTRAL BODY

## LEVEL 12 NASTRAN EXPERIENCES

AT GENERAL DYNAMICS,  
CONVAIR AEROSPACE DIVISION,  
FORT WORTH OPERATION

Merle Allen  
Project Structures Engineer

### SUMMARY

The level 12 NASTRAN has been used to support the NASA/LaRC Advanced Transport Technology study, a predesign, short-response-time effort. Aeroelastic analyses were performed. NASTRAN calculated the vibration modes for the supported airfoil components and the entire unsupported vehicle. Other procedures were then used for the aeroelastic analysis, with procedure interfacing accomplished through use of the NASTRAN produced restart tape. Stiffness matrices were used in static aeroelastic analyses; natural vibration modes were used for flutter and flight control system definition. Various level 12 NASTRAN characteristics were discovered and are discussed; e.g., the ability to solve singular matrices in rigid format 1, run times using multipoint constraints, restart tape problems, and the inaccurate stresses from the quad membrane when used with anisotropic materials.

15

### INTRODUCTION

Two versions of NASTRAN have been acquired at the Convair Aerospace Division, Fort Worth operation, from COSMIC at the University of Georgia. Level 8.1.0 was implemented 5 May 1970 and was used until 12 March 1971, at which time the implementation of level 12.0.0 was finalized. Implementation was initially on an IBM 360/65/65/50 computing system. Current utilization is on an IBM 370-155 computing system.

To date, the most significant application of level 12 has been to perform an analysis for the natural modes of vibration of the baseline configuration of an Advanced Transport Technology (ATT) airplane. This was a predesign, short-response-time effort. The vibration modes were necessary for use in flutter analysis and as an aid in defining the flight control system. The stiffness matrices used in calculating the modes were also used for a static aeroelastic analysis.

The flutter and static aeroelastic analyses were performed in procedures foreign to NASTRAN. The interfacing between these procedures and NASTRAN was accomplished via the use of the NASTRAN-produced restart tape.

The following discussion centers around the NASTRAN ATT analysis. It is presented as Part I. However, validation of level 12 NASTRAN was being performed prior to, during, and following the ATT analysis. This revealed several NASTRAN characteristics, which are presented and discussed in Part II.

## PART I

### ATT SYMMETRIC VEHICLE NORMAL MODES

Prior to calculation of the normal modes for the symmetric vehicle, the stiffness matrices for the supported wing and tail components were calculated in NASTRAN and then used in a different procedure to perform static aeroelastic analyses. Vibration modes for the wing, tail and fin components were then calculated after the weights were defined. The idealization used for the wing is illustrated in Figure 1. Four frames have been used for the wing plots in order to better illustrate the details of the idealization and the grid sequencing.

The idealization for the horizontal tail is shown in Figure 2. The tail component stiffness matrix was calculated in a separate problem, but the grid-point numbers start at 301. This numbering sequence was used so that the same input data cards could be re-used in calculating modes for the unsupported vehicle.

The vehicle representation used to calculate symmetric vibration modes is illustrated in Figure 3. Advantage has been taken of the symmetry, and only one half the vehicle is represented. The wing and tail representations are the same as previously shown in Figures 1 and 2, respectively. As expected, the lines for these components are so numerous as to produce a smeared appearance. The fuselage, engine pylon, and nacelle were represented with a simple bar arrangement.

Multipoint constraints were used to tie the tail, wing, and fuselage together. Single-point constraints were applied along the vehicle plane of symmetry to suppress the antisymmetric modes. The SUPORT card was used to enhance the extraction of the zero frequency roots, and the Inverse Power Method was used to calculate the first seven flexible modes. The flexible modes are illustrated in Figure 4. The plot element (PLOTTEL) was used to reduce the density of lines.

The problem used 331 grids, 956 degrees of freedom after fixing, 1193 elements (which include 89 lumped masses read in from CMASS 2 cards), 11 sets of multipoint constraints and 350 omitted coordinates. The CPU time was 41.3 minutes (69.9 minutes wall clock). Execution was on the IBM 360/65/65/50 computing system.

Four factors in the run time deserve mention. Modules MCE1 and MCE2, which perform the multipoint constraints required 3.3 minutes CPU time. This is considered excessive, and their use in the future will be avoided wherever possible. Module SMP1, which omits the coordinates, required 14.3 minutes CPU time. Module READ, which calculates the frequencies and modes, used 10.9 minutes. Module SDR1, which backfigures for the deflections omitted, used 2.1 minutes. The time required for calculation of the stiffness matrix was insignificant.

Because the omitted coordinates decrease the dynamic matrix size, the execution time could probably have been reduced by omitting more coordinates. This would extend the execution times for SMP1 and SDR1 but should be more than offset by the decreased time in READ. In fact, had the dynamic matrix been reduced to the same size as the number of lumped masses (i.e., 89), then the transformation method would probably have calculated all the frequencies in less time than that required for the Inverse Power Method to calculate seven.

## PART II

### SOME LEVEL 12 CHARACTERISTICS

The decision to use NASTRAN for the ATT analysis was made primarily on the basis of the experiences with level 8 (see Reference 1). Since level 12 had been implemented for use at this time, it was quickly explored with some small inexpensive sample problems to validate that it could satisfactorily handle the task. The results were positive, but some characteristics of interest were discovered. These characteristics, together with those which became apparent during and following the ATT analysis, are presented.

#### Checkout Preliminary to the ATT Analysis

##### Use of the Inverse Power Method

The first check problem run was a simple unsupported-beam vibration problem. The beam frequencies were known in advance, the first being 3.5 Hz. Because the Inverse Power Method would be used for the ATT, it was stipulated for use in the check problem, and a tight frequency band (3.4 to 3.7 Hz) was defined on the EIGR card. To economize on computing time, two modes were requested (to insure that multiple roots could be extracted). However, only one mode was calculated because the procedure shifted four times (maximum number allowed in the algorithm) while tracking the root that was correctly calculated. Two items contributed to the large number of shifts: (1) The decomposition time estimate used in NASTRAN is less than the actual time used. (2) The user-stipulated frequency band was too small. This caused the starting point to be positioned close to the root and the shifted eigenvalues, calculated during iteration, to be small. The small numerical values obtained for the shifted eigenvalues made it difficult for the algorithm to sense convergence. Also, the tight frequency band restricted the amount of shift.

The stipulated frequency band was then changed to 3.4 to 6.0 Hz and a restart made. One root was estimated to lie within the band; two roots were requested. This time three roots were obtained, two of which were rigid-body or zero-frequency roots. The correct flexible root was first obtained, and the two rigid-body roots were next obtained by iteration. According to the documentation (Reference 2), the procedure should have moved outside the stipulated band during the search procedure, but should have searched down to approximately 3.2 and up to approximately 6.1 Hz. Hence, moving all the way down to the zero-frequency level was a surprise and is undesirable because not only is it too far outside the stipulated band, but to extract repeated roots by a root-tracking method is computationally expensive.

#### Use of the SUPORT Card

Because of these results, it was determined that the SUPORT card should always be used when calculating modes for unsupported structures, even though the frequency band stipulated on the EIGR card may be well removed from the zero-frequency position. Use of this card allows the extraction of zero-frequency roots by a direct method (i.e., without iteration), which saves on computer time, and then reverts to iteration for extraction of the flexible modes. The disadvantage is that a price (however small) is paid for the roots even though they may not be desired for use.

A subsequent restart, using this type card, validated that it yielded satisfactory results and does prohibit the iteration for the repeated (zero-frequency) roots.

#### Backfiguring for Deflections

In performing the modal analysis on the simple beam, the OMIT card was used to eliminate several coordinates that did not have lumped masses attached. The deflections for these eliminated coordinates form a subset of the deflections in the eigenvector and were not needed for subsequent analysis. In NASTRAN, the eigenvectors for those remaining coordinates (the active set) are first calculated and then a backfiguring operation is used to calculate the deflections for those eliminated. Since the user

has the option of requesting deflections for either the "deflection" set or the "solution" set, it was reasoned that requesting the "solution" set would save the computer time used in backfiguring. (The "solution" set means those coordinates used in the solution, e.g., modal coordinates, grid points and extra points, etc.) This was done with the result that no eigenvectors were printed. Hence, it is necessary to pay the price for the backfiguring computations, even though the deflections for the eliminated coordinates may not be desired.

It was later determined that the module which performs the backfiguring operation, i.e., SDR1, used only 129 seconds of CPU time during the ATT modal analysis. This is relatively inexpensive.

#### Failure to Punch Modes

Initially, it was desired to cause NASTRAN to punch the calculated modes of vibration in card deck form. It was planned that these would be used as input data to other digital procedures that use the NASTRAN results in calculating static and dynamic aeroelastic response. However, a check problem revealed that NASTRAN will not currently punch modes. Because of this, and because the format of the punchout was unknown, it was decided to code a small procedure that would read the NASTRAN-produced magnetic tape, normally used for restarts, and extract the desired information.

The small coding task was accomplished by a programmer in 4 hours. The result was a procedure that acted as a front step to the aeroelastic and flutter procedures and successfully used the NASTRAN restart tape to bridge the interface between them and NASTRAN.

#### Calculation of Masses External to NASTRAN

When using NASTRAN to calculate natural vibration modes, dynamic response, or "pseudo" static inertia relief, the easiest and most convenient approach is to allow NASTRAN to calculate its own mass matrix. Even though this approach had been operationally validated, the calculation of the mass matrix outside of the finite-element procedure in which it is to be used is sometimes desirable. It becomes desirable when (1) the design

process makes the flight vehicle weight data available in a form more suited to manual lumping of masses, and/or (2) it is necessary to match the static unbalance and pitch inertia of an airfoil structure while simulating only the "box" part or, at least, excluding the most forward part of the leading edge and the most aft portion of the trailing edge. Such was the case with the ATT study.

The most convenient means of supplying mass information to NASTRAN for the ATT was through the use of the CMASS type card; specifically CMASS2 was used. This type card was selected because the mass definition and grid connection were defined on a single card. Hence, this type approach was validated with a sample problem.

The sample problem indicated that modes are satisfactorily calculated when manually lumped masses are used. Unfortunately, it also revealed that the vehicle weight and balance information (normally available under option) is not printed upon request when the masses are calculated externally to NASTRAN.

## Evaluation During the ATT Analysis

### Solution of Singular Matrices

NASTRAN was used to generate the stiffness matrix for each of the three ATT supported airfoil structure components (i.e., wing, tail, and fin) prior to a static aeroelastic analysis. The matrices were generated by Rigid Format 1, and a single mechanical load was applied (for checking) to the structure for which deflections and reactions were calculated. The deflections and reactions obtained served to increase the level of confidence in the validity of the stiffness matrices.

In checking one component, supports were not applied in one direction (inadvertently), which allowed a rigid-body degree of freedom to exist within the horizontal plane of motion. The mechanical load condition used for validation was a force-applied normal to this horizontal plane. The inclusion of this rigid-body degree of freedom means that the stiffness matrix is singular (i.e., its determinant is zero). Algorithms designed for static analysis conventionally will not successfully solve

this type of matrix. However, NASTRAN used the singular matrix and obtained correct answers. This was a pleasant surprise.

According to Reference 3, Section 3.2, a singularity check is performed on the stiffness matrix. This check is performed by module GPSP (DMAP statement 61, Rigid Format 1). However, the check simply determines if any coordinates which do not have a finite value of stiffness assigned remain in the matrix after application of single and multipoint constraints. When all coordinates possess finite-stiffness values, module GPSP assumes the matrix to be nonsingular. Hence, a matrix which is singular because at least two rows are linearly dependent (i.e., a rigid-body mode is contained) is successfully passed through GPSP.

Module RBMG2 is then used to decompose the symmetric real matrix into upper and lower triangular form. As a result of this decomposition, the upper triangular matrix will have a zero term in the last diagonal position when the original matrix is singular. (When the original matrix is 2 times singular, the last 2 diagonals will be zero, etc.)

Deflections under load are then calculated in module SSG3 through use of the decomposed matrix and the user-supplied loads. The deflections are calculated by performing forward-backward substitution. In performing the backward pass, the calculation for the nth deflection becomes  $U_n = 0/0$ , which is indeterminate. The numerator is zero because all loads are zero in the direction of the rigid-body deflection. The denominator is zero because the matrix is singular.

It is believed that because of roundoff errors, the denominator used in NASTRAN was not exactly zero. The numerator was exactly zero because loads were user-supplied. Hence, the result would be a determinant situation, i.e., zero deflection.

Upon completion of the ATT analysis, a small check problem was run which accurately recreated the above situation while greatly simplifying the picture. The static analysis was correct and did use a singular matrix.

## Use of Multipoint Constraints

What has historically been termed "beaming" at Convair Aerospace is termed "Multipoint Constraints" (or MPC) in NASTRAN. However, the computational expense for MPC's in NASTRAN is considered by this writer to be excessive. The symmetric ATT airplane modal analysis used 10 sets of MPC's which were summed in an eleventh set. Each set involved only two degrees of freedom. The modules timed, MCE1 and MCE2, required 200 CPU seconds for execution.

## Restart Tape Problem

Two restart failures have occurred. One failure occurred during the ATT analysis, which cost a significant amount of execution time. The second failure occurred on a small check problem following the ATT analysis. The failures were of the same type and the critique printed was "System Fatal Message 36, Cannot Find File Named XVPS on Old Problem Tape." XVPS is a variable-parameter-set table printed on the restart tape during each CHKPNT operation.

The solution used for this latest restart failure was to remove from the checkpoint dictionary the cards punched from the last CHKPNT operation. This forfeited one milestone, but the subsequent restart was successful. Forfeiting one milestone was not significant since the solution of a problem will involve from 24 to 36 milestones, depending on the rigid format being used.

## Post ATT Analysis - Additional Evaluation

Following the analysis of the ATT, two additional areas were explored with small problems.

### Normal Modes by Transformation

One of the extensions made in level 12.0.0 was the addition of a transformation method to calculate vibration modes. Because this method had not been previously used, a small test problem was solved with it. The problem consisted of a flat anisotropic plate, cantilevered along one edge. Test modes and frequencies were available for comparison.

The idealization used is shown in Figure 5. Deflections were fixed to zero value at grids 1 through 6. Twenty-five quadrilateral bending plate (QDPLT) elements were used. Ninety degrees of freedom existed after fixing; sixty of these were omitted, leaving a dynamic matrix of size 30.

All 30 frequencies were extracted, and the first 12 modes were printed and plotted. Computer time required was 4.0 CPU minutes. It is interesting to note that this problem had previously been run, where the Inverse Power Method was used to calculate only the first 4 modes. However, the CPU time was 4.4 minutes.

Only the first seven modes and frequencies are available from test. The calculated/test frequency comparison is shown in Table 1. Testing was accomplished by both acoustic and holographic methods; hence, both results are shown. Note that the NASTRAN/test comparison is better than the test/test comparison. No "tuning" was performed in the analysis. Considering the crudeness of the model, this is considered excellent.

The first seven vibration modes are shown in Figure 6. Test modes were not available for inclusion in this report; however, the modes and node lines compare very well, as would be expected from the frequency comparison.

### Static Analysis of Anisotropic Membrane

This problem had previously been solved to validate level 8, wherein it was discovered that the quadrilateral membrane element produced inaccurate stresses when used with anisotropic type materials (correct stresses were calculated for isotropic materials). The analysis subject was an anisotropic membrane of rectangular shape. Stresses were correctly calculated when the triangular membrane was used.

Hence, this problem was again used to verify that the correction for the quadrilateral element had been made to level 11.1 and above (as was indicated in Software Problem Report Number 21).

The results showed that the quadrilateral element is still defective. (This was reported to NASA and logged as SPR 446.) Hence, the switch was again made to the triangular element to validate its accuracy in level 12.0.0. The results were accurate. Also, solutions were obtained in one computer pass to the multiple loads with different boundary conditions.

### CONCLUSIONS

NASTRAN continues to be the most versatile of any individual procedure. It has been successfully used to support the ATT study, a predesign, short-response-time effort. However, its execution costs are not yet competitive with its contemporaries.

Some of its operating characteristics are as follows:

1. When using the Inverse Power Method for calculating natural modes of vibration, computer time can be saved if the starting point(s) for iteration is spaced a reasonable distance away from the root(s) to be extracted (rather than too close). This is accomplished by stipulating a reasonably wide band in the input data.
2. When calculating natural modes of vibration for unsupported structures, the SUPORT card should always be used. This causes the rigid-body modes to be calculated by a direct method, whether or not the modes are desired for use. If the SUPORT card is not used, there is the danger that the repeated zero-frequency roots may be calculated by iteration, which is an expensive process. This can occur even though these roots may lie well outside the user-stipulated frequency band.

3. Backfiguring of deflections for those coordinates eliminated through use of the OMIT card cannot be avoided by requesting that displacements be printed for the solution set. The eliminated coordinates form a subset of the displacements for each eigenvector.
4. Vibration modes (eigenvectors) cannot be punched on cards at present in level 12.0.0 because of a programming error.
5. NASTRAN will solve singular matrices in performing static analysis when the matrix singularity is due to its containing a rigid-body degree of freedom and when no mechanical load component is aligned with the rigid-body degree of freedom.
6. System Fatal Message 36 occurred twice during restart and the run was aborted. A successful restart was accomplished by removing from the checkpoint dictionary those cards punched during the latest checkpoint operation. This sacrificed the most recent milestone traversed.
7. The use of Multipoint Constraints should be avoided in NASTRAN whenever possible because it is computationally expensive.

#### REFERENCES

1. Allen, M. G., "NASTRAN Experiences of Fort Worth Operations, Convair Aerospace Division of General Dynamics", paper presented at Colloquium at Langley Research Center, September 13-15, 1971 and published in NASA TM X-2378, NASTRAN: User's Experiences, September 1971.
2. MacNeal, R. H. (Editor), The NASTRAN Theoretical Manual, NASA SP-221, September 1970.
3. McCormick, C. W. (Editor), The NASTRAN User's Manual, NASA SP-222, September 1970.

Table 1 Anisotropic Cantilevered Plate Calculated/  
Test Frequency Comparison

Mode Order	Frequencies in Hz			Percent Error	
	Holographic Test	NASTRAN	Acoustic Test	<u>NASTRAN</u> Holographic	<u>NASTRAN</u> Acoustic
1	24.0	24.6	25.1	+2.5	-2.0
2	81.0	78.8	83.6	-2.7	-5.7
3	145	150	155	+3.4	-3.2
4	196	200	203	+2.0	-1.5
5	316	327	331	+3.5	-1.2
6	352	384	369	+9.1	+4.1
7		455	469		-3.0

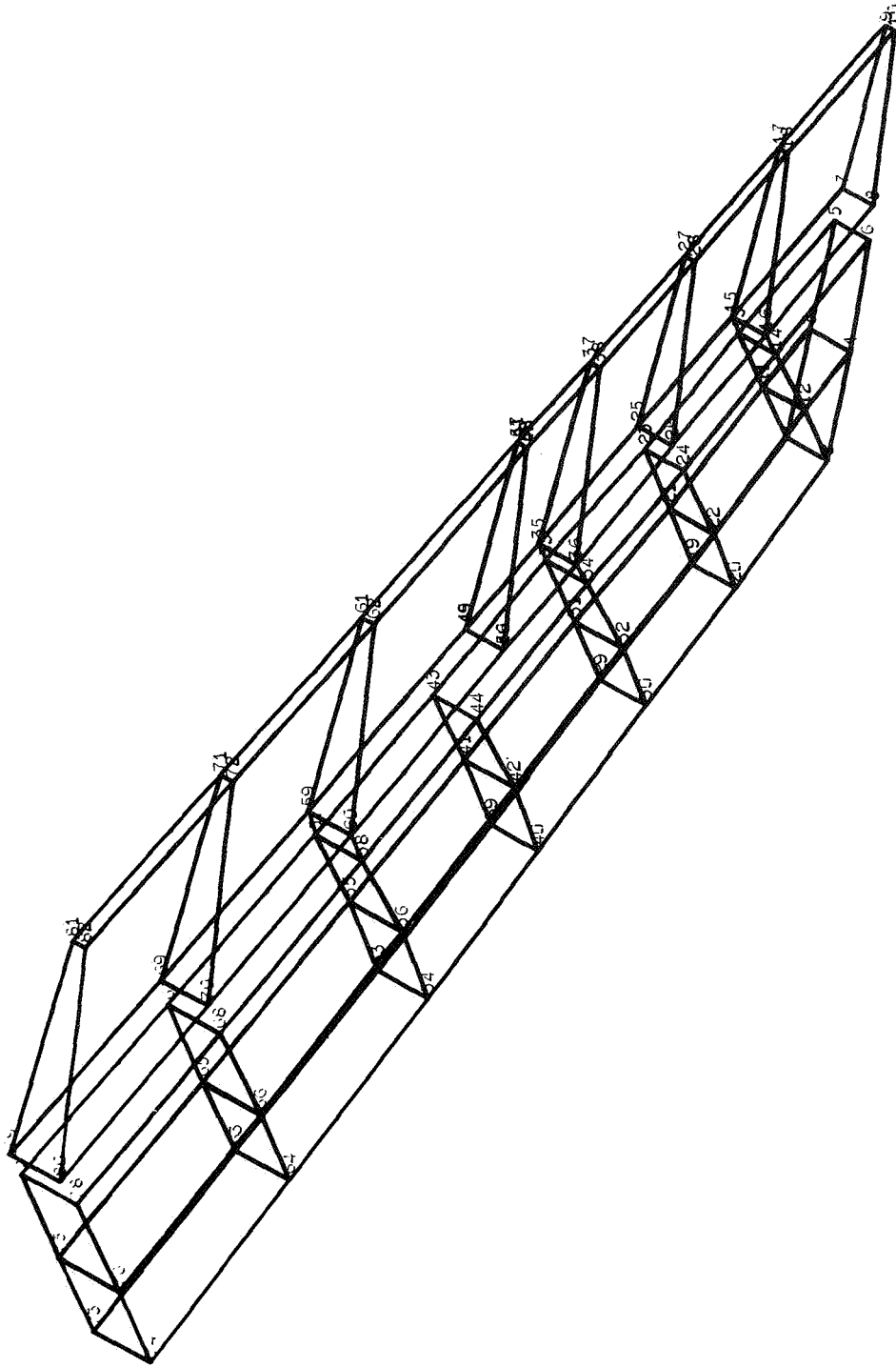


Figure 1.- ATT wing idealization (outboard section), frame 1 of 4 frames.

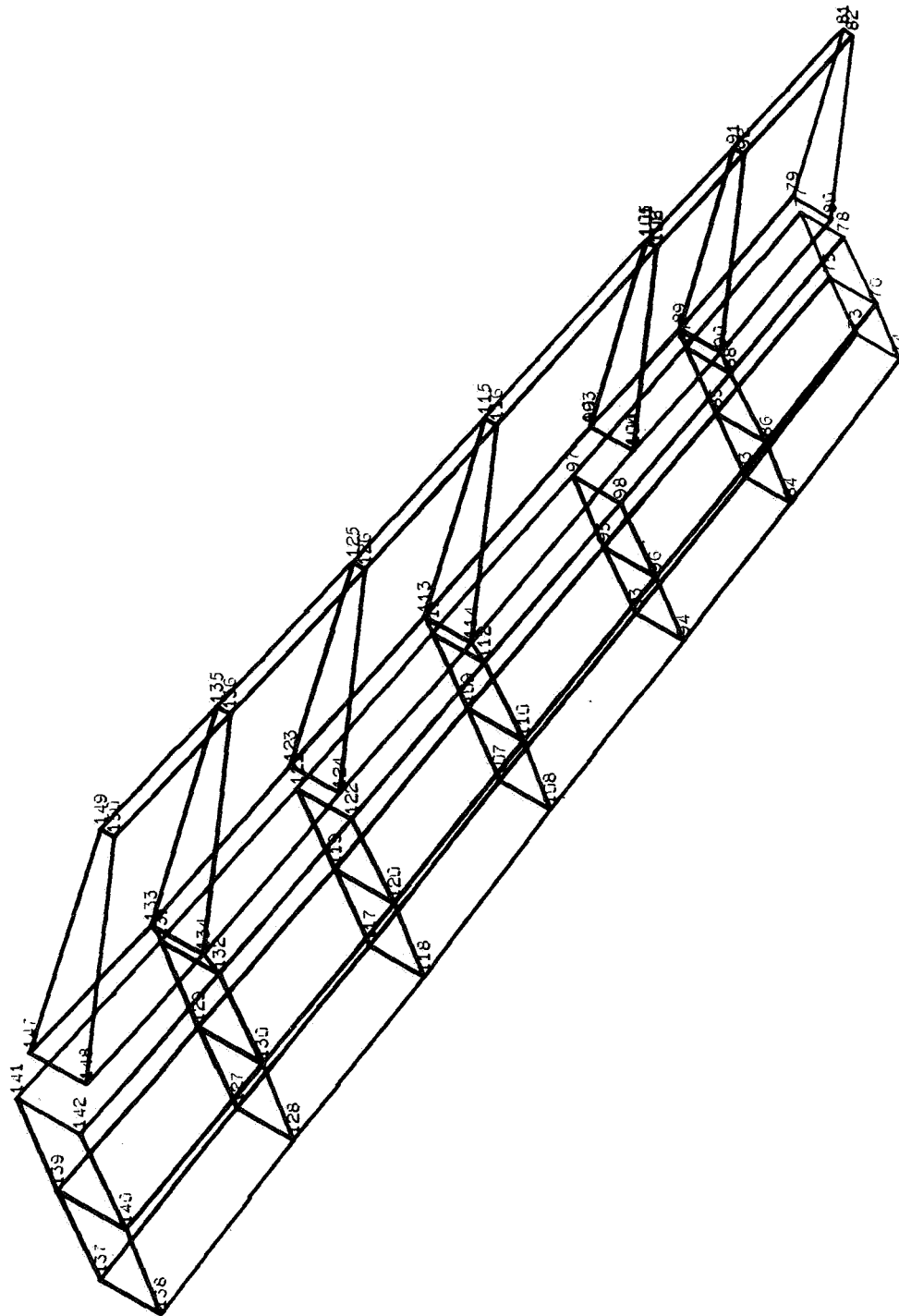


Figure 1.- ATT wing idealization (mid section), frame 2 of 4 frames - Continued.

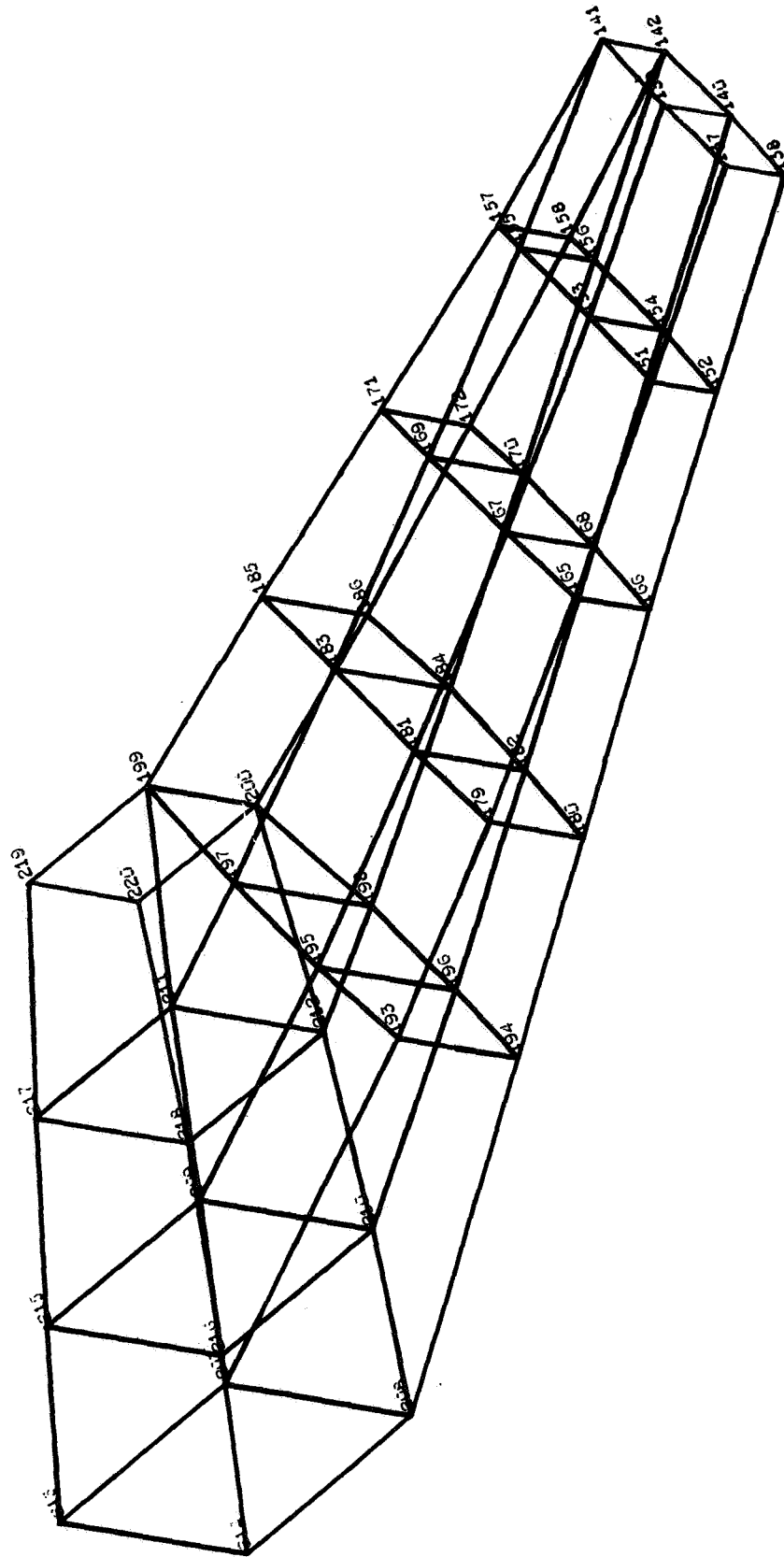


Figure 1.- ATT wing idealization (inboard-forward section), frame 3 of 4 frames - Continued.

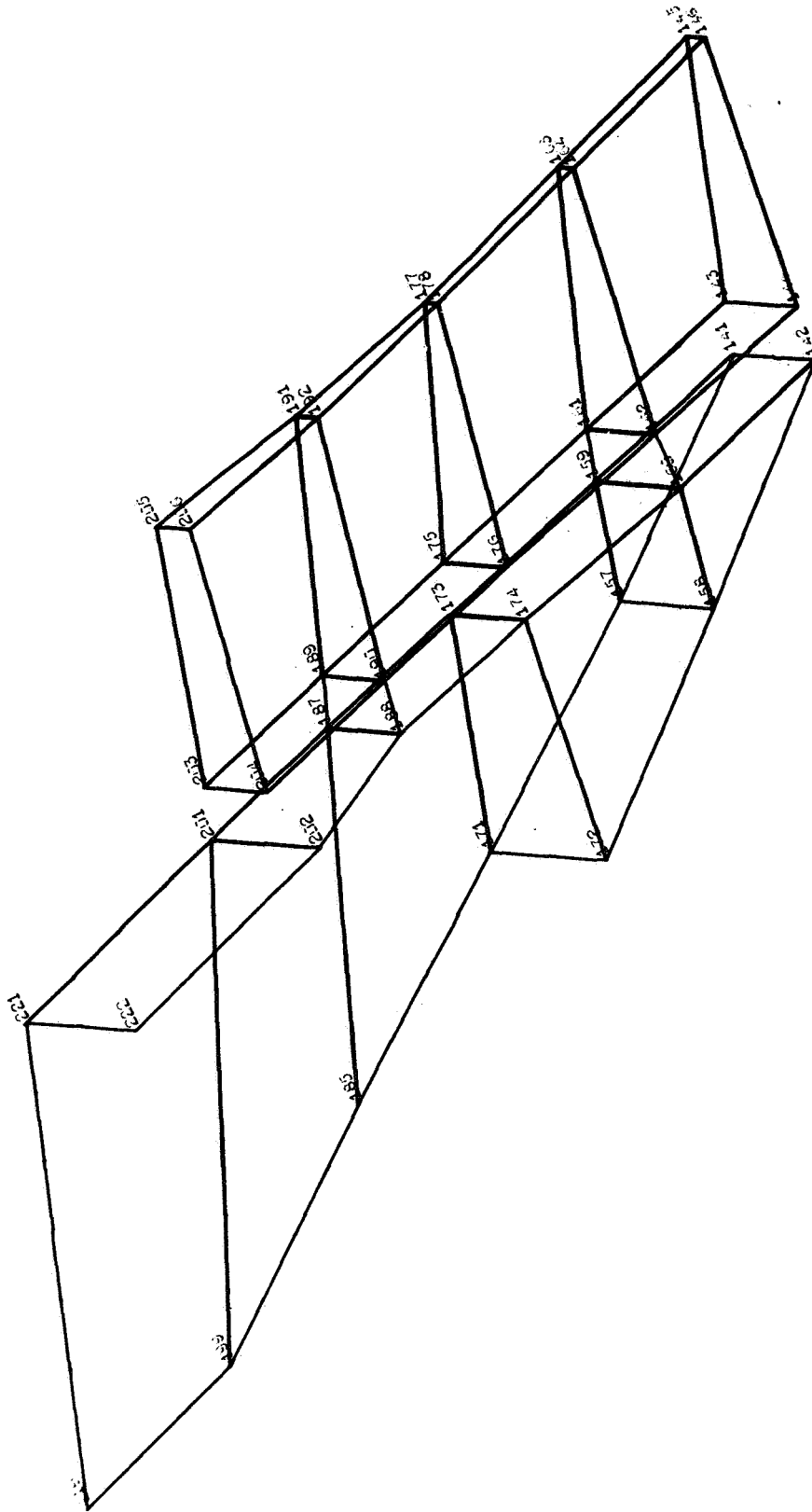


Figure 1.- ATT wing idealization (inboard-aft section), frame 4 of 4 frames - Concluded.

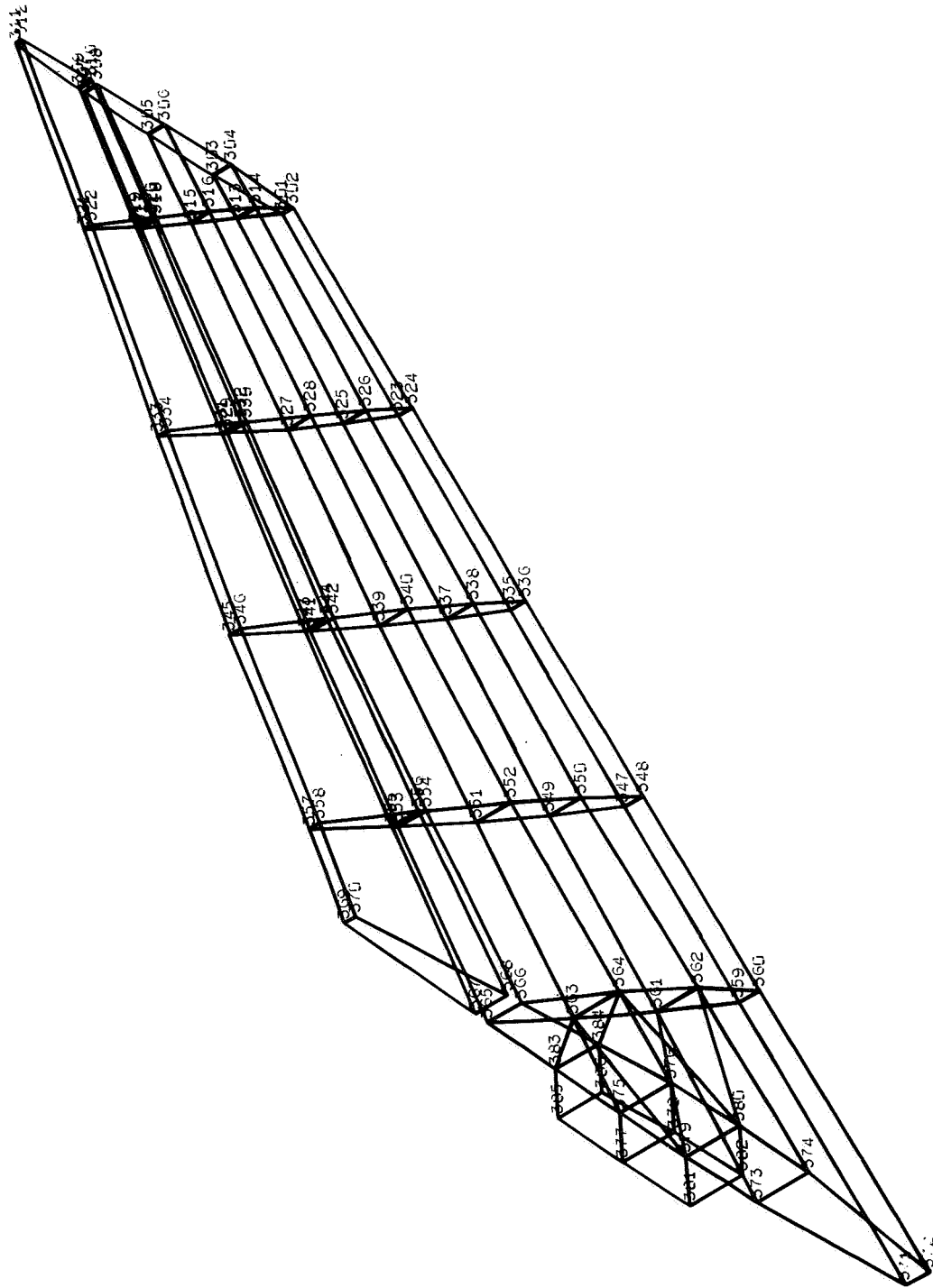


Figure 2.- ATT tail idealization.

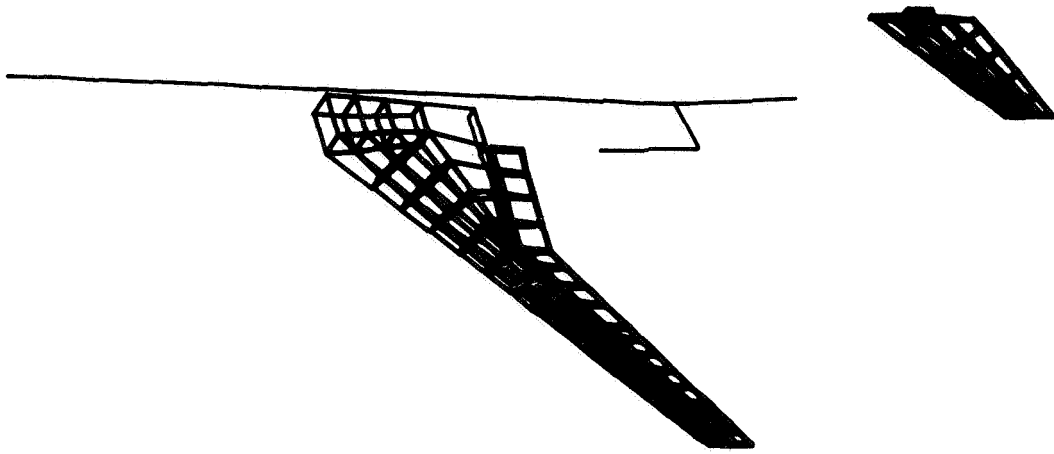
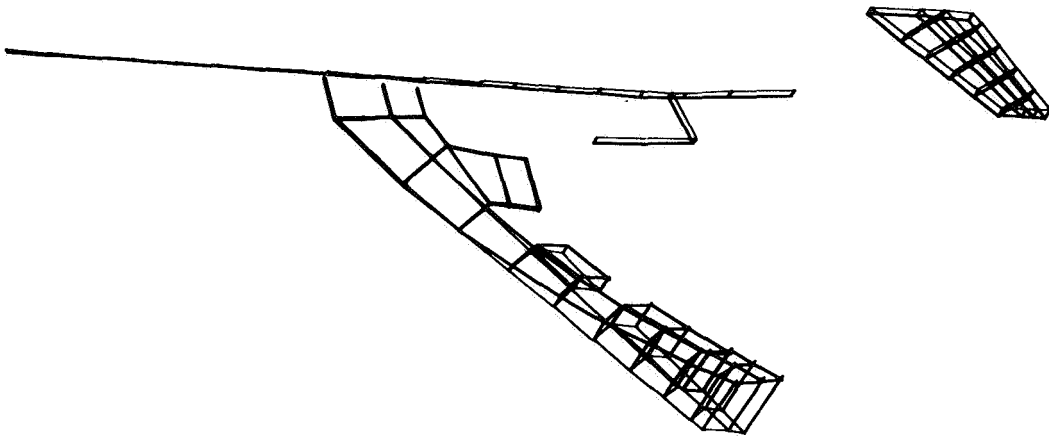
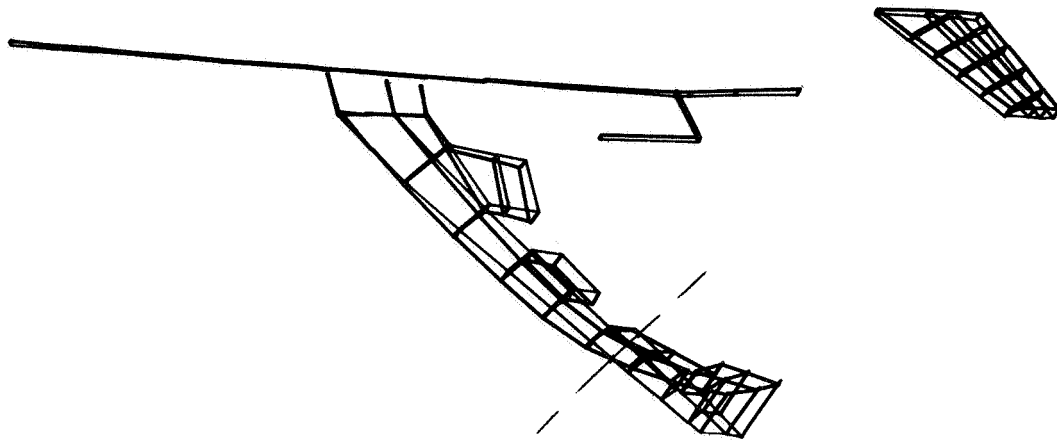


Figure 3.- ATT symmetric vehicle representation.

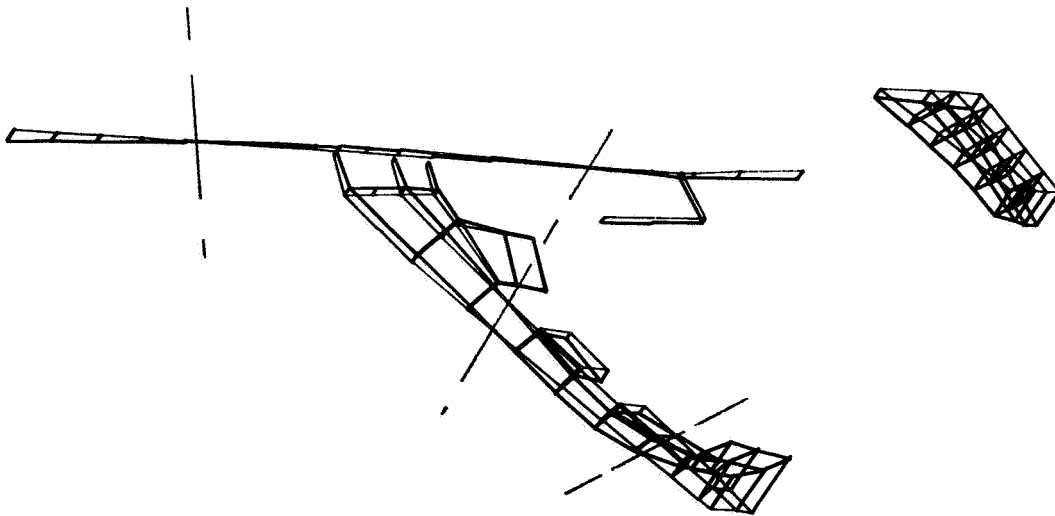


Mode 1,  $f_1 = 0.95$  Hz

Figure 4.- ATT symmetric vehicle modes.

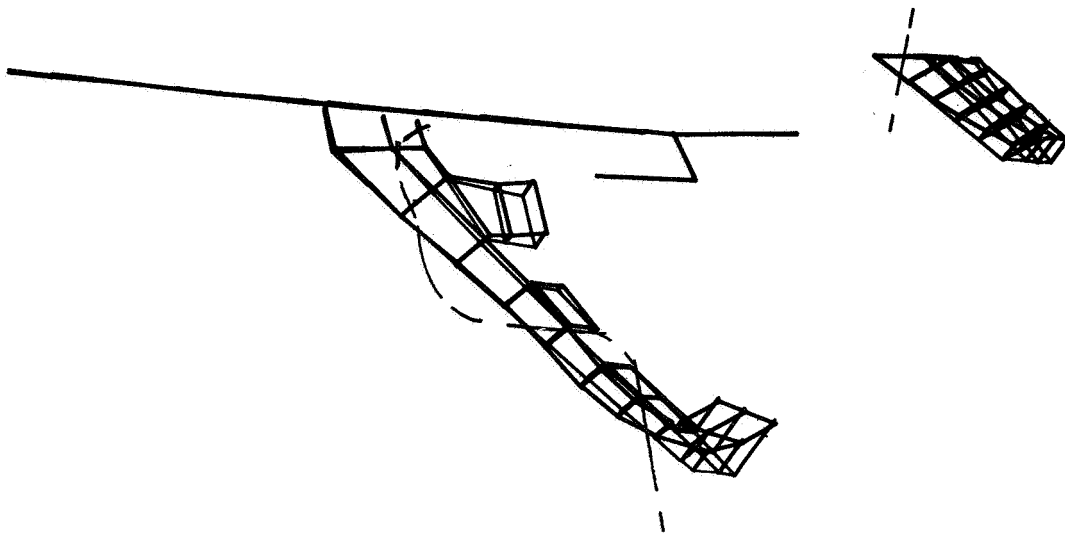


Mode 2;  $f_2 = 2.45$  Hz

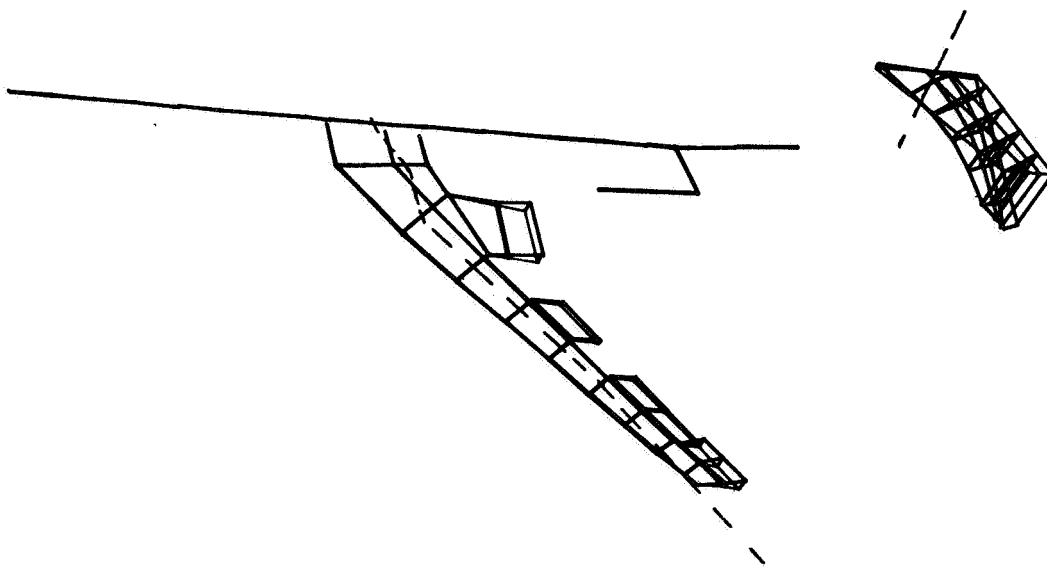


Mode 3;  $f_3 = 3.73$  Hz

Figure 4.- ATT symmetric vehicle modes - Continued.

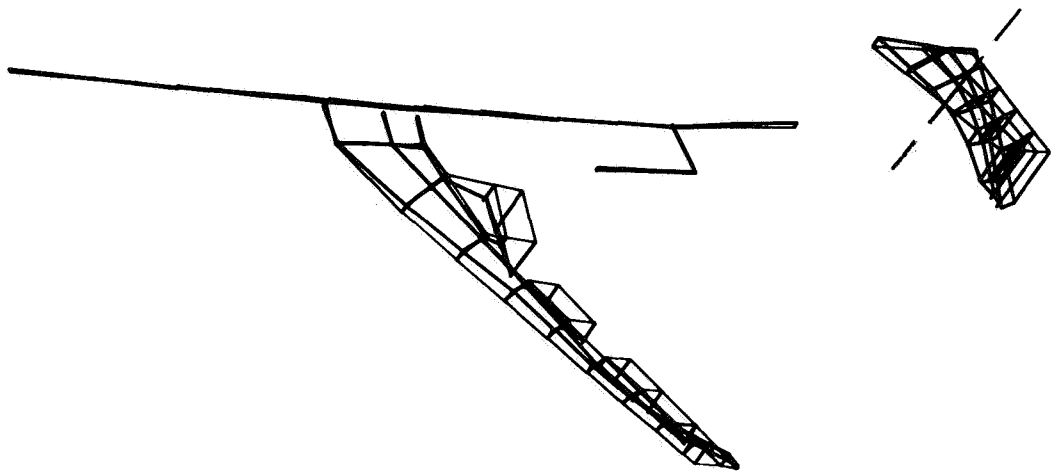


Mode 4;  $f_4 = 5.30$  Hz

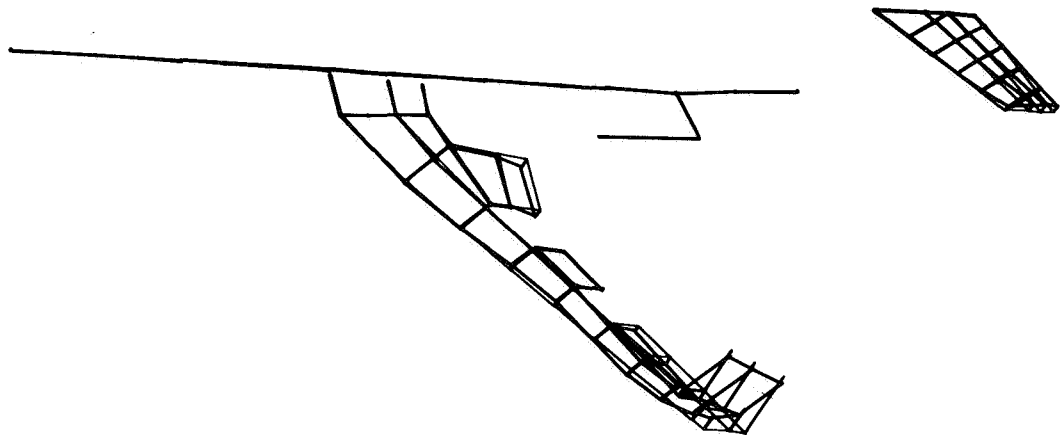


Mode 5;  $f_5 = 5.91$  Hz

Figure 4.- ATT symmetric vehicle modes - Continued.

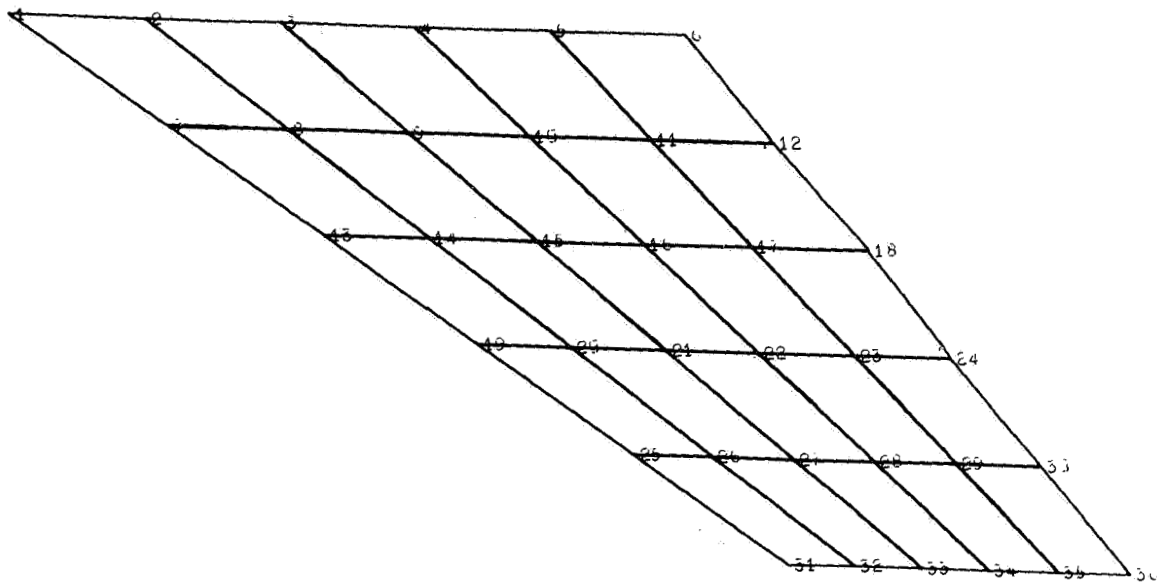


Mode 6;  $f_6 = 6.53$  Hz

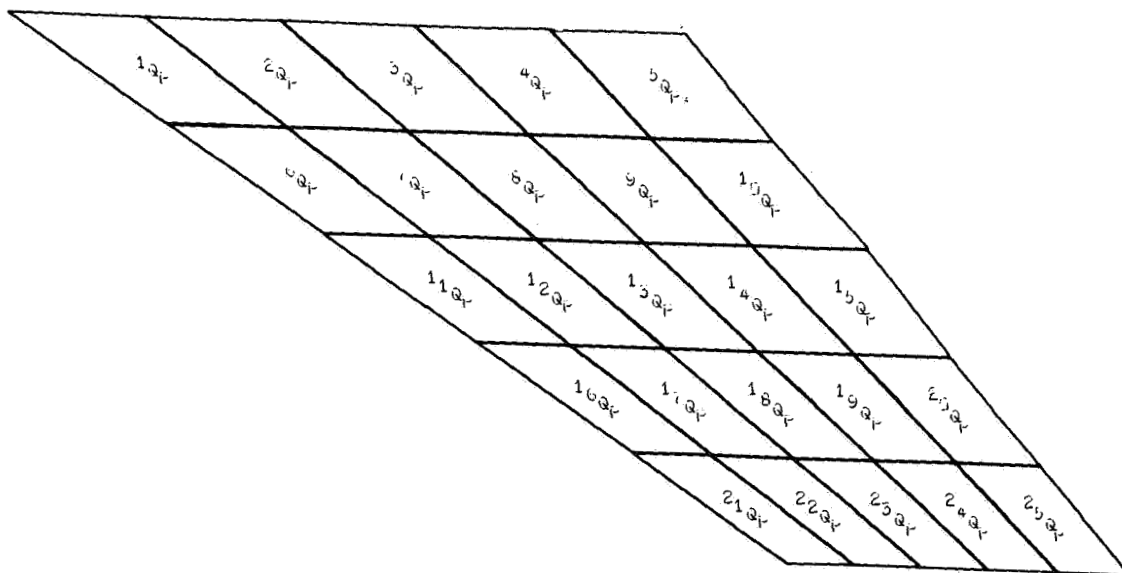


Mode 7;  $f_7 = 7.57$  Hz

Figure 4.- ATT symmetric vehicle modes - Concluded.

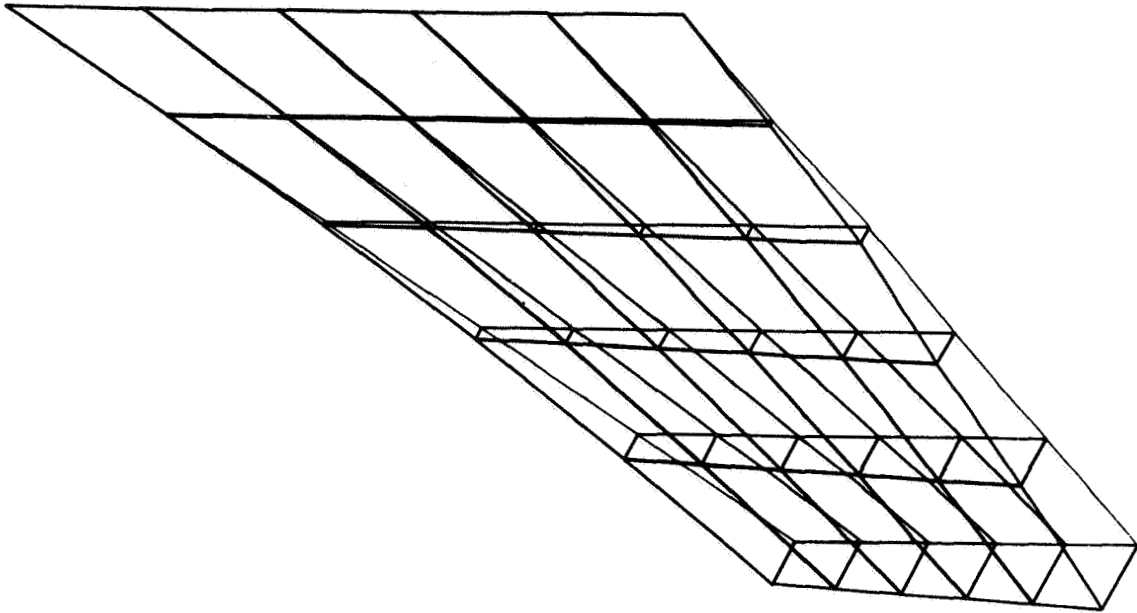


Grid-Point Locations

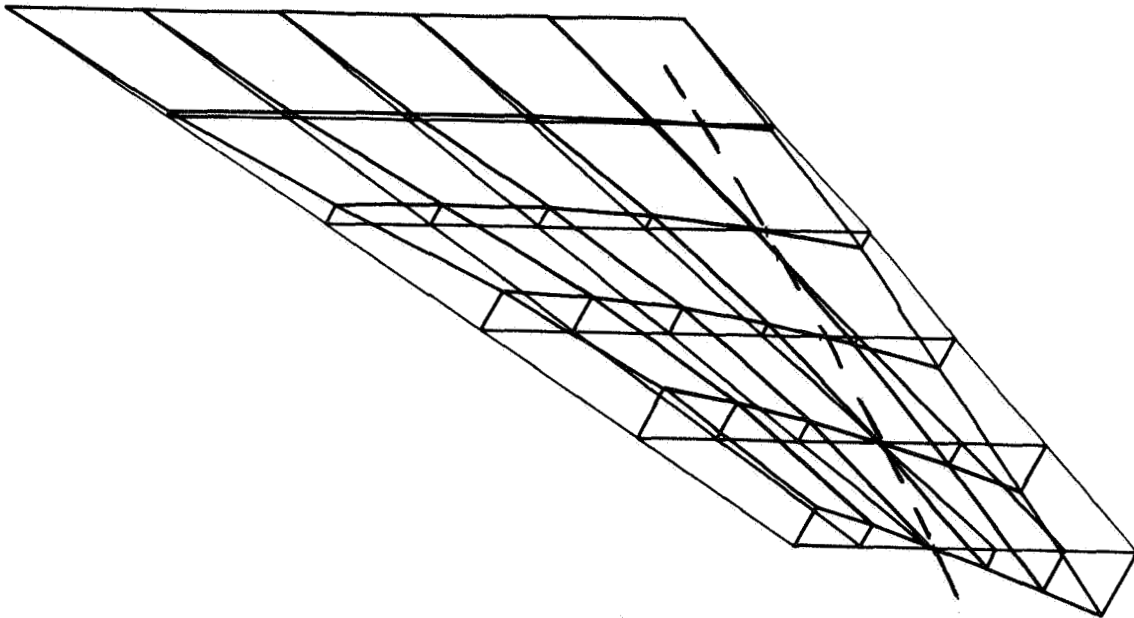


Finite-Element Locations

Figure 5.- Idealization of anisotropic plate.

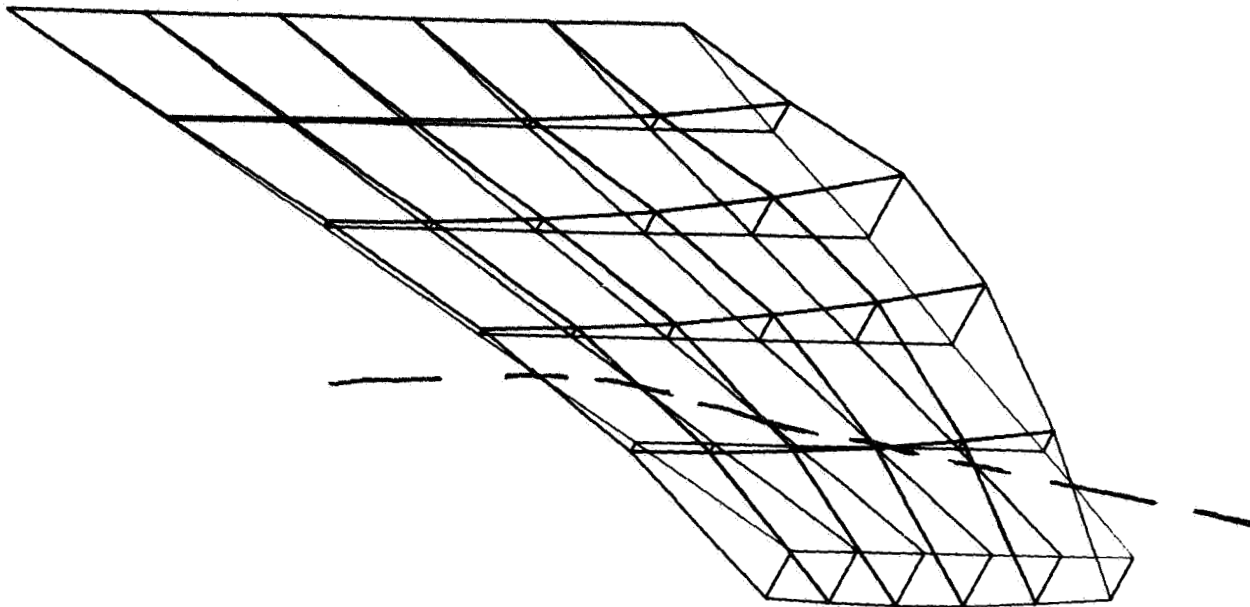


Mode 1;  $f_1 = 24.6$  Hz

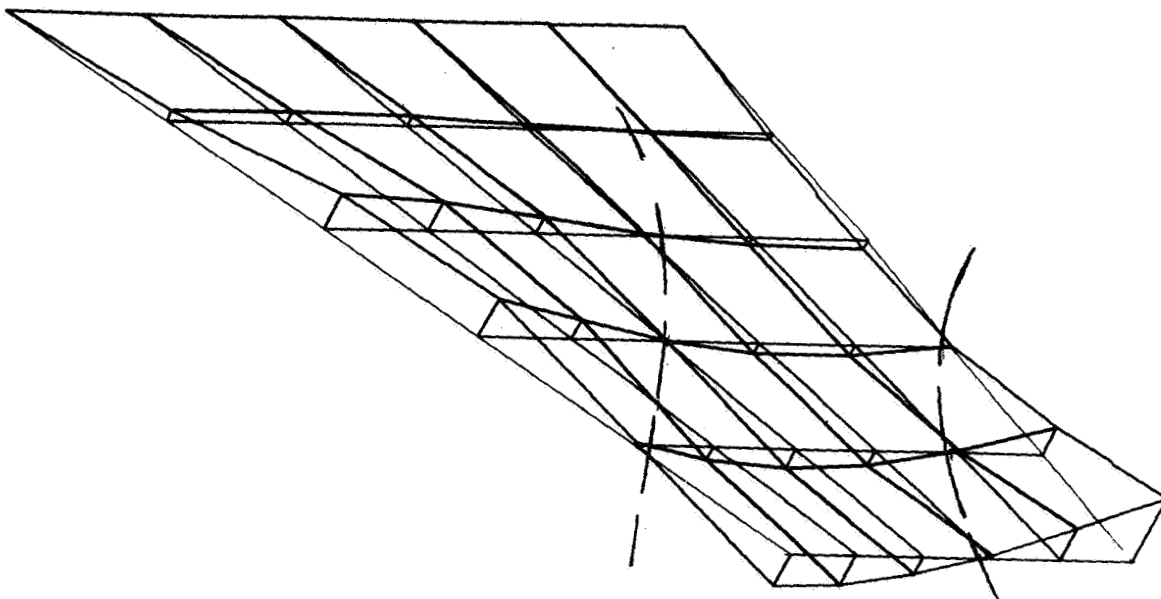


Mode 2;  $f_2 = 78.8$  Hz

Figure 6.- Anisotropic cantilevered plate modes.

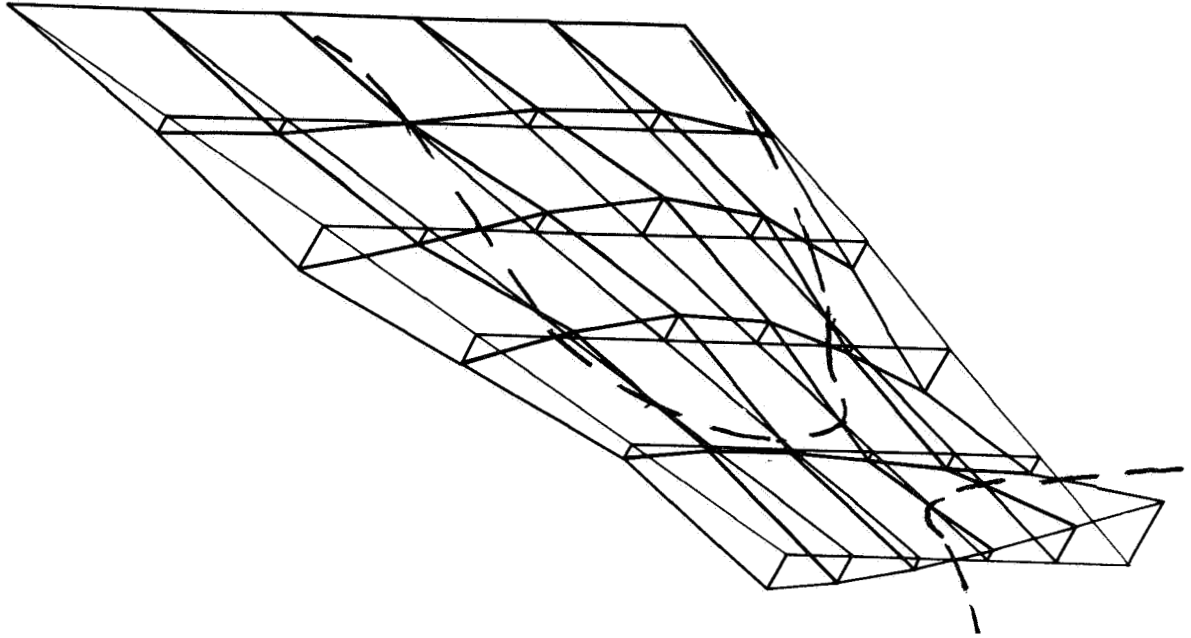


Mode 3;  $f_3 = 150$  Hz

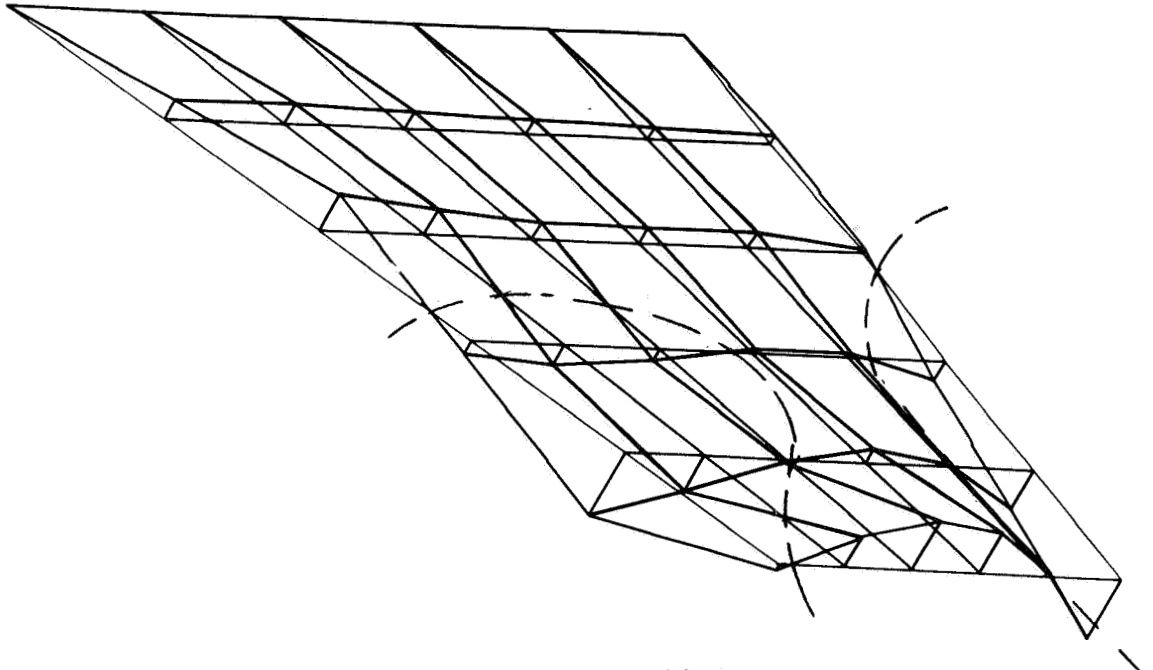


Mode 4;  $f_4 = 200$  Hz

Figure 6.- Anisotropic cantilevered plate modes - Continued.

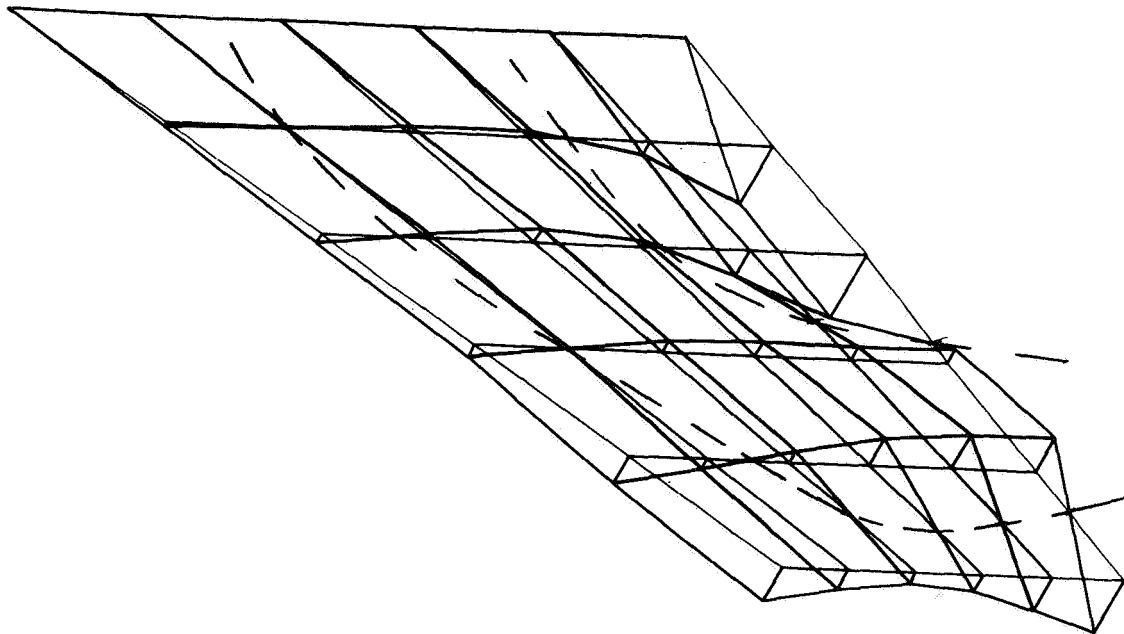


Mode 5;  $f_5 = 327$  Hz



Mode 6;  $f_6 = 384$  Hz

Figure 6.- Anisotropic cantilevered plate modes - Continued.



Mode 7;  $f_7 = 455$  Hz

Figure 6.- Anisotropic cantilevered plate modes - Concluded.



NONAPPLICABILITY OF  
LINEAR FINITE ELEMENT PROGRAMS TO THE  
STRESS ANALYSIS OF TIRES

by Michel Durand and Etienne Jankovich

KLEBER-COLOMBES, Theoretical Tire Engineering,  
COLOMBES, France

SUMMARY

A static finite element stress analysis of an inflated radial car tire is carried out. The deformed shape of the sidewall presents an outward bulging. The analysis of a homogeneous isotropic toroidal shell shows that the problem is common to all solids of this type. The study suggests that the geometric stiffness due to the inflation pressure has to be taken into account. Also, the resulting large displacements make it necessary for the geometry to be up-dated at each load step.

16

INTRODUCTION

The tire is a mass-produced industrial product, and therefore those who are not specialists tend to believe that its mechanical behavior is well known and precisely analyzed. However, the tire engineer knows that this is not the case because of the rather unique characteristics of rubber.

A survey of available literature shows that most often empirical methods are used to determine the behavior of existing tires (References 1, 2 and 3). In the design field a few analytical methods are available to determine the dimensional and inflated geometry of the tire (References 4, 5 and 6). In addition, results of wider applicability have been obtained by Zorowski using finite element shell theory type modelization which included nonlinear relations of the mid-surface strain (Reference 7).

The reasons for the lack of theoretical work are that stress analysis of tires is a rather formidable task. It involves large displacement analysis, nearly incompressible materials, viscoelasticity and thermal conduction and radiation. At the same time one must account for the heat generated under dynamic loading conditions. Heretofore it has not been possible to solve even part of the problem by the most powerful analytical methods. Recently, however, large-size finite element methods became available and were applied successfully to a number of complex problems. Because of the generality of these programs, it was thought that the method might be applicable to stress analysis of tires.

The ASKA program was selected because it has a very wide variety of finite elements which includes tridimensional elements. Some other programs, such as TITUS, developed in France by CITRA, have also been tested. However, the most significant results were obtained by means of ASKA. A singular point is encountered on the sidewall of the tire. Different solutions are proposed and their economical feasibility are discussed.

#### SYMBOLS

u displacement , m  
 $\sigma$  stress , MN/m<sup>2</sup>  
Subscript:  
R, Z and T radial, axial, and hoop components

#### ANALYSIS OF THE TIRE

The calculations were carried out on a radial type KLEBER V10 RS experimental Rallye-Racing tire. A cross-sectional view of the initial shape taken as the mold shape of the tire is shown in Figure 1. The bead wires are made of steel and the flipper is a nylon fabric with the fibers lying at  $\pm \pi/4$  rad relative to the radius. The carcass is a made of textile with fibers having a radial orientation. The belt has four layers of glass-fiber cords supplied by OWENS CORNING FIBERGLASS forming an angle of  $\pm 0.35$  rad with the equatorial plan. The tube-type tire is fitted on a 7 J 13 rim. In the course of determining the material properties, several problems had to be solved.

1 - Rubber - Experimentally it has been established that for deformations not exceeding 10-15 % mm/mm, the usual HOOKE law applies to vulcanizates. The HOOKE's coefficients are determined making allowance for the instantaneous geometry of the specimen (Reference 8). For all rubber elements, the assumed POISSON's ratio is 0.49. Tests were carried out on normalized flat uniaxial tensile test pieces cut out of the vulcanized tire.

2 - Composite Materials - The strains in composite specimens were determined by taking photographs: one before and one after deformation. A network of orthogonal lines drawn on the surface of the specimen was used as a benchmark. The aim was to investigate the material properties at low strains in the range which obeys the HOOKE's law (Reference 9).

#### Finite element idealization

The ASKA program, 4.2 Level, was selected to calculate the static stresses in the tire. The inflated tire was analyzed with the help of TRIAX 6 and TRIAXC 6 linearly varying strain ring elements. The index C is relative to a curved-edge element. Both elements can be anisotropic, have six nodes, and support only axisymmetric loads. Each node has two displacement degrees of freedom.

The idealization shown Figure 2 encompasses about 577 elements and 1300 nodes. All elements have a ratio of the smaller edge to the larger one that is at least equal to 1/7. However, in some places, such as the bead wires, the angle of two edges was much smaller than  $\pi/3$  rad.

a - Tread - Half the thickness of the tire's tread was removed. In this case, the tread grooves can be assumed to be axisymmetric, and a more realistic tread groove cracking analysis can be carried out. The material is assumed to be isotropic.

b - Belt - It is idealized by means of an orthotropic equivalent material. The generalized HOOKE's coefficients are determined using coefficients obtained by single-layer tests and the equations in Reference 10.

c - Rubber reinforcement at the edge of the belt - gum tip - isotropic.

d - The carcass is orthotropic. No provisions were made for making allowance for shaping the carcass before vulcanization. HOOKE's coefficients are determined as for the belt.

e - Sidewall - isotropic

f - Rim load transfer rubber - rim cushion - isotropic.

g - Bead filler - isotropic

h - Flipper - Idealized by means of an equivalent orthotropic material using the corrected equations in Reference 10 (page 77).

i - Bead wires are analyzed like the flipper. The equivalent material is orthotropic.

j - Inner liner - isotropic.

l - Boundary conditions - In the equatorial plane all  $u_z$  have been assumed to equal zero. The influence of the rim has been taken into account by

assuming that the rim is rigid and that the tire takes the form of the rim along the contact area.

One possibility is that the exact contact area may be determined by observing the sign of the normal contact stresses and modifying by trial and error the assumed boundary displacements.

2 - Loading cases - In the first case it was assumed that there was a pressure of 0.1 MN/m<sup>2</sup> and zero displacement within the initial rim contact area. The second case was the study at zero inflation pressure of the effect of mounting the tire on the rim. In the third case the two preceding cases are combined assuming an inflation pressure of 0.25 MN/m<sup>2</sup>.

## RESULTS

A verification of the input data was carried out by in-house plotting packages. A program, for instance, involves plotting the contour of each particular material. It is also possible to plot the mesh showing either the contour of each element or the location of the nodes. Any element that is missing appears as an inlet in the contour line of the material.

To obtain an image of the stress, ASKA gives only the elemental stresses of anisotropic materials. Thus, it was necessary to set up a program to determine the arithmetic mean for each material separately. Standard deviation was also determined. Stress contours were plotted for the  $\sigma_{RR}$ ,  $\sigma_{ZZ}$ ,  $\sigma_{TT}$  and  $\sigma_{RZ}$ . Because the stress distribution is linear across an element, the contours cross the elements in straight-line segments. Thus, the adequacy of the mesh can be assessed. The results obtained are shown in Figures 4 and 5.

There are two ways to use the information given by the stress contours. In the part of the tire where the behavior is linear, the results can be used to analyze the tire quantitatively and to predict its fatigue behavior. In the range where the behavior is nonlinear, the results can be used for a qualitative assessment of the fatigue performance of the particular detail. In this case, the magnitude of the stress concentration rather than the gross stresses are obtained. The stress concentrations are located in ranges where fatigue problems have been actually encountered.

It may be of interest to the designer to know that inflated tire results can already indicate where fatigue problems occur during the service life of the tire. For example, cracks tend to grow along the length of the groove which is next to the shoulder. However, since the abrasion of a racing tire is very rapid, there is not enough time for any cracks to grow. Figure 4 shows that at the tread groove location the highest positive stress is  $\sigma_{ZZ}$ . Cracks are generally produced normal to the largest tension stress. Furthermore, none of the other grooves have a large stress concentration. Thus, both the orientation of the crack and its location can be predicted by

a finite element stress analysis. Because of the low modulus of the rubber, it is to be noted that the strains at the shoulder groove are about 20 % mm/mm.

Another interesting result concerns the inner liner. The analysis shows that the inner liner has no effect on the deformation of the tire. Thus, to reduce the computation time the inner liner and, more generally, all non-load-carrying parts can be analyzed separately by applying to their boundary the displacements obtained in a preliminary calculation of the load-carrying elements of the tire.

### CORRELATION OF TEST AND ASKA RESULTS

Figure 3 shows a plot of the deformed and initial geometry of the tire. On the sidewall, due to small bending stiffness and the large displacements occurring in this part, the tire bulges outward. Further, the deformed tire has a point of inflection that has never been observed on a tire.

An experimental check was carried out by measuring the tire's circumference and its maximum section width. The solid-line curve shows the theoretical results and the triangles show the test points. (See Figures 6-9). At a pressure as high as the service pressure of 0.25 MN/m<sup>2</sup>, agreement between theory and tests is satisfactory on the center line of the tread and the adjacent area (Figures 6 and 7). However, as shown by Figures 8 and 9, outside this range the computed displacements do not agree with the measured ones. Notice that the tire width change is a nonlinear function of the pressure starting from pressures as low as 0.03 MN/m<sup>2</sup>.

### TOROIDAL SIDEWALL SINGULARITY

The problem of the sidewall singularity in the tire is a part of the very complex tire problem.

It was therefore decided to study a similar but much simpler solid such as a toroidal isotropic shell. The cross-section of the toroidal shell was circular, its thickness was  $10^{-3}$  m, its YOUNG's modulus was 2.5 MN/m<sup>2</sup> and its POISSON's ratio was 0.49. It was inflated to .0074 MN/m<sup>2</sup>. Figure 10 shows the initial and deformed geometry obtained by means of TRIAX 6 elements. The same type of behavior as previously observed in the tire occurs again.

Experiments are described in Reference 11 showing the deformed shape of the solid described above. A nearly perfect circular cross section was found. Thus, the bulging of the sidewall is a purely mathematical problem. At the singularity point, one radius of curvature becomes infinite. The problem is similar to that of a transversely loaded clamped membrane plate. The equili-

brium of the forces can only be obtained by taking into account the deformed surface of the membrane. In finite element analysis, however, due to the fact that curves are approximated by straight lines, the chance of obtaining an infinite radius of curvature is very slight.

The explanation for the singularity that is nevertheless observed was given in Reference 12. It was established in the above reference paper that the sidewall singularity of the membrane toroid is not removed by introducing the bending stiffness. The pressurized shell has a pressure stiffness in addition to its bending stiffness. Additional computations are carried out presently using small load step increments and up-dating the geometry following a load step. In this case, the singularity is attenuated. But the computation time increases linearly with the number of load steps chosen. The computation of one load step on CDC 6600/single precision, 3 substructures, 3 load cases, with 2 tapes takes 374 s CP, 1721 s PP and a field length of 47 K CM, for the TRIAX 6 modelization of the tire.

In the preceding discussion only linear finite element programs have been considered. However, programs with nonlinear capability are available.

In fact, several examples given at the NASTRAN Users' Colloquium show that NASTRAN's differential stiffness capability might offer more adequate means for solving the problem. Because of the lack of three-dimensional elements such a calculation could not be carried out until recently.

#### CONCLUSION

Linear finite element codes are not applicable to the analysis of toroidal solids because of the toroidal singularity. The geometric stiffness due to the inflation pressure must be taken into account. This can be done, for instance, by increasing the load step by step and up-dating the geometry.

Research is being carried out at the present time by KLEBER with the aim of developing or identifying finite element methods incorporating the above-described modifications to the classical equations.

In conclusion, the straight-forward stress analysis by means of available linear finite element programs is uneconomical, in any event, as long as the computation time cannot be reduced.

#### ACKNOWLEDGMENTS

The authors wish to express their appreciation to the Civil Engineering Section of the Société Informatique Appliquée, Metra International, and especially to their chief engineer, Mr. G. CANEVET, for their helpful advice concerning ASKA.

## REFERENCES

1. CLARK, S.K., DODGE, R.N., LACKEY J.I. and NYBAKKEN, G.H., Structural Modeling of Aircraft Tires, University of Michigan, College of Engineering, Dept. of Mechanical Engineering, Technical Report No. 10, 05608-16-T, May 1970.
2. FRANK, F. and HOFFERBERTH, W., Mechanics of the Pneumatic Tire, Rubber Chemistry and Technology, Vol. 40, No. 1, February 1967, pp 271-322.
3. KERN, W.F., Verformungs- und Spannungsmessungen an Gürtelreifen, Kautschuk und Gummi-Kunststoffe, 24. Jahrgang, Nr. 11/1971, pp 599-608; 24. Jahrgang, Nr. 12/1971, pp 666-669.
4. CLARK, S.K., BUDD, C.B. and TIELKING, J.T., Tire Shape Calculations by the Energy Method, 1971 Congress of the West German Rubber Society (DKG), Wiesbaden, May 17-19, 1971.
5. BARSON, C.W., Mathematics of Modelling of Tire Performance, Akron Rubber Group's 1971 Spring Meeting, Akron, 1971.
6. ZOROWSKI, C.F. and DUNN, S.E., A Mathematical Model for the Pneumatic Tire, Report to Office of Vehicle Systems Research National Bureau of Standards, 1970.
7. ZOROWSKI, C.F., Mathematical Prediction of Dynamic Tire Behavior, Akron Rubber Group's 1971 Spring Meeting, Akron, 1971.
8. KUCHERSKII, A.M., Deformation Properties of Certain Vulcanisates at Low Deformations, Soviet Rubber Technology, March 1969, pp 27-29.
9. ZOLUTUKHINA, L.I. and LEPETOV, V.A., The Elastic Moduli of Flat Rubber - Fabric Constructions in Elongation and Compression, Soviet Rubber Technology, October 1968, pp 42-44.
10. ASHTON, J.E., HALPIN, J.C. and PETIT, P.H., Primer on Composite Materials : Analysis, Technomic Publication, Technomic Publishing Co., Inc., Stamford, Conn., 1969.
11. MERCIER, J., FREMAU, J. and ROCHA, A., Large Deformations and Stresses of a Thin, Highly Elastic, Toroidal Shell under Internal Pressure, Int. J. Solids Structures, 1970, Vol. 6, pp 1233-1241.
12. JORDAN, P.F., Analytical and Experimental Investigation of Pressurized Toroidal Shells, NASA CR-261, July 1965.

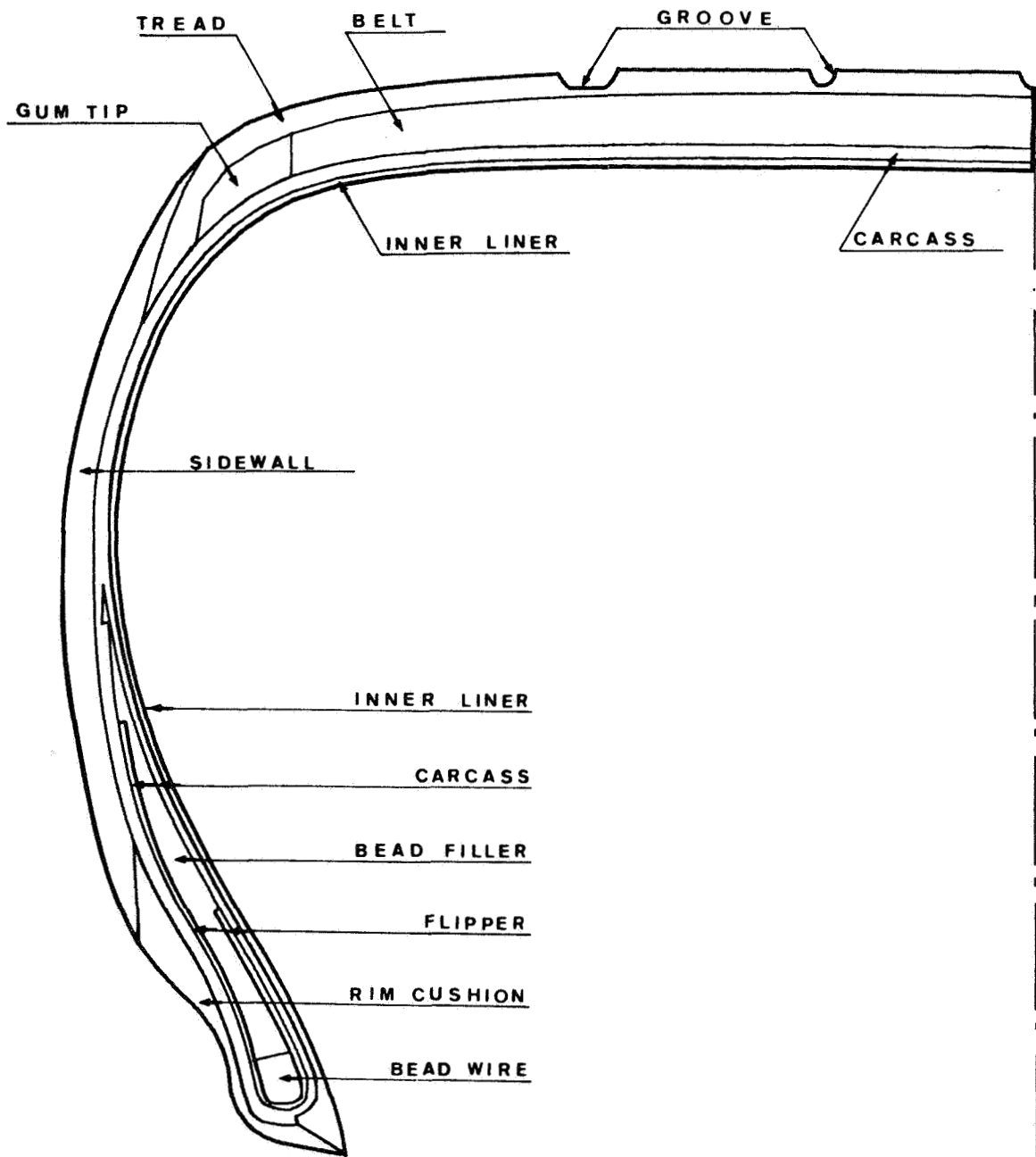


**FIG. 1**

**CROSS SECTION OF THE TIRE  
KLEBER V 10 RS 210/55-13**

Scale 1. 4/1

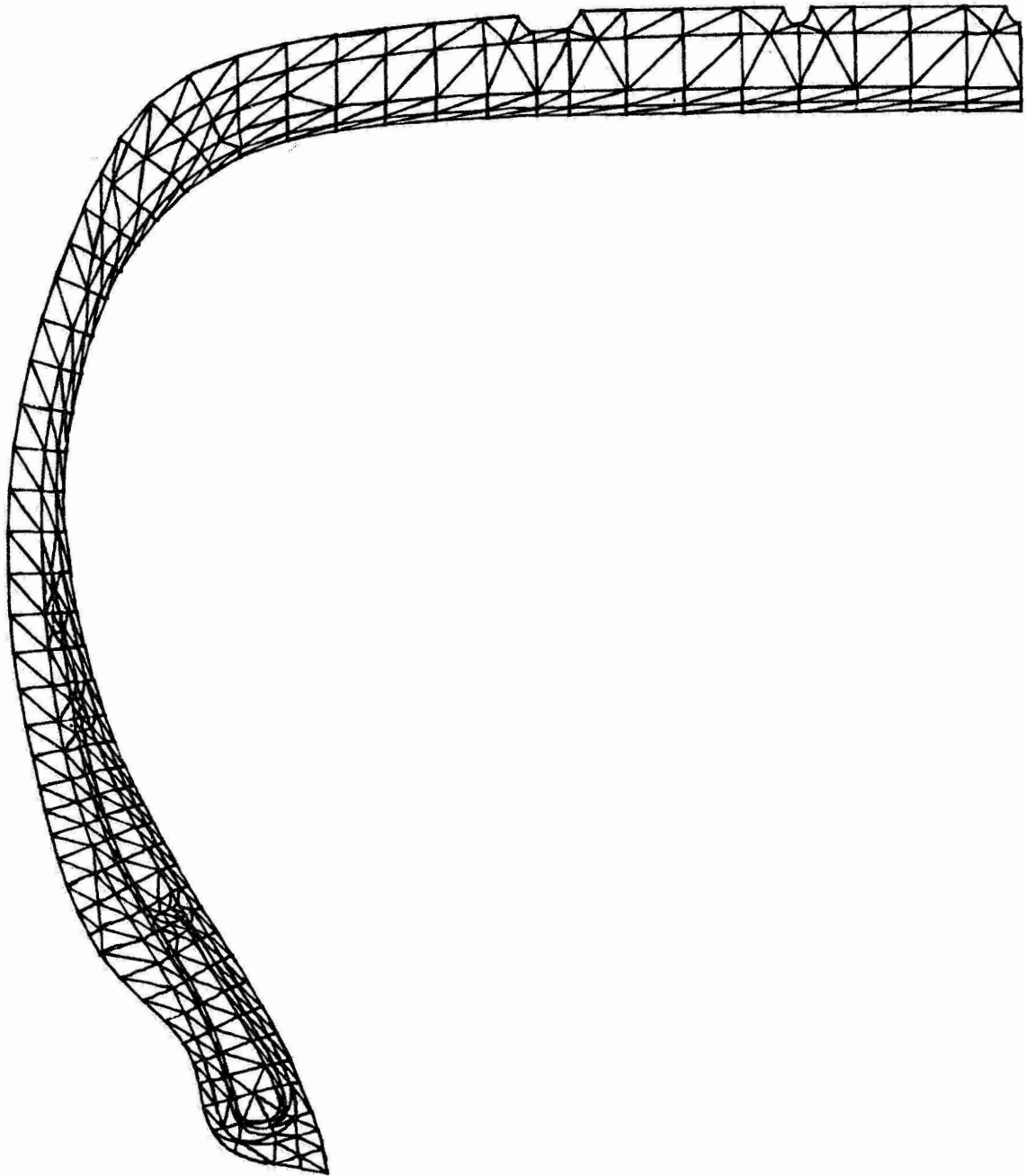


**FIG. 2**      **AXISYMMETRIC FINITE ELEMENT MODEL OF TIRE**

Scale 1.4/1

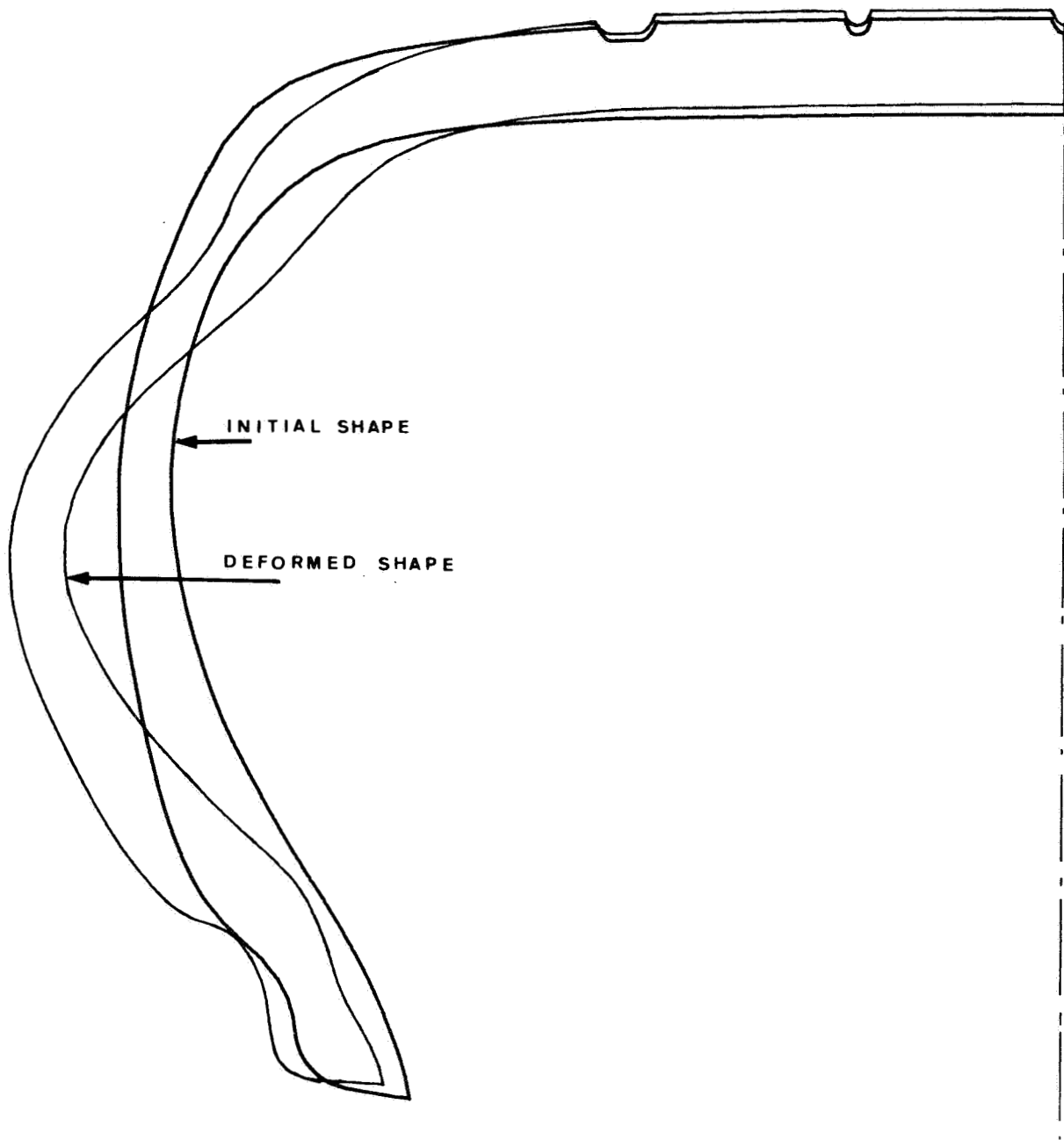


**FIG. 3**                      **INITIAL AND DEFORMED SHAPE**

**Loading case :** inflation pressure  $0.25 \text{ MN/m}^2$  and rim 7 J 13

Scale 1.4/1

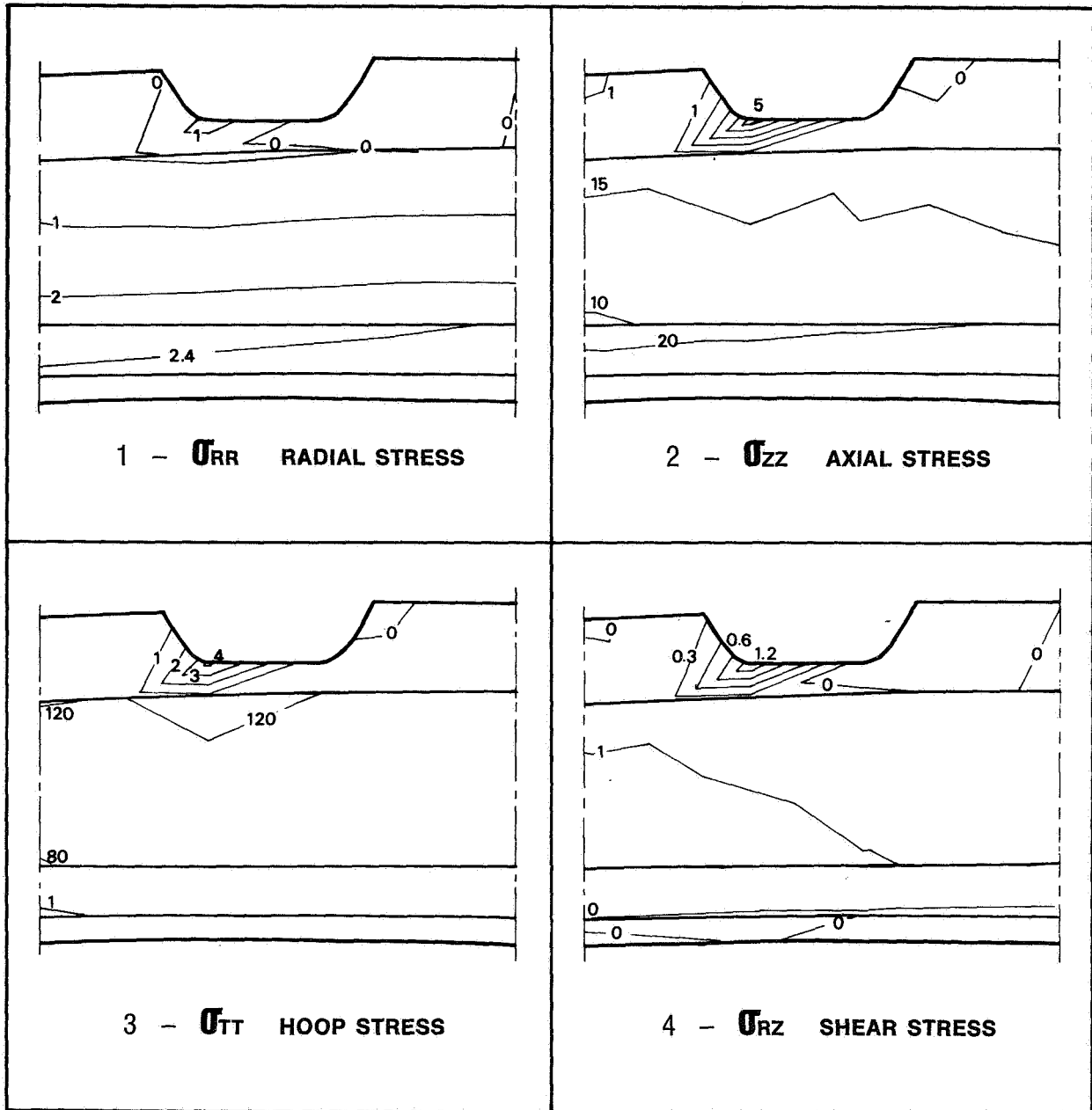
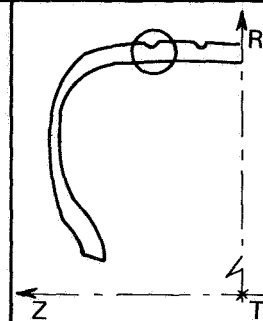


**FIG. 4 STRESS CONTOURS AROUND THE GROOVE**

Loading case : inflation pressure 0.25 MN/m<sup>2</sup>  
and rim 7 J 13

Scale 5/1

Stress unit : 0.1 MN/m<sup>2</sup>



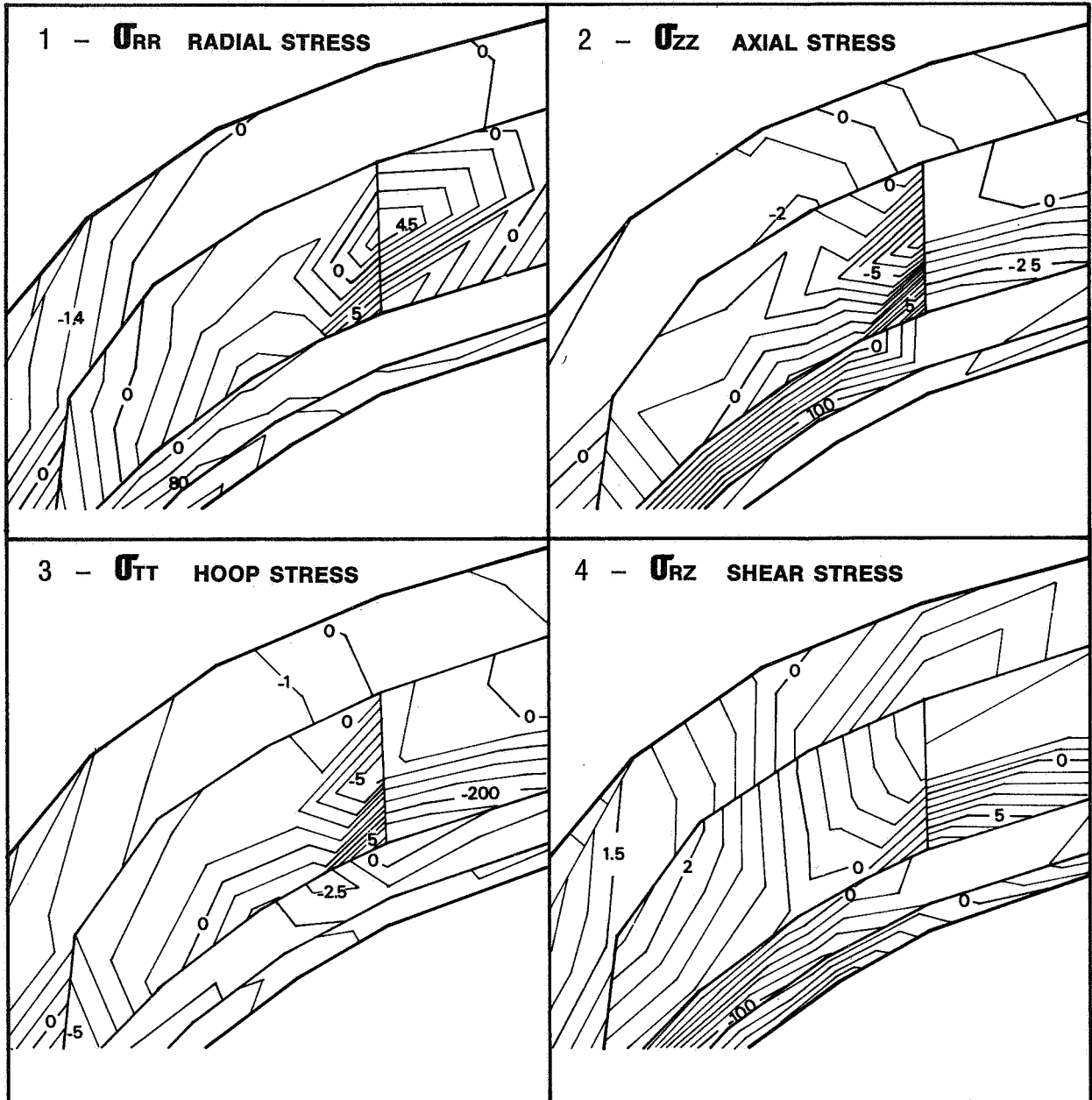
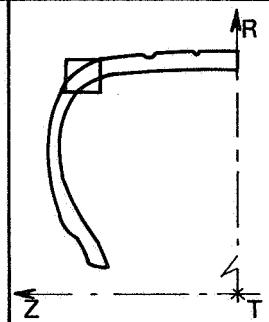


**FIG. 5 STRESS CONTOURS AT THE BELT EDGE**

Loading case : inflation pressure 0.25 MN/m<sup>2</sup>  
and rim 7 J 13

Scale 5/1

Stress unit : 0.1 MN/m<sup>2</sup>



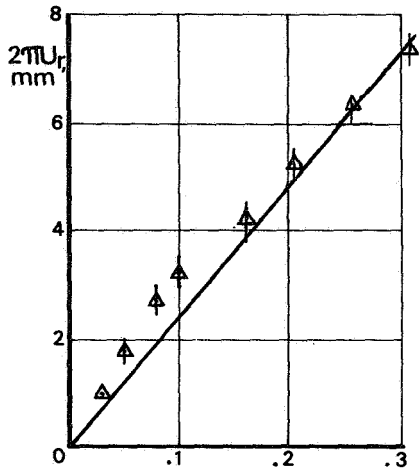


**FIG. 6** Pressure, MN/m<sup>2</sup>

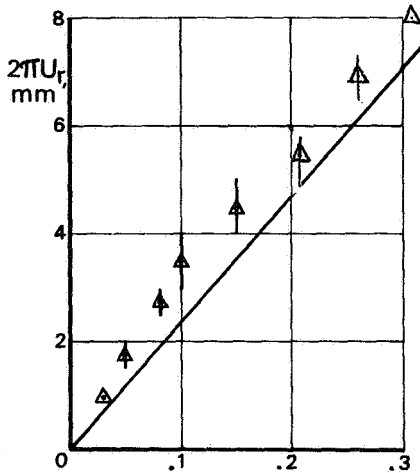


**FIG. 7** Pressure, MN/m<sup>2</sup>

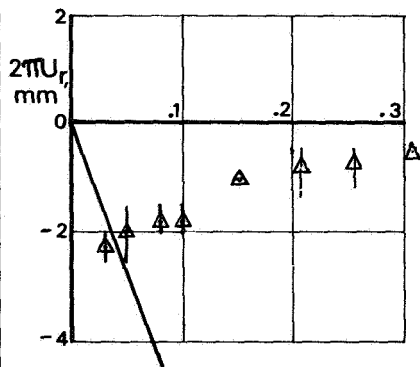
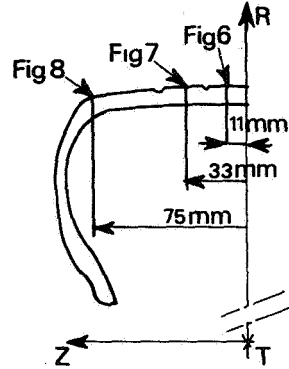


**FIG. 8** Pressure, MN/m<sup>2</sup>

**RADIAL DISPLACEMENT VS. INFLATION PRESSURE**



△ Experiment - mean of 2 parallels  
 - ASKA

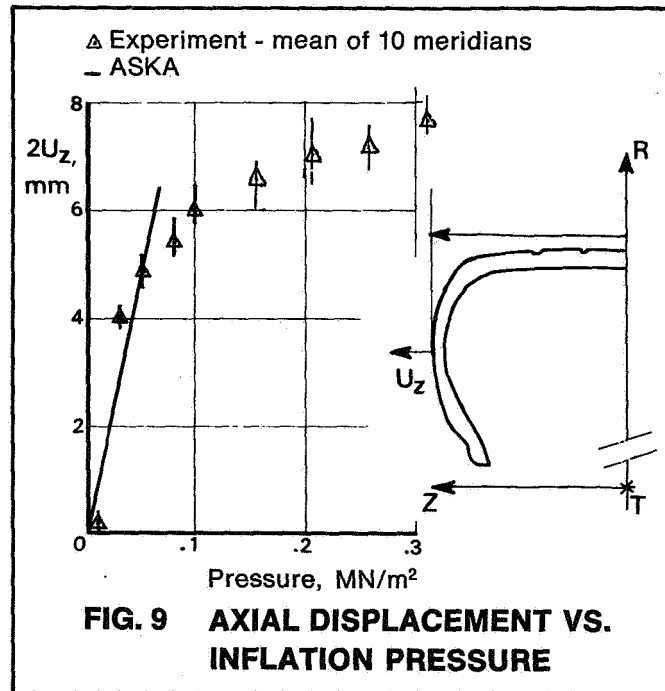


**FIG. 9** AXIAL DISPLACEMENT VS. INFLATION PRESSURE

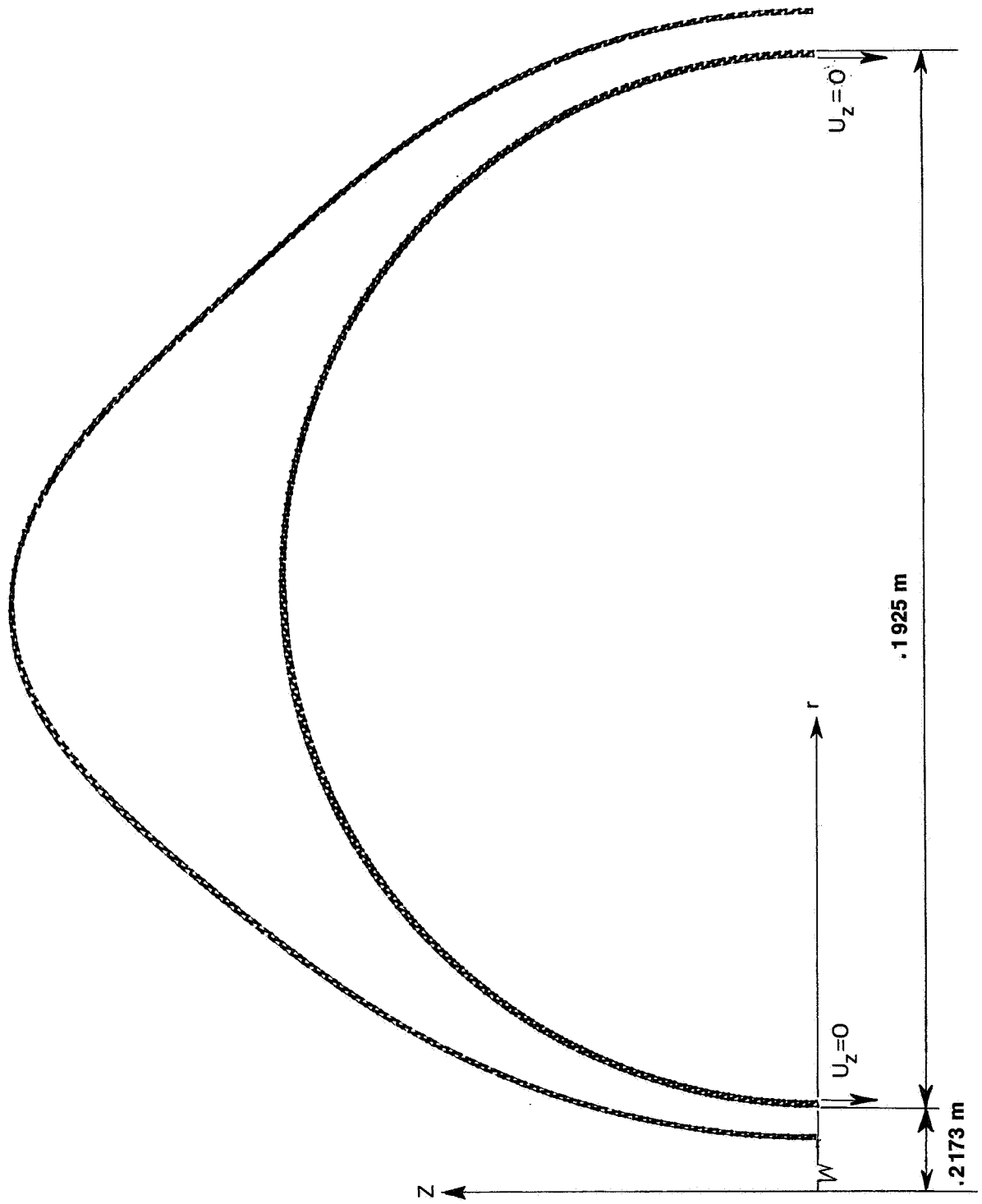


FIG. 10

TRIAx 6 MODEL OF TOROIDAL SHELL

A COMPARISON OF THE CAPABILITIES OF  
THREE FINITE ELEMENT PROGRAMS

By

David D. Loendorf  
Langley Directorate, U.S. Army Air Mobility  
Research and Development Laboratory

SUMMARY

Three finite element programs are compared to assess their capabilities as an analysis tool in a structural design process. Because of the need for repetitive analyses as an integral part of a design loop, a candidate program must be capable of handling large problems, operate efficiently and be readily adaptable for use in computer aided design. The three programs considered in the study, ELAS, SNAP, and NASTRAN, range from a relatively small finite element program limited to static structural analysis (ELAS) to a large complex general analysis system (NASTRAN). Results are given in the paper for comparative speeds and computer resources required for each program in the analysis of sample fuselage problems representative of practical aircraft design.

INTRODUCTION

During the past decade, numerous finite element programs have been developed and are available for public use. They range in size from small programs restricted to two-dimensional static analysis to large systems capable of handling virtually any type of three-dimensional structure subjected to static, dynamic, or thermal loads. Most of the finite element programs in current use were initially developed to analyze a prescribed structural design to determine, for example, if stress levels are within allowable limits. More recently, however, researchers have attempted to incorporate these finite element programs as an integral part of an automated design process. In design applications, many cycles are often required to obtain a converged design, and the efficiency of the automated design procedure is strongly dependent on the efficiency of the analysis tool.

It is the purpose of this paper to present selected analysis results obtained with three finite element programs in current use and discuss some of their assets and liabilities when considering their inclusion as the analysis phase of an automated structural design program.

## ANALYSIS REQUIREMENTS FOR AUTOMATED STRUCTURAL DESIGN

The analysis program is the backbone of any automated structural design procedure and, hence, must efficiently handle the repetitive computation of stresses and deflections following each structural modification. A very simplified schematic of a structural design process is shown in figure 1. It has been the author's experience with the development of the fuselage design program FADES, reference 1, that the analysis program is executed approximately 11 times to obtain one design and that this accounts for more than 75 percent of the total CPU time required for the design. In an effort to decrease computer cost, the finite element analysis program must be evaluated carefully to determine what design oriented finite element capabilities are needed. Since it is important that the actual structure be closely approximated, many diverse finite elements are required. At the same time, analytical results should be obtained with minimum computer costs. However, one should not look at efficiency alone, but must also consider program capabilities and interface problems associated with integrating the finite element program into the design algorithm. These general requirements lead to specific requirements for a structural analysis program in the following areas:

1. Efficiency
  - a. Core requirements
  - b. Execution time
  - c. Bandwidth minimization or sparse matrix techniques
  
2. Generality
  - a. Static, dynamic, buckling, etc., capabilities
  - b. Large problem capability
  - c. Checkpoint/restart capability
  - d. Large library of elements
  - e. Plot capability
  
3. Interfaceability
  - a. Standardized input
  - b. User determined, file oriented output
  - c. Complete, concise, and accurate documentation
  - d. Machine independence
  - e. Continued maintenance

To the author's knowledge, no finite element programs currently available are specifically tailored to efficiently meet all of the above design oriented capabilities; thus, one must consider suitable alternatives among existing programs. Three programs were considered in this study ranging from moderate to broad in capability. The programs are ELAS, reference 2, a relatively small finite element program limited to static structural analysis and presently used in the FADES program; SNAP, reference 3, a proprietary static analysis finite element program efficient for large structures; and NASTRAN, reference 4, NASA's general purpose structural analysis program. (Some of the more important capabilities are listed in Table I).

## RESULTS AND DISCUSSION

A structural configuration representative of an aircraft fuselage section was used in the studies to compare the three programs. A model of the configuration is set up so that the number of rings, stringers, and floor members was easily changed through a model generating program which prepared input to all three programs (see figure 2 for two sample configurations). This procedure facilitated running identical problems with the three programs with a minimum of intermediate effort. Ring elements and transverse floor elements were modeled using a typical beam formulation (combined bending and extension). Stringer elements and longitudinal floor elements were modeled by a rod formulation (extensional properties only). Skin sections were modeled using the constant strain membrane plate element in NASTRAN and ELAS, and the Pian hybrid membrane in SNAP. A comparison of the membrane formulations may be found in references 5 and 6. The loading in all cases was a self-equilibrating compressive force applied to each of the grid points of the end rings. Problem size ranged from 90 grid points, 360 D.O.F., and 267 elements to 1530 grid points, 6102 D.O.F., and 4415 elements.

All results were obtained using the CDC 6000 series computers at the Langley Research Center. ELAS was run using version 75, SNAP using version J, and NASTRAN using level 15.1.1, a pre-release form of level 15. Displacements for the SNAP results tended to be about 5 percent larger than for NASTRAN or ELAS and the difference is attributed to the relatively flexible hybrid element contained in SNAP. The stresses obtained for all programs agreed to within 1 percent for all cases.

The effect of problem size on core requirements for the three programs is shown in figure 3. The steep slope of the ELAS curve is due to the fact that ELAS requires the complete stiffness matrix in-core during execution. Both SNAP and NASTRAN are not limited by this requirement and, therefore, can handle fairly large problems in a minimum of core; the SNAP core requirement is the lesser of the two.

Total execution times for a number of configuration sizes are shown in figure 4 for SNAP and NASTRAN. ELAS times are not included because of problem size; however, for smaller problems, ELAS and NASTRAN execution times are similar. The top three curves indicate NASTRAN execution times increase with increasing problem size. These also show that time increases with increasing number of grid points per ring. The bottom three curves show run times for SNAP and indicate that on the contrary, execution times for SNAP decrease slightly with increase in grid points per ring.

For NASTRAN, the effect of grid points per ring on decomposition times is shown in figure 5. The sharp increase in decomposition time shows that if NASTRAN is to be efficient, the analyst must be able to minimize the problem bandwidth, preferably by the use of an automatic bandwidth minimization scheme such as BANDIT (reference 7).

The effect on solution times of using BANDIT to generate SEQGP cards for NASTRAN is shown in figure 6. The curve labeled NASTRAN 15.1.1 shows results for problem solutions without any resequencing. The curve labeled NASTRAN/BANDIT shows execution times of NASTRAN plus the execution times required by BANDIT which are shown in the curve marked BANDIT. These results show the benefits resulting from improved grid point sequencing. Also shown on the figure are execution times for SNAP which indicate that problem solution times are less than the times required to resequence grid points for NASTRAN, when SNAP is run with a good grid point elimination sequence. However, one must input the reduction sequence for SNAP as there are no available algorithms capable of doing this for the analyst.

The results discussed thus far have been restricted to computer time and storage. A more realistic comparison is to put computer resources on a cost basis. While computer cost algorithms vary among computing centers, any reasonable algorithm provides a basis for comparison. Cost presented herein was calculated by the cost algorithm currently used at the NASA Langley Research Center which takes into account operating systems calls (O/S calls), CPU time, and CORE.

A comparison of SNAP and NASTRAN computer requirements for a large problem consisting of 1530 grid points, 4415 elements, and 6106 D.O.F. is shown in figure 7. Both SNAP and NASTRAN were run in 160 000 octal core locations. As shown in the figure, NASTRAN requirements exceeded those for SNAP in all categories. In particular, the ratio of total time is about 5.3:1 while cost is approximately 4.5:1. These figures do not reflect the fact that BANDIT was run for NASTRAN to resequence the grid points in an effort to minimize NASTRAN costs, as SNAP was running under an optimum reduction sequence.

The above discussion focuses on the efficiency of the solution process. However, one must not exclude the other points made earlier (2. a-e; 3. a-e, p. 278), as they, too, must be considered in overall efficiency considerations. For example, if a design program is built around an efficient static analysis program, no capability will exist for mode shapes and frequencies. Thus, program generality may be as important as efficiency considerations. For such a case, NASTRAN is the only program of the three that has a broad range of analysis capability. The SNAP program has a free vibration counterpart, but at present, it is a separate program and requires regeneration of input.

User conveniences are also important if the analysis program is to be easily interfaced with a design algorithm. All of the programs have well documented, standardized input for which an input generating program may be developed to help reduce errors in input. All three programs also have some form of internal data checking with diagnostic error printout. However, only one of the programs, SNAP, allows the user to define desired output and on which files it should be placed. This is very desirable from the standpoint of automated design if different elements are designed at different times. Current theoretical documentation is adequate for NASTRAN only. NASTRAN and ELAS are operational on three machines, CDC, UNIVAC, and IBM, while SNAP is operational on CDC and UNIVAC. NASTRAN is being maintained under contract by

the NASTRAN System Management Office at Langley Research Center; SNAP is maintained by its developer; and ELAS is being updated by its author at Duke University.

#### CONCLUDING REMARKS

Three finite element programs were studied to determine their feasibility as the analysis tool in automated structural design. Due to problem size limitations, ELAS does not appear to be suitable for this purpose. The present speed of SNAP makes it desirable in a design environment where many repetitive analyses are required. However, the generality of NASTRAN may overshadow the fact it is less efficient than SNAP. Thus, one must weigh all present and future requirements before deciding on which program to choose. It should be clear, however, that bandwidth can have a significant effect on computer costs and perhaps NASTRAN should be extended to include a band optimization scheme, or the decomposition procedure should be improved. It is very likely that a complex design system could provide the option of using either SNAP or NASTRAN until NASTRAN is extended to provide the speed offered by SNAP.

#### REFERENCES

1. Sobieszczanski, J. E., and Loendorf, D. D.: A Mixed Optimization Method for Automated Design of Fuselage Structures. Presented at the 13th AIAA/ASME/SAE Structures, Structural Dynamics and Materials Conference, San Antonio, Texas, April 1972.
2. Utku, Senol: ELAS--A General Purpose Digital Computer Program for the Linear Equilibrium Problems of Structures. Structural Mechanics Series No. 11, School of Engineering, Duke University.
3. Whetstone, W. D.: Computer Analysis of Large Linear Frames. J. Str. Div., ASCE, ST11, Nov. 1969.
4. Butler, Thomas G., and Michel, Douglas: NASTRAN--A Summary of the Functions and Capabilities of the NASA Structural Analysis Computer System. NASA SP-260, 1971.
5. Whetstone, W. D., and Yen, C. L.: Comparison of Membrane Finite Element Formulations. Lockheed Missiles and Space Company Report #HREC 6-81-70-3, LMSC/HREC D162553, Huntsville, Alabama.
6. MacNeal, Richard H.: NASTRAN Theoretical Manual. Ed. NASA SP-221.
7. Everstine, Gordon C.: The BANDIT Computer Program for the Reduction of Matrix Bandwidth for NASTRAN. NSRDC Report #3821, March 1972.

TABLE I

## CAPABILITIES OF THREE FINITE ELEMENT PROGRAMS

<u>CAPABILITY</u>	<u>ELAS</u>	<u>SNAP</u>	<u>NASTRAN</u>
1. Complete Stiffness Matrix In-core	X		
2. Sparse Matrix Techniques		X	
3. Good Documentation	X <sup>0</sup>	X <sup>0</sup>	X
4. Static Solution	X	X	X
5. Dynamic Solution for Transient Loadings			X
6. Eigenvalue/Frequency Solution		X	X
7. Buckling			X
8. Cholesky Decomp.	X		X
9. Symmetric Gaussian Elimination		X	
10. Automatic Bandwidth Minimization	X		X <sup>1</sup>
11. Plot Capability (Undeformed & Deformed)		X	X
12. Restart/Checkpoint		X	X
13. Large Family of Users	X		X
14. Multiple Loadings		X	X
15. User Determined Output		X <sup>2</sup>	
16. Interface Capabilities Good	X		
17. Many Element Types	X	X <sup>3</sup>	X

<sup>0</sup> Input/Output only

<sup>1</sup> BANDIT is available for external re-sequencing

<sup>2</sup> Specific files may be designated

<sup>3</sup> Pian hybrid formulation for plate membrane and bending formulations

2/2/70  
11/1/70  
10/1/70  
9/1/70

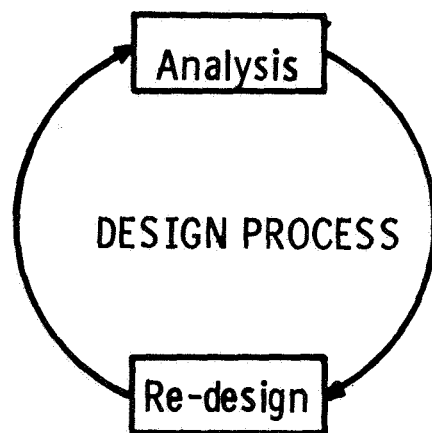
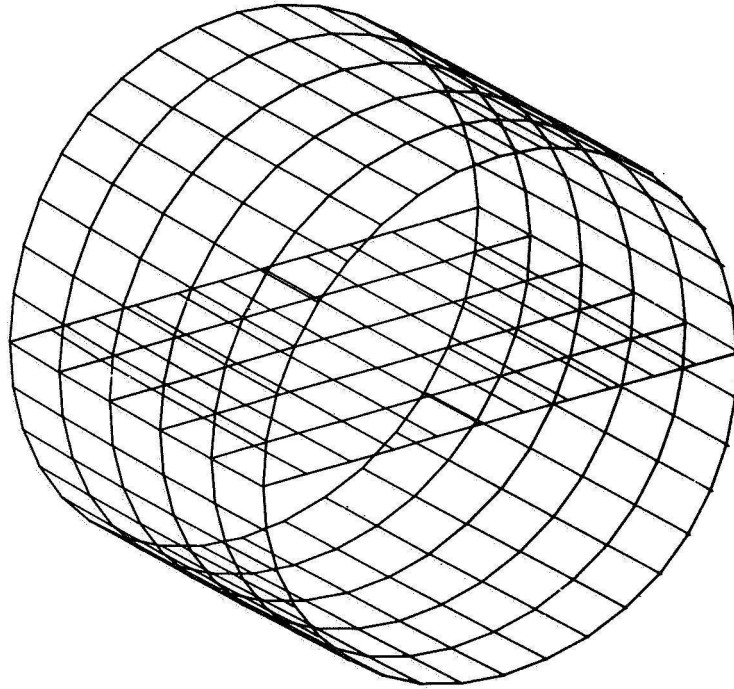
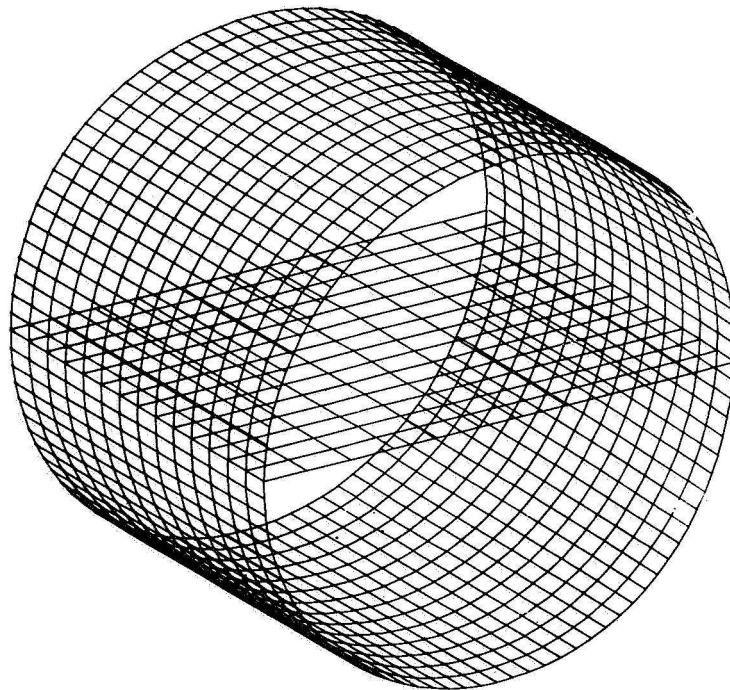


Figure 1. - Simplified schematic of the design process.



276 Nodes 1098 D.O.F. 752 Elements



1530 Nodes 6114 D.O.F. 4415 Elements

Figure 2. - General Configurations.

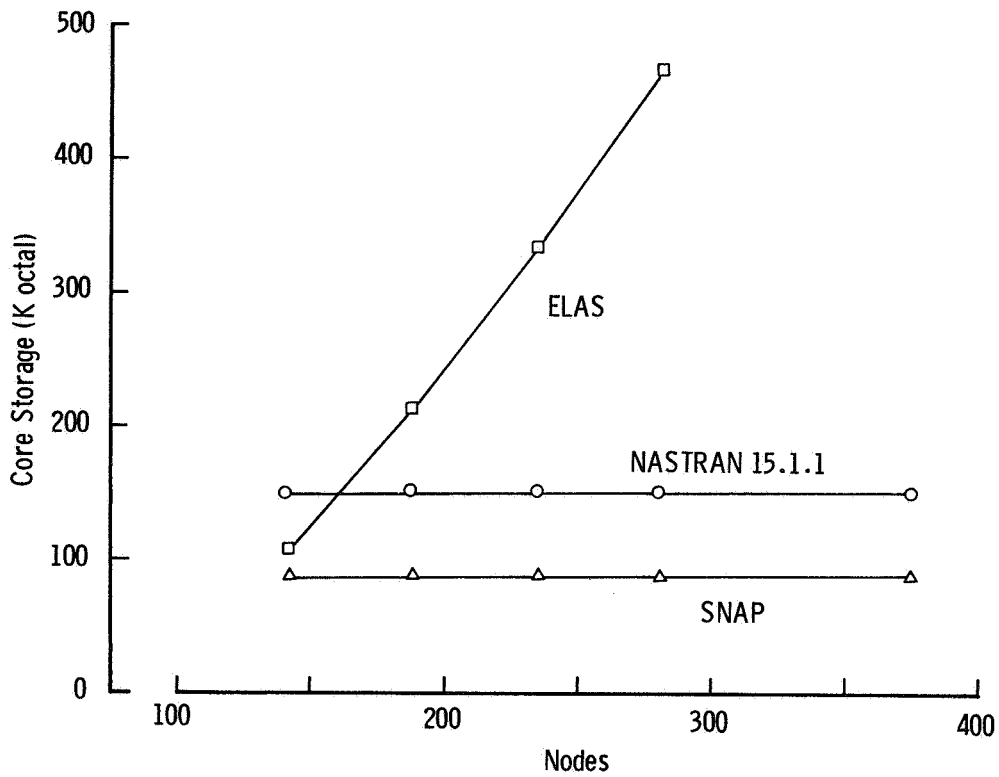


Figure 3. - Core requirements for various problem sizes.

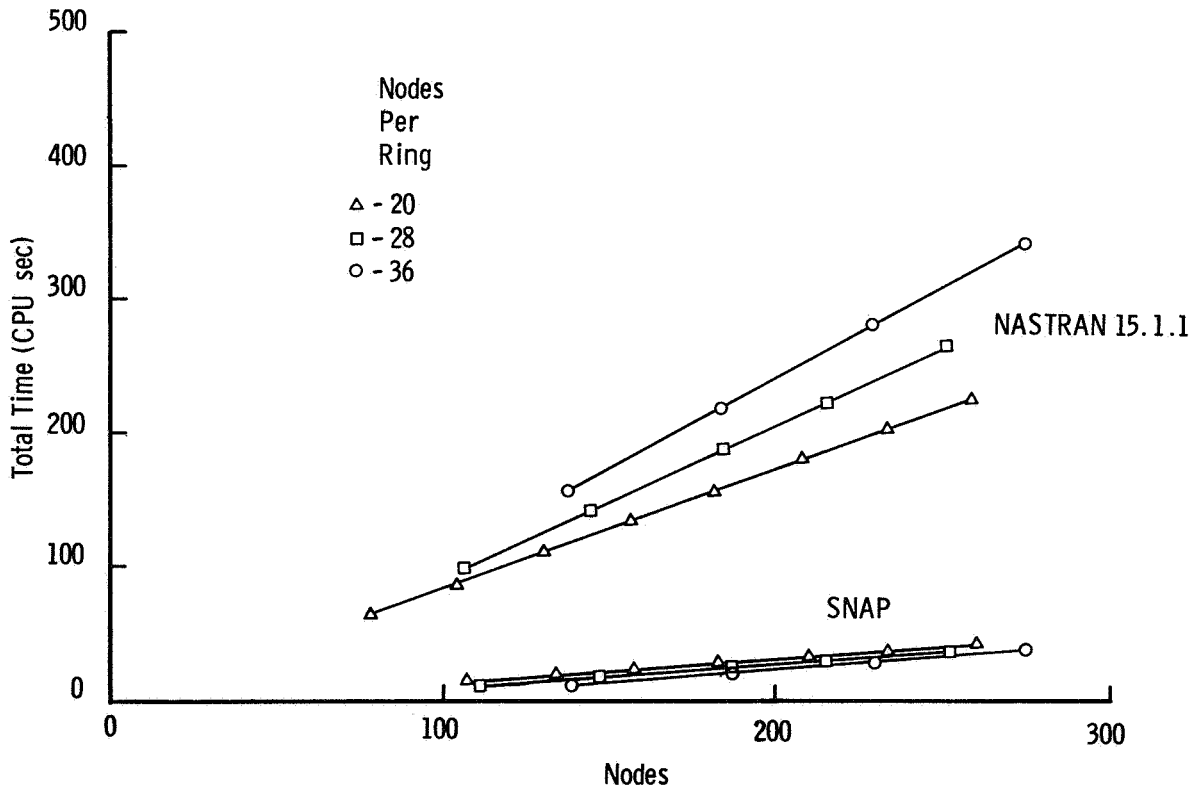


Figure 4. - Total CPU time for various numbers of circumferential nodes.

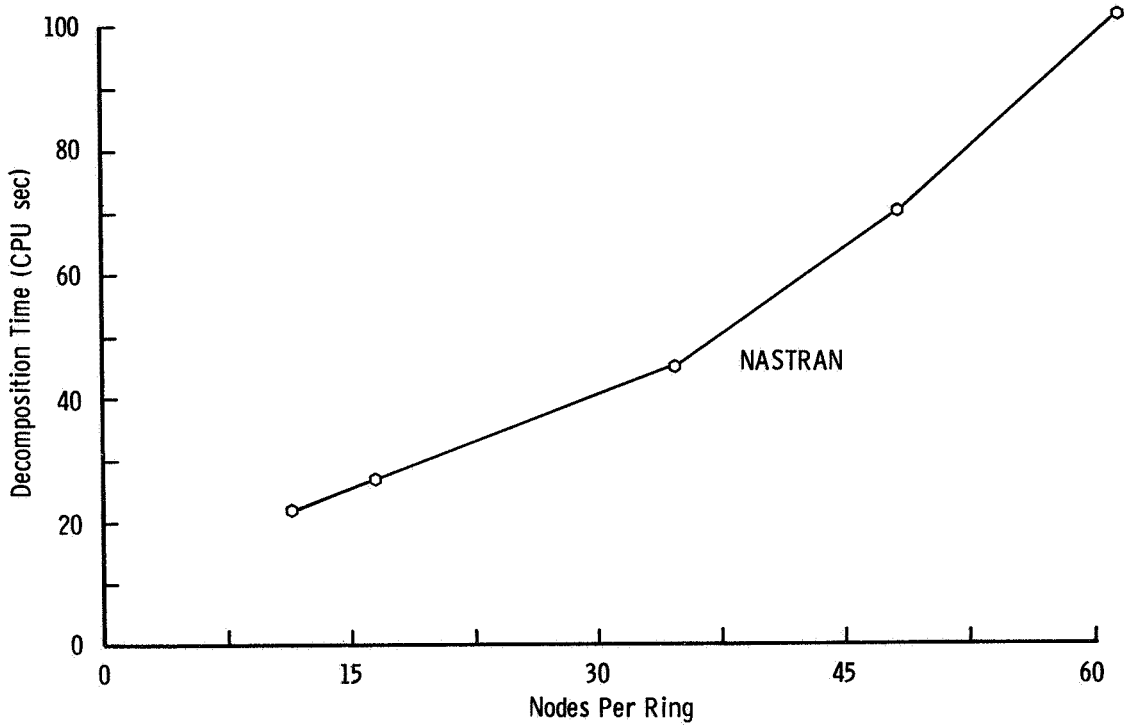


Figure 5. - Effect of nodes per ring on decomposition time.  
(Total nodes held constant)

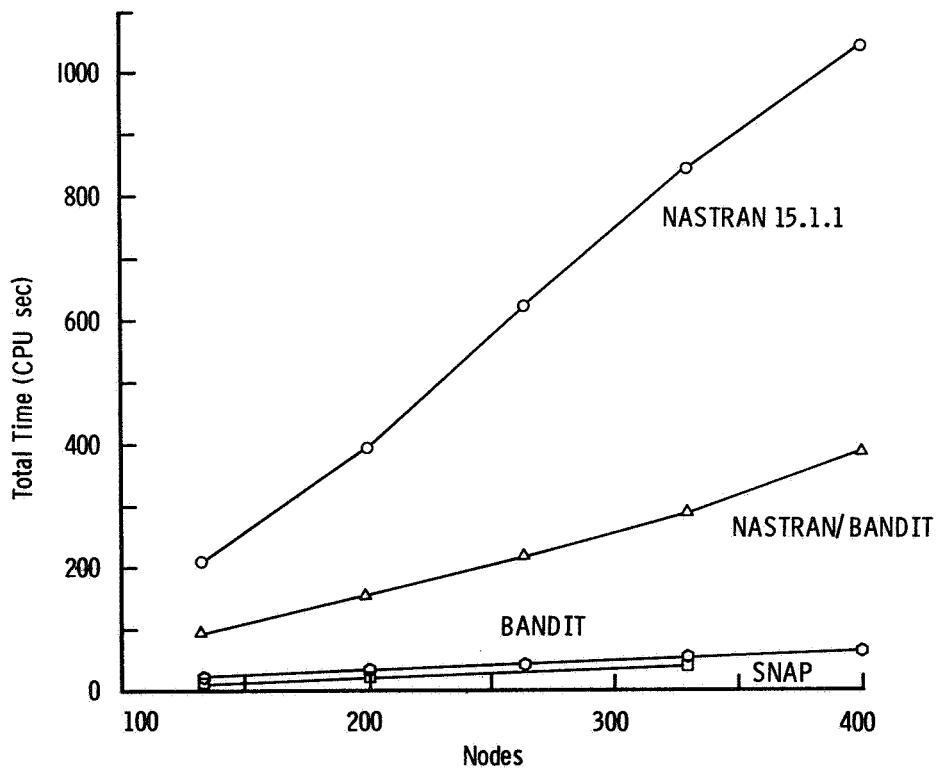
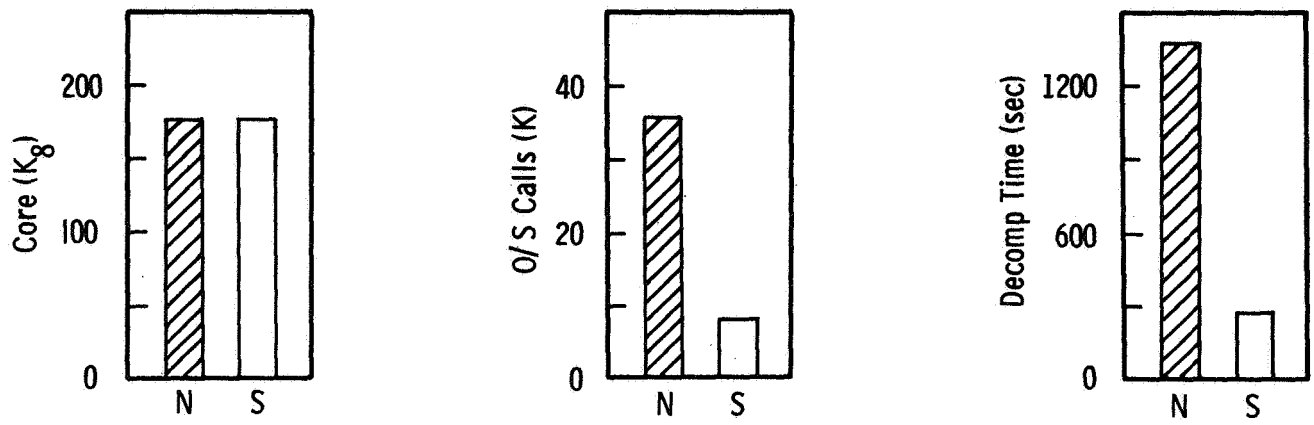


Figure 6. - Effect of BANDIT on NASTRAN 15.1.1 execution time.  
(52 nodes per ring)



N - NASTRAN 15.1.1

S - SNAP

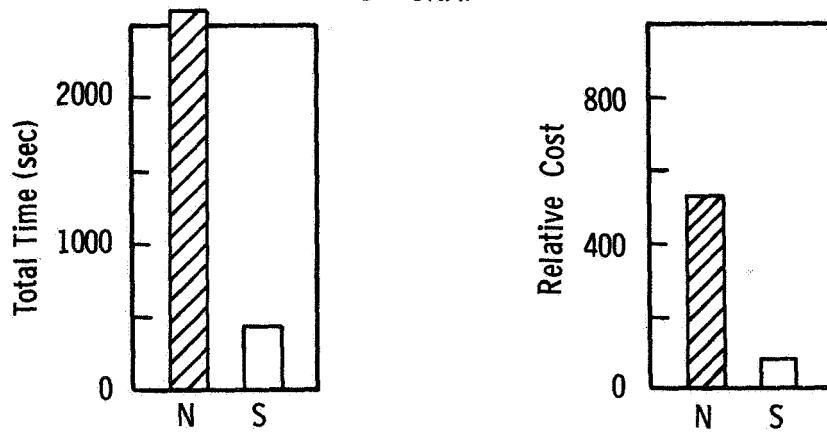


Figure 7. - Comparison of SNAP and NASTRAN computer requirements. (1530 grid points, 6102 D.O.F., 4415 elements)



ADAPTATION OF NASTRAN TO AN INTEGRATED SYSTEM OF  
STRUCTURAL DESIGN ANALYSIS

By Gernot W. Hagenmacher  
Lockheed-California Company  
Burbank, California

ABSTRACT

This paper discusses efforts to integrate NASTRAN into a complete structural analysis system for use by large airframe design projects. The Lockheed-California Company is implementing the use of NASTRAN as a major finite element structural analysis program to determine the static and dynamic behavior of complete airframes as well as structural components. This requires modifications and additions to NASTRAN, to communicate with an existing system, and to provide facilities needed to work within the integrated structural analysis. For this purpose several special DMAP modules were developed and introduced into the CALAC version of the NASTRAN system.

INTRODUCTION

The decision to use NASTRAN as a major analysis tool, implicitly leads, in our opinion, to the need for the user-company to actively pursue to a degree its own development of the program system. Regardless of the quality of the available system, the time will soon arrive when specific company priorities do not coincide with the more general priorities of the NASTRAN Systems Management Office. At this time the company will be forced to respond with either additions and/or modifications to NASTRAN, or development of its own system. In the latter case, its use of NASTRAN would tend to diminish. If used actively, it thus appears unavoidable that a company version will emerge, which deviates, in a variety of aspects, from the officially released NASTRAN level.

The introduction of NASTRAN as the major program to analyze the elastic behavior of the structure required its adaptation and connection into the complete structural system analysis process for determining the response of the aircraft. The purpose of the complete system is the analysis of the environment which has a bearing on the structural integrity of the aircraft. Analyses to be performed include flutter, steady and transient maneuver loads, gust and ground response, and their effects on internal loads, stresses and deflections.

This adaptation requires the integration of NASTRAN with the existing set of computer codes which provide these analyses and which are complementary to the NASTRAN structural analysis program. Modifications and additions to NASTRAN are made in a manner designed not to interfere with existing NASTRAN capabilities and operations nor with potential NASA directed improvements.

While it may be easy to agree on what constitutes a structural analysis system in its totality, agreement on the priorities of specific developments of NASTRAN may not. It is likely to be an entirely different affair for NASA than it is for any one of the industrial users. The readiness of any company to fully accept NASTRAN as a standard system depends on its own in-house programs and the ease with which the former can be modified and adapted without loss in efficiency.

The present paper is therefore an example only of what the Lockheed-California Company has done, and is planning to do in the immediate future, to join NASTRAN as a major (but not the only) finite element analysis program to its structural analysis system.

A discussion of this nature may serve to stimulate ideas and contribute to the formation of system specifications from the practical operation aspects of large aircraft design. It may also revive a concept voiced in last year's meeting, which proposed an industrial user organization working in conjunction with the System Management Office in matters concerning further development of NASTRAN. (See Ref. 1.)

## 1. AN INTEGRATED STRUCTURAL DESIGN ANALYSIS SYSTEM

To discuss an integrated structural design analysis system we must define its scope and then determine the role of its parts and programs which are to perform its various functions.

### 1.1 The Total System

The system which will be described here briefly has in similar form been considered throughout the industry. The total analysis system may be said to consist of the complete environment which affects the structural integrity of the aircraft. As such it must incorporate the following major design analysis facets:

1. Structural deformation and stress analysis by finite element methods
2. Weight accounting and mass matrix
3. Aerodynamic forces
4. Static and dynamic loads and design conditions
5. Flutter analysis
6. Detail stress analysis
7. Design strength allowables and margins of safety.

### 1.2 The CALAC Analysis System

To discuss the activities and the plans of the Lockheed-California Company (CALAC) for development of the NASTRAN system, we should review the structure of the in-house analysis process as it presently exists. This includes NASTRAN as a major finite element analysis tool, which is fully operational and has been used for several important analysis jobs. The concept of the completed system is shown on Table 1.

The Lockheed-California Company's structural analysis operations are based on its extensive system of matrix algebra and functional modules, called FAMAS. The FAMAS system, originally an acronym for Flutter and Matrix Algebra System,

has been developed at CALAC and has been expanded in scope far beyond these narrow limits. This system includes the CALAC finite element programs of the force method and several displacement method programs of lesser scope than NASTRAN. These are now gradually being replaced by NASTRAN.

The FAMAS system has completely compatible matrix input/output within all its programs, contains a very extensive matrix algebra and manipulation system, and a large family of functional modules for aerodynamic loads, structural response and flutter analysis, which are of prime importance in the present context. The system was extensively used during the SST design study, L-1011 and S-3A programs. It is operated by a simple program calling system, and has also a compiler for programming strings of matrix equations much like FORTRAN algebraic expressions. The general capabilities of this system are summarized on Table 2. In some algebraical and functional modules the NASTRAN and FAMAS systems contain duplicate capabilities. In general, however, they supplement each other extensively.

A variety of theories are used in FAMAS to calculate aerodynamic force influence coefficient matrices, including important procedures to update theoretical values with experimental flight and wind tunnel data. A paper given by John Lewolt of CALAC at the August 1972 meeting of the AIAA, Reference 2, discusses this capability in considerable detail.

The FAMAS input/output compatibility permits any matrix, specifically stiffness-, flexibility-, aero- and mass- matrices, resulting directly from a previously executed program module, or from data storage, to be used, as in NASTRAN, as input to subsequent vibration, load and flutter analysis. Any design load matrix thus generated can be fed into an airplane finite element structural analysis program for determining internal loads, stresses and deflections. Any matrix, for example, stress matrices, can be scanned row by row, that is, element by element, for the most critical columns (design conditions), or can further be processed. In addition, FAMAS stress matrices can be fed into special programs for comparison with data banks of design allowables to calculate margins-of-safety.

The complete analysis sequence can therefore be performed by computer operations without unnecessary human transcription or other handling of data block communication between programs. As many analyses steps as desired and practical can be performed in a single job submittal to the computer. Interruptions of the automatic computing flow are dictated principally by the need to check intermediate results and introduce human judgement. When the capabilities of the FAMAS system are joined by the finite element analysis capabilities of NASTRAN through an automatic data communication, a powerful integrated analysis system will be the result. Table 3 shows a summary of the capabilities of the combined system, which communicates through tape and disc storage without human data handling.

### 1.3 NASTRAN's Part in the System

The part which NASTRAN is playing in the combined system includes, of course, all its finite element analysis capabilities in static, dynamic, and structural stability, excepting special problems where separate programs may be preferable. There are however, some problem areas within NASTRAN itself which we feel must eventually be resolved to make its use as a tool for

finite element analysis of aircraft structures better adapted to project needs. These concern, in our view, the following major areas:

- o Extended analysis checking capabilities for force equilibrium and improvement of checking and location of matrix singularities.
- o Improved stress analysis capability primarily through the addition of finite elements with better stress definition within the standard degrees of freedoms.
- o Substructure coupling is of great importance for large airframe analysis; methods to streamline the present capability of NASTRAN in this field are being pursued at CALAC.

## 2. NASTRAN MODIFICATIONS AND ADDITIONS

Several new DMAP modules were added into NASTRAN, those which serve the specific purpose of connecting NASTRAN with FAMAS, and those which were needed to amplify its operational capability and flexibility within the CALAC analysis system. The Job Control Language (JCL) in the IBM-360 system permits a single, uninterrupted job run from either NASTRAN into FAMAS, or vice versa. This provides adequate operational flexibility, since interruptions for the purpose of intermediate data checking are required anyway.

### 2.1 The Process of Adaptation of NASTRAN

The new facilities designed to complement the integrated system were added as DMAP modules into the NASTRAN system. The following general principles were applied in adding the required features.

- o The modification of existing NASTRAN modules and their operation under the original NASTRAN calling code name was avoided. Instead a new DMAP module under a new calling code was formed, consisting, if necessary, of original subroutines as well as new subroutines. This prevents the disruption of basic NASTRAN capabilities in the rigid formats even if NASA makes changes in the basic modules at a later date.
- o Similarly, variations or additions to existing tables were given new identities, with a format identical or similar to the existing one if feasible.
- o To avoid (for the time being) the need to define many new bulk data cards, and the ensuing complications, pitfalls and delays, it was decided to input special data types by means of the direct input tables DTI. These can fairly well be accommodated to a card format similar to bulk data type cards. This method also avoids accidental collision with new bulk cards introduced by NASA. However, since bulk data cards are preferable, an agreement of NSMO, reserving some special code letter for user card types might be advantageous.
- o Since the special NASTRAN modules added will not be used frequently in the many standard applications, they have not at this time been introduced in any rigid formats, but are, when needed, inserted instead of, or in addition to, regular DMAP sequences by ALTER sets.

## 2.2 New CALAC-NASTRAN Modules

To accomplish the connection between the NASTRAN and FAMAS systems, and provide the additional operational flexibility necessary, a series of special CALAC-NASTRAN DMAP modules have been added or are in preparation for the following functions.

1. User designated data blocks for input or output onto tapes (INPUTT, OUTPUT)
2. NASTRAN-FAMAS interface matrix transcription (FAMASIO)
3. Element force and stress output table are written into NASTRAN matrix format (ELMAT).
4. Generation of a case control tables for large numbers of load cases internal to NASTRAN, based on the content of the displacement matrix (LDCONTROL).
5. Rewriting of NASTRAN matrix print output format, and punched card input in the FAMAS format (MATPRN).
6. Development of a gridpoint load matrix and mass matrix balanced for a given external load location (LOADGEN).
7. Formation of a diagonal matrix (DIAGMAT).
8. Generating multipoint constraint conditions (MPCGEN) (planning stage).

The principal function and techniques of these new modules are described in more detail below.

### 2.2.1 INPUTT and OUTPUT Modules

The user designated tape input and output, already discussed in last year's colloquium, were written for CALAC by MacNeal-Schwendler Corp. These modules are briefly discussed again. The two modules permit user designated data blocks to be written on, or input from tape at any suitable DMAP sequence location, into a NASTRAN run from other than, or in addition to, the checkpoint restart tape. With this capability previously calculated data can be read into a single run from as many different tapes as the computer equipment permits. This is a prime requirement for substructure coupling, but has many other useful operational possibilities.

### 2.2.2 NASTRAN-FAMAS Interface

The item of prime importance to the integration of NASTRAN with the CALAC system is the interface module. A DMAP module, FAMASIO, accompanied by appropriate Job Control Language, permits rewriting any set of NASTRAN matrices into the FAMAS format onto a FAMAS system tape, and subsequently continuing with any matrix operation sequence in the latter system. Similarly, it is possible to start with an operational sequence in FAMAS, transit into NASTRAN, using FAMASIO to copy the matrices into the NASTRAN format for continuation and conclusion of the run in NASTRAN with any type of rigid format or DMAP operation. The importance of this step is visible from Table 4.

In this fashion all the design load analysis capabilities of the FAMAS system are joined with the finite element analysis capabilities of NASTRAN. Similarly, NASTRAN stiffness or structural flexibility matrices, vibration mode vectors, etc., can be used in direct link with the flutter analysis system in FAMAS, as well as the aero-elastic loads calculations.

### 2.2.3 Element Force and Stress Matrices

The conversion of the NASTRAN element force and stress tables into matrix format has several applications. At present this has been completed for ROD, BAR, and SHEAR elements. The stress matrix contains a column vector for each subcase. The rows correspond to element stresses, row numbers are related to element numbers according to a key given by parameters of the module. In the simplest form the row number is identical to the element number. The most important aspect within the CALAC structural analysis system is the transcription of complete stress or force tables into matrix form for subsequent transfer, with FAMAS $\phi$ , into the FAMAS system, where they are used in an existing scanning program. This program scans each row of a matrix (the stress at one point) for, say, the six largest positive values and the six largest negative values. This provides a quick picture of critical design conditions in a given region of the structure.

The formation of NASTRAN element force and stress matrices also permits, through FAMAS, the use of a variety of margin-of-safety- programs in conjunction with data banks of stress allowables.

### 2.2.4 Case Control Module

To appreciate the significance of this module it is first necessary to explain the arrangement of design load matrices as generated in FAMAS and transcribed into NASTRAN. The total number of columns in the matrix is usually over a thousand, with each column number permanently assigned to a specific load condition. The thousand-order matrix is fairly sparse, only the few hundred columns corresponding to load conditions critical in the region analyzed being occupied. Inches or feet of meaningless output for null conditions can be avoided in NASTRAN with an extensive case control, shown below. One subcase is called out for each column of the displacement matrix UGV.

#### Case Control

MPC  
SPC

Subcase 1  
Subcase 2           Null Cases  
Subcase 3

Subcase 4  
OLOAD  
SPCFORCES           Non-null Case  
ELSTRESS  
ELFORCE

Subcase 5           Null Cases  
Subcase 6

etc., for as many subcases as columns in UGV.

Writing the control cards for these thousands of subcases would be tedious work spiked with potential errors, and requiring previous knowledge of the location of occupied columns in the load matrix transcribed from FAMAS. The module LDCONTROL is designed to eliminate the human element from writing this case control language. The solution vector matrix UGV for the load matrix, read in from FAMAS in lieu of the NASTRAN solution generator module SSG1, can be obtained by a single fictitious LOAD call in CASE CONTROL.

This new module LDCONTROL is ALTERED into the rigid format of NASTRAN just prior to the solution data recovery module SDR2. It scans the column headers of the displacement matrix UGV for null and non-null columns, and writes the extensive case control table in the format of NASTRAN CASECC, but now designated LDCASE. Using this control table in SDR2 in lieu of CASECC results in output tables for non-null conditions only, avoiding all output of zero conditions. The subcase numbers identifying the NASTRAN output table are identical to the column numbers of the non-null vectors in the original displacement vectors UGV.

The stress matrix module picks up the subcase numbers from the stress output tables to form stress columns identified, therefore, by the same numbers as the displacement vectors.

#### 2.2.5 Matrix Print Output and Card Input

The standard NASTRAN matrix input (DMI) and print output (MATPNT) were found to be somewhat inconvenient, the print identification of rows and columns not providing a clear picture. Intermediate and end result checking require an easily readable matrix print format. Non-rigid format operations require an easy tabular form for input. A new matrix card input was provided using the various CALAC matrix input forms. The NASTRAN matrix print MATPNT output was replaced by the standard CALAC-FAMAS format. This output identifies the column and row numbers of all non-zero terms, and does not print zero terms. This eliminates the need to count lines when searching for specific elements and is much easier to read. A comparison of the two matrix output formats is shown on Tables 5 and 6.

#### 2.2.6 Load and Mass Matrix Generation

A DMAP module LOADGEN has been designed to generate gridpoint load column vectors which load a given limited set of gridpoints, and which are in balance with a given general load vector at a given, non-gridpoint, location. To explain the rationale and the function of this module we review the transition from the loads or mass network to the structural network. The two networks are hardly ever congruent, and therefore a transformation is required. Also the use of the NASTRAN mass matrix generation facilities is impractical for large aircraft parts. To relate the mass with model element properties, where the structural weight is less than 25% of the total aircraft weight, and to keep the mass data for the structural-dynamic analysis consistent with the weight accounting of the vehicle is an almost insurmountable task of manual calculation and bookkeeping.

It was found necessary to form directly a gridpoint mass matrix which is consistent with weight accounting data. Coordinates of all gridpoints are available in NASTRAN, total mass and centroid locations of suitably small aircraft regions are given by the weight accounting system. The same type of

data are available for design loads, which are assumed uniform over given regions with an established load centroid; the loads network usually is established by criteria for aerodynamic loads calculations and does not correspond to the structure.

The procedure adopted in the present program to determine gridpoint loads uses the following principle: A (mass) weighting is judiciously assigned to each NASTRAN gridpoint of a selected point set. The centroid and the inertias of the weighted point set are determined, the given load vector is transformed from its location to the CG of the point set. This imparts an acceleration to the point set, which in turn determines inertia forces in the gridpoints from which the load column is formed. While this approach is very general and flexible, its successful use depends on the rationale used to input the gridpoint weighting factors, and requires careful evaluation of the resulting load vector. It can best be used in connection with an interactive or graphic input-output system. Additional work in this area is yet required to determine suitable algorithms to mechanize the determination of a rational gridpoint weighting based on the aircraft geometry and weight accounting.

The completed result of this procedure is a load matrix  $[L_p]$  in all the unconstrained D.O.F. for  $p$  unit load or unit mass regions. A linear combination of these columns results in a proper design condition for the structural model.

$$\{PG\}_{c,1} = [L_p]_{c,p} * \{Pd\}_{p,1}$$

$[L_p]$  is the transformation matrix between structural network and aero-loads network.

$\{Pd\}$  is a design load case in the loads network.

A multiplication with regional masses  $\{Ms\}$  results in a column of gridpoint masses

$$\{MG\} = [L_p] * \{Ms\}$$

Conversion of  $\{MG\}$  into a diagonal matrix results in a diagonal mass matrix  $[MGG]$  for the structural model. The module and the corresponding DMAP instructions can be ALTERed into a rigid format to replace either or both of SMA2 and SSG1 functional modules which generate the mass and the gridpoint load matrices respectively.

### 2.2.7 Diagonal Matrix

A minor but operationally useful facility was the design of DMAP module DIAGMAT which rewrites any column of a NASTRAN matrix on the diagonal of a square matrix of same order. Alternatively it generates a diagonal matrix of given size and given scalar value.

### 2.2.8 Multipoint Constraint Equation Generator

A module for this purpose is in the study stage. Final plans at CALAC will depend heavily on what the detail plans of the NSMO are. There are several requirements which should in our opinion be considered in the

generation of multipoint constraint equations. These are based on our experience with the MPC system and are summarized as follows:

- o The MPC equations facility are an extremely versatile feature with a wide range of applications. Means should be investigated to reduce the computer time expenditure for large systems.
- o It should be made possible to input the MPC equations in any of the defined coordinate systems, performing the necessary transformations into the global system internally to the program.
- o MPC equations can be generated internally based on one or more (connected) elements which are made rigid to create a full rigid body. There is however a necessary special feature, which might be called a semi-rigid body, which has significant advantages. Such a situation results when only part of the independent element variables of the elements used are declared rigid. Thus, for instance, if BAR elements are used to build the semi-rigid body, only bending in one plane of an element may be rigid.
- o Another capability to form MPC equations may be provided, which is the result of a force equilibrium condition between the loads in the independent D.O.F. and the force in the dependent freedom.

The theory of the necessary relations has been established and the detail program requirements are now being worked out. The decision to go ahead with programming will depend on NASA's plans in this area.

#### CONCLUSIONS

The previous discussions give some examples of the type of development which we at CALAC feel a user-company has to undertake if it intends to adopt NASTRAN as a major part of its structural analysis system. The use of NASTRAN at the Lockheed-California Company is steadily increasing, but so is the need for in-house development of NASTRAN.

It is evident that NASA is continuing to pursue the development of capability improvements of a general nature. However, we feel strongly that an active user-company will find it necessary to become intimately familiar with the NASTRAN system in order to enable it to successfully develop the capabilities within NASTRAN needed to fulfill its particular requirements.

#### REFERENCES

1. NASTRAN User's Experiences, September 1971, NASA TM X-2378.
2. W. A. Stauffer, J. G. Lewolt, and F. M. Hoblit, "Application of Advanced Methods to the Determination of Design Loads of the Lockheed L-1011 TriStar," AIAA 4th Aircraft Design, Operations and Flight Test Meeting. 7 August 1972. AIAA 72-775.

TABLE 1

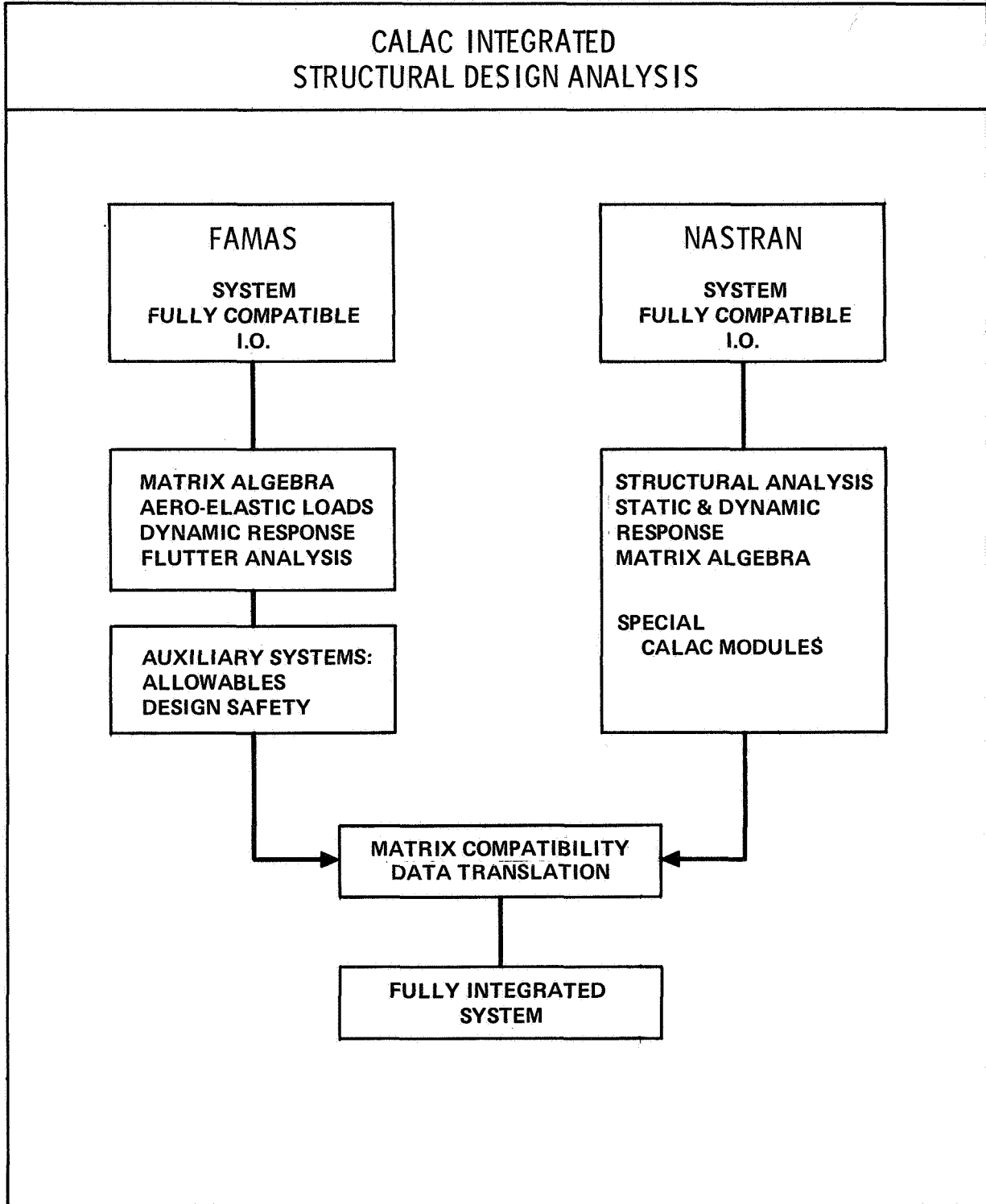


**TABLE 2**

**CALAC – FAMAS SYSTEM**

**\* EXTENSIVE MATRIX ALGEBRA & MANIPULATION APPROXIMATELY 50 MODULES**

**\* SEVERAL FAMILIES OF FUNCTIONAL MODULES FOR AERO-ELASTIC ANALYSIS  
(See Ref. 2)**

**● AERODYNAMIC LOAD-DEFLECTION INFLUENCE MATRICES**

- Lifting line theories.
- Mach Box (Supersonic)
- Kernel Function
- Doublet Lattice
- Vortex Lattice
- Piston theory
- Reduction of wind-tunnel data and subsequent correction of theoretical matrices.

**● STABILITY DERIVATIVES**

**● MASS-MATRICES**

**● MODAL ANALYSIS, VIBRATIONS**

**● FLUTTER ANALYSIS**

**● AIRCRAFT LOAD ANALYSES**

- Steady
  - Transient
- } maneuvers
- Dynamic Gust Response  
Incl. Power Spectral Density Methods
  - Ground Handling & Landing Impact Response

TABLE 3 INTEGRATED STRUCTURAL DESIGN ANALYSIS SYSTEM

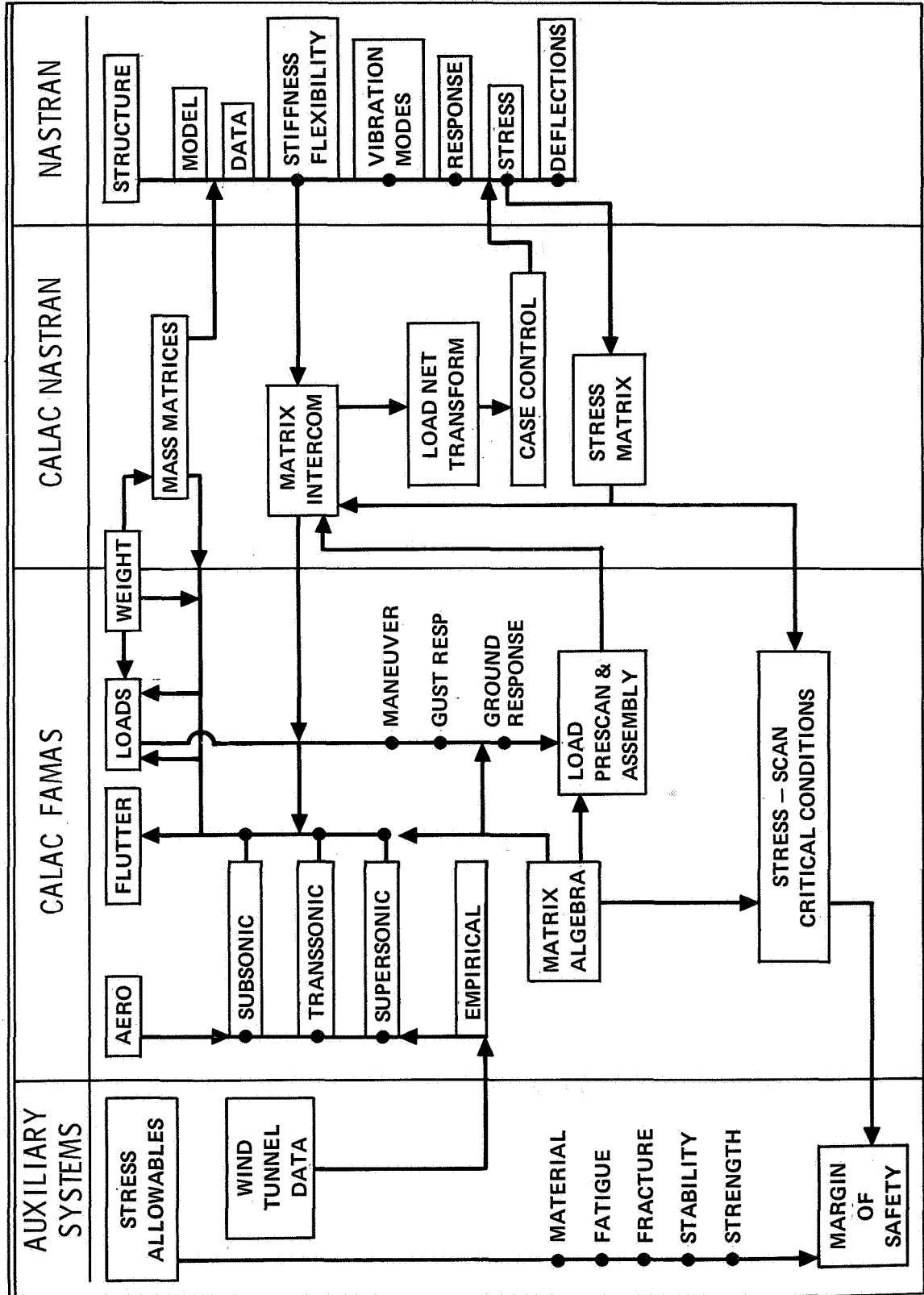


TABLE 4

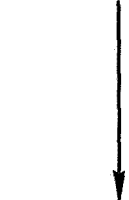
EXAMPLE OF A COMBINED NASTRAN – FAMAS OPERATION

**RUN 1**

NASTRAN CONTROL



- NASTRAN STRUCTURAL DATA
- CONSTRAINED STIFFNESS OR FLEXIBILITY MATRIX
- NASTRAN CHECKPOINT
- MATRIX OUTPUT IN FAMAS FORMAT (FAMASIØ)



NASTRAN – FAMAS  
INTERFACE

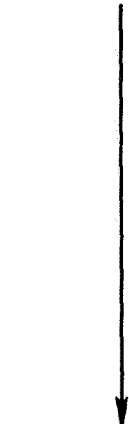
END RUN 1

**RUN 2**

FAMAS CONTROL



- FAMAS DATA
  - MASS MATRICES
  - AERO MATRICES
  - READ "NASTRAN" STIFFNESS MATRIX
  - MANEUVER
  - GUST RESPONSE
  - GROUND RESPONSE
- } PROGRAMS
- DESIGN CONDITION MATRICES



FAMAS – NASTRAN  
INTERFACE

NASTRAN CONTROL



- CHECKPOINT RESTART FROM RUN 1
- READ FAMAS LOAD MATRICES (FAMASIØ)
- CONCLUSION OF NASTRAN STATIC ANALYSIS . OUTPUT

END RUN 2



COMPARISON OF NASTRAN AND STARDYNE  
STATIC ANALYSIS OF A GRAPHITE FIBER  
REINFORCED PLASTIC TRUSS STRUCTURE

By George H. Honeycutt, Frank J. On,  
and Stuart L. Hanlein

NASA Goddard Space Flight Center

SUMMARY

A static and buckling analysis of the ATS-F&G spacecraft reflector support truss (RST) and bridge truss assembly using NASTRAN has been conducted. The RST is fabricated from a new material, graphite fiber reinforced plastic. A comparison is made with the NASTRAN results and the results of a similar analysis conducted using the STARDYNE program. The results of an actual static load test are also compared.

INTRODUCTION

The ATS-F&G are a new generation of communication spacecraft. The predominate feature of these spacecraft is a 30 foot parabolic dish high gain antenna as can be seen in Figure 1. The reflector dish must be accurately aligned with the feed system and this alignment must be held throughout the spacecraft life. Because of this rigid alignment requirement, a new material, graphite fiber reinforced plastic (GFRP), was selected for the reflector support truss (RST) between the feed system and the parabolic reflector. The GFRP was chosen because of its extremely low coefficient of thermal expansion and its high stiffness to weight ratio. Because of the newness of the material, particularly in an application as primary structure, there was concern about its capability to carry the launch loads. The present NASTRAN analysis was conducted to evaluate deflections, internal loads, and verify the adequacy of the RST design.

During launch the reflector dish is wound around a hub and the solar arrays are folded down as shown in Figure 2. In this configuration, the RST structure must support approximately 180 kilograms at the top. Static acceleration loads were applied to the RST structure as enveloping the dynamic loads during launch. The load cases were applied 9.0g thrust plus 3.9g lateral and -3.9g thrust plus 3.9g lateral. The desired results of the analysis were the buckling strength, internal member loads, and deflections.

The prime contractor for the ATS-F&G is Fairchild Industries (FI). They have used the STARDYNE program to conduct a similar analysis (Ref. 1) which allowed a comparison of results. Hercules Incorporated is the subcontractor for the RST. The results of a qualification static loads test conducted by Hercules (Ref. 2) also provided test information for comparison.

#### NASTRAN STATIC ANALYSIS

The results of the static analysis were obtained using Rigid Format One in the NASTRAN program. Figures 3 and 4 depict the finite elements used in synthesizing the NASTRAN model of the RST and bridge truss assembly. The overall model had 107 grid points, 200 elements and 618 degrees of freedom. Note that the dots (grid points) represent the selected points at which discrete masses are assumed to be concentrated, and the lines connecting these points represent bar elements.

In the analyses, the RST structure was assumed to be fixed to ground via the support fittings at the Earth Viewing Module (EVM). The material in the hub, bridge truss, reflector support ring and RST stabilizer is 6061-T6 aluminum. The material for the RST is graphite fiber reinforced plastic (GFRP). Element forces, bending moments, stresses, margins of safety and grid point deflections were obtained for two cases (Table 1) of applied loading. The two cases of loading corresponded to force and moment inputs at specific grid points and were derived from the acceleration loadings shown.

Significant results from the NASTRAN static analysis are presented in Figures 5 and 6, and Tables 2,3, and 4. Figures 5 and 6 show the deformed structure for the specified load cases. In Tables 2 and 3, the results are tabulated for the maximum compression and tension load members. Table 4 presents a summary of grid point deflections for Case 2.

#### COMPARISON OF NASTRAN AND STARDYNE STATIC ANALYSIS

A similar analysis for the same two static load cases as were investigated in the NASTRAN analysis was conducted by FI using the STARDYNE program. The STARDYNE results for the maximum compression and tension member loads and grid points deflections are also summarized in Tables 2, 3, and 4 for comparison with NASTRAN results.

In general, the NASTRAN and STARDYNE results show good agreement. Noted discrepancies in bending moment results may be attributed to differences in modeling details of the structure (e.g. in the STARDYNE analysis, the reflector hub ring was not included).

#### NASTRAN BUCKLING ANALYSIS

Buckling analysis for two maximum compression load conditions was investigated using Rigid Format Five of the NASTRAN program. These two load conditions corresponded to Cases 3 and 4 of Table 1.

From the buckling analysis results, the fundamental mode of buckling was well defined as can be seen in Figures 7 and 8. Figure 7 represents the fundamental buckling mode shape which corresponds to the eigenvalue of 4.22 for lateral load in the x direction (Case 3). For lateral load in the y direction (Case 4) the fundamental buckling mode which corresponds to the eigenvalue of 4.34 is shown in Figure 8. Since the eigenvalues are multipliers of the applied loads which will cause buckling in the fundamental mode, the results show that, in both load cases investigated, the actual applied load must be exceeded by a factor of four before buckling will occur.

#### STATIC LOAD TEST

The prototype RST was tested to qualification load levels by Hercules Incorporated (Ref. 2). The test setup is shown in Figure 9. The truss was rigidly fastened at the base and a simulated bridge truss was mounted on the top. The compression and/or tension loads were produced by the two hydraulic rams. The lower hydraulic ram produced a load in the axial direction and the upper ram produced a moment or shearing load. Dial indicators and linear potentiometers were located at the top of the RST and at the stabilizer ring to record displacements. Thirty-six strain gages were attached to the GFRP tubes and fittings at critical locations. The loading of the structure was in steps of 25%, 50%, 80%, 90% and 100% of full load. The axial and lateral loadings were applied simultaneously. The truss was tested both in axial compression and tension with transverse loading in the +x and -x directions. Then the entire truss assembly was rotated 90° and the truss was tested again in axial compression and tension with transverse loading in the +y and -y directions. Thus a total of eight combined loading tests were conducted.

## COMPARISON OF TEST RESULTS WITH ANALYSIS

Figure 10 compares the deflection test data and the NASTRAN predictions for Case 1 (see Figure 5). The test data were "normalized" since the actual test was conducted at qualification levels. The variations from the predicted values at the higher load levels are due primarily to difficulties in reading the instrumentation. The durations of the higher load levels were not long enough to allow the dial indicator gages to stabilize.

The maximum internal tube load determined from the strain gage data was 24,768 newtons which compares well with 25,760 newtons from the STARDYNE program and 24,470 newtons from the NASTRAN program. It is felt that a more detailed model of the composite material would give better values for the loads along the tubes.

## CONCLUSION

The comparison of the results between NASTRAN and STARDYNE was good. The differences in the results were due to slight differences in the modeling techniques. It must be pointed out that the model was fairly simple with bar elements only used throughout. With more complex structures and different elements, the comparison of results might not be as good.

The comparison with test results was also good. It is believed that a more detailed finite element model of the composite material would yield more accurate comparison with strain gage test data.

## REFERENCES

1. Informal Communication from Fairchild Industries. November 1971
2. "Qualification Test Report, Prototype Reflector Support Truss for Applications Technology Satellite." Hercules Incorporated, SC 71-6. November 11, 1971

TABLE 1  
Applied Load Cases

Case No.	Direction			Remarks
	X	Y	Z	
1	-3.9g	0.0g	9.0g	Force and Moment Equivalent to FI STARDYNE Input
2	-3.9g	0.0g	-3.9g	
3	-3.9g	0.0g	9.0g	Acceleration Loading Buckling Analysis
4	0.0g	-3.9g	9.0g	

TABLE 2  
Comparison of NASTRAN and STARDYNE Results for Case 1  
Maximum Compression Loads

End	Quantity		Axial F N	Shear V <sub>1</sub> N	Shear V <sub>2</sub> N	Torque T N-cm	Moment M <sub>1</sub> N-cm	Moment M <sub>2</sub> N-cm
	Element Number							
A	134	NASTRAN	-24469.7	-38.7	25.4	-50.8	-5412.0	-5570.2
		STARDYNE	-25759.7	-28.0	24.0	103.9	-5784.8	-3423.4
B	134	NASTRAN	-24469.7	-38.7	25.4	-50.8	-316.4	-3129.7
		STARDYNE	-25759.7	-28.0	24.0	103.9	-316.4	-2949.0
A	150	NASTRAN	-23.1	0.9	-12.4	7.9	474.5	90.4
		STARDYNE	-20.9	-0.9	-11.1	-10.2	418.0	22.6
B	150	NASTRAN	-23.1	0.9	-12.4	7.9	463.2	-11.3
		STARDYNE	-20.9	-0.9	-11.1	-10.2	418.0	-79.1
A	151	NASTRAN	-51.6	0.0	-37.4	-9.0	926.5	-1.1
		STARDYNE	-37.8	3.6	-39.6	11.3	971.7	101.7
B	151	NASTRAN	-51.6	0.0	-37.4	-9.0	903.9	0.0
		STARDYNE	-37.8	3.6	-39.6	11.3	972.8	67.8
A	142	NASTRAN	-24443.0	-25.4	20.0	45.2	-327.6	2022.4
		STARDYNE	-25728.5	-27.1	27.1	-33.9	-1005.6	1853.0
B	142	NASTRAN	-24443.0	-25.4	20.0	45.2	-4022.3	-7445.7
		STARDYNE	-25728.5	-27.1	27.1	-33.9	-4858.3	-7705.6

End A is the element end with the lowest numbered grid point.

TABLE 3  
Comparison of NASTRAN and STARDYNE Results for Case 2  
Maximum Tension Loads

End	Quantity		Axial F N	Shear V <sub>1</sub> N	Shear V <sub>2</sub> N	Torque T N-cm	Moment M <sub>1</sub> N-cm	Moment M <sub>2</sub> N-cm
	Element Number							
A	133	NASTRAN	22632.6	49.4	13.3	-35.0	-2282.3	7490.9
		STARDYNE	22881.6	43.6	10.7	11.3	-1604.4	6281.9
B	133	NASTRAN	22632.6	49.4	13.3	-35.0	-757.0	3705.9
		STARDYNE	22881.6	43.6	10.7	11.3	-757.0	3739.8
A	149	NASTRAN	49.8	-5.3	-38.2	2.2	915.2	-113.0
		STARDYNE	48.0	-5.8	-37.4	-1.1	903.9	-124.3
B	149	NASTRAN	49.8	-5.3	-38.2	2.2	949.1	-158.2
		STARDYNE	48.0	-5.8	-37.4	-1.1	926.5	-169.5
A	150	NASTRAN	12.0	3.1	-13.3	7.9	497.1	101.7
		STARDYNE	15.6	2.2	-12.0	-5.6	452.0	79.1
B	150	NASTRAN	12.0	3.1	-13.3	7.9	497.1	135.6
		STARDYNE	15.6	2.2	-12.0	-5.6	463.2	90.4
A	141	NASTRAN	22601.4	23.1	13.3	19.2	113.0	-2530.9
		STARDYNE	22855.0	23.1	12.0	-10.2	90.4	-2429.2
B	141	NASTRAN	22601.4	23.1	13.3	19.2	-2960.2	7490.9
		STARDYNE	22855.0	23.1	12.0	-10.2	-2711.6	7457.0

End A is the element end with the lowest numbered grid point.

TABLE 4

Comparison of NASTRAN and STARDYNE Results for Case 2  
Grid Point Deflection in Centimeters

Grid Point No.	NASTRAN X	STARDYNE X	NASTRAN Z	STARDYNE Z
9	-0.9893	-0.9968	-0.0656	-0.0722
23	-0.9899	-0.9974	0.0190	0.0209
14	-0.9970	-1.0094	-0.0717	-0.0800
28	-0.9964	-1.0087	0.0152	0.0148
29	-1.0548	-1.0748	-0.0220	-0.0213
30	-1.0547	-1.0764	-0.0226	-0.0216
33	-1.0484	-1.0685	-0.0280	-0.0244
34	-1.0500	-1.0724	-0.0200	-0.0121
4	-1.0474	-1.0677	-0.0455	-0.0607
5	-1.0492	-1.0719	-0.0376	-0.0544
19	-1.0510	-1.0728	-0.0327	-0.0414
18	-1.0516	-1.0717	-0.0321	-0.0409
37	-0.9136	-0.9153	-0.0134	-0.0150
40	-0.9969	-1.0019	-0.0212	-0.0196
38	-0.9169	-0.9188	-0.0138	-0.0154
39	-0.9885	-1.0013	-0.0016	-0.0002
53	-0.2867	-0.2780	-0.0350	-0.0371
54	-0.2815	-0.2666	-0.0170	-0.0173
55	-0.2915	-0.2774	-0.0146	-0.0133
56	-0.2992	-0.2891	-0.0333	-0.0356
57	-0.2994	-0.2893	0.0197	0.0208
58	-0.2741	-0.2763	0.0051	0.0061
59	-0.2639	-0.2668	0.0039	0.0043

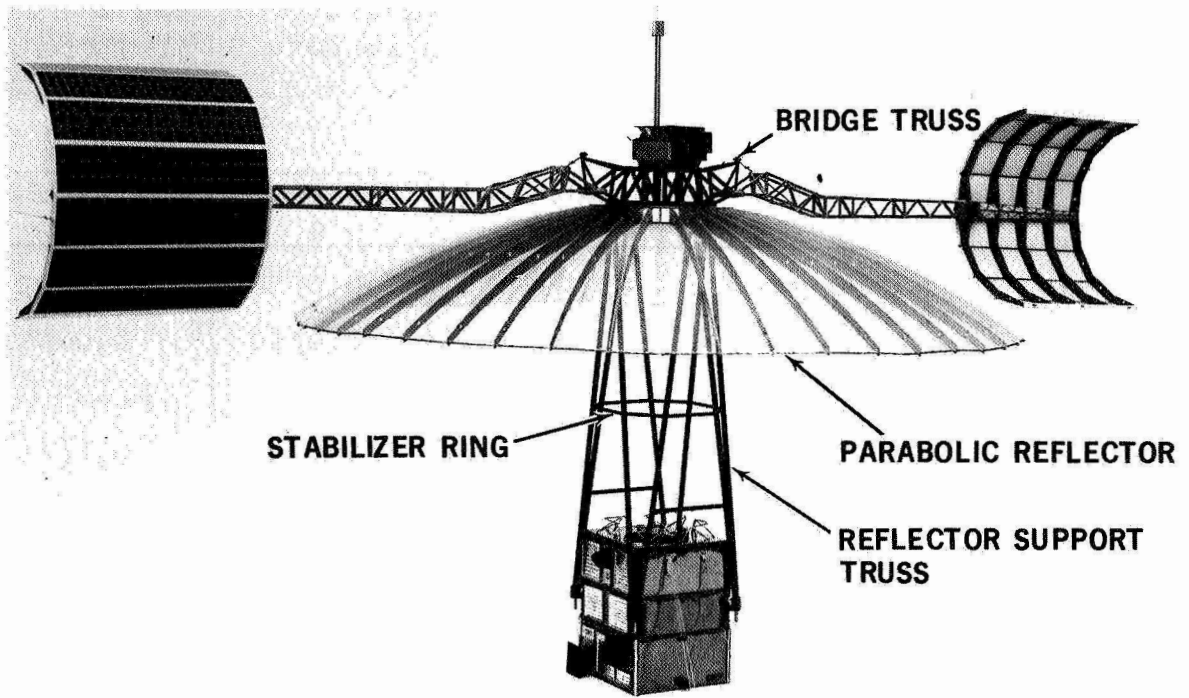


Figure 1. ATS-F/G Orbital Configuration

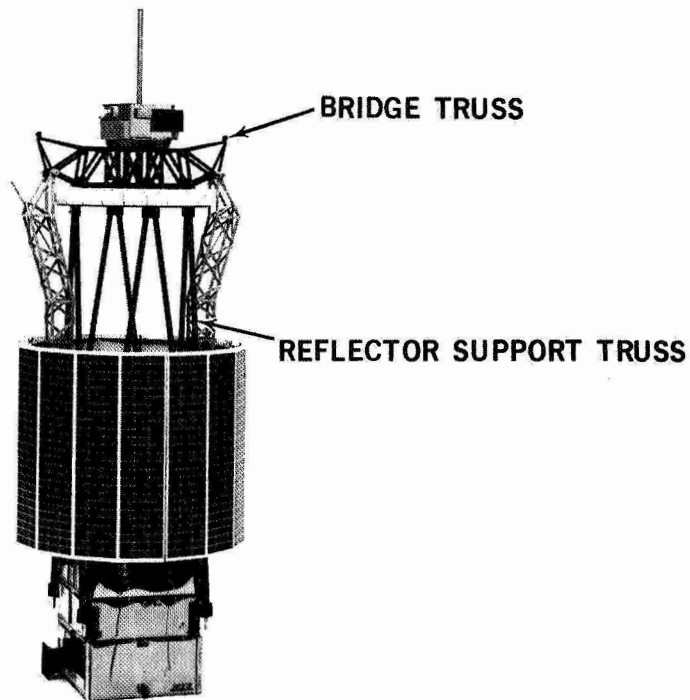


Figure 2. ATS-F/G Launch Configuration

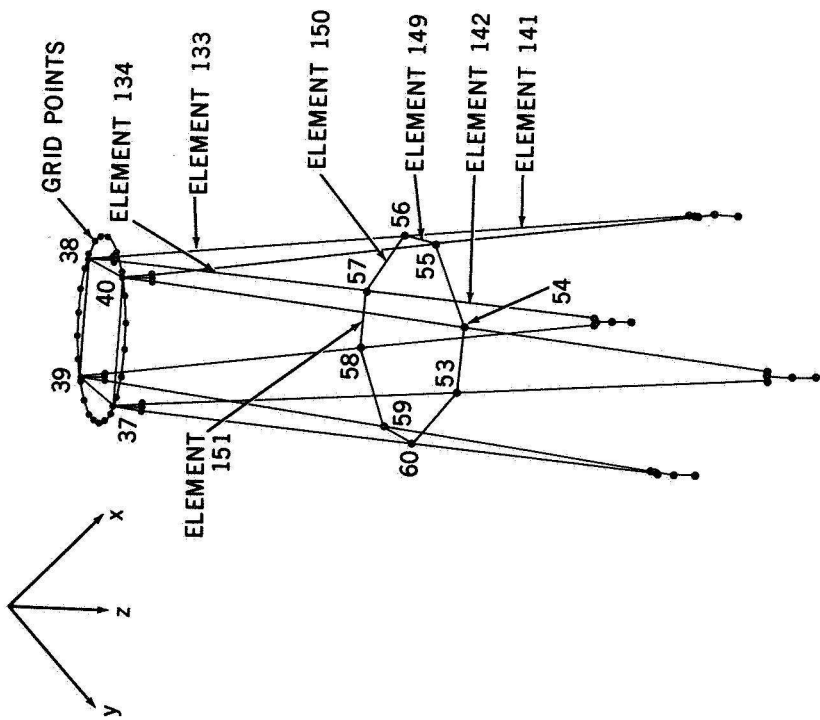


Figure 3. NASTRAN Plot Of Reflector Support Truss

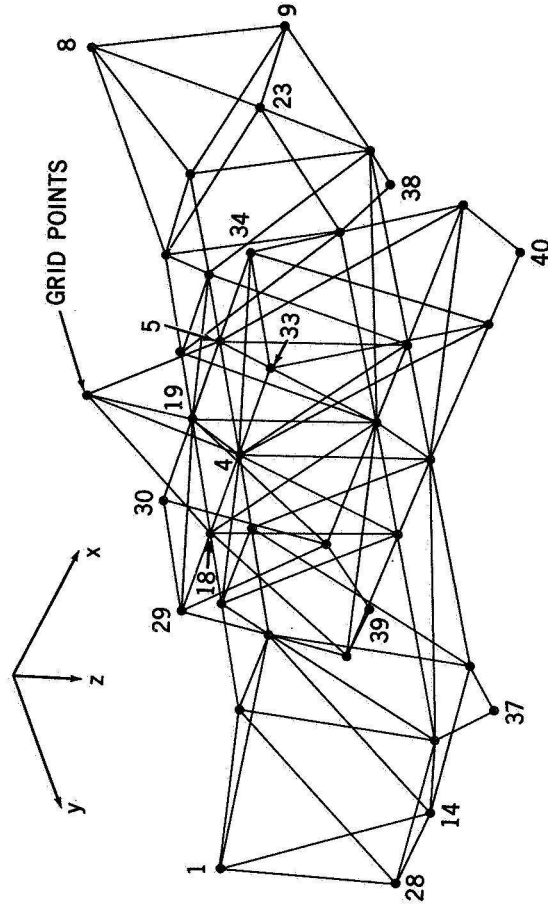


Figure 4. NASTRAN Plot Of Bridge Truss

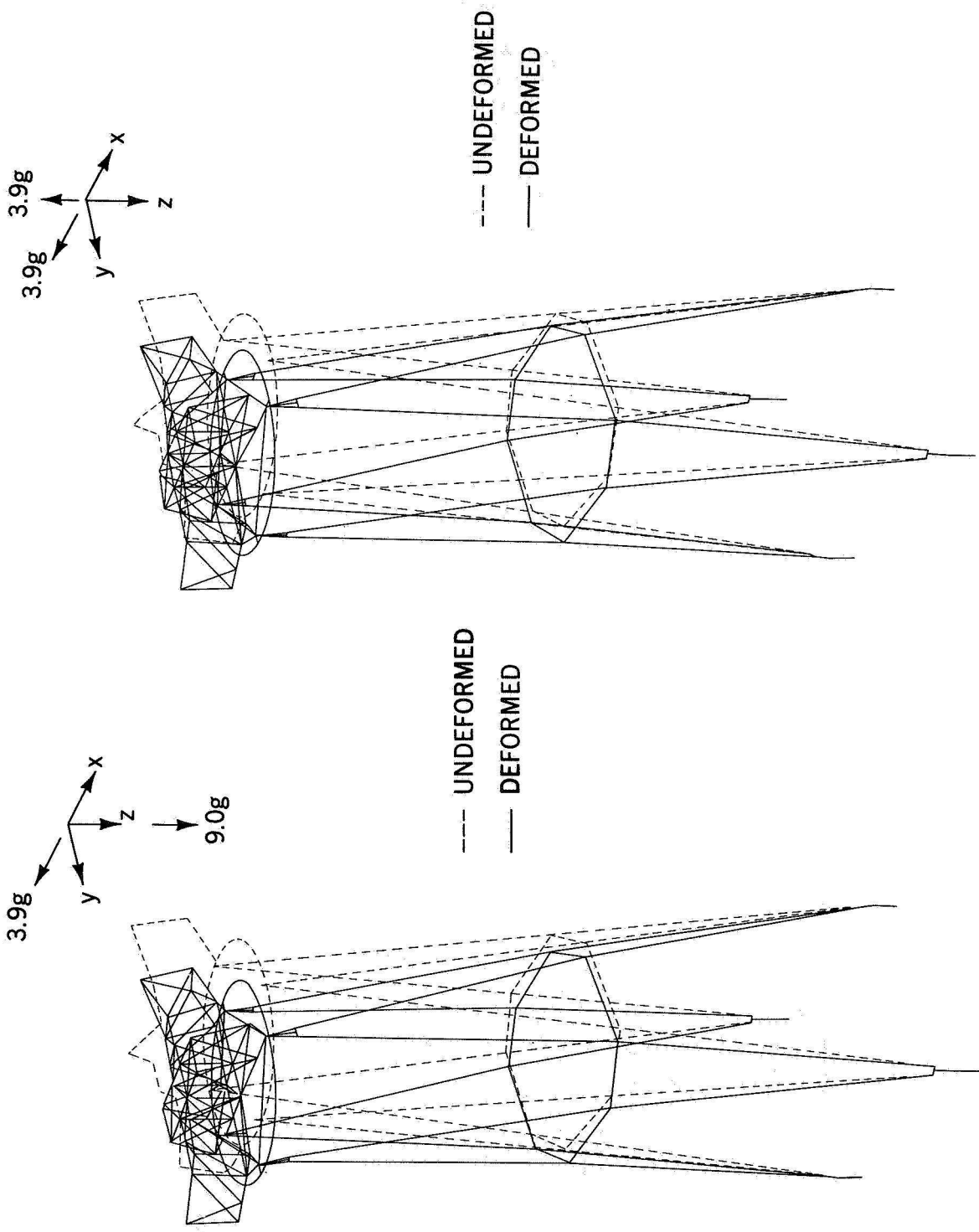


Figure 5. Deformed ATS-F/G Reflector Support Truss Structure Due To Force/Moment Input Equivalent - Case 1

Figure 6. Deformed ATS-F/G Reflector Support Truss Structure Due To Force/Moment Input Equivalent - Case 2

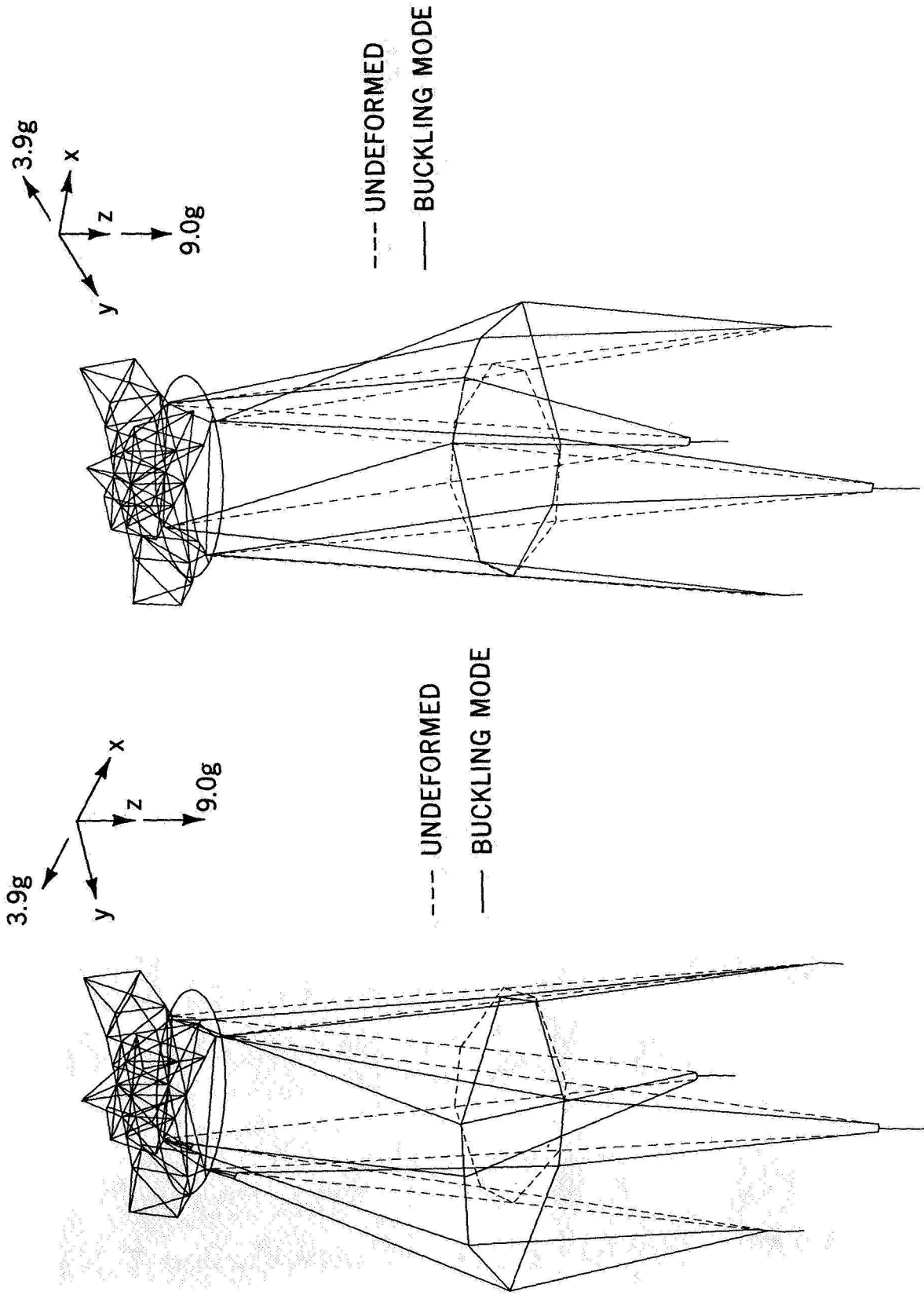


Figure 8. Fundamental Buckling Mode Shape - Case 4

Figure 7. Fundamental Buckling Mode Shape Case 3

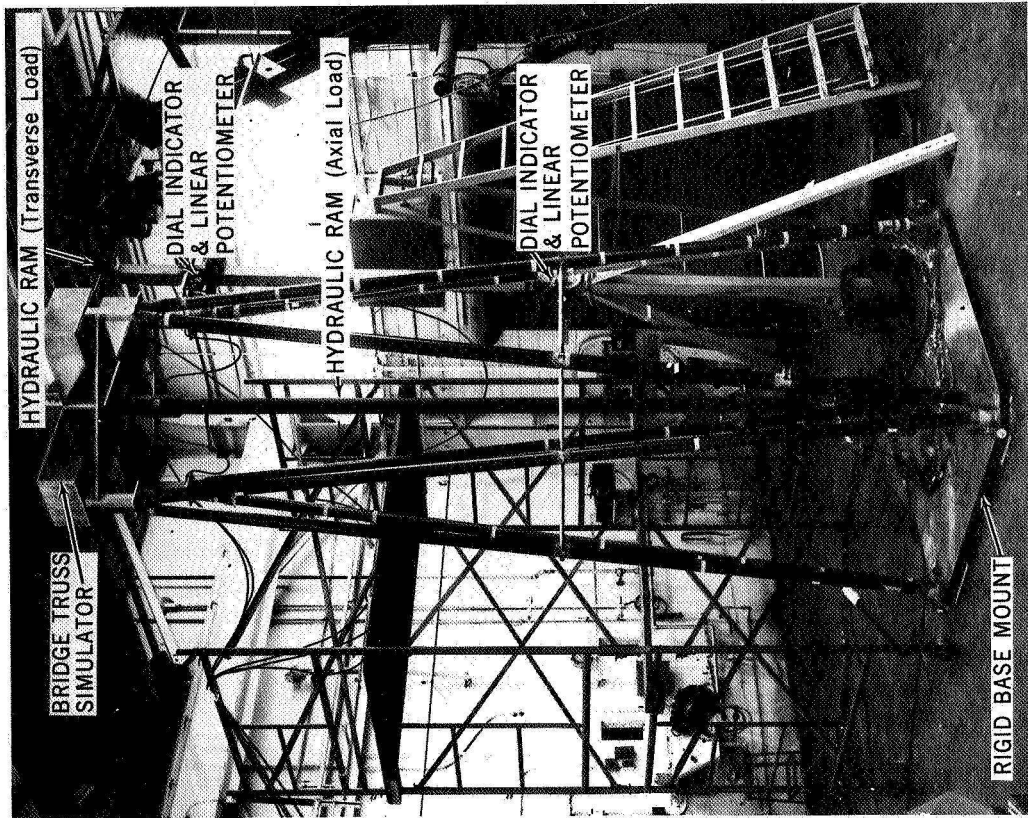


Figure 9. Load Test Set Up

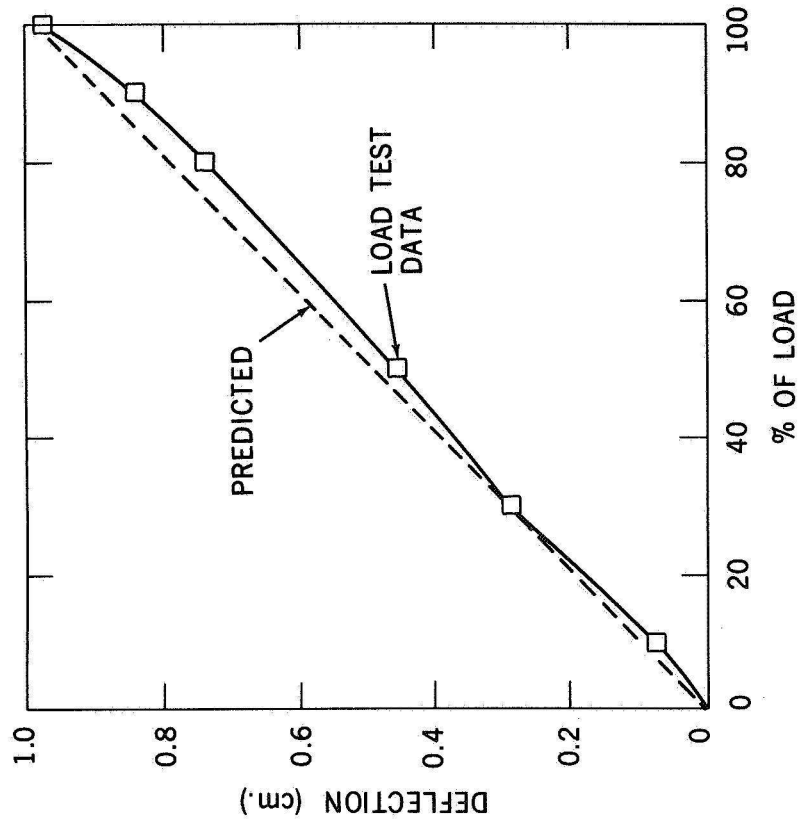


Figure 10. Comparison Of Load Test Data And NASTRAN Predictions For Case 1

# AN ISOPARAMETRIC QUADRILATERAL

## MEMBRANE ELEMENT FOR NASTRAN

By

Howard M. Adelman, Joseph E. Walz, and James L. Rogers, Jr.  
NASA Langley Research Center

### SUMMARY

This paper describes the implementation of an improved quadrilateral membrane element in NASTRAN. Descriptions of the geometrical and kinematic properties of the element are included along with development of the matrices and vectors which characterize the element. The necessity for considering small deviations from planeness of the element is discussed and the approach taken to account for these deviations for the new element is described. The improved accuracy available from the element over the existing quadrilateral membrane is indicated by a sample calculation for which an analytical solution is available from beam theory. For the same finite element idealization, the errors in maximum displacement and stress were significantly reduced by the use of the new element.

### INTRODUCTION

One of the more frequently used elements in the NASTRAN library is the quadrilateral membrane element (CQDMEM). This element is used to represent portions of structures for which membrane action constitutes the predominant contribution to the strain energy. An example of one such application is to the skin of aircraft wings. In addition, the quadrilateral membrane element is also used in conjunction with the quadrilateral bending element (CQDPLT) to form the membrane-bending elements CQUAD1 and CQUAD2 needed to represent more general deformation behavior.

The quadrilateral membrane element currently available in NASTRAN is composed of overlapping constant strain triangles as described in reference 1. It has been reported that the CQDMEM element does not accurately represent problems involving high stress gradients, suggesting that the current element

needs improvement. The reason for this difficulty is generally attributed to the constant strain field provided by this element (ref. 2). Several improved quadrilateral membrane elements have been developed which have linear strain fields (e.g. refs. 3 and 4) and these elements should provide improved results in membrane element applications. The implementation of an improved quadrilateral membrane element in NASTRAN was undertaken as an in-house project to improve the element library by attempting to overcome the noted shortcomings.

The element chosen for implementation is the linear strain isoparametric quadrilateral membrane element described in references 3 and 4. The reasons for this choice are:

- (1) The element is conforming, i.e. the displacements of adjoining elements are matched along their entire interface. As a result, the strain energy is an upper bound to the corresponding exact energy.
- (2) The stresses and strains vary within the element thus providing improved accuracy over the existing element.
- (3) The element is well-documented.

The purposes of the present report are to present a description of the element being implemented and to demonstrate the increased accuracy available through the new element by comparison with the existing quadrilateral element and an analytical solution.

#### SYMBOLS

[A]	matrix relating strains and displacements
[B]	transformation matrix relating displacements in mean plane to those at actual grid points
[C]	matrix which relates rotations of the mean plane to displacements of mean plane
[E]	matrix relating displacements in element coordinate system to those in basic coordinate system
$e_x, e_y, e_{xy}$	membrane strains
$\{f_a\}$	vector of forces at actual grid points in element coordinate system

$\{f_e\}$	vector of forces in mean plane
$[G_e]$	matrix relating stresses and strains
H	distance from actual grid point to the mean plane
h	thickness of membrane
J	Jacobian of transformation from x-y coordinates to $\xi-\eta$ coordinates
[K]	stiffness matrix referred to global coordinate system
$[K^d]$	differential stiffness matrix referred to global coordinate system
$[K_{ee}]$	stiffness matrix in element coordinate system
$[K_{ee}^d]$	differential stiffness matrix in element coordinate system
$\{P\}$	thermal load vector referred to global coordinate system
$\{P_e\}$	thermal load vector in element coordinate system
[S]	matrix relating element stresses to global displacements
$[S_e]$	matrix relating element stresses to element displacements
$\{S_t\}$	vector relating element temperature to element stress
[T]	basic to global coordinate transformation matrix
$t_o$	reference or stress-free temperature of the element
$\bar{t}$	temperature of the element above the reference or stress-free temperature
u,v,w	displacements in x-, y-, and z-directions, respectively
$\bar{u}, \bar{v}, \bar{w}$	displacements in X-, Y-, and Z-directions, respectively, see table I
$\{u_a\}$	vector of displacements at actual grid point in element coordinate system
$\{u_e\}$	vector of displacements in mean plane
X,Y,Z	cartesian coordinates used in table I
x,y,z	element cartesian coordinate directions, see figure 1
$\eta, \xi$	element parametric coordinates, see figure 1
$\omega_x, \omega_y, \omega_z$	rotations of the mean plane element about x,y and z axes, respectively

Subscripts:

1, 2, 3, 4 refer to grid points 1, 2, 3 and 4 respectively, of the element

A subscript preceded by a comma indicates partial differentiation with respect to the subscript.

#### DESCRIPTION OF THE ELEMENT

In this section of the paper, descriptions of the geometry and kinematic behavior of the isoparametric element (figure 1) will be given. The element, since it is defined by four points, need not be planar; however the development of the necessary matrices is carried out for a flat element. The treatment of the case for which the four points are not coplanar will be discussed in a later section of the paper. The element parametric coordinates  $\xi$  and  $\eta$  shown in figure 1 vary linearly between zero and one with the extreme values occurring on the sides of the quadrilateral. Further, lines of constant  $\xi$  and  $\eta$  are straight as indicated in the figure. A set of element cartesian coordinates  $x, y, z$  is defined as follows: the x-axis is along the line connecting the first two grid points; the y-axis is perpendicular to the x-axis and lies in the plane of the element; and the z-axis is normal to the plane and forms a right handed system with the x- and y-axes. Displacement components in x, y, and z directions are denoted by u, v, and w, respectively. As given in reference 3, the displacement field is assumed to have the following form:

$$\left. \begin{aligned} u(\xi, \eta) &= (1 - \xi)(1 - \eta) u_1 + \xi(1 - \eta) u_2 + \xi\eta u_3 + (1 - \xi) \eta u_4 \\ v(\xi, \eta) &= (1 - \xi)(1 - \eta) v_1 + \xi(1 - \eta) v_2 + \xi\eta v_3 + (1 - \xi) \eta v_4 \end{aligned} \right\} \quad (1)$$

where the subscript on a displacement component denotes the grid point value of the component.

It may be observed that on lines of constant  $\xi$ , u and v vary linearly with  $\eta$  and on lines of constant  $\eta$ , u and v vary linearly with  $\xi$ . In particular u and v vary linearly on each edge between grid points and as a result the displacements of adjacent elements are matched all along their common edges. The element is therefore of the "conforming" type which guarantees that the element will converge as an upper bound on the strain energy.

The required membrane strains are related to the displacements  $u$  and  $v$  by the familiar relations

$$e_x = u_{,x} \quad e_y = v_{,y} \quad e_{xy} = u_{,y} + v_{,x} \quad (2)$$

where the comma indicates partial differentiation. Since the displacements are expressed in terms of  $\xi$  and  $\eta$ , the operations in equations (2) cannot be carried out without knowing the relationships between the  $(x,y)$  coordinates and the  $(\xi,\eta)$  coordinates. These relations are given in reference 3 as

$$\left. \begin{aligned} x &= (1 - \xi)(1 - \eta) x_1 + \xi(1 - \eta) x_2 + \xi\eta x_3 + (1 - \xi) \eta x_4 \\ y &= (1 - \xi)(1 - \eta) y_1 + \xi(1 - \eta) y_2 + \xi\eta y_3 + (1 - \xi) \eta y_4 \end{aligned} \right\} \quad (3)$$

By use of familiar relations involving partial derivatives, the operations indicated in equations (2) may be performed. Thus, for example,

$$u_{,x} = u_{,\xi} \xi_{,x} + u_{,\eta} \eta_{,x} \quad (4)$$

where

$$\xi_{,x} = \frac{1}{J} y_{,\eta} \quad \eta_{,x} = -\frac{1}{J} y_{,\xi} \quad (5)$$

and

$$J = \begin{vmatrix} x_{,\xi} & x_{,\eta} \\ y_{,\xi} & y_{,\eta} \end{vmatrix} \quad (6)$$

It is noted in passing that equations (1) which relate displacements within the element to its grid point values or "parameters" are identical in form to equations (3) for coordinates  $x$  and  $y$ . Thus the term "isoparametric" is applied to characterize the element.

For the special case of a rectangle it can be shown that the  $x$  and  $\xi$  directions are identical as are the  $y$  and  $\eta$  directions. In this case  $e_x$  is linear with respect to  $y$  and constant with respect to  $x$ , whereas  $e_y$  is linear with respect to  $x$  and constant with respect to  $y$ . The shear

strain varies linearly with respect to both  $x$  and  $y$ . In contrast to the strains, all three stress components vary linearly in both the  $x$  and  $y$  directions. This is a direct consequence of the constitutive equations. For nonrectangular shapes the behavior of the stress and strain components is more complicated and is not easily characterized.

#### IMPLEMENTATION OF THE ELEMENT

The addition of an element to NASTRAN requires the derivation of a set of characteristic matrices and vectors as described in reference (1) and those necessary for the new element are:

stiffness matrix,  $[K_{ee}]$   
lumped mass matrix,  $[M_{ee}]$   
thermal load vector,  $\{P_e\}$   
stress recovery matrices,  $[S_e]$  and  $\{S_t\}$   
differential stiffness matrix,  $[K_{ee}^d]$

The development of these matrices is presented in this section along with a description of the procedure used when the four grid points defining the element are not coplanar. Finally, this section contains an outline of the matrix transformations required so that the new element will be compatible with others in NASTRAN.

#### Stiffness Matrix

Using equations (1) through (5) results in the following relation between strains and grid point displacements

$$\begin{Bmatrix} e_x \\ e_y \\ e_{xy} \end{Bmatrix} = [A] \begin{Bmatrix} u_1 \\ v_1 \\ u_2 \\ v_2 \\ u_3 \\ v_3 \\ u_4 \\ v_4 \end{Bmatrix} = [A] \{u_e\} \quad (7)$$

where the elements of the 3x8 matrix  $[A]$  are functions of  $\xi$  and  $\eta$ . The stress-strain relation is given by

$$\begin{Bmatrix} \sigma_x \\ \sigma_y \\ \sigma_{xy} \end{Bmatrix} = [G_e] \begin{Bmatrix} e_x \\ e_y \\ e_{xy} \end{Bmatrix} - [G_e] \begin{Bmatrix} \alpha_x \\ \alpha_y \\ \alpha_{xy} \end{Bmatrix} \bar{t} \quad (8)$$

where the 3x3 matrix  $[G_e]$  represents most generally a completely anisotropic material. The terms  $\alpha_x$ ,  $\alpha_y$  and  $\alpha_{xy}$  are thermal expansion coefficients and  $\bar{t}$  is the average temperature of the element above the stress-free temperature, given by

$$\bar{t} = \frac{1}{4} (t_1 + t_2 + t_3 + t_4) - t_0 \quad (9)$$

The strain energy,  $V$ , (apart from thermal effects) is

$$V = \frac{h}{2} \int_0^1 \int_0^1 \{u_e\}^T [A]^T [G_e] [A] \{u_e\} J d\xi d\eta \quad (10)$$

and from this expression, the stiffness matrix can be identified as

$$[K_{ee}] = h \int_0^1 \int_0^1 [A]^T [G_e] [A] J d\xi d\eta \quad (11)$$

The required integration is performed numerically by the use of Gaussian quadrature using a 4x4 grid. For a discussion of Gaussian quadrature as used for isoparametric elements, see references 3 and 4.

#### Lumped Mass Matrix

The mass matrix developed for the isoparametric element is a lumped mass matrix since coupled mass matrices for membrane elements generally result in overly stiff representations in dynamic problems (see ref. 1 p. 5.5-5). One method of lumping is to assign one quarter of the mass of the element to each of the four grid points. However, this method usually does not preserve the location of the center of mass of the element. Accordingly, the method used to generate the mass matrix for the new element is that presently used in NASTRAN for the existing quadrilateral membrane element. This later method is based on an averaging procedure which always preserves the center of mass.

#### Thermal Load Vector

For the purpose of developing the thermal load vector, the contribution to the potential energy,  $U$ , of the element temperature above some stress-free value is written as

$$U = h \int_0^1 \int_0^1 \begin{Bmatrix} \sigma_x \\ \sigma_y \\ \sigma_{xy} \end{Bmatrix}^T \begin{Bmatrix} \alpha_x \\ \alpha_y \\ \alpha_{xy} \end{Bmatrix} \bar{t} J d\xi d\eta \quad (12)$$

Using equations (7) and (8) in equation (12) and discarding an irrelevant constant term not involved in the solution, results in

$$U = h \int_0^1 \int_0^1 \{u_e\}^T [A]^T [G_e] \begin{Bmatrix} \alpha_x \\ \alpha_y \\ \alpha_{xy} \end{Bmatrix} \bar{t} J d\xi d\eta \quad (13)$$

and the thermal load vector is then recognized as

$$\{P_e\} = h \int_0^1 \int_0^1 [A]^T J d\xi d\eta [G_e] \begin{Bmatrix} \alpha_x \\ \alpha_y \\ \alpha_{xy} \end{Bmatrix} \bar{t} \quad (14)$$

### Stress Recovery Matrices

Expressions for the element stress components  $\sigma_x$ ,  $\sigma_y$ , and  $\sigma_{xy}$  at any point written in terms of displacements measured in the element cartesian coordinate system are obtained by combining equations (7) and (8) to give

$$\begin{Bmatrix} \sigma_x \\ \sigma_y \\ \sigma_{xy} \end{Bmatrix} = [S_e] \{u_e\} - [S_t] \bar{t} \quad (15)$$

where

$$[S_e] = [G_e][A] \text{ and } [S_t] = [G_e] \begin{Bmatrix} \alpha_x \\ \alpha_y \\ \alpha_{xy} \end{Bmatrix} \quad (16)$$

Although the stress components may vary within the element, they are computed only at the intersection of the element diagonals for the purpose of stress output. Once the stress components are obtained, they are used to compute the principal stresses and directions by appropriate formulas given in reference 5.

### Differential Stiffness Matrix

The differential stiffness matrix, which is used in NASTRAN primarily for linear buckling analyses, is developed by a consideration of the work done by stress components  $\sigma_x$ ,  $\sigma_y$ , and  $\sigma_{xy}$  during small rotations  $\omega_x$ ,  $\omega_y$ , and  $\omega_z$  about the three element cartesian axes. The expression for the work done is taken from reference 1 (section 7.1, equation (16)) given as

$$W = -\frac{h}{2} \int_0^1 \int_0^1 \begin{Bmatrix} \omega_x \\ \omega_y \\ \omega_z \end{Bmatrix}^T [K_{\omega\omega}^d] \begin{Bmatrix} \omega_x \\ \omega_y \\ \omega_z \end{Bmatrix} J \, d\xi \, d\eta \quad (17)$$

where

$$[K_{\omega\omega}^d] = \begin{bmatrix} \sigma_y & -\sigma_{xy} & 0 \\ -\sigma_{xy} & \sigma_x & 0 \\ 0 & 0 & \sigma_x + \sigma_y \end{bmatrix} \quad (18)$$

and the rotation components are given by

$$\begin{aligned} \omega_x &= w_{,y} & \omega_y &= -w_{,x} \\ \omega_z &= \frac{1}{2} (v_{,x} - u_{,y}) \end{aligned} \quad (19)$$

In order to evaluate  $\omega_x$  and  $\omega_y$ , the behavior of  $w$  in the element is required, and for this purpose  $w$  is assumed to have the same parametric variation as  $u$  and  $v$ , thus

$$w = (1 - \xi)(1 - \eta) w_1 + \xi(1 - \eta) w_2 + \xi\eta w_3 + (1 - \xi)\eta w_4 \quad (20)$$

Combining equations (1), (19), and (20) results in

$$\begin{Bmatrix} \omega_x \\ \omega_y \\ \omega_z \end{Bmatrix} = [C] \{u_e\} \quad (21)$$

where the elements of the 3x8 matrix  $[C]$  are functions of  $\xi$  and  $\eta$ . Substituting equation (21) into equation (17) gives

$$W = -\frac{h}{2} \int_0^1 \int_0^1 \{u_e\}^T [C]^T [K_{\omega\omega}^d] [C] \{u_e\} J \, d\xi \, d\eta \quad (22)$$

and the differential stiffness matrix is recognized as

$$[K_{ee}^d] = h \int_0^1 \int_0^1 [C]^T [K_{\omega\omega}^d] [C] J \, d\xi \, d\eta \quad (23)$$

The integration is performed by use of Gaussian quadrature using a  $4 \times 4$  grid. The values of  $\sigma_x$ ,  $\sigma_y$ , and  $\sigma_{xy}$  at each of the sixteen quadrature points are obtained from equation (15) for appropriate values of  $\xi$  and  $\eta$ .

#### Use of the Mean Plane

As mentioned previously, the matrices and vectors associated with the new quadrilateral membrane element were derived for a planar element. If the four grid points are not coplanar they are projected onto a so-called mean plane which is defined in the following manner (see figure 2). Two skewed lines whose end points are grid points 1 and 3 and grid points 2 and 4, respectively, are defined to be the diagonals of the element. The mean plane is defined so that it passes through the midpoint of the perpendicular connector of the two diagonals and parallel to them (see ref. 5 p. 4.87-105.). As shown in figure 2, if the length of the perpendicular connector is  $2H$ , then the user defined grid points are alternatively  $H$  units above and below the mean plane as one progressively moves around the element. Once the actual grid points are projected onto a mean plane, a planar element is defined and the previously derived matrices are applicable.

The authors would like to emphasize that the use of the mean plane concept does not finally resolve the question of how to deal with a quadrilateral element whose grid points are not coplanar and that further research on this subject is warranted. One alternative to the mean plane is to assume the element to be planar with the plane defined by three of the grid points. This alternative was found to be undesirable for the new element because numerical results were sensitive to the grid point numbering sequence in a single element. This numerical experiment to determine this sensitivity is described in the Appendix.

Transformation of Matrices and Vectors  
to Global Coordinates

Up to this point the characteristic matrices and vectors for the element have been derived in terms of displacements in the element cartesian coordinate system. In order that the new element be compatible with other elements in NASTRAN, it is necessary to transform the matrices and vectors so that they are expressed in the global coordinate system. This procedure involves three transformations:

- (1) transformation from displacements in the mean plane in the element cartesian system to the displacements at the user-defined grid points in the element cartesian system
- (2) transformation from displacements in the element coordinate system to displacements in the NASTRAN basic coordinate system
- (3) transformation from the NASTRAN basic coordinate system to the NASTRAN global coordinate system.

The first transformation is based on replacing the set of forces in the mean plane  $\{f_e\}$  by a statically equivalent set at the user defined grid points  $\{f_a\}$ . The first set consists of forces in the x and y directions only, whereas the second set consists of forces in the x, y, and z directions. This statement of static equivalence can be written as

$$\{f_a\} = [B]\{f_e\} \tag{24}$$

where

$$\{f_a\} = \begin{Bmatrix} f_{x1} \\ f_{y1} \\ f_{z1} \\ f_{x2} \\ \cdot \\ \cdot \\ \cdot \\ f_{z4} \end{Bmatrix} \text{ and } \{f_e\} = \begin{Bmatrix} f_{x1} \\ f_{y1} \\ f_{x2} \\ f_{y2} \\ f_{x3} \\ f_{y3} \\ f_{x4} \\ f_{y4} \end{Bmatrix} \tag{25}$$

The matrix [B] depends on the geometry of the element and H which is a measure of the nonplaneness of the element. This same matrix is used to transform displacements, thus

$$\{u_e\} = [B]^T \{u_a\} \quad (26)$$

The second and third transformations are required of all elements in NASTRAN and are discussed fully in reference 1. In terms of the notation of reference 1 the transformation matrix from element coordinates to NASTRAN basic coordinates is denoted by a 12x12 matrix [E], and the transformation matrix from NASTRAN basic coordinates to NASTRAN global coordinates is denoted by a 12x12 matrix [T]. The relation between element and global displacements may finally be written as

$$\{u_e\} = [B]^T [E]^T [T] \{u_g\} \quad (27)$$

All that is now required to express the matrices and vectors in the global coordinate system is to substitute equation (27) into equations (10), (13), (15), and (22). The results are summarized below

Stiffness matrix:

$$[K] = [T]^T [E][B][K_{ee}][B]^T [E]^T [T] \quad (28)$$

Thermal load vector:

$$\{P\} = [T]^T [E][B]\{P_e\} \quad (29)$$

Stress recovery matrix:

$$[S] = [S_e][B]^T [E]^T [T] \quad (30)$$

Differential stiffness matrix:

$$[K^d] = [T]^T [E][B][K_{ee}^d][B]^T [E]^T [T] \quad (31)$$

## PRELIMINARY RESULTS

At the time of writing, the element is in the early stage of being verified. A stand-alone program has been written for the purpose of testing the element in a NASTRAN-like environment. The first available test case for this element is a cantilever beam modeled by 16 equal elements as shown in figure 3. Displacements and stresses were computed using the existing CQDMEM element and the new isoparametric element based on the same finite element idealization. The finite element results are then compared to an analytical solution based on elementary beam theory. In figure 3 the analytical solution for displacements is indicated by the solid line and the finite element results by dashed lines. The new element is seen to be a significant improvement over the CQDMEM element. When comparison is made with the analytical solution, the largest error exhibited by CQDMEM is 50% whereas the corresponding error for the new element is 9%. The comparison of stresses is presented in figure 4 where the results have been normalized to the maximum stress predicted by elementary beam theory. Although the finite element stresses were computed at a single point in each element, these stresses are presented as continuous curves. Again the exact solution is shown by the solid line and the finite element results by dashed lines. The results indicate a significant improvement in accuracy by using the new element. The maximum error in stress using the CQDMEM element is about 49% whereas that for the improved element is 14%.

## CONCLUDING REMARKS

An isoparametric quadrilateral membrane element which is being implemented in NASTRAN by the NASTRAN Systems Management Office is described. Included are descriptions of the basic geometry and deformation characteristics of the element, as well as an outline of the derivation of each of the required matrices and vectors for the element. Derivations of the stiffness matrix, thermal load vector, stress recovery matrices, and differential stiffness matrices are given. A discussion of the need for some method of accounting for deviations from planeness is included along with a description of the method used for this purpose in the new element. Finally, a sample

calculation is carried out in which the displacements and stresses in a cantilever beam are computed by the new element and by the existing quadrilateral membrane (CQDMEM) and compared with an analytical solution from beam theory. The significant increase in accuracy obtainable with the new element is demonstrated by the calculation.

## APPENDIX

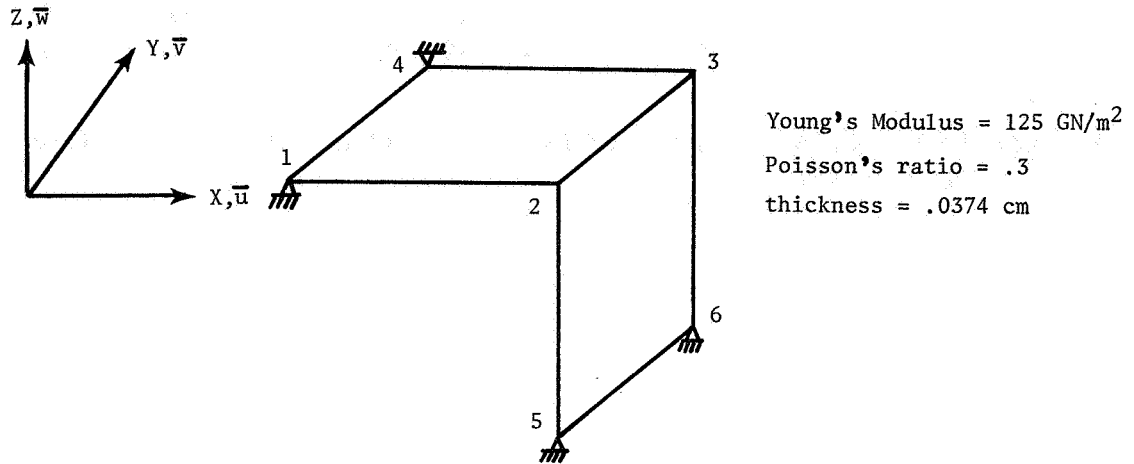
### SENSITIVITY OF MEMBRANE RESULTS TO ELEMENT GRID POINT NUMBERING SEQUENCE

A numerical experiment suggested by Dr. Raphael Haftka, currently a National Research Council postdoctoral Fellow at the Langley Research Center, is performed on the structure sketched at the top of table I. The top member is non-planar and the vertical member is planar. Both members were represented by the new quadrilateral membrane element assumed to be planar with the plane of each element being defined by three of its grid points. Displacements under two loading conditions were computed by means of a stand-alone program. In the calculations, the grid point sequence for the top member was varied as shown in table I, and the effects of these variations are shown in table II. Examination of table II (a) shows that for a load applied in the X-direction, the displacements both in the X-Y plane and normal to it are sensitive to the grid point numbering. For example, there is a 12% difference among the displacements in the Y-direction as well as among the displacements in the Z-direction at grid point 3. For the case of loads in the Z-direction there is a difference among the displacements in the Y-direction of 46%. The consequences of these percentage errors are tempered by the observation that the large errors noted always occurred in displacement components which were not in the direction of the applied load. By contrast the maximum difference was 1.5% for a displacement in the X-direction at grid point 2 in the first loading condition. Although the difference for displacements in the direction of the load is small, it is felt that the existence of a situation where different answers can be obtained with the same finite element model by merely changing the grid point numbering sequence for individual elements should be avoided.

#### REFERENCES

1. MacNeal, Richard H., editor: The NASTRAN Theoretical Manual, NASA SP-221, Sept. 1970.
2. Bergmann, H. W.; Robinson, J. C.; and Adelman, H. M.: Analysis of a Hot Elevon Structure, NASTRAN Users Experiences, NASA TM X-2378, 1971, pp. 163-180.
3. Przemieniecki, J. S.: Theory of Matrix Structural Analysis, McGraw-Hill, 1968, pp. 102-107.
4. Zienkiewicz, O. C., and Cheung, Y. K.: The Finite Element Method in Structural and Continuum Mechanics, McGraw-Hill, 1968, pp. 67-70.
5. Douglas, F. J., editor: The NASTRAN Programmer's Manual, NASA SP-223, Sept. 1970.

TABLE I.- STRUCTURE USED TO DETERMINE EFFECT OF NONPLANENESS



(a) Gridpoint Locations  
 (all coordinates given in centimeters)

Gridpoint	X	Y	Z
1	1280.45	480.44	9.38
2	1367.30	480.44	7.36
3	1391.87	536.68	5.52
4	1305.01	536.68	5.78
5	1367.30	480.44	-87.00
6	1391.87	536.68	-87.00

(b) Loading

Loading condition 1	$F_{X2} = F_{X3} = 1N$
Loading condition 2	$F_{Z2} = F_{Z3} = 1N$

(c) Grid Numbering Sequence for Top Element

Case	1st Point	2nd Point	3rd Point	4th Point
I	1	2	3	4
II	2	3	4	1
III	3	4	1	2
IV	4	1	2	3

Table II.- Effect of Grid Point Numbering on Displacement of a Warped Quadrilateral. (All Displacements are in cm.)

(a) Displacement due to loads in X-direction						
Grid point Sequence (table I)	$\bar{u}_2 \times 10^6$	$\bar{v}_2 \times 10^6$	$\bar{w}_2 \times 10^6$	$\bar{u}_3 \times 10^6$	$\bar{v}_3 \times 10^6$	$\bar{w}_3 \times 10^6$
I	5.46	1.59	1.46	6.85	.498	-1.07
II	5.49	1.57	1.48	6.84	.526	-1.08
III	5.44	1.56	1.35	6.86	.511	-1.20
IV	5.41	1.57	1.33	6.88	.470	-1.19

(b) Displacements due to loads in Z-direction						
Grid point Sequence	$\bar{u}_2 \times 10^6$	$\bar{v}_2 \times 10^6$	$\bar{w}_2 \times 10^6$	$\bar{u}_3 \times 10^6$	$\bar{v}_3 \times 10^6$	$\bar{w}_3 \times 10^6$
I	.485	.535	6.41	-.095	-.298	6.05
II	.506	.365	6.33	-.099	-.447	6.12
III	.377	.421	6.33	-.223	-.392	6.12
IV	.354	.591	6.41	-.217	-.246	6.05

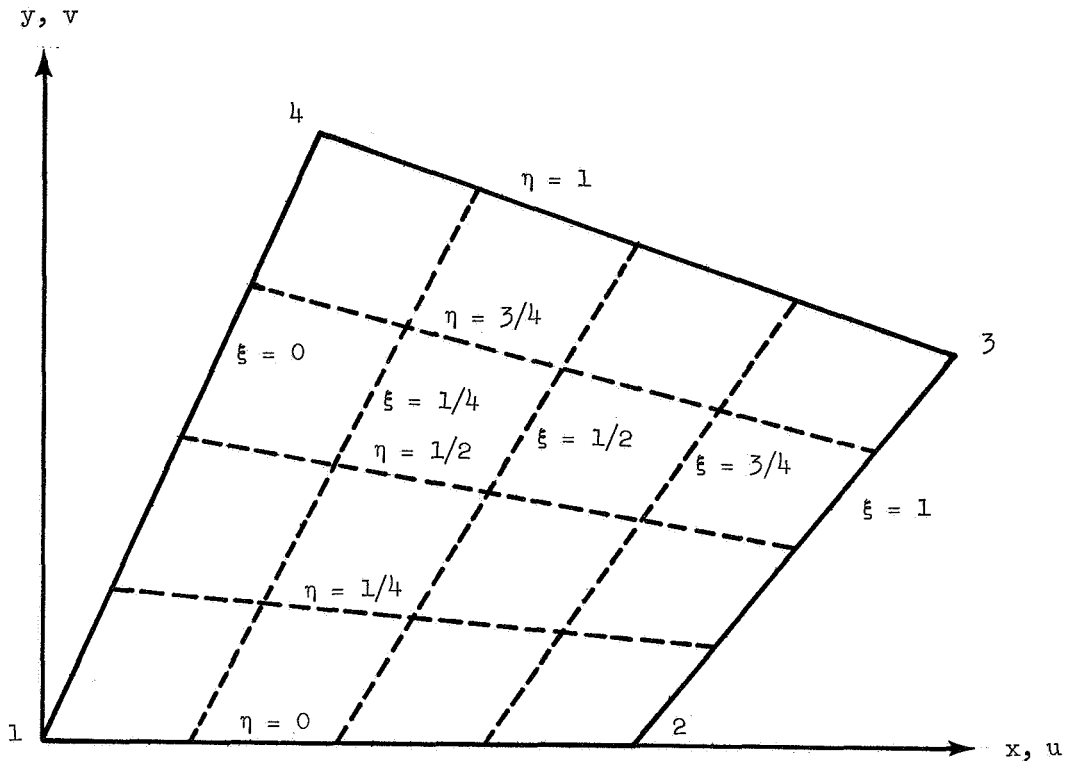


Figure 1. - Coordinate systems for quadrilateral membrane element.

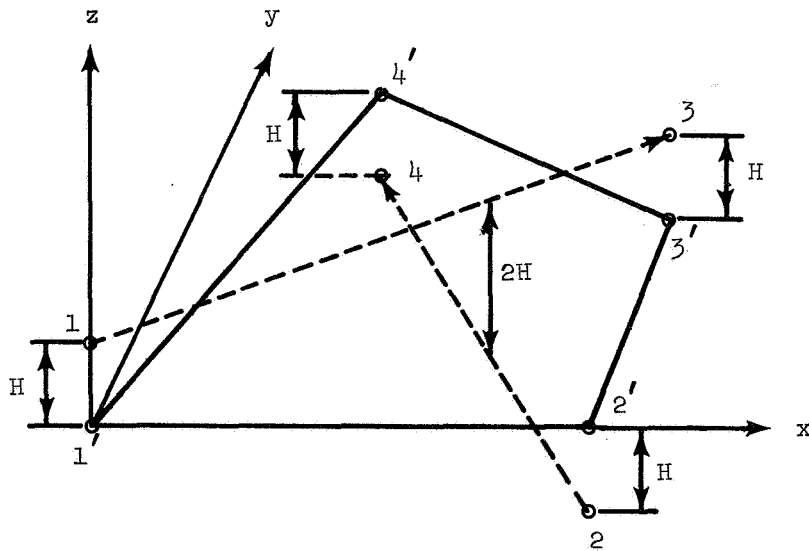


Figure 2. - Mean plane for quadrilateral membrane element. (Actual grid points are indicated by unprimed numbers and projection of grid points onto mean plane are indicated by primed numbers.)

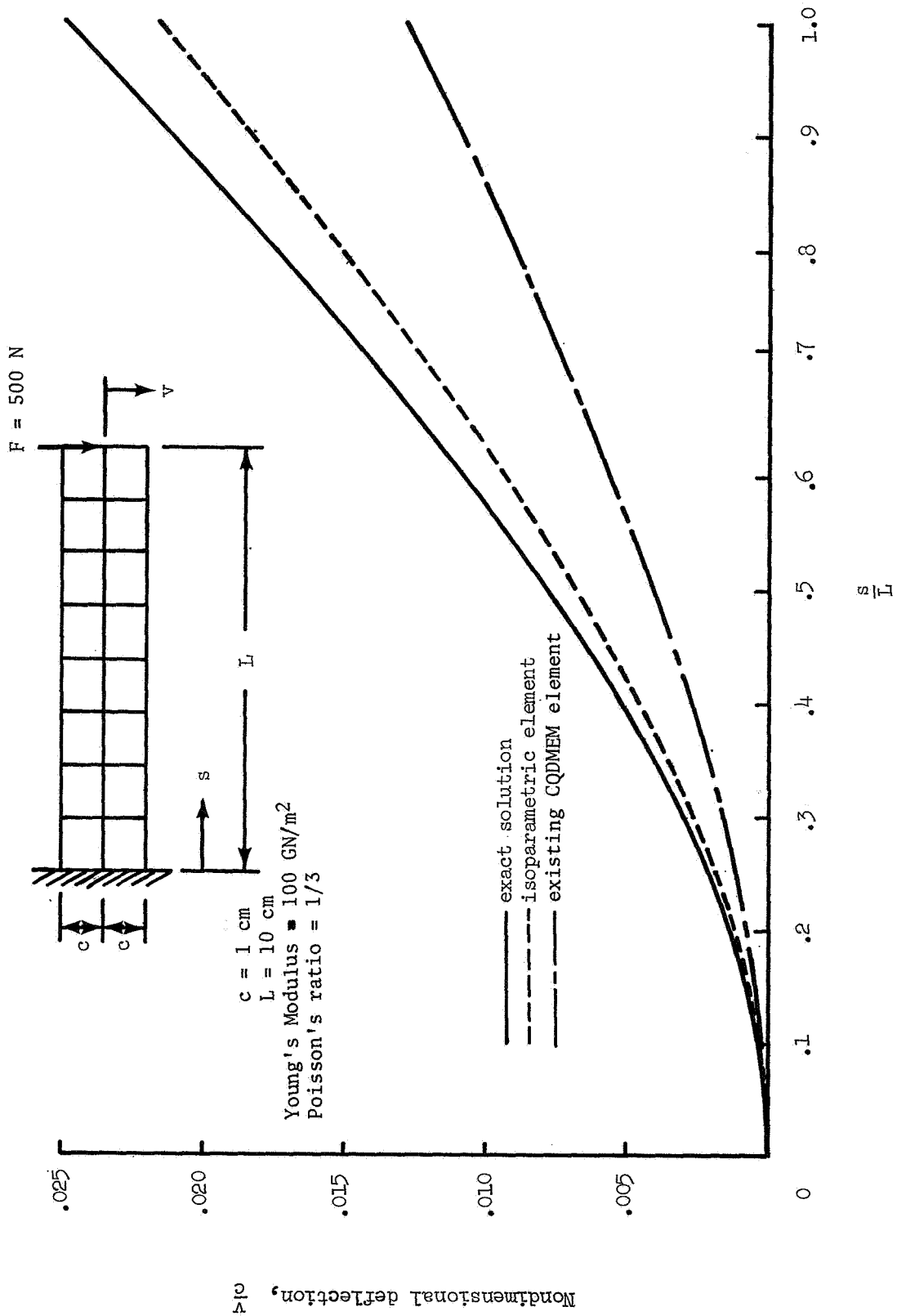


Figure 3.- Deflection of cantilever beam idealized by quadrilateral membrane elements.

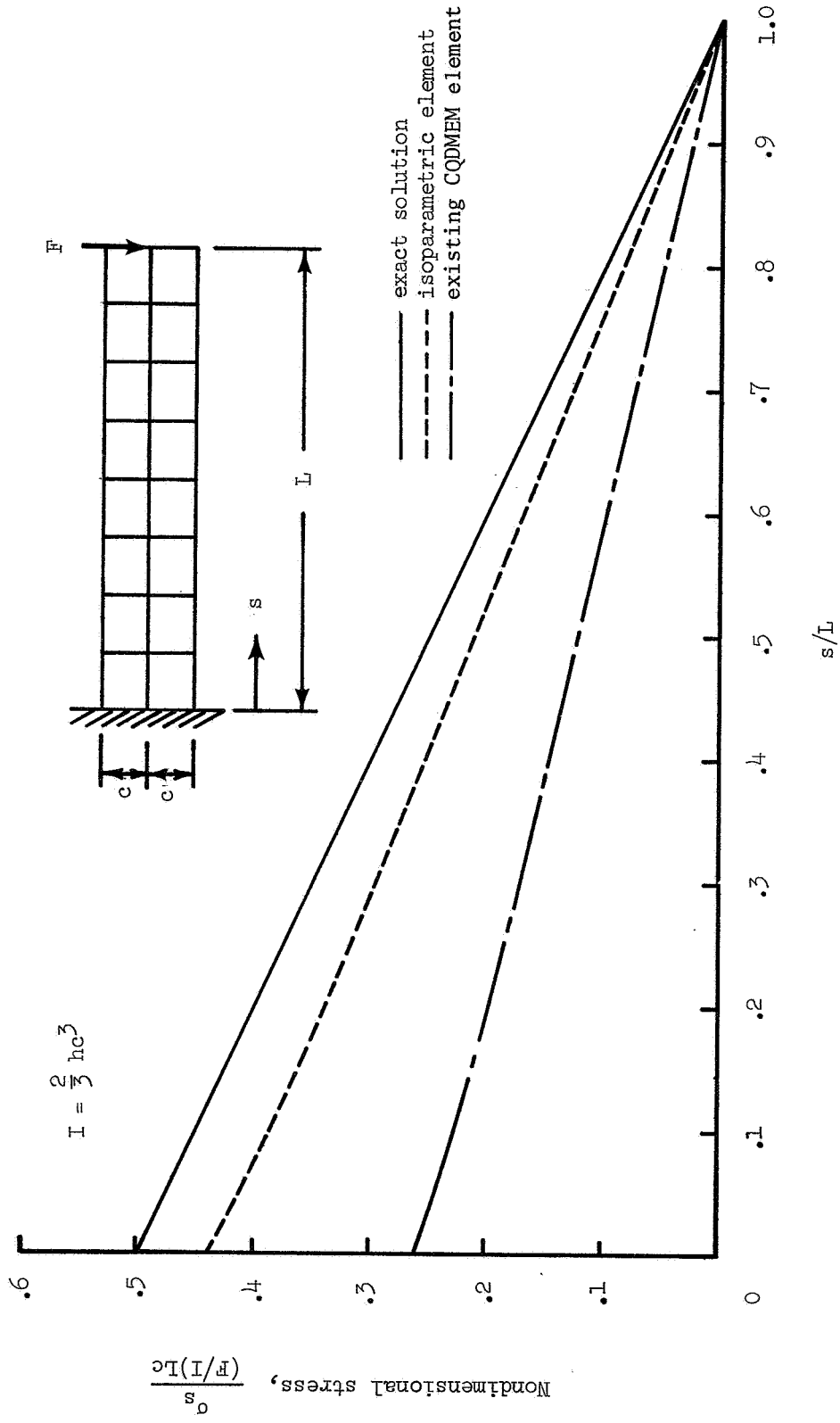


Figure 4. - Longitudinal stress at distance  $c/2$  above neutral axis in cantilever beam idealized by quadrilateral membrane elements.

## SOME ASPECTS OF THE NASTRAN PROGRAM OUTPUT

By David J. Gregory Grumman Aerospace Corporation

### Summary

*This paper discusses the Nastran Program Output from a structural analysts point of view, and describes the simple modifications which have been made to the program in order to improve it in certain areas. In particular, the convenience of the output for use in original design work is critically appraised and compared with the output from Astral.\* It is shown that considerable hand calculation is necessary in order to extract useful load distribution data from the available Nastran output. For this reason, some effort has been directed towards providing additional force output for the Nastran shear panel element.*

### Introduction

*The output from any finite element structural analysis program must be in a form which is immediately useful to the stress or design engineer. The most sophisticated program is not being used efficiently if lengthy hand calculations are necessary before useful loads data can be extracted from the computer output. It is for this reason that Astral has been refined in a design environment over several years to provide a "Force" type output. This is the output that Grumman Engineers have found preferable to a stress output in most design situations where the structural model only approximates to the real structure. The output from Nastran is definitely not in a convenient form and this paper describes some of its shortcomings and the modifications made to the program in order to provide a force type output for the shear panel element. Similar modifications should also be made to the membrane and plate elements.*

### SYMBOLS

$b$	Shear panel width	in.
$d$	Shear panel depth	in.
$F$	Shear panel corner forces	#
$n$	Number of loading conditions	
$N_x$	Wing chordwise load distribution	#/in.
$P$	Shear panel diagonal forces	#
$q$	Shear flow	#/in.
$r$	Number of members in idealization	
$t$	Shear panel thickness	in.
$x, y$	Local coordinates	in.
$\phi$	} Angles defining geometry of shear panel (See Figure 13)	
$\psi$		
$\theta_2$		

### NASTRAN OUTPUT: COMPARISON WITH ASTRAL

*In this section of the paper, Nastran Output is compared with Astral "M Print" for output format and form.*

\* Automated Structural Analysis Program developed by Grumman

Output Format. Nastran output is grouped by loading conditions whereas Astral groups output by member or grid point number. Grouping by loading condition is far less convenient when many loading conditions may be present as is often the case in a fuselage analysis. Also, grouping by member number enables a maximum minimum search to be made by the program with a minimum of additional programming. This maximum minimum output for loads and deflections is an indispensable feature of Astral "M Print" output.

As an example of the different grouping strategies, consider a hypothetical structure with  $r$  members and  $n$  loading conditions. Figure 1 compares the output formats for this structure.

Output Form. Figure 2 indicates the main differences in output between Nastran and Astral for some of the most commonly used finite elements. In general, Nastran provides average stresses and scant loads data, whilst Astral provides a comprehensive force output on a "node force" basis. Nastran also provides a Margin of Safety output for some elements if an allowable stress is specified by the user. This margin is based upon average stresses in idealized members and assumes a uniaxial stress field. As such it is a "misleading" output and should be disregarded in all but the most elementary truss type structure. Of more use, would be a stress ratio of the form:

$$\text{Stress Ratio} = \frac{\text{Stress}}{\text{Allowable Stress}}$$

Any stress output should be treated with caution, especially in final design work, since stresses output by Nastran are only correct if the idealized structure is identical to the real structure – rarely the case. In most cases, the Structural Analyst prefers to work with load distributions.

Axial Force Output. Nastran outputs average forces in rod elements, diagonal forces in shear panels and no forces for the membrane element. Hence, the element node forces can not be calculated when using membranes, but can be calculated from rod and shear panel output at the expense of tedious hand calculations. The following procedure shows how node forces are obtained from rectangular shear panels and rods. Note that for the more general case of non rectangular panels, the required calculations are more tedious and an approximate graphical approach would be used in most cases.

Assume a situation were a rod is bounded by two rectangular shear panels as shown in Figure 3:

Nastran Output:	Panel 1 Diagonal forces $P_1$ and $P_2$	(#)
	Rod Average Force $P_3$	(#)
	Panel 2 Diagonal Forces $P_4$ and $P_5$	(#)

Required: Node Forces at Rod Ends  $F_1$  and  $F_2$  (#)  
 Shear Flows Adjacent to Rod  $q_1$  and  $q_2$  (#/in)

Resolving diagonal forces along panel edges, adding and dividing by length of rod:

$$q_1 = \frac{(P_1 + P_2)}{\sqrt{b^2 + d_1^2}} \text{ \#/IN}$$

$$q_2 = \frac{(P_4 + P_5)}{\sqrt{b^2 + d_2^2}} \text{ \#/IN}$$

Summing corner forces and rod average force at each end of rod:

$$F_1 = P_3 + \frac{P_1 b}{\sqrt{b^2 + d_1^2}} - \frac{P_5 b}{\sqrt{b^2 + d_2^2}}$$

$$F_2 = P_3 - \frac{P_2 b}{\sqrt{b^2 + d_1^2}} + \frac{P_4 b}{\sqrt{b^2 + d_2^2}}$$

These equations would be modified appropriately if more than two shear panels were adjacent to the rod. Typically, for a wing rib and beam intersection, four panels would be involved.

### H3-T Orbiter Wing Analysis

This analysis has been chosen to illustrate how loads are extracted from both Nastran and Astral for use in design work.

Briefly, the idealization consists of quadrilateral and triangular membranes for the upper and lower covers, and rods and shear panels for the ribs, beams (spars) and vertical studs (posts). A drawing of the idealization is shown in Figure 4.

Main features of the idealization are as follows:

- 130 Grid Points
- 80 Quadrilateral Membranes
- 14 Triangular Membranes
- 107 Shear Panels
- 71 Rods
- 364 Degrees of Freedom

*The Nastran Bulk Data Deck used for the analysis was generated automatically from the Astral Input Deck using an in house conversion program. Only the Control Decks were produced by hand. A comparison of computer running times for the two analyses is shown in Figure 5.*

*Load distributions useful to the Structural Analyst and Designer are shown at sample wing sections, and the method of deriving them from the raw program output is detailed. The general agreement between the two analyses, as indicated by overall wing flexibility, is good as expected, since both use the stiffness method of finite element analysis and both have approximately equivalent elements. The difference in wing tip deflection for one typical loading condition amounted to less than .02%.*

### **Wing Cover Axial Loads**

*Cover axial loads are most often presented at Grumman as a series of chordwise running load distributions(#/in.) along each rib line. As an example, the distribution for the upper cover at rib 10 is determined in Figures 6 and 7 and shown plotted in Figure 8. The Astral node or cap loads are divided by the effective panel width. The Nastran average stresses in panels on the inboard and outboard sides of the rib must be converted to running load and then averaged.*

*Note that both analyses require a finer grid in the area adjacent to the rear beam due to the discontinuity at grid points 91 and 92. Additional stringers between the beams which carry through to the airplane center line are also needed, in order to predict the shear lag effect caused by the cover discontinuity across rib 11.*

### **Rib and Beam Shear Flows**

*All shear flows are output directly by Astral "M Print". Nastran output consists of maximum and average shear stresses which may be converted to shear flows by multiplying by the panel thickness. If, however, all four shear flows are required, then the procedure outlined previously for rectangular panels or the procedure below for extracting stud loads must be used. Figure 9 shows the extraction of maximum shear flows only, for rib 10.*

### **Stud Cap Forces**

*Stud forces or cap forces are the most difficult to extract from Nastran output. In this example the cap forces for stud 85 at the intersection of rib 10 and beam 5 will be determined. None of the adjacent four shear panels are rectangular; therefore, the simplified equations of the Appendix may not be used. Instead, an approximate graphical approach is taken. First the four shear panels are drawn to scale on Figure 10 with the diagonal forces and rod average forces as shown. Next, the components of the diagonal forces acting along the stud are scaled and added:*

$$\begin{aligned} \text{At the upper cover: Force} &= 3055 + 16292 \times \frac{1.67}{2.49} - 2514 \times \frac{1.43}{3.17} + 4393 \times \frac{1.39}{1.87} - 10911 \times \frac{1.78}{2.06} \\ &= 6660 \# \end{aligned}$$

$$\begin{aligned} \text{At the lower cover: Force} &= 3055 + 2626 \times \frac{1.71}{3.30} - 15416 \times \frac{1.45}{2.35} + 12199 \times \frac{1.55}{1.84} - 3960 \times \frac{1.67}{2.09} \\ &= 1990 \# \end{aligned}$$

*These stud forces are not in good agreement with the corresponding forces output directly by Astral which are 7610# at the upper cover and 710# at the lower cover. This is probably due partly to the graphical approach used, and partly to the relative insensitivity of wing flexibility and deflection to stud loading. A Nastran wing solution with rigid studs, imposed by multipoint constraints, showed only a 4.6% reduction in wing deflections.*

#### **Program Modifications to Improve the Shear Panel Output**

*This section of the paper describes in detail the changes made in Nastran Module SDR2 as a first step in providing an improved "force" type output. Perhaps the most inconvenient aspect of the present output is the use of shear panel diagonal forces, and it was decided to improve this output as quickly as possible. This has been accomplished by modifying the appropriate routines and subroutines in Module SDR2 and outputting the additional data directly from this module, without recourse to User Modules or changes in the Output File Processor. The additional output includes corner forces (#), shear flows(#/in), panel edge lengths and internal node numbers. This output in no way affects the regular Nastran printout which follows it. (See Appendix.)*

*In order to make these changes, the necessary equations were derived for resolving diagonal forces into corner forces and combining corner forces into shear flows. Next, a working knowledge of how Nastran interfaces "horizontally" between routines and "vertically" between modules was obtained, mostly on a trial and error basis, since this information is not specifically given in the Programmers Manual. The layout chart for Module SDR2 shown in Figure 11 was then drawn and proved invaluable when modifying routines and deciding on the best data paths between routines. At first it was hoped to accomplish all data transfer by means of common blocks; however, it was soon realized that due to the looping that takes place within the module this was not possible. Instead, use was made of the data file ESTA when necessary. The necessary changes to module SDR2 are described in some detail below and summarized in Figure 12. (See Appendix.)*

*The basic problem consists of bringing together the diagonal forces and local mean plane coordinates, performing the necessary calculations and printing the results. The diagonal forces are calculated in subroutine SPANL2 and the local coordinates in subroutine SPANL1. A convenient place to calculate the forces and shear flows and print them is in routine SDR2E. The following list of modifications to the routines have been made.*

- The local coordinates of the four corners of each panel are loaded into common block SDR2X5 as SPOUT (8) in subroutine SPANL1 for transfer to SDR2B. These coordinates are X and Y values for corners 1 to 4 (Figure 13).
- In routine SDR2B, the local coordinates from common block SDR2X5 are transferred to Data File ESTA for the “vertical” transfer to SDR2E (Figure 11). ESTA assembles a block of data for each shear panel element processed, whereas the common blocks are rewritten for each pass through a loop.
- The block data subroutine SDR2BD must be updated to redimension the enlarged ESTA file. The block size is increased from 25 to 33 words to include the coordinates.
- The shear panel diagonal forces P13 and P24 are loaded into common block SDR2X7 in SPANL2 and transferred to SDR2E where they are available as BUFB(2) and BUFB(3) respectively. This does not require any additional coding.
- Data file ESTA is moved into common as ELESTA in routine SDR2E and element numbers and internal grid point numbers are already available as BUFB(1) and ELESTA(2-5) respectively. Hence, all the necessary data is assembled in SDR2E.

Local Coordinates	ELESTA (25-32)
Node Number	ELESTA (2-5)
Diagonal Forces	BUFB (2-3)
Member Number	BUFB (1)
Subcase Number	Z (ICC + 1)

- In routine SDR2E the corner forces, shear flows and panel edge lengths are calculated.
- The calculated data is output with appropriate headings.

Appendix A summarizes the equations used, shows a listing of the major SDR2E module coding changes and provides an example of the additional program output.

### Recommended Changes in Nastran Output

The following changes in the form and format of Nastran Output would greatly ease the task of the Structural Analyst in design work. They would reduce the amount of hand calculation necessary, eliminate the likelihood of not designing to the most critical loading condition and increase the accuracy of most load distributions.

#### Output Format

- The output should be grouped by member or grid point number, not by loading condition.
- The maximum and minimum loads for each member should be output if more than two loading conditions are present.
- Loads should be output in decimal form, not in exponential form, when of a suitable size. For example, a load of 5650# should be output as 5650.0 or 5650, not as 5.650000E 03 which is far more difficult to read correctly.

## Output Form

- *The shear panel should have a shear flow (#/in.) output for all four sides, and the resolved corner forces should be used in a "Force" type output including "kick" loads due to warping.*
- *Rod and bar elements should have cap or grid point forces output, not average forces. These are determined using the above panel corner forces.*
- *The membrane element should have a "force" type output consisting of shear flows (#/in.) along all four sides and cap forces along imaginary rod elements.*
- *The Margin of Safety output should be deleted.*
- *The length of all sides of all panels should be output, together with their direction cosines in the global coordinate system.*
- *A check on the free body equilibrium of the structure is essential output for any finite element analysis. This should be a summation of all forces and moments about the origin.*

## Recommended Additions to Documentation

- *Inclusion of Module Layouts in the Programmers Manual (see Figure II).*
- *Inclusion of full instructions for implementation of user modules in the programmers manual.*

## Concluding Remarks

*The output from these two finite element analyses, Nastran and Comap Astral, differ in concept. Nastran in general outputs average stresses in elements and some forces which are not in an immediately usable form. Comap Astral provides no stress output (unless specifically requested) but gives a comprehensive force type output. Generally in all but the most elementary of structures, the force type output is preferred by structural analysts at Grumman. The Nastran Shear panel output is particularly difficult to use and the necessary modifications to the program to quickly provide a more suitable output have been described. At this time work is under way to provide a better output form and format for all the commonly used Nastran Elements.*

## Reference

*AFFDL-TR-70-118 An Automated Procedure for the Optimization of Practical Aerospace Structures. Section 4.3 "Nodal Stress Method."*

## APPENDIX

Summary of Equations:

Trigonometric Functions:

$$\cos \varphi_1 = \frac{y_4}{\sqrt{x_4^2 + y_4^2}}$$

$$\sin \varphi_1 = \frac{x_4}{\sqrt{x_4^2 + y_4^2}}$$

$$\cos \varphi_2 = \frac{y_3}{\sqrt{x_3^2 + y_3^2}}$$

$$\sin \varphi_2 = \frac{x_3}{\sqrt{x_3^2 + y_3^2}}$$

$$\cos \psi_1 = \frac{y_3}{\sqrt{(x_2 - x_3)^2 + y_3^2}}$$

$$\sin \psi_1 = \frac{(x_2 - x_3)}{\sqrt{(x_2 - x_3)^2 + y_3^2}}$$

$$\cos \psi_2 = \frac{y_4}{\sqrt{(x_2 - x_4)^2 + y_4^2}}$$

$$\sin \psi_2 = \frac{(x_2 - x_4)}{\sqrt{(x_2 - x_4)^2 + y_4^2}}$$

$$\cos \theta_2 = \frac{(y_3 - y_4)}{\sqrt{(x_3 - x_4)^2 + (y_3 - y_4)^2}}$$

$$\sin \theta_2 = \frac{(x_3 - x_4)}{\sqrt{(x_3 - x_4)^2 + (y_3 - y_4)^2}}$$

$$F_{12} = P_{13} \cdot \frac{\sin \varphi_2 \cos \varphi_1 - \cos \varphi_2 \sin \varphi_1}{\cos \varphi_1}$$

$$F_{11} = P_{13} \cdot \frac{\cos \varphi_2}{\cos \varphi_1}$$

$$F_{22} = P_{24} \cdot \frac{\cos \psi_2}{\cos \psi_1}$$

$$F_{21} = P_{24} \cdot \frac{\sin \psi_2 \cos \psi_1 - \cos \psi_2 \sin \psi_1}{\cos \psi_1}$$

$$F_{32} = P_{13} \cdot \frac{\sin \varphi_2 \cos \psi_1 + \cos \varphi_2 \sin \psi_1}{\sin \theta_2 \cos \psi_1 + \cos \theta_2 \sin \psi_1}$$

$$F_{31} = P_{13} \cdot \frac{\sin \theta_2 \cos \varphi_2 - \cos \theta_2 \sin \varphi_2}{\sin \theta_2 \cos \psi_1 + \cos \theta_2 \sin \psi_1}$$

$$F_{42} = P_{24} \cdot \frac{\sin \psi_2 \cos \theta_2 + \cos \psi_2 \sin \theta_2}{\sin \theta_2 \cos \varphi_1 - \cos \theta_2 \sin \varphi_1}$$

$$F_{41} = P_{24} \cdot \frac{\sin \varphi_1 \cos \psi_2 + \cos \varphi_1 \sin \psi_2}{\sin \theta_2 \cos \varphi_1 - \cos \theta_2 \sin \varphi_1}$$

$$q_1 = \frac{F_{21} - F_{12}}{l_{12}} = \frac{F_{21} - F_{12}}{x_2}$$

#/IN

$$q_2 = \frac{F_{22} - F_{31}}{l_{23}} = \frac{F_{22} - F_{31}}{\sqrt{y_3^2 + (x_2 - x_3)^2}}$$

#/IN

$$q_3 = \frac{F_{41} - F_{32}}{l_{34}} = \frac{F_{41} - F_{32}}{\sqrt{(y_3 - y_4)^2 + (x_3 - x_4)^2}}$$

#/IN

$$q_4 = \frac{F_{42} - F_{11}}{l_{41}} = \frac{F_{42} - F_{11}}{\sqrt{y_4^2 + x_4^2}}$$

#/IN

## APPENDIX - Continued

S H E A R   P A N E L   O U T P U T   F O R   S U B C A S E   1												
SHEAR PANEL NUMBER	CORNER 1		CORNER 2		CORNER 3		CORNER 4		SIDE 1-2	SIDE 2-3	SIDE 3-4	SIDE 4-1
	NODE NO.	NODE NO.	NODE NO.	NODE NO.	NODE NO.	NODE NO.	NODE NO.	LENGTH SHEAR	LENGTH SHEAR	LENGTH SHEAR	LENGTH SHEAR	
	FORCE 11	FORCE 21	FORCE 31	FORCE 41	FORCE 12	FORCE 22	FORCE 32	FORCE 42				
40	1	31	25	7	204.523	-81.809	204.523	-81.809	J.500	1.250	0.500	1.250
	204.523	-81.809	-204.523	81.809	81.809	-204.523	-204.523	-327.237	-327.237	-327.237	-327.237	
41	7	25	19	13	204.539	-81.815	204.539	-81.815	J.500	1.250	0.500	1.250
	204.539	-81.815	-204.539	81.815	81.815	-204.539	-204.539	-327.262	-327.262	-327.262	-327.262	
42	37	67	61	43	-42.758	32.891	-42.758	32.891	1.250	1.625	1.250	1.625
	-42.758	32.891	42.758	-32.891	42.758	-32.891	42.758	52.625	52.625	52.625	52.625	
43	43	61	55	49	-42.748	32.883	-42.748	32.883	1.250	1.625	1.250	1.625
	-42.748	32.883	42.748	-32.883	42.748	-32.883	42.748	52.612	52.612	52.612	52.612	
44	1	31	67	37	3348.872	-167.273	3348.872	-167.273	J.500	10.010	1.250	10.010
	3348.872	-418.184	-3348.872	167.273	167.273	-3348.872	-3348.872	-1572.739	-669.096	-669.096	-669.096	
45	25	31	67	61	-2006.089	250.565	-2006.089	250.565	1.250	10.010	1.625	10.008
	-2006.089	325.735	2006.089	-250.566	2006.089	-250.566	2006.089	521.177	400.905	308.338	400.905	
46	19	25	61	55	-513.731	64.091	-513.731	64.091	1.250	10.008	1.625	10.019
	-513.731	83.319	513.731	-64.091	513.731	-64.091	513.731	133.310	102.546	78.882	102.546	
47	13	19	55	49	655.799	-32.726	655.799	-32.726	J.500	10.019	1.250	10.019
	655.799	-81.815	-655.799	32.726	32.726	-655.799	-655.799	-327.261	-130.905	-52.362	-130.905	
48	13	7	43	49	513.731	-64.091	513.731	-64.091	1.250	10.008	1.625	10.019
	513.731	83.319	-513.731	64.091	64.091	-513.731	-513.731	-133.310	-102.546	-78.882	-102.546	
49	7	1	37	43	2006.089	-250.565	2006.089	-250.565	1.250	10.010	1.625	10.008
	2006.089	325.735	-2006.089	250.566	250.566	-2006.089	-2006.089	-521.177	-400.905	-308.338	-400.905	
50	37	67	103	73	1001.758	-125.092	1001.758	-125.092	1.250	10.010	2.000	10.010
	1001.758	200.148	-1001.758	125.093	125.093	-1001.758	-1001.758	-327.237	-200.148	-125.093	-200.148	

## APPENDIX – Continued

51	61 -743.416 -148.567	67 148.567 743.567	103 -743.567 -120.711	97 120.711 743.416	1.625 182.852	10.010 148.567	2.000 120.711	10.008 148.567
52	55 -403.849 -80.613	61 80.613 403.377	97 -403.377 -65.498	91 65.498 403.849	1.625 99.215	10.008 80.613	2.000 65.498	10.020 80.613
53	49 -0.764 -0.153	55 0.153 0.764	91 -0.764 -0.095	35 0.095 0.764	1.250 0.244	10.020 0.153	2.000 0.095	10.020 0.153
64	49 403.849 80.613	43 -80.613 -403.377	79 403.377 65.498	95 -65.498 -403.849	1.625 -99.215	10.008 -80.613	2.000 -65.498	10.020 -80.613
65	43 743.414 148.567	37 -148.567 -743.567	73 743.567 120.710	79 -120.710 -743.414	1.625 -182.851	10.010 -148.567	2.000 -120.710	10.008 -148.567

## APPENDIX - Continued

```

C INITIALIZE ESTA POINTERS.                                0000109
C*****                                                    0000110
ISN 0045      IF( STRESX.EQ.0 .AND. FRCCEX.EQ.0 ) RETJRN    0000111
C HEADINGS = FCLLCW LINE 111 IN ROUTINE SDRZE
WRITE(6,101) Z(ICC61)
ISN 0047      101 FORMAT(1H1,63H SHEAR PANEL OUTPUT FOR SU
ISN 0048      1B C A S E ,110,/)
ISN 0049      WRITE(6,102)
ISN 0050      102 FORMAT(1X,9H SHEAR ,12H CORNER 1,12H CORNER 2,12H CORNER
1 3,12H CORNER 4,12H SIDE 1-2,12H SIDE 2-3,12H SIDE 3-
24,12H SIDE 4-1)
ISN 0051      WRITE(6,103)
ISN 0052      103 FORMAT(1X,5H PANEL ,12H NCOE NO.,12H NODE NO.,12H NODE
IND.,12H NCOE NO.,12H LENGTH ,12H LENGTH ,12H LENGTH
2 ,12H LENGTH )
ISN 0053      WRITE(6,104)
ISN 0054      104 FORMAT(1X,9H NUMBER,12H FRCCE 11,12H FORCE 21,12H FORCE
1 31,12H FRCCE 41,12H SHEAR ,12H SHEAR ,12H SHEAR
2 ,12H SHEAR )
ISN 0055      WRITE(6,105)
ISN 0056      105 FORMAT(10X,12H FRCCE 12,12H FORCE 22,12H FORCE 32,12H F
ORCE 42,/)
C THIS COMPLETES HEADINGS FOR SHEAR PANEL OUTPUT AS OF 3/17/72
ISN 0057      IC ESTAND = IESTA                                0000112
ISN 0058      I) = ICC & HARMS                                0000113
ISN 0059      AGAIN = .FALSE.                                0000114
ISN 0060      OHARMS = Z(IX)                                  0000115
ISN 0061      IF( OHARMS .LT. C ) CHARMS = NHARMS            0000116
ISN 0063      ISAVE = IVEC                                    0000117
ISN 0064      ELTYPE = Z(ESTAND)                              0000118
ISN 0065      FILE = ESTA                                     0000119
ISN 0066      IX = ICC & ISTR & 2                             0000120
ISN 0067      SPHASE = IABS( Z(IX) )                          0000121
ISN 0068      IX = ICC & IELF & 2                             0000122
ISN 0069      FPHASE = IABS( Z(IX) )                          0000123
ISN 0070      IF( NESTA .NE. 0 ) GO TO 30                     0000124
ISN 0072      CALL REWIND ( ESTA )                             0000125
ISN 0073      20 CALL READ( $950, $990, ESTA, ELTYPE, 1, 0, FLAG ) 0000126
C*****                                                    0000127
C ELEMENT PARAMETERS FOR NEW ELEMENT TYPE                    0000128
C*****                                                    0000129
ISN 0074      30 IELEM = (ELTYPE-1)*INCF 61                   0000130
ISN 0075      NNOEA = ELEM(IELEM64)                           0000131
ISN 0076      NPTSTR = ELEM(IELEM67)                           0000132
ISN 0077      NPTFOR = ELEM(IELEM68)                           0000133
ISN 0078      NNDSTR = ELEM(IELEM65)                           0000134
ISN 0079      NNDFOR = ELEM(IELEM66)                           0000135
ISN 0080      LSTRES = NNCSTR.                                 0000136
ISN 0081      LFORCE = NNCFOR.                                 0000137
ISN 0082      IDSTRS = .FALSE.                                0000138
ISN 0083      IDFORC = .FALSE.                                0000139
ISN 0084      IF( KTYPE.NE.1 .AND. NPTSTR.EQ.0 .AND. NPTFOR.EQ.0 ) GO TO 40 0000140
ISN 0086      IF( NNDSTR & NNDFOR .GT. 0 ) GO TO 70           0000141
C*****                                                    0000142
C NO STRESS OR FORCE WORDS POSSIBLE FOR THIS ELEMENT TYPE IF FAIL HERE 0000143
C*****                                                    0000144
ISN 0088      40 IF( NESTA ) 60,50,60                          0000145
C                                                            0000146

```



## APPENDIX - Concluded

```

C WRITE OUT DATA IN ROUTINE SDF2E -- FOLLOWS LINE F41=P24*(SA1*CA4....
ISN 0239      AL1=X2
ISN 0240      AL2=SQRT(Y3*Y3*(X2-X3)**2)
ISN 0241      AL3=SQRT((Y3-Y4)**2*(X3-X4)**2)
ISN 0242      AL4=SQRT(Y4*Y4*(X4**2))
ISN 0243      S1=(F21-F12)/AL1
ISN 0244      S2=(F22-F31)/AL2
ISN 0245      S3=(F41-F32)/AL3
ISN 0246      S4=(F42-F11)/AL4
ISN 0247      WRITE(6,106) IIDD,NCDE1,NCDE2,NODE3,NODE4,AL1,AL2,AL3,AL4
ISN 0248      106 FORMAT(1X,I5,1X,4(I10,2X),4F12,3)
ISN 0249      WRITE(6,107) F11,F21,F31,F41,S1,S2,S3,S4
ISN 0250      107 FORMAT(10X,8F12,3)
ISN 0251      WRITE(6,108) F12,F22,F32,F42
ISN 0252      108 FORMAT(10X,4F12,3,/)
C THIS COMPLETES DATA CALCULATION AND OUTPUT      3/17/72
ISN 0253      GO TO 620
ISN 0254      450 K= 3
ISN 0255      GO TO 550
ISN 0256      460 K= 0
ISN 0257      GO TO 510
ISN 0258      470 K= 3
ISN 0259      GO TO 510
ISN 0260      480 K= 1
ISN 0261      GO TO 530
ISN 0262      490 CALL SELAS2
ISN 0263      GO TO 620
ISN 0264      500 K= 4
ISN 0265      510 CALL SBSPL2(K)
ISN 0266      GO TO 620
ISN 0267      520 K= 2
ISN 0268      530 CALL STQME2(K)
ISN 0269      GO TO 620
ISN 0270      540 K= 4
ISN 0271      550 CALL STRGD2(K)
ISN 0272      GO TO 620
ISN 0273      560 CALL SBAR2
ISN 0274      GO TO 620
ISN 0275      570 AGAIN = .FALSE.
ISN 0276      CALL SCCNE2( SORC )
ISN 0277      GO TO 620
ISN 0278      580 CALL STRIR2(TGRID)
ISN 0279      GO TO 620
ISN 0280      590 CALL STRAP2(TGRID)
ISN 0281      GO TO 620
ISN 0282      600 CALL STORD2(TGRID)
ISN 0283      GO TO 620
ISN 0284      610 GO TO 500
C*****
C CALL ELEMENT 2 TIMES FOR COMPLEX VECTOR. IMAGINARY FIRST, REAL SECOND
C CALL ELEMENT ROUTINE TWICE IF AXIC PROBLEM
C ONCE FOR EACH OF THE 2 VECTORS IN CORE
C*****
ISN 0285      620 IF( AXIC .AND. MIDVEC.NE.0 .AND. IPART.EQ.1 ) GO TO 625
ISN 0287      IF( IPART .GE. KTYPE ) GO TO 615
ISN 0289      625 IVEC = MIDVEC
C*****
C FOR CONICAL SHELL ONLY

```

Output Format Comparison

<i>Nastran</i>	<i>Loading Condition</i>	<i>Member</i>
	1 2 . . . n	1 → r 1 → r . . . 1 → r
<i>Astral</i>	<i>Member</i>	<i>Loading Condition</i>
	1 2 . . . r	1 → n 1 → n . . . 1 → n

FIG. 1

*Member Output Form Comparison*

<i>Element Type</i>	<i>Astral M Print Output</i>	<i>Nastran Output</i>
<i>Astral Bar</i> <i>Nastran Rod</i>	<i>Node forces at each end of bar</i>	<i>Average force in bar</i> <i>Average stress in bar</i>
<i>Astral Beam</i> <i>Nastran Bar</i>	<i>Node forces at each end of Beam.</i> <i>Moments, torque and shear at each end of beam</i>	<i>Average force in beam</i> <i>Moments, torque and shear as for Astral. All respective stresses</i>
<i>Shear Panel</i> <i>(Astral Type 6)</i> <i>(Nastran Shear)</i>	<i>Shear flow (#/in.) along all four sides</i> <i>Length of each side</i>	<i>Four diagonal forces on shear panel</i> <i>Average and maximum shear stress #/in<sup>2</sup></i>
<i>Quadrilateral Membrane</i> <i>(Astral Type 8)</i> <i>(Nastran QDMEM)</i>	<i>Node cap forces along each side</i> <i>Shear flow (#/in.) along each side</i> <i>Length of each side</i>	<i>No force type output</i> <i>Average stresses in local x and y directions and shear stress</i> <i>Principal stresses and maximum shear stress</i>
<i>Triangular Membrane</i> <i>(Astral Type 4)</i> <i>(Nastran TRMEM)</i>	<i>Node cap forces only</i>	<i>No force type output</i> <i>Stress output as for Quadrilateral membrane</i>

FIG. 2

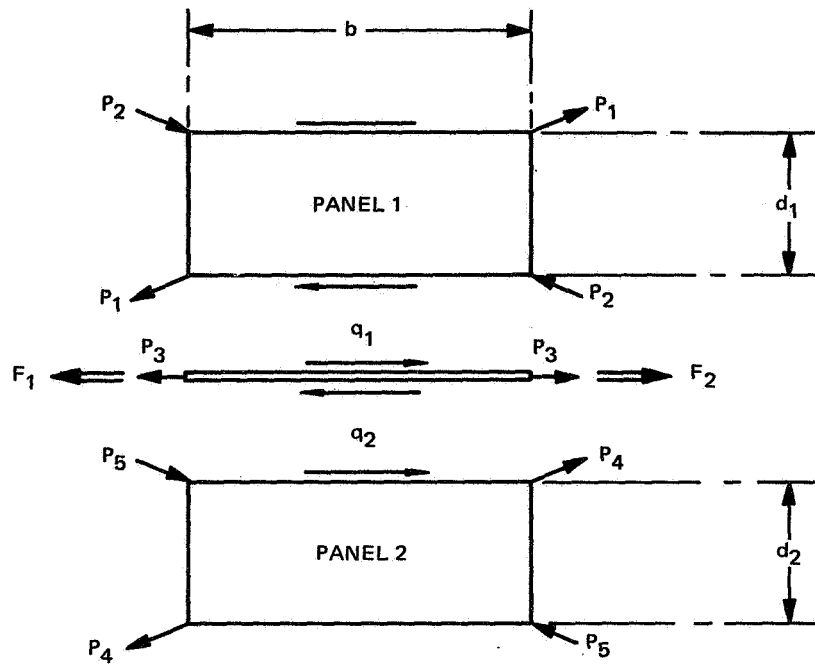


FIG. 3 ROD AND RECTANGULAR PANEL—EXAMPLE

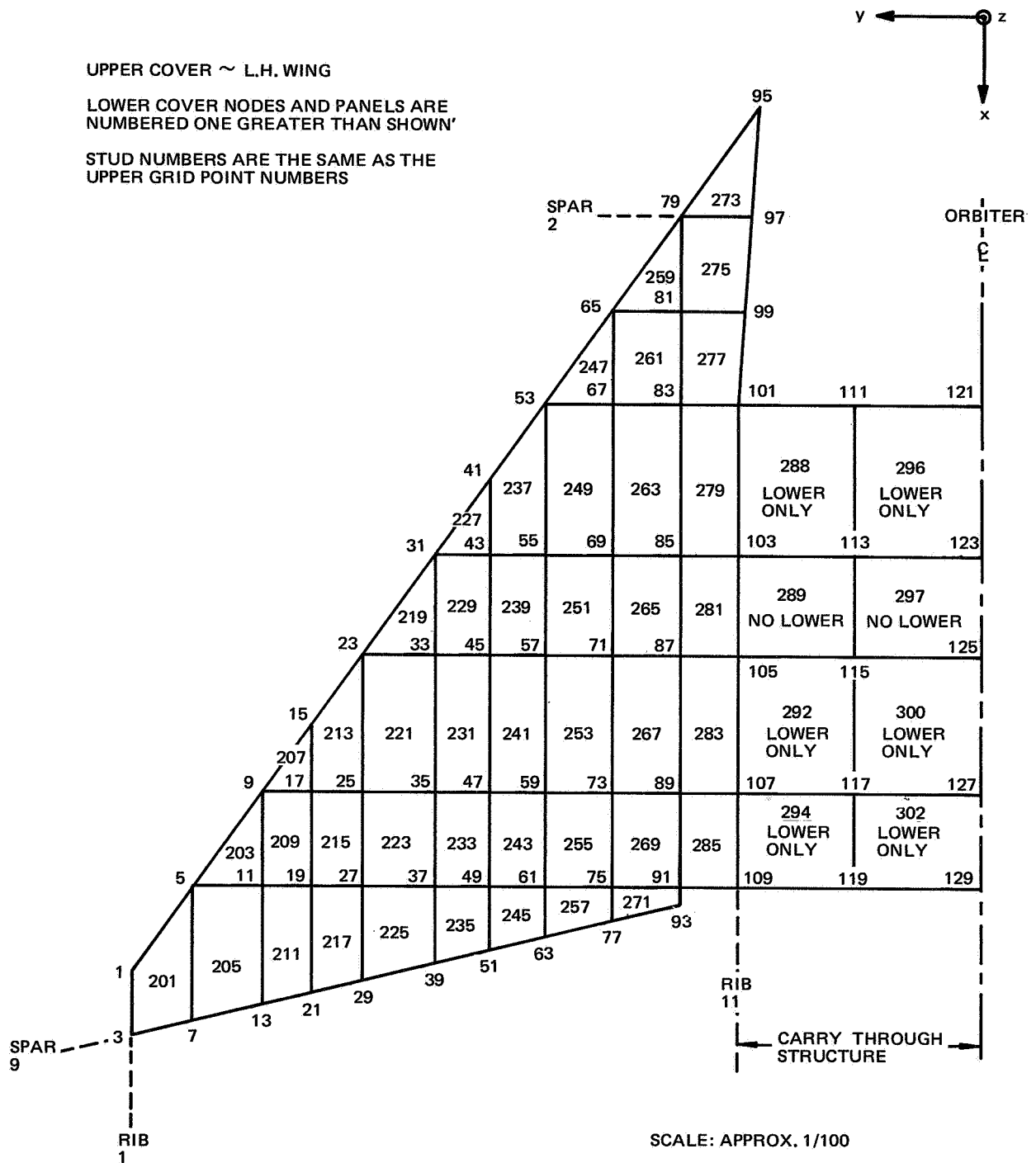


FIG. 4 ORBITER WING IDEALIZATION

*Program Running Times - Comparison*

<i>Time in Seconds</i>	<i>Comap Astral</i>	<i>Nastran</i>
<i>CPU</i>	<i>101.2</i>	<i>214.3</i>
<i>Job</i>	<i>157.7</i>	<i>241.3</i>

*FIG. 5*

Spanwise Load Intensity Distribution

Astral Results (M Print)

Node Number	Spanwise Load #	Effective* Width in.	$N_x$ #/in	Distance From F. Bm in.
79	+1100	35.63	+31	0
81	-4133	70.66	-59	71.3
83	-69980	91.57	-764	141.3
85	-130990	93.66	-1399	254.4
87	-150400	88.43	-1701	328.6
89	-118790	86.62	-1370	431.3
91	-93280	41.57	-2240	501.9
93	0	6.26	0	514.4

\* Effective width is equal to the sum of half the panel widths on each side of the node.

Fig. 6

Nastran Results

Panels	Inbd of	Panel	$N_x$	Panels	Inbd of	Panel	$N_x$	Average	Distance
Rib 10	$F_x^*$ #/in <sup>2</sup>	t in	#/in	Rib 10	$F_x^*$ #/in <sup>2</sup>	t in	#/in	$N_x$	Aft of Front Beam
259	-7680	.025	-192	275	-4210	.0250	-19	-105	35.6
261	-12990	.025	-325	277	-16510	.0250	-500	-412	106.3
263	-35350	.025	-884	279	-39820	.0256	-1134	-1009	197.8
265	-49500	.0277	-1371	281	-52060	.0317	-1732	-1552	291.5
267	-50000	.0282	-1410	283	-51800	.0307	-1646	-1528	379.9
269	-51400	.0294	-1511	285	-57820	.0369	-2371	-1942	466.6

\*  $F_x$  is the average membrane stress in the panel, in the local coordinate system x direction.

Fig. 7

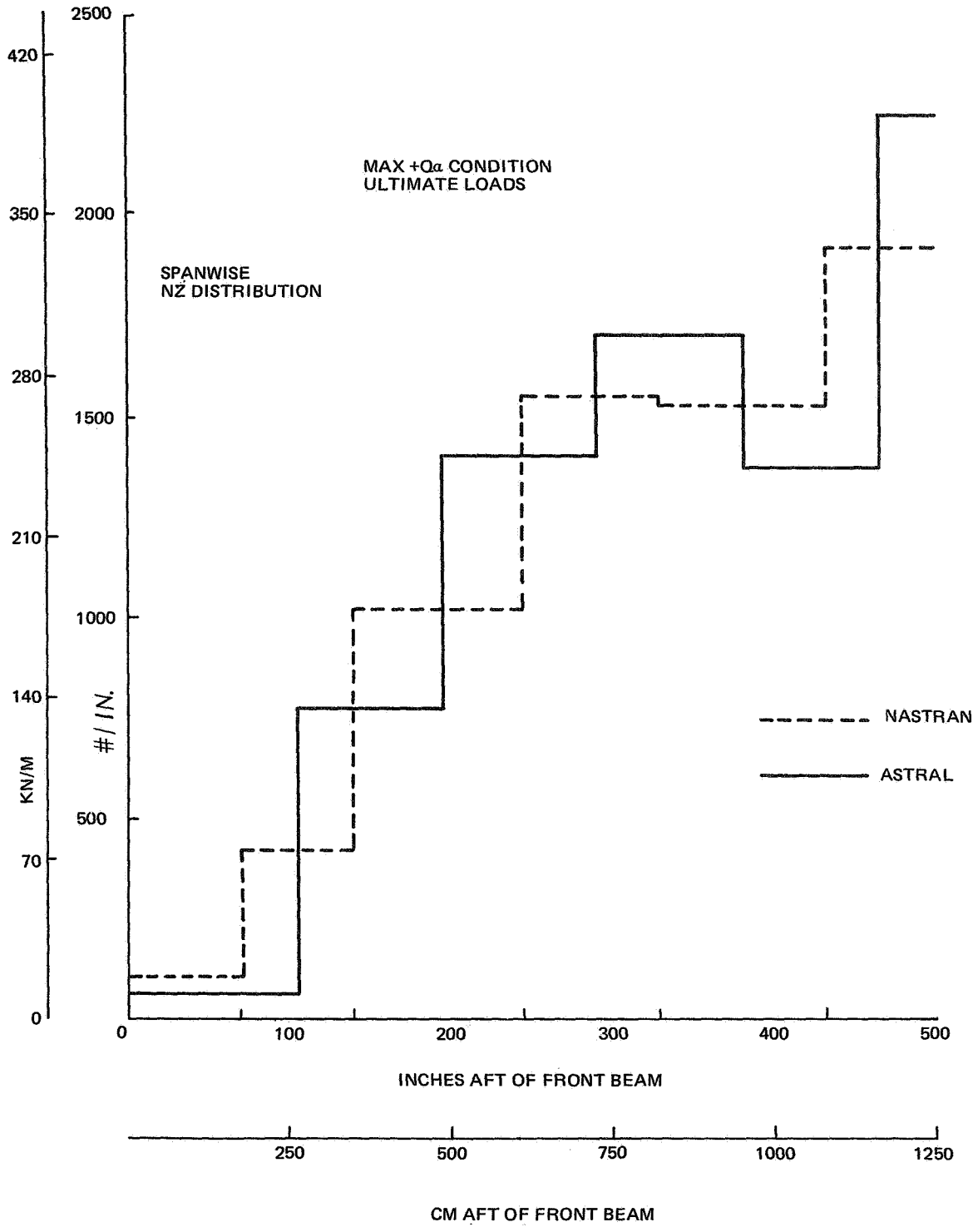


FIG. 8 ORBITER WING – ASTRAL/NASTRAN COMPARISON  
UPPER COVER RIB 10 LOAD DISTRIBUTION

*Nastran and Astral Maximum Shear Flows in Rib 10*

<i>Panel Number</i>	<i>Nastran Max. Shear Stress #/in.</i>	<i>Panel Thickness in.</i>	<i>Nastran Max. Shear Flow #/in.</i>	<i>Astral Max. Shear Flow #/in.</i>
461	11212	.02	224	233
463	10473	.02	210	244
465	2086	.02	42	37
467	17297	.02	346	327
469	9235	.02	185	160
471	10915	.02	218	289
473	19476	.02	389	343

*FIG. 9*

RIB AND SPAR PANELS, TO SCALE, WITH APPROPRIATE  
DIAGONAL LOADS AND AVERAGE STUD LOAD SHOWN

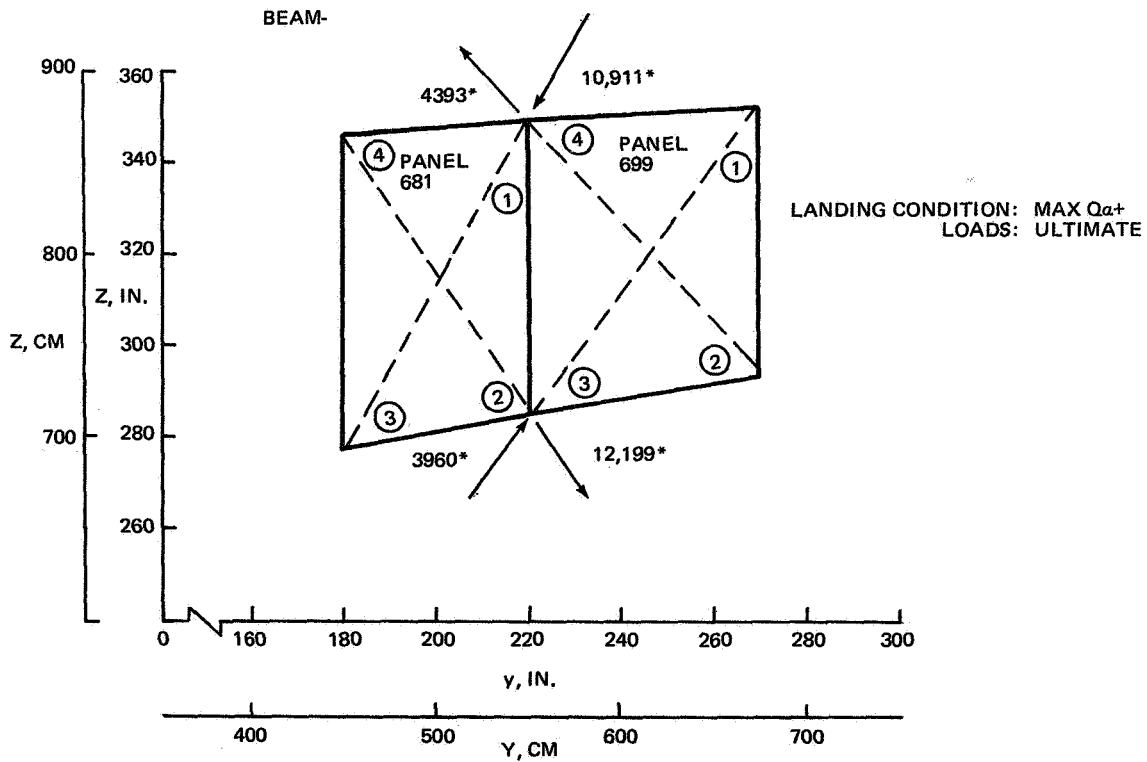
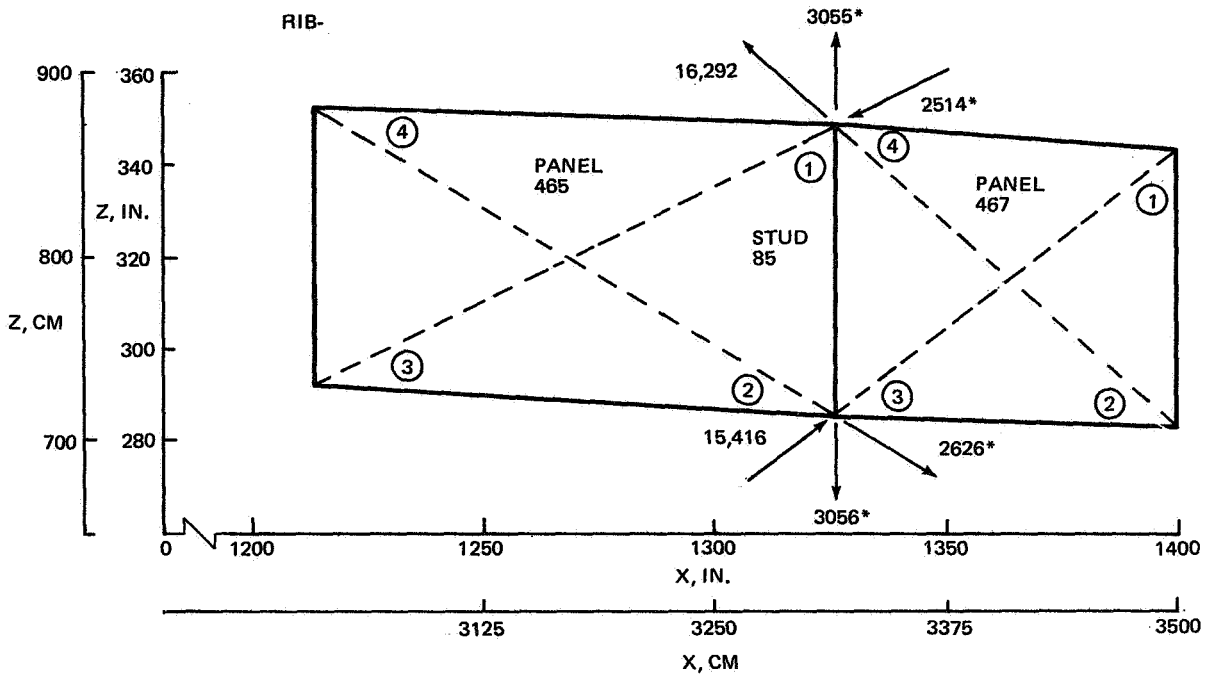
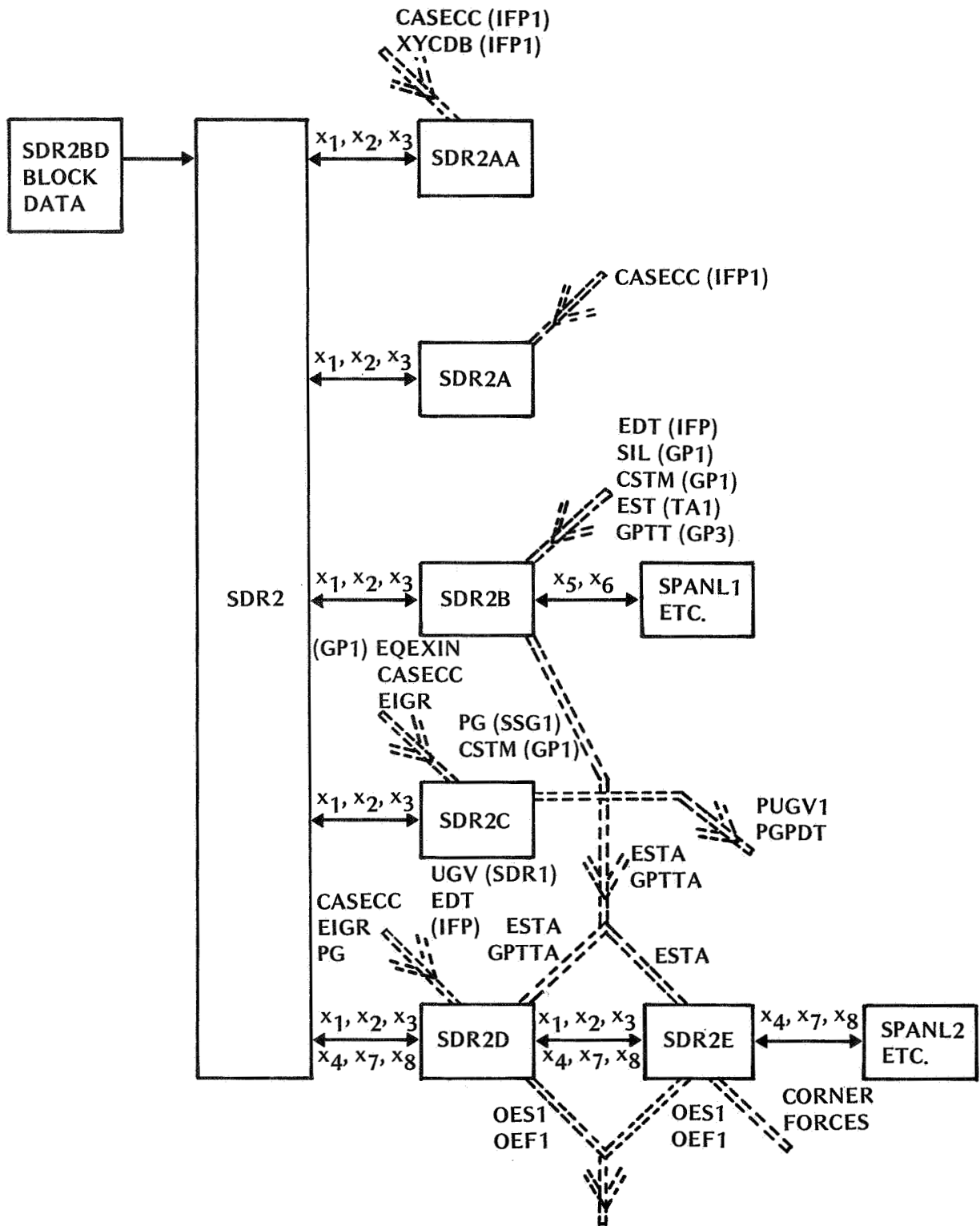


FIG. 10 NASTRAN-EXTRACTION OF STUD LOADS

NASTRAN MODULE SDR2



ADDITIONAL DATA FOR  
CORNER FORCE MODIFICATIONS

Fig. 11

*Summary of Changes to SDR2 Module to Provide Shear Panel Corner Force Output*

<i>Routine</i>	<i>Location</i>	<i>Change or Inclusion</i>
<i>SDR2BD</i>	<i>Line 88 "Data Elem 1"</i>	<i>Increase "ESTA" block for "shear" element by number of words being added (8 in this case) column 40 . . . 33 (was 25)</i>
<i>SDR2E</i>	<i>Line 36</i>	<i>Add: "Dimension XLESTA (100), XBUFB (200)" These are 'real' array equivalents of integer arrays 'ELESTA' and BUFB</i>
<i>SDR2E</i>	<i>Line 96</i>	<i>Add: "Equivalence (ELESTA (1), XLESTA (1)), (SBUFB (1), BUFB (1))"</i>
<i>SDR2E</i>	<i>Line 111</i>	<i>Add Headings for each subcase. This output will appear at the beginning of each subcase.</i>
<i>SDR2E</i>	<i>Line 289</i>	<i>Add: a) calculations for shear flows, etc. b) output of shear flows, etc.</i>
<i>SPANL1</i>	<i>Line 69 "common"</i>	<i>In common "/SDR2X5/" and SPOUT (8) (to hold corner coordinates) Continuation card 3: "3, SPOUT (8), yyyyy (94)"</i>
<i>SPANL1</i>	<i>Line 191</i>	<i>Add: SPOUT (1),,,, SPOUT (8) = 0.0, 0.0, X2, 0.0, X3, Y3, X4, Y4</i>

*Fig. 12*

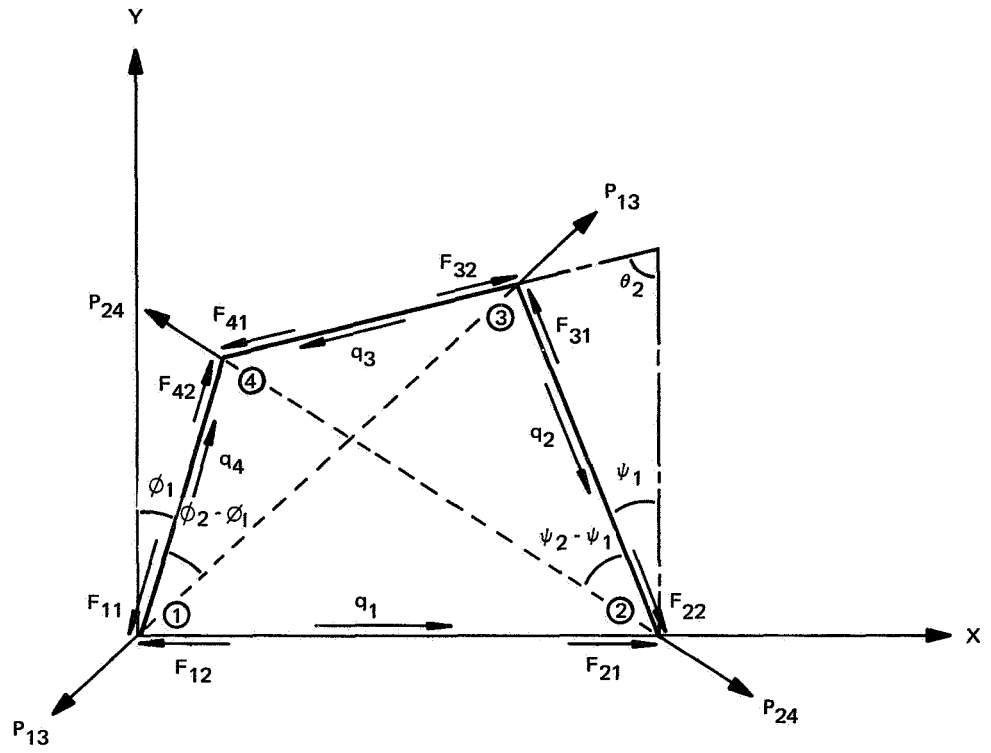


FIG. 13 SHEAR PANEL NOMENCLATURE, LOCAL COORDINATES

A DESIGN STUDY FOR THE ADDITION OF HIGHER-ORDER  
PARAMETRIC DISCRETE ELEMENTS

TO NASTRAN\*

By E. L. Stanton

McDonnell Douglas Astronautics Company  
Huntington Beach, California

SUMMARY

Higher-order parametric discrete elements are a significant modeling advance over similar elements with straight-sided triangular or quadrilateral planforms. However, the addition of such discrete elements to NASTRAN poses significant interface problems with the Level 15.1 assembly modules and geometry modules. The present paper systematically reviews potential problems in designing new modules for higher-order parametric discrete elements in both areas. An assembly procedure is suggested that separates grid point degrees of freedom on the basis of admissibility. New geometric input data are described that facilitate the definition of surfaces in parametric space.

SYMBOLS

$C^k$	Denotes continuity through $k$ derivatives
$f_{,\alpha\beta}$	The partial derivative of $f$ with respect to $\alpha$ and $\beta$
$df$	Total differential of $f$
$R$	Cylindrical radius
$S$	Arc length
$u^\alpha$	Elastic displacement in the curvilinear coordinate direction $\alpha$
$u^3$	Elastic displacement normal to the midsurface
$UA$	Grid point displacement parameters required for admissibility

\*This work was performed under the sponsorship of the McDonnell Douglas Astronautics Company Independent Research and Development Program.

UH	Grid point displacement parameters not required for admissibility
$x^i$	Grid point coordinates in a reference coordinate system
$\theta^i$	Rotations about the $x^i$ coordinate directions
$(\xi, \eta)$	Patch parameters analogous to curvilinear coordinates
Subscripts:	
FP	Flat plate
CP	Cylindrical panel

## INTRODUCTION

In the main, joining problems arise with higher-order discrete elements because the additional grid point degrees of freedom contain terms directly proportional to element strains. A complete one-to-one joining of displacement parameters between geometrically similar elements implies a strain continuity that is erroneous if the elements are of different materials. A complete one-to-one joining of displacement parameters between geometrically dissimilar elements implies a strain discontinuity that is erroneous if the elements are of similar materials. An example of this latter behavior will be given in which the in-plane displacement gradients are erroneously linked between cylindrical panel elements and flat plate elements. To obtain the correct solution these parameters must either be allowed to vary independently or be joined by a constraint equation for in-plane strain continuity. In general, any variational problem can be solved by using only the minimum constraints required to produce an admissible displacement field for the Ritz procedure. As a practical matter this approach is of little help if used uncritically since it can add many unnecessary degrees of freedom. At the intersection of four MDAC parametric discrete elements, for example, there are 48 degrees of freedom that are reduced by admissibility constraints to 22 independent degrees of freedom. When strain continuity constraints are applied these are reduced to 12 independent degrees of freedom. In this case there is nearly a 50 percent reduction when strain continuity is valid. Any modification of the NASTRAN assembly modules to process higher-order discrete elements must be flexible enough to take advantage of this situation if it is to be efficient.

The basic geometric entity used by NASTRAN is the grid point. The basic geometric entity need for parametric discrete elements is a mapping of two surface coordinates into points on the surface in three dimensions. This mapping, called a patch, is approximated locally by interpolation functions. These functions must be input to NASTRAN in order to generate element matrices (stiffness, etc.). It is, of course, feasible to input the patch for each element directly as part of the property data for the element. This has the obvious disadvantage of requiring a great deal of input data; up to 48 items for a bicubic patch. To reduce input data requirements, the MDAC parametric plate element program uses the boundary curve for the entire plate to generate patches for each discrete element once a topological mesh has been specified (Reference 1). The present paper considers new geometric input data for NASTRAN to facilitate the introduction of parametric discrete elements.

#### ADMISSIBLE DISPLACEMENT FIELDS

Admissibility conditions for discrete element displacement functions are an especially important topic for higher-order discrete elements. In classical variational mechanics the material properties are usually assumed either constant or continuously differentiable functions of the spatial coordinates. This leads to simple smoothness requirements based on the order of the differential operator in the equilibrium equations (Reference 2). The displacement  $u^3$  in a homogeneous plate bending problem, for example, must be  $C^4$  in the interior and  $C^3$  on a free edge. The latter condition is a consequence of the natural boundary condition for shear. These are of course conditions on the continuum displacement solution that the discrete element model must converge to in the limit. Convergence is measured by an energy norm and it is the existence of this norm that sets the admissibility conditions for the piecewise polynomial displacement function formed by assembling individual discrete elements. Returning to the plate example, the energy norm is derived from the strain energy density which involves at most second derivatives of  $u^3$ . As long as the discrete element displacement field is at least  $C^1$  between elements the energy norm is well defined. Physically this condition corresponds to the absence of a hinge between plate elements and it is imposed at the grid points to assemble or build a discrete element model of a plate structure. How closely the assumed displacement functions approach

this condition between nodes is a problem in approximation theory that is intimately related to the question of completeness. This is another issue entirely and for the present discussion completeness will be assumed. Again returning to the plate example if there are no line moments between elements and the material is continuous, then the strains are continuous. Additional constraints can then be used to impose inter-element strain continuity but these conditions are not required for admissibility. The solutions obtained with and without these additional constraints will often have the same mean error (Reference 3) but the solution with strain continuity will require solving fewer equations. When dealing with higher-order elements the constrained stiffness matrix may be less than one-half the dimension of the original.

When higher-order discrete elements with distinctly different strain-displacement equations must be assembled, a clear understanding of the admissibility conditions is essential. Perhaps the best way to describe the possible pitfalls is with an illustrative example. Consider adjacent flat plate and cylindrical panel elements from the discrete element model of the pear-shaped cylinder shown in Figure 1. Using the Bogner, Fox, Schmit (BFS) plate and cylindrical panel elements (Reference 4), there are 12 degrees of freedom per grid point per element, the three displacement components relative to a local curvilinear coordinate frame  $u^\alpha$ ,  $u^3$  and the nine gradients of these displacement components  $u^\alpha, 1$ ,  $u^\alpha, 2$ ,  $u^\alpha, 12$ ,  $u^3, 1$ ,  $u^3, 2$ ,  $u^3, 12$ . There is a tendency to erroneously assume the plate displacement gradient components are equal the panel displacement gradient components at a common node, in particular  $(u^2, 2)_{FP} = (u^2, 2)_{CP}$ . A substantial error in the normal displacement component  $u^3$  is caused by this assumption as shown in Figure 2 for the pear-shaped cylinder under a uniform axial load. The admissibility conditions merely require  $(u^\alpha)_{FP} = (u^\alpha)_{CP}$  and  $(u^3, \alpha)_{FP} = (u^3, \alpha)_{CP}$  where the curvilinear coordinates have been parameterized such that  $d\alpha = dS$  in each element. This allows discontinuities in  $u^2, 2$  which of course must exist if we are to have continuous midsurface strains,

$$\left(u^2, 2\right)_{FP} = \left(u^2, 2\right)_{CP} + \frac{u^3}{R} \quad (1)$$

It should be noted that it is not necessary to use Equation (1) as a constraint. The minimum potential energy theorem ensures that the Ritz procedure for admissible displacement fields will find  $(u^2, 2)_{FP}$  and  $(u^2, 2)_{CP}$  such that equilibrium is satisfied in the limit. In this problem equilibrium implies strain continuity and Equation (1) can be used as in Reference 5 as an additional constraint which reduces the number of equations to be solved. If we modify the pear-shaped cylinder such that the flat panel material is different from the cylindrical panel material then Equation (1) cannot be used since equilibrium now requires a strain discontinuity.

There are at least two other situations in the assembly of higher-order discrete elements that deserve attention. Consider the stiffened cylindrical panel shown in Figure 3 again modeled using the BFS discrete elements. In this case, even though adjacent cylindrical panel elements have the same strain displacement equations and are made of the same material, there can be discontinuities in  $u^1, 2$  caused by load transfer between the stiffener and the cylindrical panel. Consider next an error that can occur when constraining the three rotations to be equal between adjacent higher-order plate elements. Let  $x^1 = \text{constant}$  be the common edge between two BFS plate elements and recall that the elastic rotations are one-half the curl of the displacement vector. Using a Cartesian coordinate system, the rotations are

$$\begin{aligned}\theta^1 &= \frac{1}{2} u^3, 2 \\ \theta^2 &= -\frac{1}{2} u^3, 1 \\ \theta^3 &= \frac{1}{2} (u^2, 1 - u^1, 2)\end{aligned}\tag{2}$$

To ensure the same displacement along the common edge requires  $u^{\alpha}, 2$  and  $u^3, 2$  to be continuous. If, in addition, we now require  $\theta^3$  to be continuous this will imply  $u^2, 1$  is continuous. This in turn implies the shear strains are continuous which is erroneous if the plates are of different materials. Admissibility requires only that  $\theta^1$  and  $\theta^2$  be continuous.

These examples illustrate the pitfalls that can occur in the assembly of high-order discrete elements when constraints are used that exceed those

necessary for admissibility. Unfortunately it is not practical to use only admissibility constraints when strain continuity or other grid point constraints are valid. These constraints not only reduce the number of equations, they usually do not change the structure of the stiffness matrix (if it was banded it will remain banded) and in most cases they do not increase the mean error. The design of a new structural matrix assembly module for use with higher-order elements in NASTRAN must take these factors into account.

## STRUCTURAL MATRIX ASSEMBLY MODULE

The structural matrix assembly module in Level 15.1 of NASTRAN cannot process discrete elements with more than six degrees of freedom per grid point. A new module is required for higher-order elements that accounts for accurate and efficient design requirements. Assembly based on simply the admissibility conditions must be available as a default and grid point constraints must be available for efficiency. The module should be able to assemble the existing general elements in NASTRAN with higher-order elements of different types. This suggests two categories of grid point degrees of freedom for each element; those directly involved in admissibility conditions, UA, and all others, UH. All grid point degrees of freedom (in element coordinates) for all general elements now in NASTRAN fall in the first category. The new grid point degrees of freedom, UH, are somewhat like scalar point variables except they are elastically coupled to all the other grid point degrees of freedom for an element. As a default value, the number of UH at a grid point is equal the sum of the UH associated with that grid point from each element connected to that grid point. This corresponds to assembly based simply on admissibility. Next, it is necessary to provide for grid point constraints that are linear equations, usually identities, among the UH and UA at a grid point. This is analogous to multipoint constraint equations with all the degrees of freedom occurring at the same grid point. As a practical matter a unique identification scheme for the UH will be needed. The UA of course already are identified uniquely by component numbers 1 to 6. Also, as a practical matter, an automated grid point constraint generator is needed; one that could set all UH components equal for elements of the same type at a grid point. To fix some of these ideas consider a BFS plate element (Reference 4),

a CKLO plate element (Reference 5) and a QODPLT plate element (Reference 6) all modeling the behavior of a plate having one common grid point. At the element level the QODPLT element has five degrees of freedom per grid point, the BFS element has twelve and the CKLO element has twelve. These are listed in Table 1, divided into UA and UH degrees of freedom.

Table 1. Grid Point Degrees of Freedom

Element	UA <sub>1</sub>	UA <sub>2</sub>	UA <sub>3</sub>	UA <sub>4</sub>	UA <sub>5</sub>	UA <sub>6</sub>	UH <sub>1</sub>	UH <sub>2</sub>	UH <sub>3</sub>	UH <sub>4</sub>	UH <sub>5</sub>	UH <sub>6</sub>	UH <sub>7</sub>
BFS	u <sup>1</sup>	u <sup>2</sup>	u <sup>3</sup>	u <sub>2</sub> <sup>3</sup>	-u <sub>1</sub> <sup>3</sup>		u <sub>1</sub> <sup>1</sup>	u <sub>2</sub> <sup>1</sup>	u <sub>12</sub> <sup>1</sup>	u <sub>1</sub> <sup>2</sup>	u <sub>2</sub> <sup>2</sup>	u <sub>12</sub> <sup>2</sup>	u <sub>12</sub> <sup>3</sup>
CKLO	u <sup>1</sup>	u <sup>2</sup>	u <sup>3</sup>	u <sub>2</sub> <sup>3</sup>	-u <sub>1</sub> <sup>3</sup>		u <sub>1</sub> <sup>1</sup>	u <sub>2</sub> <sup>1</sup>	u <sub>1</sub> <sup>2</sup>	u <sub>2</sub> <sup>2</sup>	u <sub>11</sub> <sup>3</sup>	u <sub>22</sub> <sup>3</sup>	u <sub>12</sub> <sup>3</sup>
QODPLT	u <sup>1</sup>	u <sup>2</sup>	u <sup>3</sup>	u <sub>2</sub> <sup>3</sup>	-u <sub>1</sub> <sup>3</sup>								

The two higher-order elements have elastic rotations about the x<sup>3</sup> axes (c.f. Equation 2) but these are not UA degrees of freedom as described earlier. If the UA<sub>6</sub> degree of freedom is removed with an SPC1 card there are 19 degrees of freedom at the common grid point. If the elements are all of the same material then grid point constraint equations can reduce this to 14. Suppose there is a rod normal to the plate that transmits torsion. This does not add a degree of freedom since UA<sub>6</sub> in this case is related to UH<sub>2</sub> and UH<sub>4</sub> of the BFS element by Equation (2) or equivalently UH<sub>2</sub> and UH<sub>3</sub> of the CKLO element. As is obvious from this example, admissibility cannot be determined for all combinations of general elements without the analyst making judgments about load paths in his structure. These decisions will be input via grid point constraint equations. An analogous situation now exists with frame structures when the analyst uses pin flags (cuts and releases) on the CBAR card to input his decisions about joints.

## PARAMETRIC DISCRETE ELEMENT GEOMETRY

The initial geometric representation of a complicated structure is a formidable design problem but it is one that has been solved by the time a discrete element analysis is required. Some form of a geometric model (loft lines, offsets, etc.) has been prepared and serves as a data base for

the analyst. Increasingly these models are computer generated and in several industries piecewise polynomial surface representation is now used (Reference 7). This form of surface representation is the same as that used for parametric discrete element models and consists of patches that map two parameters  $(\xi, \eta)$  into spatial coordinates  $(x^1(\xi, \eta), x^2(\xi, \eta), x^3(\xi, \eta))$ , on the midsurface of the discrete element. The patches are constructed such that the edges of the element coincide with constant values of the patch parameters  $(\xi, \eta)$  as Figure 4 illustrates. The data required to define a patch with curved edges is obviously more than the grid point coordinates of the corners. If bicubic Hermite polynomials (Coons' surface patches) are used then  $x^i, x^i_{,\xi}, x^i_{,\eta}$  and  $x^i_{,\xi\eta}$  are required at each corner. To a large extent the increased data per grid point is offset by a reduction in the number of grid points required to model the geometry but this is a separate issue. The immediate problem is how to efficiently introduce into NASTRAN the geometric data required by parametric discrete elements. This data can be input as property data for each element or as a separate entity like grid point coordinates that can then be referenced on a broader basis by all elements. The first approach would require a minimum change to NASTRAN but could be very inefficient in that the same boundary data might be input over and over again, once for each element sharing a common edge. Primarily for this reason only the second approach will be considered further.

The patches used for parametric discrete elements are almost always bivariate polynomials although other interpolatory functions are possible. These polynomials can be uniquely determined in several different ways, each related to the other by a linear transformation. A bicubic Hermite polynomial interpolate determined from corner coordinates and derivatives also can be uniquely determined by the coordinates of sixteen points (Reference 1) where four of these must be interior points for the  $x^i_{,\xi\eta}$ . Boundary curves can also be used to define patches. Mallet provides an excellent example (Reference 8) using piecewise cubic interpolation of a grid line to obtain  $C^1$  continuity. This approach uses grid line data in much the same way grid point data is now used in NASTRAN. Another useful representation is the super patch that defines several patches within its boundaries. The super patch is constructed using spline constraints (Reference 9) and has been used by Timmer (Reference 10) to form bicubic patches for aerodynamic surface modeling. Both the grid line modeling and super patch modeling offer the additional

benefit of  $C^1$  continuity along the entire common boundary between adjacent patches. Patches derived with the spline constraints of Reference 9 also have  $C^2$  continuity and require far less input data. This suggests a simple way of constructing grid line data from a near minimal data base. The parametric slopes at the two end points,  $x^i, \xi_1$  and  $x^i, \xi_N$  and the grid point identification numbers  $G_1, G_2, \dots, G_N$  of points on the line are all that's required to define the line. If cross derivative data is desired for Coons surface patches then  $x^i, \xi\eta_1$  and  $x^i, \xi\eta_N$  are also required but only at the four corners of a super patch. A prototype data card for generating a grid line from spline constraints is shown in Figure 5. There are of course situations where spline constraints produce a wavy line that does not model the initial geometry well. In this instance the parametric slopes should be input for every grid point on the line. Although no mention of grid line parameterization has been made, it will be necessary to adopt some standard such as  $0 \leq \xi \leq 1$  between adjacent grid points.

#### REFERENCES

1. Palacol, E. L. and Stanton, E. L.: Anisotropic Parametric Plate Discrete Elements. McDonnell Douglas Astronautics Company Paper WD 1656, March 1972.
2. Mikhlin, S. G.: Variational Methods in Mathematical Physics. Macmillan, New York, Chapter 2, 1964.
3. Stanton, E. L. and Schmit, L. A.: A Discrete Element Stress and Displacement Analysis of Elastoplastic Plates. AIAA Journal, Vol. 8, No. 7, July 1970, pp. 1245-1251.
4. Schmit, L. A., Bogner, F. K., and Fox, R. L.: Finite Deflection Structural Analysis Using Plate and Shell Discrete Elements. AIAA Journal, Vol. 6, No. 5, May 1968, pp. 781-791.
5. Lindberg, G. M. and Cowper, G. R.: An Analysis of a Cylindrical Shell With a Pear-Shaped Cross Section-Lockheed Sample Problem No. 1. National Research Council of Canada, NAE Lab., Memo. ST-139, June 1971.
6. MacNeal, R. H. (Editor): The NASTRAN Theoretical Manual. NASA SP-221, September 1970.

7. Birkhoff, G. and De Boor, C.: Piecewise Polynomial Interpolation and Approximation. Approximation of Functions, edited by H. L. Garabedian, Elsevier, New York, 1965, pp. 164-190.
8. Mallett, R. H.: Formulation of Isoparametric Finite Elements with  $C^1$  Continuity. Bell Aerospace Co. Report No. 9500-920209, Jan. 1972.
9. De Boor, C.: Bicubic Spline Interpolation. Journal of Mathematics and Physics, Vol. 41, 1962, pp. 212-218.
10. Timmer, H. G.: Ablation Aerodynamics for Slender Reentry Bodies. AFFDL-TR-70-27, Vol. 1, March 1970.

MATERIAL PROPERTIES:

$E = 68.95 \times 10^9$  NEWTONS/METER<sup>2</sup>

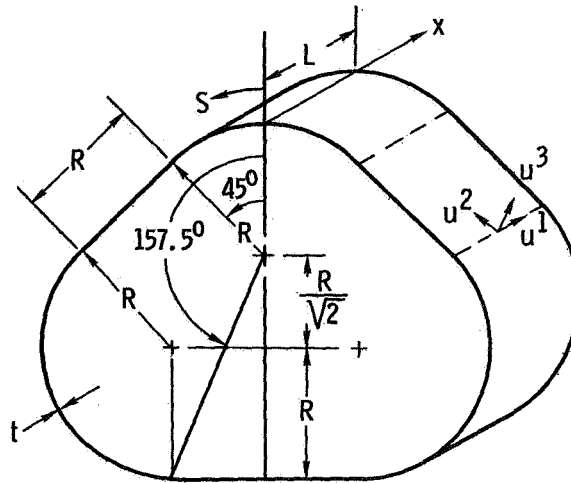
$\nu = 0.3$

$\rho = 689.5$  NEWTONS/METER<sup>2</sup>

$R = 2.54$  CM

$L = 2.032$  CM

$t = 0.254$  CM



UNIFORM AXIAL LOAD = 1.751 NEWTONS

Figure 1 Cylindrical Shell with Pear-Shape Cross-Section

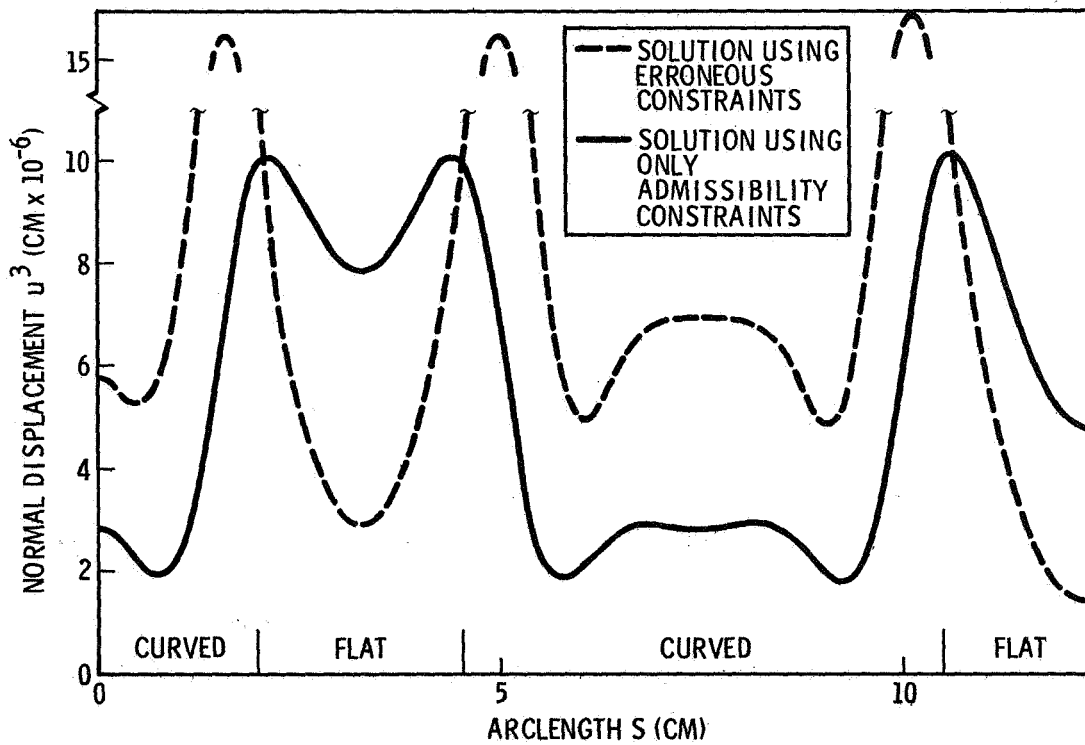


Figure 2 Effect of Erroneous Constraints Between Higher-Order Curved and Flat Discrete Elements

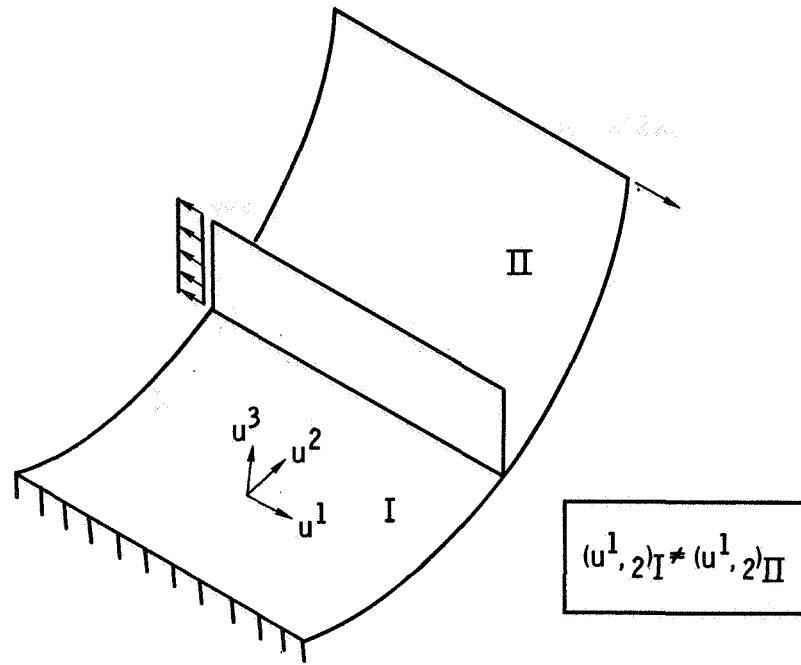


Figure 3 Stiffened Panel Joining Example

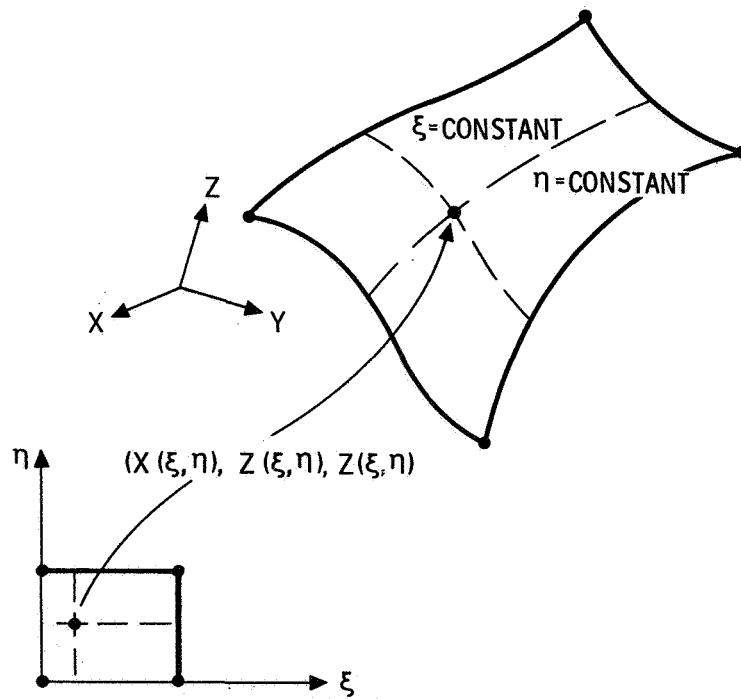


Figure 4 Discrete Element Geometry Represented by a Patch

BULK DATA DECK

INPUT DATA CARD SPLINI GRID LINE SPLINE CONSTRAINTS

DESCRIPTION: DEFINE END SLOPES AND INTERMEDIATE GRID POINTS FOR  
A TYPE I SPLINE CONSTRAINT EQUATION

SPLINI	GLID	CD	X1C1	X2C1	X3C1	X1CN	X2CN	X3CN	abc
+bc	G1	G2	.	.	.	GN			

FIELD	CONTENTS
GLID	GRID LINE IDENTIFICATION NUMBER
CD	IDENTIFICATION NUMBER OF COORDINATE SYSTEM IN WHICH THE PARAMETRIC SLOPES ARE INPUT
X1C1	PARAMETRIC SLOPE $x^1_{,\xi}$ AT GRID POINT 1
X3CN	PARAMETRIC SLOPE $x^3_{,\xi}$ AT GRID POINT N
G1, G2, .. GN	GRID POINT IDENTIFICATION NUMBERS OF POINTS ON GRID LINE GLID IN SEQUENCE

Figure 5 Prototype Bulk Data Card for Spline Constraints



MODIFICATIONS AND ADDITIONS TO NASTRAN  
AT MARSHALL SPACE FLIGHT CENTER

1969 - 1972

By Archie J. Jordan, Jr., and William G. Ward  
Computer Sciences Corporation

SUMMARY

Modifications made to NASTRAN at Marshall Space Flight Center, Huntsville, Alabama, can be grouped into two general classes:

1. Those modifications to NASTRAN code which result from the location, identification, and correction of errors or operational problem areas.
2. Addition of new capability which is structural, executive system oriented, or utility in nature.

In addition to these modifications to NASTRAN, several important studies have been conducted at MSFC relative to NASTRAN efficiencies and inefficiencies.

INTRODUCTION

A brief description on some of the major modifications to NASTRAN will be discussed. These are modifications which have been made to various levels of NASTRAN and which are currently incorporated into MSFC's version of Level 12. Because of the significance of two studies conducted relative to NASTRAN efficiencies and inefficiencies, more time will be allotted to discussion of these studies and their results.

Modifications and Additions

- (1) A post-processor was written to stack SC-4020 plot commands generated by NASTRAN onto drum, preceded by the MSFC standard identification frame and followed by the MSFC standard end job frame. This was written in the form of a utility subroutine, but performs as a post-processor in that it is executed after all other NASTRAN activities have been completed. This modification

was made at the request of MSFC Computation Laboratory management in order to solve SC-4020 tape labeling problems on NASTRAN runs coming in from remote terminals.

- (2) The method of obtaining accumulated CPU time for triangular decomposition "time-to-go" checks and other time checks in NASTRAN was changed due to a change in the 1108 Executive System's PCT (Program Control Table). Accumulated CPU time is now found by interrogating a locally maintained system routine since the format of the PCT appears to be highly evolutionary.
- (3) Additions and modifications to the NASTRAN Executive System were made to allow the capability of inputting NASTRAN Executive, Case Control, and Bulk Data decks from magnetic tape instead of cards. The user may also require the flexibility of inputting the Executive and Case Control decks from cards and the Bulk Data decks from a non-UMF formatted tape. This case often occurs when a user has generated a large amount of bulk data in a small FORTRAN data conversion program and the number of punched cards is prohibitively large. Both of these options were made available.
- (4) A NASTRAN DMAP functional module, OUTPUT 2, was developed to write on magnetic tape the non-zero terms of the lower triangular portion of a NASTRAN symmetric matrix. Options have been recently included in this module which allow for writing on tape or punching on cards non-zero terms of a general matrix in a user specified FORTRAN format.
- (5) A NASTRAN DMAP functional module was developed to punch out NASTRAN matrices in the NASTRAN Bulk Data DMI card format. A module similar to this will be delivered in Level 15 by NSMO. However, the module developed here will punch out single and double precision values instead of just single precision values and will also punch complex matrices, such as complex eigenvectors.
- (6) Modifications to appropriate subroutines in NASTRAN's Executive System have been made which will generate a forced checkpoint if the run time on the run card is greater than or equal to 30 minutes. The modified code will detect the run time, assign a checkpoint tape, generate the card image "CHKPNT YES" in the Executive Control deck and allow for the punching of the restart dictionary. This modification was developed at the request of the MSFC NASTRAN Technical Monitor who felt some users were not using the checkpoint feature at all and, as a result, were needlessly using CPU time in subsequent runs. This inhibits all users from getting machine time. With the automatic checkpoint feature, it is not necessary for the user to include the "CHKPNT YES" option in his run. A close kin to this capability is the development of the NASTRAN Executive System capability of forcing "undeformed structural plots" for NASTRAN runs which appear to be large (greater

than 30 minutes). Again, it was felt that too many users were creating large models and making many long runs without ever checking their model by looking at the undeformed plots. This capability is now being developed.

- (7) A modification was made to the real eigenvalue module to print out the eigenvalue iteration information as computed and to force exit from the algorithm as soon as the first root is obtained. This capability is often desirable in buckling problems where only the first mode is desired and run times are long.
- (8) Several functional modules have been developed and incorporated into MSFC's NASTRAN version which allow for a complex eigenvalue solution for a spinning flexible body such as NASA's SKYLAB. The user DMAP sequence for this capability is available, and a detailed user paper is being presented in this colloquium by Dr. Jayant S. Patel of Teledyne-Brown Engineering.
- (9) Two DMAP functional modules have been developed which will allow for the capability of substructuring in NASTRAN as defined by a segment of the MSFC structural analysis NASTRAN user community. Basically, one module unpacks and writes NASTRAN matrices on a magnetic tape; the other reads matrices from magnetic tape, packs them in NASTRAN matrix format and generates corresponding NASTRAN output data blocks. These data blocks (matrices) are then utilized in a DMAP sequence or rigid format to accomplish the substructuring task. This approach can be used to model a structure with up to eight substructures.

#### Studies on NASTRAN Efficiencies and Inefficiencies

Two significant studies will be presented relative to NASTRAN efficiencies and inefficiencies:

1. NASTRAN CPU Time Versus Available Core for Triangular Decomposition.
2. Investigation of NTRAN I/O Usage in NASTRAN.

The first study was initiated in order to discover some quantitative relationship between "core" solutions and "spill logic" solutions for NASTRAN problems requiring triangular decomposition on MSFC's UNIVAC 1108 EXEC VIII. For large NASTRAN problems, a substantial amount of the total computing time is associated with triangular decomposition. NASTRAN performs this decomposition task utilizing all available core. It dynamically allocates its large arrays at execute time by employing an "open core" concept. The use of fixed dimensions for large arrays is avoided since this automatically restricts the size of the problems that can be solved. Instead, FORTRAN routines are programmed to allocate space as required and to use all of core available to user programs. When all of core has

been allocated, NASTRAN then uses "spill logic" to transfer data to scratch files and back to core again. NASTRAN calculates the amount of available core ("open core") for allocation purposes by determining the number of words available between the origin of "open core" and the end of core.

To demonstrate the relationship between CPU time and available core for triangular decomposition, it was decided to develop a problem which would yield an "all core" decomposition for 65K on the UNIVAC 1108 and then decrease the amount of available core to NASTRAN in subsequent runs. This decrease in the amount of available core would cause the "all core" solution to become a "spill logic" solution. Comparisons of CPU run times would give some insight into the excessive run times being experienced at this center for decomposition problems.

Using Version 12 of NASTRAN, the amount of "open core" can be reduced with relative ease. By choosing appropriate options on the UNIVAC 1108 Executive Control XQT card, a user can limit the amount of core available for his own NASTRAN problem. Four runs were submitted for various size models with available core figures of:

1. 65K
2. 55K
3. 50K
4. 42K

The structural problem developed to use as a test case for this study was a rectangular panel made up of quadrilateral plate elements with a bandwidth of 169 and 480 degrees of freedom. A buckling analysis was performed on the panel, and only one eigenvalue was obtained. The CPU run times for the four test runs were evaluated by three different methods:

1. Total CPU run time versus available core.
2. CPU time spent in the NASTRAN functional module, READ, versus available core. This module performs the matrix decomposition and eigenvalue solution.
3. CPU time spent only in the decomposition portion of READ versus available core. It is this portion of the READ module which contains the "spill logic".

These run times are given in Attachment A, and the results are plotted in Figures 1, 2, and 3 to graphically illustrate the increase in CPU time in all program areas as the amount of available core is steadily decreased. Since the aim of this study was to determine the increase in CPU time due to the use of "spill logic" in triangular decomposition, it is important to note that the CPU time for

the entire program increased 2.4 times (240%) when core was decreased by 1/3 (33 1/3%). The total decomposition CPU time increased 6.5 times (650%) due to the same decrease in available core. It is also important to notice that the increase in CPU time in the three areas mentioned is not linear; i. e., the ratio of the change in CPU time to the change in available core is not constant.

#### Investigation of NTRAN I/O Usage in NASTRAN

The second study was initiated in order to determine if NASTRAN's NTRAN I/O package was hurting NASTRAN performance at MSFC since it was known that the NTRAN I/O was excessively inefficient. A series of test runs was made in which 249 word records (FORTRAN buffer size) were written from core to drum by MSFC's NTRAN, NASTRAN's NTRAN, and FORTRAN binary I/O operations. In addition, two approaches to using NTRAN were tested and were designated NTRAN 1 and NTRAN 2 as follows:

- NTRAN 1 - A method of NTRAN usage in which a wait in NTRAN occurs until all previous operations, for the specified logical unit, are complete before stacking any further operations or returning to the user's program. This approach is the method employed by NASTRAN.
  
- NTRAN 2 - A method of NTRAN usage in which the transmission status word is tested in a FORTRAN loop until an error occurs or the transmission is successfully completed.

The results from one such series of tests follow. In these tests, each I/O method was allowed to write as many records as possible (up to 4000) in two minutes (CPU).

#### 249 WORD RECORDS (MSFC NTRAN)

<u>METHOD</u>	<u>DEVICE</u>	<u>RECORDS TRANSMITTED</u>	<u>CPU TIME</u>
NTRAN 1	DRUM	577	2:00 Min.
NTRAN 2	DRUM	284	2:00 Min.
FORTRAN	DRUM	4000	1:17 (Min. Sec.)

249 WORD RECORDS (NASTRAN NTRAN)

<u>METHOD</u>	<u>DEVICE</u>	<u>RECORDS TRANSMITTED</u>	<u>CPU TIME</u>
NTRAN 1	DRUM	4000	25 Sec.
NTRAN 2	DRUM	1523	2:00 Min.
FORTTRAN	DRUM	4000	1:11 (Min. Sec.)

It was determined that NTRAN 1 or the wait and unstack approach is vastly superior to the NTRAN 2 programming approach and substantially better than FORTRAN binary I/O. It was also determined that NASTRAN's NTRAN is substantially more efficient than MSFC's NTRAN and does not inhibit NASTRAN's I/O performance.

CONCLUDING REMARKS

Modifications and additions to the local MSFC standard version of NASTRAN are only one area of NASTRAN maintenance which occurs at MSFC; however, it is probably the most significant since it hopefully plays a part in keeping NASTRAN a meaningful, useful, and evolutionary tool for the structural analysts at MSFC instead of the obsolete monster it could become if modification and addition could not be performed on this remarkable system.

## ATTACHMENT A

### A. TOTAL CPU RUN TIME

UPPER CORE LIMIT	CPU TIME
65K	20.1 MIN.
55K	25.5 MIN.
50K	31.9 MIN.
42K	48.2 MIN.

### B. CPU TIME IN READ

UPPER CORE LIMIT	CPU TIME
65K	13.5 MIN.
55K	19.3 MIN.
50K	25.2 MIN.
42K	41.3 MIN.

### C. CPU TIME IN DECOMPOSITION

UPPER CORE LIMIT	CPU TIME
65K	4.7 MIN.
55K	9.7 MIN.
50K	15.7 MIN.
42K	30.5 MIN.

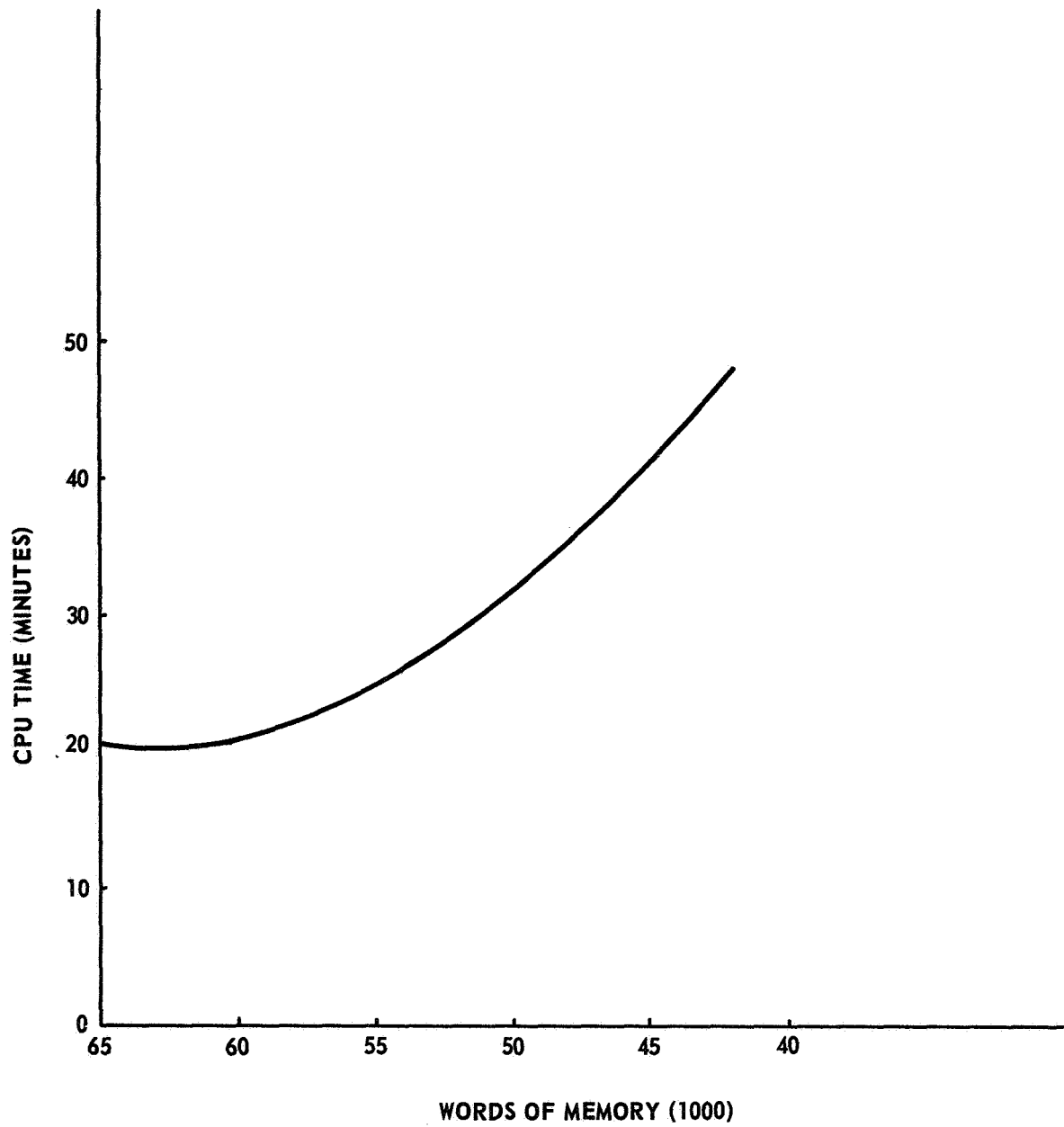


FIGURE 1.

CPU RUN TIME VERSUS AVAILABLE  
CORE (TOTAL PROBLEM RUN TIME)

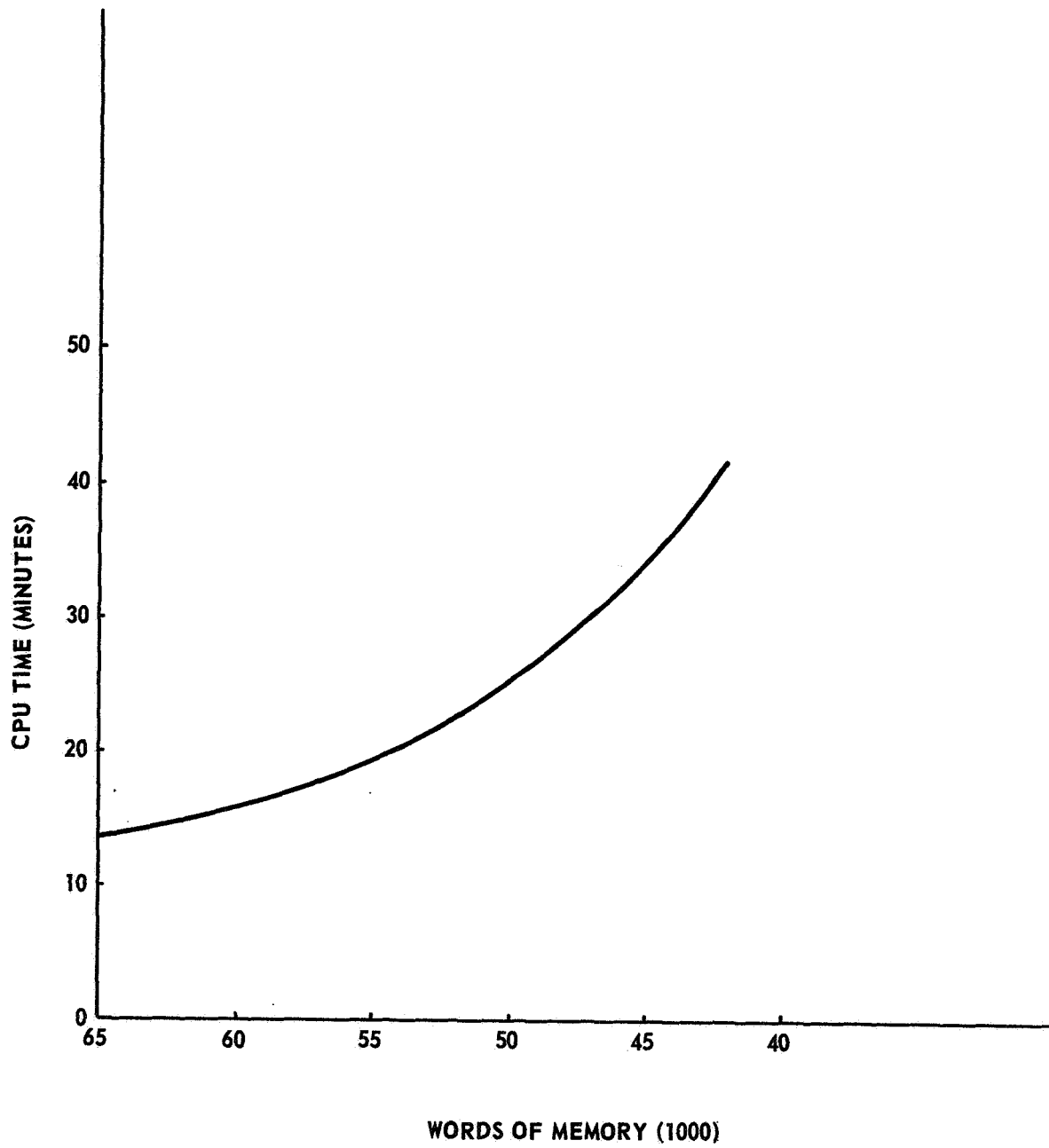


FIGURE 2.

CPU RUN TIME VERSUS AVAILABLE CORE  
(DECOMPOSITION PLUS EIGENVALUE  
EXTRACTION CPU TIME)

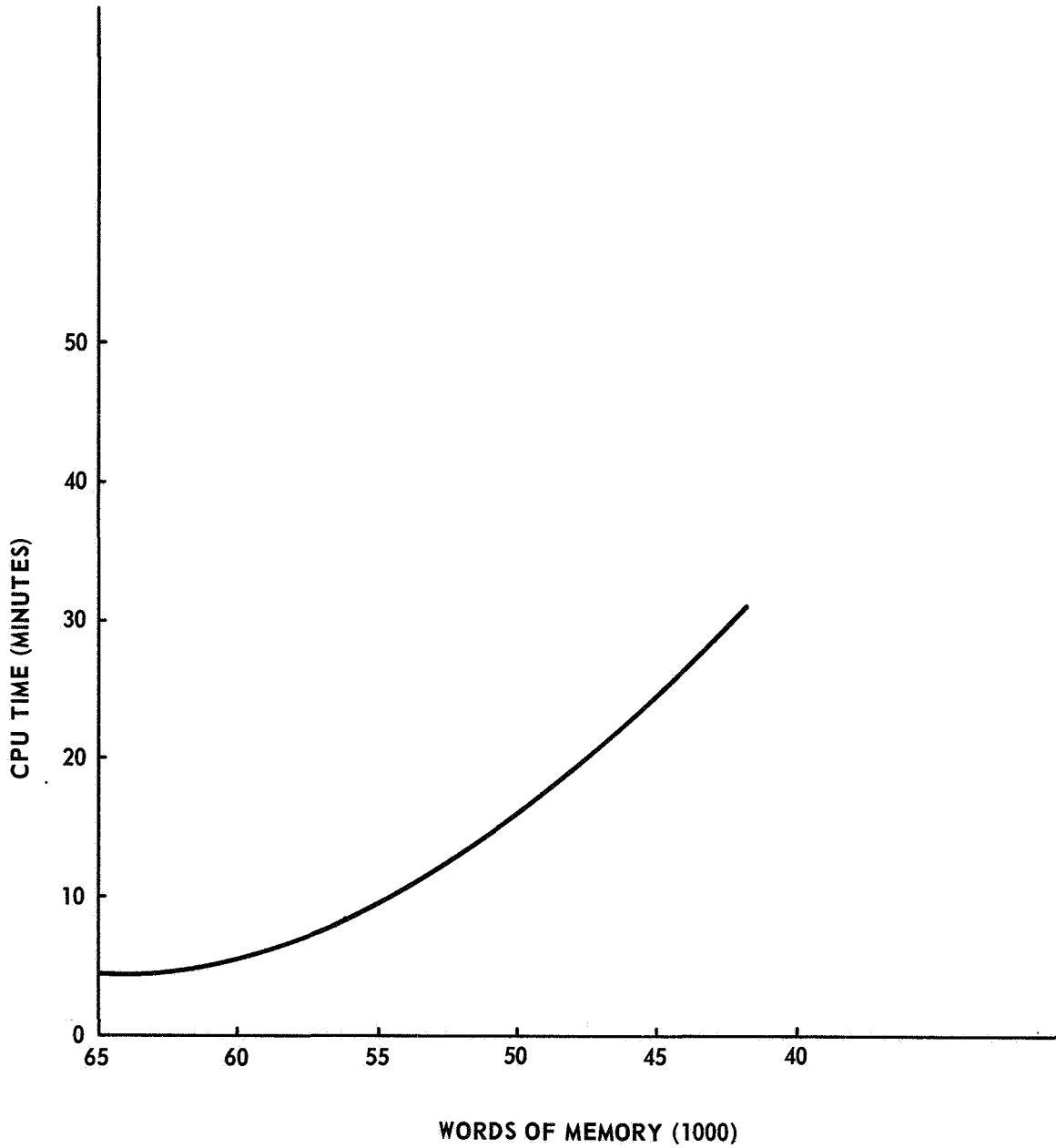


FIGURE 3.

CPU RUN TIME VERSUS AVAILABLE CORE  
(DECOMPOSITION CPU TIME ONLY)

# THE NASTRAN CONTOUR PLOTTER

By Barbara M. Kelly

Naval Ship Research and Development Center

## SUMMARY

The NASTRAN Contour Plotter, a group of subroutines and modifications to the NASTRAN Plot Module, enables contour lines to be superimposed on the plot of the structural model or on an outline of the structural model. The NASTRAN Contour Plotter can be incorporated into NASTRAN Version 12. Consistent with the NASTRAN computer program, it is operational on the IBM 360, the CDC 6000, and the UNIVAC 1108 computers on a variety of plotter hardware.

## INTRODUCTION

NASTRAN (Nasa STRuctural ANalysis) program is a general purpose digital computer program for the analysis of large complex structures. NASTRAN uses the finite element structural analysis approach which involves replacing the actual, continuous structure by an idealization composed of small elements.

NASTRAN currently provides a plotting capability to aid in the preparation of the structural model and in the interpretation of the computed results. This structure plotting capability produces both deformed and undeformed geometric projections of the structural model with or without displacement vectors at the nodal points. The X-Y plotting capability produces graphs of transient response and frequency response, and the matrix plotting capability generates topological displays of matrices.

The contour plotting capability, an enhancement to the structure plotter, will plot lines representing equal values on any deformed or undeformed geometric projection of the structural model. It was developed to aid in the interpretation of various stress and displacement results.

The contour plotting capabilities are described in terms of the data card specifications which indicate the type of contour plot and direct the contour plotter to superimpose contour lines on the structural model. These data cards are an addition to the structure plot request packet used to define and control the execution of the structural model plot (ref. 1).

Adding the contour plotting capability to the structure plot module necessitated certain modifications to existing subroutines within the module and to the plot DMAP (Direct Matrix Abstraction Program) statement in the all rigid formats. These modifications and additions are described in the format of The NASTRAN Programmer's Manual (ref. 2).

## USING THE CONTOUR PLOTTING CAPABILITY

### The Contour Plot Definition Card

The contour plot definition card (fig. 1) is used to specify the type of contour plot and the contour values to be plotted. The card is optional since all parameters may be defaulted. The card follows the format of a free-field plot request card (ref. 3).

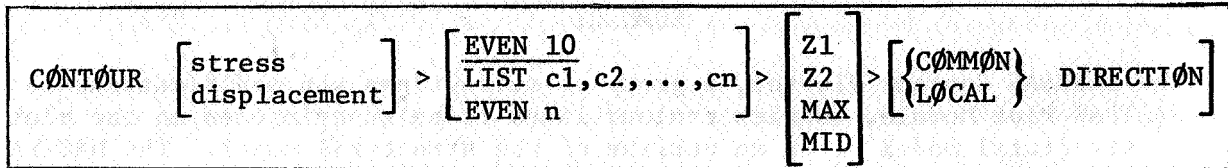


Figure 1.

Nine types of stress contour plots are available:

stress =	{	<u>MAJPRIN</u>	- Major and Minor Principal Stress	
		MINPRIN		
		MAXSHEAR		- Maximum Shear Stress
		XNORMAL		- X,Y,Z Normal Stresses
		YNORMAL		
		ZNORMAL		
		XYSHEAR		
		XZSHEAR		- Shear-XY, -XZ, -YZ .
		YZSHEAR		

Four types of displacement contour plots are available:

displacement =	{	XDISPLAC	- the X,Y,Z components of the displacement vector
		YDISPLAC	
		ZDISPLAC	
		MAGNITUD	- the magnitude of the displacement vector

Default for this parameter is MAJPRIN, Major Principal Stress.

The contour values to be plotted may be specified by supplying the parameter EVEN and the number, n, of contour values, or by supplying LIST and a list of real number contour values. If EVEN is specified, the contour plotter will calculate n contour values at (n-1) equal intervals over the range of values specified by the user. The first contour value will be the minimum and the n-th contour value the maximum of the values for the current set of elements. The number of contour values, n, must be less than or equal to 50. Default for this parameter is "EVEN 10", i.e., contour values at 10 even (i.e., equal) intervals.

Since stress may be calculated at two Fibre Distances, the Fibre Distance may be specified by designating Z1 (Fibre Distance 1) or Z2 (Fibre Distance 2). In addition, MAX, the maximum of Z1 and Z2, or MID, the average of Z1 and Z2,

may be selected. In the set of elements for which a contour plot can be executed (see The PLOT Execution Card), the average of Z1 and Z2, MID, is applicable only to the CTR1A2 and CQUAD2 elements. The default is Z1.

The Normal Stresses are directional and are calculated in the elements local coordinate system. If COMMON DIRECTION is specified, the contour plotter will transform the Normal Stresses and the Shear Stresses to a common (currently the basic) coordinate system. If LOCAL DIRECTION is specified, the contour plotter will leave these stresses in the global coordinate system. Note that the Normal Z Stress, and the Shear-XZ and Shear-YZ are assumed to be zero in the element's local coordinate system. Default for this parameter is the COMMON DIRECTION.

### The PLOT Execution Card

The PLOT Execution Card (figure 2) has been altered to include the CONTOUR and OUTLINE execution commands (ref. 4).

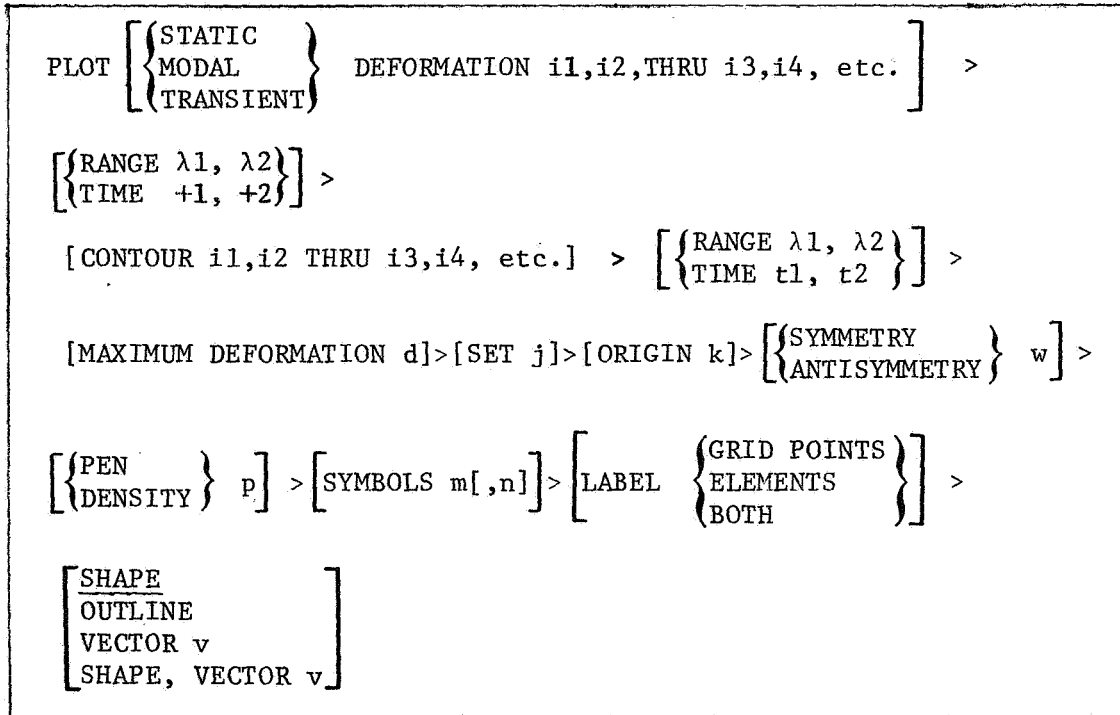


Figure 2.

The CONTOUR command will superimpose lines representing equal value on the structural model or on the outline of the structural model. The nonzero integers following the CONTOUR command refer to subcases to be plotted. Default is the subcase following the DEFORMATION parameter or, if that parameter is not specified, all subcases. In addition, the RANGE or TIME may be specified. If both DEFORMATION and CONTOUR are specified, the contour plotter will take the subcase, range, or time parameters following

DEFORMATION as applicable to the contour plot as well as to the deformed plot.

If a stress contour plot is requested, contour lines will be plotted on the following elements in SET j appropriate to the type of stress contour plot requested (ref. 5): CSHEAR, CTR1A1, CTR1A2, CQUAD1, CQUAD2, CTRMEM, CQDMEM.

If a displacement contour plot is requested, contour lines will be plotted on all two-dimensional elements plotted by the structure plotter. The type of deformation must be specified for a displacement contour plot.

The contour lines are labeled with integers indicating the contour value. The integers are listed with their associated contour values in the form of a key in the Plot Module Message section of the printed output.

The OUTLINE command has been added as an alternative to the SHAPE command. OUTLINE will plot connecting lines between those grid points which lie on the boundary of the structural model.

If DEFORMATION is specified in an addition to OUTLINE, the OUTLINE will reflect the deformed structure. If a "0" is added to the deformation subcase string, the undeformed outline will be plotted.

The OUTLINE command may be specified only in addition to the CONTOUR command.

## CONTOUR PLOT PROGRAM FUNDAMENTALS

### Modifications and Additions to the Functional Module Plot

The addition of the contour plotter enlarges the capabilities of the Functional Module Plot (ref. 6) to include the capability of superimposing contour lines on structural shapes using a variety of different plotters. In order to incorporate the contour plotter, two data blocks were added to the input string of data blocks brought into the Plot Module and modifications were made to the existing subroutines in order to add the new subroutines to the Plot Module. A page of printed output was also devised to give information on the contour plot.

The data blocks ECPT and ØES1 were added as additional input blocks to the DMAP calling sequence. The DMAP calling sequence (ref. 7) becomes:

```
PLØT  PLTPAR, GPSETS, ELSETS, CASECC, BGPDT, EQEXIN, SIL, ECPT,  
      PLTDSP1, PLTDSP2, ØES1/PLØTX/V,N,NGP/V,N,LSIL/V,N,PLTFLG/  
      V,N,PLTNUM    $
```

ECPT is the Element Connection and Properties Table and ØES1 is the Output Element Stress Table. If the ECPT data block is purged, contour plots will not be drawn. If the ØES1 data block is purged, the stress contour plots will not be drawn.

Modifications were made to existing plot module subroutines so that the contour plot definition card could be detected and so that the CONTOUR and OUTLINE commands could be executed. When the plot module is ready to generate the plot (subroutine DRAW), all the necessary parameters have been set and any necessary rotations have been made to generate the contour plot.

The subroutine CONTOR is called by the subroutine DRAW to plot contour lines. If a stress contour plot was requested, CONTOR requests that the plot set be ordered and that contour values be found for each element. The contour lines are then located on the structural model, drawn and labeled. If a displacement contour plot was requested, the contour lines are drawn by the subroutine DISPLA which returns to the subroutine CONTOR to plot the labels.

If an OUTLINE of the structural model was requested, the subroutine DRAW calls the subroutine BORDER to generate this part of the plot.

The subroutine DRAW, then, (ref. 8), has been altered so that subroutines CONTOR and BORDER can be called to generate contour lines and the structural outline. The subroutine PLOT (ref. 9) has also been altered so that a call to ROTATE can be made to transform certain stresses to a common coordinate system.

The seven subroutines comprising the contour plotting capability are described below.

(1) Subroutine Name: ROTATE

Purpose: to transform the Normal Stresses and the Shear Stresses to a common coordinate system.

Calling Sequence: CALL ROTATE(ELSETS, GPLST, X)

where ELSETS is the data block containing element connection data,

GPLST is a list of indices defining the set of grid points associated with the elements, and

X contains the corresponding coordinates of the grid points.

Common Blocks:

/XXPARAM/ (ref. 10) (see also Additions to NASTRAN Tables, page 10 ).

Method: The subroutine transforms the Normal Stresses and Shear Stresses from the local coordinate system to a common coordinate system using the following expression:

$$[T] = [\theta] [T'] [\theta]^T$$

where  $[T] = \begin{bmatrix} \sigma_x & \tau_{xy} & \tau_{xz} \\ \tau_{yx} & \sigma_y & \tau_{yz} \\ \tau_{zx} & \tau_{zy} & \sigma_z \end{bmatrix}$  is a symmetric matrix,

$\sigma_x, \sigma_y, \sigma_z$  are the Normal X,Y, and Z Stresses respectively,

$\tau_{xy}, \tau_{xz}, \tau_{yz}$  are the Shear-XY, -XZ, and -YZ Stresses respectively, and

[ $\theta$ ] is the rotation matrix which has as its components the direction cosines between the local and common coordinate systems.

Since all elements considered by the contour plotter are plate elements, the elements are all assumed to lie in the local X,Y plane with the X-axis passing from grid point one to grid point two (ref. 11). The subroutine makes use of the assumption that  $\sigma_z = \tau_{xz} = \tau_{yz} = 0$  in the local coordinate system.

A new local element stress table (NEWOES) is compiled by the subroutine ROTATE to communicate the transformed stresses to the subroutine CONTOR.

Additional Subroutines Required: None.

(2) Subroutine Name: C $\theta$ NT $\theta$ R

Purpose: to plot and label contour lines.

Calling Sequence: CALL C $\theta$ NT $\theta$ R(GPLST,X,S,U,PEN,DEF $\theta$ RM)

where GPLST is a list of indices defining the set of grid points,  
X contains the corresponding coordinates of the undeformed points,  
S contains the corresponding coordinates of the deformed points,  
U contains the displacement coordinates,  
PEN is the line density or pen number, and

DEF $\theta$ RM =  $\begin{cases} 0 & \text{if an undeformed structural model was requested} \\ 1 & \text{if a deformed structural model was requested} \end{cases}$

Common Blocks:

/XXPARAM/ (ref.12) (see also Additions to NASTRAN Tables, page 10 ).

/PLTDAT/ (ref.13)

/DRWDAT/ (ref.12) (see also Additions to NASTRAN Tables, page 10 ).

Method: If the contour plot is to be a displacement contour plot, CONTOR calls the subroutine DISPLA to plot the contour lines. If a stress contour plot was requested, CONTOR calls the subroutine CREATE to prepare a table containing the contour value and the centroid for each element in the plot set. The subroutine ORDER is then called, if necessary, to provide a table of all grid points internal to the structural shape and all elements that share a common grid point in the current plot set.

Once these tables are available, CONTOR estimates a contour value for each internal grid point using a weighted average of distance from the centroids and contour values of surrounding elements. Contour lines are found within a triangle formed by connecting an internal grid point and two

adjacent elements' centroids. Contour lines are plotted with the assumption that the contour values vary linearly between vertices of this triangle.

Labels are placed on the completed contour plot and the subroutine PLTOPR is called to print the contour plot key as part of the plot messages.

**Additional Subroutines Required:** ORDER, CREATE, DISPLA.

(3) Subroutine Name: CREATE

**Purpose:** to extract the stress contour values from the appropriate data block and calculate the centroid of each element in the plot set.

**Calling Sequence:** CALL CREATE(GPLST,X,U,DEFØRM,CØNMIN,CØNMAX,ELMTID,STØRE)  
where GPLST is a list of indices defining the set of grid points,  
X,U contain the corresponding undeformed and deformed coordinates respectively, of the grid points,

$$\text{DEFØRM} = \begin{cases} 0 & \text{if an undeformed structural shape was requested,} \\ 1 & \text{if a deformed structural shape was requested} \end{cases}$$

CONMIN,CONMAX are the minimum and maximum of the contour values, and  
ELMTID,STORE are temporary storage areas for the element identification number and the contour value found on the stress data block.

**Common Block:**

/XXPARAM/ (ref.14) (see also Additions to NASTRAN Tables, page 10 ).

**Method:** After determining which stress data block contains the contour values for this contour plot, the appropriate data block is opened and the temporary storage area is filled. The contour values are selected from the information on Fibre Distance, direction, subcase, and if applicable, range or time specified by the user. Then the ELSETS data block is read to supply information on element types, elements identification numbers, and internal grid point numbers of elements contained in the current set.

The subroutine makes two assumptions concerning the stress data block and the ELSETS data block. It assumes that element types are ordered in the same sequence and that for each element type, element information is ordered by increasing element identification number. Element types for which contour lines cannot be drawn are ignored as are elements not included in the current plot set.

Finally, the centroid is calculated for each element in the plot set and a temporary table is made containing the element identification number, the contour value, and the centroid.

**Additional Subroutines Required:** CENTRE .



(6) Subroutine Name: DISPLA

Purpose: to draw displacement contour lines.

Calling Sequence: CALL DISPLA(GPLST,X,S,U,PEN,DEFORM,LABEL,PT)

where GPLST is a list of indices defining the set of grid points,  
X,S contain the corresponding undeformed and deformed  
coordinates, respectively, of the grid points.  
U contains the grid point displacement coordinates,  
PEN is the line density or pen number,

$$\text{DEFORM} = \begin{cases} 0 & \text{if an undeformed structural shape was requested} \\ 1 & \text{if a deformed structural shape was requested,} \end{cases}$$

LABEL contains the contour line labeling information, and  
PT contains the coordinates of the triangle formed to calculate  
contour lines.

Common Blocks:

/XXPARM/ (ref.15) (see also Additions to NASTRAN Tables, page 10 ).

/PLTDAT/ (ref.15) (see also Additions to NASTRAN Tables, page 10 ).

Method: The subroutine DISPLA uses the ELSETS data block to extract the two dimensional elements in the plot set. Each element is then broken down to one or more triangles and contour lines are drawn within the triangles with the assumption that the contour values vary linearly between grid points.

It is assumed in the DISPLA subroutine that the user's coordinate system is a right-handed coordinate system with coordinate axes X,Y,Z. If the AXES card (ref. 16) is used to change the orientation of the structural model, it will have no effect on the component of displacement used to draw the contour plot.

Labeling information is maintained on a temporary file to be added to the plot by the subroutine CONTOR.

Additional Subroutines Requested: None.

(7) Subroutine Name: BØRDER

Purpose: to draw the structural outline.

Calling Sequence: CALL BØRDER(GPLST, X, U, DEFØRM)

where GPLST is a list of indices defining the set of grid points,  
X,U contain the corresponding undeformed and deformed coordinates,  
respectively, of the grid points, and

$$\text{DEFØRM} = \begin{cases} 0 & \text{if an undeformed structural shape was requested} \\ 1 & \text{if a deformed structural shape was requested.} \end{cases}$$

Common Blocks: None.

Method: The subroutine BØRDER uses the table created by the subroutine ØRDER. BØRDER extracts from the table those grid points that lie on the plot sets boundary. All grid points connected to this grid point by element

boundary lines are sorted to find the two element boundary lines which form the structural boundary. The BORDER subroutine then draws two connecting lines for each grid point so that the structural outline will be of density two.

Additional Subroutines Required: None.

#### Additions to the NASTRAN Tables

The NASTRAN Functional Module Plot uses labeled common to communicate information concerning plot requests, plot calculation parameters, and plotter hardware characteristics among subroutines. Additional parameters have been added to two of the labeled common blocks to pass contour plotter information. These additional parameters are described here (ref. 17).

(1) COMMON/DRWDAT/SET,...,VECTOR,C0N,EDGE

where C0N is an integer indicating the contour plot option, and  
EDGE is an integer indicating the outline option.

(2) COMMON/XXPARM/PBUFSZ,...,XY(11,3),NCNTR,CNTR(50),ICNTVL,WHERE,DIRECT,  
SUBCAS,FLAG,VALUE,SET

In the following descriptions, the value in parenthesis to the right of the variable name is the default value, and the letter in parenthesis to the right of the explanation pertains to the type of variable (I is integer, and R is real).

#### Contour Plotting Data

NCNTR(10)	-	Number of contour values to be plotted (I)
CNTR	-	Contour values (R)
ICNTVL(3)	-	Type of contour plot (I)
WHERE(1)	-	Fibre Distance of stress contour value (I)
DIRECT(2)	-	Stress vector direction option (I)
SUBCAS	-	Current subcase (I)
FLAG(0.0)	-	Data identification indicator (R)
VALUE	-	Current eigenvalue or time step (R)
SET	-	Last plot set processed by contour plotter (I)

#### Local Table Descriptions

Three tables are formed for the use of the contour plot subroutines. The tables are compiled and used within the structure plot module. The description of each table follows the file name.

1. SCR1, scratch file 1 - compiled by the subroutine CREATE to be used by the subroutine CONTOR. The header record is written by the subroutine GOPEN. The table is compiled from information contained in the ELSETS data block (ref. 18) and the OES1 data block (ref. 19) or the NEWOES table (see below).

Table Format:

<u>Record</u>	<u>Word</u>	<u>Type</u>	<u>Item</u>
0			Header Record
1	1	I	Element Type
	2	I	Element Identification Number
	3	R	Stress Value
	4,5	R	Element Centroid
	⋮		⋮
	(4m+2)	I	0
2			End-of-File

repeated for each element type in contour type set

Note: m = the number of elements of current type in the plot set.

2. SCR2, scratch file 2 - compiled by the subroutine ORDER to be used by the subroutines CONTOR and BORDER. The header record is written by the subroutine GOPEN. The table is compiled from information contained in the ECPT data block (ref. 20) and the SIL table (ref. 21).

Table Format:

<u>Record</u>	<u>Word</u>	<u>Type</u>	<u>Item</u>
0			Header Record
1	1	I	Flag
	2	I	Number of elements, m.
	3	I	Grid point internal number
	4	I	repeated for each element containing the grid point. Contents dependent on Flag.
	.		
	.		
	.		

repeated for each grid point in plot set

Notes:

- 1) n = the number of grid points in the plot set.
- 2) m = the number of elements in current record.
- 3) Flag = -1:

<u>Word</u>	<u>Type</u>	<u>Item</u>
4	I	Element identification number
⋮	⋮	⋮
(3+m)	I	⋮

4) Flag = -2:

<u>Word</u>	<u>Type</u>	<u>Item</u>
4	I	Element identification number
5	I	Grid point internal number
6	I	Grid point internal number
⋮		⋮
(3m+1)	I	Element identification number
(3m+2)	I	Grid point internal number
(3m+3)	I	Grid point internal number

3. NEWOES - compiled by the subroutine ROTATE to be used by the subroutine CREATE. There is no header record. The table is compiled using stress values contained in the OES1 data block (ref. 22).

The first record in each set of two records on NEWOES is a copy of the corresponding record of the OES1 data block. The second record of each set contains changes in content for the following element types:

Element types CTRIA1, CQUAD1, CTRIA2, CQUAD2

<u>Word</u>	<u>Contents</u>
2	Z1
3	Normal X Stress at Z1
4	Normal Y Stress at Z1
5	Normal Z Stress at Z1
6	Shear XY at Z1
7	Shear XZ at Z1
8	Shear YZ at Z1
9	Maximum Shear at Z1
10	Z2
11	Normal X Stress at Z2
12	Normal Y Stress at Z2
13	Normal Z Stress at Z2
14	Shear XY at Z2
15	Shear XZ at Z2
16	Shear YZ at Z2
17	Maximum Shear at Z2

Element types CTRMEM, CQDMEM

<u>Word</u>	<u>Contents</u>
2	Normal X Stress
3	Normal Y Stress
4	Normal Z Stress
5	Shear XY
6	Shear XZ
7	Shear YZ
8	Maximum Shear

## REFERENCES

1. "The NASTRAN User's Manual," edited by Caleb W. McCormick, Office of Technology Utilization, National Aeronautics and Space Administration, Washington, D.C. (1970), Section 4.2.
2. "The NASTRAN Programmer's Manual," edited by Frank J. Douglas, Office of Technology Utilization, National Aeronautics and Space Administration, Washington, D.C. (1970), Section 4.24.
3. "The NASTRAN User's Manual," Section 4.2.1.
4. "The NASTRAN User's Manual," Section 4.2.2.3.
5. "The NASTRAN User's Manual," pages 4.3-12 through 4.3-14.
6. "The NASTRAN Programmer's Manual," Section 4.24.
7. "The NASTRAN Programmer's Manual," Section 4.24.3.
8. "The NASTRAN Programmer's Manual," Section 4.24.8.6.
9. "The NASTRAN Programmer's Manual," Section 4.24.8.3.
10. "The NASTRAN Programmer's Manual," Section 4.24.9.2.
11. "The NASTRAN User's Manual," Section 1.3.5.
12. "The NASTRAN Programmer's Manual," Section 4.24.9.2.
13. "The NASTRAN Programmer's Manual," Section 2.5.
14. "The NASTRAN Programmer's Manual," Section 4.24.9.2.
15. "The NASTRAN Programmer's Manual," Section 4.24.9.2.
16. "The NASTRAN User's Manual," Section 4.2.2.2.
17. "The NASTRAN Programmer's Manual," Section 4.24.9.2.
18. "The NASTRAN Programmer's Manual," Section 2.3.5.4.
19. "The NASTRAN Programmer's Manual," Section 2.3.28.15.
20. "The NASTRAN Programmer's Manual," Section 2.3.8.3.
21. "The NASTRAN Programmer's Manual," Section 2.3.3.6.
22. "The NASTRAN Programmer's Manual," Section 2.3.28.15.



# NASTRAN DATA GENERATION AND MANAGEMENT USING INTERACTIVE GRAPHICS\*

By M. Smoot Katow  
and Barry M. Cooper

Jet Propulsion Laboratory

## SUMMARY

For effective use of NASTRAN, the input bulk data must accurately model the structure to be analyzed and result from a minimum of time and money expended. A method of using an interactive graphics device to generate a large portion of the input bulk data with visual checks of the structure and the card images is described. The generation starts from GRID and PBAR cards. The visual checks result from a three-dimensional display of the model in any rotated position. By detailing the steps, the time saving and cost effectiveness of this method may be judged, and its potential as a useful tool for the structural analyst may be established.

## INTRODUCTION

The generation of NASTRAN input bulk data to correctly simulate or model a large structure to be analyzed usually consumes many man hours and much time. Sketches and/or drawings are necessary to define the GRID numbers connected by structural elements identified with EID numbers and their property identification PID numbers. After the constraints are organized, a list for keypunching must be prepared. After the cards are keypunched and inputted to the computer, more time is required to debug the input data for compliance with the NASTRAN formats before an answer is outputted. Debugging procedures usually employ plotting capabilities available in NASTRAN to provide visual checks of the structural model. Normally, further checking follows by noting values in the load vectors generated by gravity loadings, the coordinates of the center of gravity, and symmetry or equating of the single-point constraint values to the input load vectors.

Besides the schedule time deadlines, the total cost of the analysis must be considered. Procedures or processes that can reduce the time of preparing input data invariably reduce costs. If during these processes the correctness of the model can be raised to a high level before input to a computer, the NASTRAN computing costs can be reduced.

---

\* This paper presents the results of one phase of research carried out at the Jet Propulsion Laboratory, California Institute of Technology, under Contract No. NAS 7-100, sponsored by the National Aeronautics and Space Administration.

At JPL, with the installation of the UNIVAC Advanced Graphics Display System to the UNIVAC 1108 - EXEC 8 time-sharing computer used for scientific computing purposes, the development of the use of interactive graphics to generate and check NASTRAN bulk data has proceeded.

## CONFIGURATION DESCRIPTION

The UNIVAC Advanced Graphics Display System is composed of two major units: the display controller minicomputer (Type 1557) and the display console (Type 1558). The purpose of the minicomputer is to provide computing and control capabilities to handle, internally, display functions and programs that are tailor-made by the user to meet NASTRAN bulk data requirements. It also serves as an interactive device to the UNIVAC 1108 processor to provide additional large-scale processing capabilities.

The display console consists of a cathode ray tube (CRT) display, keyboard, display control, and light pen. The unit is designed for display of grid points, line vectors, alphanumeric characters, and special symbols necessary for the NASTRAN program. It features a high-speed, high-precision CRT to accommodate the wide variety of graphic displays.

The basic configuration of the system interfaces directly with an input/output channel of the UNIVAC 1108 processor. The basic storage for the minicomputer contains 8192 locations.

## GRAPHICS PROGRAMMING LIBRARY

A primary purpose of the UNIVAC 1108 - EXEC 8 computer and Graphics Programming Library (GPL) is to provide easily manipulated data structures that describe and define a displayable image for the 1557/1558 graphics minicomputer/display console.

The GPL permits both the graphics entities which constitute the images to be displayed and nongraphic associated or managerial data to be defined and stored in the data base. Entities of both types can be grouped to form single higher level or parent groups capable themselves of being grouped to form still higher-level groups, giving rise to a hierarchically organized data structure.

A large central data base is required to support the NASTRAN package; thus many automatic facilities are included in the system to make management of this data both convenient and efficient. In order to maintain the integrity of the data file, it is accessible only through the GPL subroutines. These subroutines permit total flexibility in defining, manipulating, and displaying images on the display screen.

Interaction control tables (ICTs) provide a unique approach to the problem of defining and accomplishing the processing to be performed in the

minicomputer. These tables handle the function of basic attention handling, analyze and change both its data base and display file, and send and request information to and from the central computer as required. The ICTs are a hardware-independent, interpretively executed, interactively oriented language in which processing performed by the minicomputer is programmed by the user.

## THE USE OF INTERACTIVE GRAPHICS

### Structure Development Program

In the normal analysis, the preparation of the input bulk data cards starts with the GRID cards. The grid point numbers of these cards are defined on a sketch or drawing. Also, from these pictures the coordinate values are ascertained directly or by calculations on a desk machine. Normally, these coordinate values are described within the precision limits of the computer, although in the real structure there are larger errors. These errors can be evaluated as to their effects on the answers from the analysis as one more separate problem in structural analysis to be considered. Because of the symmetrical nature of many structures, precise coordinate values usually aid in debugging as well as enhancing the use of partial section analysis, thereby reducing the time and cost of analysis.

For this method of interactive graphic adaptation, the GRID cards are keypunched to suit NASTRAN format. For this discussion we will assume that only CBARs are used, so PBARs are keypunched next.

At this point, these NASTRAN cards are input to a catalog file in the 1108, and the 1557/1558 unit through GPL is activated so that the CBARs can be generated or completely listed and keypunched for observation and updating by interactive graphics. The NASTRAN graphics package consists of three subprograms: a structure development subprogram for the CBAR generation, a rotation subprogram for visual demographics, and a data edit subprogram for card image alterations. Each subprogram can be used in a stand-alone mode or can be subroutinized to operate interchangeably.

The graphics tube face layout has been designed from a human engineering standpoint, with speed and efficiency coordinated at each user/hardware operation. The tube face is divided and overlaid by windows, each representing a segment of the visual data structure. One window contains a "menu" which informs the user of his current status in the program. These window and menu concepts can be seen in figure 1.

In the left window, the grid point identification numbers from the catalog file are listed in columns. Above it are listed the PID numbers of the PBARs. To the right side of the grid ID, there is space for displaying the generated CBAR data.

The right window of the tube displays, as point vectors, the grid point locations initially as they appear normal to the XY plane. Then by pressing either X, Y, or Z on the keyboard, the views in XY, XZ, or YZ planes, respectively, can be displayed.

The light-sensitive pen is then pointed to the first GA of the desired CBAR. The screen responds by displaying a  $\pm$  "local indicator" next to the listed GA as well as the point vector on the right window. When in succession, the GB, PID, and GO are selected via light pen interaction; then a "C" in the keyboard enters the CBAR, which is shown by an entry in the CBAR connection list data in the left window and a directional vector between the point vectors of the GA and GB. The formats described are shown by a photograph of the screen after some CBARs have been developed (fig. 1).

At any time during this development of the structural model the rotation subprogram may be called and the model can be visually checked from any oblique angle. Figure 2 shows the model of figure 1 viewed by rotations around the X and Z axes of 30 degrees each. Figure 3 shows the complete development at a -30 deg angle about the X axis.

#### Rotation Subprogram

This monitor (a 1557 software operating system) performs three-dimensional rotation on the two-dimensional screen, which gives the user complete control of visual structure demographics: rotation about any axis, at any incremental angle, at any speed. This combination of control leads to "animated" movement in three dimensions for visual analysis and to hard copy graphics of the structure.

If at this time the card images of a GRID or CBAR require changes, the grid data may be edited by a call to the data edit subprogram. A typical display is shown in figure 4. By use of the keyboard, specific changes can be made in the card image inputs.

#### Data Set Edit Subprogram

The data set edit routine can be utilized as a stand-alone procedure to update an existing NASTRAN data package or as a subroutine in a structure development production.

The data set edit routine presents the "card image" run stream by paging data and control messages across the screen at the user's discretion. On each page, the user has control or editing options and can direct the program direction. The user can change a card image, delete a card image, and add a card image which represents a CBAR or PBAR, while maintaining all structure credibilities connected to the member unless entirely deleted.

The user can switch the rotation monitor on and visually check his structure, flag a member, and automatically have the program page to the card image representing the member for further analysis and editing.

To prevent loss of completed connections a page of 25 CBARs is automatically stored in the user's FASTRAND file. In turn, the next 25 CBARs may be entered. This program has restart capabilities in case of computer failure or "current" analysis changes.

When the visual checks of the interactive graphics output signal a good set of GRID, CBAR and PBAR cards, the final exit can be made by requesting the 1108 to punch out the edited cards as presently programmed, or, in the 1108, it is possible to have data files read into a catalog file so that an immediate NASTRAN run can be made from the remote terminal used for the 1557/1558 unit.

### ADVANTAGES OF INTERACTIVE GRAPHICS

The replacement of the normal listing of CBARs and subsequent keypunching with the use of interactive graphics will save time. However, the greatest values should result from the opportunity to make intermittent three-dimensional visual checks of the structural model. The analyst can insure the accuracy of the model as well as provide an opportunity for study to optimize the geometric arrangement.

As the system is now working, using many satellite ICT routines and self-contained monitors with the minicomputer, minimum demand time is required of the 1108. The current cost of working the system is approximately \$50/hr. This includes "roll-in/roll-out" of the three monitors and full user utilization in a demand environment.

### ACKNOWLEDGEMENT

Appreciation is expressed to Larry Bauer of UNIVAC for advanced developments of the GPL and to Robert Patton for research and development of the rotation subprogram.

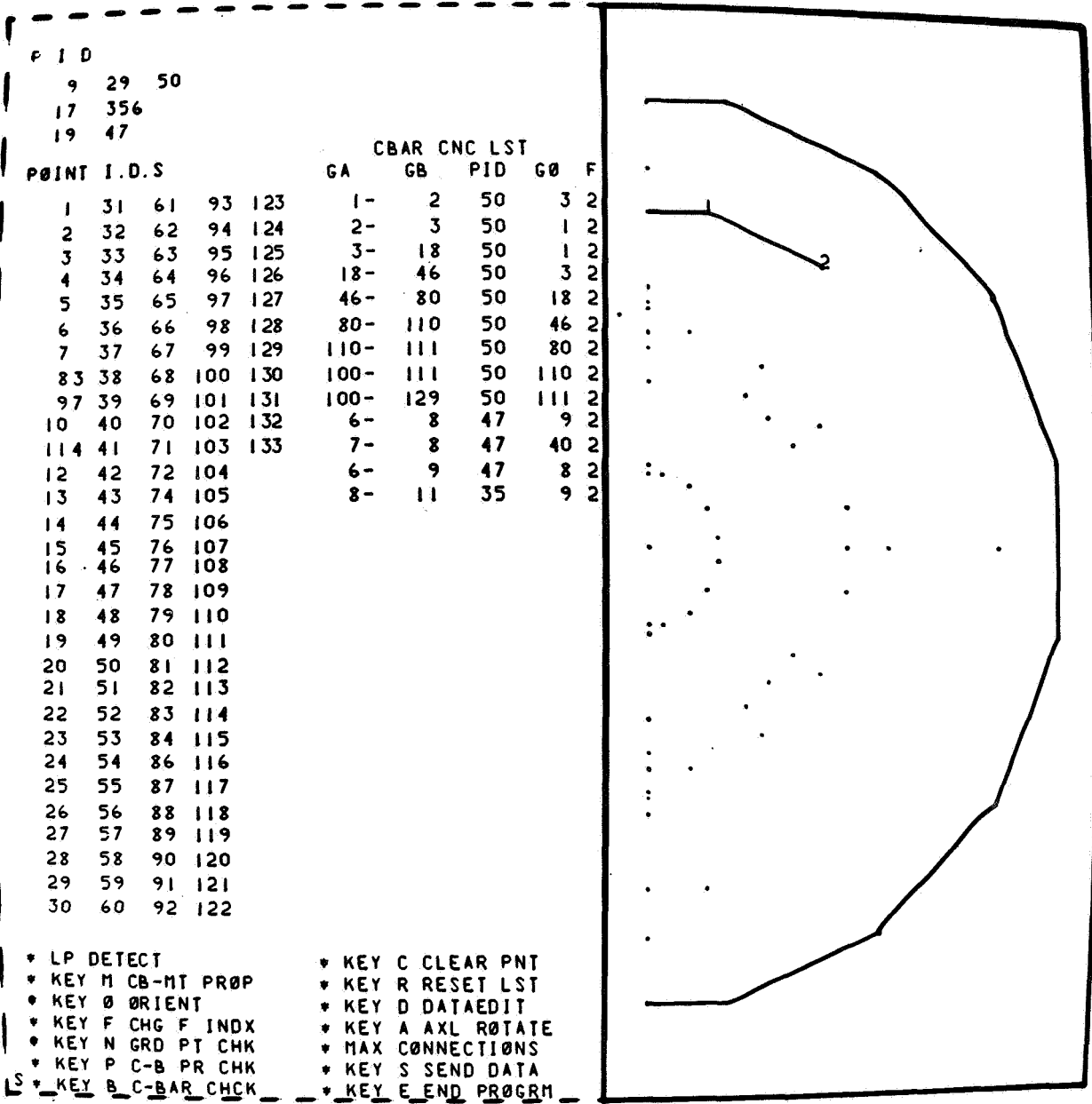


Figure 1. -The XY plane image, data development program

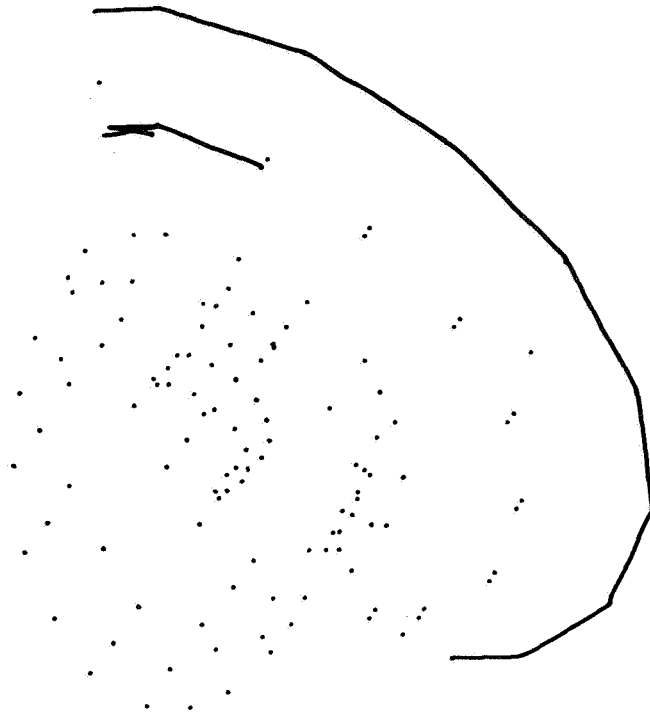


Figure 2. -Rotated partial development, rotation subprogram

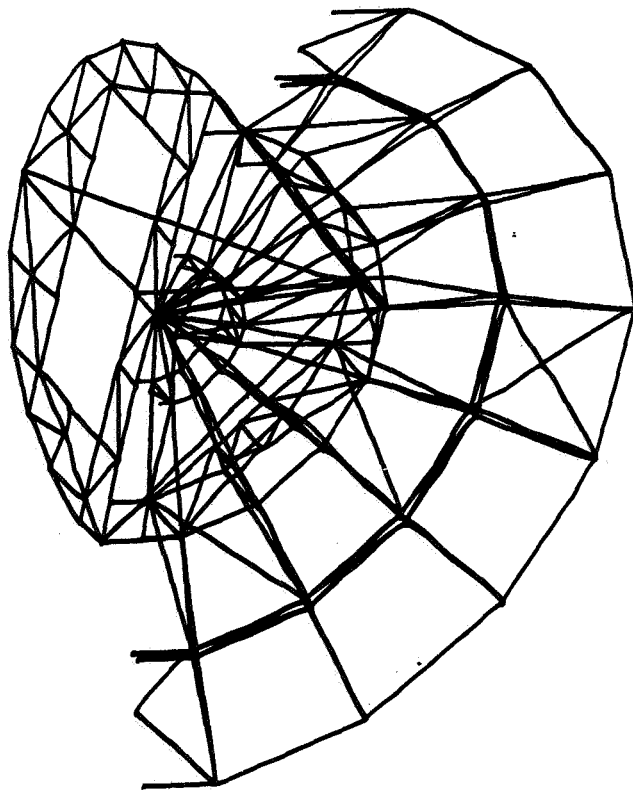


Figure 3. -Rotated full structure, rotation subprogram

```

CBAR      EID  PID  GA   GB   GØ      F
*CBAR     61   35   20   22   19      2
*CBAR     44   35   19   21   22      2
*CBAR     65   35   20   42   33      2
*CBAR     69   35   21   33   42      2
*CBAR    129   35   42   49   33      2
*CBAR    107   35   33   50   42      2
*CBAR    152   35   49   64   77      2
*CBAR    156   35   50   64   76      2
*CBAR    157   35   50   77   76      2
*CBAR    199   35   64   77   76      2
*CBAR    198   35   64   76   77      2
*CBAR    238   35   76  106   77      2
*CBAR    243   35   77  107   76      2
*CBAR    308   35  106  115  116      2
*CBAR    310   35  107  116  115      2
*CBAR *****

      * ØLD PAGE      * LIST
      * NEW PAGE     * RETURN

PL

```

Figure 4. -CBAR listing, data set edit subprogram

The BANDIT Computer Program for the Reduction of  
Matrix Bandwidth for NASTRAN

By Gordon C. Everstine

Computation and Mathematics Department  
Naval Ship Research and Development Center  
Bethesda, Maryland 20034

SUMMARY

This paper describes a computer program called BANDIT, which has been developed for use as a preprocessor to NASTRAN to automatically resequence the grid point numbers for reduced matrix bandwidth. The BANDIT program accepts a standard NASTRAN data deck as input, resequences the grid point numbers for reduced bandwidth (if possible), and generates a set of SEQGP cards for insertion into the NASTRAN bulk data deck. BANDIT uses the Cuthill-McKee strategy for resequencing grid points. The program is operational on the CDC 6000 series of computers, the IBM 360, and the UNIVAC 1108.

INTRODUCTION

The structural matrices formed during a NASTRAN analysis are normally both symmetric and sparse. With a suitable choice of the numbers (labels) assigned to the grid points, the matrices are also banded (i.e., the non-zero entries in each matrix are clustered about the main diagonal). Matrix bandwidth is important to the NASTRAN user for both computer storage and running time considerations. Indeed, many of the routines used in NASTRAN for the solution of linear equations and for the extraction of eigenvalues operate most efficiently when the bandwidths of the structural matrices are minimum. In such routines, the number of calculations required (and hence the computer running time) is of order  $NB^2$  for large  $N$  and  $B$ , where  $N$  and  $B$  are the matrix order and bandwidth\*, respectively.

Thus, it is clearly essential to the NASTRAN user to have matrices with small bandwidth. On the other hand, NASTRAN currently places the burden on

---

\* For a structure with grid points numbered 1 through  $N$ , the bandwidth (BW) is defined as the maximum numerical difference between any two connected grid point numbers. A pair of grid points are "connected" if there is an explicit connection between them or if they appear in the same element.

the user to number his structure so as to provide such a bandwidth. In many cases, this is an excessive burden, particularly for large, complex structures or for those emanating from automatic data generators. In any case, the burden is unnecessary since several algorithms have been developed for the express purpose of permuting grid point sequences to reduce matrix bandwidth.

Although there might be merit in including such an algorithm within NASTRAN, the desired effect can be achieved externally by means of the SEQGP bulk data cards. These cards define a look-up table giving the correspondence between the original grid numbers used by a structural analyst in defining his problem and a new set of numbers to be used internally for all calculations.

This paper describes a computer program called BANDIT (ref. 1) developed for use as a preprocessor to NASTRAN to automatically resequence the grid point numbers for reduced matrix bandwidth. BANDIT accepts a standard NASTRAN data deck as input, resequences the grid point numbers for reduced bandwidth (if possible), and generates a set of SEQGP punched cards for insertion into the NASTRAN bulk data deck.

#### THE RENUMBERING STRATEGY

The heart of any bandwidth-reduction program is its renumbering strategy. The need to resort to "strategies" at all becomes evident when one considers that  $N$  grid points can be sequenced in  $N!$  distinct ways. Thus, with any strategy, there is no guarantee that an optimum numbering will be achieved at acceptable cost.

The renumbering strategy used in BANDIT is a fast, direct method developed by Cuthill and McKee (ref. 2). Considerable experience gained over the past two years has shown this strategy to perform well consistently for the types of structures of interest to the Navy users of NASTRAN. Consistency is emphasized since, by its very nature, the business of bandwidth reduction is very heuristic. Indeed, no algorithm is best for all structures. Comparisons between the Cuthill-McKee approach and other schemes appear both in reference 2 and a sequel by Cuthill (ref. 3).

Although a complete discussion of the Cuthill-McKee strategy appears in the source paper (ref. 2), the main ideas are presented here for completeness.

For the purposes of this discussion, the degree of a grid point (or node)\* is defined as the number of neighboring nodes to which it is connected. A starting node is one given the new label 1. The strategy first involves the selection of one or more possible starting nodes. Although these nodes are normally of low degree, the one eventually chosen to be the starting node

---

\* Throughout this paper, "grid point" and "node" are used interchangeably.

need not be of minimum degree.

After the selection of a starting node, the remaining nodes are relabeled according to the following prescription: The nodes adjacent (i.e., adjoining) to the starting node are labeled in sequence in the order of their increasing degree. These nodes are said to be at Level 1. (The starting node constitutes Level 0.) In general, Level n is the set of all nodes adjacent to Level n-1 nodes and not previously assigned to a level.

Once Level 1 nodes have been sequenced, the Level 2 nodes are numbered as follows: For each node of Level 1 and in sequence, the Level 2 nodes are numbered in the order of their increasing degree. The numbering continues in this fashion, level-by-level, until all nodes have been numbered. In the event of a "tie" among several nodes to receive a given label, the first node to qualify is chosen.

The above procedure is carried out for each possible starting node previously selected. The sequence yielding the lowest bandwidth is finally chosen.

It is apparent that, in the absence of ties for a given label, the relabeling sequence is independent of the original numbering once a starting node has been selected. Thus the original nodal numbering has almost no effect on the final numbering.

This, rather simple approach to bandwidth reduction has proved to be surprisingly effective in production use.

#### PROGRAM CAPABILITIES

BANDIT's primary reason for existence is the generation of the NASTRAN SEQGP data cards to effect low matrix bandwidth. As a by-product, BANDIT can also be used to right-adjust a NASTRAN bulk data deck. In either case, following the execution of BANDIT, the complete right-adjusted data deck is available on disk file. In addition, the user can elect to have punched card output for either the entire deck or the SEQGP cards alone.

The input data deck for BANDIT consists of a standard NASTRAN data deck (ID card through ENDDATA card, inclusive) with the addition of appropriate \$ cards (comment cards to NASTRAN) indicating what the user wants BANDIT to do.

Although BANDIT accepts an entire NASTRAN deck as input, resequencing requires only the following NASTRAN cards: BEGIN BULK, ENDDATA, and all "connection" cards. GRID cards are not processed by BANDIT. Input bulk data cards may have either 8- or 16-column field widths. In general, the deck can be unsorted, except that each continuation to a connection card must immediately follow the parent card.

The user is also allowed to specify grid points which he wants ignored during the resequencing. Such points appear last in the new nodal sequence, and hence would normally be assigned by NASTRAN to active columns. This feature lets the user specify points which he feels should be relegated to active columns by NASTRAN. Unfortunately, it is often very difficult to identify such points.

#### COMPUTER CONFIGURATIONS

The BANDIT program was developed principally for use on the CDC 6000 series of computers and hence has some machine-dependent features. However, for use on other computers, a "machine-independent" version has also been developed. This version is currently operational on the IBM 360 and UNIVAC 1108.

On CDC machines, BANDIT functions as a variable-core program. Hence, it is essentially open-ended with respect to the number of grid points that can be handled. The program will load with less than 50000<sub>8</sub> words of core, in which space typical structures of less than 500 grid points can be handled. For larger structures, more core is usually required, although rarely are more than 60000<sub>8</sub> words needed.

Typical running times on a CDC 6400 computer are of the order of two to three minutes. For example, a 1000-grid-point structure was recently processed in four minutes. As a rough rule-of-thumb, run times increase in proportion to the number of grid points.

#### DISCUSSION AND EXAMPLES

It would be appropriate to include at least one example of BANDIT's performance. Comparisons among the various algorithms for realistic large structures are rare. Equally rare (at NSRDC, at least) are structures which demonstrate a meaningful "before and after" comparison. The latter is due to the natural tendency of structural analysts to make no serious manual attempt at achieving small bandwidth when aware of the existence of an automatic capability.

The example included here (Figure 1) is a solid structure containing 1686 grid points. It was analyzed on a program other than NASTRAN. Although both manual and automatic renumbering attempts were made, the smallest bandwidth obtained was 202. Subsequent use of the Cuthill-McKee approach further reduced the bandwidth to 151.

Examples such as this tend to gloss over the important role played by the modeler in achieving a small matrix bandwidth. Even with good automatic

direct resequencing capabilities available, it still is undesirable for the analyst to disregard bandwidth considerations in his modeling. Some of the complications can be illustrated by two simple examples.

The first example (Figure 2) shows the reduction of bandwidth possible merely by switching from quadrilaterals to triangles. Here the bandwidth has been cut almost in half. This example was reported at the first NASTRAN Users' Colloquium by R.H. Broliar (ref. 4), who indicated a central processor time saving of 78%.

The second example, obtained from Livesley (ref. 5), shows that bandwidths can sometimes be reduced by the addition of extra nodes. This is illustrated in Figure 3, where the addition of three nodes effected a bandwidth reduction from 4 to 3.

These two examples serve to illustrate that the structural analyst has control over bandwidth considerations that are beyond the scope of automatic bandwidth reduction programs.

#### REFERENCES

1. Everstine, G.C., The BANDIT Computer Program for the Reduction of Matrix Bandwidth for NASTRAN, NSRDC Report 3827, March 1972.
2. Cuthill, E.H., and McKee, J.M., Reducing the Bandwidth of Sparse Symmetric Matrices, Proceedings of the 24th National Conference, ACM, 1969, pp. 157-172.
3. Cuthill, E.H., Several Strategies for Reducing the Bandwidth of Matrices, Sparse Matrices and Their Applications, edited by D.J. Rose and R.A. Willoughby, Plenum Press, New York, 1972, pp. 157-166.
4. Broliar, R.H., A NASTRAN Buckling Analysis of a Large Stiffened Cylindrical Shell with a Cutout, NASTRAN: Users' Experiences, Vol. I, NASA TM X-2378, September 1971, pp. 65-84.
5. Livesley, R.K., The Analysis of Large Structural Systems, The Computer Journal, vol. 3, 1960, pp. 34-39.

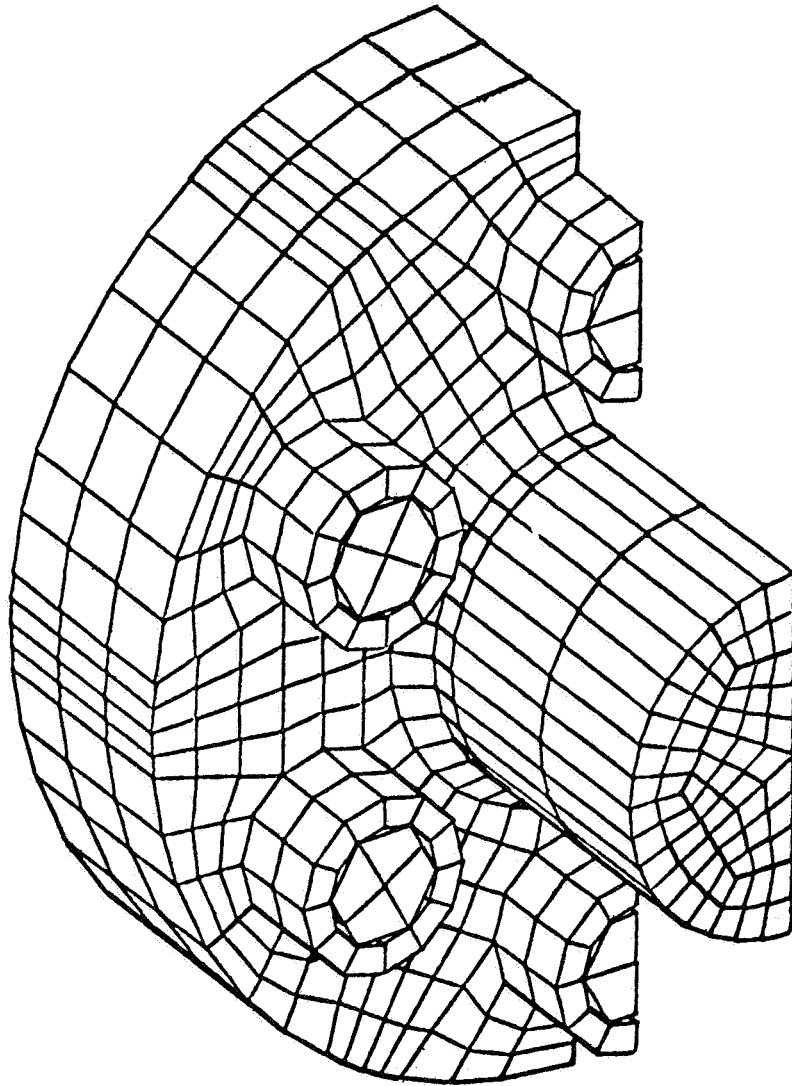
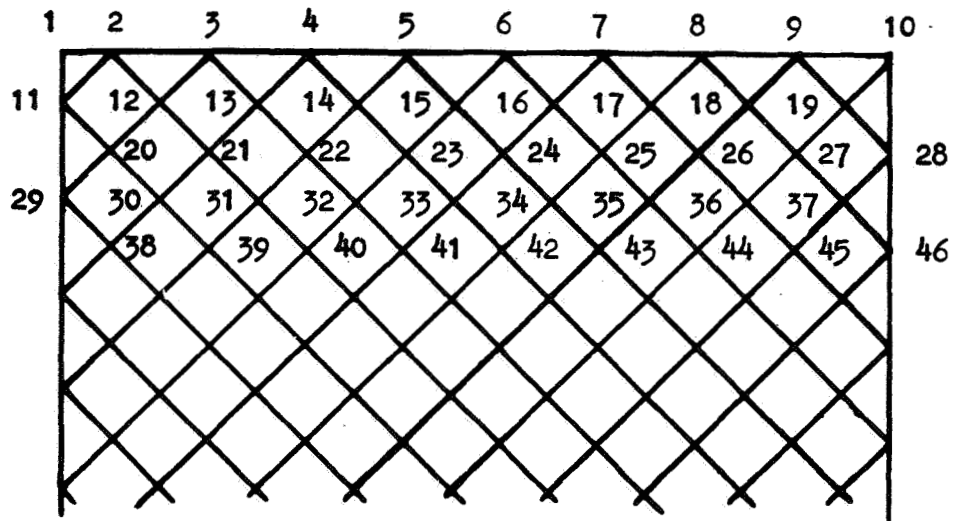
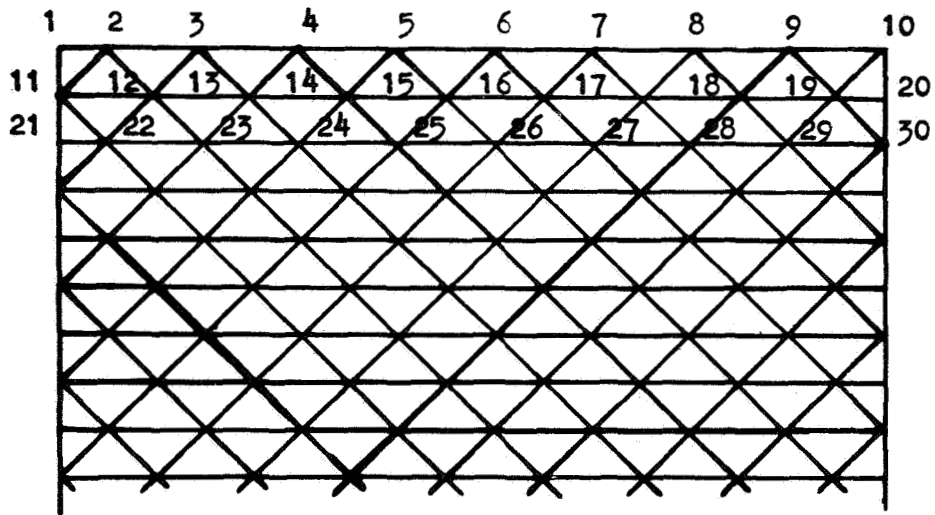


**Figure 1. Example with 1686 Nodes.**

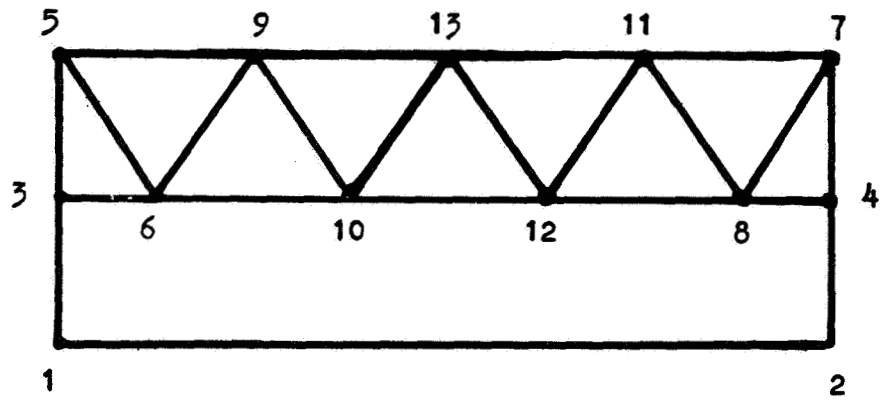


(a) Quadrilateral Modeling (BW = 18).

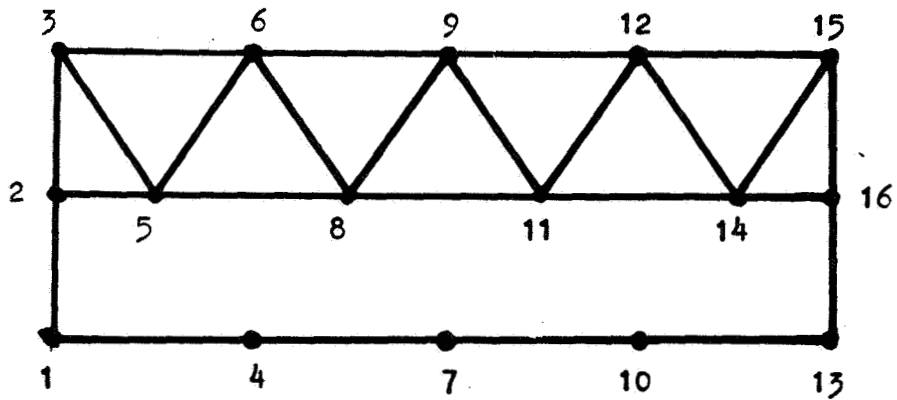


(b) Triangle Modeling (BW = 11).

Figure 2. Example Showing Bandwidth Reduction Possible by Using Triangles Rather than Quadrilaterals.



(a) Without Extra Nodes ( $N = 13$ ,  $BW = 4$ ).



(b) With Extra Nodes ( $N = 16$ ,  $BW = 3$ ).

Figure 3. Example Showing Bandwidth Reduction Possible by Addition of Extra Nodes.

## USE OF NASTRAN AS A TEACHING AID

By Michael T. Wilkinson

Louisiana Tech University

### SUMMARY

Recent experiences with incorporating NASTRAN as a teaching tool in undergraduate courses has been found pedagogically sound. Students with no previous computerized structures background are able to readily grasp the program's logic and begin solving realistic problems rapidly. The educational benefit is significantly enhanced by NASTRAN's plotting feature. However, the cost of operating the level 12 version presently makes the program difficult to justify.

### SELECTION OF A FINITE ELEMENT PROGRAM

Undergraduate instruction in the area of structural analysis must begin by placing major emphasis on the fundamentals such as stress, strain, Mohr's circle, flexure formula, etc. However, all too often the undergraduate's progress does not extend far beyond problems in which a beam is either bent, sheared, twisted or buckled under a wide variety of end conditions.

It seems highly desirable that the undergraduate should also be exposed to more realistic structural problems such as are encountered in practice. These realistic problems generally present two major obstacles -- 1) they are usually too large for hand calculations and 2) they often cannot be analyzed using the simple formulas with which the student is familiar.

It is, of course, clear that the addition of large structural problems into the undergraduate curriculum should not precede a study of the fundamentals. However, realistic problems not only give the senior-level student a practical feel for the results but also provide a significant motivation factor. That is, students generally feel a greater sense of achievement when they successfully solve a significant engineering problem.

With this purpose in mind, the general finite element programs have significant potential as a teaching aid. In the selection of a

finite element program, the instructor must consider the following characteristics of the programs:

- 1) Is it easy to use?
- 2) Will it handle a sufficiently broad class of problems?
- 3) Is it a program the student could be expected to encounter after graduation?
- 4) Is it expensive to use?

With regard to the first question, it is important that a minimum amount of classroom time is spent "checking out" the student on the program. Consequently, the program must be user oriented with easy input and extensive error checks. A corollary to this question is a requirement for a program which is dependable -- nothing dampens student enthusiasm like a program which fails to work!

The second question concerns the versatility of the program. This requirement arises for several reasons. If the program is used for senior level design work, the variety of problems will almost certainly require a general program. Furthermore, many students remain for graduate school and want to use the program as a research tool. Thus, while it is not mandatory, it certainly is desirable to acquaint the undergraduate student with a program which can also be used for graduate research.

The third question asks not only is the program presently widely used by structural engineers, but also is it one of lasting quality? This question is very difficult to answer and tends to be more of an opinion than anything else. All too frequently the answer is biased with how well the instructor can use the program in comparison to similar programs with which he is familiar. Fortunately, it is not imperative that the student be "trained" on a universal program, provided the program used has the same major characteristics of the more commonly used ones.

The final question is more pragmatic and is one which cannot be ignored in view of the current financial pressure on institutions of higher learning. The cost of operating the program depends significantly on the type of computer installation and the method of charging for computer services. It is important that the instructor monitor the computer expenses to ensure they do not get out of hand.

While several excellent finite element programs are available (Ref. 1), the NASTRAN program was selected for the present study for the following reasons. First and foremost, the author felt NASTRAN

struck a proper balance between easy usage and versatility (Ref. 2). It was also felt that the government's commitment (Ref. 3) to maintain and improve the program will assure an even wider acceptance of NASTRAN in the future. With regard to the question of cost, it is acknowledged that NASTRAN is an expensive system to operate (Ref. 2). However, with the significant time savings available between Levels 12 and 15, it appears the cost of operation can still be reduced.

#### PROGRAM UTILIZATION

The presentation of computer methods of structures primarily consists of three topics with which the student is unfamiliar:

- 1) Structural theory
- 2) Computer code
- 3) User experience

The instructor is faced with the problem of maintaining a proper balance between the three. If he devotes his time exclusively to presenting structural theory, he creates an "ivory tower" product who may make an excellent graduate student but a poor prospect for industry. On the other hand, total emphasis on user experience produces a "technician" who knows how to use a "black box" but who knows very little about how the "black box" works.

A balanced approach has been taken by the author in two separate senior-level courses -- one in aircraft structures and another in machine design in mechanical engineering. The two courses differ in that the aircraft structures course has an assigned problem of a small aircraft component whereas the machine design course allows the students to select individual projects. Typical projects which have been selected by students are:

- 1) Automobile brake drum
- 2) Concrete beam with spliced reinforcing steel
- 3) Automobile car roof
- 4) Railroad tank car
- 5) Motorcycle helmet
- 6) Outboard motor propeller

The diversity of subjects points out the wide variety of interests and backgrounds among engineering students.

In each course it has been found possible to start with a sequence of lectures on how to use NASTRAN for static analysis. By relying upon the physical concepts of the finite elements, it has been found that three periods are sufficient to check out students who have had no previous structural programming experience. This initial check out enables the students to spend the remainder of the course working on their particular structural problem. Following the first three periods, the remaining lectures are devoted to structural theory and computer coding.

The topic of computer coding is covered with a presentation of a simple finite element program written by the instructor to illustrate the major steps in program code development. Explanation of this simple program is intended to show the student the art of building a program. Thus, the student is spared the time consuming labors of writing his own computer code, debugging it, and finally trying to obtain some practical results before the course ends. The fact that the student can understand how to use NASTRAN before he has the structural theory and coding background significantly increases the amount of time he can spend developing first-hand experience. Thus, in a sense, he is able to see the "big picture" before becoming entangled in the details.

Based upon student accomplishments, understanding, and endorsement, this particular approach has apparently been successful. Its greatest shortcoming is that NASTRAN is expensive to operate. The program was run on an IBM 370/145 computer with 256K core. The charges for this machine are figured at \$400 per CPU hour. The average student in the aerospace structures course used approximately one hour of CPU time, whereas the machine design students required an average of two CPU hours. Thus, the computer costs per student fell within the range of \$400-\$800. For comparison, a similar study on course instruction in basic FORTRAN was found to cost less than \$40 per student.

The author's experience has also shown that use of NASTRAN's plotting feature dramatically improves student acceptance of the results. The importance of the student seeing a scaled model of the structure, as opposed to simply scanning pages of numbers, cannot be over-emphasized. After gaining a feel for his problem, he is much more willing to study the tabulated results.

#### PROPOSED WORK

At first glance, students tend to be overwhelmed by the magnitude and bulk of the NASTRAN User's Manual. This initial shock could be eased

with the availability of a "Mini-Manual" which describes the essential steps for writing a NASTRAN program. This manual should also contain simple example problems. After graduating from the "Mini-Manual," the student can then use the more extensive documentation contained in the present User's Manual.

#### REFERENCES

1. T. G. Butler, "On the Reduction of Proliferation of Finite Element Programs," paper contained in "NASTRAN: Users' Experiences," NASA X-2378, 1971.
2. J. L. Tocher and E. D. Herness, "A Critical View of NASTRAN," paper presented at the International Symposium on Numerical and Computer Methods in Structural Mechanics, Urbana-Champaign, Ill., Sept. 8-10, 1971.
3. J. P. Raney, D. J. Weidman, and H. M. Adelman, "NASTRAN: Status, Maintenance, and Future Development of New Capability," paper contained in "NASTRAN: Users' Experiences," NASA TM X-2378, 1971.



# STRUCTURAL ANALYSIS FOR A 40-STORY BUILDING

By Lo-Ching Hua

Professional Services Division  
CONTROL DATA CORPORATION

## SUMMARY

NASTRAN was chosen as the principal analytical tool for structural analysis of the Illinois Center Plaza Hotel Building in Chicago, Illinois. The building is a 40-story, reinforced concrete structure utilizing a monolithic slab-column system. The displacements, member stresses, and foundation loads due to wind load, live load, and dead load were obtained through a series of NASTRAN runs. These analyses and the input technique are described in this paper.

## INTRODUCTION

The demands of a prosperous economy, combined with advancements in material technology, have created a high-rise building boom all over the world. In most cases, these buildings have complicated structural configurations for the purpose of accommodating the multiple functions required. The traditional structural analysis of buildings has been limited to simplified methods, such as plane frame or truss analysis. These methods often lead to erroneous results. To improve solution accuracy, manual iteration has been used at the expense of higher computation and labor costs. Occasionally, model testing techniques have been employed. However, the measured results did not necessarily yield better accuracy. They are more generally accepted as an indication to insure the conservatism of the designer.

In the last few years, the finite element method has gained wide recognition in this field. Unfortunately, most of the finite element programs available do not have the capabilities necessary to analyze a theoretically desirable model of a large building. They are either insufficient in capacity, or lacking essential finite elements. The emergence of the NASTRAN program has served to alleviate these shortcomings.

The Illinois Center Plaza Hotel is located near Lake Michigan in downtown Chicago. It is a 40-story reinforced concrete building which includes 1,000 guest rooms, several restaurants, parking facilities, and large conference rooms and ballrooms. The structural system of the building is the unique slab-column system, in which, the thin floor slabs are poured monolithically with the columns. There are no drop panels or haunches at the slab-column junctions. The savings in construction costs associated with this simplification makes the slab-column system a very competitive one in comparison to the conventional beam-column-slab system. However, more analytical work is necessary to insure an adequate design of this type

of system. The stress concentrations at the junctions, and the interaction between the slab and column become a necessary part of the analysis.

The hotel building is symmetrical about its short axis (X-axis) as shown in Figure 1. Therefore, only one-half of the structure was analyzed. The mathematical model representing this half building consisted of 1718 GRID points; 5000 CBAR elements, with maximum nodal difference of 81; and 3600 concentrated forces and moments. NASTRAN was chosen for this application on the basis of solution accuracy, problem capacity, and multiple constraint and restart capabilities. The analysis and results are described herein.

#### SLAB-COLUMN INTERACTION ANALYSIS

Structurally, the slabs of a high-rise building have two functions. They support the live and dead load and transfer them to the columns and footings. On the other hand, they also resist shear forces due to wind pressure on the building.

The models used in this analysis are shown in Figures 2 and 3. The model in Figure 2 consists of 777 GRID points, 124 CBAR's, 618 CQUAD2's, and one CTRIA2. CBAR elements were used to represent columns, while CQUAD2 and CTRIA2 elements were used to represent floor slab and shear walls. Because the point of inflection of a column is approximately midway between two floor slabs, the length of the columns were taken to be half of the floor height. The model shown in Figure 3 is similar to the first one, with 152 GRID points and 234 CBAR's. The columns are the same as in the first model, whereas, the slabs are represented by an equivalent beam system. The equivalent beams are fictitious beams with the slab thickness as their depth, and the reduced slab width as their width. The amount of width reduction is determined by the means of the displacement analysis which is described in the following paragraphs. In the case of the shear walls, the total cross section was considered to be effective in formulating the replacement CBAR elements.

Since the inplane rigidity of the slab is relatively stiff, the lateral displacements of the column ends which are not connected to slabs are tied together with multiple constraints. This constraining condition yields a more realistic distribution of shearing force among the columns.

The slab-column model was analyzed with three loading conditions; live load, dead load, and wind load. The individual results were also combined in accordance with local building codes. The live load and dead load analysis determined the related bending and shearing stresses, as well as displacements of the slab. It also provided the distribution of column loads. In the wind load analysis, the total accumulation of wind load was applied at the top of the model, and the wind load of the particular story was applied at the slab level. This resulted in the computation of shearing displacement of the particular story, and the shearing and bending stresses in slabs and columns due to wind load. By inspection of the stress variation across the width of the slab, an initial width was determined for the equivalent beams in the beam-column model.

Then, the same wind load was applied to obtain the shearing displacement. The width of the beams was varied to search for a configuration which provided the same displacement as the slab-column model. These two models are displacement compatible models. Obviously, the motivation for this is strictly economical. In this investigation, the size of the problem was reduced by 80%. Yet, it still provided a reasonably reliable wind stress analysis.

#### SPACE FRAME BUILDING STRUCTURE ANALYSIS

Once the simple equivalent model was obtained through the analysis described in the previous paragraphs, the task of assembling the model for the whole building was a straight forward one. It resulted in the space frame shown in Figure 1. Because the building has one plane of symmetry, only half of the building was necessary for this model.

There were two NASTRAN runs in this analysis. The first one was to analyze the displacements and stresses due to live load, dead load, and wind load acting in the direction of the short axis of the building, with symmetrical boundary conditions at the grid points along the short axis. The second run was to analyze the displacements and stresses due to wind load acting along the direction of the long axis (Z-axis) of the building, with anti-symmetrical boundary conditions along the short axis.

The results showed that the building shortens about 3.6 centimeters under combined live and dead load. It also drifts 8.6 centimeters and 17.8 centimeters under wind load in the direction of long and short axis, respectively. The profiles of the drift of the building are shown in Figure 4. They all conform to Chicago building code. The amount of drift is considered to be an important criteria for design. It determines the natural frequencies of the building and, hence, the response of the building to wind loads. The stress results were used for design purposes such as determining reinforcing, sizing concrete sections, and required material strengths. The Single Point Constraint Forces at the base of the building were used for the design of the foundation system.

#### PREPROCESSOR

Since a large portion of the building layout was uniform, there was a great deal of repetition of the bulk data. In order to take advantage of this and simplify data preparation, a short preprocessor was written to generate bulk data cards from a few key cards. Essentially, the preprocessor was a collection of counters and bulk data Formats. The function of the counters was to repeat and extrapolate the data on key cards. The bulk data Formats were required to generate card images. Approximately 11,000 input card images were generated on magnetic tape from 1,500 cards input to the preprocessor program.

The operation of linking the preprocessor, storing and transferring data, as well as executing NASTRAN, were done on a CDC 6600 computer under the SCOPE 3.3 operating system. All together, seven SCOPE control cards were required for this entire operation. Therefore, the amount of data preparation work was minimal. It represented an approximate reduction of 86% when compared to all manual work.

#### CONCLUDING REMARKS

The slab column interaction analysis presented herein is believed to be the first of its kind in the field of high-rise building analysis. It bypassed the requirement of conventional assumptions and, therefore, provided more reliable results.

The average nodal difference in the building model was 41, with a maximum of 81 occurring at the transfer girder floor. However, the maximum nodal difference occurred only in a few elements. This made it ideal for the application of the active column approach utilized in NASTRAN. As a result, the solution times were competitive with some of the fastest finite element codes in the field.

In addition to being fast and accurate, the flexibility on NASTRAN's I/O routines and data management, coupled with a simple preprocessor, greatly reduced input time. This is essential in solving large structural problems. The current version of NASTRAN may not have the best elements being developed in research institutions, nevertheless, the present degree of sophistication is generally consistent with current procedures used in the design and construction of a high-rise building.

STRUCTURE OF THE HOTEL BUILDING

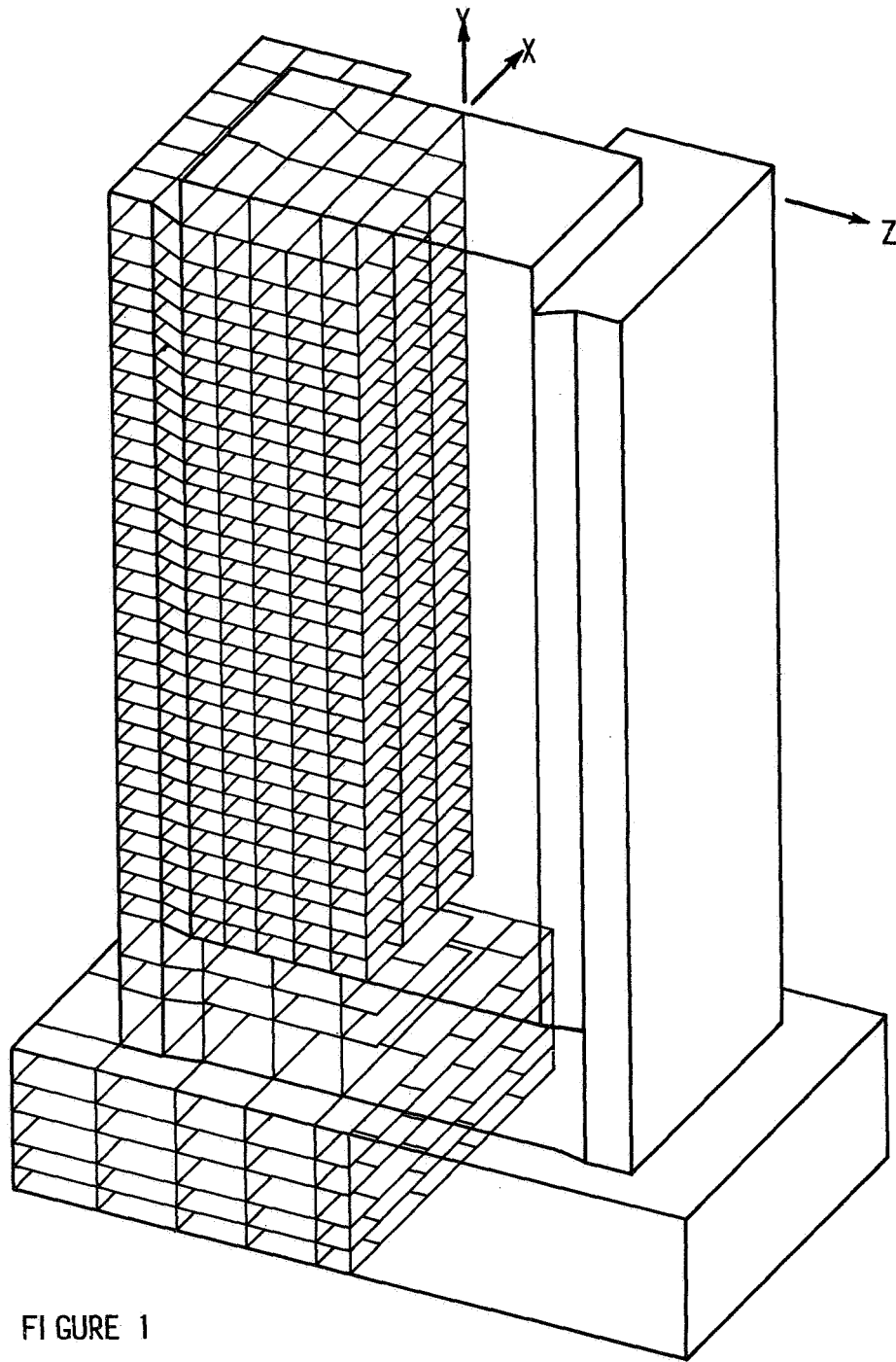


FIGURE 1

SLAB-COLUMN MODEL

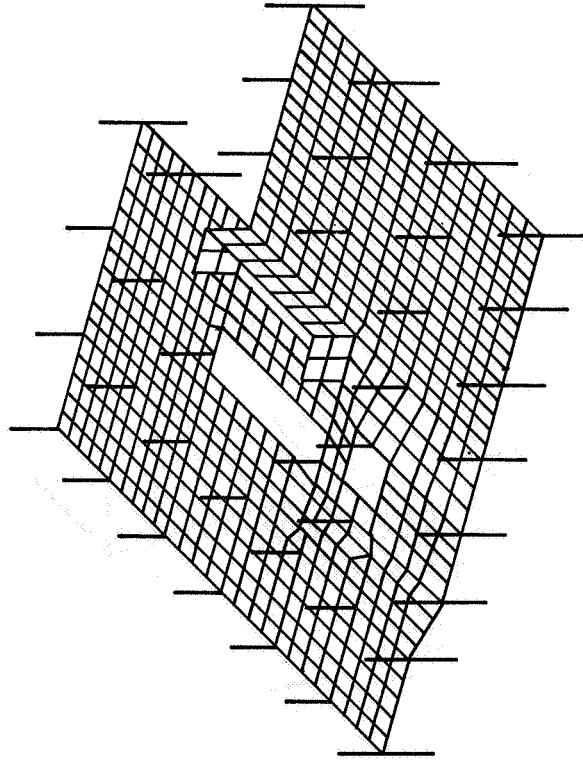


FIGURE 2

SLAB-BEAM-COLUMN MODEL

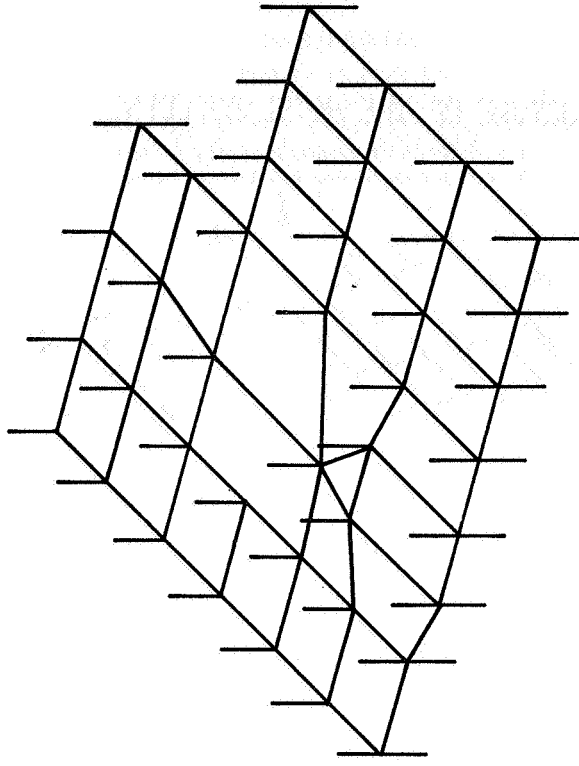


FIGURE 3

DRIFT OF THE BUILDING

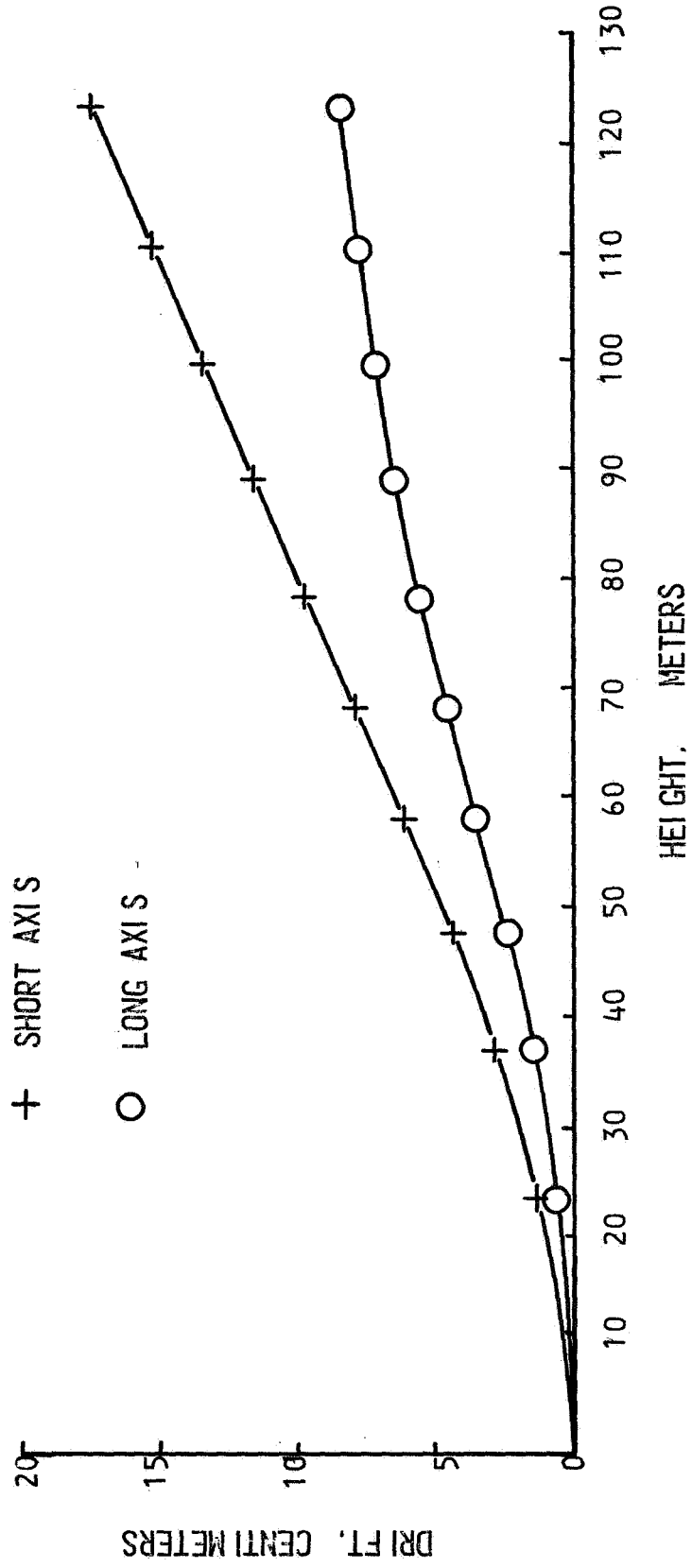


FIGURE 4



# APPLICATIONS OF NASTRAN TO NUCLEAR PROBLEMS

By Embertus Spreeuw\*  
NASA Langley Research Center

## SUMMARY

The usefulness of NASTRAN for nuclear applications has been investigated. For this purpose the extent to which suitable solutions may be obtained for one physics problem and two engineering type problems is traced. NASTRAN appears to be a practical tool to solve one-group steady-state neutron diffusion equations. Transient diffusion analysis may be performed after new levels that allow time-dependent temperature calculations are developed.

NASTRAN Piecewise Linear Analysis may be applied to solve those plasticity problems for which a smooth stress-strain curve can be used to describe the nonlinear material behavior. The accuracy decreases when sharp transitions in the stress-strain relations are involved. Improved NASTRAN usefulness will be obtained when nonlinear material capabilities are extended to axisymmetric elements and to include provisions for time-dependent material properties and creep analysis. Rigid Formats 3 and 5 proved to be very convenient for the buckling and normal-mode analysis of a nuclear fuel element.

## INTRODUCTION

In addition to NASTRAN finding its way into leading U.S. aerospace industries and research institutes, it is also more and more used in other areas of structural analysis such as civil engineering and the automotive industry. In the past much duplication has occurred with respect to the development of finite-element computer programs, but at present it is worthwhile to investigate the applicability of NASTRAN before deciding to write a finite-element routine or to add large extensions to existing programs. NASTRAN is an easy-to-use general-purpose program with assured continuous management and maintenance and is available at a low price.

The domain of nuclear problems is an important field of application outside the area for which NASTRAN was originally developed, and the present paper discusses the use of NASTRAN for some characteristic nuclear engineering and physical problems. The recently released Level 15 allows the solution of physical problems since a functional for neutron diffusion calculations, which shows a close relationship to one used for thermal analysis, was derived. Except for the computation of a neutron-flux distribution, the paper deals with two structural example problems; one discusses the elastic and plastic deformation of nuclear fuel cladding, and the other concerns the normal-mode and buckling analysis of a fuel element.

---

\*Postdoctoral Research Fellow, European Space Research Organization.

The example problems chosen do not cover the whole area of finite-element applications suitable for nuclear research and design nor are all details of them investigated. Therefore, the paper cannot provide sufficient information needed to decide whether to use NASTRAN or not and may only serve as a guideline to more directed research.

### ONE-GROUP NEUTRON DIFFUSION

Recently, different authors (refs. 1, 2, and 3) have applied finite-element techniques to solve problems from nuclear physics. The equations used to describe heat transfer and neutron diffusion show a close similarity, and only a few minor modifications of heat transfer programs are necessary to allow neutron diffusion calculations. Functionals for both phenomena will be discussed and NASTRAN alterations to give neutron-flux distributions will be outlined. The results for one particular application are presented.

For the case in which all neutrons are assumed to belong to the same energy (velocity) group, the equation of neutron diffusion reads (ref. 4)

$$-\frac{1}{v} \frac{\partial \phi}{\partial t} + D \frac{\partial^2 \phi}{\partial x_i \partial x_i} - \sigma \phi + S = 0 \quad (1)$$

Here the summation convention is used while  $v$  stands for velocity,  $D$  for the diffusion coefficient,  $\phi$  for the scalar flux,  $\sigma$  for the macroscopic absorption cross section, and source term  $S$  for the rate of production of neutrons per unit volume per second.

The boundary conditions applied to equation (1) involve continuity of flux and current at interfaces, and vanishing of flux at extrapolated boundaries or return current at the actual boundaries. The general form of the boundary conditions reads

$$D \frac{\partial \phi}{\partial n} + \gamma \phi + q = 0 \quad (2)$$

where  $\gamma$  and  $q$  are constants. Equations (1) and (2) can be combined to obtain the functional:

$$F = \iiint \left( \frac{1}{v} \frac{\partial \phi}{\partial t} \phi + \frac{D}{2} \frac{\partial \phi}{\partial x_i} \frac{\partial \phi}{\partial x_i} + \frac{\sigma}{2} \phi^2 - S \phi \right) dV + \iint \left( q \phi + \frac{\gamma}{2} \phi^2 \right) dA \quad (3)$$

where the triple integrals are to be extended over the volume  $V$ , and the double integrals over the surface  $A$  of this volume. Functional  $F$  reaches a minimum value with respect to all admissible variations of flux distribution  $\phi$ .

The functional most commonly used for finite-element heat conduction computation is

$$P = \iiint \left( \rho c \frac{\partial \theta}{\partial t} \theta + \frac{\lambda}{2} \frac{\partial \theta}{\partial x_i} \frac{\partial \theta}{\partial x_i} - Q^o \theta \right) dV + \iint \left( \frac{\alpha}{2} \theta_m^2 - \alpha \theta_m \theta + \frac{\alpha}{2} \theta^2 \right) dA \quad (4)$$

which reaches a minimum value with respect to all admissible variations of temperature distribution  $\theta$ . The symbol  $Q^o$  is used for volumetric heat generation rate,  $\rho$  for density, and  $c$  for specific heat while  $\lambda$  stands for the coefficient of heat conductivity. The coefficient of heat transfer between the structure and its surrounding medium is represented by  $\alpha$  and the temperature of the surrounding medium by  $\theta_m$ . Comparison of expressions (3) and (4) shows that duality of finite-element temperature programs is obtained when for neutron

diffusion calculations the following substitutions are made:  $\frac{1}{v}$  for  $\rho c$ ;  $D$  for  $\lambda$ ;  $S$  for  $Q^o$ ;  $-\frac{q}{\gamma}$  for  $\theta_m$ ; and  $\gamma$  for  $\alpha$ . Moreover, the heat

capacity matrix has to be generated using a coefficient of thermal capacity equal to  $\sigma$  and added to the heat conduction matrix. As yet NASTRAN heat flow capability can be used for stationary problems only and in this way applications to the calculation of neutron-flux distributions have to be restricted to steady-state conditions. The calculations can be performed by carrying out the substitutions mentioned and the insertion of an ALTER package (fig. 1). In Level 15.1.1 the heat capacity matrix cannot be generated directly. However MAT1, MAT2, or MAT3 cards can be used to submit values for the mass density equal to those desired for the thermal capacity and module SMA2 can be executed to obtain the mass matrix. The ALTER package allows the generation of matrix MGG and the addition of it to the heat conduction matrix KGGX. Module SCE2 removes additional matrix elements implied by MGG and undesired in the heat capacity matrix. The method described has been used to determine the flux distribution in the basic area of symmetry in a fuel-moderator mixture located between a square array of cruciform control rods. The rods are black to thermal neutrons and a uniform slowing density has been assumed. Figure 2 shows the geometry together with the idealization and calculated lines of constant neutron flux. The problem has also been investigated by Semenza et al. (ref. 2) and the agreement looks reasonable.

#### DEFORMATION OF NUCLEAR-FUEL CLADDING

One of the most important problems in the design of nuclear fuel elements is the interactive deformation of fuel pellets and the surrounding cladding (fig. 3). For most of the current cladding and fuel materials, the temperatures at which the loadings are applied will cause creep and plasticity to occur. Moreover, the nuclear irradiation leads to swelling, introduced by helium bubble formation, and embrittlement of the materials; thus, two more complications must be dealt with in analyzing the deformations.

With the exception of contact forces implied by the cladding, the pellet is only loaded thermally. The cladding is subject to

- (1) Differential pressure between coolant on the outside and released fission gas on the inside
- (2) Contact pressure and axial forces due to swelling and thermal deformation of the fuel
- (3) Thermal load caused by heat transfer through the clad wall

The magnitude of these loadings depends on time, neutron dose, and power output of the reactor.

NASTRAN permits the calculation of deformations both elastically and plastically. A static solution could be obtained by use of solid-of-revolution elements. After a choice has been made with respect to the grid points where contact occurs, multipoint-constraint equations could provide expressions for the displacements of internal cladding grid points in terms of external pellet grid points and the undeformed gap. The idealization and the deformed shape are given in figure 4, and the results show close agreement with solutions obtained from other programs (ref. 5).

Plasticity calculations of cladding deformations as a result of mechanical loading have been performed using Piecewise Linear Analysis. Because this feature is as yet not applicable for solid-of-revolution elements, the cladding wall has been idealized by parallel plate elements (fig. 5). In using this model, all axial displacements were restrained and all elements were kept parallel during deformation while interelement distances remained constant. Moreover all collinear grid points remained collinear and on the same radii. All these restrictions could easily be accomplished by multipoint and single point constraints leading to a number of independent degrees of freedom equal to 1. The application of this model means that radial stresses are neglected. These, however, proved to be of minor importance and are partly counterbalanced by the assumption of constant interelement distances.

During each pass through the Piecewise Linear Analysis loop a new value for the stress-strain slope is estimated by using

$$E^i = \frac{\sigma_a^{i+1} - \sigma_a^i}{\epsilon_a^{i+1} - \epsilon_a^i} \quad (5)$$

where  $\sigma_a^i$  and  $\epsilon_a^i$  are the uniaxial equivalences of stress and strain obtained after application of the  $i$ th load increment and

$$\epsilon_a^{i+1} = \epsilon_a^i + \frac{\Delta\alpha_{i+1}}{\Delta\alpha_i} (\epsilon_a^i - \epsilon_a^{i-1}) \quad (6)$$

$$\sigma_a^{i+1} = F(\epsilon_a^{i+1}) \quad (7)$$

where  $\Delta\alpha_i$  denotes the load increment during the  $i$ th load factor and  $F$  denotes a user-supplied tabular function of stresses and strains.

If a strain-hardening law is applied, the model requires that within a small increase of load, all elements deform beyond the elastic limit. The overall rigidity decreases considerably in the plastic stage and a load increment beyond the yielding point causes a strain increment which may be many times greater than that registered during the elastic deformation.

This is why the use of expression (6) to predict the strain due to the next load factor can lead to greatly underestimating the strain and, in such cases, the value used for  $E^i$  will be much too large. The present levels of NASTRAN do not contain a check on the accuracy of  $E^i$ . For the model described, acceptable results could only be obtained by choosing the piecewise linear factors in such a way that each of the nonlinear elements will be loaded up to the yielding point for one particular load factor.

This approach is of course very laborious and not feasible for structures with many nonlinear elements. However, the accuracy can be improved if the relationship between stresses and strains can be described by a smooth curve and if small load increments are used.

Thermal stresses are an important factor in the analysis of the cladding. When these stresses alternate, as is the case during startups and shutdowns of the reactor, they become of even more importance and a stepwise increase of the cladding diameter, called "thermal ratchetting," may be observed.

In Piecewise Linear Analysis (PLA), thermal loading can be taken into account by generating the relevant load vector separately and adding it stepwise to the mechanical loading after the mechanical loading has been fully accumulated during repeated execution of the PLA loop. The deviating values of  $E^i$  and the alternate direction of strain increments for elements compressed by the thermal strain could be accomplished by application of Direct Table Input. These tables can substitute the regular element summary, connection, and property tables for nonlinear elements, but once again the approach proved to be laborious and useless for practical applications. NASTRAN did not allow creep calculations or the consideration of time-dependent material properties introduced by the influence of nuclear irradiation.

#### BUCKLING AND NORMAL-MODE ANALYSIS OF FUEL ELEMENT

In many types of nuclear reactors, the heat generated by nuclear fission is removed by a gaseous or liquid coolant flowing longitudinally along the fuel rods. Considering the buckling of these rods when subjected to the flowing environment, it does not matter whether the fluid is assumed to flow through or along the tube, and the critical value of the fluid velocity can be found by solving the differential equation for steady flow of the fluid through the tube:

$$EI \frac{\partial^4 z}{\partial x^4} + \rho v^2 \frac{\partial^2 z}{\partial x^2} = p$$

Here  $z$  stands for the transverse displacement,  $v$  for fluid velocity, and  $EI$  for the bending stiffness of the tube. This agrees (ref. 6) with the equation for a pipe carrying a lateral load  $p$  and an axial load of  $\rho v^2$ . When  $\lambda$  is used for the length it means that buckling of the pipe will occur when

$$\rho v^2 = EI \left( \frac{\pi}{\lambda} \right)^2$$

therefore, the critical velocity is

$$v = \frac{\pi}{\lambda} \sqrt{\frac{EI}{\rho}}$$

NASTRAN allows accurate<sup>1</sup> determination of the buckling load, and therefore the critical velocity, when the pipe is idealized by only a few collinear BAR elements. Therefore, this program may also be used for the computation of critical velocities in complete fuel elements. In order to reduce the number of degrees of freedom, a NASTRAN fuel-element analysis has been performed by use of an artificial element with fewer fuel rods than usual but with a length-to-width ratio in agreement with existing fast-breeder reactor designs. The element considered contains 37 fuel rods arranged in a hexagonal pattern with an 8-mm pitch. The 6-mm-diameter rods occupy the full 800-mm length of the element.

To support the rods in the transverse directions, the element is equipped with four intermediate honeycomb-like grids; thus, all transverse displacements are equated at grid locations. The element is assumed to be clamped in the lower element supporting plate, whereas only longitudinal displacements are possible in the upper plate.

Every fuel rod is idealized by 10 collinear BAR elements of equal length while each side of the hexagonal prismatic container is modeled by a rectangular pattern of QUAD1 elements with 10 elements over the length and four elements over the width. Figure 6 gives the undeformed element together with normal modes 1, 2, and 5. The first four modes show vibrations of the fuel rods and mode 5 represents the impact of the lowest container frequency on the behavior of the fuel element also. When liquid sodium is used for cooling, the critical velocity is found to be 5.7 m/sec. Matrix partitioning has been applied to obtain 195 degrees of freedom in the a-set. For the problem concerned, this figure is too high to produce a significant reduction in CPU time. Checkpointing with restarting proved to be profitable when other eigenvalue ranges of interest had to be investigated.

---

<sup>1</sup>0.16 percent deviation for three elements.

## CONCLUDING REMARKS

The use of NASTRAN for the solution of three nuclear problems has been investigated. In view of the fact that NASTRAN was developed for solution of problems in aerospace structures, it is not astonishing that it is somewhat limited in the scope of nuclear problems that it will solve and requires more user effort than special-purpose nuclear programs. In summary, the conclusions from the analysis of the chosen examples can be stated as follows:

1. Steady-state one-group neutron-flux distributions can be computed very conveniently by the use of NASTRAN. One of the next official levels featuring transient-temperature calculations will also permit the solution of time-dependent diffusion equations. The applicability to multigroup diffusion and other problems from nuclear physics may be investigated.

2. At this time, Rigid Format 6 seems unsuitable when a strain-hardening law is used and alternating thermal loads are involved. In order to improve the present approach used in Piecewise Linear Analysis (PLA) it may be advisable to repeat the calculation in those cases where a large deviation between the estimated and actual strains occurs. Reference 7, 8, or 9 may be useful if an alternative approach is shown to be desirable. Other areas of interest for nuclear users will be to have PLA available for solid-of-revolution elements also and to be able to apply NASTRAN for creep calculations.

3. Buckling and normal-mode analysis can be applied directly to nuclear problems and to permit calculations of critical fluid velocities. The use of matrix partitioning reduces the number of independent degrees of freedom without loss of accuracy. More emphasis on creep applications is also desirable for these rigid formats, and a provision to perform creep-buckling analysis would mean a considerable improvement.

The criticism expressed did not show to full advantage the many important features such as checkpointing, substructuring, and multipoint constraints which are not found in any known computer code for nuclear use. These features give NASTRAN the lead over its competitors. The general and flexible applicability of NASTRAN constitutes its main power, and especially when more effort can be spent to improve nonlinear material capabilities, NASTRAN will have a large potential in the area of nuclear research and design.

## ACKNOWLEDGEMENT

The author is thankful for the ESRO fellowship that enabled the performance of this research. Gratitude is also extended to NASA and its NASTRAN Systems Management Office for the opportunity offered and for the beneficial assistance given.

## REFERENCES

1. Kang, C. M.; and Hansen, K. F.: Finite Element Methods for the Neutron Diffusion Equations, ANS Annual Meeting, Boston, June 1971.
2. Semenza, L. A.; Lewis, E. E.; and Rossow, E. C.: A Finite Element Treatment of Neutron Diffusion, Trans. Am. Nucl. Soc., 14,200, 1971.
3. Ohnishi, T.: Application of Finite Element Solution Technique to Neutron Diffusion and Transport Equations, ANS National Topical Meeting, Idaho Falls, Idaho, March 1971.
4. Weinberg, A. M.; and Wigner, E. P.: The Physical Theory of Neutron Chain Reactors, The University of Chicago Press, Chicago, Ill., 1958.
5. Spreeuw, E.: Fiesta: Finite Element Temperature and Stress Analysis, RCN-Report 149, Petten (1971) the Netherlands.
6. Roth, W.: Oelhydraulik and Pneumatik, 1961, p. 307.
7. Cyr, A. M.; and Teter, R. D.: Finite Element Elastic-Plastic-Creep Analysis of Two Dimensional Continuum with Temperature Dependent Material Properties, Nat. Symp. on Computerized Structural Analysis and Design, Washington, D.C., Mar. 1972.
8. Swedlow, J. L.: A Procedure for Solving Problems of Elasto-Plastic Flow, Nat. Symp. on Computerized Structural Analysis and Design, Washington, D.C., Mar. 1972.
9. Noor, A. K.; Stephens, W. B.; and Fulton, R. E.: An Improved Numerical Process for Solution of Solid Mechanics Problems, Nat. Symp. on Computerized Structural Analysis and Design, Washington, D.C., Mar. 1972.

NASTRAN EXECUTIVE CONTROL DECK ECHO

```

TD      STEADY ONE GROUP NEUTRON DIFFUSION
APP     DISPLACEMENT
SQL     1,0
DIAG 1,14
ALTER 22,22
$ SKPMGG = 1 WILL AVOID PUPPING OF MGG
$ AND ENABLE EXECUTION OF SMA2
PARAM   //C,N,NOP/V,N,SKPMGG=1 $
ALTER 37
$ ADD THE DIFFUSIVITY MATRIX TO THE ABSORPTION MATRIX
ADD     KGGX,MGG/KGG1/C,Y,ALPHA=(1.0,0.0)/C,Y,BETA=(1.0,0.0) $
CHKPNT  KGG1 $
ALTER 44,44
EQUIV   KGG1,KGG/NOGENL $
ALTER 47,47
SMA3    GE1,KGG1/KGG/V,N,IUSET/V,N,NOGENL/V,N,NOSIMP $
ENDALTER
TIME    2
CEND
    
```

Figure 1.- Executive Control Deck for neutron diffusion calculations.

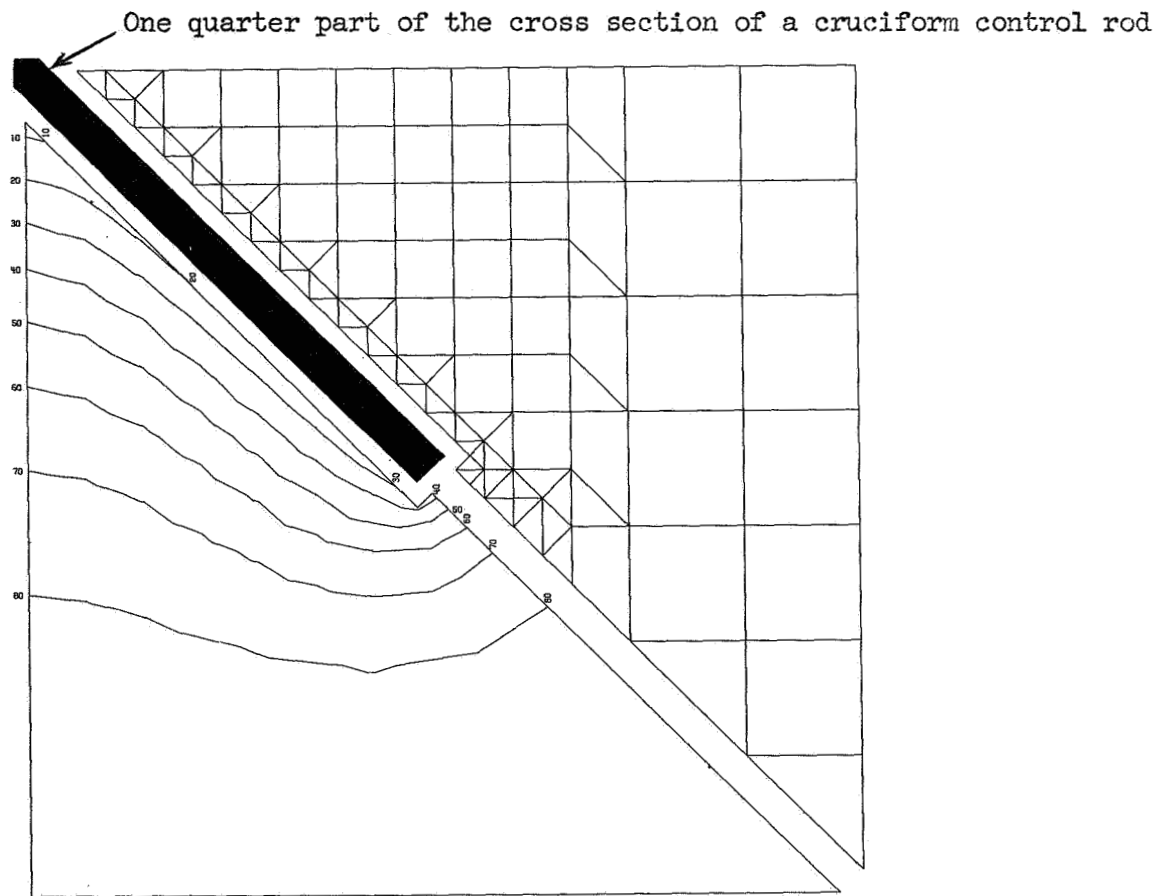
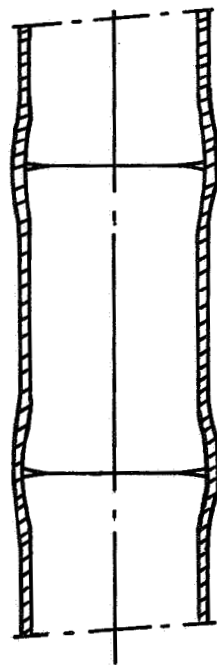
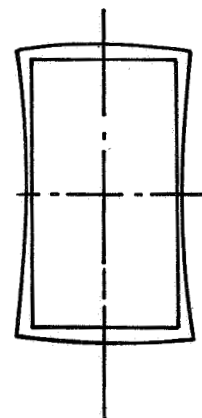


Figure 2.- Idealization and lines of constant neutron flow in a fuel-moderator mixture area between cruciform control rods.



(a) Interactive deformation.



(b) Thermally expanding pellet.

Figure 3.- Pellet and cladding.

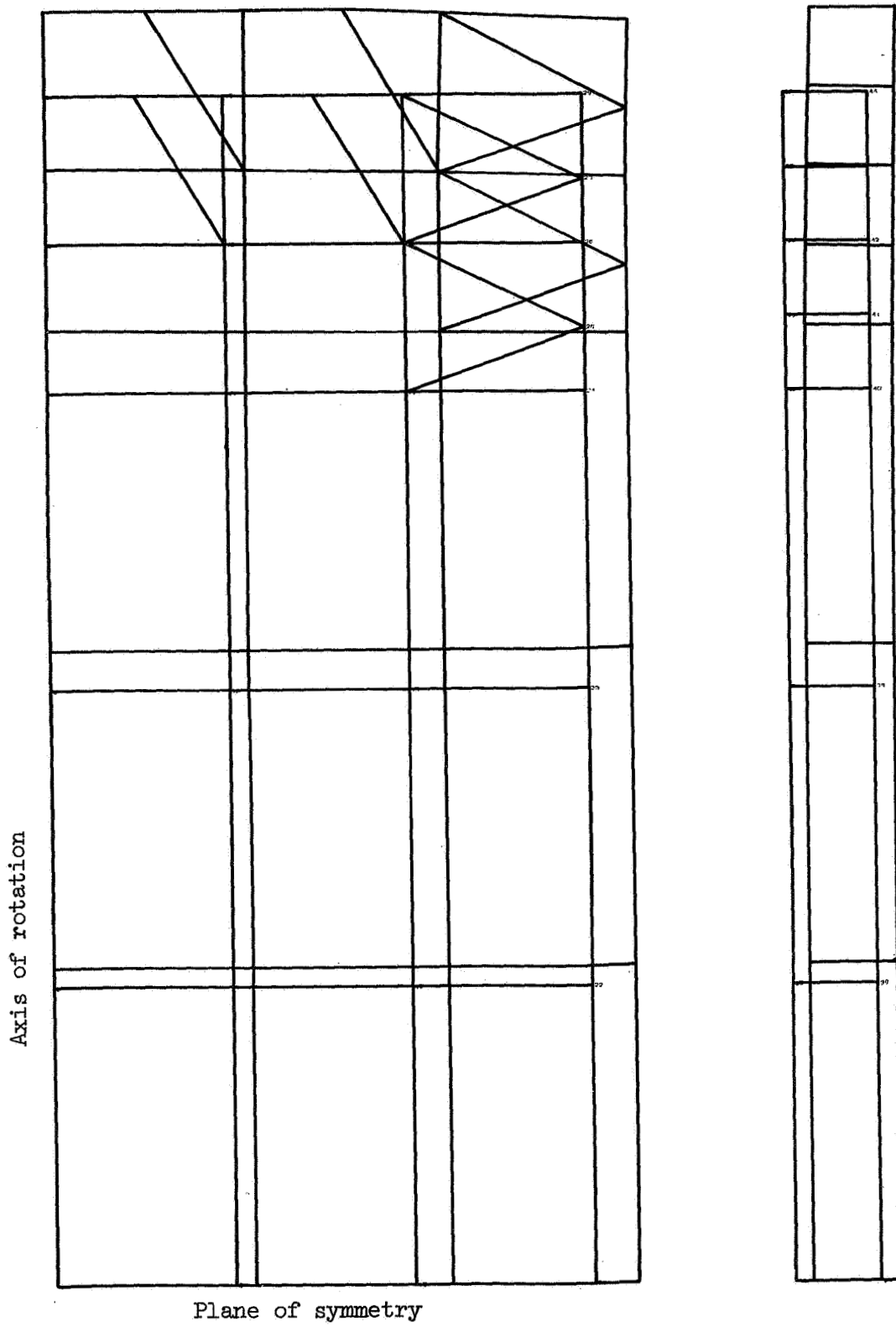


Figure 4.- Computed interactive deformation of pellet and cladding.

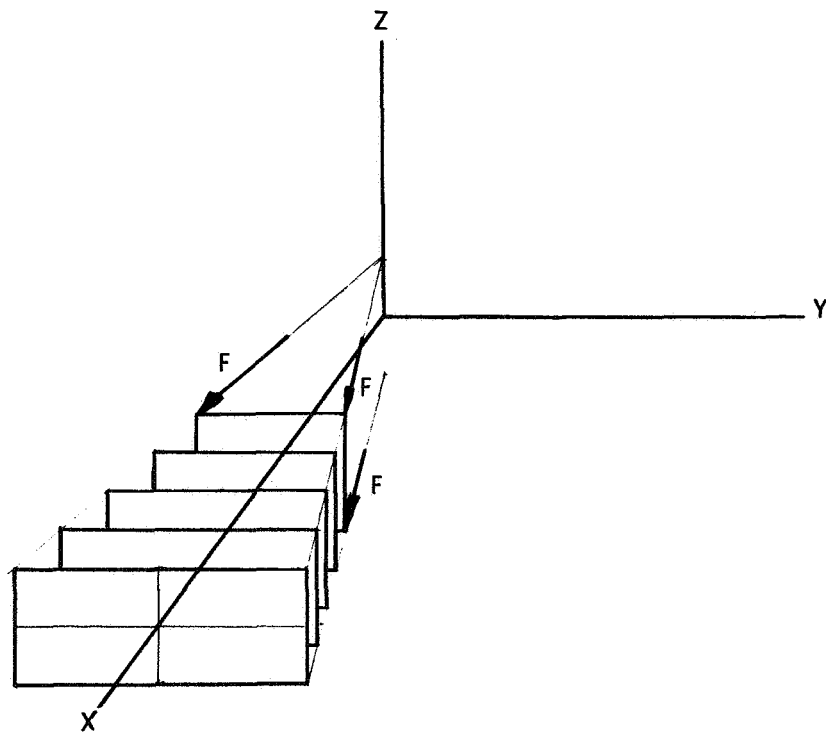


Figure 5.- Idealization of a tube for Piecewise Linear Analysis.



Figure 6.- Normal modes of nuclear fuel element.



## NASTRAN THERMAL ANALYZER

### A GENERAL PURPOSE FINITE-ELEMENT HEAT TRANSFER COMPUTER PROGRAM

Hwa-Ping Lee and James B. Mason

NASA Goddard Space Flight Center

#### SUMMARY

A general purpose heat transfer analysis capability based on the finite-element method has been added to the NASTRAN system. The program not only can render temperature distributions in solids subjected to various thermal boundary conditions, including effects of diffuse-gray thermal radiation, but is fully compatible in capacity and in the finite-element model representation with that of its structural counterpart in the NASTRAN system. The development history of the finite-element approach for determining temperatures is summarized. The scope of analysis capability, program structure, features, and limitations are given with the objective of providing NASTRAN users with an overall view of the NASTRAN Thermal Analyzer.

#### INTRODUCTION

The NASTRAN Thermal Analyzer is a general purpose heat transfer computer program based on the finite-element approach. It is fully capable of rendering temperature distributions and heat flows in solids subjected to various boundary conditions, including the modes of convection and radiation, in both steady-state and transient problems. This computer program has been achieved by the addition of new capabilities to NASTRAN including new elements and solution algorithms. The resulting Thermal Analyzer is both self-contained and user-oriented but remains totally compatible in capacity and in the finite-element model representation with that of its structural counterpart in the NASTRAN system. Therefore, thermal and structural analyses of large and complex structural configurations utilizing a unified finite-element representation have become a reality.

The purpose of this paper is to provide the NASTRAN users with an overall view of the NASTRAN Thermal Analyzer describing its scope, program structure, features and limitations. The practical needs which motivated the development of this thermal analysis capability are given. A brief survey of early works with regard to heat transfer analysis by the finite-element method is included. Also described are studies conducted at GSFC which investigated element behaviors, obtainable accuracy and solution efficiency of various schemes used in conjunction with the finite-element method, the feasibility of adding thermal analysis capability to the NASTRAN system, and the various approaches for treating problems with emphasis on radiative exchanges.

## BACKGROUND OF DEVELOPMENT

The main objective of a research and development program at GSFC, titled the Structural-Thermal-Optical Program (STOP) (ref. 1), is the development of analytical methods and procedures which can yield reliable predictions of thermal deformation and optical degradation in an orbiting spacecraft (ref. 2), or in a simulated environment. This multi-disciplinary project is intended to render analytical services to projects such as LST (Large Space Telescope), SAS (Small Astronomy Satellite), EOS (Earth Observatory Satellite), etc. To predict alignment or optical performance of a large spacecraft-telescope system, NASTRAN is relied upon for structural analysis to compute thermally induced deformations and stresses. For a reliable structural solution, the thermoelastically uncoupled structural analysis requires accurate temperature data as an input to the NASTRAN structural model. Prior to the existence of the NASTRAN Thermal Analyzer, available general purpose thermal analysis computer programs were designed on the basis of the lumped-node thermal balance method (e.g. ref. 3). They were not only limited in capacity but seriously handicapped by incompatibilities arising from the model representations inherent in the two distinct approaches. The intermodel transfer of temperature data was found to necessitate extensive interpolation and extrapolation. This extra work proved not only a tedious and time-consuming process but also resulted in compromised solution accuracy. To minimize such an interface obstacle, the STOP project undertook the development of a general purpose finite-element heat transfer computer program.

Preliminary studies were then conducted at GSFC to investigate the feasibility of achieving such a computer program as an integrated part of the NASTRAN system. When this task began, the theoretical foundation of the finite-element approach had been established for both steady-state and transient thermal field problems (ref. 4-6). Efforts aimed at broadening its scope were found in literature such as an extension to axis-symmetric problems (refs. 7, 8), a consideration of inhomogeneous material using higher order elements (ref. 9), a demonstration of procedure enabling the achievement of an efficient solution by reducing the order of the set of equations (ref. 10), and many special applications (ref. 11-13). All of these studies, however, were limited to thermal conduction with linear boundary conditions. Since radiation is a dominant mode of the heat transfer process in space-oriented applications and introduces a fourth-power nonlinear temperature term in the boundary conditions, the in-house studies were directed principally to include these nonlinear radiation effects. Other investigations into solution feasibility, accuracy and efficiency, and element behaviors in combined modes of heat transfer analysis were also undertaken. The in-house studies consisting of two parallel efforts were:

- (1) the structural version of NASTRAN was employed directly to solve heat transfer problems by utilizing mathematical analogies together with manipulations of available elements and solution routines (refs. 14, 15). The concept of treating the radiative fluxes as nonlinear loads was demonstrated successfully for simple radiative problems. The solution scheme, however, was restricted in that all nonlinear radiation problems had to be solved using the direct transient integration algorithm available in the program.

- (2) the derivation of heat elements including radiative effects from the governing equation and boundary conditions approached via a variational principle, and studies centered on heat elements with associated different solution schemes (ref. 16). Two distinct approaches to nonlinear radiative problems were investigated and studies of radiative exchanges between element surfaces of known and unknown temperatures were included. A direct steady-state solution via the consistent linearization method and using an iterative process proved to be able to yield a solution more efficient than using a transient route. The other approach, the direct energy distribution method, which had been illustrated independently in a simple problem (ref. 17), in fact, shares the same theoretical basis as that employed by a direct use of the structural version of NASTRAN (ref. 14, 15). A prototype computer program based on the direct energy distribution method was coded (ref. 18), and studies of element behaviors and solution accuracy were also conducted.

While the NASTRAN System Management Office at Langley Research Center planned the extension of the NASTRAN system to include linear conductive heat transfer analysis capability only, GSFC-STOP was seeking the implementation of a full-fledged finite-element heat transfer computer program. The software capability was finally developed and implemented by the MacNeal-Schwandler Corporation under a subcontract from Bell Aerospace Company. It must be stressed, however, that a cooperative financial and technical effort between these two NASA centers made possible the emergence of this vital new capability.

#### SCOPE OF ANALYSIS CAPABILITY

The NASTRAN Thermal Analyzer is capable of solving both steady-state and transient heat transfer problems in large size systems of arbitrary configuration. The governing heat equation together with the boundary conditions may be expressed, following the finite-element technique, in matrix form as

$$[B] \{\dot{u}\} + [K] \{u\} = \{P\} + \{N\} \quad (1)$$

where

$\{u\}$  = vector of grid point temperatures

$\{\dot{u}\}$  = rate change of temperature vector

$[K]$  = thermal conductance matrix

$[B]$  = thermal capacitance matrix

$\{P\}$  = vector of grid point heat fluxes

$\{N\}$  = vector of temperature-dependent nonlinear heat fluxes

With appropriate interpretation of the matrices appearing in Eq. (1), three basic types of problem can be identified. They are distinguished by the numerical solution algorithms required for their solutions.

### (1) Linear Steady-State Problems

Letting  $\{\dot{u}\} = \{N\} = \{O\}$  and  $[K] = [K_1]$ , Eq. (1) is reduced to a linear steady-state equation of the form

$$[K_1] \{u\} = \{P\}$$

where  $[K_1]$  is a constant thermal conductance matrix. This equation is analogous to the basic linear static analysis of the structural version and is treated by the solution algorithm present in Rigid Format 1, (Ref. 19).

### (2) Nonlinear Steady-State Problems

Letting  $\{\dot{u}\} = \{O\}$  and  $[K] = [K_2]$ , Eq. (1) has the form

$$[K_2] \{u\} = \{P\} + \{N\}$$

where  $[K_2]$  may be temperature-dependent. The permitted nonlinearities may arise from temperature-dependent conduction and convection properties as well as diffuse radiation. A new iterative solution algorithm, which includes test for convergence, has been added to the program for this type of problem.

### (3) Linear and Nonlinear Transient Problems

Equation (1) directly represents the general transient heat transfer problem in which  $\{P\}$  is allowed to be a time-dependent heat flux vector. The permitted nonlinearities may arise from the effects of radiation or from user specified nonlinear elements. The new solution algorithm accommodated for this type of problem is implicit and is a combination of forward and backward differencing embracing a free parameter  $\beta$  that allows the user to select the amount of each. While a default value exists for the parameter which assures stability in linear problems, an override option is provided which allows the user to trade stability for efficiency. An option is also available which permits the user to linearize the effects of radiation.

## PROGRAM STRUCTURE

The NASTRAN Thermal Analyzer has been designed to perform thermal analysis utilizing input and output formats compatible with those of the structural version. This

capability has been achieved by making maximum use of existing elements and system capabilities needed to satisfy the unique requirements posed by thermal problems. All input quantities as well as output displays are physically meaningful to users in the thermal field.

Features such as nonlinear and scalar elements, multipoint constraints, transfer functions, DMAP, etc. are automatically inherited from NASTRAN. The user, therefore, is provided with a powerful tool to include effects not normally modeled by other elements as long as those effects can be described by zero or first order system of equations

The essential points which characterize this thermal analyzer are summarized as follows:

(1) Geometry Description

The body to be analyzed is idealized as an assemblage of appropriate finite elements. NASTRAN grid, scalar, and extra points remain valid for use in this description. However, only one degree-of-freedom is associated with a grid point because of the nature of the scalar temperature field problem.

(2) Types of Elements

The program contains elements in three general categories:

- (a) Heat conduction elements – The constant gradient line, triangle and tetrahedra are the basic elements and utilize linear temperature gradients in one, two and three dimensions, respectively. All elements share common descriptions with their structural counterparts and are summarized in Table 1. Quadrilateral elements are composed of overlapping triangles, and wedges and hexahedra from sub-tetrahedra. Solid-of-revolution elements of triangular and trapezoidal cross-section are available for analyzing axisymmetric problems. Lumped capacitance matrices are used with all conduction elements to account for the effect of heat storage.
- (b) Boundary elements – XHBDY elements are used to define surface heat flux input and to describe convective and radiative exchanges between boundary elements. More than one boundary element can be connected to any one heat conduction element to account for multiple boundary heat inputs, including convection and radiation. A special cylindrical element with an arbitrary user specified elliptic cross-section is included for convenience in treating vector heat inputs. With this one dimensional element the effects of directional radiant heat inputs are automatically included in that peripheral energy inputs over the lateral surfaces are integrated internally.
- (c) Special elements – Several element types are available for the indirect inclusion of effects which cannot be otherwise modeled if only heat conduction

elements together with boundary elements were used. These special elements may be employed to enhance the analysis capability of the program. Scalar elements, nonlinear elements, transfer functions, and direct matrix inputs are included in this category. In heat transfer problems, scalar spring elements are analogous to thermal conductors and scalar dampers to thermal capacitance.

### (3) Material Properties

Isotropic and anisotropic material behaviors are included. The treatment of nonlinearities arising from temperature-dependent thermal conductivity and convective film coefficient requires an iterative solution algorithm and this has been automated for steady-state problems only. The process involves the supply of temperature-dependent data in the form of tabulated functions which are interrogated at the beginning of each iterative step. In transient cases, however, the user must rely on the use of nonlinear elements to treat the nonlinear effects as additional thermal loads that are evaluated at the previous integration time step.

### (4) Constraints and Partitions

Constraint and partitioning features of the structural version remain valid. Single-point constraints are used for the specification of prescribed temperatures, and multipoint constraints are used to describe known temperature dependency between temperature degrees of freedom. The omitted degree-of-freedom capability employs the well-known Guyan reduction technique to reduce the problem size of the solution set.

### (5) Boundary Conditions, Initial Conditions, and Thermal Loading

Convective exchange along the boundary can be specified between a surface and an ambient zone of known temperature, or between two or more surfaces or zones of unknown temperatures. Constant temperatures are specified directly by using constraints while temperatures which are arbitrary functions of time are specified indirectly by using simple modeling procedures which avoid unnecessary retriangularization when solving transient problems. Arbitrary initial temperature distributions can be specified in transient analysis.

Several options are available to users for the specification of thermal flux input. Steady or time varying scalar heat flux can be described at the element and/or grid point level. Vector heat flux, such as that of radiant flux from a distant source, is described by specifying the flux intensity and vector direction. Both the flux intensity and vector direction may be time dependent and this allows, for example, the automated accommodation of rotating bodies in a vector heat flux field. Volumetric heat generation can be specified at the element level.

Required input data for diffuse-gray thermal radiation problems consists of the Stefan-Boltzmann's constant, reference absolute temperature, thermo-physical properties

and an array of exchange coefficients together with a list which identifies the elements that are radiatively interacting. The array of radiative exchange coefficients  $AF$  is a symmetric matrix according to the reciprocity rule. It is the product of the emitting surface area  $A$  and the geometric view factor  $F$  between the emitting and receiving surfaces. The Thermal Analyzer accepts radiation data via card or tape.

#### (6) Graphics Capability

The structural plotting feature for data checkout is available. Included options are orthotropic, perspective or stereoscopic projection capabilities. Time-history data of element heat flux, thermal loads, and temperatures at grid points can all be graphically shown in x-y plots.

#### (7) Integrated Thermo-Structural Analysis

The thermo-elastically uncoupled thermal and structural analyses are performed in two passes through the NASTRAN System, but may be made to appear as a single continuous run by the use of computer system control language. In the case of transient analysis, temperature distributions computed by the NASTRAN Thermal Analyzer are recorded on magnetic tape or punched cards at predetermined time intervals and, subsequently, employed for static structural analysis. Back-to-back thermal and structural analyses require that the grid point locations must be identical in both models on a point-to-point basis.

### A VIEW FACTOR GENERATION COMPUTER PROGRAM

In computing temperatures involving radiative interchanges between surfaces, the geometric view factors between any two radiatively active element surfaces are necessary to form the exchange coefficients as input to the Thermal Analyzer. In an in-house STOP project effort, GSFC has developed an IBM-360 program named "VIEW" which computes the view factors and the required exchange coefficients between radiating boundary elements. VIEW has compatible input-output formats with the Thermal Analyzer and possesses other programming features similar to those of NASTRAN. A detailed description of this program is presented in an associated paper titled "VIEW - A Modification of the RAVFAC View Factor Program for Use with NASTRAN Level 15."

### FURTHER STUDY IN EFFECT OF VIEW FACTOR COMPUTATIONS

In studying accuracy, one of the factors that might influence the result of solution involving radiative exchanges between elements is the method that computes the amount of net radiant energy on the element level which is then evenly distributed to its vertices. This approximation involves the computation of view factors which are computed on the element surface to element surface basis associated with the element temperature which is an average of those temperatures at the vertices. An alternate approach is to form an isothermal area of the temperature at the grid point by dividing the origin elements into subelements and assembling the subelements from the adjoining elements to that grid

point while subelements are formed by connecting the centroid to each midpoint on the side of an element. The difference of the view factor results from these two approaches is evident in view of a demonstration of the view factor  $F_{A-B}$  between two shaded areas as shown in Figure 1.

A direct computation of  $F_{A-B}$  gives 0.23344, the result obtained from a summation of one-third of the view factors computed on the basis of element surface to element surface is 0.12471, and the result obtained from summing up the view factors on the basis of subelement to subelement following the rule of the view factor algebra is 0.233989. It is to be noted, however, that these computations took into consideration the view factor alone. A study combining the effects of temperatures and view factors which involves a modification of a prototype computer program to assess the quantitative influence to the solution accuracy is in progress and will be reported separately.

### ILLUSTRATIVE PROBLEM

Since the delivery of the IBM-360 NASTRAN Thermal Analyzer to GSFC in June of 1972, the system check-out phase has proceeded. A problem was designed to demonstrate program capabilities and features including: inter-element and inter-program (with regard to VIEW program) compatibilities, coordinate transformations, combined thermal modes of operation, vector heat flux input description, and the application of the different solution algorithms. The problem is that of a fin-like bent plate, whose dimensions, thermophysical properties and finite-element model are shown in Figure 2 where the input parameters with the subscript t refer to the tube and those without any refer to the plate. The underside of the plate is insulated thermally, and the upper face is exposed to a directional heat flux of S. The flowing fluid has a temperature  $T_{in} = 1200$  K at the entrance and a linear temperature drop of 60 K across the tube which has a wall thickness  $\tau = 1$  cm and an outer radius  $r_0 = 20$  cm. Determine temperature distributions in the plate for the following cases:

- (1) The upper face dissipates heat to the surroundings of  $T_{air} = 300$  K with a convective film coefficient  $h_{air} = 1.135$  W/cm<sup>2</sup> -°K.
- (2) A radiative enclosure of a temperature  $T_{\infty}$  replaces the convective environment in the preceding case, and radiative interchanges between all surface elements are taken into consideration. The solution is approached by the direct nonlinear steady-state solution algorithm.
- (3) The plate has a uniform temperature at  $T_0 = 300$  K initially. The temperature response of the plate is determined by the nonlinear transient solution algorithm. The process starts with an activation of the flow into the tube which has identical tube-fluid conditions as previously described.

In view of the length that would be required to embed the complete meaningful computer print out of this problem, which consists of detailed card descriptions of the control and input data decks and the output results, solutions are not included in this report

but have been prepared in a separately bound copy (ref. 20) which will be made available to the audience of this colloquium as well as to any interested reader who will make a request to the authors.

#### REFERENCES

1. Lee, H. P.: Structural-Thermal-Optical-Program (STOP), Paper presented at NASA-GSFC 1970 Science and Technology Review, NASA-Goddard Space Flight Center, Jan. 13-14, 1971; also appears in: Significant Accomplishments in Technology: Goddard Space Flight Center, 1970, NASA SP-295, Washington, D.C., pp. 36-40.
2. Mason, J. B.: Thermal Deformation Prediction in Orbiting Observatory Structures, NASA SP-233, 1970, Washington, D.C., pp. 401-415.
3. Thermophysics Branch: Nodal Network Thermal Balance Program, NASA Goddard Space Flight Center, February 1968.
4. Zienkiewica, O. C., and Cheung, Y. K.: Finite Elements in the Solution of Field Problems, The Engineer, Vol. 220, Sept. 1965, pp. 507-510.
5. Visser, W.: A Finite Element Method for the Determination of Non-Stationary Temperature Distribution and Thermal Deformations, Proceedings of Conference on Matrix Methods in Structural Mechanics, AFFDL-TR-66-80, Air Force Flight Dynamics Lab., Wright-Patterson Air Force Base, Ohio, December 1965, pp. 925-943.
6. Wilson, E. L., and Nickell, R. E., Application of the Finite Element Method of Heat Conduction Analysis, Nuclear Engineering and Design, Vol. 4, 1966, pp. 276-284.
7. Brocci, R. A.: Analysis of Axis-symmetric Linear Heat Conduction Problems by Finite Element Method, ASME Paper 69-WA/HT-37, Winter Annual Meeting, Los Angeles, Calif., 1969.
8. Adelman, H. M. and Catherines, D. S.: Calculation of Temperature Distributions in Thin Shells of Revolution by the Finite-Element Method, NASA TN D-6100, Langley Research Center, Hampton, Va., February 1971.
9. Rybicki, E. F., and Hopper, A. T.: Higher Order Element Method for Transient Temperature Analysis of Inhomogeneous Materials, ASME Paper 69-WA/HT-33, Winter Annual Meeting, Los Angeles, Calif., 1969.
10. Gallagher, R. H., and Mallett, R.: Efficient Solution Processes for Finite Element Analysis of Transient Heat Conduction, ASME-Journal of Heat Transfer, Vol. 93, No. 3, August 1971, pp. 257-263.

11. Becker, E. B., and Parr, C. H.: Application of the Finite Element Method to Heat Conduction in Solids, T.R. S-117, Rohm and Haas Co., Philadelphia, Pa., 1967.
12. Chaloupka, A. B.: A Computer Program for the Analysis of Two-Dimensional Heat Conduction using the Finite Element Technique, AD-690450, M. S. thesis, Naval Postgraduate School, Monterey, Calif., June 6, 1969.
13. Mote, C. D., Jr., Unsymmetrical, Transient Heat Conduction: Rotating Disk Applications, ASME-Journal of Engineering for Industry, Vol. 92, No. 1, February 1970, pp. 181-190.
14. Mason, J. B., The Solution of Heat Transfer Problems by the Finite Element Method Using NASTRAN, NASA-GSFC, Test and Evaluation Div. Rept. X-321-70-97, Greenbelt, Md., 1970.
15. Mason, J. B.: Heat Transfer Analysis Using NASTRAN, Paper presented at NASTRAN Colloquium, NASA-Langley Research Center, September 13-15, 1971.
16. Lee, H. P.: Application of Finite-Element Method in the Computation of Temperature with Emphasis on Radiative Exchanges, Paper presented at AIAA 7th Thermophysics Conference, San Antonio, Texas, April 10-12, 1972; also to appear in: Thermal Control and Radiation, Thermophysics Progress Volume, AIAA Progress Series Vol. 31, 1972.
17. Richardson, P. D., and Shum, Y. M.: Use of Finite Element Methods in Solution of Transient Heat Transfer Conduction Problems, ASME Paper 69-WA/HT-36, Winter Annual Meeting, Los Angeles, Calif., 1969.
18. Heuser, J. S.: Finite Element Method for Thermal Analysis, NASA-GSFC Test and Evaluation Div. Program STOP-Documents, Greenbelt, Md., 1971.
19. McCormick, C. W.: The NASTRAN User's Manual, NASA SP-222, September 1970, Washington, D.C.
20. Lee, H. P. and Mason J. B.: NASTRAN Thermal Analyzer Solutions of a Bent Fin-Tube Configuration, NASA-GSFC Test and Evaluation Div., Program STOP-Documents, Greenbelt, Md., 1972.

**TABLE-1**  
**HEAT CONDUCTION ELEMENTS**

DIMENSION	TYPE	ELEMENTS
1-D	Linear	BAR, R $\phi$ D, C $\phi$ NR $\phi$ D, TUBE
2-D	Membrane	TRMEM, TRIA1, TRIA2, QDMEM, QUAD1, QUAD2
	Solid of Revolution	TRIARG, TRAPRG
3-D	Solid	TETRA, WEDGE, HEXA1, HEXA2

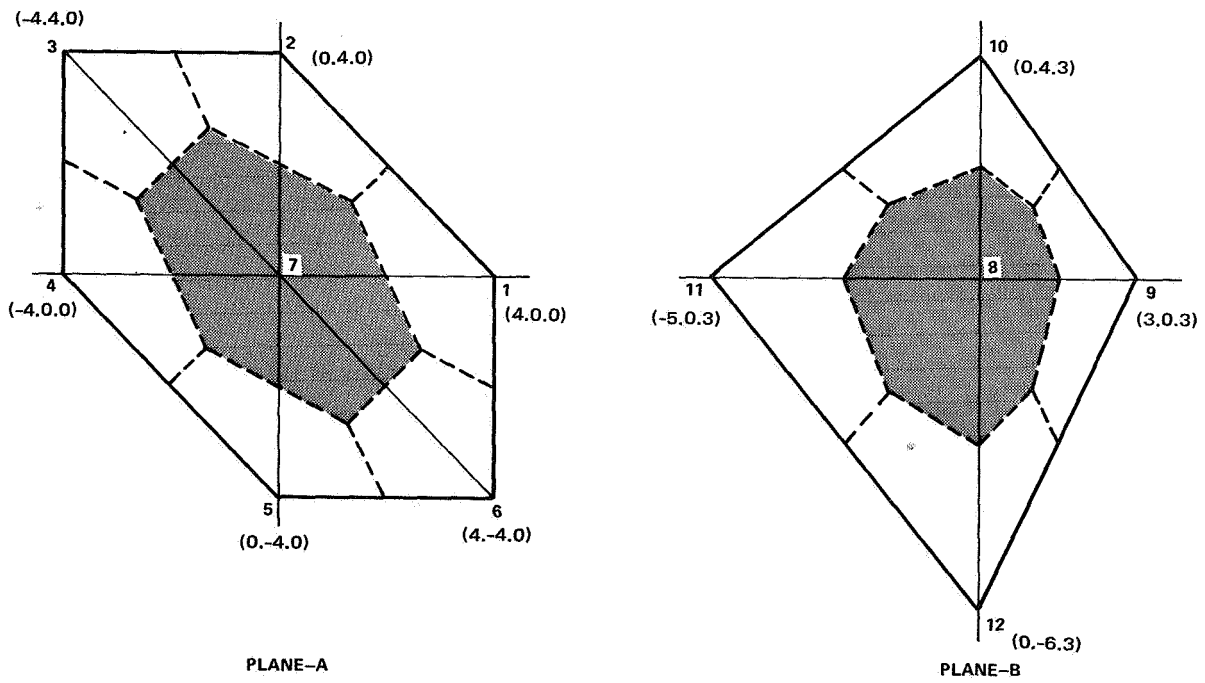


Figure 1. Sub-elements joined at two common vertices to form two isothermal radiative surfaces.



VIEW - A MODIFICATION OF THE RAVFAC VIEW FACTOR PROGRAM  
FOR USE WITH THE NASTRAN THERMAL ANALYZER

By Edward F. Puccinelli and Clifton E. Jackson, Jr.

NASA Goddard Space Flight Center

INTRODUCTION

The NASTRAN Thermal Analyzer will include the capability to perform complete thermal analyses on structures. One of the inputs to NASTRAN required to simulate radiative heat transfer between surfaces will be the view factors (also called shape factors, form factors, configuration factors) between those surfaces. The purpose of the VIEW program is to compute these view factors and produce appropriate RADMTX and RADLST output to be used as NASTRAN Bulk Data.

VIEW assumes that the view factors between surfaces is a function only of their geometries and relative locations in space. The effects of emissivity, absorptivity, transmissivity, and multiple reflections are not taken into account, though provision has been made in the program design for their incorporation in a future version.

The view factor from surface S1 to S2 (these surfaces of area S1 and S2, respectively) may be found by considering the orientation of two infinitesimal surfaces  $dS_1$  and  $dS_2$ , located respectively on S1 and S2 (see figure 1).

The derivation of the view factor formula for computing  $dF_{dS_1 \rightarrow dS_2}$  (the view factor between  $dS_1$  and  $dS_2$ ) can be found in reference 1 as:

$$dF_{dS_1 \rightarrow dS_2} = \frac{\cos(\theta_1) \cos(\theta_2)}{\pi r_{12}^2} dS_2 \quad .$$

Integrating over both surfaces the view factor from  $S_1$  to  $S_2$  becomes

$$F_{S_1 \rightarrow S_2} = \frac{1}{S_1} \int_{S_1} \int_{S_2} \frac{\cos(\theta_1) \cos(\theta_2)}{\pi r_{12}^2} dS_1 dS_2$$

Program VIEW can compute view factors by integrating this equation using either finite difference or contour integration (reference 1). The former method requires less computer time, while the latter gives more accurate solutions in certain cases. The user is allowed three options in selecting the method to be used:

1. He may request finite difference integration only,
2. He may request contour integration only,
3. He may allow the program to make its own selection on the basis of a user specified area-to-distance ratio.

The third option is the most common user selection.

#### INPUT DESCRIPTION

The majority of the input to the program consists of a description of the surface shapes and their locations in space. The VIEW program allows the user a choice of two distinct input formats. First, one may describe the surface shape and locations using NASTRAN formatted input (that is, using GRID cards, CORD cards, CHBDY cards, etc., see figures 2 and 4). Second, he may describe the problem using the same input format required by the RAVFAC program (see figure 3). Third, he may elect to combine the two types of input data. In addition, several cases may be run at once, as shown in figure 4.

The control cards required are very simple. The first control card of every case is a title card. This consists of any eighty characters and is printed out as the output heading.

The second control card is the VIEW case control card, which is not to be confused with NASTRAN case control cards. On this card the user specifies such items as the method of integration

to be used, the input data device to be used (cards or tape), the output data device(s), and other program variables. These are all described in greater detail in the program documentation.

The third control card identifies the type of data which is to follow. If NASTRAN data is being used as input, the user punches "NASTRAN DATA" in columns one through twelve. If it is RAVFAC data, he punches "RAVFAC DATA" in columns one through eleven.

This card is followed by either the NASTRAN or RAVFAC bulk data deck, which in turn is followed by a control card specifying the end of the case (the user punches "ENDCASE" in columns one through seven). If no other cases are to follow, the next control card signals the end of the run and has "ENDRUN" punched in columns one through six.

If another case is to follow, the control card following "ENDCASE" would be a new title card. The input format would then repeat itself as described. See figures 2, 3 and 4.

We now come to the heart of the input: those cards which describe the surfaces and their positions in space. The RAVFAC input format will be ignored in this paper but can be found in reference 1. However, it is worth noting that the surface shapes which may be described by RAVFAC input are:

- a. rectangular
- b. disk (ring and/or section)
- c. trapezoidal
- d. cylindrical (ring and/or section)
- e. conical (ring and/or section)
- f. spherical (ring and/or section)
- g. circular parabolic (ring and/or section)

NASTRAN input allows for the description of the following surface shapes:

- a. solid disk (POINT element)
- b. rectangle (LINE element)
- c. cone or cylinder (REV element)

- d. triangle (AREA3 element)
- e. quadrilateral (AREA4 element)

At this point it is necessary to define the following terminology:

"elements" - The units in which a structure is modeled (called finite elements in NASTRAN)

"sub-elements" - The units into which an element may be divided (used only in VIEW).

Therefore, the surface shapes previously defined will henceforth be referred to as element shapes, or just elements.

Basically, the NASTRAN user models (approximates) his structure by reconstructing it in space using NASTRAN elements. For an analysis involving radiation the user is allowed the use of the elements described previously.

The NASTRAN input acceptable to the VIEW program is therefore: \*

- a. CHBDY cards - which describe the element shape
- b. PHBDY cards - which describe properties of the elements
- c. GRID, CORD, and GRDSET cards - which describe the location in space of the elements
- d. ENDDATA card - defines the end of the surface description cards. Any other type of card (with one exception to be explained later) is ignored by the program, and a message is printed stating how many cards were ignored.

The exception just mentioned is a card designed specifically for the VIEW program called, appropriately, a VIEW card. On this card the user specifies whether an element can be shaded by another element and whether it can shade some other element. This is not required input (as the program can determine such relationships automatically), but its use can save computer time. Also on the VIEW card the user may specify that an element is to be divided into nxn sub-elements. The default is 1x1, meaning

\*No double field input allowed.

that each element is to be considered as a sub-element. View factors are computed between sub-elements and recombined to yield view factors between elements. The division of an element into sub-elements is used to increase the accuracy of the answers. It should be used whenever two elements share a common boundary and are known to have a non-zero view factor between them.

Once a run has been made all the NASTRAN Bulk Data cards may be recovered from the VIEW input deck. These cards, along with the RADLST and RADMTX cards just produced, may then be used as input to NASTRAN to provide radiative coupling information for a heat transfer analysis.

#### COMPARISON OF VIEW TO CONFAC II

Several of the sample problems presented in the Confac II manual (reference 2) were modeled with NASTRAN elements and run using the VIEW program. Excellent agreement was obtained in all cases, and the results for one of the most complex cases (involving shading) is shown below (see figure 5 on the following page).

CASE F1	CONFAC (7x7)	VIEW (10x10) (588 SUB-ELEMENTS)
1PLA10 → 8COPLA	.27337	.27556
1PLA10 → 1PLA11	.21136	.21339
1PLA10 → 1PLA9	.06201	.06157
1PLA12 → 8COPLA	.11370	.11278
1PLA12 → 1PLA9-9R	.07183	.07227
1PLA12 → 1PLA11	.04187	.04051
1PLA11 → 1PLA10	.30435	.30815
1PLA9-9R → 1PLA12	.06733	.06773

These results satisfactorily demonstrate the ability of the VIEW program to account for shading relationships in view factor calculation.

#### PROGRAMMING REMARKS

As a final note, it should be mentioned that the VIEW program has been designed to be as much like NASTRAN as possible, in that it (1) has a restart capability, (2) is organized in overlays to minimize the core required to load the program, and (3) dynamically allocates core space so that the user may run any

size problem he desires, if he requests a sufficient amount of core space. A major difference which remains is that the VIEW program is written in Fortran IV and assembly language for IBM 360 computers, and conversion would be necessary for its use on CDC or Univac machines.

#### REFERENCES

1. Lovin, J. K., and Lubkowitz, A. W.: User's Manual for 'RAVFAC,' A Radiation View Factor Digital Computer Program. Contract #NAS 8-30154, Huntsville Research and Engineering Center, Huntsville, Ala., 1969.
2. Toups, K. A.: A General Computer Program for the Determination of Radiant Interchange Configuration and Form Factors. SID 65-1043-2, North American Aviation, Inc., October, 1965.

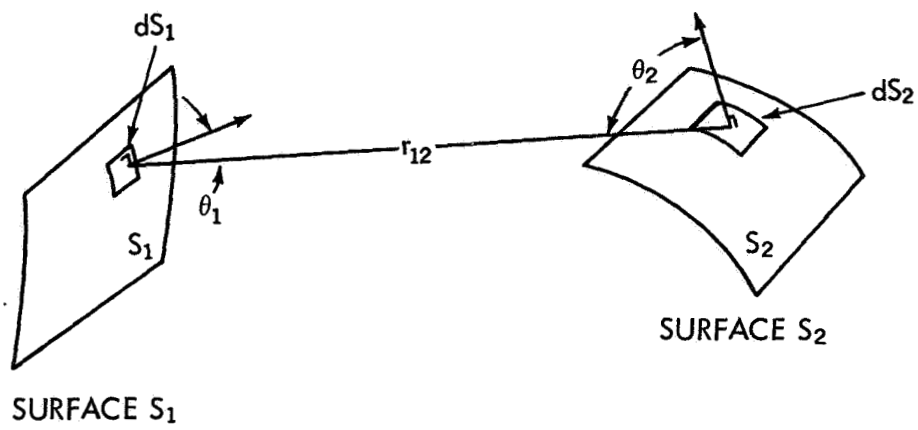


Figure 1. Orientation of Two Arbitrary Surfaces  $S_1$  and  $S_2$

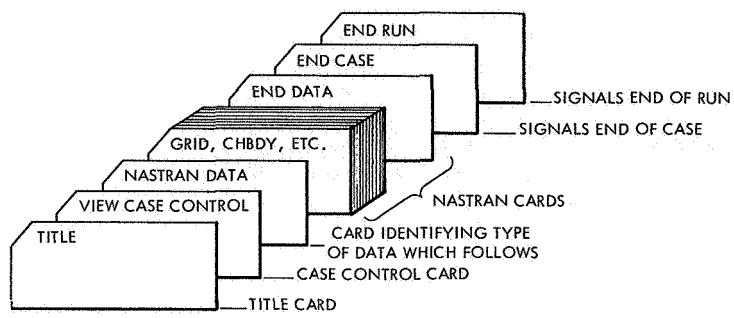


Figure 2. Typical Run, 1 Case, NASTRAN Input Only.

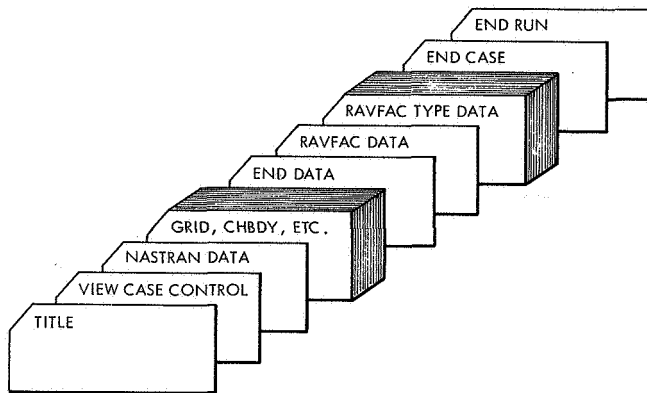


Figure 3. Run One Case Using NASTRAN and RAVFAC Input Combined.

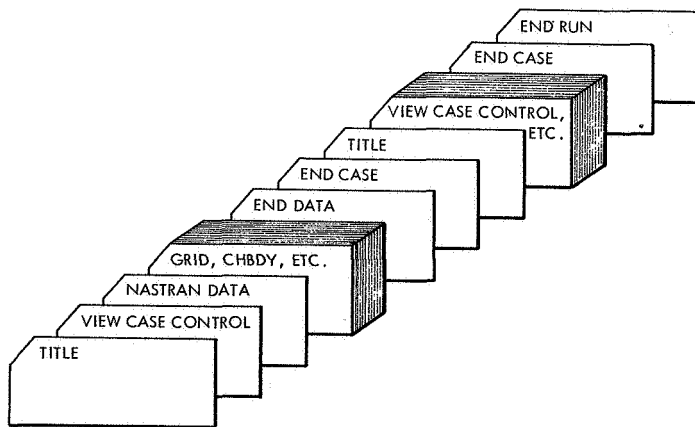


Figure 4. Run 2 Cases, both NASTRAN Input.

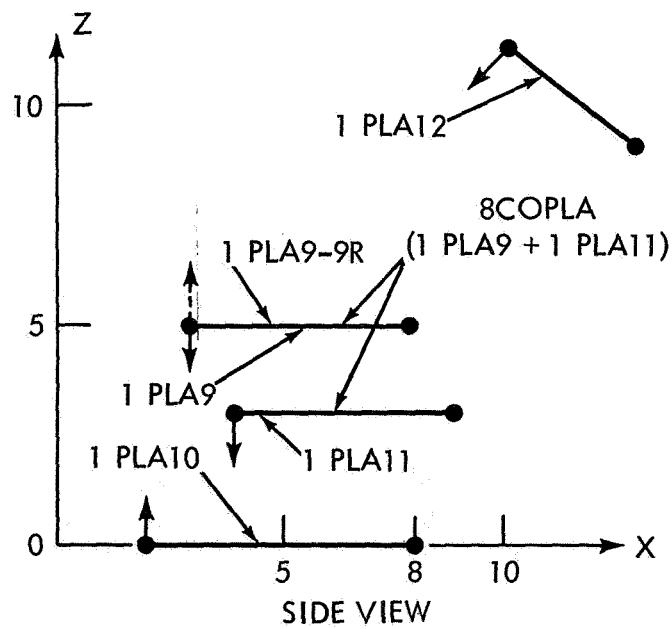
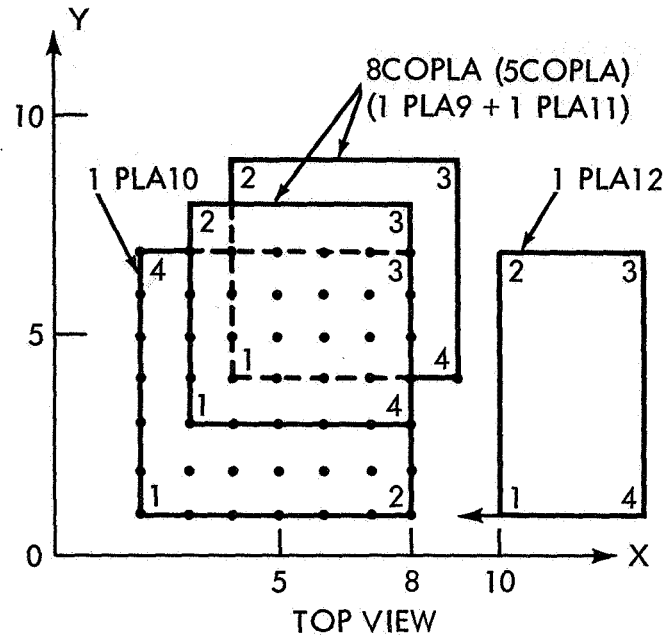


Figure 5. Case F1



# Structural Dynamic and Thermal Stress Analysis of Nuclear Reactor Vessel Support System

By

Dr. James Chi-Dian Go  
Computer Sciences Corp.

32

## ABSTRACT

A nuclear reactor vessel is supported by a Z-ring and a box ring girder as indicated in Figures 1 and 2.

The two proposed structural configurations to transmit the loads from the Z-ring and the box ring girder to the foundation are shown in Figures 3 and 4. Figure 3 illustrates the cantilever concrete ledge transmitting the load from the Z-ring and the box girder via the cavity wall to the foundation while Figure 4 depicts the loads being transmitted through one of the six steel columns. Both of these two supporting systems were analyzed by using rigid format 9 of NASTRAN for dynamic loads and the thermal stresses were analyzed by AXISOL Ref. 1. The six column configuration was modeled by a combination of plate and bar elements and the concrete cantilever ledge configuration was modeled by plate elements. Both configurations were found structurally satisfactory; however, nonstructural considerations favored the concrete cantilever ledge.

Each of the NASTRAN models has about 600 dynamic degrees of freedom. Because of structural and loading symmetry, only 30 and 15 degree, circumferentially, models as shown in Figures 3 and 4 were required. The bulk data was re-sequenced by BANDIT to minimize the run time. Time steps in the range of 2 to 10 MS were used for different runs and the total response times were kept at about 130 MS. Various structural damping coefficients were applied in this analysis. Many structural and X-Y plots were produced. Average run time was about 20 minutes CPU and 40 minutes wall clock.

The basic computer hardware consists of a UNIVAC 1108 central processor with 131K core memory, 2-22, 020, 096 words FASTRAND, 5-FH432 drums, 8-UNISERVO VIII magnetic tapes and two 30-inch CALCOMP drum plotters.

## STRUCTURAL CONFIGURATIONS

The 6-column configuration is shown in Figures 1, 2 and 4. These steel columns are built up sections with two horizontal supports at the third points. Each column is bolted to the Z-ring. The concrete cantilever ledge configu-

ration is shown in Figure 3. The box ring girder shown in Figure 2 is supported by the concrete ledge.

### STRUCTURAL MODELING

In a 30 degree column configuration model, the Z-ring is modeled by 7 plate elements per 2 degrees of azimuth for a total of 150 plate elements while the box ring girder and column are modeled by 15 and 18 bar elements respectively. The concrete cantilever configuration was modeled by 18 plate elements per 3.75 degrees of azimuth or total of 72 plate elements. All the connecting bolts are assumed rigid.

### DYNAMIC LOADING

The dynamic loads consist of an up load and a down load as shown in Figure 5. The load paths for the two proposed structural concepts are shown in Figures 2 and 3. These dynamic loads are specified on TLOAD1 cards and combined on DLOAD cards.

### DYNAMIC RESPONSE

The transient dynamic stresses, element forces, deflections, velocities and accelerations were printed and plotted for selected critical elements and grid points.

The dynamic load factor, DLF, is the ratio of the peak dynamic displacement to the static displacement produced by a static load with magnitude equal to the peak dynamic load. The DLF for the 6-steel columns and the concrete cantilever ledge are calculated to be about 1.6 and 1.2 respectively. The results are summarized in Tables 1 and 2.

### THERMAL STRESSES ANALYSIS

AXISOL, which is a finite element computer program for stress or strain structural problems, was used for the thermal analysis. The structural model and resulting thermal stresses are shown in Figure 6. The thermal stresses in the concrete ledge are significant. These stresses were combined with the dynamic stresses and shown in Table 1.

## SUMMARY

The analyses reported in this paper pertain to the preliminary structural design phase. The results obtained from NASTRAN and AXISOL are satisfactory for this purpose. Due to the versatility of the NASTRAN input format, design changes, additional analyses or modeling refinement can easily be effected. Some simple lumped mass models with one to five degrees of freedom with nonlinear material properties were analyzed independent of NASTRAN. The basic structural dynamic responses were within 10 - 20% of NASTRAN results. The satisfactory results of this analysis clearly indicate the applicability and usefulness of NASTRAN to heavy civil engineering type of structural design and analysis.

### Reference

1. Prof. E. Wilson, University of Calif. AXISOL Axisymmetric Solid Finite Element Structural Analysis Program.

Summary of Maximum Deflections, Stresses and Dynamic Load Factors

1% and 2% uniform structural damping

$E = 23.0 \times 10^6$

Poisson's ratio = .3

Mass density =  $.000733 \frac{\#-Sec^2}{In^4}$

Box girder filled with concrete

\* Static load set equal to peak dynamic down load

\*\* - Compression, + Tension

Location	Max Stress (ksi)		MAX Deflection (in)			Power, megawatt-sec	DLF, Ratio of Dynamic and Static Deflections
	Max Force (10 <sup>6</sup> #)		Beam (ksi)	Column (in)	Beam (in)		
	Column Forces	Stress					
Support	-49.1	-43.0**	14.8	.93	.93	350	1.2
Quarter Span	+34.7	+30.5**					
	Base	Base					
Mid Span	-45.5	-40.0	6.7	.97	.97	2% Damping	
	+38.8	+28.8					
	TOP	TOP			(.81)		
Support	-46.1	-40.5	14.3	.88	.88	150	1.5
Quarter Span	+41.5	+36.4	2.8	.91	(.58)	2% Damping	
	Base	Base					
Mid Span	-43.6	-38.3	6.3	.92	.92	.92	
	+39.0	+34.1					
	TOP	TOP			(.61)		
Support	-53.0	-46.7	15.9	1.00	1.00	350	1.3
Quarter Span	+35.0	+31.1	3.1	1.03	(.77)*	1% Damping	
	Base	Base					
Mid Span	-48.9	-42.8	7.0	1.05	(.80)	.80	
	+33.1	+29.1					
	TOP	TOP			(.81)		
Support	-51.0	-43.8	15.7	.95	.95	150	1.66
Quarter Span	+51.7	+45.3	2.9	1.00	(.58)	1% Damping	
	Base	Base					
Mid Span	-46.7	-41.0	6.6	1.01	(.60)	.60	
	+47.4	+41.0					
	TOP	TOP			(.61)		

Table 1

MAXIMUM PRINCIPAL STRESSES

<u>Case Number &amp; Description</u>	<u>KIPS/Sq. In.</u>				<u>Remarks</u>
	$\sigma_r$	$\sigma_\theta$	$\sigma_z$	$\tau$	
A. 150 megawatt-sec	-3.2 +2.3	-1.0 + .9	-.4	1.65	Maximum Shear at 40" Ledge & Max. Bending Stress, $\sigma_r$ , in Cavity Wall.
B. 350 megawatt-sec	-3.3 +2.55	-1.0 + .9	-.4	1.70	
C. 20 x 10 <sup>6</sup> # Static Load at the Cantilever Ledge Tip	-2.21 +1.60	-.72 + .56	-.25	1.16	
D. Thermal with Heating	-.19 +.19	-2.1 +1.0	-.04	.05	At Upper Cantilever Tip.
E. Thermal without Heating	-.08 +.08	-.9 +.4	-.04	.01	
F. Combination of A&D	-3.39 +2.49	-3.1 +1.9	-.44	1.70	
G. Combination of A&E	-3.28 +2.38	-1.9 +1.3	-.44	1.66	
H. Combination of B&D	-3.49 +2.64	-3.1 +1.9	-.44	1.75	
I. Combination of B&E	-3.38 +2.63	-1.9 +1.3	-.44	1.71	
J. Combination of C&D	-2.40 +1.79	-2.82 +1.56	-.29	1.21	
K. Combination of C&E	-2.29 +1.68	-1.62 + .96	-.29	1.17	

$\sigma_r$  is the radial bending stress.  
 $\sigma_z$  is the vertical bending stress.  
 $\sigma_\theta$  is the hoop stress.  
 $\tau$  is the shear stress.  
 -compression.  
 +tension

Table 2

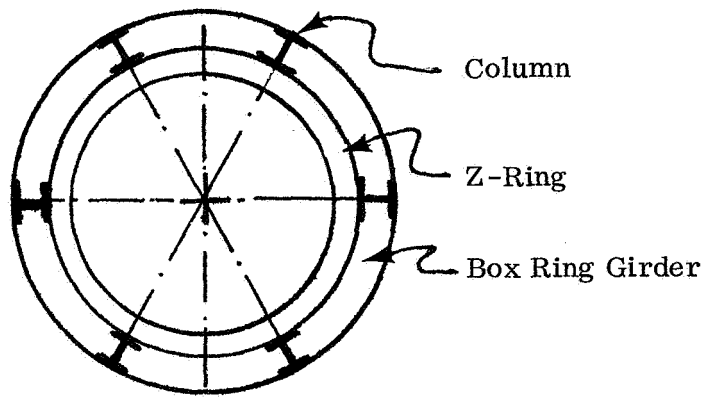


Figure 1  
Key Plan

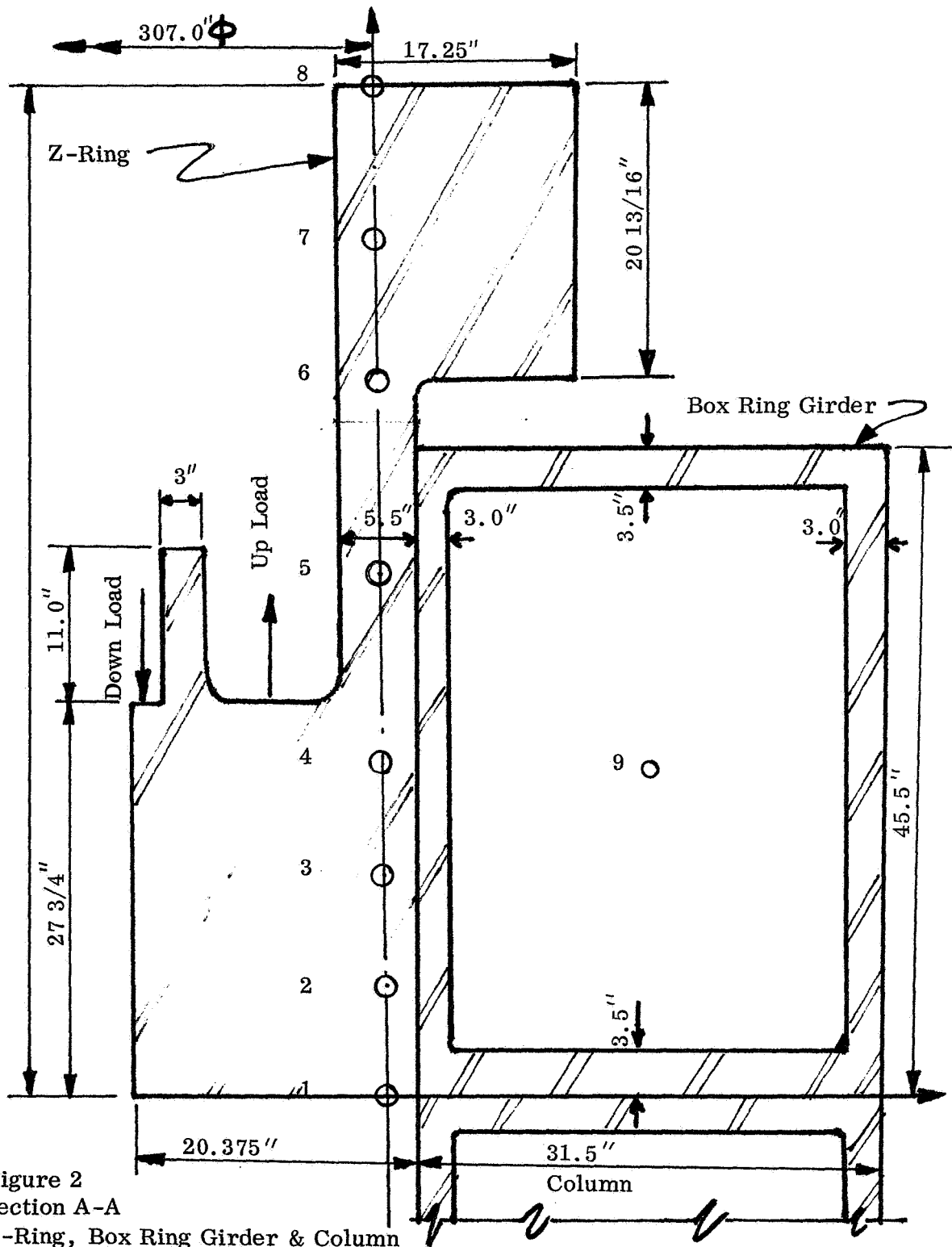


Figure 2  
 Section A-A  
 Z-Ring, Box Ring Girder & Column

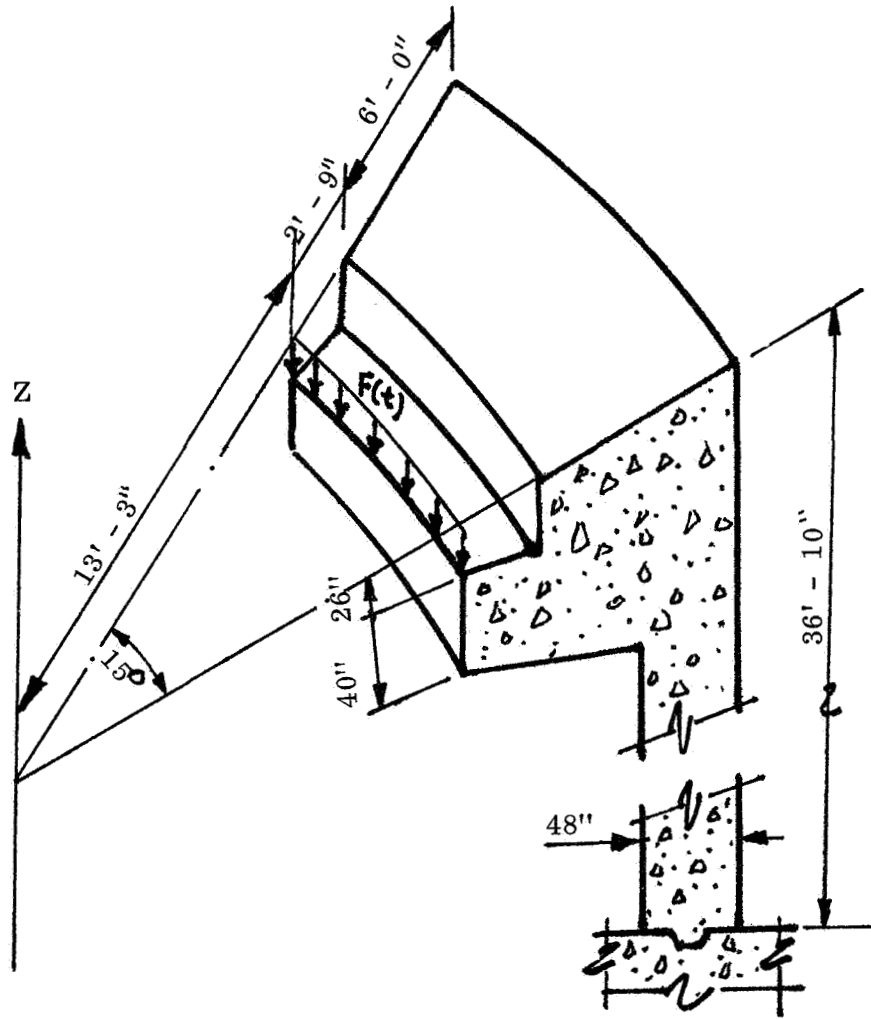
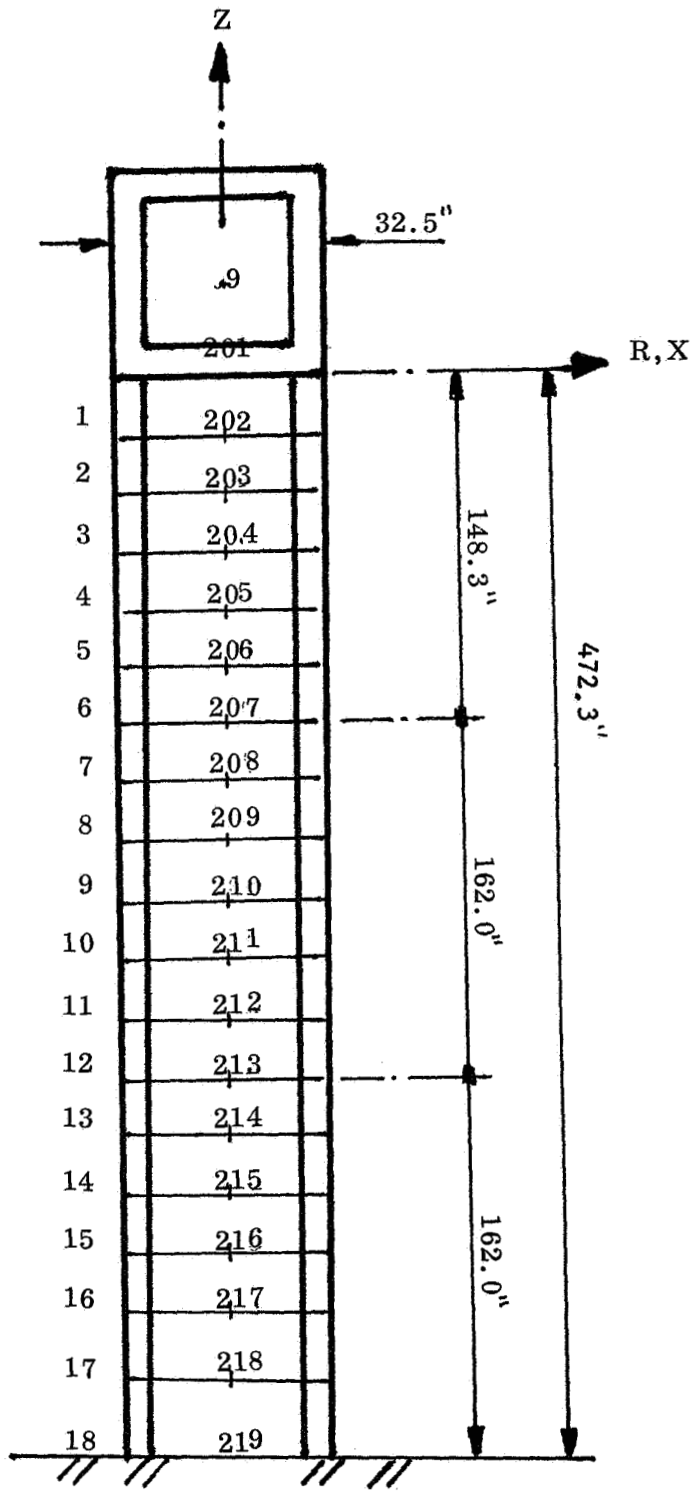


Figure 3  
Concrete Cantilever Ledge



COLUMN ELEVATION

Figure 4  
 Fixed at 219 pinned at 207 & 213 MPC at 9 & 201

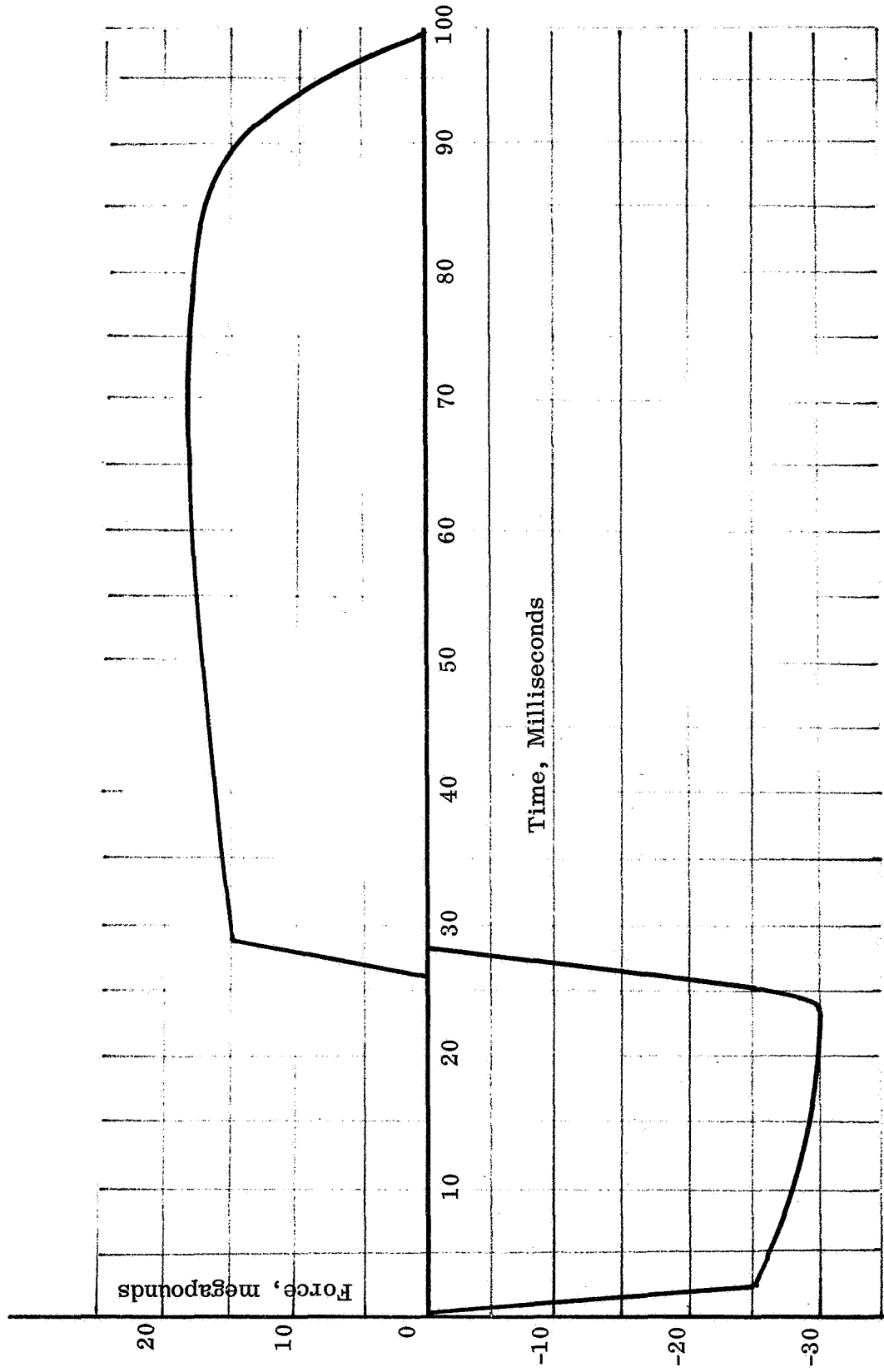


Figure 5  
Dynamic Load

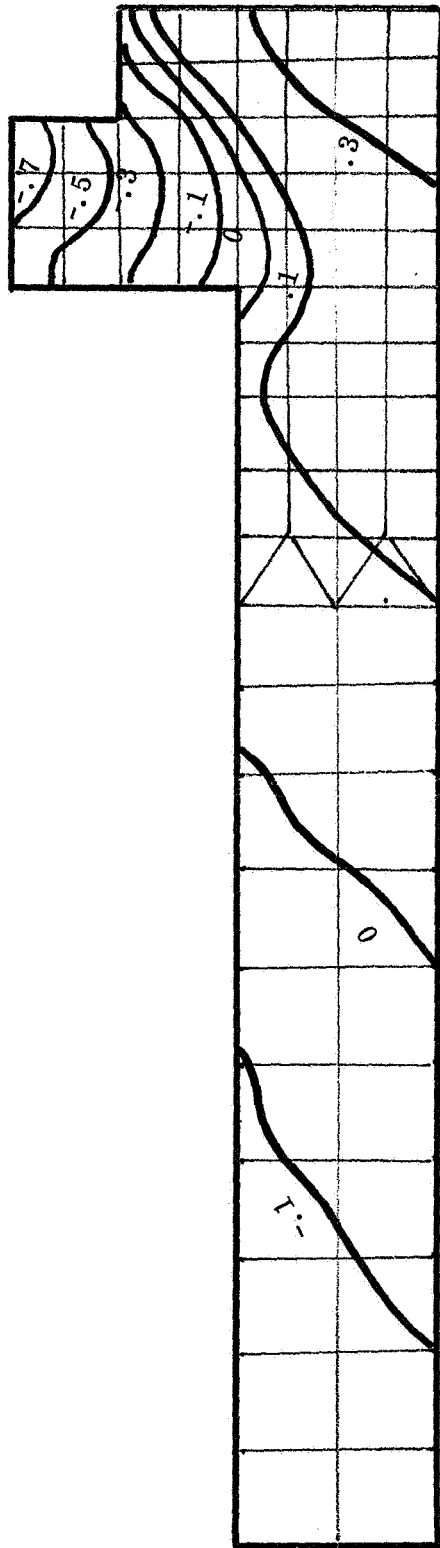


Figure 6  
 Concrete Ledge Thermal Stress  
 Hoop Stress Contour  
 KIPS/Sq. In.



# HIGH PRESSURE TURBINE BLADE STRESS ANALYSIS

Robert R. Van Nimwegen and Samuel Tepper  
AiResearch Manufacturing Company  
Torrance, California

## Summary

One of the critical areas in jet engine design is the high pressure turbine (fig. 1). Combinations of high temperature gradients associated with strong transients in both temperature and rotational speed fields, make the stress analyst conscientious about constructing a reasonably good model to study this particular area. The present report pertains to the blade definition and results of the analysis.

Since the same model should later be used to define some dynamic characteristics and certain areas would require a non-linear analysis, NASTRAN was chosen as a convenient program to manage the several alternatives. Previous experiences with the program were highly satisfactory in other areas of jet engine design.

## Introduction

The Garrett ATF3 fan jet engine has a high pressure turbine with rotor blade cooling configuration basically a three-cavity, convection-cooled design. The cooling air is distributed to each blade by inserted tubes which also serve the purpose of locking the blades in the disk. The cavities must be designed in such way that the cooling path is optimum for the overall performance of the blade, under centrifugal loads and temperature field, especially considering the transients in both fields.

At design turbine inlet temperature the metal temperature map at 3 sec transient, for a 5-second acceleration in a standard day at sea level condition, is indicated in Figure 2.

The blade has a large amount of twist with a low hub-tip ratio. The object of the present study is to obtain the best mechanical design compatible with the several conditions abovementioned.

## Mechanical Design and Model

Due to the strong twist and the centrifugal load a significant torque is developed. Shear stresses resulting from this torque are reduced by the addition of two shear webs in the blade.

A previous stress analysis of the disk fir-tree area defined the blade root stress characteristics (Figure 3). Considering the particular

blade configuration it was decided to analyze the part by using the NASTRAN program selecting the PTRIA2 plate element to constitute the shell-like structure.

The blade was divided into 915 triangular plate elements shown in Figure 4.

### NASTRAN Analysis

The analysis consisted of the following three parts:

- a) Stress distribution due to centrifugal forces only, to obtain the rotational speed participation in the overall analysis.
- b) Stress distribution due to combined steady-state thermal and centrifugal loads. This case corresponds to the normal operating conditions.
- c) Stress distribution due to combined transient thermal and centrifugal loads. This case was the particular interest considering both creep and low cycle fatigue analysis and the possibility of defining non-linear material characteristics at local points to establish blade life characteristics.

In Figures 5 and 6 several of the stress maps obtained from the computer runs are depicted.

### Conclusions

As a result of the analysis, minor modifications have been made to reduce the stresses in two critical areas. The forward shear web has been scalloped at the root section to reduce the high shear stresses at the base of the web. Additional material has been added to the trailing edge of the blade by cutting back the core trailing edge at the root of the blade to reduce the peak stress.

With respect to the use of the NASTRAN program itself, several considerations could be summarized. Within an environment where numerous computer programs are in use during the last ten years, there is a natural inertia against starting the use of another large program, especially of the NASTRAN size. However, once the analyst has become more familiar with the several features of NASTRAN he becomes more aware and conscious of the strong analytical possibilities of the present program. For example, in the analysis mentioned above the capability of having a model to run dynamic analysis and non-linear material behavior, plus plotting the model and shapes, was a decisive factor in the use of this program.

# TURBINE ROTOR ASSEMBLY

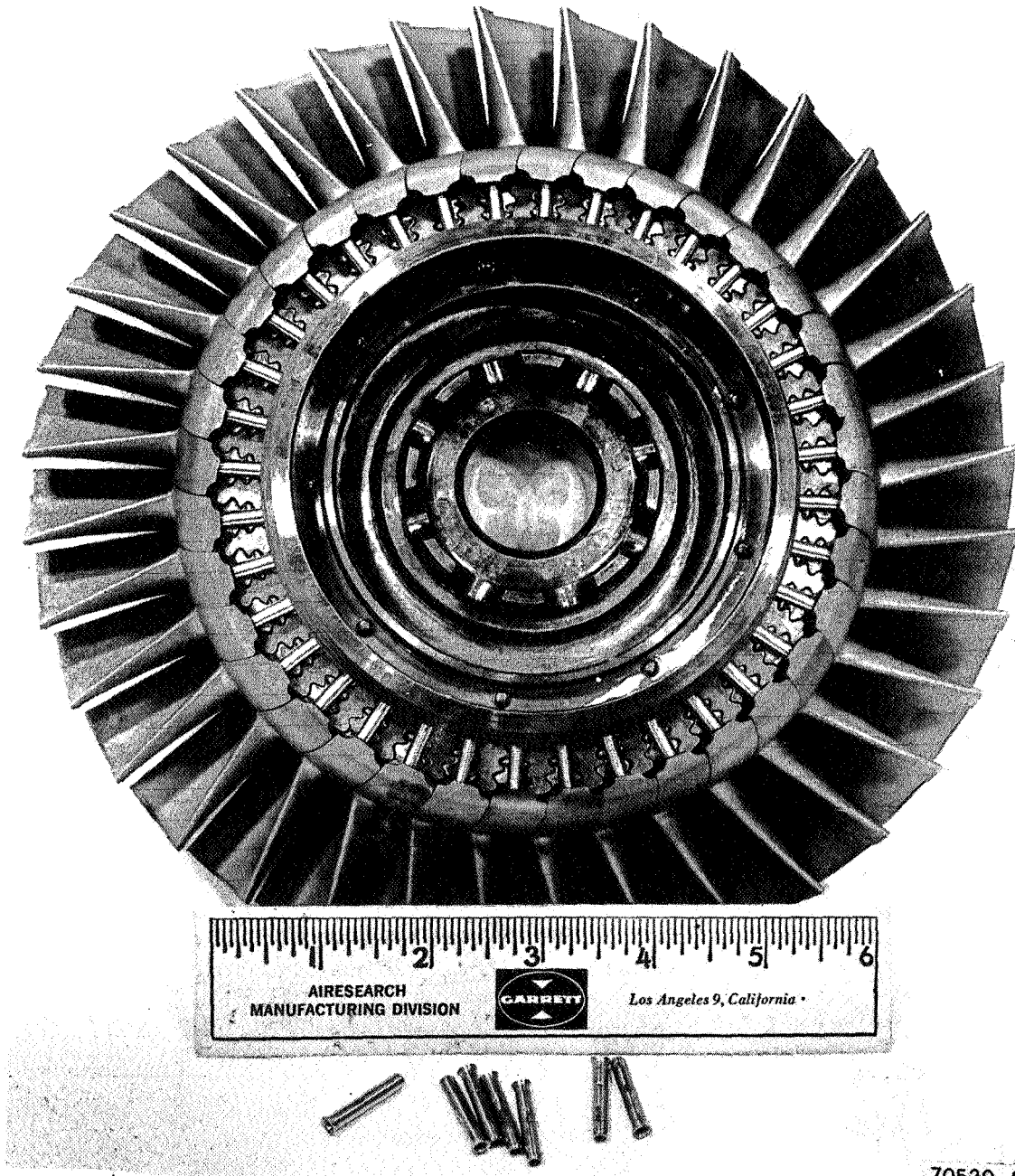


FIGURE 1

# 3-SECOND TRANSIENT TEMPERATURES

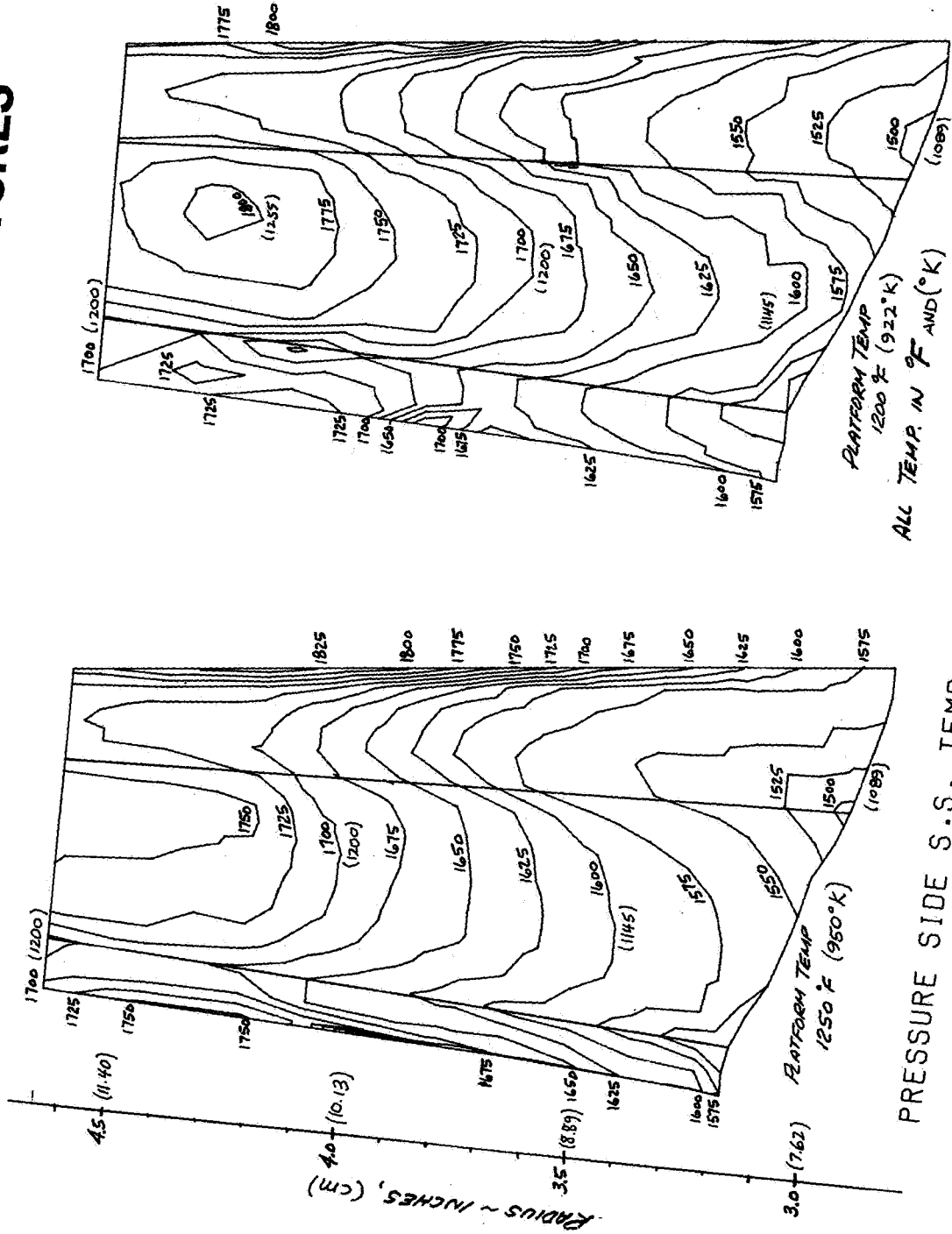


FIGURE 2  
PRESSURE SIDE S.S. TEMP  
SUCTION SIDE S.S. TEMP

S-60324

# EFFECTIVE STRESS LINES FOR HIGH-PRESSURE TURBINE BLADE & DISK FIR-TREE CONNECTION - KSI & (N/m<sup>2</sup>)

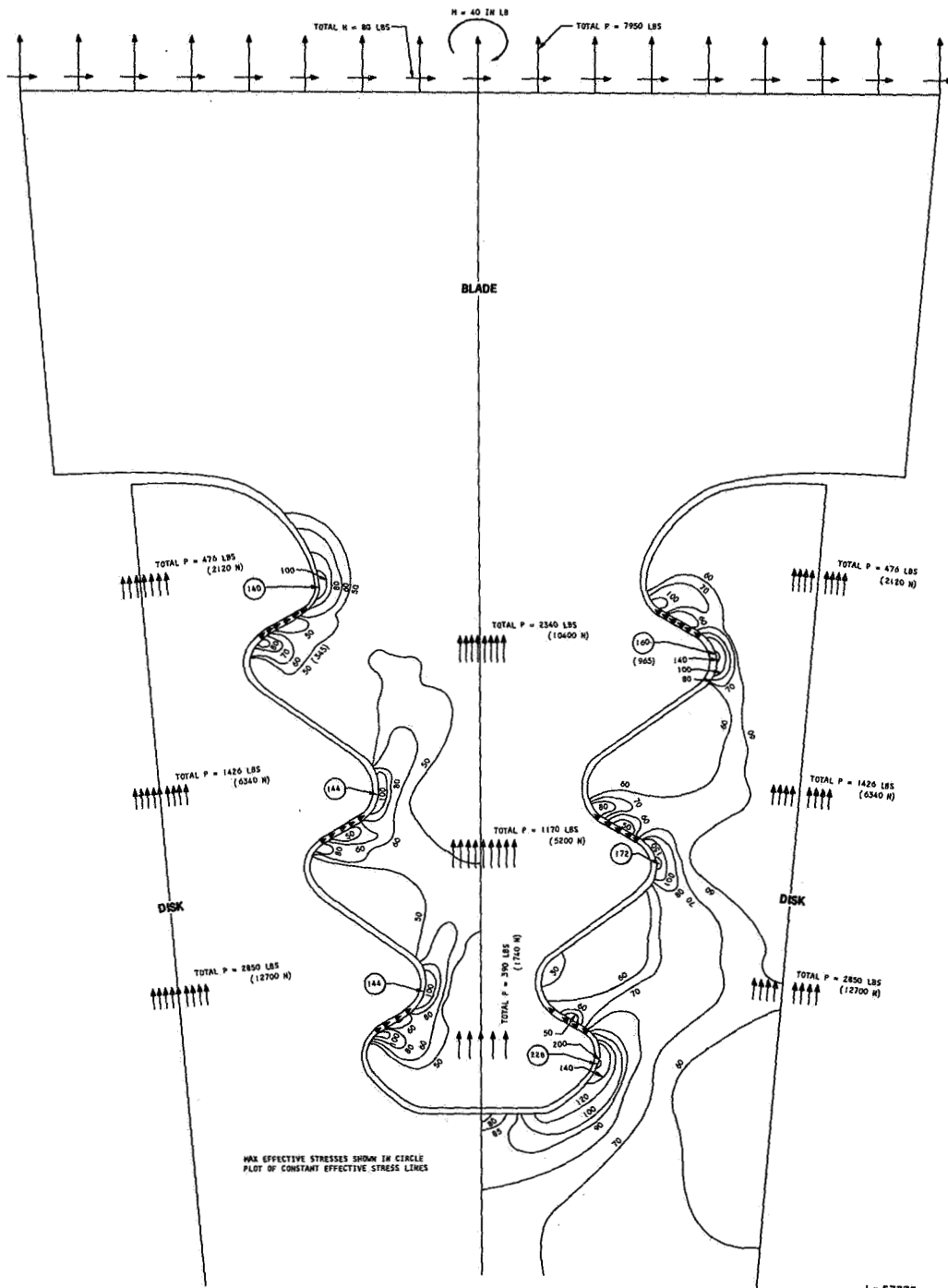
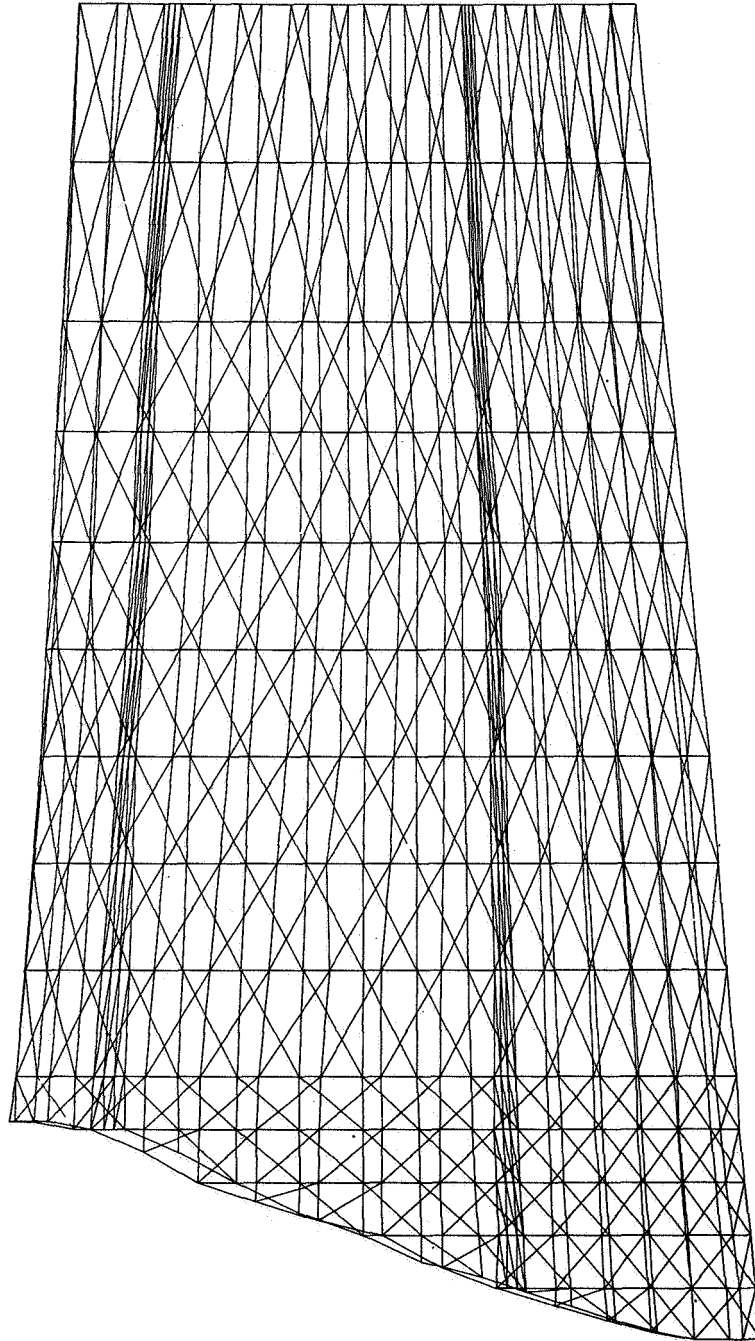


FIGURE 3

# ANALYTICAL MODEL OF THE THREE CAVITY HIGH-PRESSURE TURBINE BLADE



S-66274

FIGURE 4

# HIGH-PRESSURE TURBINE BLADE CENTRIFUGAL STRESS

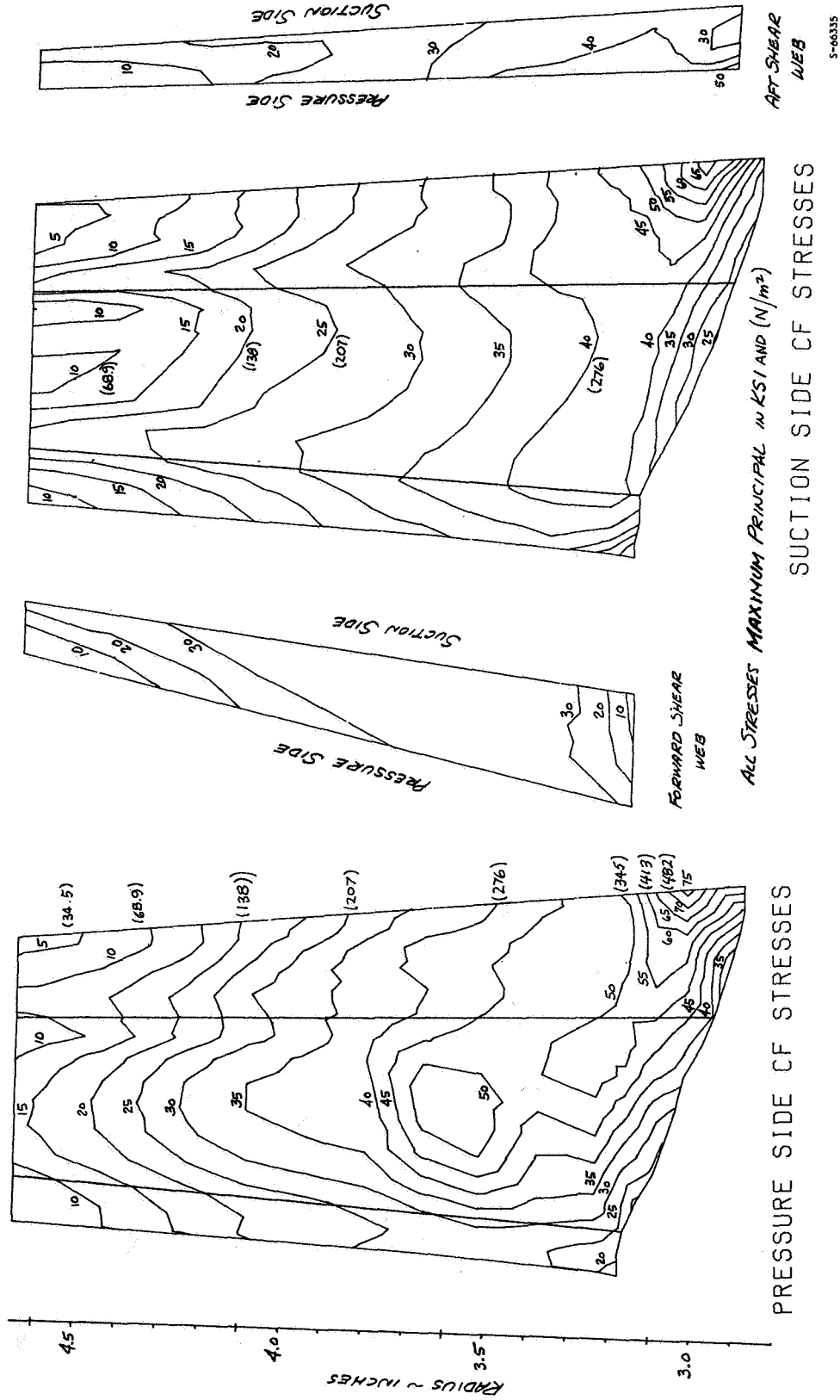


FIGURE 5

# 3-SECOND TRANSIENT THERMAL & CENTRIFUGAL STRESS

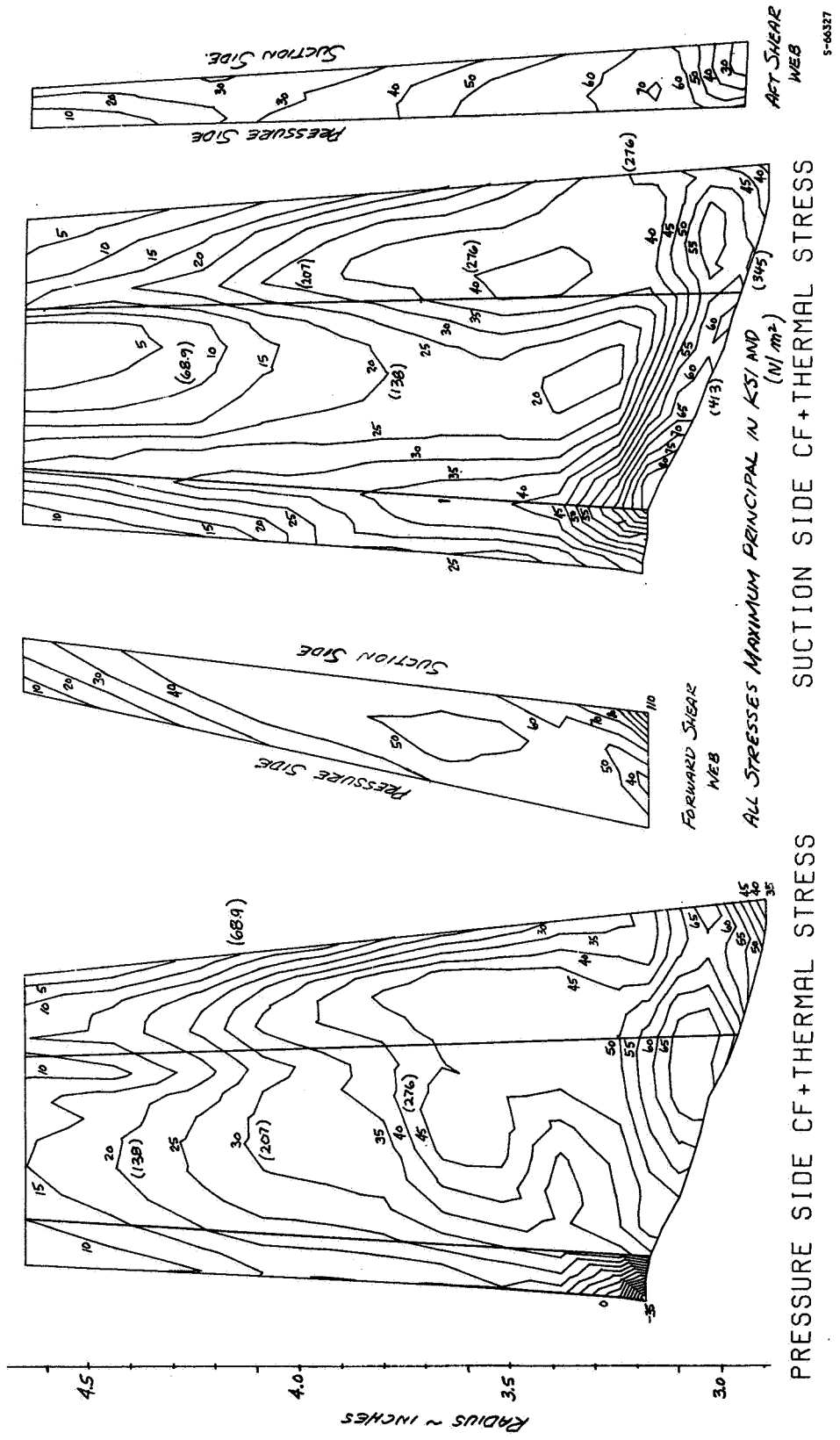


FIGURE 6

## APPLICATIONS OF NASTRAN SUBSTRUCTURING

By R. Narayanaswami\*  
NASA Langley Research Center

### SUMMARY

This paper describes the application of substructuring techniques for two example problems, (i) a square plate and (ii) the static analysis of a frame-wall interaction problem in multistory structures. Presently, multipoint constraint forces are not retrieved in NASTRAN. A DMAP routine for calculating the multipoint constraint forces is also presented herein.

34

### INTRODUCTION

The use of substructuring techniques in NASTRAN is well documented (references 1 and 2). However, it is felt that example problems involving large degree of freedom (d.o.f.) systems would bring out the advantages of substructuring in greater detail and will be of help to the NASTRAN user community. This is attempted in this paper.

There are several cases where the analyst will be interested in evaluating the multipoint constraint forces - for example, the frame-wall interaction problem in multistory structures or the nuclear fuel pellet-cladding problem in nuclear engineering. These forces are not presently retrieved in NASTRAN. A DMAP routine, based on the Lagrange multiplier technique, is presented herein for the calculation of multipoint forces of constraint. When this DMAP routine is applied for large d.o.f. problems, the computing effort needed is so great as to make it impracticable. The substructuring feature in NASTRAN overcomes this difficulty. This paper uses the substructure partitioning and the Lagrange multiplier technique to retrieve the interaction forces between the shear wall and frame of a multistory structure.

### DESCRIPTION OF PROCEDURE

The details of substructure partitioning are explained in the NASTRAN User's Manual (ref. 2) and will not be described here. With reference to static analysis, the method is briefly outlined in the following paragraphs.

---

\*NAS-NRC Post-Doctoral Resident Research Associate.

The complete structure is divided into a number of substructures, the boundaries of which may be specified arbitrarily; however, for convenience, it is preferable to make structural partitioning correspond to physical partitioning. Each substructure is first analysed separately, assuming that all common boundaries (joints) with the adjacent substructures are completely fixed. (In NASTRAN, this is called the Phase I operation.) From this analysis, the displacements of all interior points in each substructure with the adjacent substructure boundaries fixed are evaluated. These boundaries are then relaxed simultaneously and the boundary displacements are determined from the equations of equilibrium at the boundary joints (the Phase II NASTRAN operation). Each substructure can now be analysed for boundary displacements. Adding these to the Phase I displacements, (displacements of interior points in each substructure with adjacent boundaries fixed) we get the final displacements. (This is achieved in NASTRAN in Phase III operation.)

The addition of the reduced substructure boundary loads and stiffness matrices to obtain the total boundary load and stiffness matrix for the complete structure, and the partition of the boundary displacement of the complete structure into the boundary displacements of the separate substructures is achieved with the aid of partitioning vectors. The partitioning vector for each substructure is a vector of size  $n \times 1$  where  $n$  is the total degrees of freedom in the a-set. The various steps in the construction of the partitioning vectors are explained in ref. 2. For cases where all the grid points in the total structure have been numbered distinctly, the partitioning vectors can be formed as follows:

1. Arrange the grid points in the a-set, in ascending sequence. List the connected degrees of freedom at these grid points (the components of the a-set) as scalar point internal indices in ascending numerical sequence starting with 1. This gives the size  $n$  of the partitioning vector.
2. The partitioning vector for each substructure is obtained by entering real 1's in all locations where the substructure under consideration has connection components with any other substructure.

The formation of the partitioning vector when one substructure has connection with two or more substructures and when the grid point numbering for the total structure shows discontinuities is illustrated in Example Problem Number 2.

## EXAMPLE PROBLEMS

### Problem Number 1

The structural problem consists of a square plate with hinged supports on all boundaries. The  $10 \times 20$  model, as shown in Fig. 1, uses one-half

of the structure and symmetric boundary constraints on the midline in order to reduce the order of the problem and the band width by one-half. Because only the bending modes are desired, the inplane deflections and rotations normal to the plane are constrained. This is the same problem as that solved in the NASTRAN demonstration manual (ref. 3).

The model is divided into five substructures. (This is not the best division of the problem; however, since the purpose herein is to demonstrate the use of identical substructures and the second stiffness reduction in Phase II, no attempt is made to choose the best subdivision.) The a-set points consist of (i) points on the boundaries of the substructures, 12 thru 22, 88 thru 98, 154 thru 164, 220 thru 230 and (ii) additional points in each substructure needed to define the dynamic response (this is largely based on the analyst's judgement), 55, 60, 65, 121, 126, 131, 187, 192, and 197. Note that Phase I runs are made only for two substructures, substructure 1 and substructure 2 (Sub-5 is identical to Sub-1; Sub-3 and Sub-4 are identical to Sub-2). There are 53 a-set points with 3 d.o.f. per grid point (Total d.o.f. = 159). Applying the boundary condition  $y = 0$  along  $X = 0$ , 7 d.o.f. are eliminated; applying the condition  $u_z = \theta_x = 0$  along  $X = 10$ , 14 d.o.f. are eliminated; this leaves 138 d.o.f. in a-set. Since all the grid points in the boundaries are not needed for reasonably satisfactory dynamic response of the structure, a second stiffness reduction is done in Phase II. The grid points omitted are 13 thru 16, 18 thru 21, 89 thru 92, 94 thru 97, 155 thru 158, 160 thru 163, 221 thru 224, and 226 thru 229 (total of 32 points each of 3 d.o.f.). There are thus only 42 d.o.f. in the final solution of the pseudo-structure in Phase II. The natural frequency comparisons with and without the second stiffness reduction of Phase II is given in Table 1.

#### Problem Number 2

This problem deals with the analysis of a multistory structure. The shear wall and frame are treated as separate structures and they are discretized and divided into substructures as shown in Figures 2 through 5. The shear wall is divided into 30 substructures (three for each story). The frame is divided into 10 substructures. Phase I analysis is performed for 7 of the 30 substructures of the shear wall and 2 of the 10 substructures of the frame (due to the repetitive geometry, it is enough if 3 substructures of shear wall and 1 of frame are analysed for Phase I; however, to reduce the a-set points, the former approach is used).

Substructure 1 has connection points with substructures 2 and 4; substructure 4 has connection points with substructures 1, 2, 5, and 7. The grid point numbering for the total structure is available, even though it is not continuous serially. Under these conditions, the partitioning vectors for all the substructures can be formed as shown below.

- (1) Arrange the grid points in the boundaries in ascending sequence: 49-56, 105-112, 161-168, 217-224, 273-280, 329-336, 385-392, 441-448, 497-504, 1749-1756, 1805-1812, 1861-1868, 1917-1924, 1973-1980, 2029-2036, 2085-2092, 2141-2148, 2197-2204, 2905-2907, 2912-2914, 2919-2921, 2926-2928, 2933-2935, 2940-2942,

2947-2949, 2954-2956, 2961-2963, 2968-2970, 3105-3107, 3112-3114, 3119-3121, 3126-3128, 3133-3135, 3140-3142, 3147-3149, 3154-3156, 3161-3163, 3168-3170. Since each point has 2 degrees of freedom (u and v), the components of the a-set are listed as scalar point internal indices in ascending numerical sequence starting with 1 as follows:

A-Set grid point	Scalar point internal index
49	1
	2
50	3
	4
51	5
	6
.	.
.	.
.	.
1749	145
	146
1750	147
	148
.	.
.	.
.	.
2905	289
	290
2906	291
	292
.	.
.	.
.	.
3105	349
	350
3106	351
	352
.	.
.	.
.	.
3170	407
	408

- (2) The partitioning vector for each substructure is obtained by entering real 1's in all locations where the substructure under consideration has connection components with any other substructure. The partitioning vectors for 2 sample substructures is shown on the following pages (size of partitioning vectors  $408 \times 1$ ):

Scalar point Internal Index	Substructure 1	Substructure 4
1	1.0	1.0
2	1.0	1.0
3	1.0	1.0
4	1.0	1.0
5	1.0	1.0
6	1.0	1.0
7	1.0	1.0
8	1.0	1.0
9	1.0	1.0
10	1.0	1.0
11	1.0	1.0
12	1.0	1.0
13	1.0	1.0
14	1.0	1.0
15	1.0	1.0
16	1.0	1.0
17		1.0
18		1.0
19		1.0
20		1.0
21		1.0
22		1.0
23		1.0
24		1.0
25		1.0
26		1.0
27		1.0
28		1.0
29		1.0
30		1.0
31		1.0
32		1.0
33		
34		
35		
36		
37		
38		
39		
40		
41		
42		
43		
44		
45		
46		
47		
48		

Scalar point Internal Index	Substructure 1	Substructure 4
49		
50		
51		
52		
.		
.		
289	1.0	
290	1.0	
291	1.0	
292	1.0	
293	1.0	1.0
294	1.0	1.0
295		1.0
296		1.0
297		1.0
298		1.0
299		1.0
300		1.0
301		
302		
303		
304		
.		
.		
408		

The a-set points for the frame are 5, 9, 13, 16, 20, 24, 27, 31, 35, 38, 42, 46, 49, 53, 57, 60, 64, 68, 71, 75, 79, 82, 86, 90, 93, 97, 101, 104, 108, 112. Since there are 3 d.o.f. per grid point, (u, v, and  $\theta_z$ ) the a-set components total 90. The partitioning vectors for the substructures of the frame (size  $90 \times 1$ ) can be formed easily.

Since it is of interest to know how the frame and the wall acting alone will resist the lateral wind load, the frame and the shear wall are analysed separately at first.

This example will also be used to illustrate the use of multiple level substructuring. The multistory structure is to be analysed for different first story heights of 12 ft, 13 ft, 15 ft, and 20 ft. In order that the entire calculations are not to be repeated, a Phase II (Initial) run is made where substructures 4 thru 30 of the shear wall are combined into a "super-substructure"; so also substructures 2 thru 10 of the frame. The Phase II (Final) run consists of combining the first story substructures to the super-substructures of shear wall and frame, respectively. The data recovery of substructures of interest is achieved in Phase III. For a different first-story height of the multistory structure, the Phase I run for the substructures of

the first story and Phase II (Final) runs are repeated with the necessary Phase III runs.

The stiffness matrices with respect to the active degrees of freedom of the wall and frame, respectively, are merged by means of vector of size  $498 \times 1$ . The interaction of the wall and frame is studied using multipoint constraint equations; the conditions to be satisfied being (i)  $u$  and  $v$  displacements at corresponding points of wall and frame are equal and (ii)  $\theta_z$  of frame at connection points with the wall should be equal to the fictitious  $\theta_z$  values of the wall obtained by dividing the difference of the vertical displacements at the two ends of the left wall at each floor level by the width.

The value of the maximum displacement for wall alone, frame alone, and frame-wall interaction for the case of the lateral wind load is given in Table 2. It is to be pointed out that without substructuring, each of the cases investigated would have involved considerably more computing effort. For example, the frame-wall interaction problem has a total of 3210 degrees of freedom. In a direct analysis of the total structure the stiffness matrix of  $3210 \times 3210$  has to be decomposed; whereas in substructuring, 6 substructures in each of which the size of matrix does not exceed  $112 \times 112$ , 2 of size  $30 \times 30$ , 1 of size  $54 \times 54$ , and 1 of size  $468 \times 468$  are solved.

As seen from Table 2, for solving six different problems, a total time of about 900 sec is only needed while using substructuring techniques whereas for the solution of one shear-wall problem alone, about 2450 sec is needed without substructuring. The total time for solving all the cases without substructuring will be exorbitantly high (the bulk of the time is spent on decomposition of the large stiffness matrix). It should be mentioned that this wide discrepancy in time with and without substructuring is largely due to the repetitive nature of the structure geometry of this problem and also that Phase III runs are performed only at the portion of interest in the structure. Nonetheless, time savings are bound to result, in general, with the use of substructuring.

#### EVALUATION OF MULTIPOINT CONSTRAINT FORCES

In NASTRAN, the multipoint constraint forces are not retrieved. A DMAP program is written here to retrieve these forces. The theoretical basis for this DMAP routine lies in the use of the Lagrange multiplier technique.

From the minimum potential energy principle, we have the functional

$$\pi_p = 1/2 \int_V \{\epsilon\}^T [E] \{\epsilon\} dV - \int_{s_\sigma} \Delta \bar{T} dS$$

where  $s_\sigma$  is the surface upon which the tractions  $\bar{T}$  are prescribed.

The collection of multipoint constraint equations can be written in the form

$$\begin{bmatrix} \mathbf{C} \end{bmatrix} \begin{Bmatrix} \Delta \end{Bmatrix} = 0$$

To account for such constraints, we invoke the method of Lagrange multipliers, and defining the vector  $\{\lambda\}$  of these multipliers, we have the augmented functional

$$\pi_p = \left\{ \frac{\Delta}{2} \right\}^T \begin{bmatrix} \mathbf{K} \end{bmatrix} \begin{Bmatrix} \Delta \end{Bmatrix} - \begin{Bmatrix} \Delta \end{Bmatrix}^T \begin{Bmatrix} \mathbf{P} \end{Bmatrix} + \begin{Bmatrix} \Delta \end{Bmatrix}^T \begin{bmatrix} \mathbf{C} \end{bmatrix}^T \begin{Bmatrix} \lambda \end{Bmatrix}$$

After applying the first necessary conditions, we have

$$\begin{bmatrix} -\mathbf{K} & -\mathbf{C}^T \\ \mathbf{C} & \mathbf{O} \end{bmatrix} \begin{Bmatrix} \Delta \\ \lambda \end{Bmatrix} = \begin{Bmatrix} \mathbf{P} \\ \mathbf{O} \end{Bmatrix}$$

This equation can now be solved for  $\left\{ \frac{\Delta}{\lambda} \right\}$ . Note that the system of equations, in general, is not now positive definite, and hence the unsymmetric decomposition routine of NASTRAN has to be used for the solution. From the stand point of units,  $\lambda$ 's have the unit of lb/in. or in-lb/in. depending on whether the particular multipoint constraint equation equates displacements or rotations. This discloses that from a purely physical standpoint, the  $\lambda$ 's represent the average value of the distributed force or moment needed to satisfy the multipoint constraint equation.

For this problem the a-set stiffness matrix for the wall is of size  $408 \times 408$ ; that for the frame is  $90 \times 90$ ; and there are 30 multipoint constraint equations. Thus the augmented matrix is the size  $528 \times 528$ . An unsymmetric decomposition of this matrix on CDC 6600 machine with 14OK (octal) storage will require about 18.5 minutes. Since this is very expensive, an alternative formulation is used herein. The  $408 \times 408$  a-set stiffness matrix of the wall is reduced to  $20 \times 20$  (retaining only the d.o.f. at each connection point with the frame); the  $90 \times 90$  a-set stiffness matrix of the frame is reduced to  $30 \times 30$  (retaining only the d.o.f. at each connection point with the wall); thus, with 30 multipoint equations, the augmented matrix of size  $80 \times 80$  need only be unsymmetrically decomposed. The reduction of a-set stiffness and load matrices and the solution of the augmented matrix took only about 88 sec on CDC 6600 with 14OK (octal) storage. The DMAP package for this frame-wall interaction problem, including the stiffness reductions mentioned above, is given in the Appendix.

Even though the procedure described herein for the calculation of multipoint constraint forces is general and can be used for problems that do not involve and/or necessitate substructuring techniques, it has to be emphasized that for large problems, the method can be used only with substructuring. Even then, an additional stiffness reduction would considerably shorten the computing effort. This is because unsymmetric decomposition of large matrices will involve unacceptably high computing costs.

## CONCLUDING REMARKS

The NASTRAN substructuring techniques have been applied for the solution of a static and a dynamic problem. In both problems, substructuring is found to result in considerable saving of computing effort. The multiple level substructuring technique, which facilitates the efficient reanalysis of the structure when only a portion of the structure is modified, has been applied for a frame-wall interaction problem. In NASTRAN, the multipoint constraint forces are not presently retrieved. A DMAP routine for retrieving the multipoint constraint forces has been written and has been successfully used in calculating the interactive forces between the frame and shear wall of a multistory structure.

## REFERENCES

1. MacNeal, R. H., ed.: The NASTRAN Theoretical Manual, NASA SP-221, Sept. 1970 (Revised 1972).
2. McCormick, C. W., ed.: The NASTRAN User's Manual, NASA SP-222, Sept. 1970 (Revised 1972).
3. NASTRAN Demonstration Problem Manual, NASA SP-224, Sept. 1970.



Table 1. Natural Frequency Comparisons, CPS.

Mode	Theoretical	NASTRAN 10 x 20	5 Substructures (No stiffness reduction in Ph. 2)	5 Substructures (Stiffness reduction in Ph. 2)
1	0.9069	0.9056	0.9063	0.9068
2	2.2672	2.2634	2.2707	2.2812
3	4.5345	4.5329	4.6070	4.6629
Total (Phase 1 and Phase 2) time on CDC 6600 machine			258.5 sec	238.5 sec

Table 2. Value of maximum displacement, in. ft.,  
due to lateral wind load of 1 kip/sq. ft.

	Frame Alone	Shear-wall Alone	Frame-Wall interaction problem
Case 1-First story height = 12'	0.051145	0.019336	0.018901
Case 2-First story height = 13'	0.052557	0.019855	0.019448
(Total time for Ph. 1 and Ph. 2 on CDC 6600)	50 + 30 = 80 sec	290 + 220 = 510 sec	160 + 140 = 300 sec

Total time on CDC 6600 for solving the problem of shear wall alone  
(with a First story height of 13') without the use of substructuring } 2450 sec.  
but using omit d.o.f.

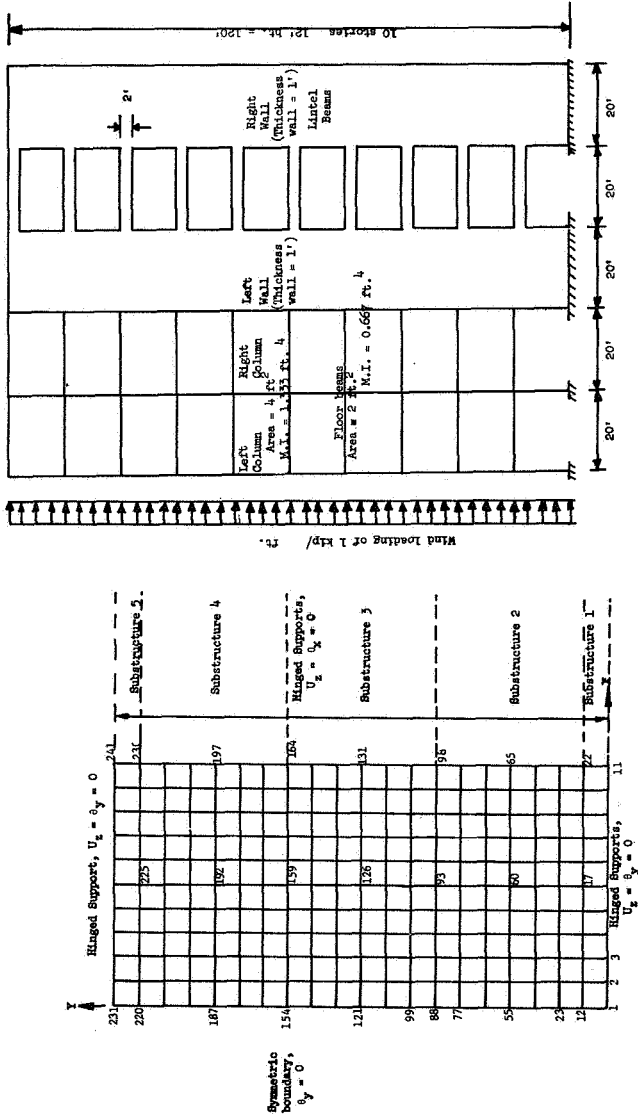


Figure 1. 10 x 20 Half plate model.

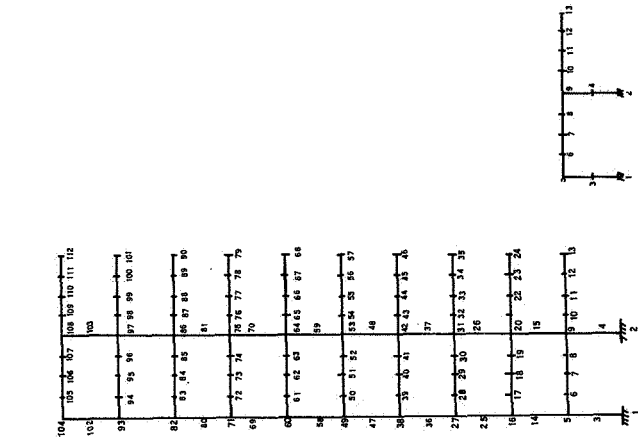


Figure 2. Multistory frame and shear wall.

(a) Discretization (All C-Bar elements) (b) Substructure 1

Figure 3. Frame details

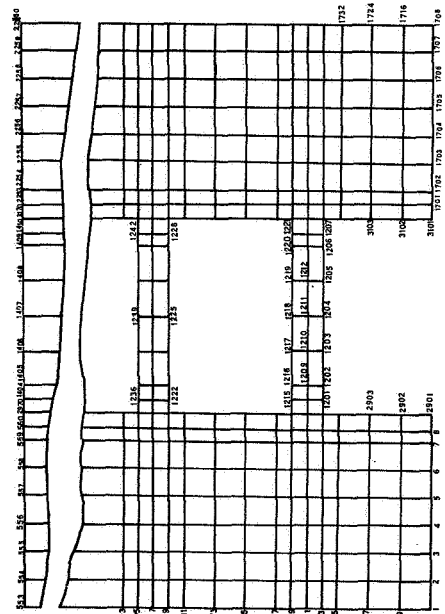


Figure 3. Shear wall Discretization (All elements are COMBO)

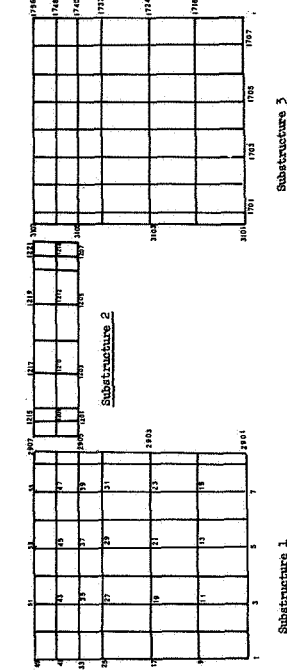


Figure 4. Division of First story into Substructure

## DESIGN OF NASTRAN DEMONSTRATION PROBLEMS

By Alvin Levy\*  
Grumman Aerospace Corporation, Bethpage, New York

### SUMMARY

Criteria and procedures are supplied for the selection, evaluation and maintenance of an optimum set of demonstration problems to be used for the purposes of checking out the NASTRAN program and demonstrating NASTRAN's capabilities. Also, suggestions are made for a new Demonstration Problem Manual that will better assist the user community in the selection of NASTRAN options and preparation of input data as well as allow the user to isolate the various options used in the set of demonstration problems.

### INTRODUCTION

The versatility and scope of NASTRAN are large and increasing with each new release. For this reason a set of demonstration problems is used to checkout the NASTRAN program as well as to demonstrate its capabilities. The use of demonstration problems in this manner is a good practice and should be continued in the future as new features are added on to NASTRAN. However, care must be taken in the construction of this set of problems. Because of the many options available in NASTRAN, the set of demonstration problems should be both complete and efficient, i.e., it should utilize all the options of NASTRAN in a limited number of problems. It is the intention of this paper to supply criteria and procedures for the selection, evaluation and maintenance of an optimum set of demonstration problems. In order to carry out our objective a catalogue is constructed which lists all the NASTRAN options which are to be explicitly checked out. This catalogue is then used to evaluate the present set of demonstration problems and a procedure is outlined for the construction of an optimum set of demonstration problems.

It is also suggested that a new Demonstration Problem Manual be supplied which will assist the user community in the selection of NASTRAN options and preparation of input data. This will be a useful supplement to the User's Manual (ref. 1). To this end the present paper includes, as a by-product of the aforementioned objective, a complete listing of the options available in NASTRAN in an organized format. Also a complete catalogue of the present demonstration problems is constructed in a matrix form. This catalogue is displayed in the Appendix and can be used as a reference to locate the use of a particular option in the set of demonstration problems.

---

\*Grumman-Langley Industry Associate, NASA Langley Research Center

## CONSTRUCTION OF CATALOGUE

The first step in constructing a catalogue is to organize the NASTRAN features into general groups. These general groups, shown in Figure 1, are based on the flow through the NASTRAN data deck and represent the main features that the user is concerned with in order to set up his problem correctly and completely. The present Demonstration Problem Manual (ref. 2) contains a similar listing.

Next, an evaluation is made to determine which options must be explicitly checked out. This will help insure completeness and avoid duplication and unnecessary bookkeeping. This evaluation leads to the following considerations:

1. All the modules in NASTRAN must be thoroughly evaluated. However, only those modules not used in the rigid formats will be listed in the catalogue (See A5.DMAP of Appendix). These modules can then be altered into the rigid formats or included in a separate DMAP program. In this way we will guarantee that all the modules are being used. In addition, all parameter options should be checked in a separate DMAP program.
2. The case control cards that are used for selecting bulk data input are not explicitly included in the list of data cards. These will automatically be checked when the corresponding bulk data cards are used. The case control cards necessary for selecting bulk data cards are listed in the Appendix under C. Bulk Data Deck Options. Also see section 2.3.1 of the User's Manual for this purpose. The case control cards TITLE, SUBTITLE, and LABEL are used in most problems and are therefore deleted from the list to be demonstrated.
3. Those bulk data cards that are necessarily referred to by other bulk data cards are not included in the catalogue. Generally, these are property cards. Other bulk data cards that fall in this category are EIGP, AXIC, AXSLOT, AXIF, ADUMi, DAREA and RANDPS.
4. Denoted by (\*) in the catalogue list are those bulk data cards that are necessarily required for one or more rigid formats. This included the following cards (along with the corresponding rigid formats): EIGR (3, 11, 12), DSFACT (4), EIGB (5), PLFACT (6), EIGC (7), and TSTEP (9, 12).

All the NASTRAN options are listed under their appropriate headings. The final product, listed in the Appendix, contains a complete and efficient listing of all the options in NASTRAN which have to be explicitly checked out. Also, the catalogue is constructed in an easily usable manner, e.g., under any category of structural consideration the user can see at a glance the options available and which data cards are necessary for each option.

## CONSTRUCTION OF OPTIMUM SET OF DEMONSTRATION PROBLEMS

### Selection of Problems

In general, small prototype problems will be selected. This will enable the user to analyze prototype problems before attempting the solution of large-scale problems. A number of large-scale problems will also be included to checkout such things as spill logic. An individual problem will be kept realistic while utilizing as many different options as feasible. This is in keeping with the desired objective, namely, to utilize all the options available in NASTRAN in an efficient manner.

The initial set of demonstration problems will be comprised of those presently being used to checkout NASTRAN. Figure 2 represents three typical problems that will be considered as additions to or replacements for the initial set. In problem 1 subcase definitions are demonstrated on a simple truss. This problem uses all the static subcase options. In problem 2 we are considering the buckling of a simply supported square plate under edge compression. Instead of using just one element we incorporate all the plate elements into one problem. There are nine such elements. This problem checks out the reliability of the static stiffness and differential stiffness matrices of plate elements. We note that in both these problems there are many options (in a given category) used in a single problem, making it possible to use all the options in fewer problems, or, more appropriately, in less computer time. In problem 3 we are analyzing the nonlinear behavior of a rotating beam under axial compression. In addition to demonstrating the differential stiffness of the CBAR element, as presently demonstrated in demonstration problem 4-1, the present problem also includes the following; (1) the use of CELAS1 and CELAS2 elements, which have not been demonstrated in any current demonstration problem, (2) the use of a negative spring to simulate a rotating mass, and (3) an ALTER which allows the load factors, specified on the DSFACT bulk data card, to be applied to load P while not affecting load q (presently all loads are multiplied by the load factors).

### Evaluation

A table is now set up in matrix form and can be used to evaluate a set of demonstration problems. A similar idea was suggested by Cuthill et al. in ref. 3. The rows of the matrix are the NASTRAN options, listed in the catalogue, while the columns refer to the different demonstration problems. For each problem we check off the options used. After a set of demonstration problems is catalogued, we can easily see from our matrix which options are used for a given problem, which problems utilize a given option, and in particular, which options have not been used. An evaluation of the demonstration problems used to check out level 15 has been made, and the complete evaluation matrix is given in the Appendix. The general observation is

that the present set of demonstration problems utilizes most of the main features of NASTRAN, but that there are many minor options which are not used.

### Construction and Maintenance

We can see at the outset that there is no unique set of optimum problems feasible. In fact it would be very inefficient to try to find the most efficient set of problems. The method outlined here is an iterative procedure, as shown in Figure 3. Starting with a given set of demonstration problems, catalogue and evaluate them as outlined previously, then update them by altering and deleting old problems and adding new problems. The updated set of problems can then be made more efficient by combining options in different ways, or possibly by combining problems. The cycle of evaluating and updating can be repeated as often as necessary. We must also make sure that we can easily maintain the set of demonstration problems. As new features are added to NASTRAN, the cataloguing tables are updated and the demonstration problems are altered or added to and the cycle repeated. This will lead to an efficient set of demonstration problems which can be maintained with a minimum of effort.

Once we have a set of problems we can demonstrate them on NASTRAN. With our cataloguing procedure we will know exactly which options are being checked out and which options remain to be checked out. Ultimately, we will have a complete set of problems, that is to say, a set of problems that utilizes all the features of NASTRAN.

### DEMONSTRATION PROBLEM MANUAL

The proposed Demonstration Problem Manual will consist of a description of the demonstration problems, as appears presently (ref. 2). A useful addition will be the catalogue of NASTRAN options. This will enable the reader to follow and understand the selection of options used for a given problem. Also included, for easy reference, should be the evaluation matrix of the present set of demonstration problems. This will allow the user to isolate the use of a given option in the set of problems. It is suggested that the data decks for the demonstration problems also be included in this manual for easy reference and completeness. This has also been suggested by Cuthill, et al. in reference 3. Whether the data decks are included in the manual, since they are supplied to the user from COSMIC, they should include comments to help explain any misunderstandings that might arise in the preparation of data.

## CONCLUDING REMARKS

The present text outlines procedures for constructing an optimum set of demonstration problems (one which utilizes all the options in an efficient manner) and a format for a new Demonstration Problem Manual (one which readily lends itself to isolating the use of individual options). This will allow both the management and user community of NASTRAN to take better advantage of the use of demonstration problems.

## REFERENCES

1. The NASTRAN User's Manual, McCormick, C. W., ed., NASA SP-222, September 1970.
2. The NASTRAN Demonstration Manual, NASA SP 224, September 1970.
3. Cuthill, E.; Matula, P.; Hurwitz, M.; McKee, J.; and Messalle, R.: NASTRAN Evaluation Report, Naval Ship Research and Development Center, AML-49-70, August 1970.

APPENDIX

CATALOGUE OF NASTRAN OPTIONS, LEVEL 15

A. Executive Control Deck Options

1. Rigid Format - APP DISP/SOL K1, K2
  - 1.1 Static Analysis
  - 1.2 Static Analysis with Inertia Relief
  - 1.3 Normal Mode Analysis
  - 1.4 Static Analysis with Differential Stiffness
  - 1.5 Buckling Analysis
  - 1.6 Piecewise Linear Analysis
  - 1.7 Complex Eigenvalue Analysis, Direct Formulation
  - 1.8 Frequency and Random Response Analysis, Direct Formulation
  - 1.9 Transient Response Analysis, Direct Formulation
  - 1.10 Complex Eigenvalue Analysis, Modal Formulation
  - 1.11 Frequency and Random Response Analysis, Modal Formulation
  - 1.12 Transient Response Analysis, Modal Formulation
2. User's Master File
  - 2.1 Create or Edit - UMFEDIT
  - 2.2 Use in Execution - UMF K1, K2
3. Checkpoint and Restart
  - 3.1 Checkpoint - CHKPNT
  - 3.2 Restart - RESTART
    - 3.2.1 Restart with Rigid Format Change
    - 3.2.2 Restart with Case Control Change
    - 3.2.3 Restart with Bulk Data Change
4. Alter Rigid Format  
ALTER K/ALTER K1, K2/ENDALTER
5. Direct Matrix Abstraction Programming (DMAP)  
APP DMAP/BEGIN/END
 

<ol style="list-style-type: none"> <li>5.1 Utility Modules               <ul style="list-style-type: none"> <li>MATPRN</li> <li>MATPRT</li> <li>SEEMAT</li> <li>TABPRT</li> <li>TABPT</li> <li>VEC</li> </ul> </li> <li>5.3 User Generated I/O               <ul style="list-style-type: none"> <li>INPUT (a = 1, 7)</li> <li>OUTPUT3</li> </ul> </li> </ol>	<ol style="list-style-type: none"> <li>5.2 Matrix Operation Modules               <ul style="list-style-type: none"> <li>ADD PARTN</li> <li>ADD5 SOLVE</li> <li>DECOMP SMPYAD</li> <li>FBS TRNSP</li> <li>MERGE UMERGE</li> <li>MPYAD UPARTN</li> </ul> </li> <li>5.4 User Tape Modules               <ul style="list-style-type: none"> <li>INPUTT1 OUTPUT1</li> <li>INPUTT2 OUTPUT2</li> </ul> </li> </ol>
--------------------------------------------------------------------------------------------------------------------------------------------------------------------------------------------------------------------------------------------------------------------------------------------------------------------------------------------------------------	--------------------------------------------------------------------------------------------------------------------------------------------------------------------------------------------------------------------------------------------------------------------------------------------------------------------------------------------------------------------------------------------------------------
6. Diagnostic Output - DIAG K (K = 1, 31)
7. Time - TIME N

B. Case Control Deck Options

1. Subcase Definition
 

SUBCASE	SYM	REPCASE
SUBCOM	SYMCOM	MODES
SUBSEQ	SYMSEQ	



C. Bulk Data Deck Options (cont.)	Case Control	Bulk Data
2.4 Shear Panel		CSHEAR
2.5 Twist Panel		CTWIST
2.6 Two-Dimensional Membrane		CQDMEM CTRMEM
2.7 Two-Dimensional Bending		CQDPLT CTRBSC CTRPLT
2.8 Two-Dimensional Combined Membrane and Bending		CQUAD1 CQUAD2 CTRIA1 CTRIA2
2.9 Conical Shell, Isotropic		CCONEAX
2.10 Toroidal Shell, Isotropic or Orthotropic		CTORDRG
2.11 Revolved Ring, Isotropic or Orthotropic		CTRAPRG CTRIARG
2.12 Scalar Spring		CELAS1 CELAS2 CELAS3 CELAS4
2.13 Fluid		CAXIF2 CAXIF3 CAXIF4 CFLUID2 CFLUID3 CFLUID4
2.14 Slot-Acoustic Cavity Analysis		CSLOT3 CSLOT4
2.15 Three-Dimensional, Isotropic		CHEXA1 CHEXA2 CTETRA CWEDGE
2.16 General		GENEL
2.17 Heat Boundary		CHBDY
2.18 Direct Input Matrices and Input Tables		DMI DTI
2.19 Plot		PLOTEL
3. Material Properties		
3.1 Linear, Temperature Independent; Isotropic		MAT1 MAT2 MAT3
Anisotropic		TABLEM1 TABLEM2 TABLEM3 TABLEM4
Orthotropic		
3.2 Linear, Temperature Dependent;		
Isotropic	TEMPERATURE	MATT1
Anisotropic	(MATERIAL)	MATT2
Orthotropic	TEMP (MAT)	MATT3
3.3 Conduction Properties;		
Isotropic		MAT4
Anisotropic		MAT5
3.4 Nonlinear Material		TABLES1 MATS1

C. Bulk Data Deck Options (cont.)	Case Control	Bulk Data
4. Static Loads		
4.1 Concentrated Load	LOAD	FORCE
	LOAD	FORCE1
	LOAD	FORCE2
	LOAD	MOMENT
	LOAD	MOMENT1
	LOAD	MOMENT2
	LOAD	SLOAD
4.2 Pressure Load	LOAD	PLOAD
	LOAD	PLOAD2
4.3 Gravity Load	LOAD	GRAV
4.4 Combined Load	LOAD	LOAD
4.5 Centrifugal Load	LOAD	RFORCE
4.6 Thermal Load	TEMPERATURE	TEMP
	(LOAD)	TEMPD
	TEMP (LOAD)	TEMPP1
	TEMP (LOAD)	TEMPP2
	TEMP (LOAD)	TEMPP3
	TEMP (LOAD)	TEMPRB
4.7 Conical Shell Load	LOAD	FORCEAX
	LOAD	MOMAX
	LOAD	POINTAX
	LOAD	PRESAX
	TEMP (LOAD)	TEMPAX
4.8 Enforced Deformation	DEFORM	DEFORM
4.9 Heat Conduction	LOAD	QHBDY
4.10 Differential Stiffness Scale	DSCO	DSFACT
Factor, *(4)		
4.11 Piecewise Linear Scale Factor, *(6)	PLCOEFF	PLFACT
5. Dynamic Modeling		
5.1 Structural Mass, MATi		St. Mass
5.2 Nonstructural Mass		CMASS1
		CMASS2
		CMASS3
		CMASS4
5.3 Concentrated Mass		COMM1
		COMM2
5.4 Structural Damping, MATi or Prop.		St. Damp.
5.5 Viscous Damping		CVISC
5.6 Modal Damping	SDAMP	TABDMP1
5.7 Direct Input Matrices	B2PP	DMIG
	K2PP	DMIG
	M2PP	DMIG
	TFL	TF
5.8 Transfer Functions		EPOINT
5.9 Extra Points		SEQEP
		CDAMP1
		CDAMP2
		CDAMP3
		CDAMP4
5.10 Scalar Damping		
6. Constraints and Partitioning		
6.1 Multipoint Constraints	MPC	MPC
	MPC	MPCADD
	MPC	MPCAX

C. Bulk Data Deck Options (concluded)	Case Control	Bulk Data
6.2 Single Point Constraints	SPC SPC SPC SPC	SPC SPC1 SPCADD SPCAX
6.3 Partitioning		OMIT OMIT1 OMITAX ASET ASET1 Guyan SUPPORT SUPAX
6.4 Free Body Support		FILSYM BDYLIST SLBDY
6.5 Fluid Constraints		
6.6 Fluid-Structure Boundary		
6.7 Slot Boundary List		
7. Eigenvalue Extration Method, *(3,5,7,11,12)		
7.1 Determinant (DET)		EIGm
7.2 Inverse Power with Shifts (INV)		EIGm
7.3 Givens (GIV)		EIGm
8. Dynamic Excitation		
8.1 Frequency Response Dynamic Load	DLOAD DLOAD	RLOAD1 RLOAD2
8.2 Transient Response Dynamic Load	DLOAD	TLOAD1 TLOAD2
8.3 Dynamic Load Tabular Function		TABLEDi
8.4 Loading Phase Angels		DPHASE
8.5 Loading Time Lags	DLOAD	DELAY
8.6 Combined Loads	DLOAD	DLOAD
8.7 Transient Initial Condition	IC	TIC
8.8 Transient Time Step,*(9, 12)	TSTEP	TSTEP
8.9 Random Analysis Power Spectral; Density Table	RANDOM	RANDT1 TABRND1
8.10 Frequency Selections for Frequency Response Problem	FREQUENCY FREQUENCY FREQUENCY	FREQ FREQ1 FREQ2
8.11 Nonlinear Transient Response Load	NONLINEAR	NOLINI
9. Rigid Format Optional Parameters, PARAM		
Grid Point Weight Generator		GRDPNT
Structural Mass Coefficient		WIMASS
Generates Coupled Mass Matrices,(Also CPelement)		COUPMASS
Uniform Structural Damping Coefficient		G
Pivotal Frequencies for Damping, Rigid Format9		W3, W4
Printing of Residual Vectors		ITRES
Frequency Range of Modes, *(10,11,12) }		L,HFREQ LMODES
Mode Acceleration Method, Rigid Format 11, 12		MODACC
Optional Decomposition for Frequency Response		DECOMOPT
Generates Conductivity Matrix		OPT. HEAT
10. Miscellaneous		
10.1 Delete from OPTP or UMF		/
10.2 Comment		\$
10.3 Large Field Bulk Data Card		TYPE*

DEMONSTRATION PROBLEMS

PROB. NO.	DESCRIPTION *
1A	1-1 Delta wing with biconvex cross section
1B	1-1A Delta wing - Restart, load change
1C	1-1B Delta wing - Restart, real eigenvalue analysis
2A	1-2 Spherical shell with pressure loading
2B	1-2A Spherical shell - Restart, boundary condition change
3A	1-3 Free rectangular plate with thermal loading
3B	1-3 Free rectangular plate - User generated input
4A	1-4 5x50 long, narrow, orthotropic plate
4B	1-4 5x50 plate - User generated input
4C	1-4A 5x50 plate - Restart, modified output
4D	1-4 5x60 long, narrow, orthotropic plate
4E	1-4 5x60 plate - User generated input
4F	1-4A 5x60 plate - Restart, modified output
5	1-5 Nonsymmetric bending of a cylinder of revolution
6	1-6 Solid disc with radially varying thermal load
7	1-7 Spherical shell, external pressure loading
8	1-8 1x4x10 cantilever beam using cubic CHEXA1 elements
9	1-9 2x2x10 fixed-free beam using rectangular CHEXA2 elements
10	1-10 Thermal bending of a bar
11	1-11 Simply supported rectangular plate with thermal gradient
12	1-12 Heat conduction through a washer, surface film heat transfer
13	2-1 Inertia relief analysis of a circular ring
14A	3-1 Vibration of a 10x20 plate
14B	3-1 Vibration of a 10x20 plate - User generated input
14C	3-1 Vibration of a 20x40 half plate
14D	3-1 Vibration of a 20x40 half plate - User generated input
15	3-2 Vibration of a compressible gas in a rigid spherical tank
16	3-3 Vibration of a liquid in a half filled rigid sphere
17	3-4 Acoustic cavity analysis
18	4-1 Differential stiffness of a 100 cell beam
19	5-1 Symmetric buckling of a cylinder
20	6-1 Piecewise linear analysis of a cracked panel
21A	7-1 Complex eigenvalues of a 500 cell string
21B	7-1 Complex eigenvalues of a 500 cell string - User generated input
22A	7-2 Complex eigenvalues analysis of a gas-filled thin cylinder-harmonics 3
22B	7-2 Complex eigenvalues analysis of a gas-filled thin cylinder-harmonics 5
23A	8-1 Frequency response of a square plate - 10x10 mesh
23B	8-1 Frequency response of a square plate - User generated input
23C	8-1 Frequency response of a square plate - 20x20 mesh
23D	8-1 Frequency response of a square plate - User generated input
24	9-1 Transient analysis with direct matrix input
25A	9-2 Transient analysis of a 1000 cell string
25B	9-2 Transient analysis of a 1000 cell string - User generated input
26	9-3 Transient analysis of a fluid-filled elastic cylinder
27	10-1 Complex eigenvalue analysis of a rocket control system
28A	11-1 Frequency response and random analysis of a 10 cell beam
28B	11-1A 10 cell beam - Restart, static analysis
29A	11-2 Frequency response of a 500 cell string
29B	11-2 Frequency response of a 500 cell string - User generated input
30	12-1 Transient analysis of a free 100 cell beam
31	1972 User Master file - demonstration problems

\* Descriptions refer to listing of demonstration problems for level 15.



		1	2	3	4	5	6	7	8	9	10	11	12	13	14	15	16	17	18	19	20	21	22	23	24	25	26	27	28	29	30	31					
	THERMAL												●																								
	VELOCITY																									●											
	(SORT2)																								●				A	●							
3.1	PLOTTER =	1													2 <sub>3</sub>		3	1						1	1			1	1	1							
3.2	PLOT														B <sub>D</sub>		●																				
3.3	PLOT																																				
3.4	PLOT														B <sub>D</sub>		●	●																			
3.5	PLOT																																●				
3.6	PLOT	A																																			
3.7	PLOT																												A	●							
3.8	PLOT																								●	●								●			
3.9	PERSPECT	A																																			
	ORTHO																																	●			
	STEREO																																	●			
	PROJ SEP																																				
	OCULAR																																				
	VANTAGE	A																																			
	AXES	A																●	●																		
	ORIGIN																																				
	VIEW	A																	●	●																	
	FIND	A													B <sub>D</sub>		●	●																●			
C. Bulk Data Deck Options																																					
1.1	CORDIC																																				
	CORDIR																																				
	CORDIS																																				
	CORD2C												●	●											●												
	CORD2R																																				
	CORD2S		●																																		
1.2	GRDSET	●	●	●	A <sub>D</sub>	●	●				●	●	●	●	●	●								A <sub>C</sub>			●	●		●							
	GRID	●	●	●	●	●	●	●	●	●	●	●	●	●	●	●								●			●	●		●							
1.3	SPOINT																																				
1.4	SEQGP			●																																	
1.5	FREEPT																																				
	FSLIST																																				
	GRIDB																																				
	GRIDF																																				
	RINGFL																																				
1.6	GRIDS																																				
1.7	RINGAX				●																																
	SECTAX																																				
2.1	BAROR										●		●																								
	CBAR										●		●																								
	Offset												●																								
2.2	CONROD	●																																			
	CROD	●																																			
2.3	CTUBE																																				
2.4	CSHEAR	●																																			
2.5	CTWIST																																				
2.6	CQDMEM	●	A																																		



	1	2	3	4	5	6	7	8	9	10	11	12	13	14	15	16	17	18	19	20	21	22	23	24	25	26	27	28	29	30	31
FORCE2																															
MOMENT							●												●												
MOMENT1																															
MOMENT2																															
SLOAD																															
4.2 PLOAD																															
PLOAD2			●																												
4.3 GRAV																															B
4.4 LOAD														●					●												
4.5 RFORCE														●																	
4.6 TEMP			●			●							●																		
TEMPD									●				●																		
TEMPP1											●																				
TEMPP2																															
TEMPP3																															
TEMPRB											●																				
4.7 FORCEAX																															
MOMAX						●																									
POINTAX					●																										
PRESAX																															
TEMPAX																															
4.8 DEFORM																															B
4.9 QHBDY																															
4.10 DSFACT																			●												
4.11 PLFACT																				●		●									
5.1 St. Mass	C												●	●															●	●	
5.2 CMASS1																															
CMASS2																															
CMASS3																						A			A				A		
CMASS4																					B			B		A		B			
5.3 CONM1																															
CONM2																												A		●	
5.4 St. Damp.																						●									
5.5 CVIS C																															
5.6 TABDMP1																												●		●	
5.7 DMIG(B2)																									●						
DMIG(K2)																									●						
DMIG(M2)																									●						
5.8 TF																												●			
5.9 EPOINT																									●			●			
5.10 CDAMP1																															
CDAMP2																															
CDAMP3																															
CDAMP4																															
6.1 MPC																													●		
MPCADD																													●		
MPCAX																															
6.2 SPC			B	B	BC		●	●	●		●		●						●	●										●	
SPC1	●	●	A		D			●	●		●																				

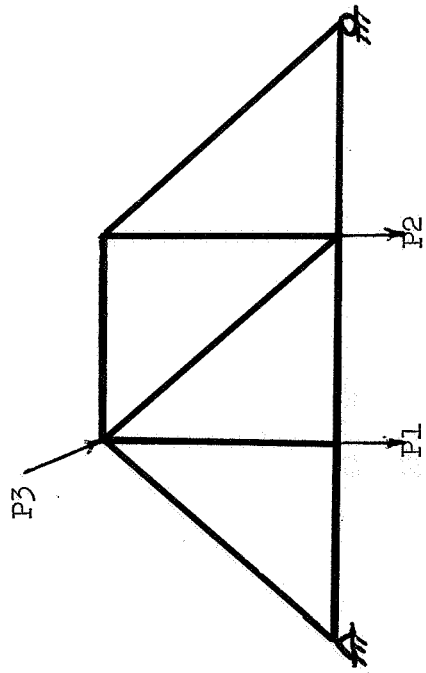
© 2000 Bentley Systems, Incorporated. All rights reserved.

		1	2	3	4	5	6	7	8	9	10	11	12	13	14	15	16	17	18	19	20	21	22	23	24	25	26	27	28	29	30	31					
	SPCADD			A						•										•																	
	SPCAX			D																																	
6.3	OMIT																																				
	OMIT1																			•													•				
	OMITAX																																				
	ASET																																				
	ASET1																																				
	Guyan																																•				
6.4	SUPPORT												•																				•				
	SUPAX																																	•			
6.5	FLSYM																																				
6.6	BDYLIST																																				
6.7	SLEBY																																				
7.1	EIGm(DET)																																				
7.2	EIGm(INV) C																																				
7.3	EIGm(GIV)																																				
8.1	RLOAD1																																				
	RLOAD2																																				
8.2	TLOAD1																																				
	TLOAD2																																				
8.3	TABLED1																																				
	TABLED2																																				
	TABLED3																																				
	TABLED4																																				
8.4	DPHASE																																				
8.5	DELAY																																				
8.6	DLOAD																																				
8.7	TIC																																				
8.8	TSTEP																																				
8.9	RANDT1																																				
	TABRND1																																				
8.10	FREQ																																				
	FREQ1																																				
	FREQ2																																				
8.11	NONLIN1																																				
9.	GRDPNT																																				
	WTMASS																																				
	COUPMASS																																				
	G																																				
	W3,W4																																				
	IRES			A	B																																
	L, HFREQ																																				
	LMODES																																				
	MODACC																																				
	DECOMOPT																																				
	OPT HEAT																																				
10.1	/																																				
10.2	\$																																				
10.3	TYPE *																																				

- A. EXECUTIVE CONTROL DECK OPTIONS
  - 1. RIGID FORMATS
  - 2. USER'S MASTER FILE
  - 3. CHECKPOINT AND RESTART
  - 4. RIGID FORMAT ALTER
  - 5. DIRECT MATRIX ABSTRACTION (DMAP)
  - 6. DIAGNOSTIC OUTPUT
- B. CASE CONTROL DECK OPTIONS
  - 1. SUBCASE DEFINITIONS
  - 2. PRINTED OUTPUT SELECTION
  - 3. PLOTTED OUTPUT SELECTION
- C. BULK DATA DECK OPTIONS
  - 1. GEOMETRY
  - 2. ELEMENTS
  - 3. MATERIAL PROPERTIES
  - 4. STATIC LOADS
  - 5. DYNAMIC MODELING
  - 6. CONSTRAINTS AND PARTITIONING
  - 7. EIGENVALUE EXTRACTION
  - 8. DYNAMIC EXCITATION
  - 9. RIGID FORMAT OPTIONAL PARAMETERS
  - 10. MISCELLANEOUS

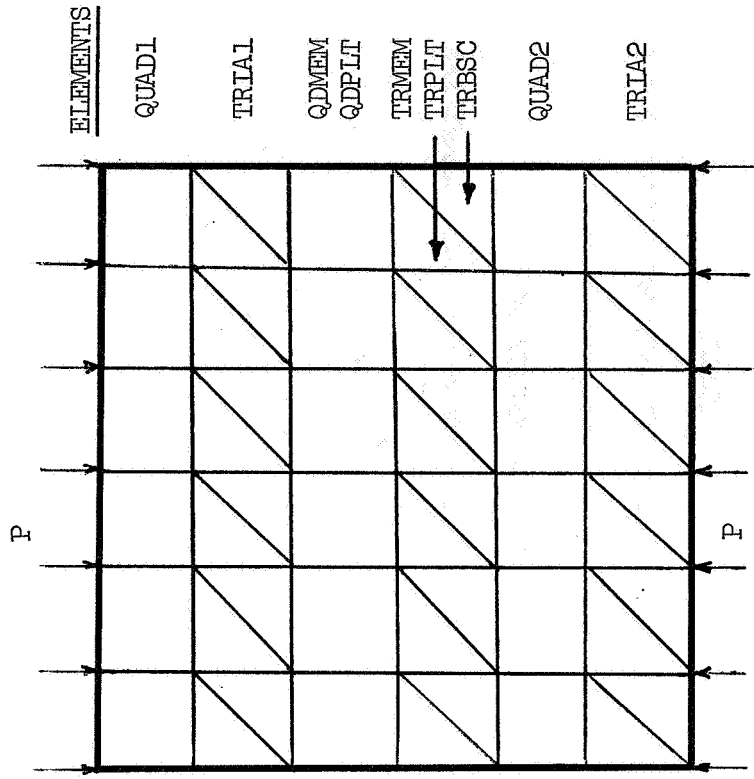
Figure 1. Catalogue-General Groups.

SAMPLE PROBLEM 1



- SUBCASE 1, Load P1
- SUBCASE 2 Load P2
- SUBCASE 3 Load P3
- REPCASE 4
- SYM 5 Output Request
- SYM 6 Load b1\*P1
- SYM 7 Load b2\*P2
- SYM 8 Load b3\*P3
- SUBCOM 8 } Linear Combinations
- SUBCOM 9 } of SUBCASE's and SYM's
- SUBCOM 10 }

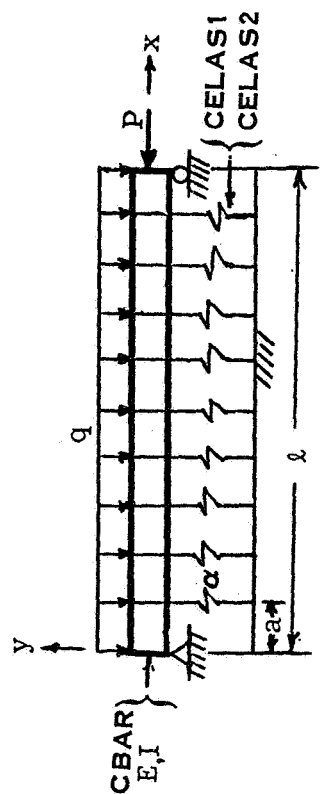
SAMPLE PROBLEM 2



BUCKLING OF A S.S. PLATE  
USING 9 TWO-DIM. ELEMENTS

Figure 2. Sample Demonstration Problems.

SAMPLE PROBLEM 3



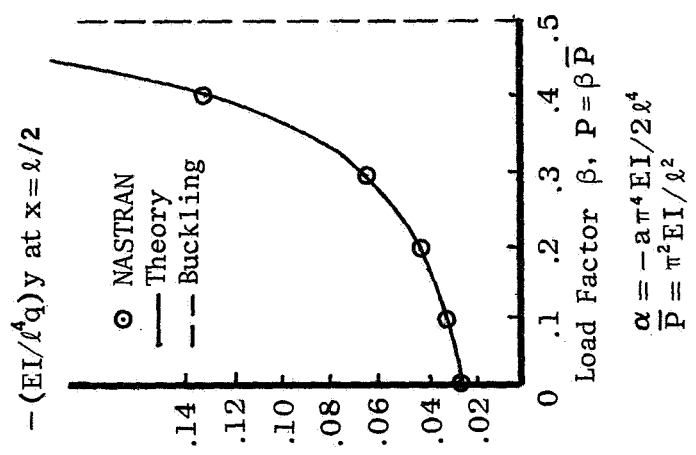
Load factors on DFACT card multiply  
load P but not load q

```

SOL 4,0
ALTER 135
PARAM //C,N,NOP/V,N,TRUE=-1 $
PARTN PL,, Q/A11,A21,,/C,N,1/C,N,1 /C,N,2/C,N,1 $
PARTN PBL,,Q/B11,B21,,/C,N,1 /C,N,1 /C,N,2/C,N,1 $
MERGE A11,B21,,,Q /PPP/C,N,1/C,N,1/C,N,2 $
EQUIV PPP,PBL/TRUE $
ENDALTER

DMI Q 0 2 1 1 m 1
DMI Q 1 n 1.0
    
```

where m = number of d.o.f. in L set  
and n specifies location of P load



Nonlinear analysis of a rotating  
beam ( $\rho\omega^2 = -\alpha/a$ ) under axial compression.

Figure 2. Concluded

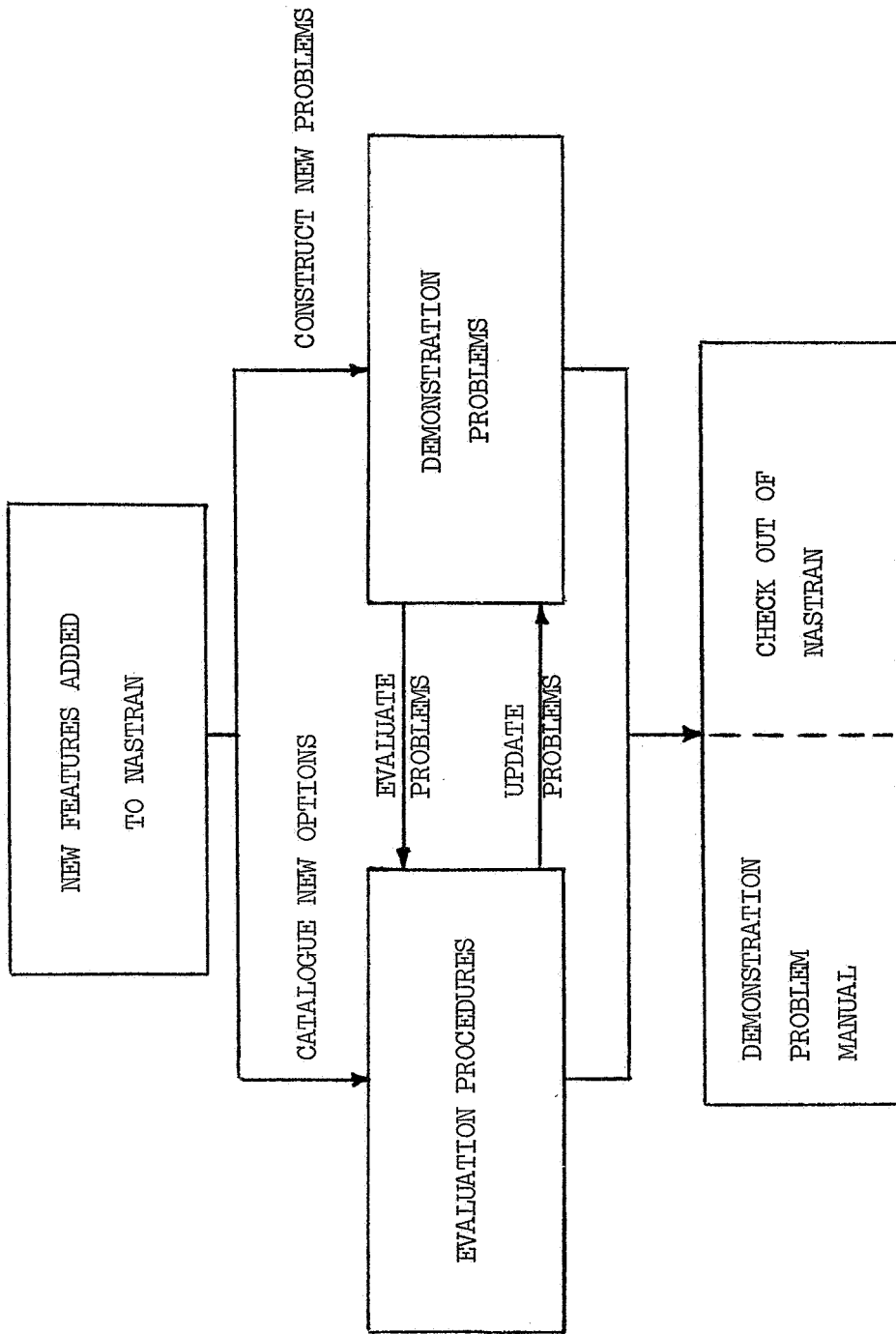


Figure 3. Construction and Maintenance of an Optimum Set of Demonstration Problems.

NATIONAL AERONAUTICS AND SPACE ADMINISTRATION  
WASHINGTON, D.C. 20546

OFFICIAL BUSINESS  
PENALTY FOR PRIVATE USE \$300

FIRST CLASS MAIL

POSTAGE AND FEES PAID  
NATIONAL AERONAUTICS AND  
SPACE ADMINISTRATION  
451



POSTMASTER: If Undeliverable (Section 168  
Postal Manual) Do Not Return

*"The aeronautical and space activities of the United States shall be conducted so as to contribute . . . to the expansion of human knowledge of phenomena in the atmosphere and space. The Administration shall provide for the widest practicable and appropriate dissemination of information concerning its activities and the results thereof."*

—NATIONAL AERONAUTICS AND SPACE ACT OF 1958

## NASA SCIENTIFIC AND TECHNICAL PUBLICATIONS

**TECHNICAL REPORTS:** Scientific and technical information considered important, complete, and a lasting contribution to existing knowledge.

**TECHNICAL NOTES:** Information less broad in scope but nevertheless of importance as a contribution to existing knowledge.

**TECHNICAL MEMORANDUMS:** Information receiving limited distribution because of preliminary data, security classification, or other reasons. Also includes conference proceedings with either limited or unlimited distribution.

**CONTRACTOR REPORTS:** Scientific and technical information generated under a NASA contract or grant and considered an important contribution to existing knowledge.

**TECHNICAL TRANSLATIONS:** Information published in a foreign language considered to merit NASA distribution in English.

**SPECIAL PUBLICATIONS:** Information derived from or of value to NASA activities. Publications include final reports of major projects, monographs, data compilations, handbooks, sourcebooks, and special bibliographies.

**TECHNOLOGY UTILIZATION PUBLICATIONS:** Information on technology used by NASA that may be of particular interest in commercial and other non-aerospace applications. Publications include Tech Briefs, Technology Utilization Reports and Technology Surveys.

Details on the availability of these publications may be obtained from:

SCIENTIFIC AND TECHNICAL INFORMATION OFFICE

NATIONAL AERONAUTICS AND SPACE ADMINISTRATION

Washington, D.C. 20546